UNIVERSITÀ DEGLI STUDI DI MILANO

DOCTORATE SCHOOL OF CHEMICAL SCIENCES AND TECHNOLOGIES

DEPARTMENT OF CHEMISTRY

PHD COURSE IN CHEMICAL SCIENCES, XXVI CYCLE

SYNTHESIS AND BIOLOGICAL EVALUATION OF POTENT INTEGRIN LIGANDS CONTAINING A DIKETOPIPERAZINE SCAFFOLD, AND OF THEIR DUAL-ACTION CONJUGATES

MICHELE MINGOZZI

R09022

Tutor: Prof. Cesare GENNARI

Co-Tutor: Prof. Umberto PIARULLI (Università dell'Insubria)

Coordinator: Prof. Emanuela LICANDRO

A.Y. 2012/2013

The present work was led by:	Prof. C. Gennari and Prof. U. Piarulli
Doctoral Final Oral Examination:	January, 14th 2014
Examination Committee:	Chairperson: Prof. M. Botta
	Second Member: Prof. D. Passarella
	Third Member: Prof. K.-H. Altmann

The work herein described was performed at the Department of Chemistry of the University of Milan in the period from January 2011 to December 2013 under the supervision of Prof. Cesare Gennari and Prof. Umberto Piarulli, whom I sincerely wish to thank.

"The important thing is not to stop questioning"
A. Einstein

Grazie a chi mi induce a non essere mai quieto nel mio sapere.

Table Of Contents

1 | Integrin Ligands

Part of the work described in this Chapter was published in the following articles:

M. Marchini, M. Mingozzi, R. Colombo, C. Gennari, M. Durini, U. Piarulli, *Tetrahedron* **2010**, *51*, 4278-4280.

M. Marchini, M. Mingozzi, R. Colombo, I. Guzzetti, L. Belvisi, F. Vasile, D. Potenza, U. Piarulli, D. Arosio, C. Gennari, *Chemistry: European Journal* **2012**, *18*, 6195 -6207.

M. Mingozzi, A. Dal Corso, M. Marchini, I. Guzzetti, M. Civera, U. Piarulli, D. Arosio, L. Belvisi, D. Potenza, L. Pignataro, C. Gennari, *Chemistry: European Journal* **2013**, *19*, 3563-3567.

1.1 TARGETING INTEGRINS

Integrins are the major family of adhesion receptors known in the kingdom Animalia, being involved in cell adhesion to extracellular matrix proteins and also playing important roles in cell-cell adhesion. In addition to mediating cell adhesion, integrins make transmembrane connections to the cytoskeleton and activate many intracellular signaling pathways. Since the recognition of the integrin receptor family around 20 years ago,[1] they have become the best-understood cell adhesion receptors. Integrins and their ligands play key roles in the pathogenesis of inflammatory diseases, leukocyte traffic, aggregation, tumor progression as well as osteoporosis and macular degeneration. The role of integrins in pathological conditions makes them attractive as pharmacological targets.[2]

Research in the last two decades has been directed to the discovery and the development of integrin antagonists for clinical applications.[3] The early discovery of the structural basis of the recognition between integrins and their natural ligands by means of short amino acid sequences,[4] together with outstanding crystallographic, electron microscopy, and computational analyses[5,6] on selected integrin subfamilies provided a breakthrough for the rational design of a wide variety of class-selective or promiscuous integrin inhibitors.

1.1.1 - Integrins: family, function, structure

Integrins are heterodimeric membrane glycoproteins comprising non-covalently associated α- and β-subunits, mediating dynamic linkages between extracellular adhesion molecules and the intracellular actin cytoskeleton. They are expressed by all multicellular animals, but their diversity varies widely among species; for example, 18 α and 8 β subunit genes are present in mammals, encoding for 25 different heterodimers, whereas the Drosophila and Caenorhabditis genomes encode only five and two integrin α and β subunits, respectively.

Each integrin subunit consists of an extracellular domain, a single transmembrane region, and a short cytoplasmic region (~30–40 amino acids). Figure 1.1.1 depicts the mammalian subunits and their αβ associations; 8 β subunits can assort with 18 α subunits to form 24 distinct integrins.[7]

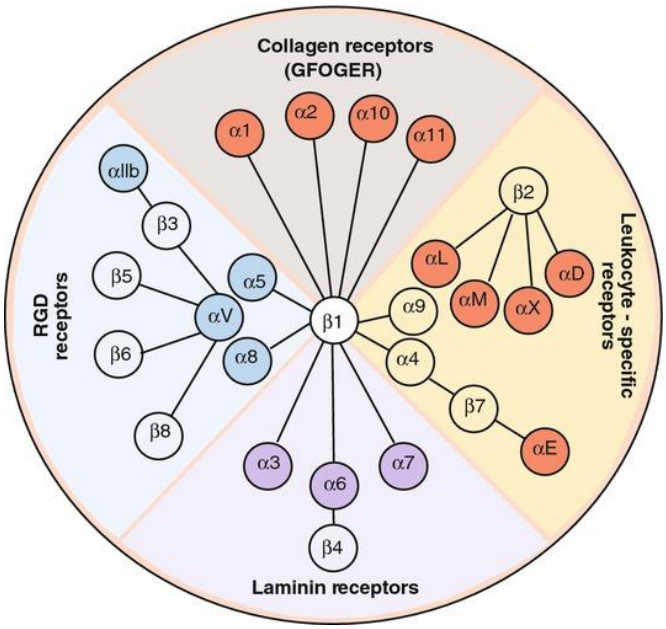

Figure 1.1.1 - Integrin family.

The N-terminus of the α-chain consists of a β-propeller domain that is formed by seven repeats of 60 amino acids each.[8] The β-propeller domain is linked to the transmembrane domain by three regions that have been named the Thigh, Calf-1, and Calf-2 domains (Figure 1.2 a). In addition, a highly flexible region is present between the Thigh and Calf-1 domains.5 Half of all α-chains have an additional 200-amino acid inserted domain between repeats two and three of the β- propeller (the I-domain, Figure 1.1.2 a).[9] The I-domain functions as the major ligand-binding site in those integrins where it is present, whereas the β-propeller serves as the ligand binding in integrins without I-domains.[10] Cytoplasmic tail domains of individual α-subunits are well-conserved across species boundaries.[11]

The N-terminal region of the β-subunit consists of a cysteine-rich region termed the plexin-semaphorin-integrin (PSI) domain. C-terminal to this domain is an evolutionarily conserved I-like domain flanked on either side by immunoglobulin folds called hybrid domains. The membrane proximal region of the α-subunit contains four EGF-like repeats. The α-subunit also has a flexible "knee" region, which is formed by the hybrid domain and the first two EGF-like repeats (Figure1.1.2 b).[10] The intracellular regions of the β-subunits are more conserved between subunits than are the α-subunit cytoplasmic tails.[12] These β-chain cytoplasmic tails play significant roles in regulating integrin activity.[5b]

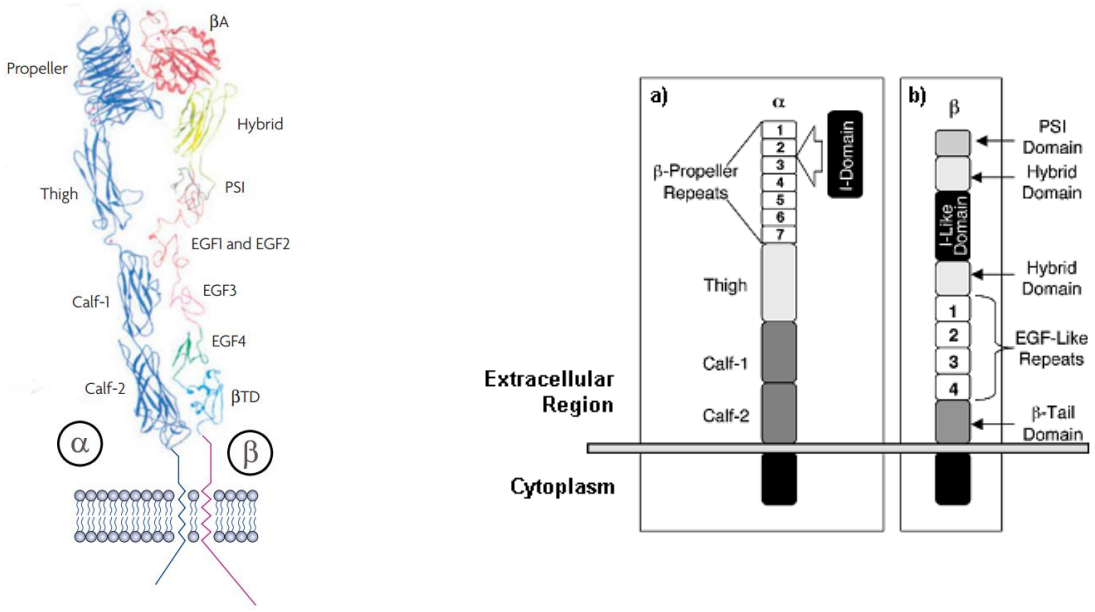

Figure 1.1.2 - Integrin structure. a) Primary structure of integrin α-subunits. Half of the α-subunits also have an I-domain inserted between β-propeller repeats 2 and 3; b) Primary structure of integrin β-subunits.

Each α-chain combines with a β-chain to form a unique heterodimer with selectivity for ECM proteins, cell surface molecules, plasma proteins, or microorganisms.[13] Integrins bind to their ligands in a divalent cation-dependent fashion.[14] Although some integrins recognize primarily a single ECM protein ligand (e.g., $\alpha_5\beta_1$ recognizes primarily fibronectin), others can bind several ligands (e.g., integrin $\alpha_v\beta_3$ binds vitronectin, fibronectin, fibrinogen, denatured or proteolyzed collagen, and other matrix proteins). Many integrins recognize the tripeptide Arg–Gly–Asp (RGD) (e.g. $\alpha_v\beta_3$, $\alpha_5\beta_1$, $\alpha_{IIb}\beta_3$, $\alpha_v\beta_6$, and $\alpha_3\beta_1$), but sequences flanking the RGD peptide are also important for selectivity.[13a,b] Other integrins recognize alternative short peptide sequences (e.g., integrin $\alpha_4\beta_1$ recognizes Glu lle Leu Asp Val [EILDV] and Arg Glu Asp Val [REDV] in alternatively spliced CS-1 fibronectin and $\alpha_{IIb}\beta_3$ binds KQAGDV in the fibrinogen γ chain).[15] In addition, some integrins can also bind cell surface receptors to induce cell–cell adhesion.[13b,c]

The ligands bound by common integrins and integrin clinical targets are shown in Table 1.1.1.[16]

Table 1.1.1 - Integrin subfamilies cluster major therapeutic indications and main ligands.

Integrin class	*Clinically targeted in:*	*Main ligands*[a]
α4- Family		
α4β1	MS, autoimmune, Crohn's, IBD	VCAM-1, FN
α4β7	MS, autoimmune, arthritis	MAd-CAM-1
α9β1	Cancer	VCAM-1, Opn, VEGF-C,-D
Leukocyte cell adhesion		
αLβ2	Inflammation, psoriasis, stroke, ischemia, fibrosis	ICAM-1,-2,-3
αMβ2	Inflammation, autoimmune	iC3b, Fbg
αXβ2	Inflammation	iC3b, Fbg
αDβ2	Inflammation	ICAM-3, VCAM-1
αEβ7	Inflammation	E-cadherin
RGD-binding		
gpIIbIIIa	Thrombosis, stroke, myocardial ischemia	Fbg, vWf
α5β1	Cancer, AMD	FN
α8β1	None	Npn, FN, VN
αnβ1	Cancer	VN, FN
αnβ3	Cancer, osteoporosis	VN, Opn, vWf, FN, Fbg[b]
αnβ5	Cancer	VN
αnβ6	Fibrosis, transplant rejection, cancer	FN, TGF-b1,-3
αnβ8	Cancer	FN, TGF-b1,-3
I domain: collagen binding		
α1β1	Fibrosis, cancer	Col
α2β1	Fibrosis, cancer	Col
α10β1, α11β1	None	Col
LN binding		
α3β1	None	LN-5
α6β1, α7β1	None	LN-1, -2
α6β4	None	LN-2, -4, -5

[a] Abbreviations: VCAM-1, vascular cell adhesion molecule 1; Mad-CAM-1, mucosal vascular addressin cell adhesion molecule 1; ICAM, Intercellular Adhesion Molecule 1; iC3b, complement regulatory protein; TGF, transforming growth factor; Col, collagens; Fbg, fibrinogen; FN, Fibronectin; LN, laminin; Npn, nephronectin; Opn, osteopontin; VN, vitronectin; vWF, von Willebrand factor.
[b] Among many other ligands.

Integrins are not constitutively active, but rather exist in multiple activation states (Figure 1.1.3).[17] Integrin activation status is regulated by the delicate balance in a bidirectional signaling mechanism which drives reversible changes in integrin conformation and affinity for their ligands. Both extra- and intracellular stimuli are allowed to regulate activation.[7,18]

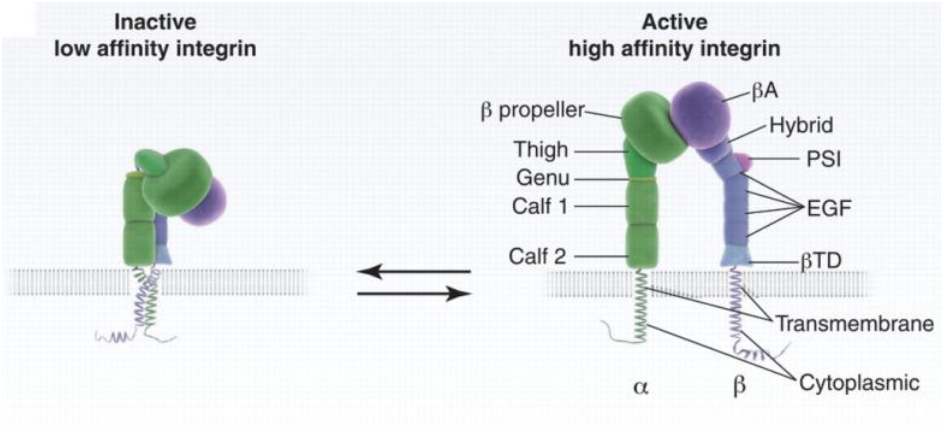

Figure 1.1.3 - Representation of integrin activation states.

High affinity binding of integrins to ligands is promoted in response to intracellular signaling events converging on the cytoplasmic domain that alter the tertiary and quaternary structure of the extracellular region, making the integrin ligand-competent (inside-out signaling).

Extracellular factors that influence integrin activation are ligand binding, divalent cation concentration, chemokine signaling and mechanical stress. Integrins transmit signals to the cell interior, which regulate organization of the cytoskeleton, activate kinase signaling cascades, and modulate the cell cycle and gene expression (outside-in signaling). Through this mechanism, integrins behave as mechanochemical transducers, orchestrating a synergic cross-talk with other extracellular matrix constituents and providing anchorage for endothelial cells.

The integrin tails serve as a site for the docking of various kinases and related adaptor proteins that comprise focal adhesions. Signals emanating from focal adhesions have been shown to promote survival, differentiation and proliferation.[19] In the absence of integrin ligation, these processes are abrogated, and therefore pharmacological inhibition of integrin ligation is of great interest for the therapy of numerous diseases resulting from aberrant integrin mediated signaling.

Integrins are transducing information both into and out of the cell to promote cell adhesion, spreading and motility. Disruption of focal adhesions prevents integrin-mediated cell adhesion and impairs cell motility and migration. Prolonged integrin inhibition in adhesion-dependent cells results in anoikis, apoptotic cell death due to ECM deprivation.[20]

1.1.2 Role in Human Diseases

1.1.2.1 Role in Angiogenesis

Angiogenesis is the process whereby new vessels form from pre-existing vessels. The growth of new blood vessels promotes embryonic development, wound healing, the female reproductive cycle, and also plays a key role in the pathological development of solid tumors, hemangiomas, diabetic retinopathy, age-related macular degeneration, psoriasis, gingivitis, rheumatoid arthritis, and possibly osteoarthritis and inflammatory bowel disease.[21]

Several cell types within tumors, including tumor cells, monocytes, and fibroblasts, secrete growth factors, such as VEGF, that induce blood vessel growth into tumors (Figure 1.1.4).[22]

Studies have shown that angiogenesis plays a major role in tumor growth and that inhibiting angiogenesis can inhibit tumor progression and metastasis. Although growth factors and their receptors play key roles in angiogenic sprouting, adhesion to the ECM also regulates angiogenesis.

Formation of new vasculature requires endothelial cell attachment and migration on ECM proteins. One ECM protein, fibronectin, is associated with vascular proliferation.[23]

As integrins are critical for the cell to bind ECM, many integrins play crucial roles in regulating vascular growth, both during embryonic development and in various pathologies. Proliferating endothelial cells express several integrins that are not expressed on quiescent blood vessels.

Recent studies suggest that inhibition of both $\alpha_v\beta_3$ and $\alpha_5\beta_1$ may be required for optimal effects on angiogenesis.[24]

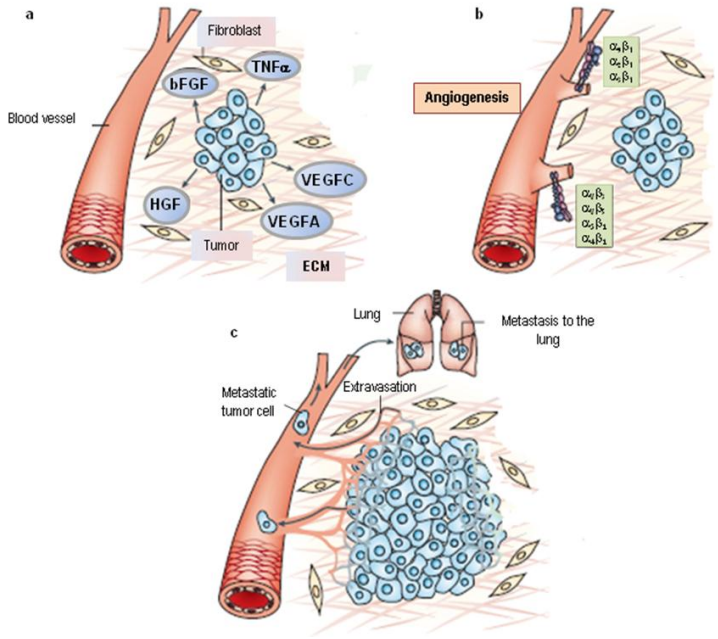

Figure 1.1.4 - Angiogenesis: a) secretion of growth factors and Chemokines from tumor cells in vicinity of already existing blood vessels; b) activation or expression upregulation of integrins such as $\alpha_1\beta_1$, $\alpha_2\beta_1$, $\alpha_4\beta_1$, $\alpha_5\beta_1$ and $\alpha_v\beta_3$ on blood vessels; c) integrins promoting endothelial cell migration and survival during invasion of tumour tissue. New vessel sprouts are produced promoting tumour growth and providing a way to metastasis to local and distant sites, such as lung.

Integrins $\alpha_{IIb}\beta_3$

$\alpha_{IIb}\beta_3$ integrin (GPIIa/IIIb) is highly expressed on the surface of platelets,[25] comprising approximately 80% of the total surface proteins found on platelets. The final common pathway in blood coagulation involves the engagement of this integrin induced by platelet activation. Under normal conditions integrin $\alpha_{IIb}\beta_3$ is maintained in the inactivated state. Soluble factors in the blood such as thrombin, bind their respective platelet receptors to activate inside-out signalling pathways that cause conformational changes in $\alpha_{IIb}\beta_3$ integrin.[25] Changes in conformation lead to increases in receptor affinity and avidity, which promote platelet aggregation and clot formation through increased cell-to-cell contacts and cell-matrix contacts. Aberrant platelet aggregation or thrombosis is central to the pathophysiology of multiple Acute Coronary Syndromes (ACS), unstable angina, ischemic stroke and sickle cell anemia. Inhibition of $\alpha_{IIb}\beta_3$ prevents platelet aggregation and therefore has shown efficacy in the prevention of thrombosis for the treatment of ACS. Some $\alpha_{IIb}\beta_3$ integrin targeted drugs have already been approved so far.

The complete ectodomain structure of integrin $\alpha_{IIb}\beta_3$ was determined,[26] thus living information about its binding site, better understanding its binding mode and conformation (Figure 1.1.5). The binding mode of RGD-based $\alpha_{IIb}\beta_3$ antagonists was established through mutagenesis experiments[27] and crystallographic analysis of the platelet fibrinogen receptor.[28]

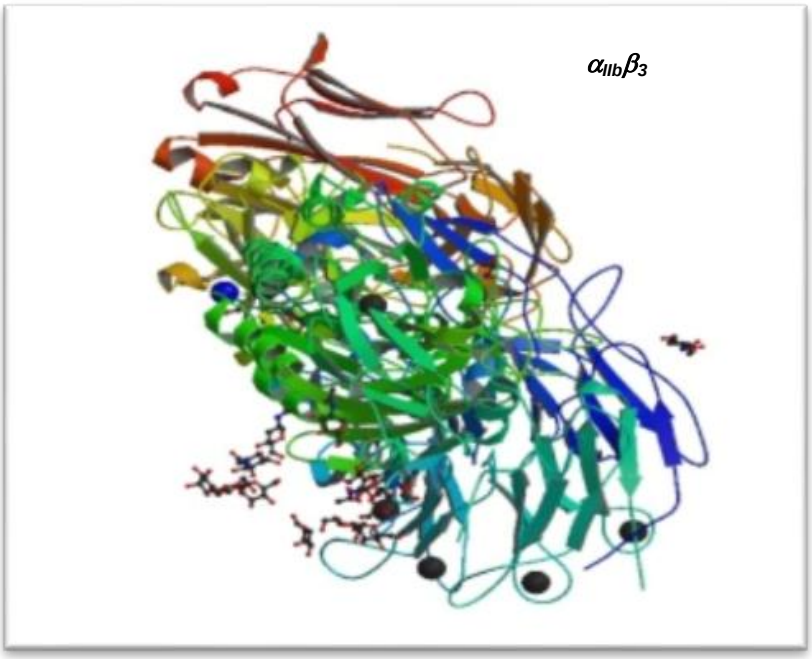

Figure 1.1.5 - Crystal structure of the extracellular segment of integrin $\alpha_{IIb}\beta_3$.

Integrins $\alpha_v\beta_3$ and $\alpha_v\beta_5$

Integrin $\alpha_v\beta_3$ is expressed on angiogenic blood vessels but not on resting vessels.[29] Antibodies that inhibit $\alpha_v\beta_3$ block angiogenesis in a variety of animal models. A key role of $\alpha_v\beta_3$ in vasculogenesis and angiogenesis has been outlined. Peptide and antibody antagonists of $\alpha_v\beta_3$ also block tumor angiogenesis and growth. Further analysis showed tumor regression related to apoptosis in the vasculature, induced by these antagonists.[30] Different members of the integrin α_v subfamily transduce angiogenic signals by different growth factors. *In vivo* angiogenesis assays showed that bFGF or TNF-α depend on $\alpha_v\beta_3$ to initiate angiogenesis, whereas $\alpha_v\beta_5$ is required for TGF-α- and VEGF-mediated angiogenesis.[31] These data, taken together, have established a role for $\alpha_v\beta_3$ integrins in angiogenesis and as important therapeutic targets.

One study showed that animals lacking β_3 or β_3 and β_5 subunits displayed increased tumor angiogenesis.[32] This led to the controversial conclusion that $\alpha_v\beta_3/\alpha_v\beta_5$ integrins might actually be involved in suppressing angiogenesis. However, it is likely that the apoptotic mechanism, which is generally induced by unligated integrins and controls tumor vascular growth, is responsible for the increased vascularization in β_3 - and β_5 - deficient tumors.[16,33]

The complete crystal structure of $\alpha_v\beta_3$ integrin ectodomain including an αβ transmembrane fragment has been very recently determined.[34] The earlier determination of the crystal structure of the ectodomain of $\alpha_v\beta_3$ (ΔTM- $\alpha_v\beta_3$, Figure 1.1.6a) in the absence and presence of a prototypical RGD ligand (Cilengitide, Figure 1.1.6b), already revealed the modular nature of integrins and pivotal information on its divalent cation–mediated binding interactions with extracellular ligands.

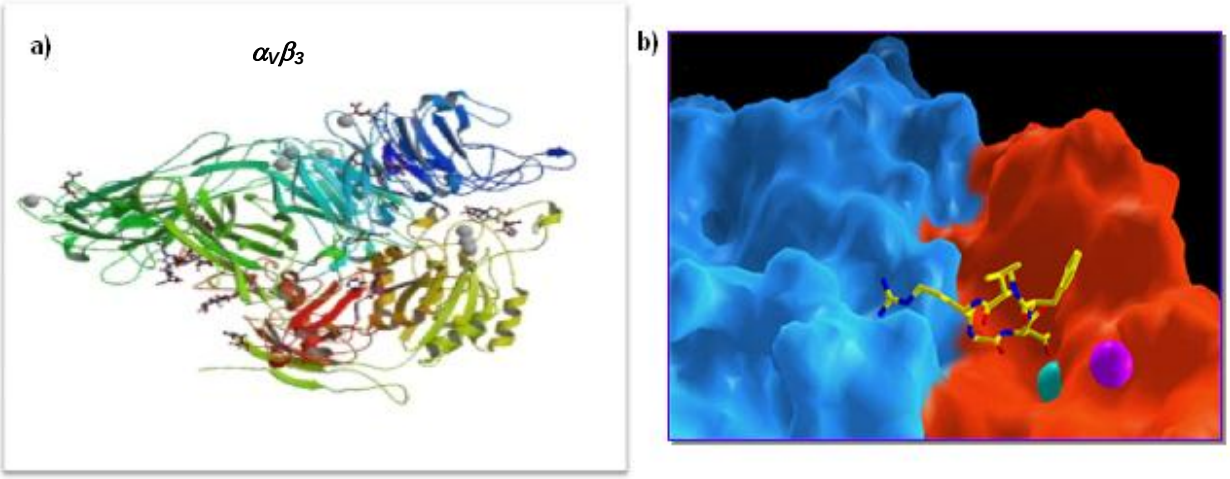

Figure 1.1.6 - Crystal structures of $\alpha_v\beta_3$ integrin: a) Crystal structure of the extracellular segment of integrin $\alpha_v\beta_3$; b) Crystal structure of the extracellular segment of $\alpha_v\beta_3$ integrin in complex with the cyclic pentapeptide ligand Cilengitide, in its binding conformation.

A homology model for the closely related $\alpha_V\beta_5$ receptor was developed. The two integrins were found to mostly differ in the region comprising residues 159-188 in the β_3 subunit. A 'roof' was described for $\alpha_V\beta_5$ integrin featuring Tyr and Lys residues, which would hamper the binding of compounds containing bulky substituents nearby their Asp-mimicking group. Because of this difference, a few inhibitors of $\alpha_V\beta_3$ integrin displaying selectivity over $\alpha_V\beta_5$ have actually been found,[35] but specific inhibitors of $\alpha_V\beta_5$ integrins have not been described yet.

Integrin $\alpha_5\beta_1$

Integrin $\alpha_5\beta_1$ is significantly upregulated in tumor angiogenesis in both mice and humans, but is not expressed on quiescent endothelium. Antagonists of $\alpha_5\beta_1$ also inhibited tumor angiogenesis in chicks and mice, thus leading to tumor regression.[23] Integrin $\alpha_5\beta_1$-mediated adhesion promotes endothelial cell survival *in vivo* and *in vitro*[33] by suppressing the activity of protein kinase A (PKA). Integrin $\alpha_5\beta_1$ antagonists activate both PKA and caspase-8, thereby inducing apoptosis and inhibiting angiogenesis.[36] Although inhibition of integrin ligation can prevent cell attachment to the ECM, recent studies show that integrin $\alpha_5\beta_1$ antagonists also actively suppress signal transduction that leads to cell survival. Antagonists of $\alpha_5\beta_1$ suppress cell migration and survival on vitronectin, but not cell attachment to vitronectin, indicating that these antagonists affect the migration and survival machinery rather than integrin receptors for vitronectin.[16,37] The three-dimensional structure of the ligand-binding headpiece of integrin $\alpha_5\beta_1$ complexed with fragments of its physiological ligand fibronectin was determined by means of a molecular electron microscopy. The density map for the unliganded $\alpha_5\beta_1$ headpiece shows a 'closed' conformation similar to that seen in the $\alpha_V\beta_3$ crystal structure. By contrast, binding to fibronectin induces an 'open' conformation (Figure 1.1.7).[38]

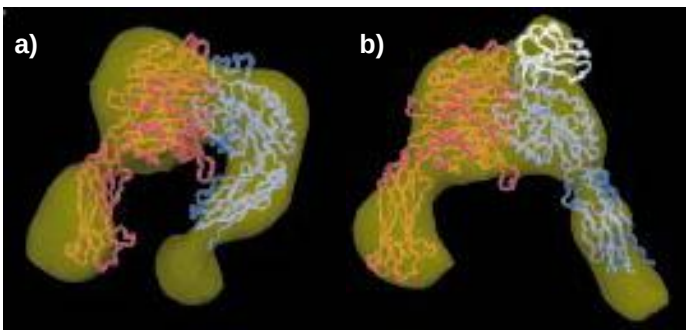

Figure 1.1.7 - Surface-rendered density maps of the $\alpha_5\beta_1$ headpiece: a) the unliganded closed and b) the ligand-bound open conformation.

The lack of reliable structural data in the past, however, excluded $\alpha_5\beta_1$ as target for structure based drug design. However, the high homology between the different integrin subtypes makes them promising targets for homology modeling, which was achieved for $\alpha_V\beta_5$ integrin by Kessler and co-workers.[39,35b] Homology modeling of proteins is considered to be possible for a homology of 40% or greater.[40] This precondition is met by the integrins $\alpha_V\beta_3$ and $\alpha_5\beta_1$ with 53% homology for α_V/α_5 and 55% for β_3/β_1. Recently the $\alpha_5\beta_1$ crystal structure was published, providing the necessary knowledge for structure based drug design.[41] In particular Takagi and coworkers reported the crystal structure of a ligand-binding fragment of human $\alpha_5\beta_1$ integrin, a prototypic integrin that functions as an RGD-dependent fibronectin receptor. The structure, solved as a complex with a Fab fragment of the anti-$\beta_1$inhibitory antibody SG/19, revealed high similarity to the ligand unbound form of $\alpha_V\beta_3$ and $\alpha_{IIb}\beta_3$ integrins (Figure 1.1.8). Surprisingly, the RGD peptide can be introduced into the binding pocket by soaking, without causing any conformational change in integrin except for an ~1 Å shift of one residue and the dissociation of Ca^{2+} from the adjacent to the MIDAS (ADMIDAS). Docking simulations and structure-based mutagenesis identified a single α_5 residue responsible for the strong preference of $\alpha_5\beta_1$ for fibronectin, establishing a basis for the combinatorial roles played by each subunit during the specific recognition of protein ligands.

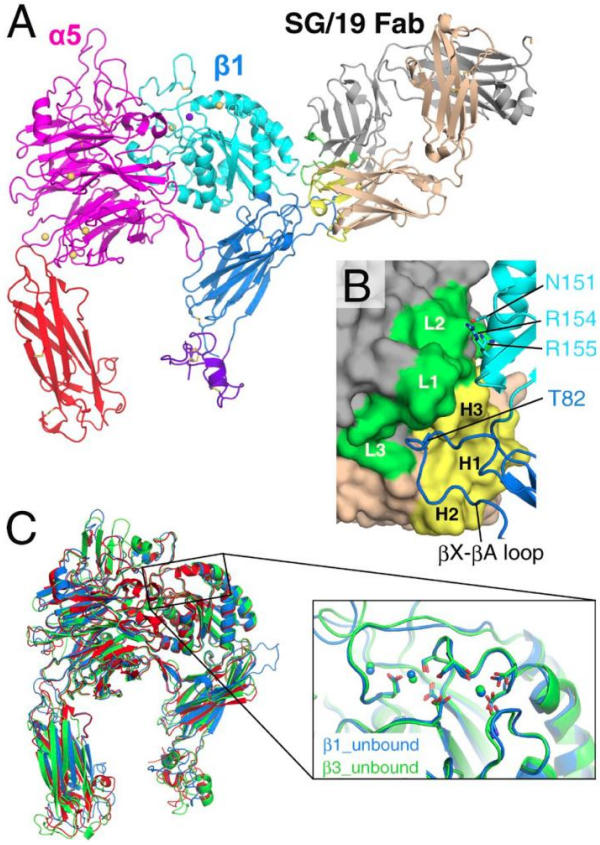

Figure 1.1.8 - Structure of the $\alpha_5\beta_1$ integrin headpiece in complex with SG/19Fab: A) Ribbon presentation of the overall structure with disulfide bonds in stick model. Individual domains are differently colored in magenta (β-propeller), red (thigh), cyan (βA), blue (hybrid), and purple (PSI), and bound metal ions are shown as spheres (yellow for Ca^{2+} and purple for Mg^{2+}). SG/19 Fab is colored in gray (light chain) and wheat (heavy chain), with their CDR loop regions highlighted in green and yellow, respectively. B) Close-up view of the SG/19-binding interface. SG/19 Fab and β_1 chain are shown in surface and ribbon presentations, respectively, with the same color code used in A. CDR regions and important interface residues are labeled. C) Superposition of three integrin headpiece structures in the ligand unbound form. Blue, $\alpha_5\beta_1$; red, $\alpha_V\beta_3$ (3IJE); green, $\alpha_{IIb}\beta_3$ (3FCS). On the right is a blowup of the region around the metal-binding sites in the β_1 (blue) and β_3 (green; 3FCS) βA domains.

1.1.2.2 Role in hemostasis and thrombosis

Thrombosis is a disease-related process consisting in the formation of a blood clot inside a blood vessel. It occurs when platelets adhere to damaged blood vessels and become activated.[42] These activated platelets recruit other platelets, resulting in the formation of a haemostatic plug. This is an essential mechanism for preventing blood loss, but inappropriate thrombus formation can lead to a stroke or to a heart attack. It is probably the first clearly integrin associated process.

In this context, integrin $\alpha_{IIB}\beta_3$ is responsible for platelet aggregation and this feature made it the first integrin to be identified as therapeutic target. In the 1990s, three $\alpha_{IIB}\beta_3$ integrin inhibitors were approved to reduce the risk of ischaemic events in patients with acute coronary syndromes and those undergoing percutaneous coronary intervention. They were the antibody fragment abciximab and the small-molecule inhibitors eptifibatide **1** and tirofiban **2** (Figure 1.1.9), all of which are administered intravenously.[43]

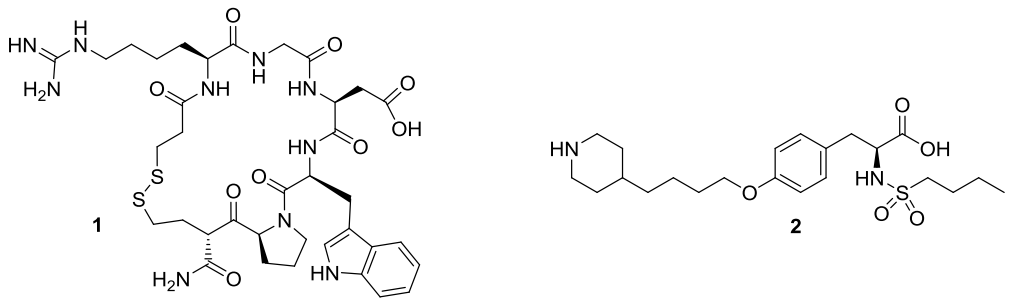

Figure 1.1.9 - $\alpha_{IIB}\beta_3$ integrin inhibitors.

However, despite initial expectations that antagonists targeting this integrin would be blockbuster drugs, attempts to develop oral antagonists for more convenient administration were not successful, and the use of the approved intravenous inhibitors has largely been restricted to high-risk patients.

Instead, clopidogrel (commercially known also as PLAVIX®), an orally active ADP receptor antagonist, filled the market that was expected for $\alpha_{IIB}\beta_3$ integrin antagonists and became the second biggest-selling drug globally.[44]

The failure of oral $\alpha_{IIB}\beta_3$ antagonists was probably due to multiple factors.[45] There were severe problems, in particular a poor bioavailability and the lack complete understanding of the $\alpha_{IIB}\beta_3$ integrin role in thrombosis and signalling.

1.1.2.3 Immune system disorders

Beside the studies on blood diseases, a great number of attempts have been made to find efficient antagonists of integrins involved in immune system disorders.
In particular, both β_1 and β_2 integrins are important in immune function, where they have essential roles in localizing the immune response to the site of inflammation.[46] Moreover a defect in β_2 integrins leads to a life-threatening immune dysfunction (that is, leukocyte adhesion deficiency).[47]
In this context, $\alpha_L\beta_2$ and $\alpha_4\beta_1$ have been the first integrins to be therapeutically targeted. In particular Karin and coworkers reported that $\alpha_4\beta_1$ integrin has a key role in the migration of lymphocytes to inflamed regions of the central nervous system in rodent models of multiple sclerosis.[48]
Monoclonal antibody binding the α_4 integrin subunit (natalizumab, approved in 2004) was effective in the treatment of multiple sclerosis, and also for the inflammatory bowel disorder Crohn's disease.[49]Although natalizumab showed substantial efficacy in clinical trials,[50] several patients developed a fatal progressive multifocal leukoencephalopathy after treatment,[51] and the drug was withdrawn from the market in 2005. However, after reassessment in 2010, the European Medicines Agency (EMA) concluded that the benefits outweighed the risks for patients treated with natalizumab, and it was re-approved with implementation of appropriate warning and safety measures. Several small-molecule inhibitors of α_4 integrins are in development as followers of natalizumab.

1.1.2.4 Osteoporosis

Osteoporosis occurs when the balance between bone formation and degradation is disturbed. Integrins have an important role in the function of osteoclasts, which mediate bone resorption. Osteoclast $\alpha_1\beta_1$ integrin is responsible for the adhesion of osteoclasts to collagen.[52] The $\alpha_v\beta_3$ integrin is also important in osteoclast function, and polymorphisms in this receptor are also associated with increased rate of fracture.[53] An antagonist of this receptor (L-000845704) showed an increased bone density in postmenopausal women in a Phase II clinical study.[54] However, it seems that neither this antagonist or any other anti-integrin is currently in clinical development for osteoporosis.

1.1.3 RGD and *iso*DGR recognition motifs

The arginine-glycine-aspartic acid (RGD) cell adhesion sequence was discovered in fibronectin 27 years ago.[55] Other adhesion proteins such as vitronectin, fibrinogen, von Willebrand factor, thrombospondin, laminin, entactin, tenascin, osteopontin, bone sialoprotein, and, under some conditions, collagens were then discovered to include RGD sites. It was soon confirmed with regard to fibronectin and then extended to other proteins that the RGD sequence is the endogenous recognition motif for cell attachment to proteins.

Cells expressing several α_V integrins (e.g. β_1, β_3, β_5, β_6 and β_8), as well as integrins $\alpha_{IIb}\beta_3$, $\alpha_5\beta_1$ and $\alpha_8\beta_1$, recognize the ubiquitous RGD sequence in their ligands. Naturally occurring integrin inhibitor proteins bearing the RGD motif are showing an extremely varied selectivity and potency in targeting RGD-recognizing integrins. Elucidations on their structure suggest that proper restriction of the RGD flexibility can lead to integrin inhibition.[56]

Hence, monomeric linear or confomationally constrained RGD-containing cyclic peptides, pseudo-peptides, and mimetics thereof displaying high potency and selectivity were conceived. The most significant advances in this field have led to the development of agents targeting $\alpha_{IIb}\beta_3$ integrin on platelets for inhibiting thrombosis[57] and inhibitors of $\alpha_V\beta_3$ and $\alpha_V\beta_5$ integrins against angiogenesis, cancer and bone resorption.[58] Among these, it is important to recall the nanomolar $\alpha_V\beta_3/\alpha_V\beta_5$ binder cyclic pentapeptide c-RGD-(D-Phe)-*N*-methyl-V developed by Kessler (known as Cilengitide or EMD121974), which is currently tested in phase II clinical investigation ("CORE" trials) for patients with newly diagnosed glioblastoma multiforme and unmethylated MGMT gene promoter, while it has been withdrawn from phase III clinical investigation ("CENTRIC" trials, Cilengitide in combination with Temozolomide and Radiotherapy in newly diagnosed glioblastoma).[58p]

As already mentioned, a crucial enhancement in this field was achieved with the crystal structure resolution of the ectodomain of $\alpha_V\beta_3$ integrin, both unligated and complexed with Cilengitide,[5b] as well as the better crystal structure resolution of $\alpha_{IIb}\beta_3$ integrin complexed with the synthetic anti-trombotic drug *Eptifibatide*.[6d,59]

Besides the well-defined RGD and other binding motifs, it has been proposed that the NGR and DGR sequences might also have a role in integrin recognition. Controversial results have however been reported.

The importance of the *iso*DGR sequence as an integrin binding motif was discovered by serendipity by Corti research group (S.Raffaele/MolMed).[60]

The NGR sequence, present in several endogenous molecules as well as in fibronectin FN-I$_5$ and FN-I$_7$, can easily deamidate (also *in vivo*) on asparagine, giving *iso*DGR and DGR (Scheme 1.1.1). Although protein modifications typically causes loss of activity/function, it was recently suggested that *iso*DGR formation at NGR or DGR sites might result in a gain of function. The *iso*DGR sequence can in fact mimic RGD and interact with the RGD-binding site of integrins.[61]

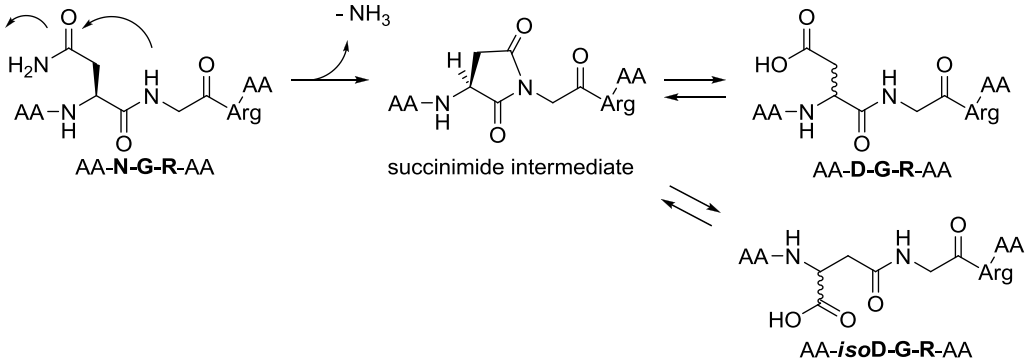

Scheme 1.1.1 - Formation of DGR and *iso*DGR sequences by asparagine deamidation.

*iso*DGR containing peptides can recognize members of the RGD-dependent integrin family, such as $\alpha_v\beta_3$, $\alpha_v\beta_5$, $\alpha_v\beta_6$, $\alpha_v\beta_8$ and $\alpha_5\beta_1$, but not other.[62] Both affinity and specificity of the interaction between *iso*DGR and integrin binding site is reported to be highly dependent on the flanking residues.

Notably, *iso*DGR docks onto the integrin binding site in an inverted orientation respect to RGD. This orientation allows *iso*DGR to bind to the $\alpha_v\beta_3$ binding pocket maintaining all the typical electrostatic-clamp interactions of the RGD motif. The acidic and basic residues are at the correct distance and orientation to engage stabilizing interactions with the polar regions of integrin: the *iso*Aspartic carboxylic side chain is interacting with MIDAS, Asn^{215}, Tyr^{122} and Arg^{214}, while Arginine guanidinium interacts with Asp^{218}, Asp^{150} and Gln^{180}. Moreover, additional stabilizing interactions are present: glycine recognizes the receptor via polar interactions and an H-bond between its amide and carbonyl of Arg^{216}.[61] Therefore, *iso*DGR can be considered as a natural fit for the RGD binding pocket of $\alpha_v\beta_3$ integrin, suggesting that the naturally occurring transformation of NGR and DGR into *iso*DGR functions as a molecular switch able to activate integrin recognition.

Although *iso*DGR- and RGD-containing ligands can share the same integrin binding site, their effects on integrin function might not be necessarily the same.[63]

1.1.3.1 RGD integrin ligands: state of the art

The potential of $\alpha_v\beta_3$ inhibitor EMD121974 (**3**, Cilengitide, Figure 1.1.10) by Kessler was soon recognized by various clinical programs, opening the era of the integrin inhibitor class as investigational agents for antiangiogenic and anticancer therapies. The crystal structure analysis of the ectodomain of $\alpha_v\beta_3$ complexed with Cilengitide offered the first clear picture of the RGD binding mode, which revealed a Cilengitide conformation featuring an inverse γ-turn centred on Asp, and a distorted βII'-turn with Gly and Asp at the i+1 and i+2 positions, respectively. A distance of 8.9 Å between the C_β of Asp and Arg, accounting for an almost extended conformation of the RGD motif were observed. The most important interactions between the ligand and the receptor involved the Arg guanidinium group, which was forming salt bridges with Asp150 and Asp218 in the α subunit, and the Asp carboxylic group of the ligand, which interacts with the Mn^{2+} ion at MIDAS (Metal-Ion-Dependent Adhesion Site) in the β subunit. Moreover, several hydrophobic interactions were engaging the Gly residue, positioned at the interface between the α and β subunits.

An earlier example of RGD-based cyclic peptide had already been identified by Kessler, c(RGDfV)[64] **4** (Figure 1.1.10), which can be considered as an ancestor of Cilengitide. This compound was selectively active against $\alpha_v\beta_3$ integrin, and its overall conformation allowed the lateral chains of Asp and Arg to adopt a unstretched arrangement (distance C_β(Asp)- C_β(Arg) 6.9 Å).

Representative examples of semipeptidic $\alpha_v\beta_3$ inhibitors, bearing a non-peptidic and rigid turn-inducing motif to appropriately constrain the RGD motif, are reported in the literature.

Classic bicyclic, but also monocyclic scaffolds and simple linear tethers have been used to properly fold the RGD sequence within a macrocyclic template, to better fit within $\alpha_v\beta_3$ integrin binding site.[65]

Bicyclic heterocycles stand among the most popular constrained mimetics of natural amino acids in the structure-based design of peptidomimetics. Various successful examples of peptide are validating their use as preferred conformation inducing scaffolds.[66]

Kessler exploited azabicycloalkane and spyrocyclic systems, traditionally known as β-turn inducers, to prepare cyclic RGD-containing peptidomimetics.[67] The most active and less constrained compound of the series (**5**, Figure 1.1.10) was a fully promiscuous antagonist.

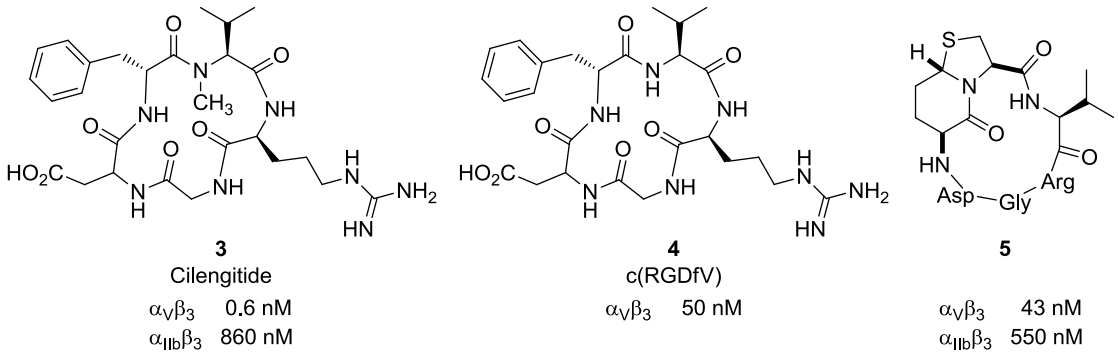

Figure 1.1.10

A library of RGD pentapeptide mimetics incorporating 5,6- and 5,7-fused azabicycloalkane amino acids was generated by the group of Scolastico.[68] Among the high affinity ligands found within the collection, the most active compounds demonstrated low nanomolar binders of $\alpha_V\beta_3$ and $\alpha_V\beta_5$ integrins. **6** was completely selective towards $\alpha_V\beta_3$ integrin respect to $\alpha_V\beta_5$ integrin. Moreover, significant antiangiogenic activity of this compound emerged from *in vitro* experiments showing inhibition of the proliferation of endothelial cells.[69]

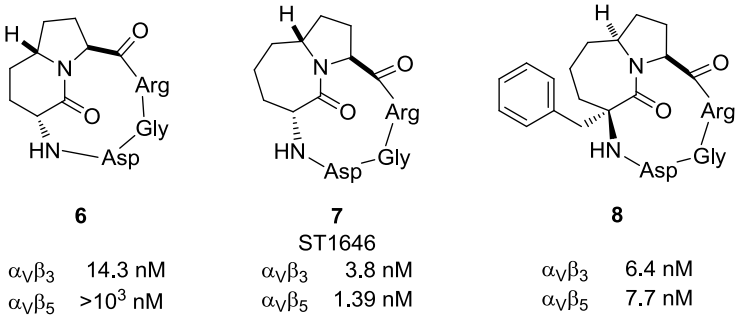

Figure 1.1.11

A strong dependence of the overall conformation of the cyclic peptides on the lactam ring size and stereochemistry was revealed. Almost the same interactions observed in the crystal structure of $\alpha_V\beta_3$ complexed with Cilengitide **3** were maintained. They observed an average distance between Arg and Asp C_β of 8.8 Å in the case of **6**, and 8.5 Å in **7**, indicative of an almost extended conformation of the RGD sequence.
Cyclopeptide **8** (Figure 1.1.11) emerged as a nanomolar antagonist of both $\alpha_V\beta_3$ and $\alpha_V\beta_5$ integrins comparable to ST1646 **7**. Docking studies revealed that the conformations containing an inverse γ-turn on Asp conserved the main contacts observed in the X-ray crystal structure with Cilengitide **3**.[70]

Also monocyclic turn-inducing scaffolds were used in the search for non peptidic RGD-containing systems, based on βII'/γ arrangement with the γ-turn centered on Gly. Kessler inserted amino pyrrolidinone based motifs to hold the RGD moiety, providing macrocycles **9a** and **9b** (Figure 1.1.12).[71] A βII' turn conformation with Gly at the i+1 position was unexpectedly observed for these compounds. **9a** was a moderate and selective antagonist of $\alpha_V\beta_3$ integrin, while **9b** proved to be a more active $\alpha_V\beta_3$ inhibitor, even though aspecific. The main difference between the two analogues was the orientation of the lactam bond in the turn-motif, which was found to be rotated by 180° in the two isomers, and involved in a H-bond with the receptor in the case of **9b**.

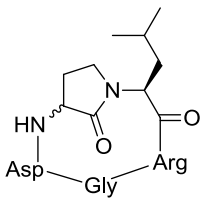

9a: (*S*) $\alpha_V\beta_3$ 40 nM
$\alpha_{IIb}\beta_3$ 2.8 μM
9b: (*R*) $\alpha_V\beta_3$ 0.8 nM
$\alpha_{IIb}\beta_3$ 8.5 nM

Figure 1.1.12

D- and L-morpholines were exploited by Guarna and co-workers to replace the *N*-Me-Val motif of Cilengitide **3**, grafting compounds **10** (Figure 1.1.13).[72] The different conformation of the peptide bond between D-Phe and the morpholine scaffold provided distinct structural arrangements for the two compounds. **10b** showed in particular a *cis* conformation in the docking analysis, with an RGD sequence arrangement comparable to that observed in the $\alpha_V\beta_3$-Cilengitide complex.

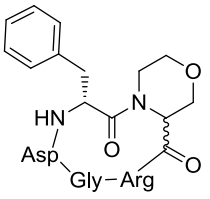

10a: (*S*) $\alpha_V\beta_3$ 157 nM
$\alpha_V\beta_5$ 15.1 nM
10b: (*R*) $\alpha_V\beta_3$ 32.6 nM
$\alpha_V\beta_5$ 21 nM

Figure 1.1.13

Kessler and Overhand designed several pyranoid and furanoid sugar δ- and ε-amino acid based compounds. Due to their high flexibility, they proved to be aspecific antagonists of $\alpha_V\beta_3$ and $\alpha_{IIb}\beta_3$ integrins. This aspecificity was also supported by the conformational analysis of this compounds, which showed an arrangement standing in between the typical kinked conformation of $\alpha_V\beta_3$-selective antagonists and the extended one required for targeting $\alpha_{IIb}\beta_3$ integrin. The two most representative members of this class of compounds are sketched in Figure 1.1.14 (**11**, **12**).[73,58k]

Casiraghi and colleagues, following an analogous inspiration, exploited furanoid carbasugar γ-amino acid equivalents to generate four stereoisomeric macrocycles (most active members **13**, Figure 1.1.14). Although an improvement in the affinity towards $\alpha_V\beta_3$ and $\alpha_V\beta_5$ was observed, their activity surprisingly proved to be almost irrespective of the configuration at the carbons bearing the amino acid functions. An inverted γ-turn, centered on Asp was revealed by NMR, displaying a C_β(Asp)- C_β(Arg) distance in the range of 8.0-8.4 Å.[74]

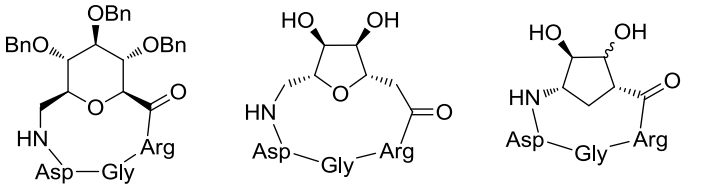

11

$\alpha_V\beta_3$ 25 nM
$\alpha_V\beta_5$ >10^4 nM
$\alpha_{IIb}\beta_3$ 13.4 nM

12

$\alpha_V\beta_3$ 1.49 μM
$\alpha_V\beta_5$ 0.38 μM

13

a (*S*): $\alpha_V\beta_3$ 51.4 nM
$\alpha_V\beta_5$ 165.5 nM
b (*R*): $\alpha_V\beta_3$ 44.7 nM
$\alpha_V\beta_5$ 125.4 nM

Figure 1.1.14

The same group incorporated 4-amino proline (Amp) scaffolds into a library of RGD peptides, to further extend these findings.[75] The compounds reported in Figure 1.1.15 (**14 a-d**) displayed exceptionally high affinity towards $\alpha_V\beta_3$ and $\alpha_V\beta_5$ integrins. A picomolar activity was observed for $\alpha_V\beta_3$ integrin in the high affinity status. A preferential conformation featuring an inverse γ-turn motif around Asp for the macrocycles containing a *cis*-disposed γ-amino acid motif was detected by NMR conformational analysis. On the contrary the macrocycles proved to be more flexible when a *trans* γ-amino acid was present. All the macrocycles showed a C_β(Asp)- C_β(Arg) distance in the 7.8-8.2 Å range. The most active analogues maintain the relevant key interactions observed for Cilengitide **3**. Compound **14a** was stabilized by a strong H-bonding contact between the NH in the aminoproline motif and Tyr178. Quite interestingly, the alkyl and acyl chains of **14 b** and **c** provided additional contacts for binding, pointing towards a large hydrophobic hollow rich with aromatic residues.

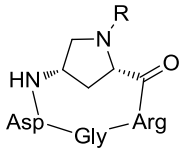

14

a: R= H
$\alpha_V\beta_3$ 4.4 nM
$\alpha_V\beta_5$ 80.2 nM

b: R= n-Heptyl
$\alpha_V\beta_3$ 2.84 nM
$\alpha_V\beta_5$ 36.1 nM

c: R= Propionyl
$\alpha_V\beta_3$ 5.60 nM
$\alpha_V\beta_5$ 94.0 nM

d: R= Bz
$\alpha_V\beta_3$ 5.15 nM
$\alpha_V\beta_5$ 86.6 nM

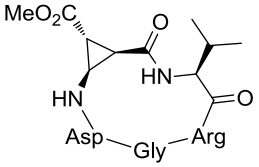

15

$\alpha_V\beta_3$ 20 nM
$\alpha_5\beta_1$ 1.5 μM

Figure 1.1.15

Pseudopentapeptides containing both enantiomers of *cis*-β-aminocyclopropanecarboxylic acid (β-Acc) were conceived, the most interesting of the two being sketched in Figure 1.1.15 (**15**).[58e]
Compound **15** resulted more active towards both $\alpha_V\beta_3$ and $\alpha_5\beta_1$ integrins, respect to the reference compound c(RGDfV) **4**. The C_β(Asp)- C_β(Arg) distance found for compound **15** resulted considerably shorter than expected (7.06 Å). Moreover, a γ-turn centered on Gly and a pseudo β-turn wherein (+)-β-Acc occupied the i+1 position were observed.

Despite the impressive work dedicated to the identification of semipeptide analogues, Cilengitide (**3**) is the only investigational agent of this class that has been developed for clinical testing on cancer patients. The growth inhibitory activity of Cilengitide observed in the clinic is likely due to a combination of multifaceted mechanisms. These might depend on whether the drug is administered alone or in combination, and include inhibition of angiogenesis, direct cytotoxic activity on tumor cells, increase of endothelial cell permeability, and inhibition of cell adhesion, migration and invasion.[65,76] Very recently, a paradoxical proangiogenic activity of low doses of Cilengitide was observed in certain preclinical studies (see also Chapter 2.1 for further discussion).[77]

1.1.3.2 isoDGR integrin ligands

As regards *iso*DGR-containing cyclic peptides or pseudo-peptides, not many examples appeared in the literature so far.

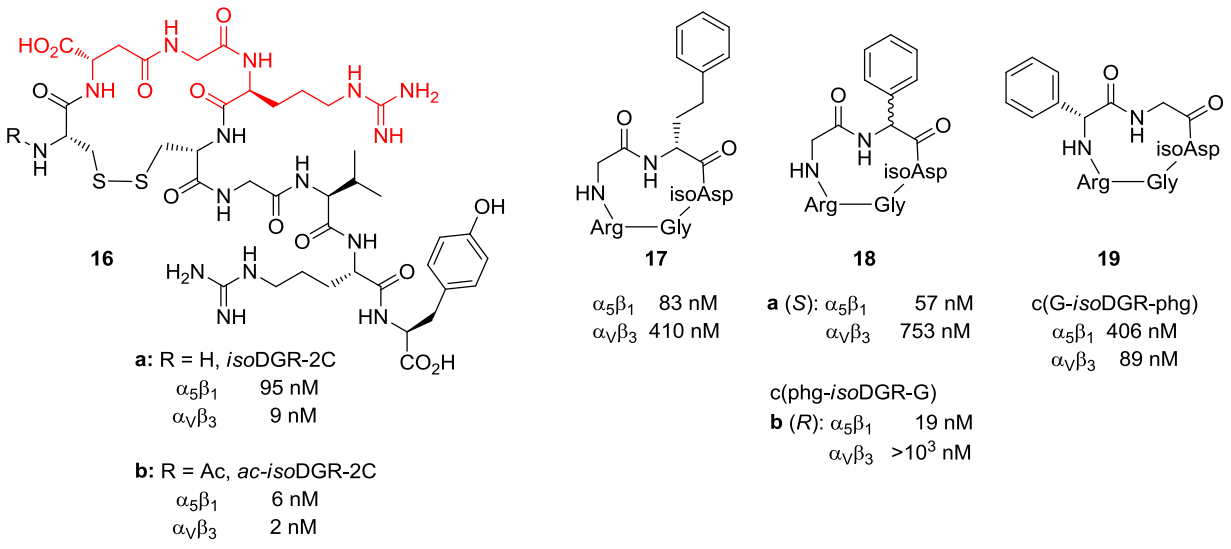

Figure 1.1.16

Being a relatively young research field (the earliest evidences dating back to 2006),[78] there is still a need to understand the structural basis for the interaction of *iso*DGR with the RGD-binding site of integrins, the molecular switch ability of the NGR sequence to

*iso*DGR and its possible applications in the discovery of innovative drugs. Still, extensive efforts in the understanding of the *iso*DGR motif potential need to be profused.

The most interesting examples appeared in the literature are reported in Figure 1.1.16.

Compound **16a** was the first to be discovered, by Corti and co-workers.[60,61] The efficacy of the cyclic motif C*iso*DGRC was demonstrated exchanging cysteine residues with glycine, and analogues such as **16b** were also prepared, obtaining enhanced affinity towards most of the integrins tested.[62]

These compounds have been tested for their competitive binding with ACDCRGDCFC-TNF to $\alpha_v\beta_3$ integrin. Being ACDCRGDCFC-TNF a quite weak ligand of $\alpha_v\beta_3$ integrin, the strikingly low nanomolar activity of these compounds should not be compared to other already shown activities.

Kessler and colleagues started an investigation in the field, synthesizing a small library of compounds based on the retrosequence of the highly active integrin-binding cyclic peptide c(RGDfV) **4**, for example c(Vf*iso*DGR), obtaining moderate to poor results. Far better results were obtained flanking the *iso*DGR moiety with an aromatic amino acid and a glycine (**17-19**, Figure 1.1.16). Hints on the importance of the flanking residues and, in particular, on the effects of a flanking aromatic moiety were given, and interesting selectivity towards $\alpha_5\beta_1$ integrin respect to $\alpha_v\beta_3$ integrin were obtained.[79]

1.2 Previous Work of Our Research Group in the Field

1.2.1 Diketopiperazines (DKP) scaffolds

Recently, our group developed the synthesis of a new class of bifunctional DKP scaffolds (**DKP-1**, **DKP-2**, **DKP-3**, Figure 1.2.1), formally derived from aspartic acid and 2,3-diaminopropionic acid, bearing a carboxylic acid and an amino functionalities.[80,81] As a consequence of the absolute configuration of the two α-amino acids forming the cyclic dipeptide unit, the two reactive functionalities (amino and carboxylic acid) are locked in a *cis*- (**DKP-1**) or *trans*-configuration (**DKP-2**, **DKP-3**). In addition, while being derived from α-amino acids, these DKP scaffolds can be seen as a conformationally constrained dipeptide formed by two β-amino acids (see Figure 1.2.1), and in particular a β^2- and a β^3-amino acids (following Seebach's nomenclature).[82]

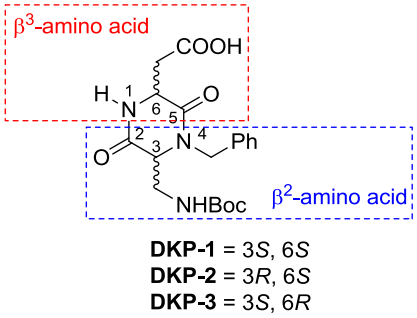

Figure 1.2.1 - Structure of bifunctional DKP scaffolds highlighting the conformationally constrained β2–β3 dipeptide sequence.

DKP-1, **DKP-2** and **DKP-3** (bearing a benzyl group at nitrogen N-4, Figure 1.2.1) were prepared making use of the serine ligation strategy exemplified in Scheme 1.2.1.[83] These scaffolds differs into the stereocenters at C3-C6 (Figure 1.2.1) and the synthetic sequence started from either (*R*)- or (*S*)-*N*-(tert-butoxycarbonyl)aspartic acid β-allyl ester **20**[84] and either (*R*)- or (*S*)-*N*-benzylserine methyl ester **21** (Scheme 1.2.1).[85] Direct coupling of these fragments (HATU, *i*Pr$_2$NEt or EDC, DMAP) led to the isopeptides **22** in high yield, rather than forming the expected dipeptides **23**. As a matter of fact, selective *O*-acylation of the unprotected β-hydroxyl group of *N*-benzylserine methyl ester is preferred to the formation of the tertiary amide and the resulting ester bond is stable in solution to *O,N*-acyl transfer.[83] The *O,N*-acyl migration was then triggered by cleavage of the Boc protecting group and treatment with a base, which also promoted the simultaneous cyclization to the diketopiperazines **24**. The introduction of the nitrogen functionality was then realized through a Mitsunobu-type reaction using HN$_3$·Tol in a toluene / dichloromethane solution, thus obtaining azides **25** in a moderate (51%; *cis*: *S,S*) to good yield (80%; *trans*: *S,R* or *R,S*).[86] Finally, a one pot Staudinger reduction –

Boc protection[87] yielded the DKP scaffold allyl esters **26**, which was de-allylated[88] to give the amino acid derivatives **DKP-1**, **DKP-2** and **DKP-3** in a quantitative yield.

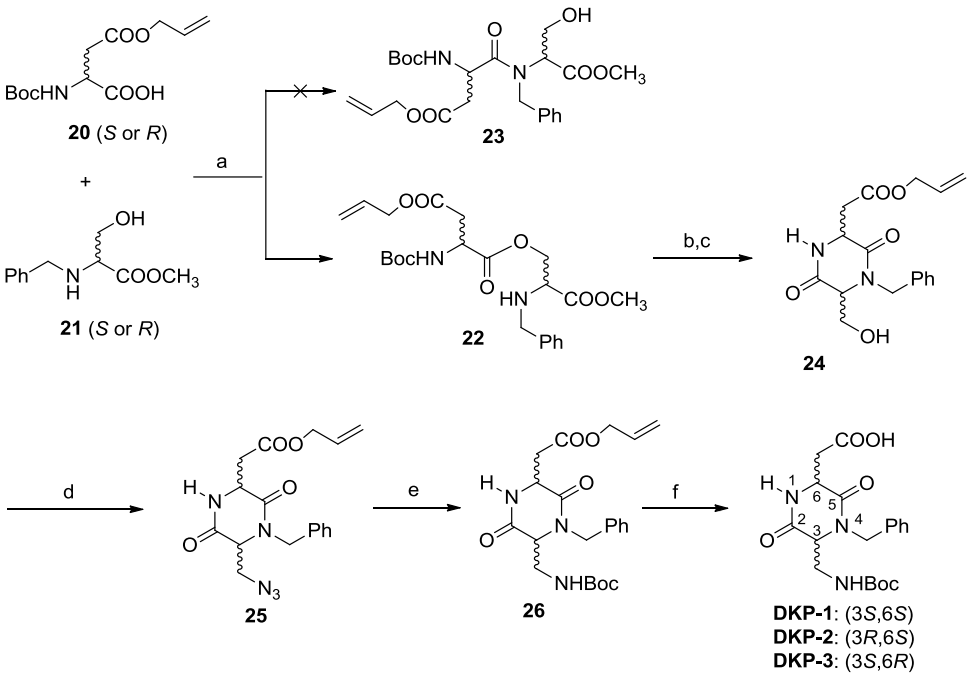

Scheme 1.2.1 - Synthesis of **DKP-1**, **DKP-2** and **DKP-3** *via* the serine ligation strategy. a) EDC·HCl, DMAP, CH_2Cl_2, 94%; b) TFA/CH_2Cl_2 1:2; c) DIPEA, *i*PrOH, 90% over two steps; d) HN_3, DIAD, PPh_3, CH_2Cl_2/toluene, 51% (*S*,*S*), 80% (*S*,*R* or *R*,*S*); e) Me_3P, BocON, THF, 76%; f) pyrrolidine, PPh_3, $[Pd(PPh_3)_4]$, CH_2Cl_2, 99%.

In addition, our group developed the synthesis of two functionalized (*f*) *trans* diketopiperazines (*i.e.*, **DKP-*f*2** and **DKP-*f*3**), varying the absolute stereochemistry at C-3 and C-6 (Figure 1.2.2).[89] These DKPs were used for the synthesis of *cyclo*[DKP-*f*-RGD] integrin ligands (Chapter 1.4), bearing a *p*-aminomethylbenzyl *N*-substituent as anchoring point for further conjugation for the synthesis of dual action compounds (Chapter 2). The Mtr protecting group for the *p*-aminomethylbenzyl *N*-substituent (Figure 1.2.2) was chosen because of its stability and orthogonality with the methyl, benzyl, allyl, *t*Bu, Boc, and Cbz protecting groups.

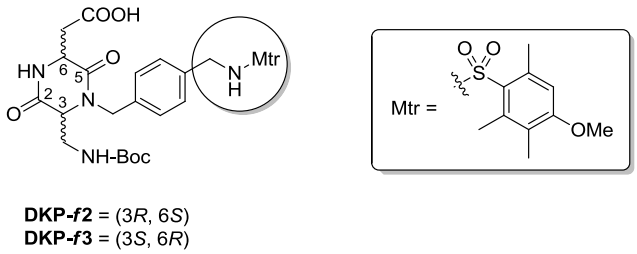

Figure 1.2.2 - Structure of functionalized (*f*) DKP-*f* scaffolds highlighting the *p*-aminomethylbenzyl *N*-substituent as anchorage point for further conjugations.

Also in this case, for the preparation of the functionalized *trans* diketopiperazines **DKP-*f*2** and **DKP-*f*3**, the serine ligation strategy was used (Scheme 1.2.2). (*R*)- and (*S*)-Serine were protected as methyl ester and reductively alkylated with aldehyde **27** and sodium triacetoxyborohydride to afford the amines **28** (Scheme 1.2.2). From this step, the synthesis is identical to that described in Scheme 1.2.1 (Scheme 1.2.2, yields are also comparable).

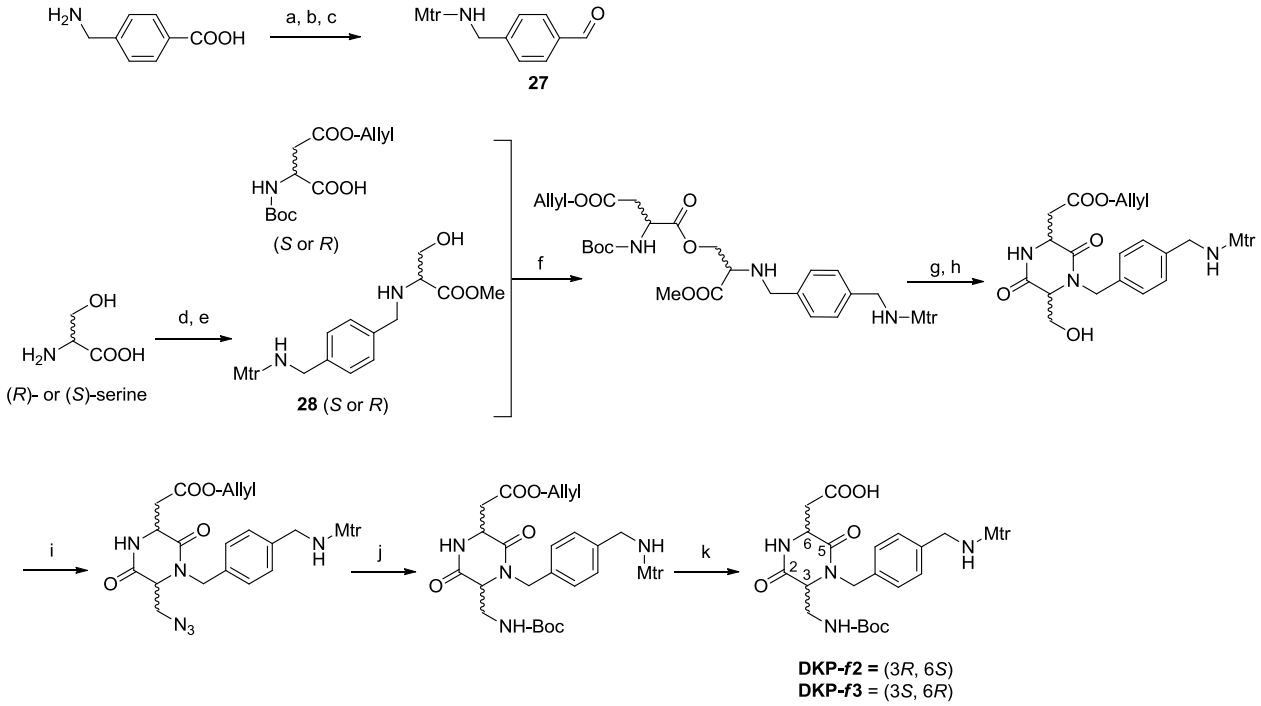

Scheme 1.2.2 - Synthesis of **DKP-*f*2** and **DKP-*f*3** *via* the serine ligation strategy. a) $LiAlH_4$, THF, 8 h, reflux, 70%; b) Mtr-Cl, *i*-Pr_2NEt, THF, 6 h, room temp., 85%; c) MnO_2, THF, overnight, room temp., quant.; d) MeOH, AcCl, quant.; e) aldehyde **27**, $NaBH(OAc)_3$, THF, 3 h, room temp., quant.; f) HATU, HOAT, *i*Pr_2NEt, DMF, 3 h, 0 °C to room temp., 86%; g) TFA/DCM 1:2, 3 h, 0 °C to room temp.; h) *i*Pr_2NEt, *i*PrOH, 6 h, room temp., 93% over two steps; i) HN_3·Tol, DIAD, Ph_3P, DCM/Tol 1:2, 7 h, -20 °C, 86%; j) Me_3P, BOC-ON, THF, 6 h, -20 °C to room temp., 88%; k) pyrrolidine, PPh_3, [$Pd(PPh_3)_4$], DCM, 4 h, room temp., quant.

1.2.2 c[DKP-RGD] integrin ligands

Starting from these scaffolds, our group previously developed the synthesis of cyclic RGD-peptidomimetics **c[DKP-1-RGD]**, **c[DKP-2-RGD]**, **c[DKP-3-RGD]**, **c[DKP-*f*2-RGD]** and **c[DKP-*f*3-RGD]** (Figure 1.2.3), containing the bifunctional diketopiperazine scaffolds **DKP-1**, **DKP-2**, **DKP-3**, **DKP-*f*2** and **DKP-*f*3** (Figure 1.2.3).[81,89,90]

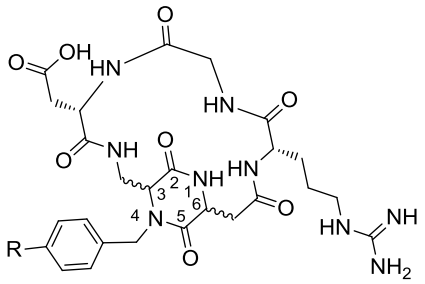

c[DKP-1-RGD]: (3*S*,6*S*), R = H
c[DKP-2-RGD]: (3*R*,6*S*), R = H
c[DKP-3-RGD]: (3*S*,6*R*), R = H
c[DKP-*f*2-RGD]: (3*R*,6*S*), R = CH_2NH_2
c[DKP-*f*3-RGD]: (3*S*,6*R*), R = CH_2NH_2

Figure 1.2.3 - Cyclic RGD peptidomimetics containing scaffolds **DKP-1**, **DKP-2**, **DKP-3**, **DKP-*f*2** and **DKP-*f*3**.

Diketopiperazines **DKP-1**, **DKP-2**, **DKP-3**, **DKP-*f*2** and **DKP-*f*3** were used as scaffolds for the synthesis of functionalized c[DKP-RGD] integrin ligands, following a solution-phase strategy (Scheme 1.2.3).

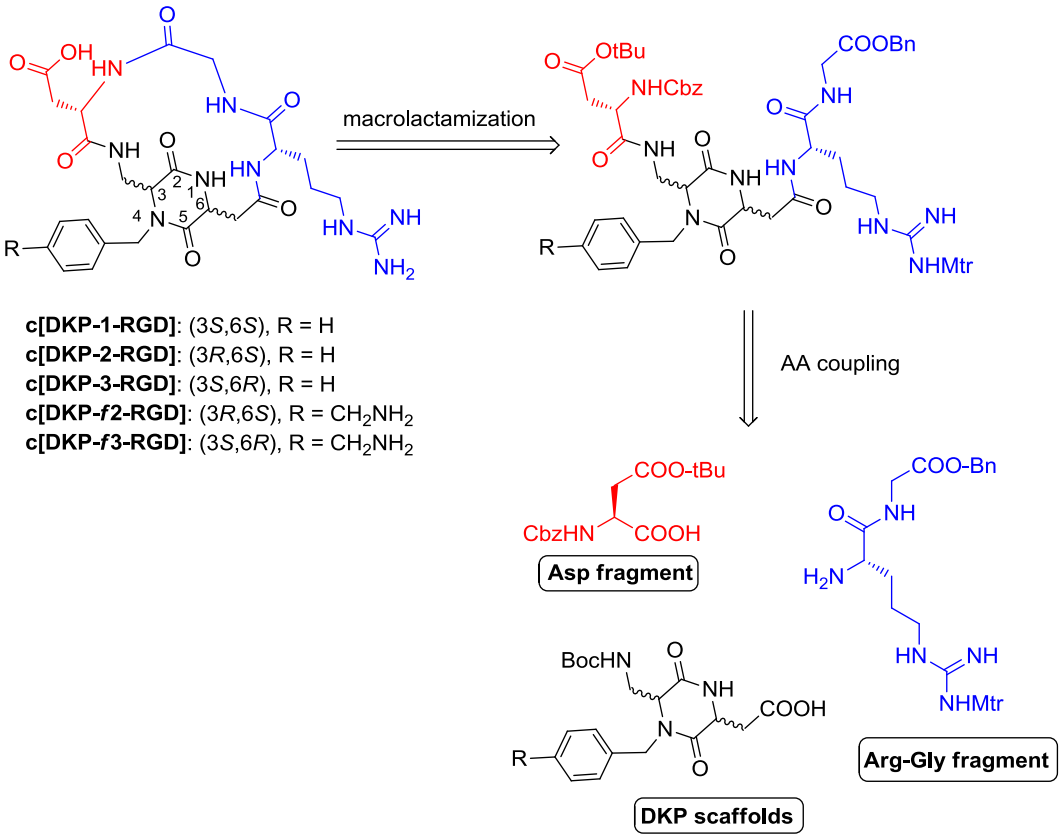

Scheme 1.2.3

Conformational studies of cyclic RGD peptidomimetics **c[DKP-1-RGD]**, **c[DKP-2-RGD]**, **c[DKP-3-RGD]** were performed by NMR spectroscopy (^{1}H-NMR and NOESY spectra of dilute H_2O/D_2O 9:1 solutions) and by computational methods [Monte Carlo/Stochastic Dynamics (MC/SD) simulations]. Their biological activities were evaluated in $\alpha_v\beta_3/\beta_5$ isolated receptor binding assay (see chapter 1.4.3 and 1.4.4 for more details).

During my PhD thesis I expanded this library of previously developed ligands, developing new DKP scaffolds (Chapter 1.3) and new corresponding c[DKP-RGD] integrin ligands (Chapter 1.4). The 7 new scaffolds of the prepared library were used as templates in the synthesis of cyclic integrin ligands containing either the RGD-recognition sequences. The development of this library has provided a detailed SAR analysis of new integrin ligands based on DKP scaffolds, affording to a comprehensive view for this new class of integrin ligands.

Furthermore, the functionalized ligands **c[DKP-*f*2-RGD]**, **c[DKP-*f*3-RGD]** and the new functionalized ligands described in Chapter 1.4.2 were used to synthesize integrin-targeting compounds conjugated to Paclitaxel and other dual-action conjugates (Chapter 2).

1.3 New DKP Scaffolds

1.3.1 Design of the library

On the basis of the goals previously achieved by our research group (see Chapter 1.2), the library of bifunctional diketopiperazines reported in Figure 1.3.1 was expanded, with the second-generation scaffolds **DKP-4-8** and **DKP-*f*4-6**, each differing in their stereochemistry and substitution pattern, to be used as templating moiety for the RGD sequence. Since the *cis* stereochemistry provided low affinity integrin ligand (see Chapter 1.4.3 for further discussion), the new scaffolds were developed only with the *trans* stereochemistry.

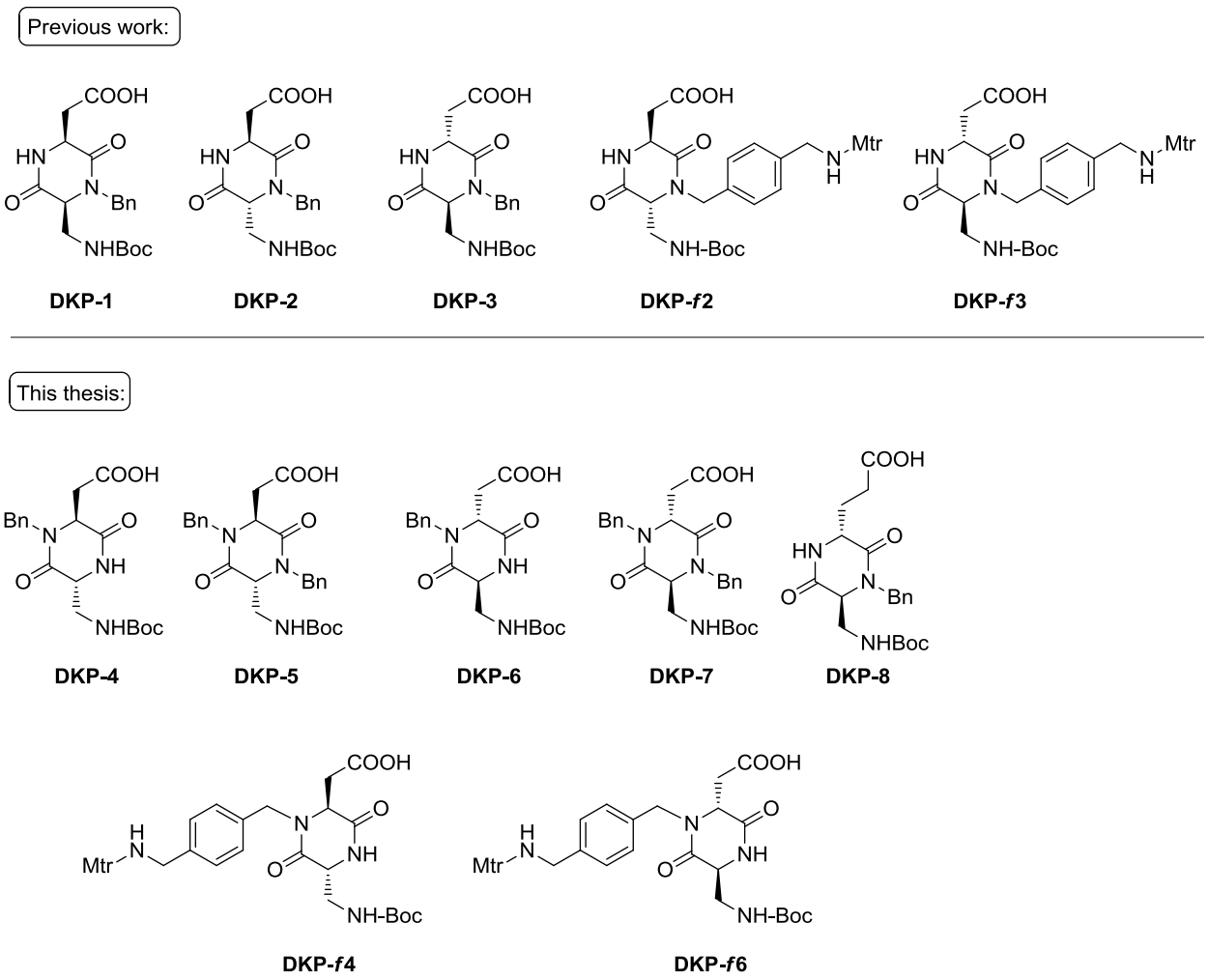

Figure 1.3.1 - Previously developed library of bifunctional diketopiperazine scaffolds (either functionalized or not) and second generation scaffolds (either functionalized or not).

DKP-1, **DKP-2**, **DKP-3**, **DKP-*f*2** and **DKP-*f*3** already turned out to be interesting and valuable constrained rigid scaffolds which, owing to their carboxylic acid and amino functionalities, could be successfully employed as secondary structure inducers for the RGD sequence. Moreover, functionalized scaffolds bear also a protected amino moiety that could be further employed for the synthesis of dual action compounds (Chapter 2). Tiny variations in their stereochemistry, ring substitutions or degrees of freedom, may dramatically change the behavior of these scaffolds when inserted into a peptidomimetic moiety. Having a wide range of scaffolds available may be of great impact expecially when aiming at the modulation of a biological target. For these reasons a library of new seven diketopiperazines (Figure 1.3.1) was conceived.
The new five unfunctionalized *trans* scaffolds differ for their absolute stereochemistry [either 3*R*,6*S* (**DKP-4, DKP-5**) or 3*S*,6*R* (**DKP-6**, **DKP-7**, **DKP-8**)], for the substitution at the endocyclic nitrogens, which can be either hydrogen or benzyl (**DKP-4**, **DKP-6, DKP-8**, **DKP-5**, **DKP-7**), and for the length of side-arm bearing the carboxylic group, which can be either carboxymethyl (**DKP-4-7**) or carboxyethyl (**DKP-8**). The new two functionalized *trans* scaffolds **DKP-*f*4** and **DKP-*f*6** differ for their absolute stereochemistry [3*R*,6*S* for (**DKP-*f*4**) and 3*S*,6*R* for (**DKP-*f*6**)].

1.3.2 Synthesis of DKP-4, DKP-6, DKP-*f*4 and DKP-*f*6

A retrosynthetic analysis of scaffolds **DKP-4** and **DKP-6** (bearing a benzyl group at nitrogen N-1) suggested that, also in this case, the diketopiperazine ring could be obtained from suitably protected aspartic acid and serine in the correct relative configuration (Scheme 1.3.1, see for comparison Scheme 1.2.1 and Scheme 1.2.2):

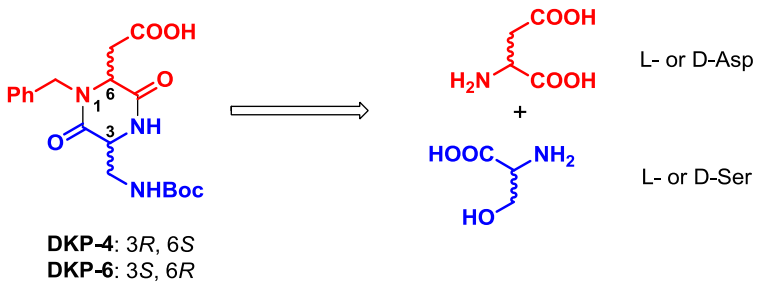

DKP-4: 3*R*, 6*S*
DKP-6: 3*S*, 6*R*

Scheme 1.3.1

Since the isopeptide route (see Scheme 1.2.1 and ref. 83) could not be applied for these scaffolds, the coupling of commercially available Boc-D-serine *tert*-butyl ether to *N*-benzyl-L-aspartic acid dimethylester **29a**[91] was initially developed for the preparation of diketopiperazine **DKP-4** (bearing a benzyl group at nitrogen N-1) (Scheme 1.3.2). Among the different coupling methodologies used (from the "classic" ones, based on

HATU and PyBrOP, till the more sophisticated such as cyanuric fluoride), the only one that was effective consisted in the pre-formation of the symmetric Boc-D-Ser(O*t*Bu) anhydride (using DCC)[92] and then coupling to *N*-Bn-L-Asp dimethyl ester **29a**, leading to the corresponding dipeptide **30a** in a satisfactory 75% yield. Treatment of dipeptide **30a** with trifluoroacetic acid (to deprotect both the amino and the hydroxy group of serine) and subsequent ring closing reaction in methanol, led to diketopiperazine **31a** (Scheme 1.3.2).

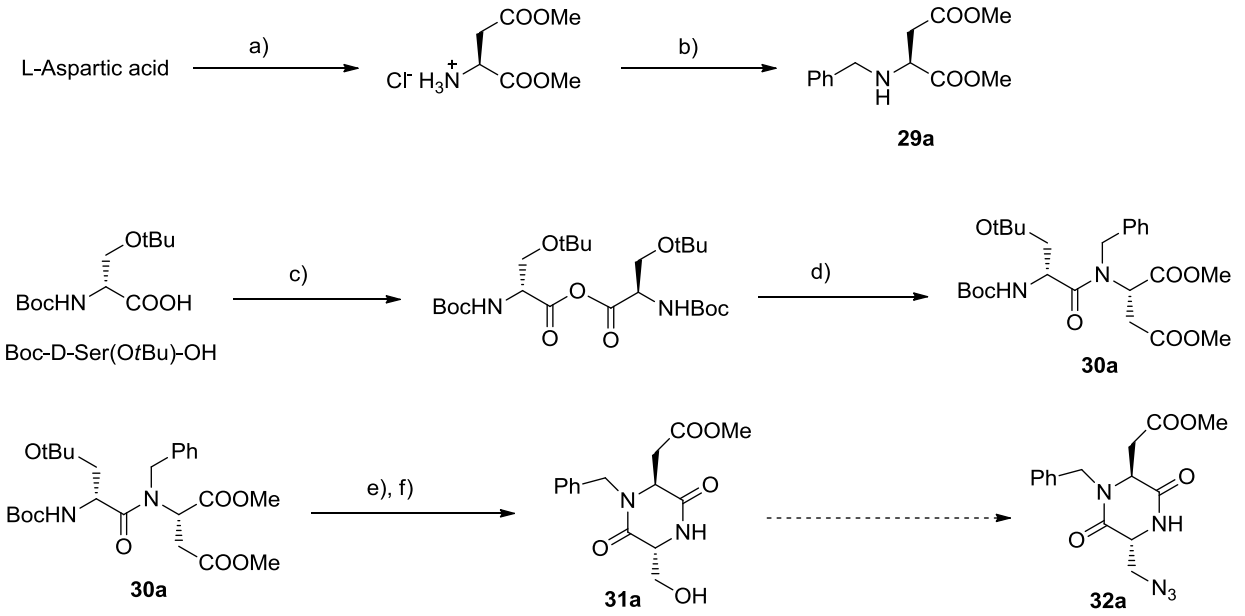

Scheme 1.3.2 - First-generation synthesis of diketopiperazine **31a**; Reagents and conditions: a) CH_3COCl, MeOH, 24h, 100%; b) PhCHO, $NaCNBH_3$, MeOH, 4h, 67%; c) DCC, CH_2Cl_2, 1h, 100%; d) **29a**, CH_2Cl_2, 18h, 75%; e) TFA/CH_2Cl_2 1:1, 2h; f) *i*Pr_2NEt, MeOH, 85% over two steps.

With the aim to transform the hydroxy group of **31a** in a protected amino group, we ran a Mitsunobu reaction under the same conditions used for the synthesis of scaffolds **DKP-1-3** (toluene/DCM, -20 °C, Scheme 1.2.1), but we only recovered starting material. Hence we tried to run the reaction again increasing temperature gradually, from -20 °C to 0 °C, without any results. Finally, the Mitsunobu reaction performed at r.t. led to azide **32a**, although major product resulted to be the β-elimination derivative **33a** (ratio **32a**/**33a** 1:4) (Scheme 1.3.3).

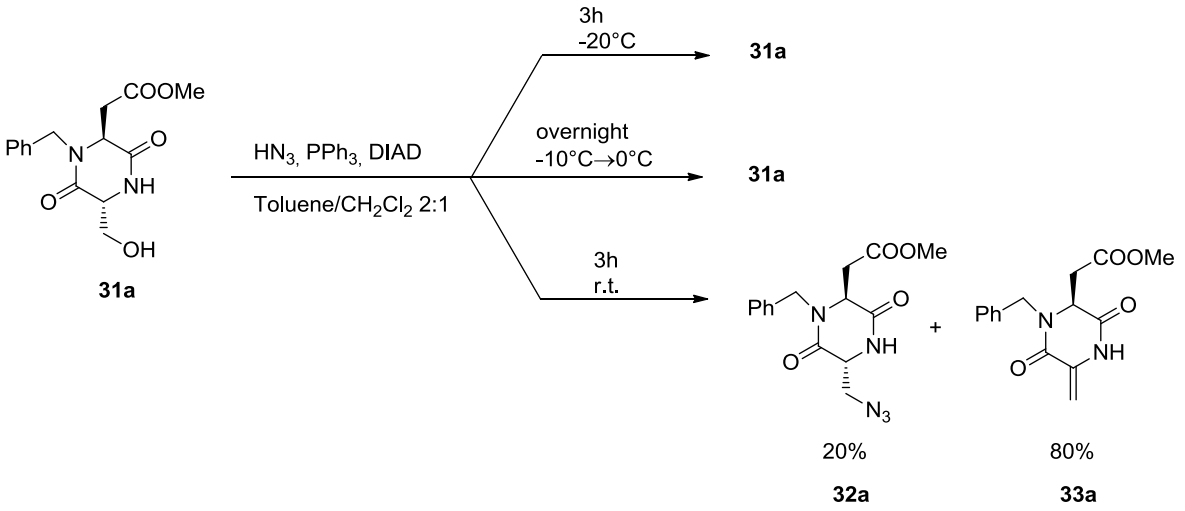

Scheme 1.3.3

Aiming at improving the poor yield obtained with the Mitsunobu reaction, we tried to introduce the azido moiety through the mesylate/sodium azide synthetic route (Scheme 1.3.4). Unfortunately, also in this case 21% of conversion was obtained at best, with the β-elimination derivative **33a** as major product.

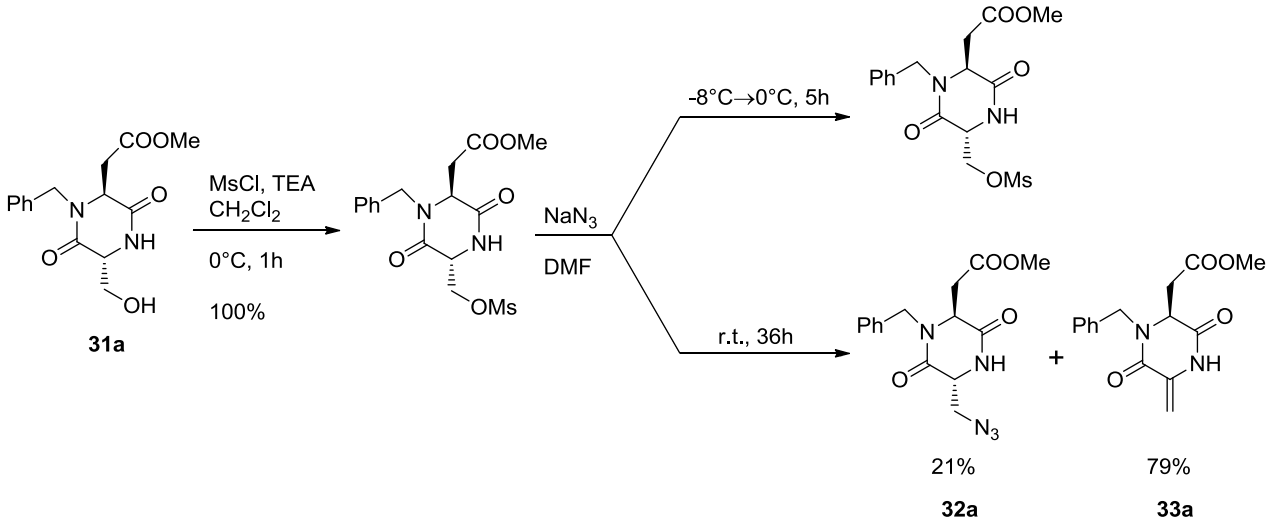

Scheme 1.3.4

At this point, aiming at scaling up the syntheses of both **DKP-4** and **DKP-6**, we tried to circumvent the problem of β-elimination, by performing the Mitsunobu reaction on Boc-Ser-OMe (either L or D)[93] (**34**), thus directly transforming the Ser OH group into the azide. This could also contribute to simplify the synthetic sequence avoiding the use of an additional protecting group (O*t*Bu). These scaffolds differs into the stereocenters at C3-C6 (Scheme 1.3.1) and the synthetic sequence was carried out starting from both the enantiomeric forms of serine (Scheme 1.3.5).

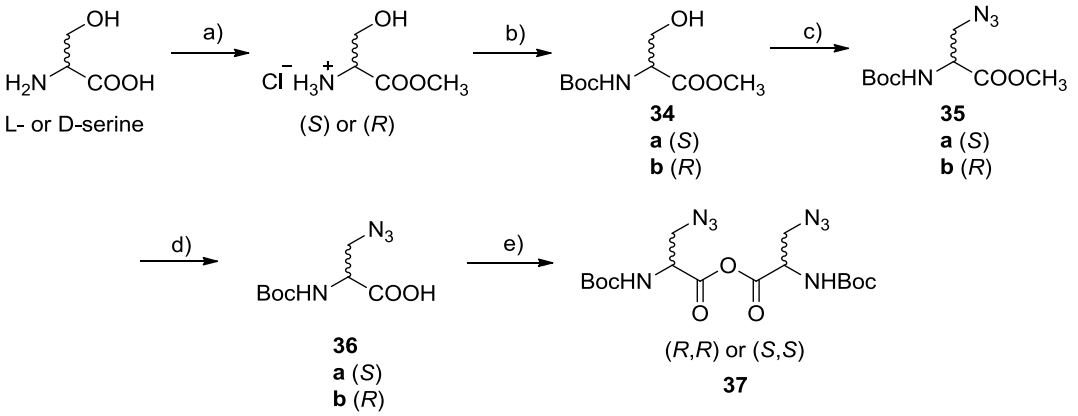

Scheme 1.3.5 - Synthesis of symmetric anhydrides **37**: a) CH_3COCl, MeOH, 95%; b) Boc_2O, THF/H_2O 1:1, 85%; c) HN_3, DIAD, PPh_3, THF, 78%; d) LiOH, THF/H_2O 1:1, 100%; e) DCC, CH_2Cl_2, 100%.

The Mitsunobu reaction with HN_3 proceeded uneventfully in good yield (78%) to give compounds **35**, which were then saponified with LiOH.[94] Treatment of freshly prepared acids **36** with DCC afforded the symmetric anhydrides **37** in a quantitative yield, which were isolated by filtering off DCU and evaporating the solvent, and immediately used in the next synthetic step without further purification (Scheme 1.3.5).

Coupling of 3-azido-2-*N*-*tert*-butoxycarbonylaminopropionic anhydrides (**37**) to either (*S*)- or (*R*)- *N*-benzyl-aspartic acid dimethylester (**29**) to give dipeptides **38** occurred in a very good 80% yield, while the subsequent Boc cleavage and cyclization to diketopiperazines **39** were nearly quantitative (Scheme 1.3.6).

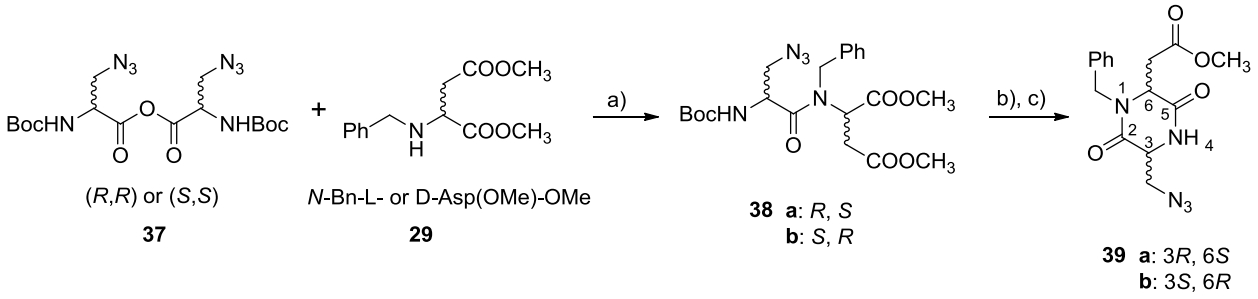

Scheme 1.3.6 - Synthesis of diketopiperazines **39**: a) CH_2Cl_2, 80%; b) Et_3SiH, TFA/DCM 1:2; c) *i*Pr_2NEt, *i*PrOH, 90% over two steps.

Dipeptides **38** were now obtained easily in gram scale, allowing thus a significant scale up of scaffolds **DKP-4** and **DKP-6**, but also **DKP-5** and **DKP-7** (see Chapter 1.3.3). Spectroscopic analysis (^1H and ^{13}C NMR) on dipeptides **38** revealed the presence of two rotamers (4:1 ratio in CD_2Cl_2 at r.t., see also the Experimental Section) due to the hindered rotation of the tertiary amide bond (*cis* and *trans* amide bond rotamers).

The same Staudinger-type reaction used for the synthesis of **DKP-1-3** (see Scheme 1.2.1) could be employed to reduce azides **39**. Moreover, the absence, in this case, of an allyl ester, allowed us to use the more reliable catalytic hydrogenation, which provides

amines **40**, followed by a Boc protection, giving compounds **41**. A final hydrolysis of the methyl ester provided diketopiperazines **DKP-4** and **DKP-6** in 90% overall yield (Scheme 1.3.7).

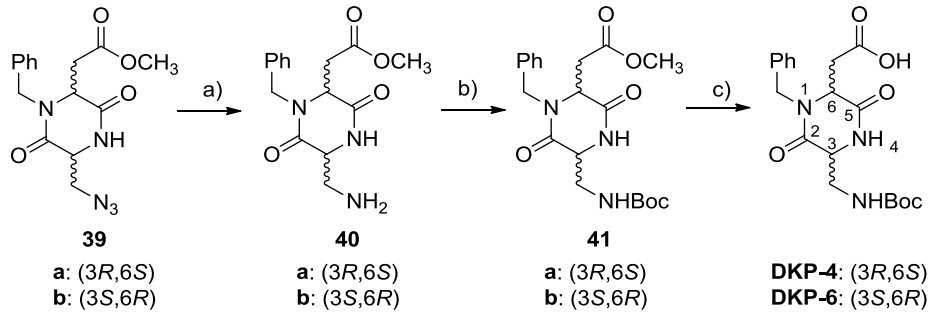

39
a: (3*R*,6*S*)
b: (3*S*,6*R*)

40
a: (3*R*,6*S*)
b: (3*S*,6*R*)

41
a: (3*R*,6*S*)
b: (3*S*,6*R*)

DKP-4: (3*R*,6*S*)
DKP-6: (3*S*,6*R*)

Scheme 1.3.7 - Synthesis of **DKP-4** and **DKP-6**: a) H_2, Pd/C, THF; b) Boc_2O, THF; c) LiOH, THF/H_2O 1:1, 90% over three steps.

Diketopiperazine scaffolds **DKP-4** and **DKP-6** were then employed as templating structures for the RGD sequence (see Chapter 1.4).

The symmetric anhydride synthetic route leading to dipeptides featuring an azido moiety described above, allowed us to synthesize also two new functionalized DKP scaffolds, **DKP-*f*4** and **DKP-*f*6** (Scheme 1.3.8).
The synthetic steps and the functional group interconversion were the same described for the synthesis of **DKP-4** and **DKP-6**. Detailed experimental procedures for each step and compounds characterization are reported in the Experimental Section. The only substantial difference consisted in the moderate yield (40%) for the symmetric anhydride coupling step. Yield optimization was pursued by extensively varying the reaction conditions (equivalents, solvents, temperature, time) but all the attempts were unsuccessful, in spare contrast with the analogous reaction run on *N*-benzyl-aspartic acid dimethylester (see Scheme 1.3.6) where the yield was uniformly higher (80%). A possible explanation could be attributed to the lower nucleophilicity of compounds **42**, probably due to the electronic effect of the aryl sulphonamide group (EWG) or to an intramolecular hydrogen bond between the acidic sulphonamide proton and the benzyl amine moiety.

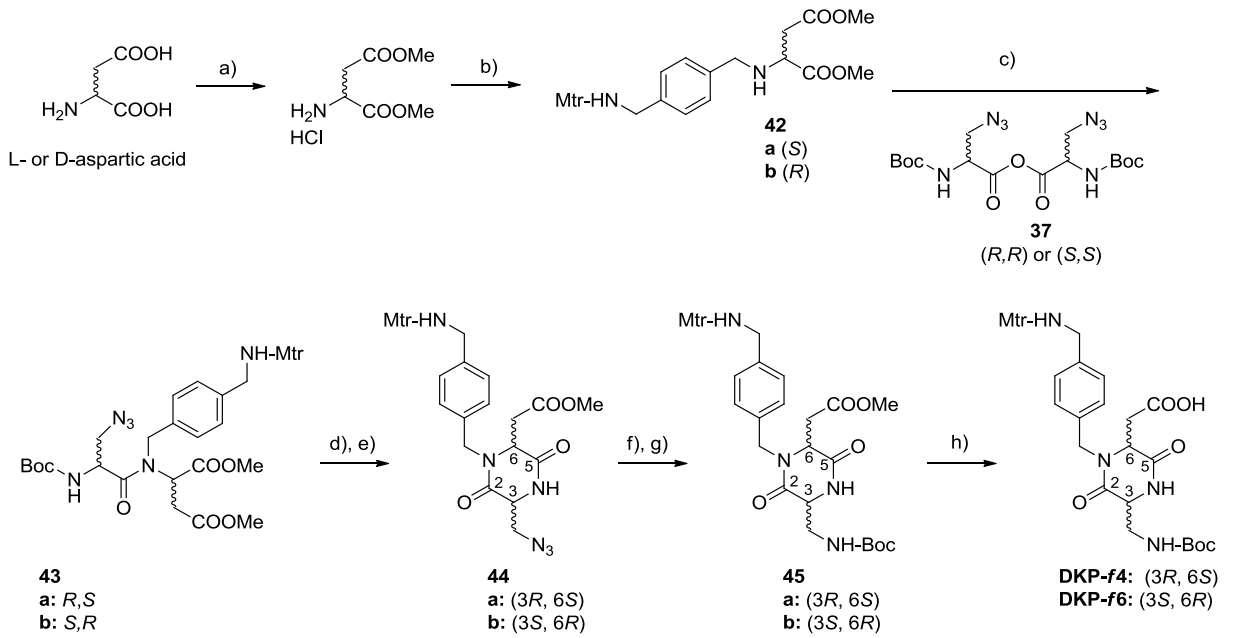

Scheme 1.3.8 - Reagents and conditions: a) MeOH, AcCl, 100%; b) aldehyde **27** [Scheme 1.2.2], $NaCNBH_3$, MeOH, 4 h, 66%; c) CH_2Cl_2, 18h, 40%; d) TFA, Et_3SiH, CH_2Cl_2; e) *i*Pr_2NEt, *i*PrOH, 6 h, 92% over two steps; f) H_2, 10% Pd/C, THF, 4 h; g) Boc_2O, *i*Pr_2NEt, DCM, 6 h, room temp., 96% over two steps; h) LiOH, THF/H_2O 1:1, 100%.

Also in this case, scaffolds **DKP-*f*4** and **DKP-*f*6** were then employed as templating structures for the RGD sequence (see Chapter 1.4), allowing further conjugation with other molecular entities.

1.3.3 Synthesis of DKP-5 and DKP-7

The synthesis of scaffolds **DKP-5** and **DKP-7** can in principle be achieved through the benzylation of the second diketopiperazine nitrogen of an advanced intermediate in the synthesis of either **DKP-2** and **DKP-4**, or **DKP-3** and **DKP-6**, respectively (Figure 1.3.2, see Scheme 1.2.1 and 1.3.7). Aiming at minimizing the use of protecting groups, the only suitable intermediate for a nitrogen alkylation was identified in the azide derivative (namely, compounds **25** and **39**). Indeed, the diketopiperazine intermediates bearing a free hydroxyl group or a Boc protected amino functionality could in fact give over-alkylated by-products. The azido group might serve as a protecting group here, being stable under the reaction conditions.

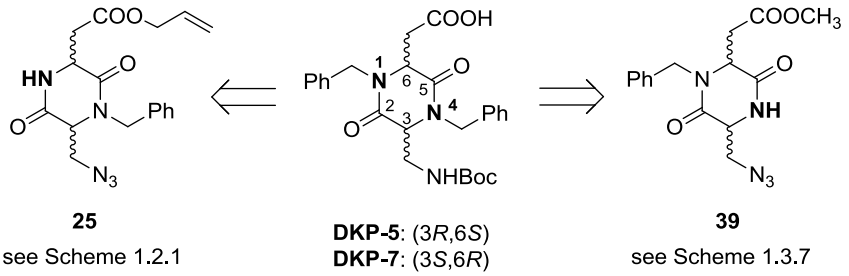

Figure 1.3.2

As we had intermediates **39** available (Scheme 1.3.7), we started to investigate *N*-benzylation on these substrates.

Nitrogen N-4 alkylation was first attempted using sodium hydride and benzyl bromide in dimethylformamide. This classic experimental procedure generally provides good yields for amide benzylation but, unfortunately, our major product proved to be an elimination derivative (compounds **33**, Scheme 1.3.4). $-N_3$ acted as leaving group in presence of a strong non-hindered base, such as NaH. Better results were obtained using hindered KHMDS (potassium bis(trimethylsilyl)amide) in presence of benzyl bromide and lowering temperature of reaction between -70°C and -40°C (Scheme 1.3.8).

Bis-benzylated azides **46** are subjected to a one pot Staudinger reduction – Boc protection, providing *N*-Boc protected amines **47**. Methyl ester hydrolysis finally afforded the desired products **DKP-5** and **DKP-7** (Scheme 1.3.8).

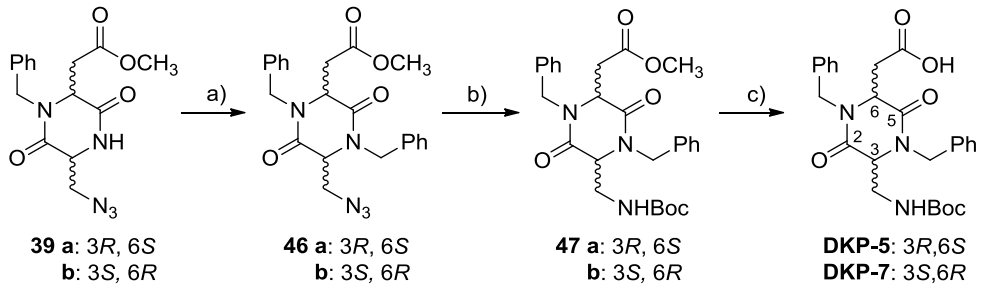

39 a: 3*R*, 6*S*
b: 3*S*, 6*R*

46 a: 3*R*, 6*S*
b: 3*S*, 6*R*

47 a: 3*R*, 6*S*
b: 3*S*, 6*R*

DKP-5: 3*R*,6*S*
DKP-7: 3*S*,6*R*

Scheme 1.3.4 - Synthesis of **DKP-5** and **DKP-7**, starting from intermediates **39a** and **39b**, respectively: a) BnBr, KHMDS, THF/DMF 7:3, 86%; b) PMe_3, Boc-ON, THF, 90%; c) LiOH, THF/H_2O 1:1, 100%.

For a synthetic comparison, azides **25** (Scheme 1.2.1) were also converted into **DKP-5** and **DKP-7** following the same protocols, a part of the last deprotection step (Tsuji-Trost-like ester deallylation, Scheme 1.3.5).

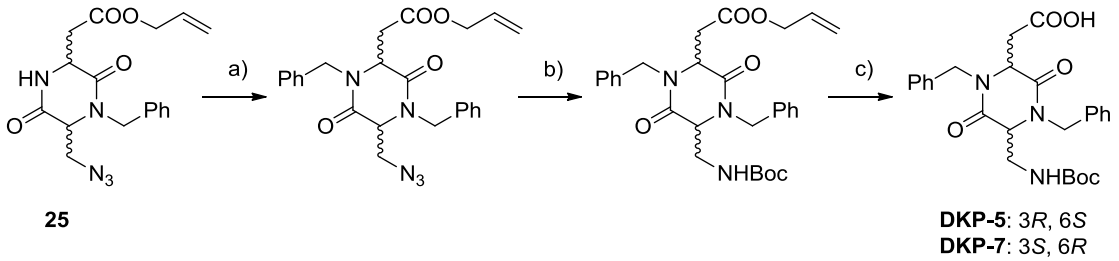

Scheme 1.3.5 - Synthesis of **DKP-5** and **DKP-7**, starting from intermediates **25**: a) KHMDS, BnBr, THF/DMF 7:3, 76%; b) Me_3P, Boc-ON, THF, 65%; c) pyrrolidine, PPh_3, $[Pd(PPh_3)_4]$, DCM, 100%.

The former approach (Scheme 1.3.4) is significantly better than the latter (Scheme 1.3.5): the overall yield for the first synthetic route is 77% over three steps, while for the second route is 49% over three steps. Moreover, methyl ester hydrolysis is an effective and transition metal free step, suitable also for substantial scale up of the synthesis.

The two bis-benzylated scaffolds **DKP-5** and **DKP-7** so obtained were then employed in the synthesis of cyclic RGD integrin ligands (Chapter 1.4)

1.3.4 Synthesis of DKP-8

Scaffold **DKP-8**, bearing a carboxyethyl side chain, was obtained through a synthetic strategy similar to the one adopted in the case of compounds **DKP-1-3** (see Chapter 1.2.1), starting from (*S*)-*N*-benzylserine methyl ester **21** (Scheme 1.2.1) and (*R*)-*N*-(*tert*-butoxycarbonyl)glutamic acid γ-methyl ester **48**.[95] In this case too, direct coupling of these fragments afforded isopeptide **49** (see scheme 1.3.6 and ref.83). Diagnostic of this outcome were the NMR spectra for compound **49**: (i) in the ^1H NMR spectrum, the O-CH_2 protons of serine were rather deshielded [δ 4.47 (dd, J = 11.0, 4.9 Hz, 1H), 4.30 (dd, J = 11.0, 4.9 Hz, 1H) ($CDCl_3$)]; (ii) in the HMBC (Heteronuclear Multiple Bond Coherence) spectrum of both compounds, a long range coupling (through three bonds) was clearly evident between the O-CH_2 protons of serine and the α-carbonyl carbon of glutamic (Figure 1.3.3).

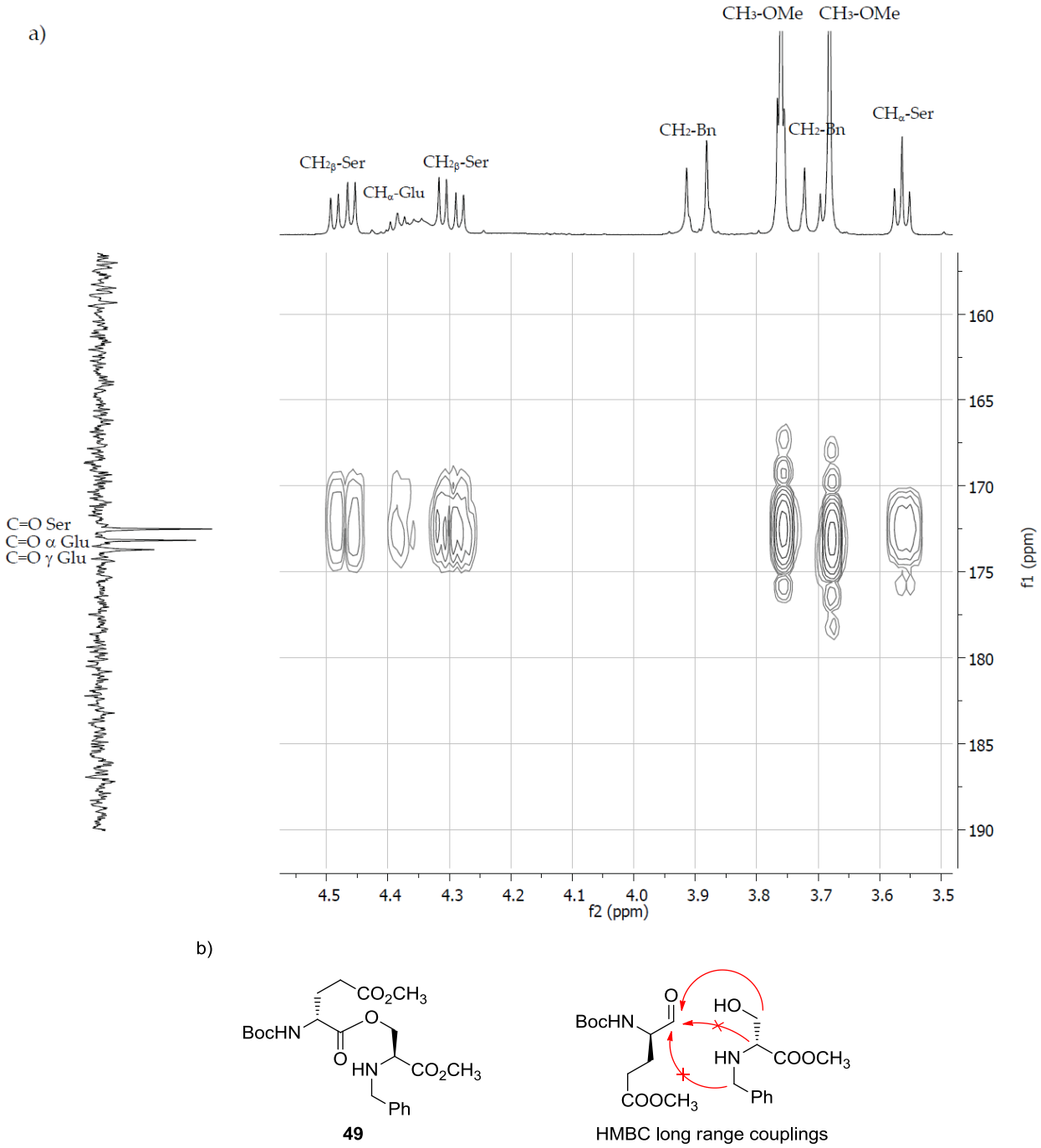

Figure 1.3.3 - a) HMBC spectra of isopeptides **49** ($CDCl_3$), highlighting the long range coupling (through three bonds) between the O-CH_2 protons of Ser and the α-carbonyl carbon of Glu; b) scheme representing the long range couplings highlighted from the HMBC spectra.

Isopeptide **49** was then deprotected and cyclized to diketopiperazine **50**. Azidation of the -CH_2OH group *via* a Mitsunobu reaction (**51**), reduction by catalytic hydrogenation (**52**), protection with Boc_2O (**53**) and final hydrolysis of the methyl ester afforded **DKP-8** (Scheme 1.3.6).

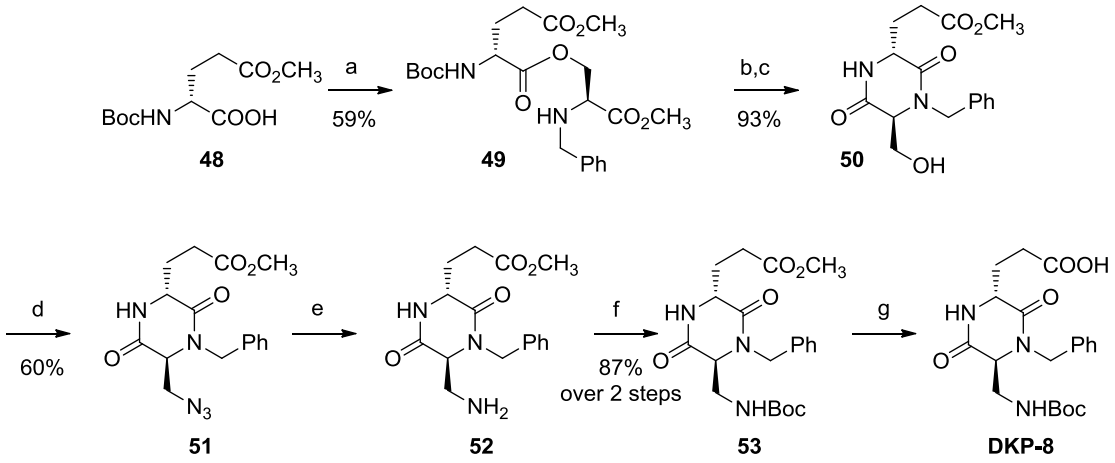

Scheme 1.3.6 - a) **21**, HATU, HOAt, DIPEA, DMF; b) TFA/CH_2Cl_2 1:2; c) DIPEA, *i*PrOH; d) HN_3, DIAD, PPh_3, CH_2Cl_2/toluene/DMF; e) H_2, Pd-C, THF; f) Boc_2O, THF; g) LiOH, THF/30% H_2O_2 1:1.

This latest step was at first performed in the conditions already described for the synthesis of **DKP-4-7**, treating **53** with LiOH in a 1:1 mixture of THF and water. The reaction did not proceed as fast and completely as observed in the other cases and, moreover, extensive racemization problems were detected in the ^{13}C spectrum of **DKP-8** thus obtained. Hence a milder yet more selective procedure involving the *in situ* formation of LiOOH was adopted. Enantiomerically pure **DKP-8** was this time obtained quantitatively.

Also this last scaffold **DKP-8** was then employed as templating structure for the RGD sequence (see Chapter 1.4).

1.3.5 Considerations on DKP scaffolds

It is noteworthy to say that scaffolds **DKP-4**, **DKP-*f*4**, **DKP-5**, **DKP-6**, **DKP-*f*6** and **DKP-7** will allow, as discussed in next chapter 1.4, a detailed SAR of this kind of diketopiperazine templating agent. However, it should be underlined that this new synthetic route (symmetric anhydride as key step) is less atom-economic compared to the previously developed isopeptide route (see 1.2.1 and 1.3.4). For this reason, in our research group it was chosen, at the end of this DKP SAR analysis, to scale up (multi-gram scale) the synthesis of **DKP-3** and **DKP-*f*3** (and its functionalized integrin ligand **c[DKP-*f*3-RGD]**, see 1.2.2), to store a relevant amount of these useful scaffolds for further applications (see 1.5 and Chapter 2).

1.4 Cyclic [DKP-RGD] Integrin Ligands

1.4.1 Synthesis of ligands c[DKP-4-8-RGD]

The synthesis of six new RGD-containing integrin ligands was performed starting from the new DKP scaffolds described in the previous chapter (1.3) (Figure 1.4.1).

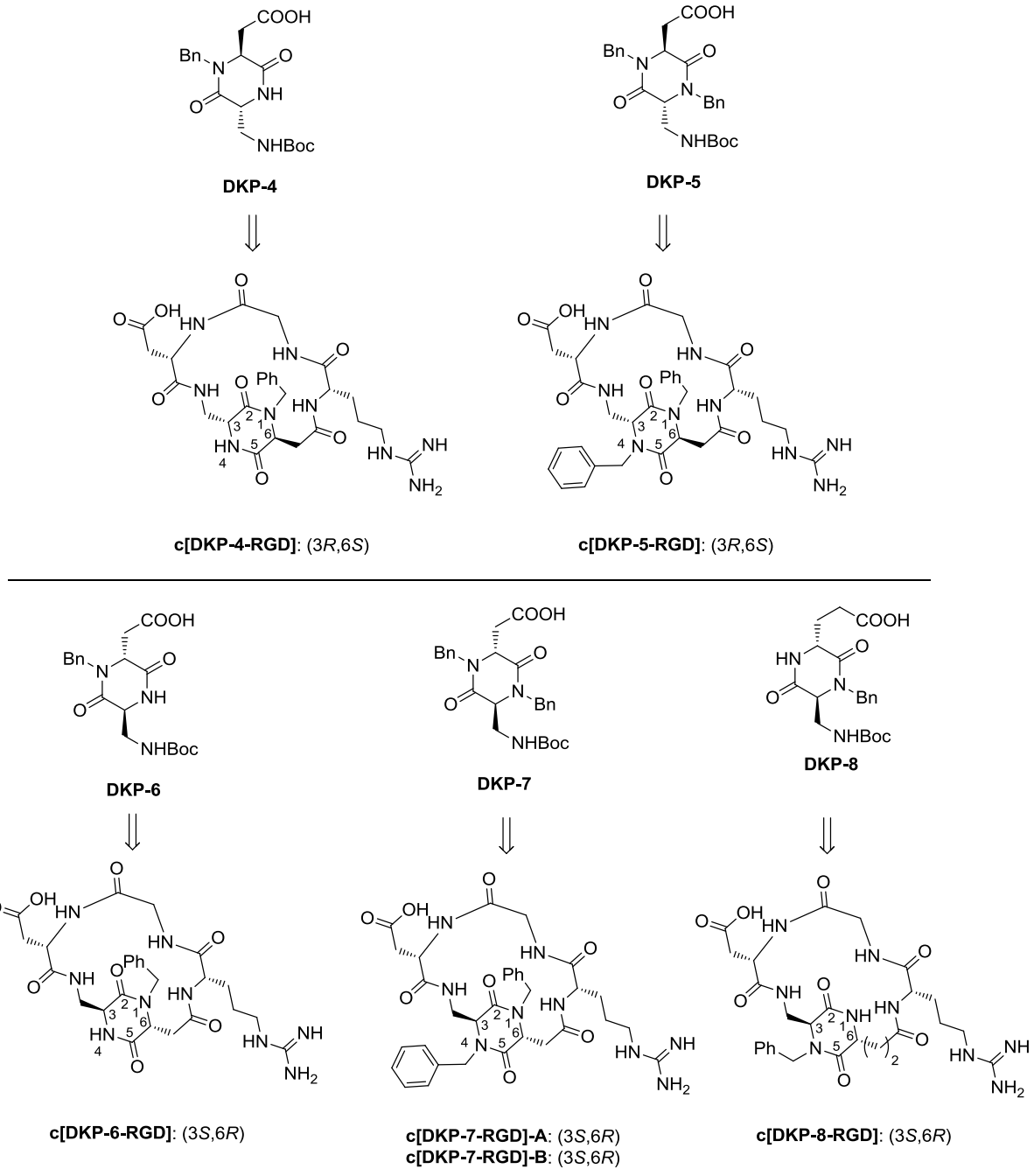

Figure 1.4.1

The presence of two diastereomers of **c[DKP-7-RGD]-A** and -**B** will be explained below.

The synthetic route leading to these new ligands was adapted from the previous work on DKP-containing integrin ligands (Scheme 1.4.1) (see Experimental Part for detailed yields and conditions):

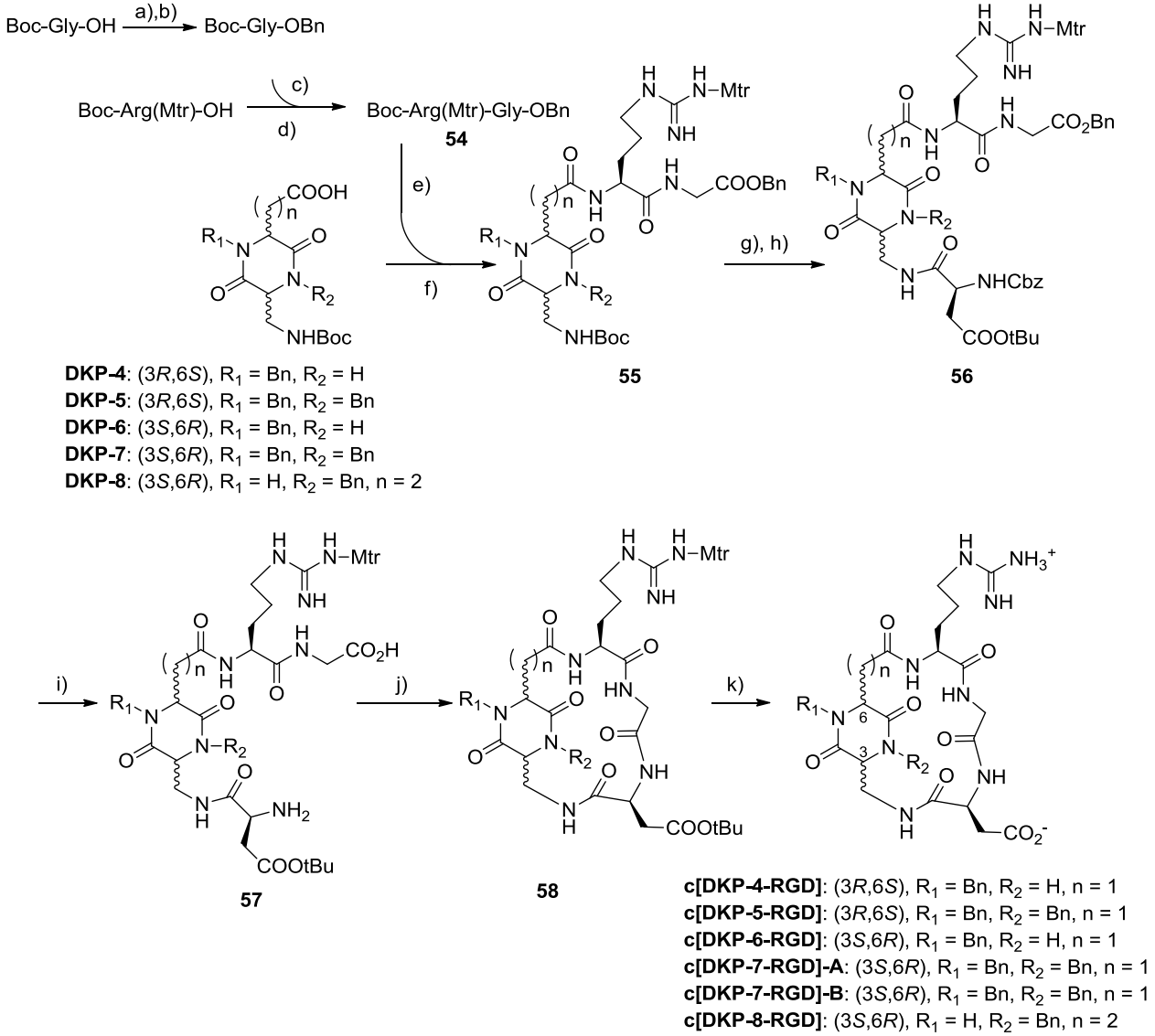

Scheme 1.4.1 - Synthesis of cyclic RGD peptidomimetics **c[DKP-4-8-RGD]** containing scaffolds **DKP-4-8**: a) Cs_2CO_3, MeOH; b) BnBr, DMF: 95% o.t.s.; c) TFA/DCM 1:2; d) HBTU, HOBt, DIPEA, DMF; e) TFA/DCM 1:2; f) HATU, HOAt, *i*Pr$_2$EtN, DMF; g) TFA/DCM 1:2; h) Cbz-Asp(O*t*Bu)-OH, HATU, HOAt, *i*Pr$_2$EtN, DMF; i) H_2, Pd/C, THF/H_2O 1:1; j) HATU, HOAt, *i*Pr$_2$EtN, DMF, 1.4mM; k) TFA 90%, thioanisol 5%, EDT 3%, anisol 2%.

Diketopiperazines **DKP-4-8** were incorporated into the cyclic RGD derivatives **c[DKP-4-8-RGD]** (Scheme 1.4.1). A solution phase synthetic strategy was adopted, using Boc-Arg(Mtr), Gly-OBn and Cbz-Asp(OtBu)-OH. The dipeptide Boc-Arg(Mtr)-Gly-OBn was Boc-deprotected and coupled to the acid of the appropriate diketopiperazine scaffold. Subsequent Boc deprotection of the DKP amino group and coupling of the aspartic derivative Cbz-Asp(OtBu)-OH afforded the linear peptidomimetic Cbz-Asp(OtBu)-

DKP-Arg(Mtr)-Gly-OBn, which was deprotected by hydrogenolysis (Cbz and Bn): initially, during the synthesis of **c[DKP-4-RGD]**, this reaction was performed in methanol and surprisingly the formation of *N*-methylated derivatives (up to 30% of the total yield) was observed (Scheme 1.4.2), leading to a troublesome HPLC separation of this byproduct after the macrolactamization step. The unexpected outcome of this reaction was then found out in literature with a similar procedure (Pd/C in methanol) specific for the synthesis of *N*-methylated amino acids.[96]

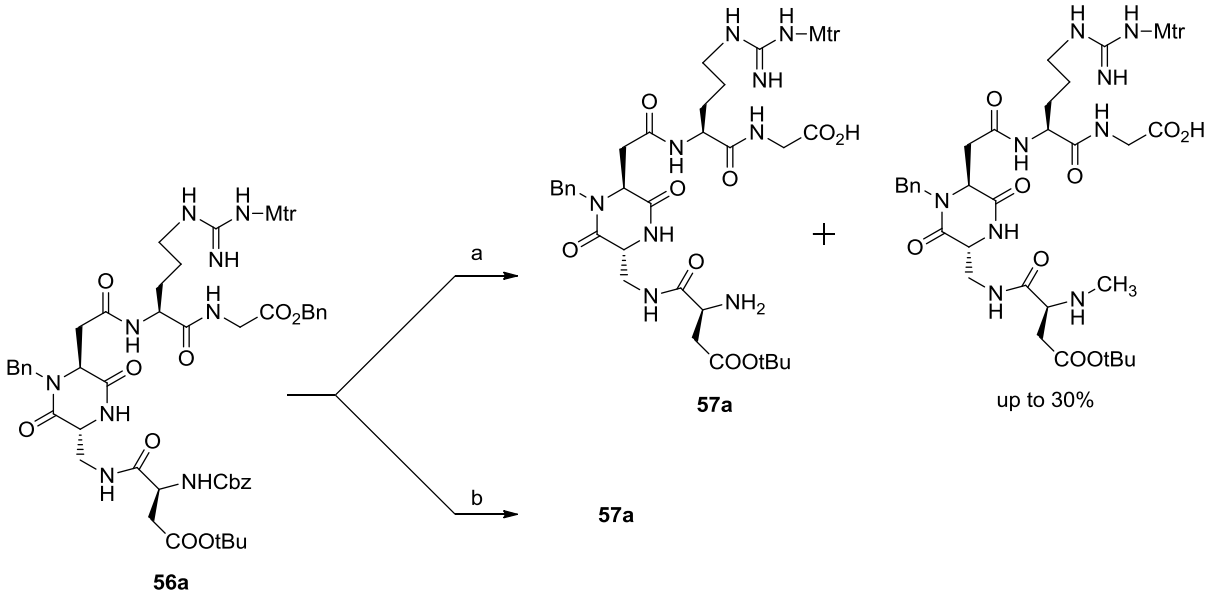

Scheme 1.4.2 - a) H_2, Pd/C, CH_3OH; b) H_2, Pd/C, THF/H_2O 1:1.

To overcome this problem, we decided to avoid the use of alcoholic solvents and we set up a solvent mixture capable of both dissolving the starting material (THF) and the hydrogenated product (H_2O) (Scheme 1.4.2).
Deprotected compounds were subjected to macrolactamization. Several methodologies were screened for the ring closure, and the best yields were obtained for all the products using HATU/HOAT as coupling agents in a 1:4:4:6 substrate/HATU/HOAT/*i*Pr$_2$*N*Et molar ratio and a substrate concentration = 1.4 mM in DMF. Purification and isolation of these products were achieved both through a simple flash column chromatography (DCM/MeOH) or through reverse phase Biotage™ purification on C18 cartridge, in case of complex mixture of formed byproducts.
A final side-chain deprotection (TFA/thioanisole/ethanedithiol/anisole 90:5:3:2) and preparative HPLC purification afforded the desired compounds **c[DKP-4-8-RGD]**.

The *N*-dibenzyl derivatives **c[DKP-5-RGD]** and **c[DKP-7-RGD]** can exist as two different separable conformers (diastereomers) due to hindered rotation of one ring around the other, in a way reminiscent of the *ansa*-cyclopeptides[97] (*i.e.*, the DKP *N*-

benzyl group cannot pass inside the macrolactam ring). In the case of **c[DKP-5-RGD]**, we were able to isolate only one diastereomer (either because it was formed exclusively or because it was formed predominantly) and the minor one was not detected.

The two diastereomers of **c[DKP-7-RGD]** (**A** and **B**), formed in the macrolactamization step, were isolated in a 2:1 ratio (Figure 1.4.2). Although two sets of peaks (2:1 ratio) were visible in the ^{1}H NMR spectrum (see Experimental Section for full peaks assignement), the two diastereomers could not be separated by HPLC because they had the same elution time. However, after protecting groups side-chain deprotection, the two diastereomers could be separated, analyzed and subjected to the binding assays (vide infra).

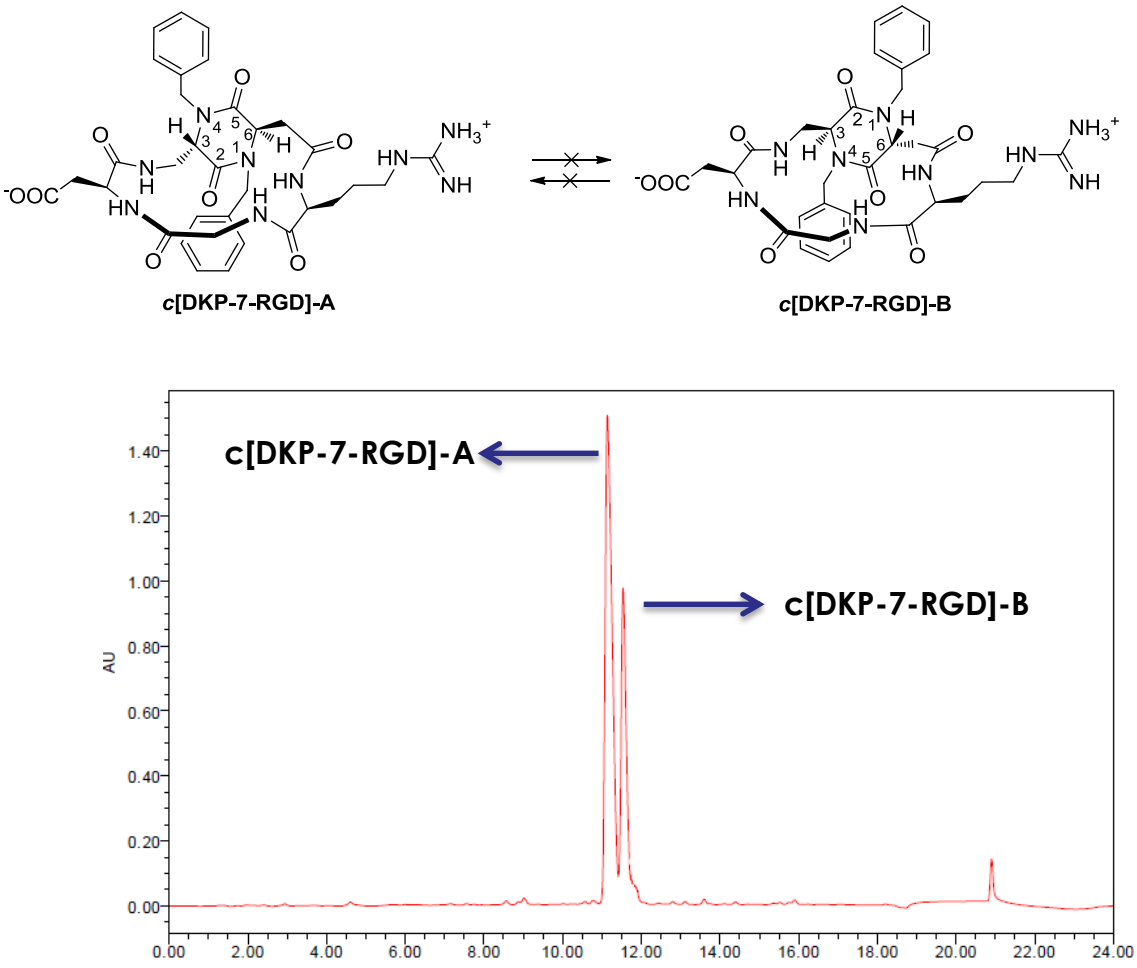

Figure 1.4.2 - Upper: non-interconverting diastereoisomers **c[DKP-7-RGD]-A** and **–B**; lower: HPLC trace after the protecting groups side-chain deprotection step.

1.4.2 Synthesis of functionalized ligands c[DKP-*f*4-RGD] and c[DKP-*f*6-RGD]

The synthesis of two new functionalized RGD-containing integrin ligands was performed starting from the new **DKP-*f*4** and **DKP-*f*6** scaffolds described in the previous chapter (1.3.2) (Figure 1.4.3).

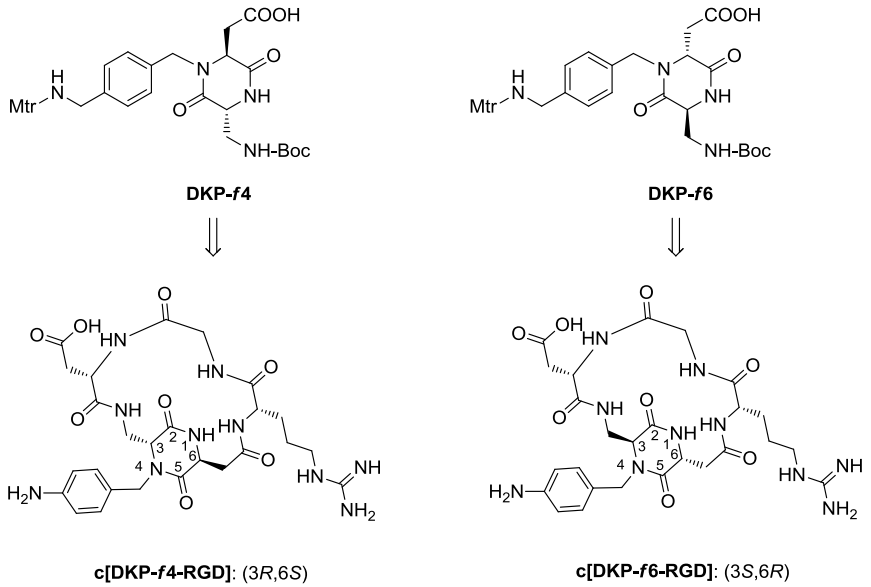

Figure 1.4.3

The tripeptide R-G-D decoration on these scaffolds was performed using the same synthetic route described in Chapter 1.4.1 (Scheme 1.4.3) (see Experimental Section for yields and detailed conditions).

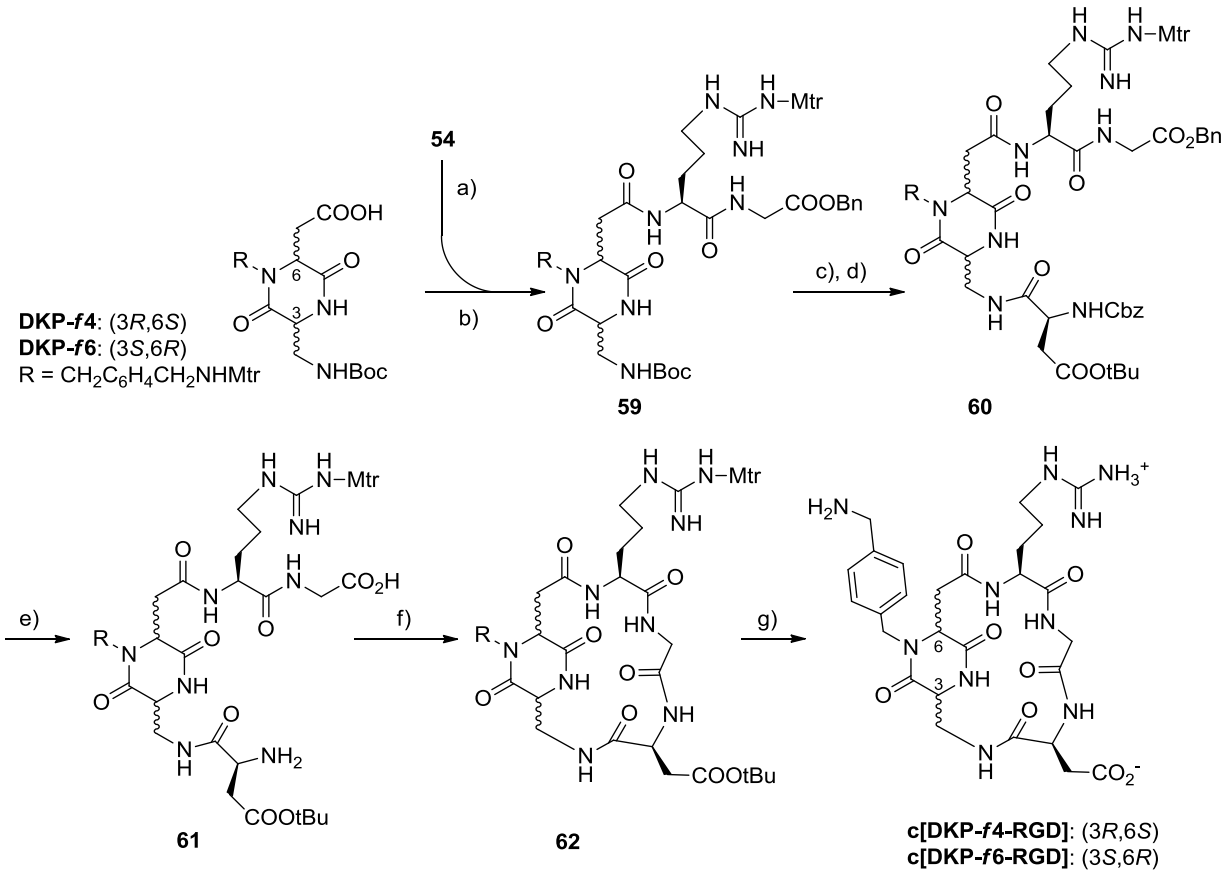

Scheme 1.4.3 - a) TFA/DCM 1:2; b) HATU, HOAT, *i*Pr2NEt, DMF; c) TFA/DCM 1:2; d) Cbz-Asp(OtBu)-OH, HATU, HOAT, *i*Pr2NEt, DMF; e) H_2, 10% Pd/C, THF/H_2O 1:1; f) HATU, HOAT, *i*Pr2NEt, 1.4 mM in DMF; g) TFA/TMSBr/thioanisol/EDT/phenol 70:14:10:5:1.

The side-chain deprotection turned out to be more challenging with respect to the previously reported unfunctionalized ligands: while the O*t*Bu and the Mtr on the arginine were easily deprotected, the Mtr on the benzylic amine turned out to be very stable (see Scheme 1.4.4).

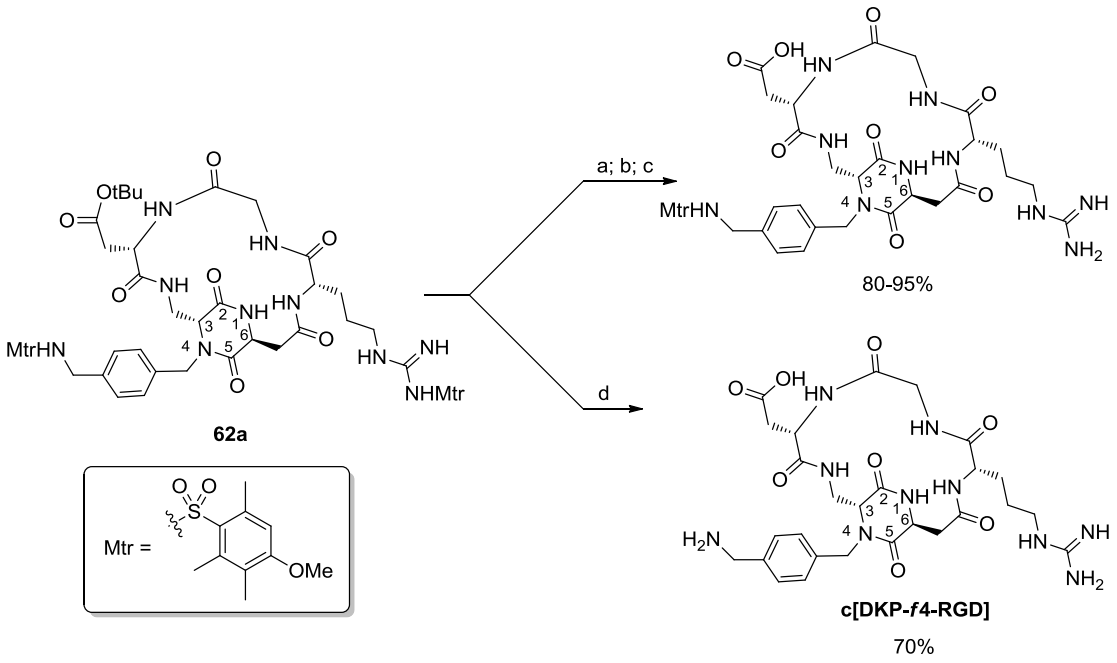

Scheme 1.4.4 - a) "Reagent K": TFA/phenol/water/TIPS, 88/5/5/2; b) "Reagent R": TFA/thioanisole/EDT/anisole, 90/5/3/2; c) "Reagent P+": TFA/phenol/methanesulfonic acid, 95/2.5/2.5; d) TFA/TMSBr/thioanisole/EDT/phenol 70/14/10/5/1.

During the synthesis of **c[DKP-*f*4-RGD]**, several cleavage cocktails were screened and the more classical ones[98] ("Reagent K", "Reagent R" and "Reagent P+") failed, giving the mono-protected compound as main product (the Mtr on the amine was still present), with a low yield (5-20%) of the desired totally deprotected product, even after 48 h. Finally, with the use of TFA/TMSBr/thioanisole/EDT/phenol (70/14/10/5/1) cleavage cocktail at room temperature for 2 h, fully deprotected compound **c[DKP-*f*4-RGD]** was obtained in 70% isolated yield.

The benzylic amine moiety contained in the **c[DKP-*f*4/*f*6-RGD]** ligands allowed, as described in Chapter 2, further conjugation with other molecular entities (dual-action conjugates). To this end, we have developed a reliable synthetic protocol to react only the free amine without side reactions on the guanidine moiety (free Arg side-chain) (Scheme 1.4.5) (see Chapter 2 and Experimental Section for further details).

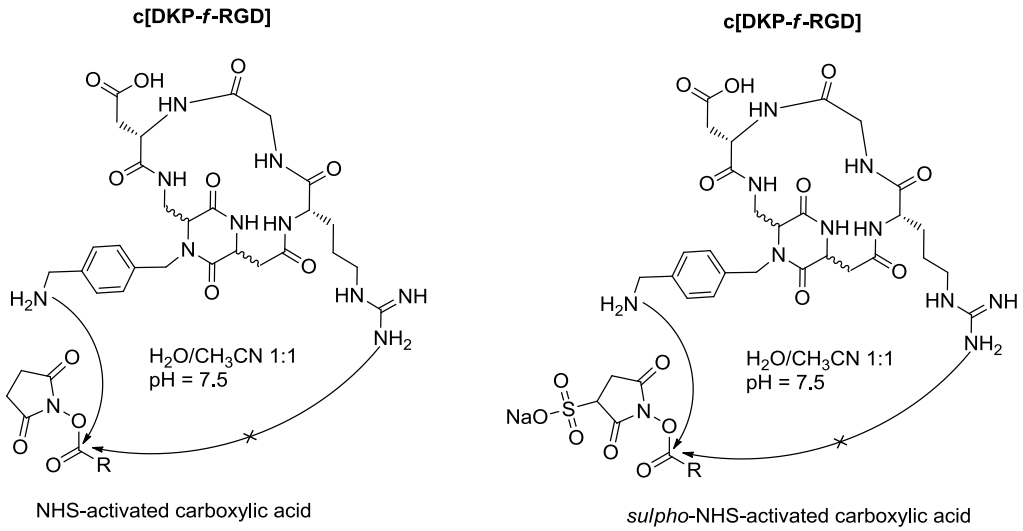

Scheme 1.4.5

The amine functionalization allows to elongate the integrin ligands through a new amide bond: the carboxylic acid can be activated both with the simple *N*-hydroxysuccinimmide (NHS) protocol or through the sulpho- *N*-hydroxysuccinimmide (sulpho-NHS) methodology, a more water soluble activating agent. In both case, the reaction must be conducted in a H_2O/CH_3CN solvent (1:1 ratio), adjusting pH = 7.5 (Scheme 1.4.5).

Integrin ligands **c[DKP-*f*4-RGD]** and **c[DKP-*f*6-RGD]** were employed in a drug-targeting approach with Paclitaxel (dual-action conjugates), further described in Chapter 2.1.

1.4.3 Biological evaluation [99]

The new cyclic RGD peptidomimetics were examined in vitro for their ability to inhibit biotinylated vitronectin binding to the purified $\alpha_v\beta_3$ and $\alpha_v\beta_5$ receptors (Table 1.4.1, in comparison with the previously reported c[DKP-RGD] ligands).

Table 1.4.1. Inhibition of biotinylated vitronectin binding to $\alpha_v\beta_3$ and $\alpha_v\beta_5$ receptors

Compound	$\alpha_v\beta_3$ IC_{50} [nM][a]	$\alpha_v\beta_5$ IC_{50} [nM][a]
c[DKP-1-RGD]	3898 ± 418	> 10^4
c[DKP-2-RGD]	3.2 ± 2.7	114 ± 99
c[DKP-3-RGD]	4.5 ± 1.1	149 ± 25
c[DKP-4-RGD]	7.6 ± 4.3	216 ± 5
c[DKP-5-RGD]	12.2 ± 5.0	131 ± 29
c[DKP-6-RGD]	2.1 ± 0.6	79 ± 3
c[DKP-7-RGD]-A	220.2 ± 82.3	> 10^4
c[DKP-7-RGD]-B	0.2 ± 0.09	109 ± 15
c[DKP-8-RGD]	7.5 ± 0.6	> 10^3
c(RGDfV)[b]	3.2 ± 1.3	7.5 ± 4.8
ST1646[b]	1.0 ± 0.5	1.4 ± 0.8

[a] IC_{50} values were calculated as the concentration of compound required for 50% inhibition of biotinylated vitronectin binding as estimated by GraphPad Prism software; all values are the arithmetic mean ± SD of triplicate determinations; [b] see Chapter 1.1.3.1.

Screening assays were performed by incubating the immobilized integrin receptors with various concentrations (10^{-10} – 10^{-5} M) of the **c[DKP-RGD]** ligands in the presence of biotinylated vitronectin (1 μg/mL), and measuring the concentration of bound vitronectin in the presence of the competitive ligands. The ability of the new compounds to inhibit the binding of vitronectin to the isolated $\alpha_v\beta_3$ and $\alpha_v\beta_5$ receptors was compared with that of the reference compounds c(RGDfV) and ST164669 (see Chapter 1.1.3.1).

Low nanomolar values were obtained with all the ligands except **c[DKP-1-RGD]**, which incorporates a *cis*-DKP and ligand **c[DKP-7-RGD]-A**. The behaviour of this last ligand is peculiar, considering that the diastereomeric compound **c[DKP-7-RGD]-B** (see 1.4.2) is the most potent ligand of this series, as it effectively inhibits the binding of vitronectin to the isolated $\alpha_v\beta_3$ receptor in subnanomolar concentration. Interestingly,

unlike reference compounds c(RGDfV) and ST1646, the RGD-peptidomimetics **c[DKP-RGD]** were ca. 10-1000-fold more selective for the $\alpha_v\beta_3$ integrin with respect to the $\alpha_v\beta_5$, in this kind of assay.

Functionalized ligands **c[DKP-*f*-RGD]** were not tested in this kind of assay, as their integrin affinity was evaluated once they were conjugated to other molecular entities (see Chapter 2).

1.4.4 Spectroscopic and computational studies [100]

The spectroscopic and computational studies are here reported for integrin ligands **c[DKP-4-8-RGD]** in comparison also with the already synthesized ligands **c[DKP-1-3-RGD]** (see 1.2.2).
The structure and connectivity of ligands **c[DKP-4-8-RGD]** and of their fully protected precursors were unambiguously assigned by means of mono- and bidimensional ^{1}H- and ^{13}C-NMR spectra.
The preferred conformations of the cyclic RGD peptidomimetics **c[DKP-4-8-RGD]** in aqueous solution were then investigated, with the aim of rationalizing the affinity of these compounds for the $\alpha_v\beta_3$ receptor at a molecular level. In fact, as already mentioned, the high activity and selectivity of Cilengitide **3** has been attributed to an extended conformation of the RGD motif displaying a distance of ca. 9 Å between the C_β atoms of Asp and Arg. In such extended conformations, the carboxylate and guanidinium groups are properly positioned to effectively exert their function of electrostatic clamp. Monodimensional ^{1}H-NMR experiments were conducted to detect intramolecular hydrogen bonds, by measuring the chemical shift of the N–H protons and their temperature coefficients ($\Delta\delta/\Delta T$). NOESY spectra were recorded to investigate both sequential and long-range NOEs that provide evidence of preferred conformations. The relevant NMR data are summarized in Table 1.4.2.

Table 1.4.2 - ^{1}H-NMR and NOE data of cyclic RGD-peptidomimetics in water.

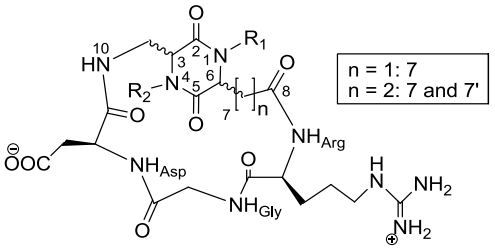

		NH_1	NH_4	NH_{10}	NH_{Arg}	NH_{Gly}	NH_{Asp}	Significant NOE contacts
c[DKP-1-RGD]	**δ** (ppm)	8,35	-	7,46	8,40	8,75	8,10	NH_{Asp}-NH_{10}; NH_{Asp}-NH_{Gly}
	$\Delta\delta/\Delta T$ (ppb/K)	-7.3	-	-2.0	-7.0	-8.0	-3.7	
c[DKP-2-RGD]	**δ** (ppm)	8.35	-	8.78	8.57	8.18	8.29	NH_{Arg}-NH_{Gly}
	$\Delta\delta/\Delta T$ (ppb/K)	-8.7	-	-10.7	-7.0	-5.7	-7.7	
c[DKP-3-RGD]	**δ** (ppm)	8.10	-	8.28	8.80	8.00	7.85	NH_{Arg}-NH_{Gly}
	$\Delta\delta/\Delta T$ (ppb/K)	-5.7	-	-8.5	-6.0	-4.5	-3.5	
c[DKP-4-RGD]	**δ** (ppm)	-	8.17	7.59	8.29	8.27	8.88	--
	$\Delta\delta/\Delta T$ (ppb/K)	-	-9.1	-0.7	-9.3	-8.2	-9.3	
c[DKP-5-RGD]	**δ** (ppm)	-	-	8.58	8.48	8.23	8.42	NH_{Arg}-NH_{Gly}
	$\Delta\delta/\Delta T$ (ppb/K)	-	-	-11.0	-7.5	-4.7	-8.2	
c[DKP-6-RGD]	**δ** (ppm)	-	8.07	7.90	8.32	8.35	8.80	NH_{Asp}-NH_{10}; NH_4-NH_{10};
	$\Delta\delta/\Delta T$ (ppb/K)	-	-4.9	-5.1	-7.6	-6.7	-8.0	
c[DKP-7-RGD] A	**δ** (ppm)	-	-	8.04	8.66	7.93	7.76	NH_{Arg}-NH_{Gly}; NH_{Asp}-NH_{Gly}
	$\Delta\delta/\Delta T$ (ppb/K)	-	-	-7.5	-5.0	-3.0	-1.0	
c[DKP-7-RGD] B	**δ** (ppm)	-	-	7.72	8.34	8.45	8.55	NH_{Asp}-NH_{10}
	$\Delta\delta/\Delta T$ (ppb/K)	-	-	-4.0	-7.0	-7.0	-5.0	
c[DKP8-RGD]	**δ** (ppm)	7.82	-	7.43	8.64	8.04	7.90	-
	$\Delta\delta/\Delta T$ (ppb/K)	-8.0	-	-6.0	-6.8	-4.4	-5.2	

As already reported in the literature,[90] ligand **c[DKP-1-RGD]** exists as an equilibrium of two different preferred conformations. The NOESY spectrum shows two mutually exclusive long-range NOE contacts. The cross peak between DKP-NH_{10} and NH_{Asp} (strong) is indicative of a β-turn conformation at Gly-Asp stabilized by a hydrogen bond between DKP-NH_{10} and Arg-C=O (Type I H-bonding pattern, Figure 1.4.4 A). The chemical shift value (7.46 ppm) and the Δδ/ΔT value (-2 ppb/K) of the amide proton

DKP-NH_{10} indicate that this proton is strongly locked in an intramolecularly H-bonded state. The cross peak between NH_{Gly} and NH_{Asp} (medium) is indicative of an alternative β-turn conformation at Arg-Gly, stabilized by a hydrogen bond between Asp-NH and C(8)=O (Type II H-bonding pattern, Figure 1.4.4 B).

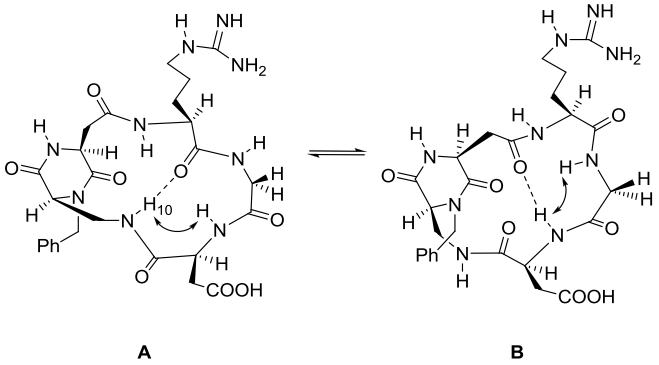

Figure 1.4.4 - Preferred intramolecular hydrogen-bonding pattern proposed for compound **c[DKP-1-RGD]** on the basis of spectroscopic data. The arrows indicate significant NOE contacts. A) Type I H-bonding pattern, Gly-Asp β-turn motif. B) Type II H- H-bonding pattern, Arg-Gly β-turn motif .

Ligands **c[DKP-2-RGD]** and **c[DKP-3-RGD]** are characterized by a high conformational equilibrium, as ascertained by the values of chemical shifts and $\Delta\delta/\Delta T$ reported in Table 1.4.2. On the other hand, the presence in both cases of a NOE contact between NH_{Gly} and NH_{Arg} suggests the formation of a β-turn motif at DKP-Arg, stabilized by a hydrogen bond between NH_{Gly} and C(5)=O (appointed as Type III H-bonding pattern, Figure 3.18). The presence of this H-bond is also supported by the rather upfield chemical shift value of NH_{Gly} in these two ligands (8.18 and 8.00 ppm for **c[DKP-2-RGD]** and **c[DKP-3-RGD]**, respectively) and the relatively low temperature dependence (-5.7 and -4.5 ppb/K, respectively). The similarity of the NMR data and hence of the conformation of these two ligands is quite surprising, considering the opposite configuration of the diketopiperazine scaffold (**DKP-2**, 3*R*,6*S*; **DKP-3**, 3*S*,6*R*) which should impart a different stereochemical orientation to the two side arms of the diketopiperazine. This conformational similarity can be interpreted in terms of a quasi-enantiomeric structure of the two ligands (excluding the configuration of the remote RD amino acid side chains, Figure 1.4.5).

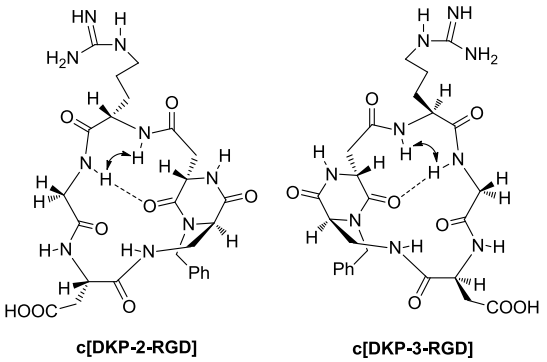

Figure 1.4.5 - Preferred intramolecular hydrogen-bonding pattern proposed for compound **c[DKP-2-RGD]** and **c[DKP-3-RGD]** on the basis of spectroscopic data. The arrows indicate significant NOE contacts. The DKP-Arg β-turn motif is referred as Type III H-bonding pattern.

Ligands **c[DKP-4-RGD]** and **c[DKP-6-RGD]**, featuring the diketopiperazine scaffolds **DKP-4** (3*R*,6*S*) and **DKP-6** (3*S*,6*R*) respectively (with the benzyl substitution at the endocyclic nitrogen N1, instead of N4), show a different NMR pattern. In particular, ligand **c[DKP-6-RGD]** is characterized by a rather strong NOE contact between NH_{Asp} and NH_{10} and a moderate/weak one involving NH_4 and NH_{10}. These two contacts are mutually exclusive and hence indicative of an equilibrium between two different conformations, respectively Type I and Type IV H-bonding patterns (Figure 1.4.6 A and B).

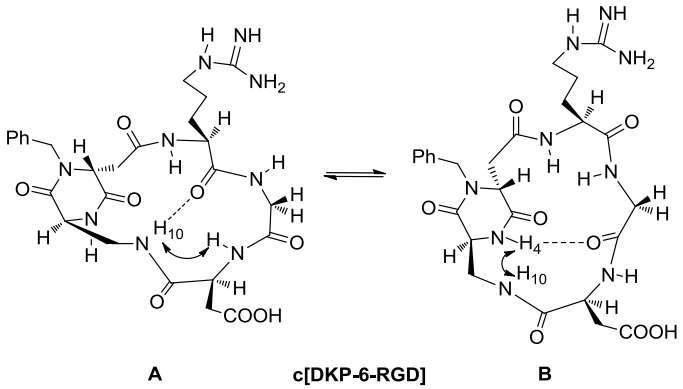

Figure 1.4.6 - Preferred intramolecular hydrogen-bonded pattern proposed for compound **c[DKP-6-RGD]** on the basis of spectroscopic data. A) Type I H-bonding pattern is characterized by a β-turn motif at Gly-Asp stabilized by a hydrogen bond between NH_{10} and Arg-C=O. B) Type IV H-bonding pattern which is characterized by a pseudo β-turn at Asp-DKP stabilized by a hydrogen bond between NH_4 and Gly-C=O. The arrows indicate significant NOE contacts.

The hydrogen bonded status of the two amide protons NH_4 and NH_{10}, as indicated by their rather low temperature dependence (-4.9 and -5.1 ppb/K, respectively) and quite upfield chemical shift values (8.07 and 7.90 ppm, respectively), corroborate this assumption. The Type IV H-bonding pattern could feature a pseudo β-turn at Asp-DKP stabilized by a hydrogen bond between NH_4 and Gly-C=O (NOE contact between NH_4 and NH_{10}).

Ligand **c[DKP-4-RGD]**, on the other hand, is characterized by the absence of relevant NOE contacts, a very low temperature dependence (-0.7 ppb/K) and a quite upfield

chemical shift value (7.59 ppm) for proton NH_{10}. These two features suggest a Type I H-bonding pattern, notwithstanding the apparent lack of NOE contact between NH_{Asp} and NH_{10}.

The dibenzylated diketopiperazine containing peptidomimetics **c[DKP-5-RGD]** and **c[DKP-7-RGD]** were eventually studied. Ligand **c[DKP-5-RGD]** shows NMR features similar to ligand **c[DKP-2-RGD]** (Type III H-bonding pattern): a NOE contact between NH_{Gly} and NH_{Arg} and a rather shielded NH_{Gly} (8.23 ppm) with a relatively low temperature coefficient (-4.7 ppb/K). As discussed above (Chapter 1.4.2), ligand **c[DKP-7-RGD]** was obtained as a mixture of two diastereomers **A** and **B**, whose conformations in solution were studied separately. In particular, **c[DKP-7-RGD]-A** displays two mutually exclusive NOE contacts between NH_{Arg} and NH_{Gly} and between NH_{Asp} and NH_{Gly}. These three protons, on the other hand, show also a rather strong hydrogen bonded status, as indicated by their low temperature dependence and, at least for NH_{Asp} and NH_{Gly}, their upfield chemical shift (Table 1.4.2). These data indicate an equilibrium between two different conformations: one displaying a Type III H-bonding pattern and a second one showing a Type II H-bonding pattern (β-turn at Arg-Gly), like the low-affinity ligand **c[DKP-1-RGD]**. Finally, ligand **c[DKP-7-RGD]-B** shows a single NOE contact between NH_{Asp} and NH_{10} and a hydrogen bonded status for NH_{10} (δ 7.72 ppm and $\Delta\delta/\Delta T$ -4 ppb/K, see Table 1.4.2). These values are indicative of a Type I H-bonding pattern.

No NOE contacts were identified for compound **c[DKP-8-RGD]**, containing the superior omologous of **DKP-3** (*i.e.* **DKP-8**). Moreover, also temperature coefficients of the amide protons are not relevant for the identification of H-bonds.

1.4.4.1 Conformational analysis

Conformational studies of the cyclic RGD-peptidomimetics were performed by mixed-mode Metropolis Monte Carlo/Stochastic Dynamics (MC/SD) simulations, using the implicit water GB/SA solvation model[2] and the OPLS_2001 force field.

As already reported in a preliminary communication,[90] three-dimensional structures satisfying long-range NOE contacts were generated for RGD peptidomimetic **c[DKP-1-RGD]** performing two 10 ns restrained MC/SD simulations and applying the DKP-NH_{10}/NH_{Asp} or the NH_{Asp}/NH_{Gly} distance restraint derived from NOESY spectra.

More than 90% of the conformations sampled during the first simulation adopted a non-extended arrangement of the RGD sequence characterized by a β-turn at Gly-Asp and the presence of the corresponding hydrogen bond between DKP-NH_{10} and Arg-C=O. In addition, the formation of a γ-turn at Gly stabilized by the hydrogen bond between NH_{Asp} and Arg-C=O was observed for 40% of the simulation. A Cβ(Arg)–

Cβ(Asp) average distance of 7.4 Å was obtained during this MC/SD calculation. A representative energy minimized conformation selected by cluster analysis and featuring both H-bonds is shown in Figure 1.4.7 A (Type I-*cis* H-bonding pattern). Approximately 60% of the conformations sampled during the simulation of **c[DKP-1-RGD]** featuring the NH_{Asp}/NH_{Gly} distance restraint, adopted a non-extended arrangement of the RGD sequence characterized by a β-turn at Arg-Gly and the corresponding hydrogen bond between NH_{Asp} and C(8)=O. In addition, the formation of a γ-turn at Arg stabilized by the hydrogen bond between NH_{Gly} and C(8)=O was observed for 40% of the simulation. The Cβ(Arg)–Cβ(Asp) average distance in this MC/SD calculation was 6.8 Å. A representative energy minimized conformation selected by cluster analysis and featuring both H-bonds is shown in Figure 1.4.7 B (Type II H-bonding pattern).

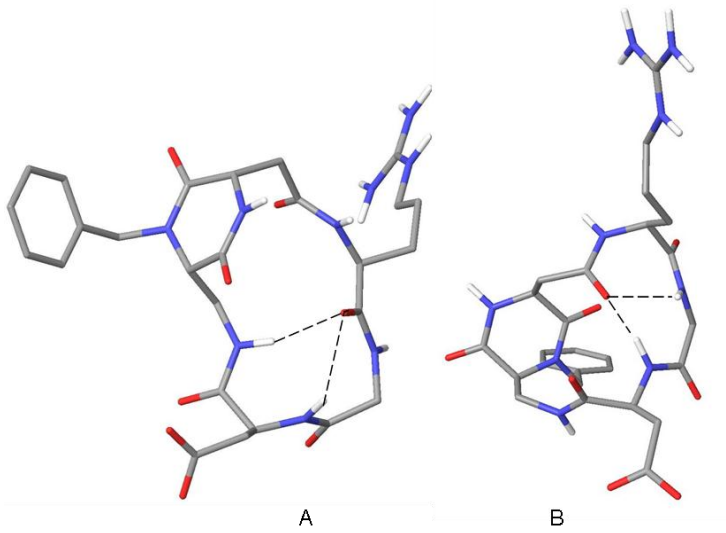

Figure 1.4.7 - Structures of **c[DKP-1-RGD]** as obtained by restrained MC/SD simulations based on experimental distance information, after energy minimization. A) Type I-*cis* H-bonding pattern, γ-turn at Gly and βII'-turn at Gly-Asp [CβArg)–Cβ(Asp)=7.9 Å]. B) Type II H-bonding pattern, γ-turn at Arg and βII'-turn at Arg-Gly [Cβ(Arg)–Cβ(Asp)=6.6 Å].

The NOESY spectra of compounds **c[DKP-2-RGD]**, **c[DKP-3-RGD]** and **c[DKP-5-RGD]** show only one relevant long-range interaction between NHGly and NHArg: this NOE is indicative of a β-turn motif at DKP-Arg stabilized by a hydrogen bond between NHGly and C(5)=O (Figure 1.4.5, Type III H-bonding pattern). The distance restraint corresponding to the NOE contact between NHGly and NHArg was applied in the 10 ns MC/SD simulations of compounds **c[DKP-2-RGD]**, **c[DKP-3-RGD]** and **c[DKP-5-RGD]**. More than 90% of the conformations sampled during each of these simulations adopted an extended arrangement of the RGD sequence characterized by a pseudo β-turn at DKP-Arg and the formation of the corresponding hydrogen bond between the NHGly and C(5)=O. Interestingly, only for compound **c[DKP-3-RGD]**, the additional

formation of a β-turn at Arg-Gly stabilized by the hydrogen bond between NHAsp and C(8)=O was observed for 15% of the simulation. These results and the NMR data (showing δ 7.85 ppm and Δδ/ΔT -3.5 ppb/K for NHAsp of **c[DKP-3-RGD]**) suggest the contribution of a Type II/Type III H-bonding pattern to the conformational equilibrium of **c[DKP-3-RGD]** (mainly populated by a Type III H-bonding pattern).
Cβ(Arg)-Cβ(Asp) average distances of 9.3, 8.8, and 9.1 Å were obtained during the MC/SD calculations of **c[DKP-2-RGD]**, **c[DKP-3-RGD]** and **c[DKP-5-RGD]**, respectively. A representative energy minimized conformation selected by cluster analysis and featuring the H-bond between the Gly-NH and C(5)=O (Type III H-bonding pattern) is shown in Figure 1.4.8 for RGD peptidomimetic **c[DKP-2-RGD]**.

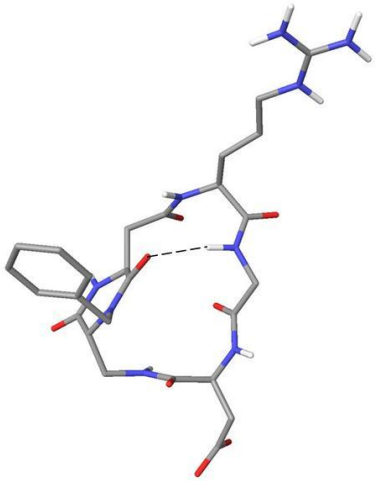

Figure 1.4.8 - Structure of **c[DKP-2-RGD]** as obtained by restrained MC/SD simulations based on experimental distance information, after energy minimization (Type III H-bonding pattern, distorted inverse γ-turn at Asp and pseudo β-turn at DKP-Arg, Cβ(Arg)–Cβ(Asp)=9.4 Å).

Due to the absence of relevant long-range NOE contacts, several 10 ns runs of unconstrained MC/SD simulations were performed for RGD peptidomimetic **c[DKP-4-RGD]** starting from different 3D structures. Most of the conformations sampled during these simulations adopted an extended arrangement of the RGD sequence (Cβ(Arg)-Cβ(Asp) average distance of 8.8 Å) and approximately 40% of them are characterized by a β-turn at Gly-Asp and the presence of the corresponding hydrogen bond between DKP-NH_{10} and Arg-C=O. These results provide a structural model in agreement with NMR data showing a low temperature dependence (-0.7 ppb/K) and an upfield chemical shift value (7.59 ppm) for proton NH_{10}. It is worth noting how the combination of the *trans* **DKP-4** scaffold with the Gly-Asp β-turn occurs by generating an extended RGD arrangement, while the combination of the *cis* **DKP-1** scaffold with the same secondary motif resulted in a non-extended RGD disposition (see above, Figure 1.4.7 A). Accordingly, two Type I H-bonding patterns have been defined, depending on the *cis* or *trans* relative stereochemistry of the diketopiperazine scaffold.

Three-dimensional structures satisfying long-range NOE contacts were generated for RGD peptidomimetic **c[DKP-6-RGD]** performing two 10 ns restrained MC/SD simulations and applying the DKP-NH_{10}/NH_{Asp} or the NH_4/NH_{10} distance restraint derived from NOESY spectra (Table 1.4.2, Figure 1.4.6).

Most of the conformations sampled during the first simulation adopted an extended arrangement of the RGD sequence (Cβ(Arg)-Cβ(Asp) average distance of 9.0 Å) and approximately 40% of them are characterized by a β-turn at Gly-Asp and the corresponding hydrogen bond between DKP-NH_{10} and Arg-C=O. A representative energy minimized conformation selected by cluster analysis and featuring this H-bond is shown in Figure 1.4.9 A (Type I-*trans* H-bonding pattern). Approximately 70% of the conformations sampled during the simulation of **c[DKP-6-RGD]** featuring the NH_4/NH_{10} distance restraint, adopted an extended arrangement of the RGD sequence (Cβ(Arg)-Cβ(Asp) average distance of 8.8 Å) characterized by a pseudo β-turn at Asp-DKP and the corresponding hydrogen bond between NH_4 and Gly-C=O. In addition, the formation of a γ-turn at Asp stabilized by the hydrogen bond between NH_{10} and Gly-C=O was observed for 50% of the simulation A representative energy minimized conformation selected by cluster analysis and featuring these H-bonds is shown in Figure 1.4.9 B (Type IV H-bonding pattern).

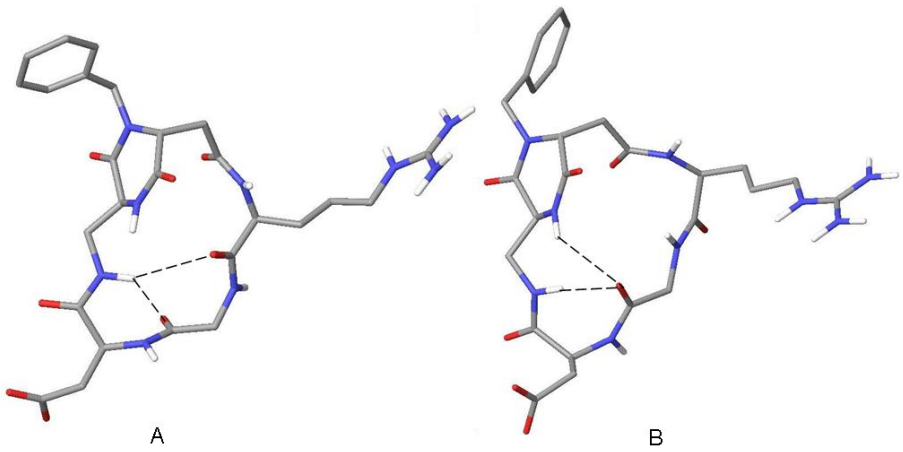

Figure 1.4.9 - Structures of **c[DKP-6-RGD]** as obtained by restrained MC/SD simulations based on experimental distance information, after energy minimization. A) Type I-*trans* H-bonding pattern, inverse γ-turn at Asp and distorted βII'-turn at Gly-Asp [CβArg)–Cβ(Asp)=9.0 Å]. B) Type IV H-bonding pattern, inverse γ-turn at Asp and pseudo β-turn at Asp-DKP [Cβ(Arg)–Cβ(Asp)=8.8 Å].

Three-dimensional structures satisfying long-range NOE contacts were generated for RGD peptidomimetic **c[DKP-7-RGD]** performing three 10 ns restrained MC/SD simulations and applying the distance restraints derived from NOESY spectra of diastereoisomers **A** and **B** (Table 1.4.2): in the first simulation NH_{Arg}/NH_{Gly} relevant in

c[DKP-7-RGD]-A, in the second simulation NH_{Asp}/NH_{Gly} also relevant in **c[DKP-7-RGD]-A**, and in the third simulation DKP-NH_{10}/NH_{Asp} relevant in **c[DKP-7-RGD]-B**.

All the conformations sampled during the first two simulations adopted a non-extended arrangement of the RGD sequence [Cβ(Arg)-Cβ(Asp) average distance of 6.6 Å] characterized by the simultaneous presence of different turn motifs (pseudo β-turn at DKP-Arg, γ-turn at Gly and pseudo β-turn centered at the DKP unit). The structural models provided by these restrained MC/SD simulations differ from the conformations hypothesized on the basis of NMR data of **c[DKP-7-RGD]-A** [equilibrium between Type III (pseudo β-turn at DKP-Arg) and Type II (β-turn at Arg-Gly) H-bonding patterns, see the NMR section]. However, also the calculated structures are able to provide an explanation for the NOE contacts and the NMR temperature coefficients observed for **c[DKP-7-RGD]-A**.

The distance restraint corresponding to the NOE contact between DKP-NH_{10} and NH_{Asp} (observed in the NOESY spectrum of **c[DKP-7-RGD]-B**) was applied in the third 10 ns MC/SD simulation of compound **c[DKP-7-RGD]**. Most of the conformations sampled during this simulation adopted an extended arrangement of the RGD sequence (Cβ(Arg)-Cβ(Asp) average distance of 9.0 Å) and approximately 50% of them are characterized by a β-turn at Gly-Asp and the corresponding hydrogen bond between DKP-NH_{10} and Arg-C=O. A representative energy minimized conformation selected by cluster analysis and featuring this H-bond is shown in Figure 1.4.10 (Type I-*trans* H-bonding pattern).

Contrary to what observed for the other cyclic RGD peptidomimetics containing DKP scaffolds, rotation of the DKP ring can not be observed during the simulations performed on compound **c[DKP-7-RGD]**, confirming **c[DKP-7-RGD]-A** and **c[DKP-7-RGD]-B** as two different separable conformers (diastereomers) due to hindered rotation of one ring around the other.

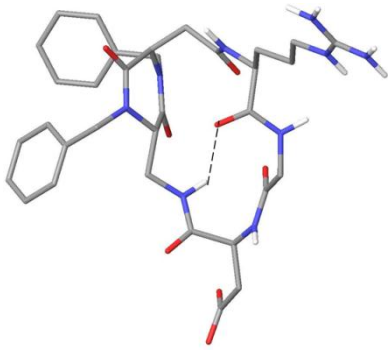

Figure 1.4.10 - Structure of **c[DKP-7-RGD]-B** as obtained by restrained MC/SD simulations based on experimental distance information, after energy minimization (Type I-*trans* H-bonding pattern, distorted inverse γ-turn at Asp and βII'-turn at Gly-Asp, Cβ(Arg)–Cβ(Asp)=9.2 Å).

Due to the absence of relevant long-range NOE contacts, two 10 ns runs of unconstrained MC/SD simulations were performed for RGD peptidomimetic **c[DKP-8-RGD]**.

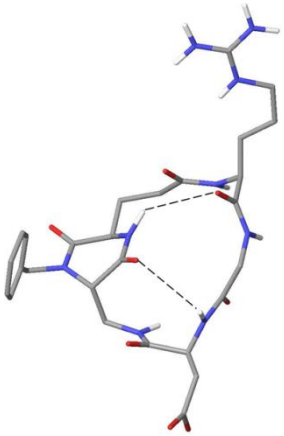

Figure 1.4.11 - Structure of **c[DKP-8-RGD]** as obtained by MC/SD simulations, after energy minimization (Cβ(Arg)–Cβ(Asp)=9.5 Å).

All the conformations sampled during these simulations adopted an extended arrangement of the RGD sequence (Cβ(Arg)-Cβ(Asp) average distance of 9.8 Å) characterized by the formation of hydrogen bonds between NH_{Asp} and C(2)=O and between NH_1 and Arg-C=O.
A representative energy minimized conformation selected by cluster analysis and featuring these H-bonds is shown in Figure 1.4.11 for RGD peptidomimetic **c[DKP-8-RGD]**.

1.4.4.2 Molecular docking

In order to rationalize, on a molecular basis, the affinity of cyclic RGD peptidomimetics for the $\alpha_v\beta_3$ receptor, docking studies were performed starting from the representative conformations obtained from the MC/SD simulations. The crystal structure of the extracellular segment of integrin $\alpha_v\beta_3$ complexed with the cyclic pentapeptide Cilengitide (1L5G, pdb code) was taken as a reference model for the interpretation of the docking results in terms of ligand-protein interactions. In the X-ray complex, Cilengitide binds to the interface of the α and β units forming specific electrostatic interactions. The acid and basic pharmacophoric groups and their orientation are essential for binding to the $\alpha_v\beta_3$ because they act like an electrostatic clamp, interacting with charged regions of the receptor binding site.
Docking calculations starting from geometries featuring the Type I-*cis* and Type II H-bonding patterns produced top-ranked poses conserving optimal interactions only with the α subunit of the $\alpha_v\beta_3$ receptor. Probably, the short Cβ(Arg)-Cβ(Asp) distances (values less than 8 Å) of these geometries prevent the guanidine and carboxylic groups

from achieving the required separation for binding to the $\alpha_v\beta_3$ integrin. On the other hand, docking calculations starting from the RGD extended conformations featuring the Type I-*trans*, Type III and Type IV H-bonding patterns, produced top-ranked poses conserving all the important interactions of the X-ray complex (Figure 1.4.12).

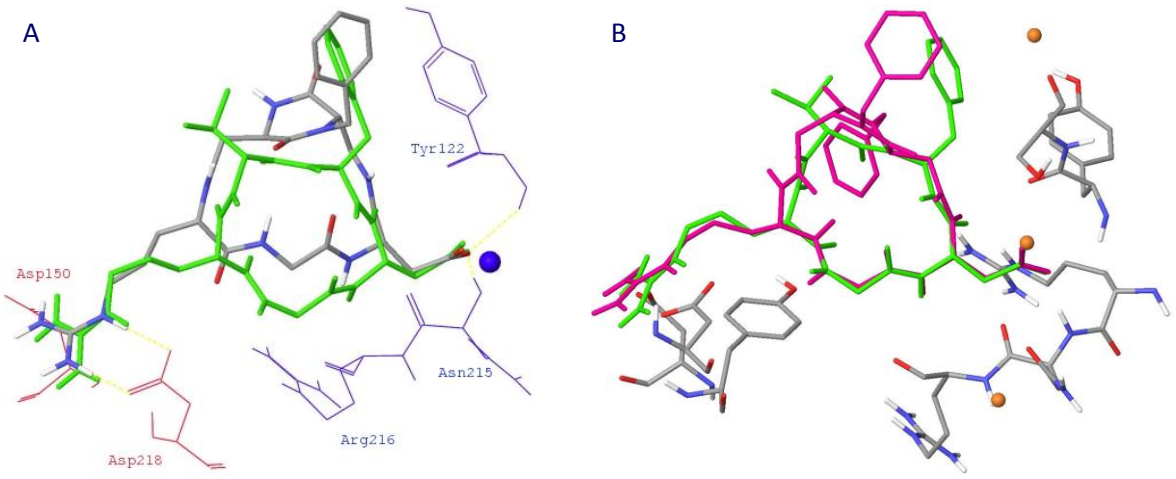

Figure 1.4.12 - Top-ranking binding mode of compounds A) **c[DKP-3-RGD]** and B) **c[DKP-7-RGD]-B** into the crystal structure of the extracellular domain of $\alpha_v\beta_3$ integrin overlaid on the bound conformation of Cilengitide (green).

The positively charged Arg guanidinium group of the ligand interacts with the negatively charged side chains of Asp218 and Asp150 in the α unit, one carboxylate oxygen of the ligand Asp side chain is coordinated to the metal cation in the metal-ion-dependent adhesion site (MIDAS) region of the β unit, while the second carboxylate oxygen forms hydrogen bonds with the backbone amides of Asn215 and Tyr122 in the β unit. Further stabilizing interaction involves the formation of a hydrogen bond between the ligand backbone NH of the Asp residue and the backbone carbonyl group of Arg216 in the β unit.

In light of all these considerations, the micromolar affinity of RGD peptidomimetics **c[DKP-1-RGD]** and **c[DKP-7-RGD]-A** (3.9 and 0.2 μM, respectively) for $\alpha_v\beta_3$ (Table 1.4.1) can be explained in terms of their low pre-organization for binding. In fact, as determined by the computational and NMR studies, these compounds in solution mainly feature non-extended RGD conformations which, according to the docking results, are not able to properly fit into the $\alpha_v\beta_3$ receptor. On the contrary, the nanomolar affinity of RGD peptidomimetics **c[DKP-2-RGD], c[DKP-3-RGD], c[DKP-4-RGD], c[DKP-5-RGD], c[DKP-6-RGD], c[DKP-7-RGD]-A, c[DKP-8-RGD]** for $\alpha_v\beta_3$ can be attributed to their high structural pre-organization. In fact, as determined by the computational and NMR studies, these compounds in solution mainly feature extended RGD conformations (principally determined by Type I-*trans*, Type III and Type IV H-bonding patterns) similar to the RGD bound conformation of Cilengitide.

1.5 Cyclic [DKP-*iso*DGR] Integrin Ligands

Given the interesting results appeared in literature recently (see 1.1.3.2), during my thesis I planned to synthesize a new class of cyclic *iso*DGR integrin ligands, starting from the already reported diketopiperazine scaffolds **DKP-2** and **DKP-3** (see 1.2.1 and 1.3.5 for the choice of DKP scaffolds).
We synthesized two cyclic *iso*DGR peptidomimetics (**c[DKP-2-*iso*DGR]** and **c[DKP-3-*iso*DGR]**; Figure 1.5.1) containing the bifunctional diketopiperazine scaffolds mentioned above, and investigated their conformation in solution and their ability to compete with biotinylated vitronectin for binding to the purified $\alpha_v\beta_3$ and $\alpha_v\beta_5$ receptors.

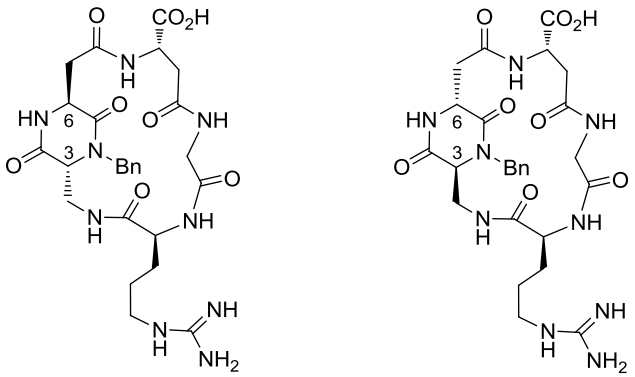

Figure 1.5.1 - Cyclic *iso*DGR peptidomimetics containing the bifunctional diketopiperazine scaffolds.

1.5.1 Synthesis of c[DKP-*iso*DGR] ligands

The synthesis was conveniently performed on solid phase (Fmoc strategy) using SASRIN™ resin, following the strategy shown in Scheme 1.5.1. Fmoc-glycine was loaded onto the resin and Fmoc-aspartic acid α-*tert*-butyl ester was coupled. The **DKP-2** and **DKP-3** scaffolds (either 3*R*,6*S* or 3*S*,6*R*) were then coupled to the supported dipeptide. The DKP-scaffolds are normally obtained as *N*-Boc protected amino acids (see 1.2.1) and thus they are unsuitable for solid phase synthetic applications. In order to avoid an exchange of the nitrogen protecting group, involving a deprotection-reprotection sequence, an intermediate of DKP synthesis, namely the azido-acids **63** were used in this case. The azide reduction on resin was performed using trimethylphosphine in dioxane-water and Cbz-Arg(Mtr) was finally coupled. The linear precursors were cleaved from the resin under controlled acidic conditions (to avoid deprotection of the *t*-butyl ester and the Mtr group) affording carboxylic acids **64** that,

after hydrogenolysis of the benzyloxycarbonyl group (**65**), were subjected to macrolactamization (**66**). Final protecting groups side-chain deprotection and purification by RP-HPLC afforded the cyclic *iso*DGR peptidomimetics **c[DKP-2-*iso*DGR]** and **c[DKP-3-*iso*DGR]** ready for biological studies and conformational analysis.

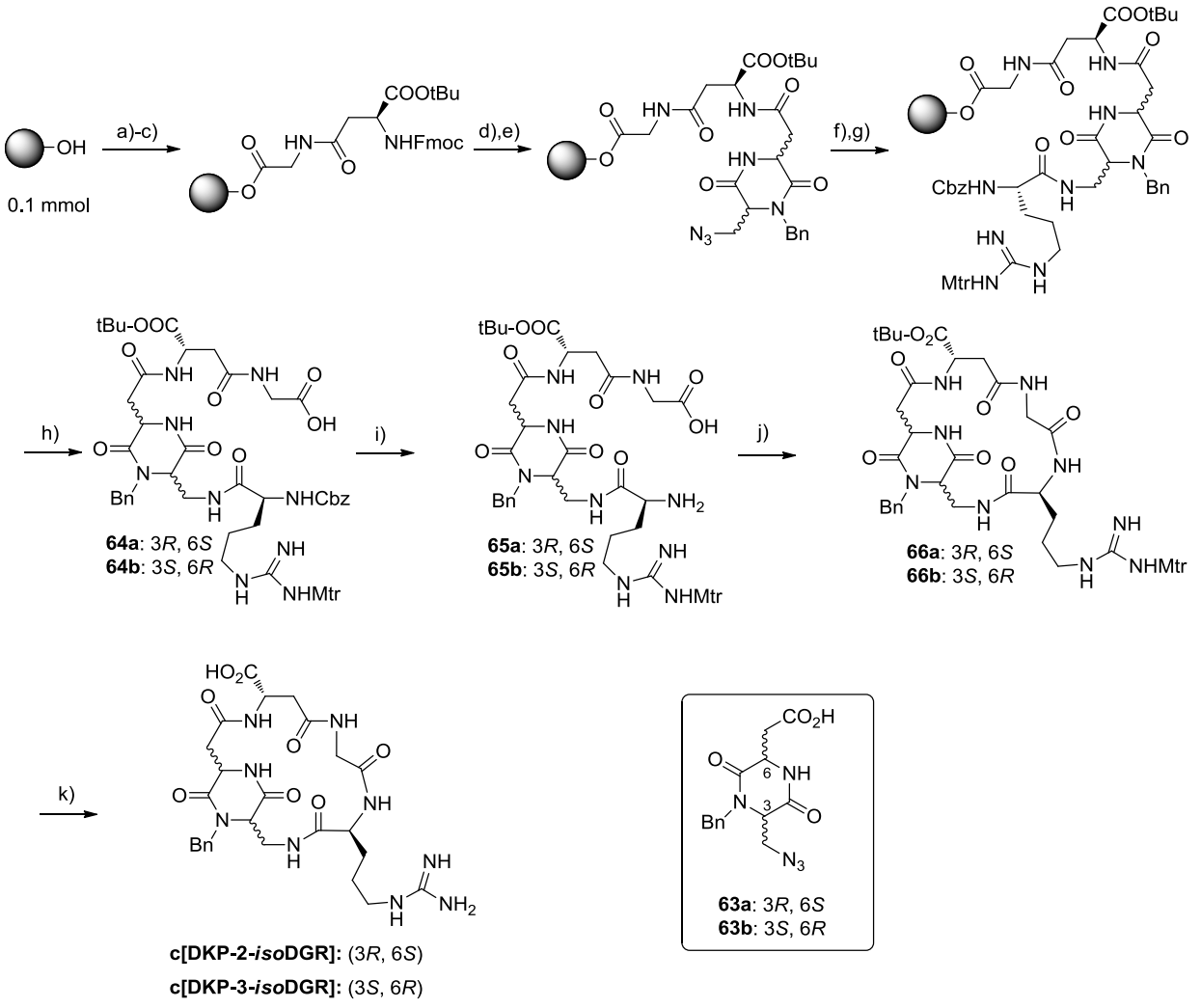

Scheme 1.5.1 - a) Fmoc-Gly-OH, DIC, cat. DMAP, DMF, 2h; b) 20% piperidine in DMF; c) Fmoc-Asp(OH)-O*t*Bu, DIC, HOAt, DMF; d) 2% piperidine and 2% DBU in DMF; e) **63a** or **63b**, DIC, HOAt, DMF, 18h; f) Me_3P, dioxane/water 4:1; g) Cbz-Arg(Mtr)-OH, DIC, HOAt, DMF; h) 1% TFA in DCM; i) H_2, 10% Pd/C, THF/water 1:1; j) HATU, HOAt, DIPEA, 1.4 mM, DMF; k) TFA/thioanisole/EDT/anisole 90:5:3:2.

1.5.2 Biological evaluation [99]

Cyclic *iso*DGR peptidomimetics **c[DKP-2-*iso*DGR]** and **c[DKP-3-*iso*DGR]** were examined in vitro for their abilities to compete with biotinylated vitronectin for binding to the purified $\alpha_v\beta_3$ and $\alpha_v\beta_5$ receptors (Table 1.5.1). Screening assays were performed by incubating the immobilized integrins $\alpha_v\beta_3$, $\alpha_v\beta_5$ and $\alpha_5\beta_1$ with increasing concentrations (10^{-12}–10^{-5} M) of the two *iso*DGR ligands in the presence of biotinylated vitronectin (for integrins $\alpha_v\beta_3$ and $\alpha_v\beta_5$) and biotinylated fibronectin (for integrin $\alpha_5\beta_1$), and measuring the concentration of bound vitronectin or fibronectin in the presence of the competitive ligands.

Table 1.5.1 - Inhibition of biotinylated vitronectin or fibronectin binding to $\alpha_v\beta_3$, $\alpha_v\beta_5$ and $\alpha_5\beta_1$ receptors.

Ligand	$\alpha_v\beta_3$ IC_{50} [nM][a]	$\alpha_v\beta_5$ IC_{50} [nM][a]	$\alpha_5\beta_1$ IC_{50} [nM][a]
c[DKP-2-*iso*DGR]	46.7 ± 18.2	220 ± 84	4246 ± 2586
c[DKP-3-*iso*DGR]	9.2 ± 1.1	312 ± 21	1066 ± 228
c[G*iso*DGRphg] [b]	89 ± 19 [c]	n.d.	406 ± 191 [c]
c[phg-*iso*DGR-G] [b]	> 10^3 [c]	n.d.	19 ± 4 [c]
c[DKP-3-RGD]	4.5 ± 1.1	149 ± 25	532 ± 35
c[RGDfV]	3.2 ± 1.3	7.5 ± 4.8	166 ± 28

[a] IC_{50} values were calculated as the concentration of compound required for 50% inhibition of biotinylated vitronectin or fibronectin binding as estimated by GraphPad Prism software; all values are the arithmetic mean ± SD of triplicate determinations; [b] See 1.1.3.2; [c] determined by a solid phase binding assay using supported vitronectin, soluble integrin, specific primary and secondary antibodies.

The $\alpha_v\beta_3$ IC_{50} values of compounds **c[DKP-2-*iso*DGR]** and **c[DKP-3-*iso*DGR]** reported in Table 1.5.1 compare favorably with other *iso*DGR ligands, such as the cyclopentapeptide c[G*iso*DGRphg] recently published by Kessler and coworkers,[79] as well as with known RGD ligands, such as our **c[DKP-3-RGD]** (see 1.2.2) and the standard cyclopentapeptide *cyclo*(RGDfV) (see 1.1.3.1). In particular, the new ligand **c[DKP-3-*iso*DGR]** is ten times more potent in binding integrin $\alpha_v\beta_3$ than c[G*iso*DGRphg] and only two-three times less potent than the powerful RGD ligands **c[DKP-3-RGD]** and c[RGDfV]. The IC_{50} value of *c*[G*iso*DGRphg] can be compared with the IC_{50} values of **c[DKP-2-*iso*DGR]** and **c[DKP-3-*iso*DGR]** despite the binding assays were realized using two different protocols. Indeed, i) vitronectin is used as a competitive natural ligand in both assays, and ii) Cilengitide, i.e. *c*[RGDf(*N*-Me)V], gives the same IC_{50} value using both assays (0.54 nM[79] and 0.58 nM[101]).

Interestingly, the synthesized ligands **c[DKP-2-*iso*DGR]** and **c[DKP-3-*iso*DGR]** show no selectivity with respect to $\alpha_5\beta_1$ integrin, unlike for some *iso*DGR ligands (i.e. c[phg-*iso*DGR-G] in Table 1.5.1) developed by Kessler and coworkers.[79]

1.5.3 Spectroscopic and computational studies [100]

The structure and connectivity of compounds **c[DKP-2-*iso*DGR]** and **c[DKP-3-*iso*DGR]** were unambiguously assigned by means of mono- and bidimensional ^{1}H and ^{13}C NMR spectra. The preferred conformations **c[DKP-2-*iso*DGR]** and **c[DKP-3-*iso*DGR]** were investigated by ^{1}H NMR spectroscopy of dilute H_2O/D_2O 9:1 solutions and by computational methods, with the aim of rationalizing the affinity of these compounds for the $\alpha_v\beta_3$ receptor at a molecular level. One-dimensional ^{1}H NMR experiments were conducted to detect intramolecular hydrogen bonds, by measuring the chemical shift of the amide N-H protons, their temperature coefficients ($\Delta\delta/\Delta T$) and their chemical exchange rate in the presence of D_2 (see Table 1.5.2). NOESY spectra were also recorded to investigate both sequential and long-range NOE signals that provide evidences of preferred conformations. Three-dimensional structures satisfying long-range NOE contacts were generated by restrained mixed-mode Metropolis Monte Carlo/Stochastic Dynamics (MC/SD) simulations, using the implicit water GB/SA solvation model.

Table 1.5.2 - List of the temperature coefficients, chemical shifts and chemical exchange rates for **c[DKP-2-*iso*DGR]** and **c[DKP-3-*iso*DGR]**.

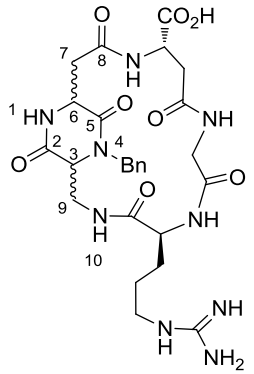

c[DKP-2-*iso*DGR]: (3*R*, 6*S*)
c[DKP-3-*iso*DGR]: (3*S*, 6*R*)

Ligand	**c[DKP-2-*iso*DGR]**			**c[DKP-3-*iso*DGR]**		
	δ(ppm)	Δδ/ΔT (ppb/K)	Chemical Exchange rates	δ(ppm)	Δδ/ΔT (ppb/K)	Chemical Exchange rates
NH_1	8.34	-6.99	0 min	7.60	-1.70	0 min
NH_{10}	8.43	-8.57	20 min	8.46	-8.02	1h27min
NH_{Asp}	8.23	-4.90	0 min	8.63	-7.03	12 min
NH_{Gly}	7.88	-4.76	0 min	8.16	-7.20	7 min
NH_{Arg}	8.26	-6.87	5-10 min	8.27	-6.92	12-17 min

The data obtained from the NMR experiments show that compound **c[DKP-2-*iso*DGR]** (Figure 1.5.2) is characterized by a high conformational flexibility. Indeed, the $\Delta\delta/\Delta T$ values range from -4.7 ppb K^{-1} (Gly-NH) to -8.5 ppb K^{-1} (DKP-NH10) and the N-H chemical shifts indicate that the amide protons of **1** are all solvent exposed. However, the strong NOE contact between *iso*Asp-NH and Gly-NH (see Figure 1.5.2, structure on the left) indicates a preferred folding through the formation of a pseudo β-turn stabilized by an intramolecular hydrogen bond between Gly-NH and DKP-C(5)=O.

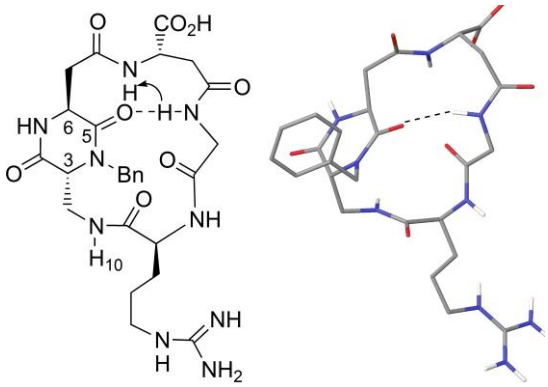

Figure 1.5.2 - Left: Preferred intramolecular hydrogen-bonded pattern proposed for **c[DKP-2-*iso*DGR]**, on the basis of spectroscopic data. The arrow indicates the NOE contact. Right: 3D structure of **c[DKP-2-*iso*DGR]** as obtained by restrained MC/SD simulations based on experimental distance information, after energy minimization [pseudo β-turn at DKP-*iso*Asp, Cβ(Arg)–COO^-(Asp) distance = 8.8 Å].

The distance restraint corresponding to the NOE contact between *iso*Asp-NH and Gly-NH was applied in the MC/SD simulations of compound **c[DKP-2-*iso*DGR]**. Approximately 50% of the conformations sampled during the simulations adopted an extended arrangement of the *iso*DGR sequence characterized by a pseudo β-turn at DKP-*iso*Asp and the formation of the corresponding hydrogen bond between Gly-NH and C(5)=O. A Cβ(Arg)–COO^-(Asp) average distance of 8.6 Å was obtained during the MC/SD calculations. A representative energy minimized conformation featuring the 11-membered ring hydrogen bond between Gly-NH and C(5)=O is shown in Figure 1.5.2 (structure on the right).

NMR experiments performed on the *iso*DGR peptidomimetic **c[DKP-3-*iso*DGR]** suggest a different conformational preference. Indeed, compound **c[DKP-3-*iso*DGR]** exists in two preferred conformations, as shown in Figure 1.5.3 (A and B). The NOESY cross peak between DKP-NH10 and Arg-NH (strong) is indicative of a β-turn conformation stabilized by a hydrogen bond between DKP-NH10 and *iso*Asp-C=O (Figure 1.5.3 A), while the NOESY cross peak between Gly-NH and *iso*Asp-NH (weak) is indicative of a pseudo β-turn motif (Figure 1.5.3 B) similar to that observed for compound **c[DKP-2-*iso*DGR]**.

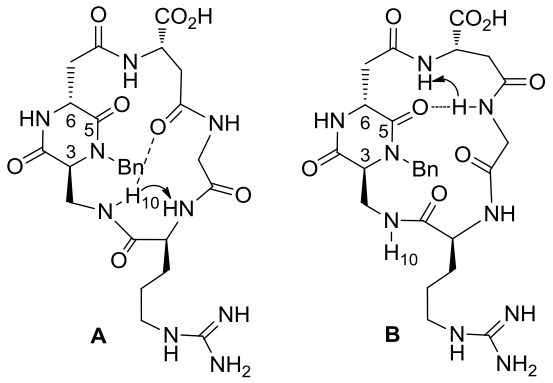

Figure 1.5.3 - Preferred intramolecular hydrogen-bonded patterns proposed for the cyclic *iso*DGR peptidomimetic **c[DKP-3-*iso*DGR]**, on the basis of spectroscopic data. The arrows indicate the NOE contacts. (A) β-turn at Gly-Arg. (B) pseudo β-turn at DKP-*iso*Asp.

Only the distance restraint corresponding to the strong NOE contact between DKP-NH10 and Arg-NH (shown in Figure 1.5.3 A) was applied in the MC/SD simulations of compound **c[DKP-3-*iso*DGR]**. It is worth noting that approximately 80% of the conformations sampled during the simulations adopted an extended arrangement of the *iso*DGR sequence, characterized by a pseudo β-turn at DKP-*iso*Asp and the formation of the corresponding hydrogen bond between Gly-NH and C(5)=O (shown in Figure 1.5.3 B). In addition, the formation of a distorted β-turn at Gly-Arg (shown in Figure 1.5.3 A), characterized by hydrogen bond distances of *ca.* 3.5 Å between DKP-NH10 and *iso*Asp-C=O, was observed for 10% of the simulations. A Cβ(Arg)–COO^-(Asp) average distance of 10.7 Å was obtained during the MC/SD calculations of compound **c[DKP-3-*iso*DGR]**. Two representative energy minimized conformations featuring the two hydrogen bond patterns compatible with the strong NOE contact between DKP-NH10 and Arg-NH are shown in Figure 1.5.4.

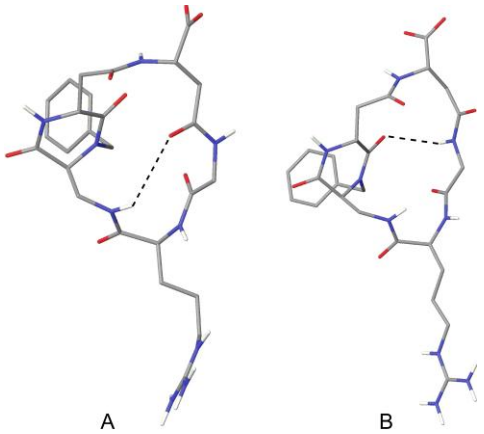

Figure 1.5.4 - 3D structures of compound **c[DKP-3-*iso*DGR]** as obtained by restrained MC/SD simulations based on experimental distance information, after energy minimization. (A) distorted β-turn at Gly-Arg, populated for 10% of the simulation, Cβ(Arg)–COO^-(Asp) distance = 10.7 Å. (B) pseudo β-turn at DKP-*iso*Asp, populated for 80% of the simulation, Cβ(Arg)–COO^-(Asp) distance = 10.8 Å.

In order to rationalize, on a molecular basis, the affinity of compounds **c[DKP-2-*iso*DGR]** and **c[DKP-3-*iso*DGR]** for the $\alpha_v\beta_3$ receptor, docking studies were performed starting from the representative conformations obtained from the restrained MC/SD simulations. The crystal structure of the extracellular segment of integrin $\alpha_v\beta_3$ complexed with the cyclic pentapeptide Cilengitide (1L5G pdb code) was taken as a reference model for the interpretation of the docking results in terms of ligand-protein

interactions. In the X-ray complex, Cilengitide (**3**) binds to the interface of the α– and β–units forming specific electrostatic interactions. The acid and basic pharmacophoric groups and their orientation are essential for binding to $\alpha_v\beta_3$ because they act like an electrostatic clamp, interacting with charged regions of the receptor binding site.

Docking calculations starting from the pseudo β-turn DKP-*iso*Asp geometries of compound **c[DKP-2-*iso*DGR]** (Figure 1.5.2, right) and from the distorted β-turn Gly-Arg conformations of compound **c[DKP-3-*iso*DGR]** (Figure 1.5.4 A), produced top-ranked poses conserving the key electrostatic interactions but lacking further stabilizing hydrogen bond interactions with the β-subunit (e.g. hydrogen bonds of ligand carboxylate oxygen with the backbone amides of Asn215 and Tyr122, and hydrogen bonds between ligand backbone N-H and protein backbone carbonyl groups).
On the contrary, docking calculations starting from the pseudo β-turn DKP-*iso*Asp geometries of compound **c[DKP-3-*iso*DGR]** (Figure 1.5.4 B) produced top-ranked poses conserving all the important interactions of the X-ray complex (see Figure 1.5.5).

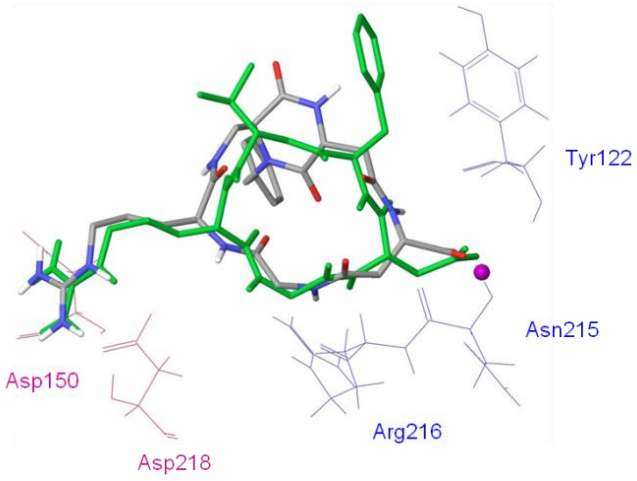

Figure 1.5.5 - Best pose of compound **c[DKP-3-*iso*DGR]** (atom colour tube representation, pseudo β-turn at DKP-*iso*Asp) into the crystal structure of the extracellular domain of $\alpha_v\beta_3$ integrin (α unit red and β unit blue wire representation) overlaid on the bound conformation of Cilengitide (green tube representation). Only selected integrin residues involved in the interactions with the ligand are shown. The metal ion in the MIDAS region is represented by a magenta sphere. Non-polar hydrogens were removed for clarity.

The positively charged Arg guanidinium group of the ligand interacts with the negatively charged carboxylates of Asp218 and Asp150 in the α unit, one carboxylate oxygen of the ligand is coordinated to the metal cation in the metal-ion-dependent adhesion site (MIDAS) region of the β unit, while the second carboxylate oxygen forms hydrogen bonds with the backbone amides of Asn215 and Tyr122 in the β unit. Further stabilizing interaction involves the formation of a hydrogen bond between the ligand backbone NH of the Gly residue and the backbone carbonyl group of Arg216 in the β unit. The *iso*DGR sequence of compound **c[DKP-3-*iso*DGR]** can fit into the RGD-binding pocket of $\alpha_v\beta_3$ integrin, establishing the same electrostatic clamp as well as additional key-interactions.

1.6 CONCLUSIONS

A library of 7 new bifunctional 2,5-diketopiperazine scaffolds (**DKP-4-8**, **DKP-*f*4, DKP-*f*6**) was designed and prepared, in addition to the previously reported scaffolds **DKP-1-3** and **DKP-*f*2-*f*3**.
All the DKP scaffolds feature a carboxylic acid functionality and a single amino moiety (**DKP-4-8**) or a double protected amino moiety (**DKP-*f*4, DKP-*f*6**). Moreover, the DKP scaffolds differ each from the other for the substitution at the intracyclic nitrogens (*N*-1, *N*-4), as they are either mono (**DKP-4, DKP-6**, **DKP-*f*4, DKP-*f*6**, **DKP-8**) or bis-benzylated (**DKP-5**, **DKP-7**). While being derived from α-amino acids, they can be seen as a constrained dipeptide formed by two β- or a β- and a γ-amino acids.

A different synthetic strategy, compared to the isopeptide strategy, was devised: the synthesis to obtain these scaffolds occurred *via* dipeptide. The β-hydroxy group of serine was converted into azide by a Mitsunobu-type reaction before the formation of the symmetric anhydride, which was used in the coupling with a *N*-benzyl dimethyl aspartate derivative. Bis *N*-benzyl substituted scaffolds (**DKP-5**, **DKP-7**) could be easily accessed by benzylation of mono-substituted advanced intermediates.

The 7 new scaffolds of the prepared library were used as templates in the synthesis of cyclic integrin ligands containing the RGD- recognition sequences.
The development of this library has provided a detailed SAR analysis of new integrin ligands based on DKP scaffolds, affording to a comprehensive view for this new class of integrin ligands.

In particular, an efficient synthesis in solution of constrained peptides containing the Arg-Gly-Asp (RGD) motif and the 7 diketopiperazine scaffolds was developed and optimized. Notably, two different separable conformers (diastereomers) formed during the cyclization of compound **c[DKP-7-RGD]**, containing bis-benzylated scaffold **DKP-7**, due to hindered rotation of one ring around the other.

Ligands **c[DKP-4-8-RGD]** were tested for their ability to inhibit biotinylated vitronectin binding to $\alpha_v\beta_3$ and $\alpha_v\beta_5$ receptors. All the ligands, except for **c[DKP-7-RGD]-A**, displayed low nanomolar affinity for both $\alpha_v\beta_3$ and $\alpha_v\beta_5$ integrins, with a slight selectivity towards the former receptor. Interestingly, the two diastereomeric compounds showing atropoisomerism (**c[DKP-7-RGD]-A**, **c[DKP-7-RGD]-B**) are the least and the most selective and potent of the series.

The conformational preferences of ligands **c[DKP-4-8-RGD]** were investigated by NMR spectroscopy in water, detecting H-bonds and long-range NOE contacts. In addition, three-dimensional structures satisfying long-range NOE contacts were generated by restrained MC/SD simulations. These high affinity ligands display well-defined preferred conformations featuring intramolecular hydrogen-bonded turn motifs and an extended arrangement of the RGD sequence [Cβ(Asp)-Cβ (Arg) average distance ca. 9 Å]. Docking studies were performed, starting from the representative conformations obtained from the MC/SD simulations and taking as a reference model the crystal structure of the extracellular segment of integrin $\alpha_V\beta_3$ complexed with the cyclic pentapeptide Cilengitide. The highest affinity ligands produced top-ranked poses conserving all the important interactions of the X-ray complex.

Besides the well-defined RGD motif, it was proposed that also the *iso*DGR sequence might be involved in integrin recognition. In fact, *iso*DGR sequence can mimic RGD and interact with RGD binding site of integrins (such as $\alpha_v\beta_3$, $\alpha_v\beta_5$ and $\alpha_5\beta_1$) in an inverted orientation, maintaining all the typical electrostatic-clamp interactions of the RGD motif and presenting additional stabilizing interactions. Hence, two constrained peptides (**c[DKP-2-*iso*DGR]** and **c[DKP-3-*iso*DGR]**) containing the *iso*Asp-Gly-Arg (*iso*DGR) motif and diketopiperazine scaffolds **DKP-2** and **DKP-3** were prepared, combining a new solid phase and an homogeneous synthetic approach. Low nanomolar values were obtained for their ability to inhibit biotinylated vitronectin binding to $\alpha_v\beta_3$ and $\alpha_v\beta_5$ receptors and also in this case the recognition sequence of compound **c[DKP-2-3-*iso*DGR]** can fit into the RGD-binding pocket of $\alpha_v\beta_3$ integrin, establishing the same electrostatic clamp as well as additional key-interactions. Interestingly, the synthesized ligands **c[DKP-2-*iso*DGR]** and **c[DKP-3-*iso*DGR]** show no selectivity with respect to $\alpha_5\beta_1$ integrin. Further studies will be conducted to develop the synthesis of **c[DKP-*iso*DGR]** ligands including also the newly prepared DKP scaffolds.

In addition, the two new functionalized integrin ligands **c[DKP-*f*4-RGD]** and **c[DKP-*f*6-RGD]** were employed in a drug-targeting approach with Paclitaxel (dual-action conjugates), further described in Chapter 2.1. These compounds were the basis for the work described in Chapter 2: since α_v integrins are involved in tumor angiogenesis and are overexpressed on the surface of cancer cells, integrin ligands can be usefully employed to design dual-action conjugates, able to exploit its integrin affinity to exert a site-directed delivery of other payloads.

References:

[1] R.O. Hynes, *Cell* **1987**, *48*, 549-554.

[2] M. Millard, S. Odde, N. Neamati, *Theranostics* **2011**, *1*, 154-188.

[3] a) M. Shimaoka, T. A. Springer. *Nature Rev. Drug Discov.* **2003**, *2*, 703-716; b) K.-E. Gottschalk, H. Kessler, *Angew. Chem. Int. Ed.* **2002**, *41*, 3767-3774; W. H. Miller, R. M. Keenan, R. N. Willette, M. W. Lark. *Drug Discovery Today* **2000**, *5*, 397-408; d) I. Ojima, *Bioorg. Med. Chem*. **1995**, *3*, 337-360.

[4] E. Ruoslahti. *Matrix Biol* .**2003**, *22*, 459-465; b) E. Ruoslahti. *Annu. Rev. Cell Dev. Biol.* **1996**, *12*, 967-715.

[5] a) J. P. Xiong, T. Stehle, B. Diefenbach, R. Zhang, R. Dunker, D. L. Scott, A. Joachimiak, S. L. Goodman, M. A. Arnaout. *Science* **2001**, *294*, 339-345; b) J. P. Xiong, T. Stehle, R. Zhang, A. Joachimiak, M. Frech, S. L. Goodman, M. A. Arnaout. *Science* **2002**, *296*, 151-155.

[6] a) W. Chen, C. Chang, M. K. Gilson.*J. Am. Chem. Soc*. **2006**, *128*, 4675-4684; b) L. Marinelli, A. Meyer, D. Heckmann, A. Lavecchia, E. Novellino, H. Kessler.*J. Med. Chem.* **2005**, *48*, 4204-4207; c) L. Marinelli, K.-E. Gottschalk, A. Meyer, E. Novellino, H. Kessler. *J. Med. Chem.* **2004**, *47*, 4166-4177; d) T. Xiao, J. Takagi, B. S. Coller, J.-H. Wang, T. A. Springer. *Nature* **2004**, *432*, 59-67; e) T. A. Springer, J. Zhu, T. Xiao.*J. Cell Biol.* **2008**, *182*, 791-800; f) T. J. You, D. S. Maxwell, T. P. Kogan, Q. Chen, J. Li, J. Kassir, G. W. Holland, R. A. F. Dixon. *Biophys. J.* **2002**, *82*, 447-457.

[7] R. O. Hynes, *Cell* **2002**, *110*, 673-687.

[8] T. A. Springer, *Proc. Natl. Acad. Sci. USA* **1997**, *94,* 65–72.

[9] M. J. Humphries, *Biochem. Soc. Trans.* **2000**, *28*, 311–339.

[10] M. Shimaoka, J. Takagi, T. A. Springer, *Annu. Rev. Biophys. Biomol. Struct.* **2002**, *31*, 485–516.

[11] S. C. Fagerholm, T. J. Hilden, C. G. Gahmberg, *Trends Biochem. Sci.* **2004**, *29*, 504–512.

[12] J. Ylanne, *Front. Biosci.* **1998**, *3*, 877–886.

[13] a) J. C. Loftus, J. W. Smith, M. H. Ginsberg, *J. Biol. Chem.* **1994**, *269*, 25235–25238; b) E. F. Plow, T. A. Haas, L. Zhang, J. C. Loftus, J. W. Smith, *J. Biol. Chem*. **2000**, *275*, 21785–21788; c) A. van der Flier, A. Sonnenberg, *Cell Tissue Res.* **2001**, *305*, 285–298.

[14] a) J. W. Smith, R. S. Piotrowicz, D. Mathis, *J. Biol. Chem.* **1994**, *269*, 960–967; b) A. P. Mould, S. K. Akiyama, M. J. Humphries, *J. Biol. Chem.* **1995**, *270*, 26270–26277.

[15] H. Jin, J. Varner, *Br. J. Cancer* **2004**, *90*, 561–565.

[16] B. A. Teicher, L. M. Ellis, *Antiangiogenic Agents in Cancer Therapy*, Humana Press, **2008**, *Chapter 3*, 49-71.

[17] M. Moser, K. R. Legate, R. Zent, R. Fässler, *Science* **2009**, *324*, 895-899.

[18] M. A. Arnaout, B. Mahalingam, J.-P. Xiong, *Annu. Rev. Cell Dev. Biol.* **2005**, *21*, 381-410.

[19] K. Legate, S. Wickström, R. Fässler, *Genes Dev.* **2009**, *23*, 397-418.

[20] J. Desgrosellier, D. Cheresh, *Nat Rev Cancer.* **2010**, *10*, 9-22.

[21] P. Carmeliet, *Nat. Med.* **2003**, *9*, 653–660.

[22] N. Ferrara, R. S. Kerbel, *Nature* **2005**, *438*, 967–974.

[23] S. Kim, K. Bell, S. A.Mousa, J. A.Varner, *Am. J. Pathol.* **2000**, *156*, 1345–1362.

[24] N. Laurens, M. a Engelse, C. Jungerius, C. W. Löwik, V. W. M. van Hinsbergh, P. Koolwijk, *Angiogenesis* **2009**, *12*, 275-285.

[25] D. Phillips, I. Charo, R. Scarborough, *Cell* **1991**, *65*, 359-362.

[26] a) J. Zhu, B. H. Luo, T. Xiao, C. Zhang, N. Nishida, T. A. Springer, *Mol. Cell* **2008**, *32*, 849-861; b) T. A. Springer, J. Zhu, T. Xiao, *J. Cell Biol.* **2008**, *182*, 791-800.

[27] T. Kamata, K. K. Tieu, T. A. Springer, Y. Takada, *J. Biol. Chem.* **2001**, *276*, 44275-44283.

[28] a) M. Hoefling, H. Kessler, K.-E. Gottschalk, *Angew. Chem. Int. Ed.* **2009**, *48*, 6590-6593; b) T. Xiao, J. Takagi, B. S. Coller, J.-H. Wang, T. A. Springer, *Nature* **2004**, *432*, 59-67.

[29] P. C. Brooks, R. A. Clark, D. A. Cheresh, *Science* **1994**, *264*, 569–571.

[30] P. C. Brooks, A. M. Montgomery, M. Rosenfeld, R. A. Reisfeld, T. Hu, G. Klier, D. A. Cheresh, *Cell* **1994**, *79*, 1157–1164.

[31] M. Friedlander, P. C. Brooks, R. W. Shaffer, C. M. Kincaid, J. A. Varner, D. A.Cheresh, *Science* **1995**, *270,* 1500–1502.

[32] L. E. Reynolds, L. Wyder, J. C. Lively, D. Taverna, S. D. Robinson, X. Huang, D. Sheppard, R. O. Hynes, K. M. Hodivala-Dilke, *Nat. Med.* **2002**, *8*, 27–34.

[33] D. G. Stupack, X. S. Puente, S. Boutsaboualoy, C. M. Storgard, D. A. Cheresh, *J. Cell Biol.* **2001**, *155*, 459–470.

[34] J.-P. Xiong, B. Mahalingham, J. L. Alonso, L. A. Borrelli, X. Rui, S. Anand, B. T. Hyman, T. Rysiok, D. Müller-Pompalla, S. L. Goodman, M. Arnaout, *J. Cell Biol.* **2009**, *186*, 589-600.

[35] a) A. Meyer, J. Auernheimer, A. Modlinger, H. Kessler, *Curr. Pharm. Des.* **2006**, *12*, 2723-2747; b) L. Marinelli, K.-E. Gottschalk, A. Meyer, E. Novellino, H. Kessler. *J. Med. Chem*. **2004**, *47*, 4166-4177.

[36] S. Kim, M. Bakre, H. Yin, J. A. Varner, *J. Clin. Invest.* **2002**, *110*, 933–941.

[37] S. Kim, M. Harris, J. A. Varner, *J. Biol. Chem.* **2000**, *275*, 33920–33928.

[38] J. Takagi, K. Strokovich, T. A. Springer, T. Walz, *EMBO J.* **2003**, *22*, 4607-4615.

[39] L. Marinelli, A. Meyer, D. Heckmann, A. Laveccia, E. Novellino, H. Kessler, *J. Med. Chem.* **2005**, *48*, 4204-4207.

[40] A. Hillisch, L. F. Pineda, R. Hilgenfeld, *Drug Discov. Today* **2004**, *9*, 659-569.

[41] M. Nagae, S. Re, E. Mihara, T. Nogi, Y. Sugita, J. Takagi, *J. Cell Biol.* **2012**, *197*, 131-140.

[42] B. Furie, *Hematology* **2009**, 255–258.

[43] M. P. Bonaca, P. G. Steg, L. J. Feldman, J. F. Canales, J. J. Ferguson, L. Wallentin, R. M. Califf, R. A. Harrington, R. P. Giugliano, *J. Am. Coll. Cardiol.* **2009**, *54*, 969-984.

[44] D. Chua, A. Ignaszewski, *BMJ* **2009**, *338*, b1180.

[45] D. Cox, *Curr. Pharm. Des.* **2004**, *10*, 1587-1596.

[46] R. Evans, I. Patzak, L. Svensson, K. De Filippo, K. Jones, A. McDowall, N. Hogg, *J. Cell Sci.* **2009**, *122*, 215-225.

[47] A. Etzioni, *Clin. Rev. Allergy Immunol.* **2010**, *38*, 54-60.

[48] T. A. Yednock, C. Cannon, L. C. Fritz, F. Sanchez-Madrid, L. Steinman, N. Karin, *Nature* **1992**, *356*, 63-66.

[49] a) G. P. A. Rice, H. P. Hartung, P. A. Calabresi, *Neurology* **2005**, *64*, 1336-1342; b) S. R. Targan, B. G. Feagan, R. N. Fedorak, *Gastroenterology* **2007**, *132*, 1672-1683.

[50] E. Havrdova, S. Galetta, M. Hutchinson, D. Stefoski, D. Bates, C. H. Polman, P. W. O'Connor, G. Giovannoni, T. Phillips, F. D. Lublin, A. Pace, R. Kim, R. Hyde, *Lancet Neurol.* **2009**, *8*, 254-260.

[51] C. Warnke, T. Menge, H. P. Hartung, M. K. Racke P. D. Cravens, J. L. Bennett, E. M. Frohman, B. M. Greenberg, S. S. Zamvil, R. Gold, B. Hemmer, B. C. Kieseier, O. Stüve, *Arch. Neurol*, **2010**, *67*, 923-930.

[52] H. -J. Lee , S. -Y. Kim , J. -M. Koh, J. Bok, K. -J, Kim, K. -S. Kim, M. -H. Park, H. -D. Shin, B. L. Park, T. -H. Kim, J. M. Hong, E. K. Park, D. J. Kim, B. Oh, K. Kimm, G. S. Kim, J. -Y. Lee, *Bone* **2007**, *41*, 979-986.

[53] C. L. Tofteng, P. Bach-Mortensen, S. E. Bojesen, A. Tybjaerg-Hansen, L. Hyldstrup, B. G. Nordestgaard, *Pharmacogenet. Genomics* **2007**, *17*, 85-91.

[54] M. G. Murphy, K. Cerchio, S. A. Stoch, K. Gottesdiener, M. Wu, *J. Clin. Endocrinol. Metab*. **2005**, *90*, 2022-2028.

[55] M. D. Pierschbacher, E. Ruoslahti, *Nature* **1984**, *309*, 30-33.

[56] a) S. Swenson, S. Ramu, F.S. Markland, *Curr. Pharm. Des.* **2007**, *13*, 2860-2871; b) J. J. Calvete, C. Marcinkiewicz, D. Monleón, V. Esteve, B. Celda, P. Juárez, L. Sanz, *Toxicon* **2005**, *45*, 1063-1074; c) Y. Fujii, D. Okuda, Z. Fujimoto, Z., *J. Mol. Biol*. **2003**, *332*, 1115-1122; d) R. J. Gould, M. A. Polokoff, P. A. Friedman, T. F. Huang, J. C. Holt, J. J. Cook, S. Niewiarowski, *Proc. Soc. Exp. Biol. Med*. **1990**, *195*, 168-171.

[57] a) D. Simon, H. Xu, S. Ortlepp, C. Rogers, N. Rao, *Arterioscler. Thromb. Vasc. Biol.* **1997**, *17*, 528-535; b) M. Dennis, W. Henzel, R. Pitti, M. Lipari, M. Napier, T. Deisher, et al.. *Proc. Natl. Acad. Sci. U. S. A.* **1990**, *87*, 2471-2475; c) I. Ojima, S. Chakravarty, Q. Dong, *Bioorg. Med. Chem*. **1995**, *3*, 337-360.

[58] a) T. Doi, S. Kamioka, S. Shimazu, T. Takahashi, *Org. Lett.* **2008**, *10*, 817-819; b) M. Ishikawa, M. Tsushima, D. Kubota, Y. Yanagisawa, Y. Hiraiwa, Y. Kojima, K. Ajito, N. Anzai, *Org. Proc. Res. Dev.* **2008**, *12*, 596-602; c) D. Heckmann, A. Meyer, L. Marinelli, G. Zahn, R. Stragies, H. Kessler, *Angew. Chem. Int. Ed.* **2007**, *46*, 3571-3574; d) D. Heckmann, A. Meyer, B. Laufer, G. Zahn, R. Stragies, H. Kessler, *ChemBioChem* **2008**, *9*, 1397-1407; e) S. Urman, K. Gaus, Y. Yang, U. Strijowski, N. Sewald, S. De Pol, O. Reiser, *Angew. Chem. Int. Ed.* **2007**, *46*, 3976-3978; f) Stupp, R., Rüegg, C, *J. Clin. Oncol.* **2007**, *25*, 1637-1638; g) A. Del Gatto, L. Zaccaro, P. Grieco, E. Novellino, A. Zannetti, S. Del Vecchio, F. Iommelli, M. Salvatore, C. Pedone, M. Saviano, *J. Med. Chem.* **2006**, *49*, 3416-3420; h) Neri, D.; Bicknell, R., *Nature Rev.* **2005**, *5*, 436-446; i) P. Vianello, P. Cozzi, A. Galvani, M. Meroni, M. Varasi, D. Volpi, T. Bandiera, *Bioorg. Med. Chem. Lett.* **2004**, *14*, 657-661; j) Schaffner, P.; Dard, M.M., *Cell. Mol. Life Sci.* **2003**, *60*, 119-132; k) E. Lohof, E. Planker, C. Mang, F. Burkhart, M. A. Dechantsreiter, R. Haubner, H.-J. Wester, M. Schwaiger, G. Hölzemann, S. L. Goodman, H. Kessler, *Angew. Chem. Int. Ed.* **2000**, *39*, 2761-2764; l) M. A. Dechantsreiter, E. Planker, B. Mathä, E. Lohof, G. Hölzemann, A. Jonczyk, S. L. Goodman, H. Kessler, *J. Med. Chem.* **1999**, *42*, 3033-3040; m) J. Wermuth, S. L. Goodman, A. Jonczyk, H. Kessler, *J. Am. Chem. Soc.* **1997**, *119*, 1328-1335; Paolillo, M.; n) M. A. Russo, M. Serra, L. Colombo, S. Schinelli, *Mini-Rev. Med. Chem.* **2009**, *9*, 1439-1446; o) Z. Liu, F. Wang, X. Chen, *Drug Dev. Res.* **2008**, *69*, 329-339; p) Merck KGaA News Release, 25/02/2013.

[59] T. A. Springer, J. Zhu, T. Xiao, *J. Cell. Biol.* **2008**, *182*, 791-800.

[60] F. Curnis, A. Sacchi, A. Gasparri, R. Longhi, A. Bachi, C. Doglioni, C. Bordignon, C. Traversari, G.-P. Rizzardi, A. Corti, *Cancer Res.* **2008**, *68*, 7073-7082.

[61] A. Spitaleri, S. Mari, F. Curnis, C. Traversari, R. Longhi, C. Bordignon, A. Corti, G.-P. Rizzardi, G. Musco, *J. Biol. Chem.* **2008**, *283*, 19757-19768.

[62] F. Curnis, A. Cattaneo, R. Longhi, A. Sacchi, A. M. Gasparri, F. Pastorino, P. Di Matteo, C. Traversari, A. Bachi, M. Ponzoni, et al., *J. Biol. Chem.* **2010**, *285*, 9114-9123.

[63] A. Corti, F. Curnis, *J. Cell Sci.* **2011**, *124*, 515-522.

[64] M. Aumailley, M. Gurrath, G. Müller, J. Calvete, R. Timpl, H. Kessler, *FEBS Lett.* **1991**, *291*, 50-54.

[65] L. Auzzas, F. Zanardi, L. Battistini, P. Burreddu, P. Carta, G. Rassu, C. Curti, G. Casiraghi, *Curr. Med. Chem.* **2010**, *17*, 1255-1299.

[66] a) S. Hanessian, L. Auzzas, *Acc. Chem. Res.* **2008**, *41*, 1241-1251; b) A. Trabocchi, D. Scarpi, A. Guarna, *Amino Acids* **2008**, *34*, 1-24; c) S. M. Cowell, Y. S. Lee, J. P. Cain, V. J. Hruby, *Curr. Med. Chem.* **2004**, *11*, 2785-98.

[67] Haubner, R.; Schmitt, W.; Hölzemann, G.; Goodman, S.L.; Jonczyk, A.; Kessler, H. *J. Am. Chem. Soc*. **1996**, *118*, 7881-91.

[68] a) L. Belvisi, A. Bernardi, M. Colombo, L. Manzoni, D. Potenza, C. Scolastico, G. Giannini, M. Marcellini, T. Riccioni, M. Castorina, P. LoGiudice C. Pisano, *Bioorg. Med. Chem.* **2006**, *14*, 169-180; b) L. Manzoni, L. Belvisi, D. Arosio, M. Civera, M. Pilkington-Miksa, D. Potenza, A. Caprini, E. M. V. Araldi, E. Monferrini, M. Mancino, F. Podestà, C. Scolastico, *ChemMedChem* **2009**, *4*, 615 –632.

[69] L. Belvisi, T. Riccioni, M. Marcellini, L. Vesci, I. Chiarucci, D. Efrati, D. Potenza, C. Scolastico, L. Manzoni, K. Lombardo, M. A. Stasi, A. Orlandi, A. Ciucci, B. Nico, D. Ribatti, G. Giannini, M. Presta, P. Carminati, C. Pisano, *Mol. Cancer Ther*. **2005**, *4*, 1670-1680.

[70] D. Arosio, L. Belvisi, L. Colombo, M. Colombo, D. Invernizzi, L. Manzoni, D. Potenza, M. Serra, M. Castorina, C. Pisano, C. Scolastico, *ChemMedChem* **2008**, *3*, 1589-1603.

[71] R. Haubner, W. Schmitt, G. Hölzemann, S. L. Goodman, A. Jonczyk, H. Kessler, *J. Am. Chem. Soc*. **1996**, *118*, 7881-7891.

[72] F. Sladojevich, A. Trabocchi, A. Guarna, *J. Org. Chem.* **2007**, *72*, 4254-4257.

[73] a) R. M. Van Well, L. Marinelli, C. Altona, K. Erkelens, G. Siegal, M. van Raaij, A. L. Llamas-Saiz, H. Kessler, E. Novellino, A. Lavecchia, J. H. van Boom, M. Overhand, *J. Am. Chem. Soc.* **2003**, *125*, 10822-10829; b) R. M. Van Well, H. S. Overkleeft, G. A. van der Marel, D. Bruss, G. Thibault, P. G. de Groot, J. H. van Boom, M. Overhand, *Bioorg.Med. Chem. Lett.* **2003**, *13*, 331-334.

[74] G. Casiraghi, G. Rassu, L. Auzzas, P. Burreddu, E. Gaetani, L. Battistini, F. Zanardi, C. Curti, G. Nicastro, L. Belvisi, I. Motto, M. Castorina, G. Giannini, C. Pisano, *J. Med. Chem.* **2005**, *48*, 7675-7687.

[75] F. Zanardi, P. Burreddu, G. Rassu, L. Auzzas, L. Battistini, C. Curti, A. Sartori, G. Nicastro, G. Menchi, N. Cini, A. Bottoncetti, S. Raspanti, G. Casiraghi, *J. Med. Chem.* **2008**, *51*, 1771-82.

[76] a) M. Weller, D. Reardon, B. Nabors, R. Stupp, *Nat. Med*. **2009**, *15*, 726; b) A. R. Reynolds, K. M. Hodivala-Dilke, *Nat. Med*. **2009**, *15*, 727.

[77] a) S. M. Weis, D. G. Stupack, D. A. Cheresh, *Cancer Cell* **2009**, *15*, 359-361; b) A. R. Reynolds, I. R. Hart, A. R. Watson, J. C. Welti, R. G. Silva, S. D. Robinson, Da Violante, M. Gourlaouen, M. Salih, M. C. Jones, D. T. Jones, G. Saunders, V. Kostourou, F. Perron-Sierra, J. C. Norman, G. C. Tucker, K. M. Hodivala-Dilke, *Nat. Med*. **2009**, *15*, 392-400. For recent examples of other antiangiogenic agents causing tumor progression in preclinical models, see: e) M. Pàez-Ribes, E. Allen, J. Hudock, T. Takeda, H. Okuyama, F. Viñals, M. Inoue, G. Bergers, D. Hanahan, O. Casanovas, *Cancer Cell* **2009**, *15*, 230-231; f) J. M. L. Ebos, C. R. Lee, W. Cruz-Munoz, G. A. Bjarnason, J. G. Christensen, R. S. Kerbel, *Cancer Cell* **2009**, *15*, 232-239.

[78] F. Curnis, R. Longhi, L. Crippa, A. Cattaneo, E. Dondossola, A. Bachi, A. Corti, *J. Biol. Chem.* **2006**, *281*, 36466–36476

[79] A. O. Frank, E. Otto, C. Mas-Moruno, H. B. Schiller, L. Marinelli, S. Cosconati, A. Bochen, D. Vossmeyer, G. Zahn, R. Stragies, et al., *Angew. Chem. Int. Ed.* **2010**, *49*, 9278-9281.

[80] A. S. M. Ressurreicao, A. Bordessa, M. Civera, L. Belvisi, C. Gennari, U. Piarulli, *J. Org. Chem.* **2008**, *73*, 652-660.

[81] M. Marchini (2011). *Peptidomimetics containing new bifunctional 2,5-diketopiperazine scaffolds: synthesis, conformational analysis and use as potent integrin ligands*. Ph.D. Thesis. Università degli Studi di Milano: Italy.

[82] The superscripted number after β specifies the position of the side chain on the corresponding β-amino acid, see: T. Hintermann, D. Seebach, *Synlett* **1997**, 437-438.

[83] M. Marchini, M. Mingozzi, R. Colombo, C. Gennari, M. Durini, U. Piarulli, *Tetrahedron* **2010**, *51*, 4278–4280.

[84] K. L. Webster, A. B. Maude, M. E. O'Donnell, A. P. Mehrotra, D. J. Gani, *Chem. Soc. Perkin Trans. 1* **2001**, 1673-1695.

[85] C. M. Thompson, J. A. Frick, D. L. C. Green, *J. Org. Chem.* **1990**, *55*, 111-116.

[86] This procedure has been reported for the successful synthesis of 2,3-diamino propionic acid starting from serine derivatives. See: a) S. H. Rosenberg, K. P. Spina, K. W. Woods, J. Polakowski, D. L. Martin, Z.Yao, H. H. Stein, J. Cohen, J. L. Barlow, *J. Med. Chem.* **1993**, *36*, 449-459; b) I. F. Pickersgill, H. Rapoport, *J. Org. Chem.* **2000**, *65*, 4048-4057.

[87] X. Ariza, F. Urpí, C. Viladomat, J. Vilarrasa, *Tetrahedron Lett.* **1998**, *39*, 9101-9102.

[88] C. David, L. Bischoff, H. Meudal, A. Mothé, N. De Mota, S. DaNascimento, C. Llorens-Cortes, M.-C. Fournié-Zaluski, B. P. Roques, *J. Med. Chem.* **1999**, *42*, 5197-5211.

[89] R. Colombo (2012). *Synthesis and biological evaluation of potent integrin ligands containing a diketopiperazine scaffold, and of their conjugates with cytotoxic agents*. Ph.D. Thesis. Università degli Studi di Milano: Italy.

[90] A. S. M. Ressurreicao, A. Vidu, M. Civera, L. Belvisi, D. Potenza, L. Manzoni, S. Ongeri, C. Gennari, U. Piarulli, *Chem.-Eur. J.* **2009**, *15*, 12184–12188.

[91] J. M. Humphrey, R. J. Bridges, J. A. Hart, A. R. Chamberlin, *J. Org. Chem.* **1994**, *59*, 2467-2472.

[92] Y. Fu, R. P. Hammer, *Org. Lett.* **2002**, *4*, 237-240.

[93] M. C. Pirrung, S.W. Shuey, *J. Org. Chem.* **1994**, *59*, 3890-3897

[94] S. H. Rosenberg, K. P. Spina, K. W. Woods, J. Polakowski, D. L. Martin, Z.Yao, H. H. Stein, J. Cohen, J. L. Barlow, *J. Med. Chem.* **1993**, *36*, 449-459

[95] V. Bavetsias, A. L. Jackman, R. Kimbell, W. Gibson, F. T. Boyle, G. M. F. Bisset, *J. Med. Chem.* **1996**, *39*, 73-85.

[96] Chu-Pei Xu,a Zhen-Hua Xiao,a Bi-Qin Zhuo,a Yu-Huang Wanga and Pei-Qiang Huang, *Chem. Commun.* **2010**, *46*, 7834–7836

[97] M. De Greef, S. Abeln, K. Belkhasmi, A. Dmling, R. V. A. Orru, L. A. Wessjohann, *Synthesis* **2006**, 3997-4004.

[98] H. Choi, J. V. Aldrich, *Int. J. Pept. Protein Res.* **1993**, *42*, 58-63.

[99] The isolated receptor binding assays in this section were carried out by Dr. Daniela Arosio from the CNR-ISTM, who I sincerely acknowledge for the kind collaboration.

[100] The NMR characterization and computational studies reported in this section were carried out by Dr. Laura Belvisi, Dr. Donatella Potenza, Dr. Monica Civera, Dr. Francesca Vasile, M.Sc. Ileana Guzzetti from the University of Milan, whom I sincerely acknowledge for the kind collaboration.

[101] M. A. Dechantsreiter, E. Planker, B. Mathä, E. Lohof, G. Hölzemann, A. Jonczyk, S. L. Goodman, H. Kessler, *J. Med. Chem.* **1999,** *42*, 3033-3040.

2 | Dual-Action Conjugates

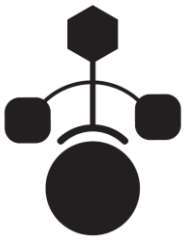

Part of the work described in this Chapter was filed in the following patent:

Nuovi Composti Antitumorali, C. Gennari, L. Belvisi, D. Potenza, R. Colombo, M. Mingozzi, M. Marchini, L. Manzoni, D. Arosio, P. Perego, N. Zaffaroni, M. De Cesare, U, Piarulli.
Italian Patent - Application **31/01/2012**, N. MI2012A000121.
PCT Int. Appl. IB2013/000116, **30/01/2013**.

and was published in the following article:

R. Colombo, M. Mingozzi, L. Belvisi, D. Arosio, U. Piarulli, N. Carenini, P. Perego, N. Zaffaroni, M. De Cesare, V. Castiglioni, E. Scanziani, C. Gennari, *Journal of Medicinal Chemistry* **2012**, *55*, 10460−10474.

2.1 Tumor Targeting Strategy

2.1.1 State of the art

Chemotherapy has been one of the main approaches for the treatment of cancer for more than half a century and is based on the administration of drugs which often interfere with fundamental cellular functions (*e.g.*, DNA replication, cell division). The antitumor efficacy of anticancer drugs is thus limited by their nonspecific toxicity to normal cells, especially to rapidly growing cells such as blood, bone marrow and mucous membrane cells, resulting in a low therapeutic index and serious side-effects. The efficacy of chemotherapy is further limited by the occurrence or development of drug resistance: tumor cells can be regarded as a rapidly changing target because of their genetic instability, heterogeneity, and high rate of mutation, leading to selection and overgrowth of a drug-resistant tumor cell population.[1] In principle, the efficiency of the treatment can be improved by increasing the doses, but this approach commonly results in severe toxicity. Therefore, selective tumor targeting of chemotherapeutic agents represents a major goal, and various drug delivery systems have been recently developed,[2] including the use of liposomes, microspheres, micelles, polymers, protein- or antibody-drug conjugates, and pro-drugs (Figure 2.1.1).[3]
Considerable efforts are currently being made in this domain to such an extent that leaders of major pharmaceutical companies foresee that >60% of all existing drugs will be targeted in less than two decades.[4]

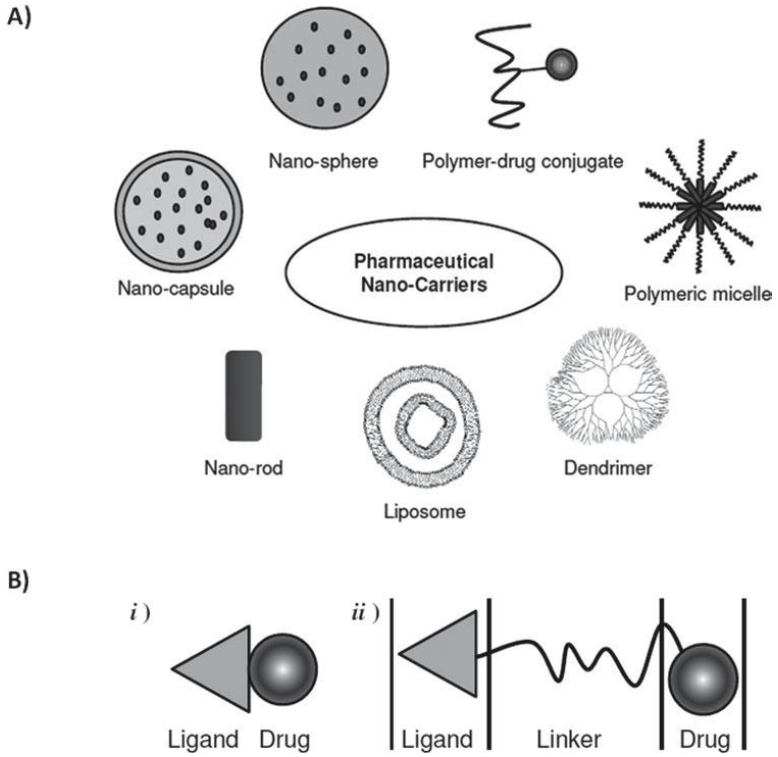

Figure 2.1.1 - Pharmaceutical nano-carriers for drug targeting: A) Structural design of a ligand-targeted drug conjugate; B) *i*) ligand-drug conjugate obtained by a direct linkage between the ligand and the drug or *ii*) connected through a linker.

Integrins are ideal pharmacological targets based on their key role in angiogenesis and tumor development and on their easy accessibility as cell surface receptors interacting with extracellular ligands.[5] They are also involved in tissue integrity and cell trafficking, growth, differentiation, proliferation and migration (see relevant discussion in Chapter 1.1).[6] As a consequence of their role in so many fundamental processes, integrin malfunction is connected to a large variety of diseases such as thrombosis, osteoporosis, inflammation, and cancer.[7] The tripeptide sequence arginine-glycine-aspartate (RGD) has been identified as the common motif used by several endogenous ligands to recognize and bind a group of integrins, including $\alpha_V\beta_3$, $\alpha_V\beta_5$, $\alpha_5\beta_1$, which are crucial in angiogenesis, tumor progression and metastasis, and $\alpha_{IIb}\beta_3$, which is involved in platelet aggregation.[8]

As mentioned in Chapter 1.1.3.1, the potent $\alpha_V\beta_3$ integrin ligand, *cyclo*[Arg-Gly-Asp-D-Phe-*N*(Me)-Val] (Cilengitide) developed by Kessler and co-workers,[9,10] is currently in phase II clinical trials ("CENTRIC") as an angiogenesis inhibitor for patients with *glioblastoma multiforme*.[11]

It is currently emerging that antiangiogenic therapy alone is not sufficient to fight and eradicate tumors: recent pre-clinical findings of a paradoxical pro-angiogenic activity of RGD-mimetic agents (like Cilengitide) at low concentrations have stimulated the debate on the use of antiangiogenetics as single drugs.[12] The presence of complex biological processes inside the cell system (among them, the integrins "cross-talk" with other extracellular receptors, Chapter 2.3.2) seems to suggest that the antiangiogenic therapy based only on integrin ligands will not lead to promising applications. After 25 years of research on integrins as pharmacological targets, only four drugs are currently on the market (cut-off: November 2012) (see Table 2.1.1 and Figure 2.1.2).

Table 2.1.1 - Integrin inhibitors in late-stage (Market, Phase III or Phase II) clinical studies.

Clinical phase	Indication[b]	Target	Drug	Synonyms	Drug class	Status
Approved	MS	a4bx[c]	Natalizumab	Tysabri, Antegren, AN-100226, BG-00002	Hu-mAb	L
	Thrombosis	gpIIbIIIa	Abciximab	ReoPro, Clotinab, CentoRx	Chi-mAb-Fab	L
	Thrombosis	gpIIbIIIa	Tirofiban	L-700462, MK-383, Aggrastat	SM	L
	Thrombosis	gpIIbIIIa	Intrifiban	Eptifibatide, SB-1, Sch-60936, Integrelin	cPep	L
Phase III	IBD, UC, Crohn's	a4bx	AJM-300		oSM	A
	UC, Crohn's	a4b7	Vedolizumab	MLN-02, LDP-02	Chi-mAb	A
	Dry eye, conjunctivitis	aLb2	SAR-1118		SM	A
	Immunosuppression	aLb2	Odulimomab		Chi-mAb	ndr
	Stroke, ischemia	aLb2	Rovelizumab	23F2G, LeukArrest	Chi-mAb	ndr
	Thrombosis	gpIIbIIIa	Alnidofibatide	RPR-109891, Klerval	Pep-der	A
	Thrombosis	gpIIbIIIa	Orbofiban	SC-57099B, CS-511	SM	A
	Diagnostics	gpIIbIIIa	DMP-444 (Tc99m)	RP-444	Diag	ndr
	Thrombosis	gpIIbIIIa	Lefradafiban	BIBU-104	SM	ndr
	Cancer	avb3, avb5	Cilengitide	EMD 121974, EMD 85189, NSC-707544	cPep	A
Phase II	Arthritis	a4b1	MDL-819767	HMR-1031	SM	A
	Crohn's	a4bx	TRK-170		oSM	A
	IBD, MS, RA, asthma, Crohn's	a4bx	firategrast	SB-683699, T-0047	oSM	A
	Arthritis, asthma	a4bx	RO-27-0608	Valategrast, R411	SM	A
	Ulcerative colitis	a4b7, aEb7	Etrolizumab	Pro-145223, RG-7413	hu-Mab	A
	Asthma, rhinitis	a4b1	RBx-7796	RBx-4638, clafrinast	SM	ndr
	HIV infection	aLb2	Cytolin		hu-mAb	A
	IS, psoriasis	aLb2	BMS-587101		oSM	ndr
	Thrombosis	gpIIbIIIa	MK-0852	L-367073	cPep	A
	AP, stroke, thrombosis	gpIIbIIIa	Cromafiban	CT-50352	SM	ndr
	Restenosis, thrombosis	gpIIbIIIa	FK-633	FR-144633	SM	ndr
	Thrombosis	gpIIbIIIa	Elarofiban	RWJ-53308	SM	ndr
	Thrombosis	gpIIbIIIa	SR-121787		SM	ndr
	Cancer, Crohn's	a5b1	ATN-161		Pep	A
	Cancer, AMD	a5b1	Volociximab	M-200, EOS-200-4	mAb	A
	Arthritis, cancer, osteoporosis, psoriasis, restenosis, RA	avb3	Etaracizumab	MED-522, hLM609, Vitaxin-2, Abegrin	mAb	A
	Cancer	avbx	Intetumumab	CNTO-95	mAb	A
	Cancer: diagnostics	avb3, avb5	Fluciclatide (^{18}F)	GE-135, [^{18}F]-AH-111585	Diag	A
	Cancer: diagnostics	avb3	^{99}mTc-Maraciclatide	NC100692	Diag	A
	Kidney TR, PF	avb6	STX-100	3G9	hu-mAb	A
	Cancer	avbx	EMD-525797	DI17E6	hu-mAb	A
	Osteoporosis	avb3	MRL-123		SM	ndr
	AMD, diabetic retinopathy	avbx, a5b1	AGR-1001		cPep	A

[b]Abbreviations: A, trials active; AP, angina pectoris; cPep, cyclic peptide; Chi-mAb-Fab, chimeric monoclonal antibody, Fab' fragment; Diag, diagnostic reagent; HIV, human immunodeficiency virus; Hu-mAb, humanized monoclonal antibody; IS, ischemic stroke; L, launched/drug approved for clinical use; mAb, monoclonal antibody; MS, multiple sclerosi, ndr, no development reported, drug not discontinued, but trials not apparently active; oSM, orally available small molecule; Pep-der, peptide derivative; PF, pulmonary fibrosis; RA, rheumatoid arthritis; SM, small molecule; TR, transplant rejection; UC, ulcerative colitis. [c]βx indicates that all associated β chains are targeted.

Although it initially appeared a promising strategy, successful therapeutic inhibition of integrins has proven to be elusive, despite the discovery of highly potent inhibitors. This is due to a number of reasons, including redundancy among the integrins, the importance of integrins in key physiological systems and antagonists that had less than optimal properties.[13]

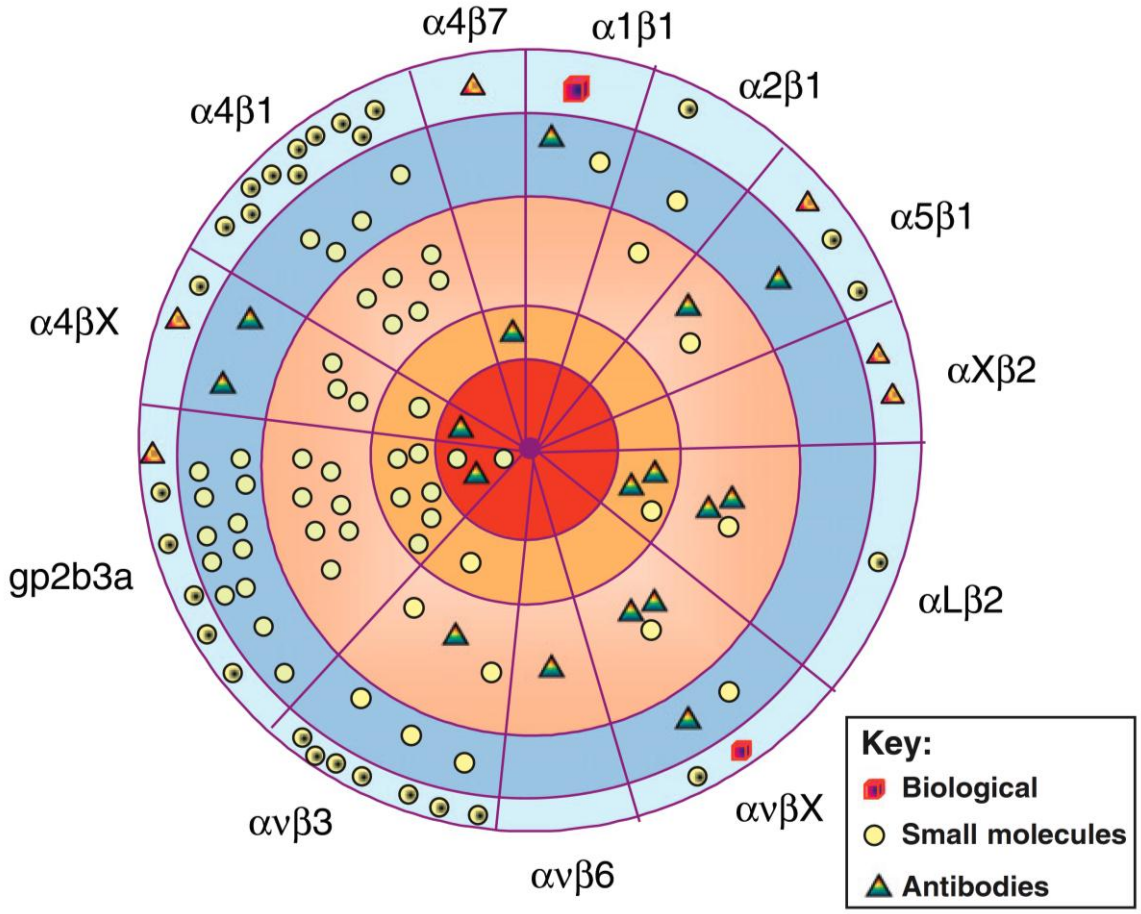

Figure 2.1.2 - The current distribution of integrins as therapeutic targets and the stages of related clinical trials. If targeting affects all α chains ('αx') or all β chains ('βx') the trial is classified accordingly (e.g., intetumumab affects all αv integrins independently of associated β chains – and is classed under αvβx). Trials discontinued (light blue); at Phase I (dark blue); at Phase II (pale orange); at Phase III (mid orange); or approved drugs (red). Symbols: small molecules and peptides (circles yellow); antibodies (triangles); biologicals (cubes). Symbols with black centers represent discontinued trials.

Since α_V integrins, which can be internalized by cells, are involved in tumor angiogenesis and are overexpressed on the surface of cancer cells, integrin ligands can be usefully employed as tumor-homing peptidomimetics for site-directed delivery of cytotoxic drugs.[14] During the past fifteen years, a number of RGD-small molecules drug conjugates have been developed (Table 2.1.2).

Table 2.1.2 - Integrin targeted delivery of therapeutic small molecules.

Therapeutic agent	Targeting motif	Experimental model	Results[a]	
			In Vitro	*In Vivo*
Doxorubicin (Dox)	RGD4C	MDA-MB-435 mammary carcinoma	+	+
Doxorubicin	RGD4C	MH134 murine hepatoma	–	+
Plasmin cleavable prodrug	RGD4C	HUVEC	=	ND
Doxsaliform (doxorubicinformaldehyde)	c[RGDf(N-Me)V]	MDA-MB-435	=	ND
Doxorubicin	RGD-containing tetrameric peptide	H2009 and H1299	+	ND
Paclitaxel	$[c(RGDyK)]_2$	MDA-MB-435	+	ND
Arabinoside C	RGDSK	B16 melanoma	–	=
PTK787 albumin	c(RGDfK)-PEG	HUVEC	+	ND
MMAE (Auristatin E)	c(RGDfK)-PEG	C26 murine colon carcinoma	+	+
MMAF (Auristatin F)	c(RGDfK)-PEG	C26 murine colon carcinoma	+	ND
SB202190 (the p38 MAPkinase Inhibitor)	c(RGDfK)-PEG	HUVEC	+	ND

[a] Efficacy compared to non-targeted chemotherapeutic agent: Improved efficacy (+), comparable efficacy (=), less efficacy (–), and not determined (ND).

In a pioneering work Arap and co-workers used a phage display library to isolate peptides that home specifically to tumor blood vessels.[15a] Recovery of phage from tumors led to identification of RGD-4C as best candidates. To determinate if this RGD-compound could be used to improve the therapeutic index of cancer chemotherapeutics, they coupled the RGD-4C ligand to doxorubicin (a well-known anticancer agent). The RGD-4C-doxorubicin conjugate (see Figure 2.1.3) was used to treat mice bearing tumors derived from human MDA-MB-435 breast carcinoma cells. An enhanced efficacy and reduced toxicity of the drug against the human breast cancer xenografts in nude mice were observed. These results demonstrated the utility of targeted chemotherapy strategies based on selective expression of receptors in tumor vasculature. The same conjugate (RGD-4C-doxorubicin) was evaluated by Lee and Kim in an orthotopic murine hepatoma model. When given intravenously to mice the construct suppressed the growth of hepatoma more effectively than free doxorubicin, confirming the previously reported results on a different tumor model.[15b]

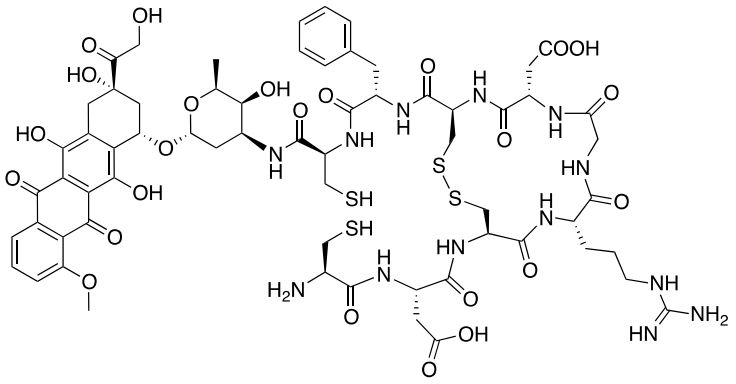

Figure 2.1.3 - RGD-4C-doxorubicin conjugate.

SF1126 (**67**, Figure 2.1.4) is an RGDS-containing prodrug of LY294002, a PI3K/mTOR inhibitor, that targets the cytotoxic portion to stromal end endothelial tumour cells and maximizes its clinical efficacy, after cellular internalization of SF1126 and its hydrolysis to give cytosolic LY294002.[16] The cyclic RGD ligand (Cilengitide)-doxorubicin conjugate **68** (Figure 2.1.4) was reported to be highly cytotoxic against cancer cells overexpressing integrins $\alpha v\beta_3/\alpha v\beta_5$ on their membrane.[17]

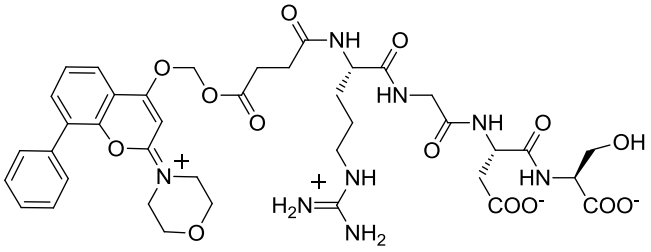

67

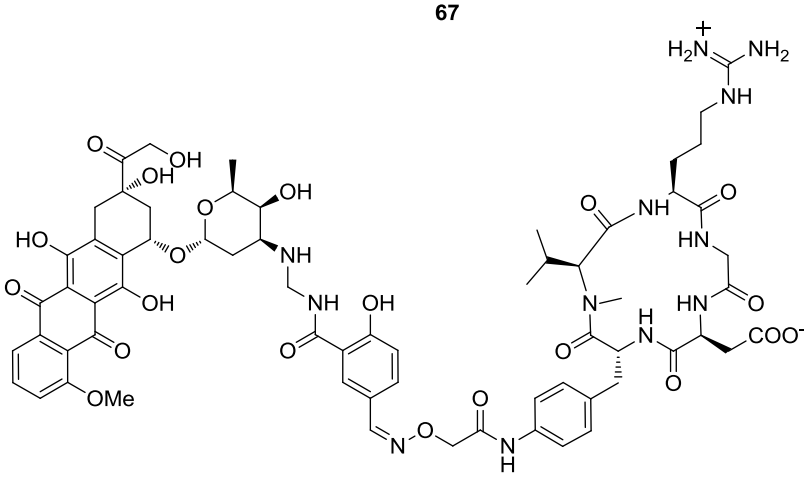

68

Figure 2.1.4 - RGD-based cytotoxic conjugates.

In this field, an attractive avenue for selective tumor targeting are hybrid molecules designed to bind to specific over-expressed receptors on cancer cells, such as integrins.[18] Clearly, the success of this approach is heavily dependent on the rational selection of appropriate biological objectives.

In the next Paragraph (2.1.2), the previous work of our research group in the tumor targeting field is presented; in Paragraph 2.2, a new class of dual-action conjugates (integrin ligand-proapoptotic compound) will be discussed.

2.1.2 Previous work of our research group in the field

Recently, our research group reported a small library of four (**69-72**, Figure 2.1.5) integrin ligand - Paclitaxel conjugates (c[DKP-RGD]-PTX), with the aim of using c[DKP-RGD] peptidomimetics as recognition motif for "tumor homing drug delivery".[19]

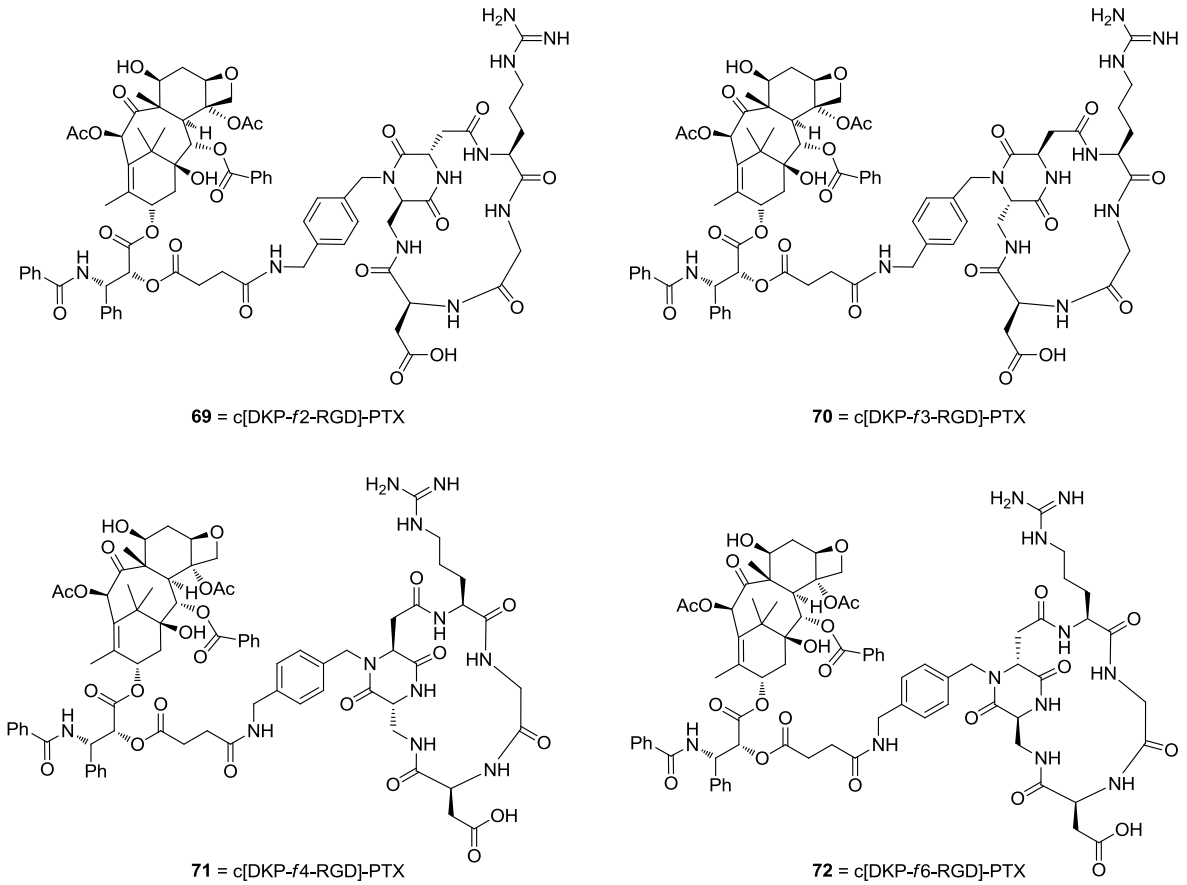

Figure 2.1.4

I contributed directly to the design and synthesis of two functionalized diketopiperazine scaffolds (**DKP-*f*4**, **DKP-*f*6**) and their relative integrin ligands (**c[DKP-*f*4-RGD]**, **c[DKP-*f*6-RGD]**) (see Chapter 1). In order to prepare cyclic RGD-peptidomimetics covalently linked to Paclitaxel, four functionalized (*f*) *trans* diketopiperazines (*i.e.*, **DKP-*f*2**, **DKP-*f*3**, **DKP-*f*4**, **DKP-*f*6**) were synthesized (see Chapter 1.2.1 and 1.3.2), varying the position of the *p*-aminomethylbenzyl *N*-substituent (*N*-1 or *N*-4) and the absolute stereochemistry at C-3 and C-6. These DKPs were used for the synthesis of c[DKP-RGD] integrin ligands (see Chapter 1.2.2 and 1.4.2), which were finally conjugated to 2′-succinyl Paclitaxel (Scheme 2.1.1).

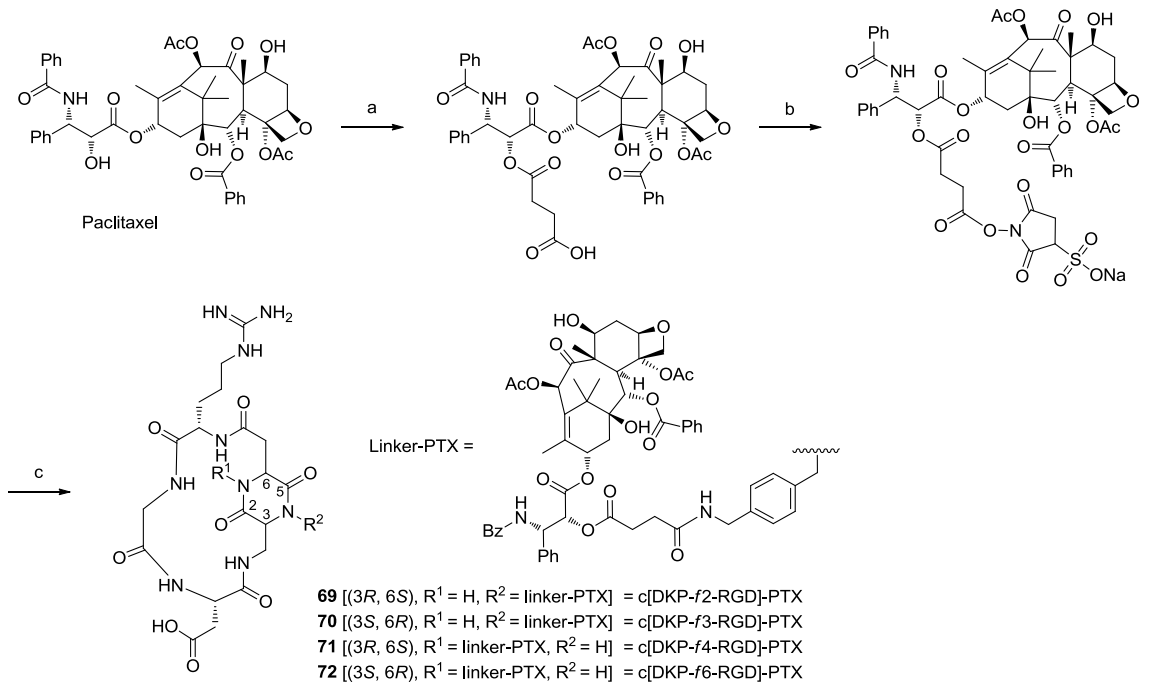

Scheme 2.1.1 - Synthesis of c[DKP-RGD]-PTX conjugates **69-72.** Reagents and conditions: a) succinic anhydride, Py, DCM, overnight, 0 °C to room temp., 94%; b) *N*-hydroxysulfosuccinimide sodium salt, DIC, DMF, overnight, room temp.; c) **c[DKP-*f*2-RGD]**, **c[DKP-*f*3-RGD]**, **c[DKP-*f*4-RGD]** or **c[DKP-*f*6-RGD]**, CH_3CN, aq. phosphate buffer, pH = 7.3, 10 h at 0 °C then 8 h at room temp., 60-70%.

All the Paclitaxel-RGD constructs **69-72** inhibited biotinylated vitronectin binding to the purified $\alpha_v\beta_3$ receptor at low nanomolar concentration (Table 2.1.3), showing that the enormous increase of steric hindrance in the conjugates, due to presence of the linker bearing Paclitaxel and of the succinate tether, did not influence the high affinity for the integrin receptors. Quite surprisingly, the worst inhibition values derive from the "unconjugated" integrin ligand **c[DKP-*f*3-RGD]** (see Chapter 2.2.2.3 for further discussion).

Table 2.1.3 - Inhibition of biotinylated vitronectin binding to $\alpha_v\beta_3$ and $\alpha_v\beta_5$ receptors.

Compound	$\alpha_v\beta_3$ IC_{50} [nM][a]	$\alpha_v\beta_5$ IC_{50} [nM][a]
69	8.5 ± 0.8	518 ± 10
70	5.2 ± 2.3	219 ± 124
71	0.9 ± 0.6	76 ± 32
72	1.1 ± 0.1	22 ± 3
c[DKP-*f*3-RGD][b]	26.4 ± 3.7	> $5 \cdot 10^3$

[a] IC_{50} values were calculated as the concentration of compound required for 50% inhibition of biotinylated vitronectin binding as estimated by GraphPad Prism software; all values are the arithmetic mean ± SD of triplicate determinations. [b] See Chapter 1.2.2.

Conjugates **69-72** showed *in vitro* cytotoxic activity against a panel of human tumor cell lines similar to that of Paclitaxel.[19] Among the cell lines, the cisplatin-resistant IGROV-1/Pt1 cells express high levels of integrin $\alpha_v\beta_3$, and thus they are an attractive target for *in vivo* tests. c[DKP-*f*3-RGD]-PTX **70** (Scheme 2.1.1) displayed sufficient stability in physiological solution and in both human and murine plasma to be a good candidate for *in vivo* testing. In tumor-targeting experiments against the IGROV-1/Pt1 human ovarian carcinoma xenotransplanted in nude mice, compound **70** exhibited better effects than Paclitaxel in terms of tumor volume inhibition, despite the lower (ca. half) molar dosage used. The superior *in vivo* activity of c[DKP-*f*3-RGD]-PTX **70** as compared to Paclitaxel supports the view that integrin ligands are promising tools to improve delivery of cytotoxic drugs.

On the base of these positive results, we designed two new classes of dual-action conjugates. The first class of conjugates (Chapter 2.2) exploits the integrin-mediated site-directed delivery of pro-apoptotic compounds for the consequent intracellular release of SMAC mimetics; the second class (Chapter 2.4) targets simultaneously two different extracellular receptors (integrin $\alpha_v\beta_3$ and VEGFR), both involved in tumor growth and angiogenesis.

2.2 *cyclo*RGD-SMAC Mimetic Dual-Action Conjugates

2.2.1 Apoptosis

Apoptosis is started by stimuli received from within the cell, or from the external environment.[20] Degradation of cellular protein components is carried out by Cysteine ASPartic acid-specific proteASEs (caspases).[21] Initiator caspases start the apoptotic process, and executioner caspases carry out protein degradation in intrinsic/mitochondrial[22] and extrinsic/death receptor-dependent[23] caspase-dependent apoptosis. The family of Inhibitor of Apoptosis Proteins (IAPs)[24] bind, through their baculovirus inhibitor repeat (BIR) domains, the initiator CASP-9 (BIR3) and the executioner CASP-3 and CASP-7 (linker-BIR2): IAP binding blocks caspases in their inactive forms and antagonizes apoptosis.[25] The endogenous SMAC protein[26,27] (Second Mitochondria-derived Activator of Caspases, also called DIABLO) binds to the primary-BIR3 domain of IAPs[28] and prevents linker-BIR2 - CASP-3/-7 interactions, through a weaker BIR2-SMAC interaction (see Figure 2.2.1).[29]
Thus, SMAC is a pro-apoptotic IAP ligand able to restore caspase-dependent apoptosis.

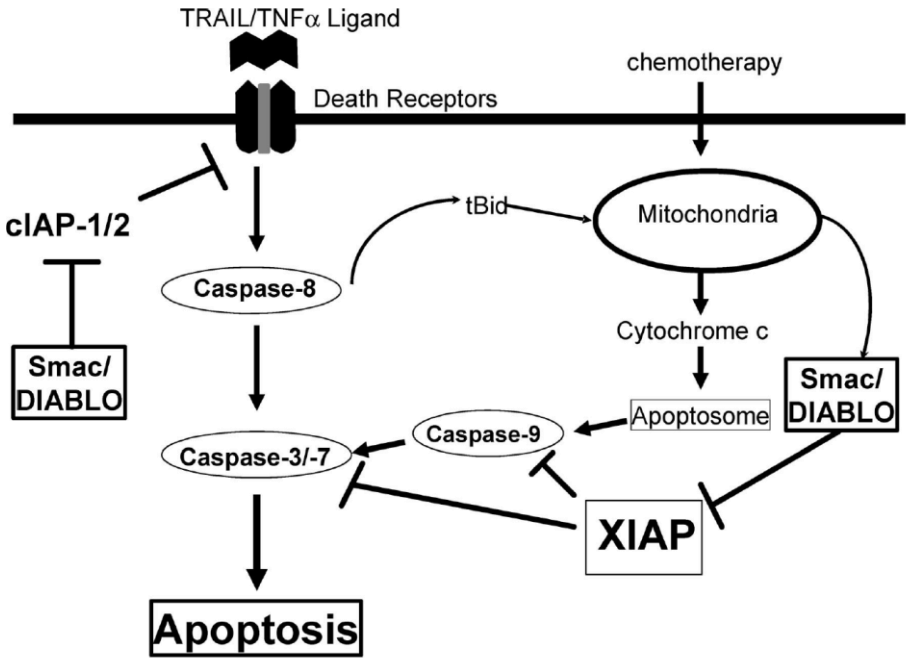

Figure 2.2.1 - The biological cycle that regulates apoptosis.

X-ray[30] and NMR studies[31] showed that the *N*-terminal sequence of SMAC (AVPI peptide sequence, see **72** in Figure 2.2.2) binds to BIR2 and BIR3 domains of XIAP, cIAP1 and cIAP2 (the most relevant IAP proteins) with nanomolar affinity.

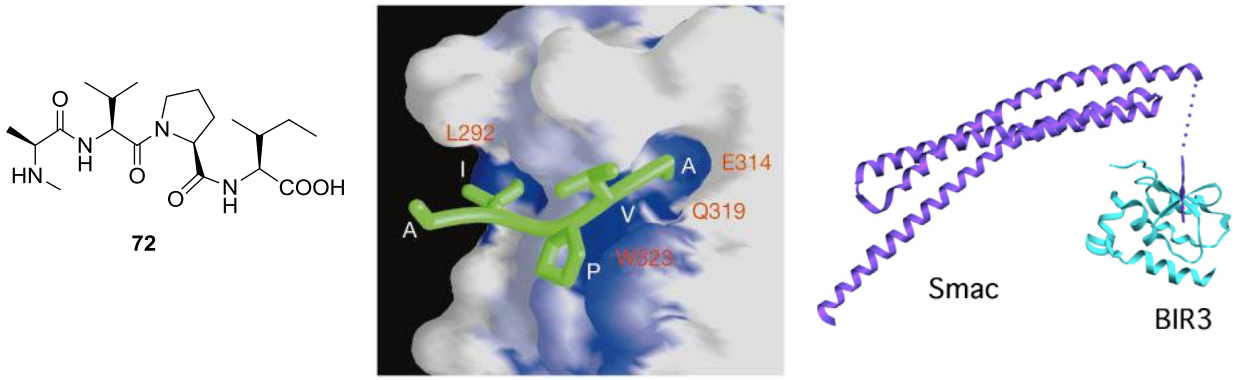

Figure 2.2.2 – AVPI binding epitope on SMAC protein and its interaction with BIR3 domain.

Starting from the natural sequence, chemists developed mimetics of the AVPI sequence, aiming at reproducing the pro-apoptotic effect.
SMAC binds XIAP as a dimer on the same binding sites of caspase 9 (BIR3 domain).[32] Smac interferes also with the XIAP binding site of caspases 3 and 7 (linker-BIR2 domain), promoting both the extrinsic and intrinsic apoptosis paths.[33] The delicate balance of this binding equilibrium is altered in various diseases; for example, several tumor cell lines show overexpression of XIAP and, consequently, a caspase-dependent resistance to enter apoptosis.[34,35] Thus, XIAP inhibition via Smac mimetics' binding is considered a validated mechanism for intervention in cancer therapy.[36]
Pro-apoptotic N-AVPI mimetics such as **73** (Figure 2.2.3) are undergoing preclinical and clinical evaluation as anticancer agents.[37] The research group of Prof. P. Seneci and colleagues introduced monomeric 4-substituted aza-bicyclo[5.3.0]decane derivatives (**74**, **75**, **76**, Figure 2.2.3), endowed with good cell-free potency against IAPs and moderate cytotoxicity.[38,39]

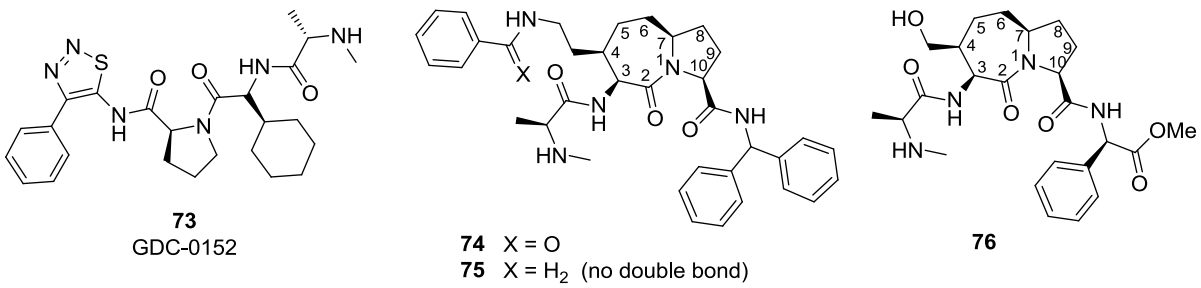

Figure 2.2.3 - Pro-apoptotic SMAC mimetics.

The dimeric SMAC mimetic **77** (Figure 2.2.4) is a potent pro-apoptotic anticancer agent where two identical N-AVPI mimetic units are connected via a suitable linker. [40] As for

the natural SMAC ligand, a first binding event between an N-AVPI mimetic unit and the BIR3 primary binding site on IAPs is followed by the intra-molecular binding of the other unit and the linker-BIR2 binding site.

Starting from monomeric SMAC mimetics **74, 75** and **76** (Figure 2.2.3), the research group of Prof. P. Seneci reported the synthesis[41] and biological evaluation[42] of head-head (**78**, Figure 2.2.4) and tail-tail dimers (**79**, Figure 2.2.4). The linker joining the monomeric units is long and flexible enough to allow binding to both IAP BIR domains. Amines and alcohols in position 4 of **74, 75** and **76** contribute to their IAP/BIR affinity.[43] Such amines and alcohols can be further reacted with bifunctional reagents without loss of IAP/BIR affinity, providing head-head SMAC dimers **78**.[44] The pro-(*S*)-phenyl group in the CONH-$CHPh_2$ amide of **74** and **75** does not participate to BIR binding[45] and can be replaced: functionalization of such group with bifunctional reagents provides access to tail-tail SMAC dimers **79**.[41]

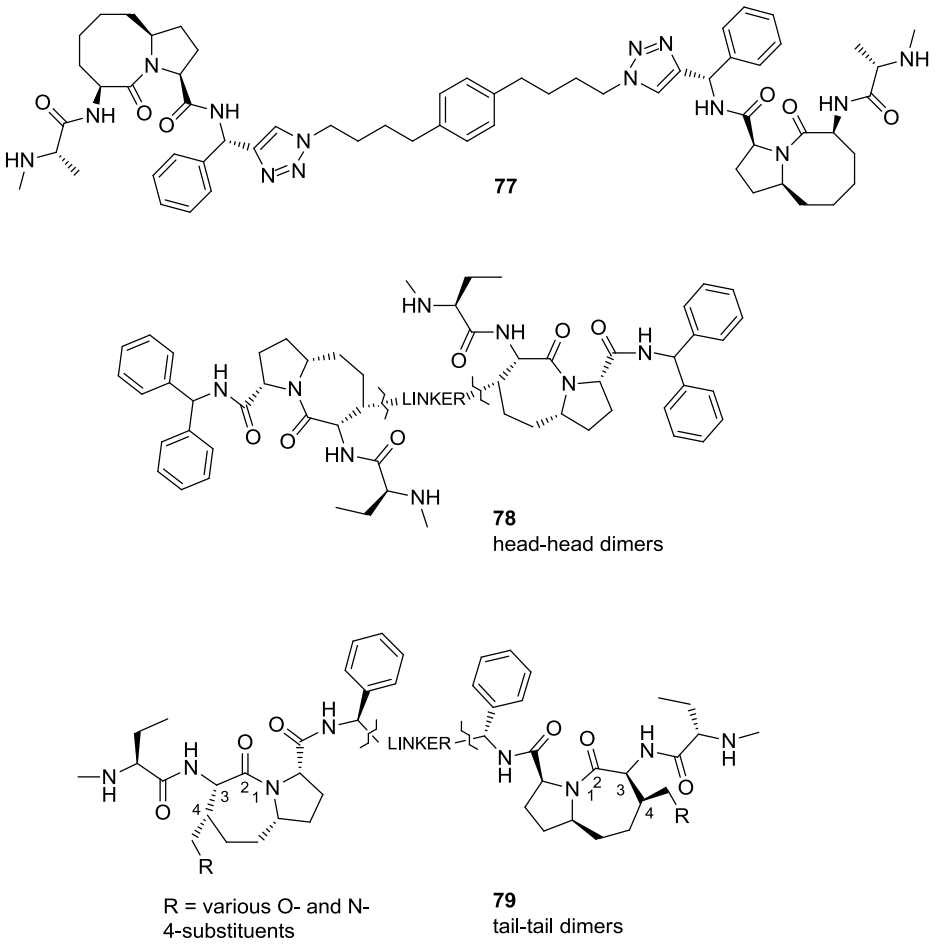

Figure 2.2.4 - Dimeric pro-apoptotic SMAC mimetics.

2.2.2 SMAC-RGD conjugates

Starting a collaboration with the research group of Prof. P. Seneci (Università degli Studi di Milano), we reasoned that, by replacing one of the N-AVPI mimetic units in **78** and **79** with a cyclic RGD ligand, dual action conjugates targeting tumor cell overexpressed receptors (cyclic RGD unit) and apoptosis (SMAC unit) could be created (Figure 2.2.5). We designed the dual-action conjugates aiming at exploring: (i) the influence of head-like (in compounds **c[DKP-RGD]-O/N-SMAC**), and tail-like (in compound **80**) connections as anchoring points on the SMAC mimetic unit, (ii) the influence of the ring size of the cyclic RGD ligand unit (15-membered in compounds **c[DKP-RGD]-O/N-SMAC** and 17-membered in compound **80**), and (iii) the presence of an ester (less stable bond, in **c[DKP-RGD]-O-SMAC**) or of an amide (more stable bond, in **c[DKP-RGD]-N-SMAC**, **80**) in the linker connecting the cyclic RGD and SMAC portions (Figure 2.2.5).

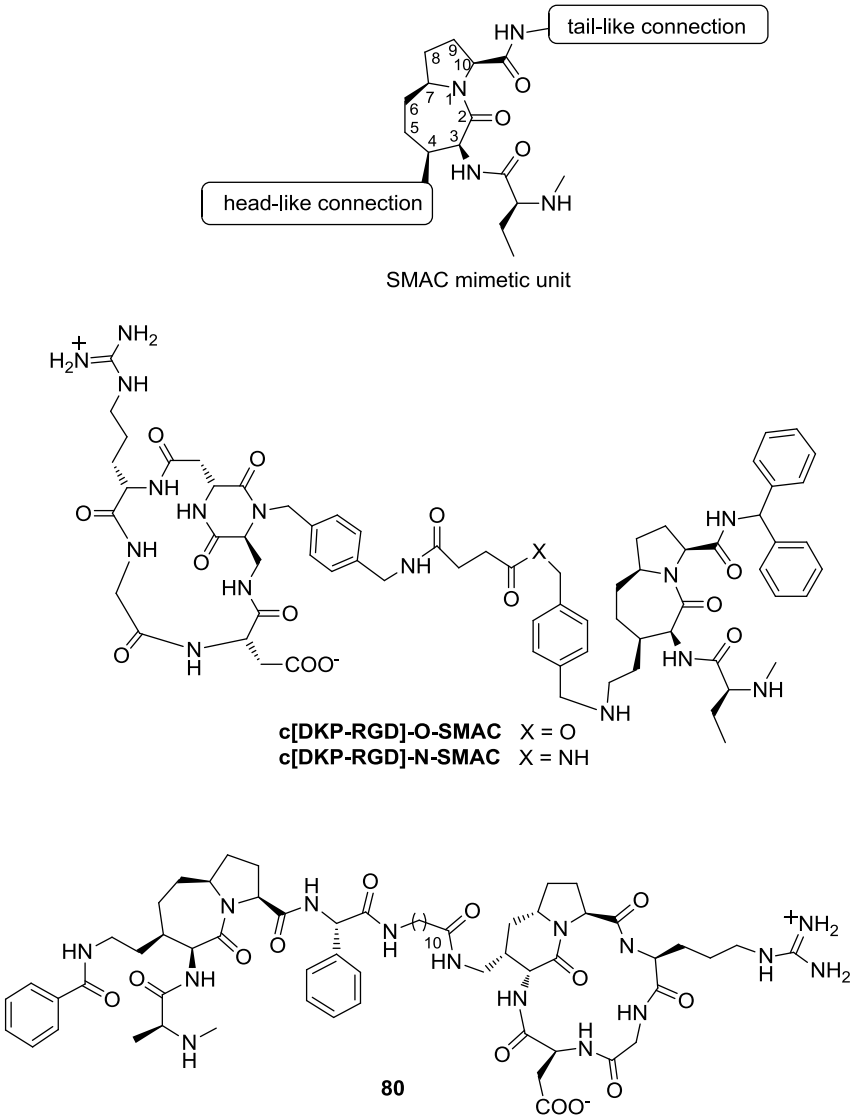

Figure 2.2.5 - Targeted cyclic RGD ligand- SMAC mimetic conjugates: head-like compounds **c[DKP-RGD]-O/N-SMAC** and tail-like compound **80**.

The targeted delivery of SMAC mimetics (cytotoxic agents) relies on the $\alpha_v\beta_3$-mediated internalization of the dual-action RGD/SMAC conjugate. Upon the binding, the complex ligand-drug-receptor is internalized by the cell (receptor-mediated endocytosis); $\alpha_v\beta_3$ integrin is internalized in a caveolin 1-dependent manner and can also enter the cell in clathrin-coated structures. Proteins caveolin and clathrin are able to interact with the integrin tails and trigger the vesicles formation. Payload compound (*i.e.*, the SMAC unit) is then released inside the cell, able to exploit its pro-apoptotic effect through the IAP proteins binding.

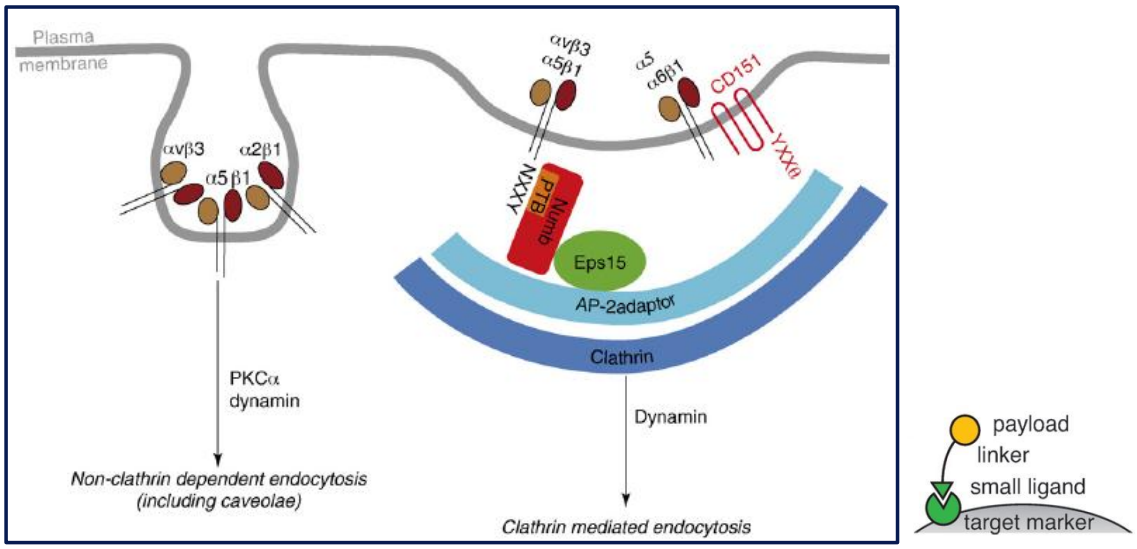

P. T. Caswell, S. Vadrevu, J. C. Norman, *Nat. Rev. Mol. Cell Biol.* **2009**, *10*, 843-853; P. Caswell, J. Norman, *Trends Cell Biol.* **2009**, *18*, 257-263.

During my PhD thesis I synthesized the two dual action conjugates **c[DKP-RGD]-O/N-SMAC**, and we performed biological evaluation on this new class of SMAC-RGD conjugates, including also compound **80** (prepared by the research group of Prof. P. Seneci).

The synthesis of **c[DKP-RGD]-O/N-SMAC** conjugates started with the analysis of a small-molecule SMAC mimetics library recently reported by Prof. Seneci' group (Figure 2.2.6).[39]

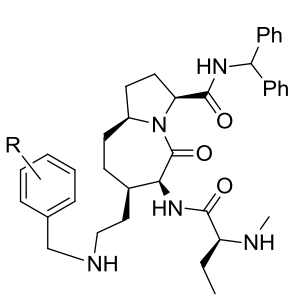

R:

H	p-F
o-Me	3,5-diCl
m-Me	3,5-diF
p-Me	p-CF_3
o-Cl	p-tBu
m-Cl	p-OMe
p-Cl	p-NO_2
o-F	p-COOMe
m-F	p-NH_2

Figure 2.2.6

We modified the synthesis of this class of ligands to introduce an anchor point for further elongation with a linker and conjugation with our functionalized integrin ligand **c[DKP-*f*3-RGD]** (see Chapter 1.2.2) (Scheme 2.2.1). 1,4-Butanedioic acid was used as a relatively short linker, because the distance between the DKP and the SMAC scaffolds (21 atoms, including two phenyl groups) was largely determined by the DKP-nitrogen *p*-aminomethylbenzyl and the SMAC *p*-O/N-methylbenzylaminoethyl substitutions.

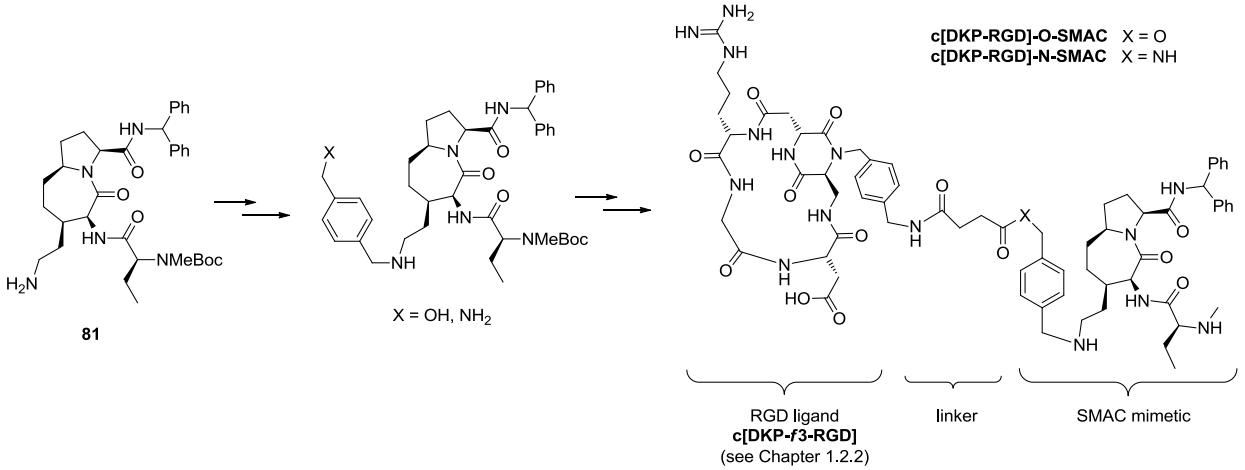

Scheme 2.2.1

The synthesis of intermediate **81** (Scheme 2.2.1) was already reported,[39] and is briefly presented at the beginning of Paragraph 2.2.2.1. We decided to use **c[DKP-*f*3-RGD]** as integrin ligand (among the other functionalized ligands prepared, see Paragraph 1.2.2 and 1.4.2), for the synthesis of SMAC-RGD conjugates, because of its good affinity to integrin receptors (see Paragraph 1.4.3) and because a multi-gram scale synthesis of this ligand was already accomplished in our laboratory.

*2.2.2.1 Synthesis of **c[DKP-RGD]-O/N-SMAC** conjugates*

As already mentioned, the synthesis of intermediate **81** was already reported: we repeated the synthetic pathway shown in Scheme 2.2.2 with an overall yield (from **82** to **81**) of 50% over 9 steps. Starting material **82** was kindly provided by research group of Prof. P. Seneci.

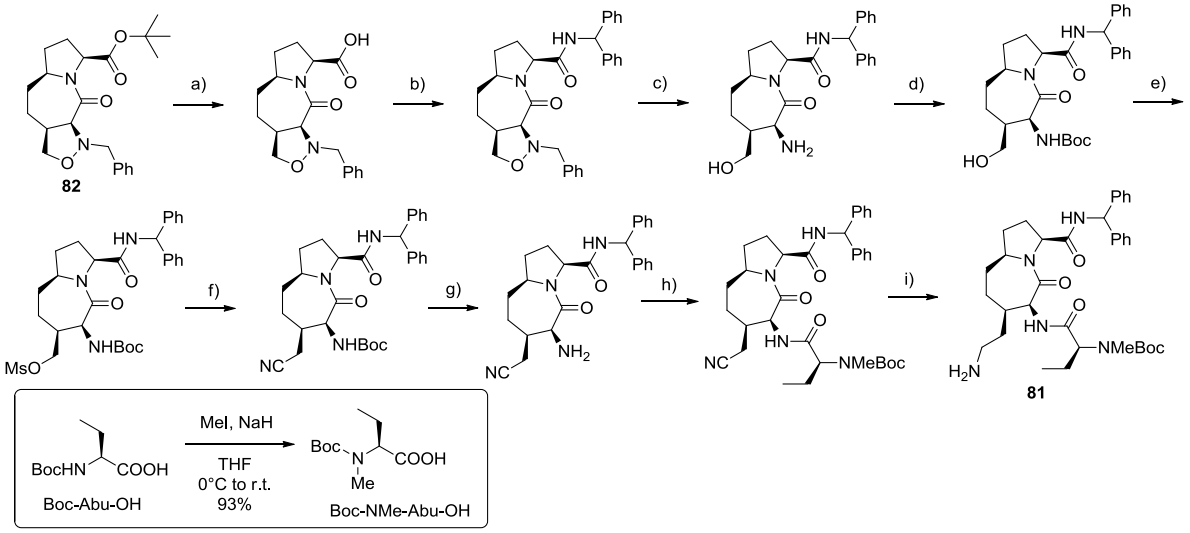

Scheme 2.2.2 - a) TFA, Et_3SiH, DCM, rt; b) $Ph_2CHNH_2 \cdot HCl$, EDC·HCl, HOAt, DIPEA, DCM, N2, rt, 82% over 2 steps; c) H_2 (H-Cube™)10bar, Pd/C, EtOH/H_2O, rt; d) $(Boc)_2O$, DIPEA, DCM, rt, 92% over 2 steps; e) MsCl, DIPEA, DCM, rt; f) *n*-$Bu_4N^+CN^-$, DMF, M.W. (80°C), 86% over 2 steps; g) MsOH, THF, 25°C; h) Boc-NMe-Abu, HATU, HOAt, DIPEA, DMF, 90% over 2 steps; i) H_2 (H-Cube™) 60bar, Ni Raney, citric acid, EtOH, H_2O, 60°C, 55% (86% b.o.r.s.m.).

The only tricky point encountered in this synthesis was the unexpected and selective formation, during the methansulfonic acid-assisted Boc removal of intermediate **83** and in the conditions described in literature, of amidine byproduct **84** (Scheme 2.2.3):

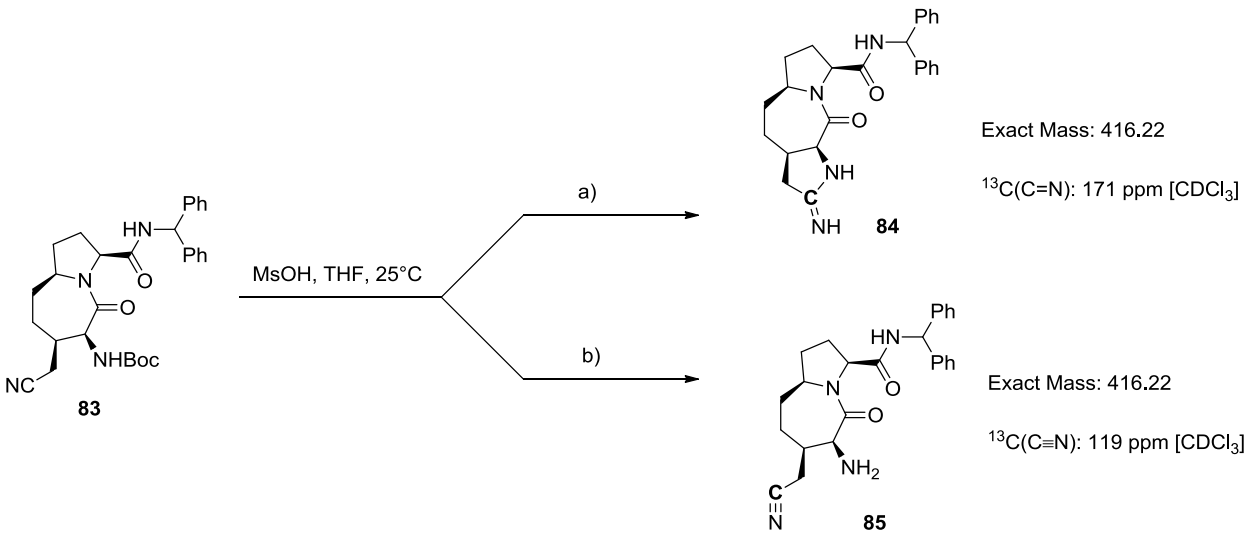

Scheme 2.2.3 - a) workup conditions: residue dissolved in CH_2Cl_2 and washed with 1 M NaOH; b) workup conditions: residue dissolved in AcOEt and washed with $NaHCO_{3\,aq.}$

Only a detailed analysis of ^{13}C NMR spectrum revealed the formation of this byproduct, since ^{1}H NMR spectrum and MS profile are identical both for the undesired amidine **84** and for the expected free amine **85**. The amidine formation seems to be linked to a too basic workup condition (Scheme 2.2.3).

Having in hands amine **81**, we synthesized the two aldehydes necessary for the ester/amide diversification strategy described in Scheme 2.2.1 (Scheme 2.2.4).

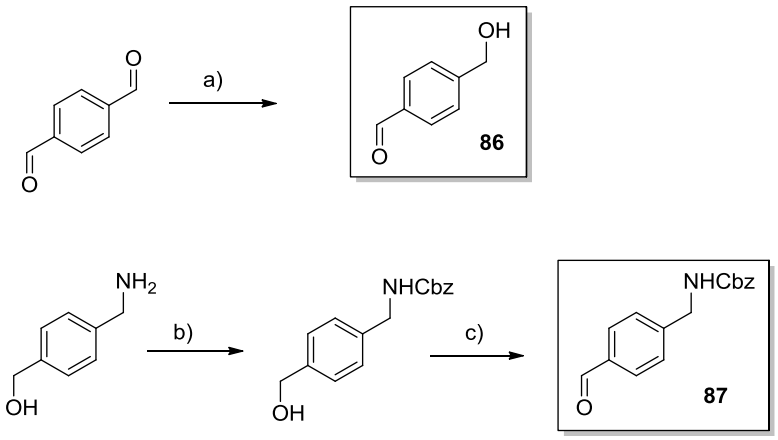

Scheme 2.2.4 - a) $NaBH_4$ (0.25 eq.), THF/EtOH/H_2O (60:38:2), 6h, -5 °C to 0 °C, 76%; b) CbzCl, *i*Pr_2Et*N*, THF, 0 °C, 71%; c) MnO_2, THF, r.t., 97%.

Our synthetic strategy to the ester-connected conjugate **c[DKP-RGD]-O-SMAC** started from amine **81** (Scheme 2.2.2). In a first approach, amine **81** was submitted to a two-steps reductive alkylation (Scheme 2.2.5) with 4-hydroxymethyl benzaldehyde **86**. The only product recovered was the amine-borane adduct **88**, that was stable also to a reported decomplexation procedure.[46]

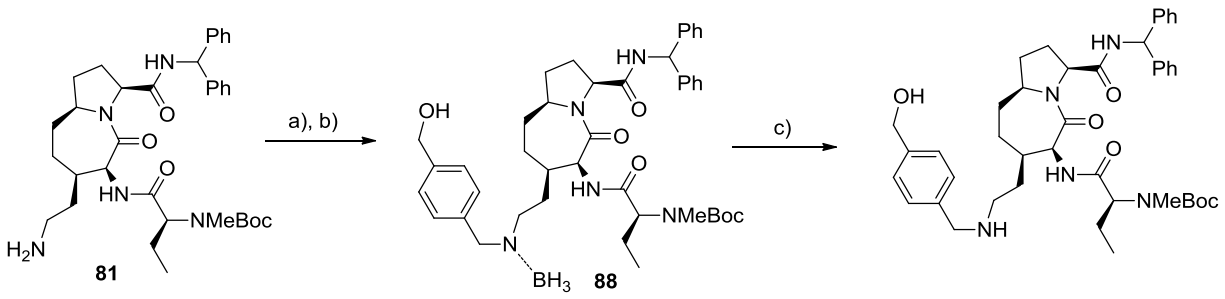

Scheme 2.2.5 - a) **86**, *i*Pr_2Et*N*, THF, r.t., 5h; b) $NaBH_4$, 5h, 43% over 2 steps; c) Raney-Ni, 1-hexene, MeOH, 18h, r.t., 5%.

Repeating the reaction changing the solvent for the imine formation step (MeOH instead of THF) and reducing time and $NaBH_4$ equivalents for the reduction step (2 eq added over 30 min instead of 10 eq left to react in 5h) afforded aminoalcohol **89** in good yield (80%) (Scheme 2.2.6). The resulting aminoalcohol **89** is chemoselectively *N*-Boc protected, and finally *bis*-*N*-Boc protected benzyl alcohol **90** is acylated with succinic

anhydride to yield the key SMAC mimetic-linker construct **91** (Scheme 2.2.6). The overall yield for the reaction steps from **81** to **91** is a rather good 62%. A single direct phase chromatographic column (step b) is needed to purify the reaction products.

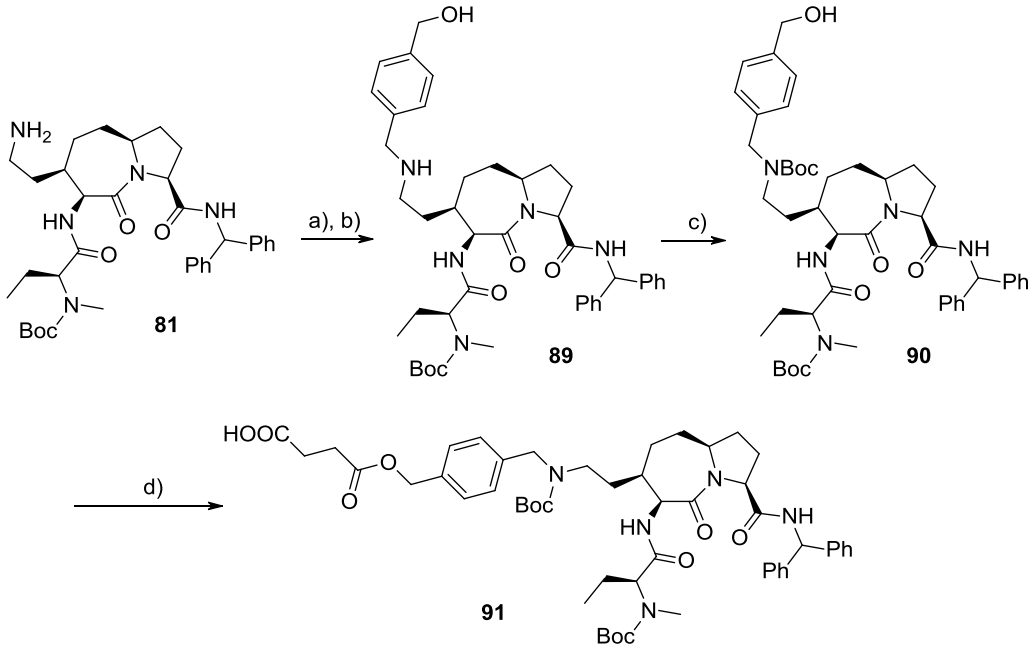

Scheme 2.2.6 – a) **86,** *i*Pr$_2$Et*N*, MeOH, r.t., 5h; b) $NaBH_4$, r.t., 30min, 80% over two steps; c) Boc_2O, *i*Pr$_2$Et*N*, CH_2Cl_2, 0°C to r.t., 24h, 87%; d) succinic anhydride, *i*Pr$_2$Et*N*, DMAP, CH_2Cl_2, 0°C to r.t., 2h, 90%.

Construct **91** is then coupled to the previously described **c[DKP-*f*3-RGD]** (see Chapter 1.2.2), to give the *bis*-*N*-Boc protected, ester-connected dual compound **92** (Scheme 2.2.7). The multi-functional nature of both coupling partners and the presence of potentially reactive functions (e.g., the guanidine and carboxylate functions in **c[DKP-*f*3-RGD]**) requires the initial activation of the carboxylic group of **91** (step a), followed by its coupling with the amino group of **c[DKP-*f*3-RGD]** (step b) under carefully controlled conditions. Namely, coupling at pH 7.5 largely prevents side reactions involving the unprotected functionalities in **c[DKP-*f*3-RGD]**, and yields an acceptable 40% overall yield. Finally, acidic hydrolysis of the *N*-Boc groups leads to quantitative deprotection and isolation of target **c[DKP-RGD]-O-SMAC** dual action conjugate (Scheme 2.2.7).

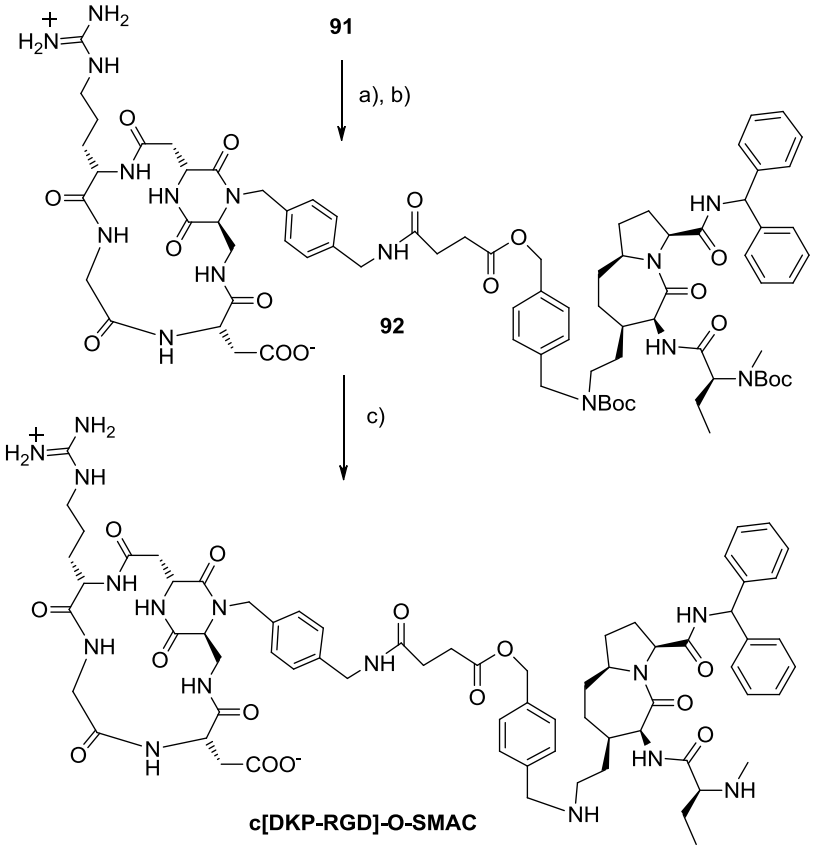

Scheme 2.2.7 - a) *N*-hydroxysulfosuccinimide, DIC, DMF, r.t., 18h; b) **c[DKP-*f*3-RGD]**, CH_3CN, phosphate buffer, pH 7.5, 0°C, 18h, 40% over 2 steps; c) TFA, CH_2Cl_2, r.t., 50min, 99%.

HPLC purification is needed to obtain *N*-protected **92** and target **c[DKP-RGD]-O-SMAC** as pure compounds. HPLC purification of step b (Scheme 2.2.7) allowed to recover both the unreacted SMAC and RGD counterpart (yield was up to 75% based on recovery of starting material) (Figure 2.2.7).

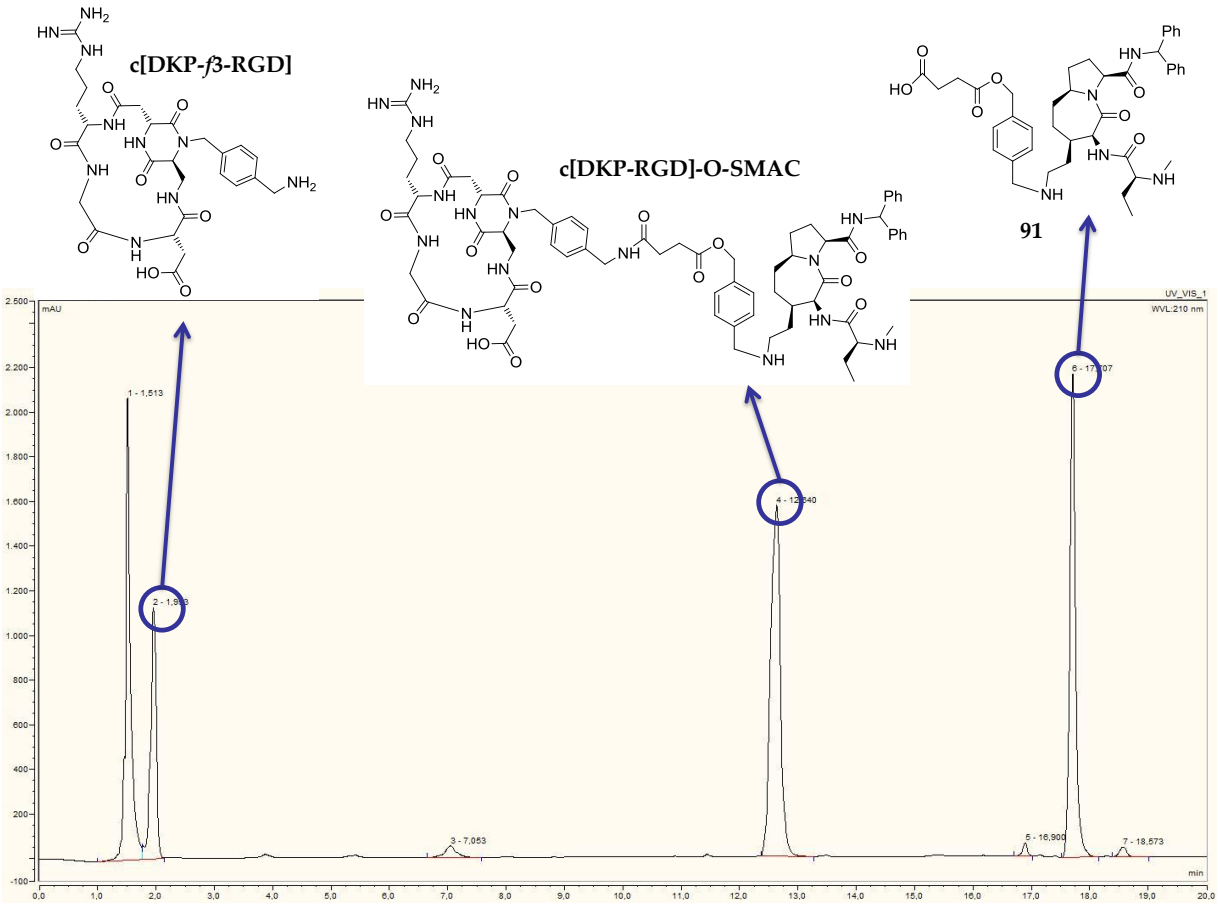

Figure 2.2.7 – HPLC trace of step b purification (See Scheme 2.2.7).

Synthesis of amide-connected conjugate **c[DKP-RGD]-N-SMAC** only differs for the aldehyde employed (**87**, Scheme 2.2.4) and for deprotection step d (Scheme 2.2.8). The overall yield for the reaction steps from **81** to **96** is an excellent 82% and amide-connected dual action conjugate **c[DKP-RGD]-N-SMAC** was obtained, in the last 3 conjugation steps, in a good 49% overall yield. However, the yield reaches 87% if the recovery of starting material for step g is taken into account (Scheme 2.2.8).

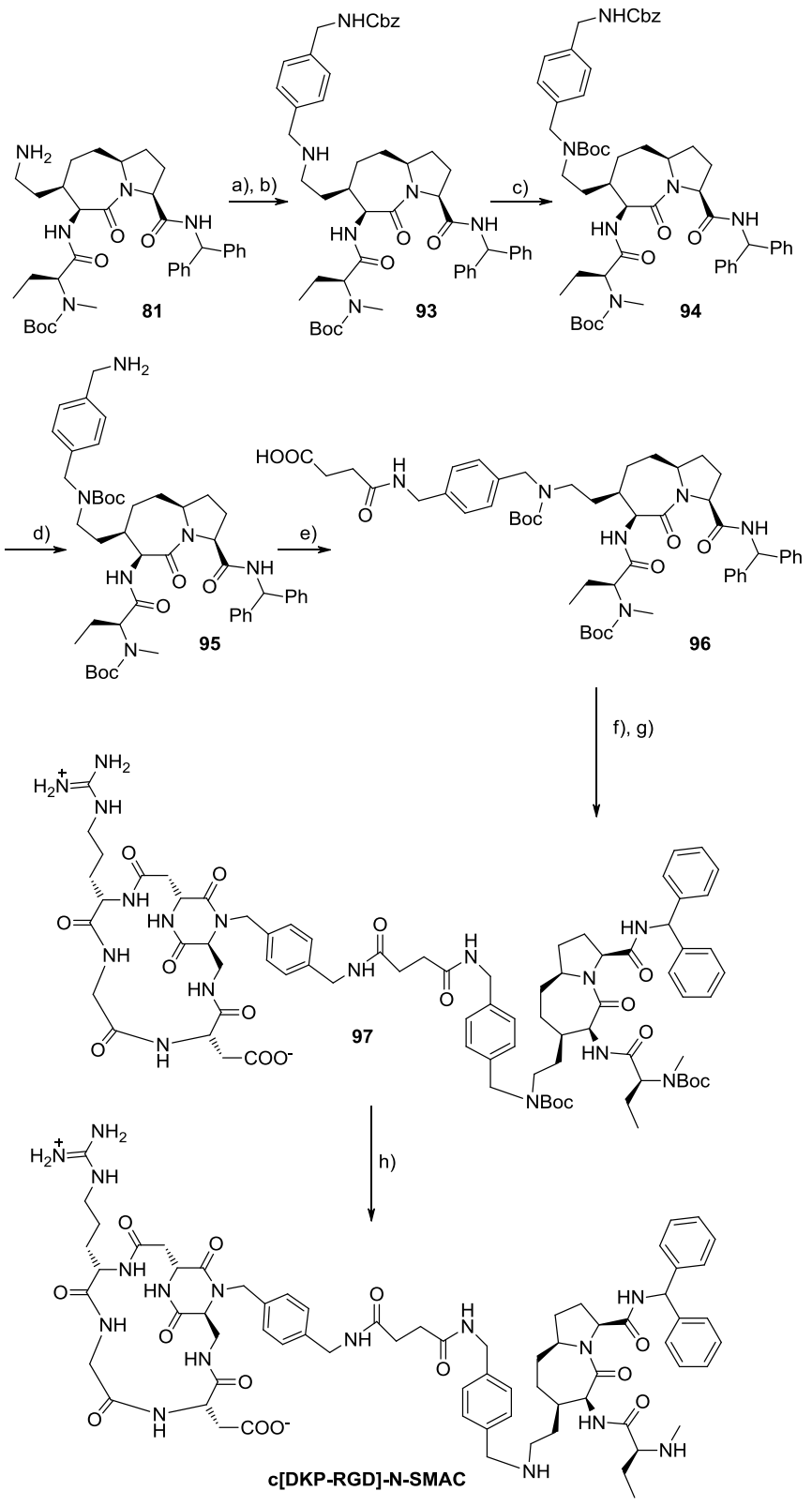

Scheme 2.2.8 - a) **87,** *i*Pr$_2$Et*N*, MeOH, r.t., 5h; b) NaBH$_4$, r.t., 30min, 83% over two steps; c) Boc$_2$O, *i*Pr$_2$Et*N*, CH$_2$Cl$_2$, 0°C to r.t., 24h, 100%; d) H$_2$, Pd/C 10%, THF/H$_2$O, r.t., 18h, 100%; e) succinic anhydride, *i*Pr$_2$Et*N*, DMAP, CH$_2$Cl$_2$, 0°C to r.t., 2h, 99%; f) *N*-hydroxysulfosuccinimide, DIC, DMF, r.t., 18h; g) **c[DKP-*f*3-RGD]**, CH$_3$CN, phosphate buffer, pH 7.5, 0°C, 18h, 49% over 2 steps; h) TFA, CH$_2$Cl$_2$, r.t., 50min, 100%.

2.2.2.2 Cell-free assays – BIR domains/IAPs [47]

Three BIR domain-based IAP portions were used to test the affinity of the cyclic RGD ligand-SMAC mimetics **c[DKP-RGD]-O-SMAC, c[DKP-RGD]-N-SMAC** and **80** (Figure 2.2.5). The primary BIR3 binding site/domain from XIAP and cIAP2 was selected to observe the affinity for two of the most therapeutically relevant IAPs.[48] The bi-functional linker-BIR2-BIR3 portion from IAP was selected to determine any SMAC dimer-like behaviour of the cyclic RGD ligand-SMAC mimetics **c[DKP-RGD]-O/N-SMAC** and **80**.[49] The standard monomeric SMAC mimetics **74, 75, 76** (Figure 2.2.3), were tested for comparison. Their IC_{50} values are reported in Table 2.2.1.

Table 2.2.1 - IC_{50} of selected compounds on BIR portions from IAPs.

Compound	BIR3, XIAP IC_{50} [nM]	l-BIR2-BIR3, XIAP IC_{50} [nM]	BIR3, cIAP2 IC_{50} [nM]
c[DKP-RGD]-O-SMAC	52.0 ± 4.5	50.5 ± 7.8	1.33 ± 0.3
c[DKP-RGD]-N-SMAC	25.5 ± 1.7	57.5 ± 5.8	0.73 ± 0.1
80 [a]	680.0 ± 77.3	504.3 ± 251.4	7.97 ± 2.8
74 [b]	120 ± 18.6	55 ± 13.1	n.t.[c]
75 [b]	110 ± 26.4	27 ± 12.4	n.t.[c]
76 [b]	760 ± 99.2	190 ± 49.1	n.t.[c]

[a] see Figure 2.2.5
[b] see Figure 2.2.3
[c] n.t.: not tested

These results clearly show that for the head-like connected cyclic RGD ligand-SMAC mimetics **c[DKP-RGD]-O/N-SMAC,** the attachment of a linker and a cyclic RGD ligand onto the SMAC mimetic unit is not affecting its affinity for IAPs. Indeed these conjugates show lower IC_{50} values than reference compounds. On the contrary, tail-like connected cyclic RGD ligand-SMAC mimetics **80** is less potent than reference compounds. In this case, we can explain this loss in affinity with the presence of a less favourable phenylglycinamide moiety – XIAP portion interaction, similar to the C-terminus phenylglycinamide ester reference compound **76**. Moreover, the higher affinity of dual action conjugates **c[DKP-RGD]-O/N-SMAC** and **80** for cIAP proteins is also common for monomeric SMAC mimetics.[39]

2.2.2.3 Cell-free assays – $\alpha_v\beta_3/\alpha_v\beta_5$ integrins [50]

The cyclic RGD ligand-SMAC mimetics **c[DKP-RGD]-O/N-SMAC** and **80** were tested *in vitro* for their ability to inhibit biotinylated vitronectin binding to the purified $\alpha_v\beta_3$ and $\alpha_v\beta_5$ receptors. The standard monomeric, integrin ligands **c[DKP-3-RGD], c[DKP-*f*3-RGD]** and **98** (Figure 2.2.8), were tested for comparison. Their IC_{50} values are reported in Table 2.2.2.

Table 2.2.2 - Inhibition of biotinylated vitronectin binding to $\alpha_v\beta_3$ and $\alpha_v\beta_5$ receptors by selected compounds.

Compound	$\alpha_v\beta_3$ IC_{50} [nM]	$\alpha_v\beta_5$ IC_{50} [nM]
c[DKP-RGD]-O-SMAC	70.1 ± 0.1	900 ± 380
c[DKP-RGD]-N-SMAC	36.5 ± 0.6	1500 ± 700
80 [a]	105.2 ± 3.4	649 ± 25
98 [b]	20.2 ± 1.9	205 ± 34
c[DKP-3-RGD] [b]	4.5 ± 1.1	149 ± 25
c[DKP-*f*3-RGD] [b]	26.4 ± 3.7	$> 5 \cdot 10^3$

[a] see Figure 2.2.5
[b] see Figure 2.2.8

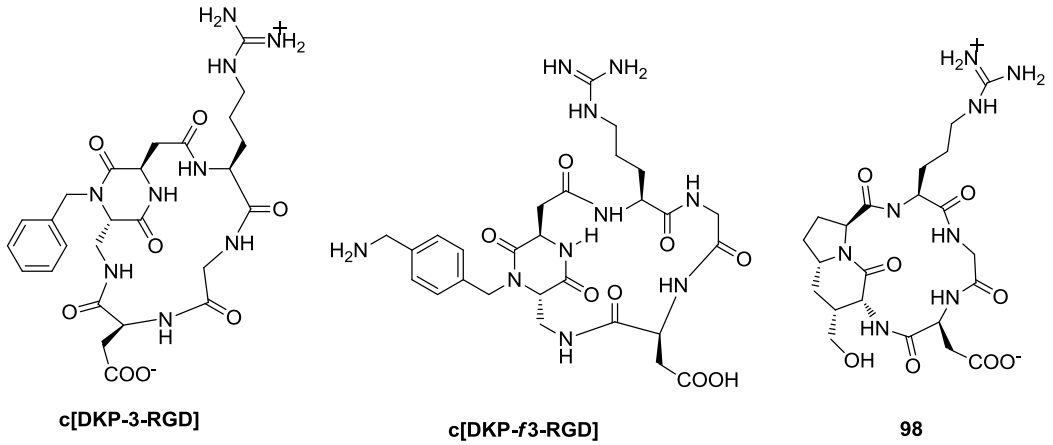

Figure 2.2.8

Although the three cyclic RGD ligand-SMAC mimetics **c[DKP-RGD]-O/N-SMAC** and **80** show nanomolar affinity for both $\alpha_v\beta_3$ (stronger interaction) and $\alpha_v\beta_5$ integrin (weaker interaction), their potency is reduced compared to the reference compounds **c[DKP-3-RGD]** and **98**. A possible explanation for this is that the free amine moiety (NMe-Abu) present in compounds **c[DKP-RGD]-O/N-SMAC** and **80** interferes with the

integrin recognition mechanism (the electrostatic clamp of the carboxylate and guanidinium groups). The free amines of the SMAC mimetic moieties could compete with the arginine guanidinium group of the RGD counterpart (see Chapter 1.1.1). This explanation is supported also by the reduced binding affinity of unconjugated ligand **c[DKP-*f*3-RGD]** (containing a free amine, see Table 2.2.2 and Figure 2.2.8) and other examples of reduced affinity of RGD ligand containing a free amine.[51] To assess if this hypothesis could be true, we tested in this kind of assay compound **97**, an available intermediate of the synthesis described in Scheme 2.2.8. Compound **97**, having both the free amine protected as Boc, should improve its binding affinity, if the hypothesis described before is correct. As shown in Figure 2.2.9, IC_{50} values for intermediate **97** turned out to be higher than reference compound **c[DKP-RGD]-N-SMAC**. Thus we could conclude that the presence of charged amines, in this specific case, is not relevant for the higher IC_{50} values measured.

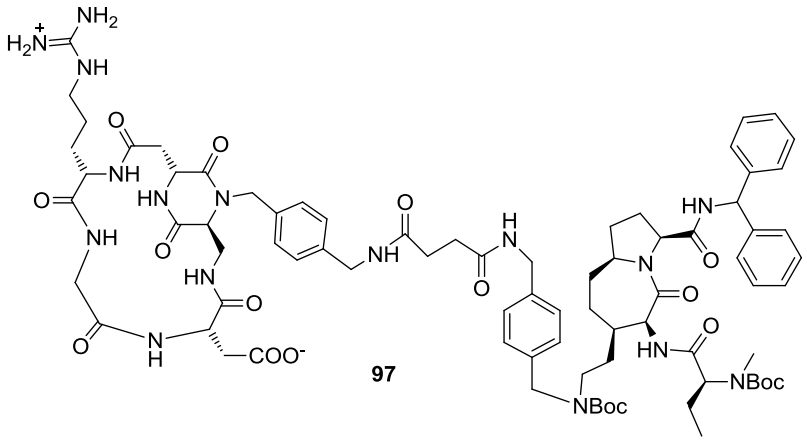

97

Compound	$\alpha_v\beta_3$ IC_{50} [nM]	$\alpha_v\beta_5$ IC_{50} [nM]
97	82.6 ± 5.7	2100 ± 600
c[DKP-RGD]-N-SMAC	36.5 ± 0.6	1500 ± 700

Figure 2.2.9

Although the affinity of the **c[DKP-RGD]-O/N-SMAC** dual-action conjugates for the $\alpha_v\beta_3$ integrin receptor is reduced with respect to the RGD ligands alone taken as reference compounds, their residual binding strength is surely sufficient to target them towards integrin-expressing tumor cells. Thus, we decided to examine the cytotoxic activity of the three cyclic RGD ligand-SMAC mimetics **c[DKP-RGD]-O/N-SMAC** and **80**.

2.2.2.4 Cytotoxicity – Tumor cells [47]

The cyclic RGD ligand-SMAC mimetics **c[DKP-RGD]-O/N-SMAC** and **80** were tested in cellular assays for their ability to kill tumor cells, either expressing integrin receptors on their surface or relying on IAP proteins to impair the physiological apoptotic process. We selected ovarian IGROV-1 carcinoma cells as representatives for the former, and breast cancer MDA-MB-231 cells for the latter group. The standard monomeric, integrin ligands **c[DKP-3-RGD]** and **98** (Figure 2.2.8) and IAP inhibitors **74, 75, 76** (Figure 2.2.3), were tested for comparison. Their IC_{50} values are reported in Table 2.2.3.

Table 2.2.3 - Cytotoxicity of selected compounds.

Compound	MDA-MB-231 IC_{50} [μM]	IGROV-1 IC_{50} [μM]
c[DKP-RGD]-O-SMAC	9.7 ± 1.6	> 25
c[DKP-RGD]-N-SMAC	> 25	> 25
80	20.5 ± 2.2	11.5 ± 2.5
98	n.t. [a]	> 25
c[DKP-3-RGD]	n.t. [a]	> 25
74	13.5 ± 1.6	> 25
75	8.1 ± 0.9	> 25
76	> 25	> 25

[a] n.t.: not tested

The results show that cyclic RGD ligand-SMAC mimetics **c[DKP-RGD]-O/N-SMAC** and **80** are endowed with moderate cytotoxic activity. Namely, cytotoxicity for ester-connected **c[DKP-RGD]-O-SMAC** and reference SMAC mimetic **74, 75** may be due to ester hydrolysis and SMAC mimetic unit release, since they are similarly potent against MDA-MB-231 cells. The loss of cytotoxicity for amide-connected **c[DKP-RGD]-N-SMAC** may be due to the non-internalization of this dual-action conjugate and consequent missed SMAC mimetic unit release. Amide connected **80** shows moderate cytotoxicity both on MDA-MB-231 and, interestingly, also on IGROV-1 cells, although no hydrolysis and SMAC unit release can easily take place. As expected, reference cyclic RGD ligands **c[DKP-3-RGD]** and **98** *per se* do not show any cytotoxicity against integrin-rich IGROV-1 cells,[19,52] and the same is true for reference SMAC mimetics **74, 75, 76**.[53] Surprisingly, amide-connected cyclic RGD ligand-SMAC mimetic **80** shows cytotoxicity on IGROV-1 cells, possibly suggesting an advantage for tail connected dual-action conjugates in terms of cellular activity: the cytotoxic activity of the dual-

action conjugate **80** on integrin-rich IGROV-1 cells indicates a possible tumor targeting effect.

In conclusion, considering the obtained results for these three dual-action SMAC/RGD conjugates, influences of linker composition, of steric hindrance and of overall physico-chemical and electronic properties (e.g., substituents on the SMAC mimetic unit, especially the RGD-unit anchoring point) seem to be of primary importance for the development of potent SMAC-RGD dual-action conjugates.

2.3 INTEGRINS AND VEGFRS

2.3.1 The VEGF-VEGFR system biology

2.3.1.1 Vascular endothelial growth factors and their receptors

Vascular endothelial growth factors (VEGFs) are crucial regulators of vascular development during embryogenesis (vasculogenesis) as well as blood-vessel formation (angiogenesis) in the adult. In mammals, five VEGF ligands, which occur in several different splice variants and processed forms, have been identified so far. These ligands bind in an overlapping pattern to three receptor tyrosine kinases (RTKs), known as VEGF receptor-1, -2 and -3 (VEGFR1–3), as well as to co-receptors (defined as VEGF-binding molecules that lack established VEGF-induced catalytic function), such as heparan sulphate proteoglycans (HSPGs) and neuropilins.[54] In certain respects, VEGFs share regulatory mechanisms with other well-characterized RTKs, such as the platelet-derived growth-factor receptors (PDGFRs) and the epidermal growth-factor receptors (EGFRs). These mechanisms include receptor dimerization and activation of the tyrosine kinase, as well as creation of docking sites for signal transducers. Moreover, the VEGFRs induce cellular processes that are common to many growth-factor receptors, including cell migration, survival and proliferation.

However, the VEGFRs also seem to be unique, for example, in their ability to transduce signals that form the three-dimensional vascular tube, and in regulating vascular permeability that leads to oedema and swelling of tissues. VEGFR1 is a positive regulator of monocyte and macrophage migration, and has been described as a positive and negative regulator of VEGFR2 signalling capacity. Negative regulation is exerted, at least in part, by an alternatively spliced soluble VEGFR1 variant that binds to VEGF and thereby prevents VEGF from binding to VEGFR2. VEGFR2 is implicated in all aspects of normal and pathological vascular-endothelial-cell biology, whereas VEGFR3 is important for lymphaticendothelial- cell development and function. Recently, tumor therapies that are based on neutralizing anti-VEGF antibodies and small-molecular-weight tyrosine-kinase inhibitors that target the VEGFRs have been developed (see Paragraph 2.3.1.2 for further discussion).

The members of VEGF family are dimeric glycoproteins of approximately 40 kDa. In mammals, the VEGF family consists of five members, VEGFA, B, C, D and placenta growth factor (PLGF). In addition, proteins that are structurally related to the VEGFs exist in parapoxvirus (VEGFE) and snake venom (a group of proteins known as VEGFFs).[55] VEGFA, B and PLGF bind to VEGFR1, VEGFA and E bind to VEGFR2, and

VEGFC and D bind to VEGFR3. Proteolytic processing of the human VEGFC and D allows for binding to VEGFR2, however, these factors bind to VEGF2 with lower affinity than to VEGFR3 (see FIG. 1a for mammalian ligand–receptor interactions). The VEGFFs interact with both VEGFR1 and 2 (Figure 2.3.1).[56]

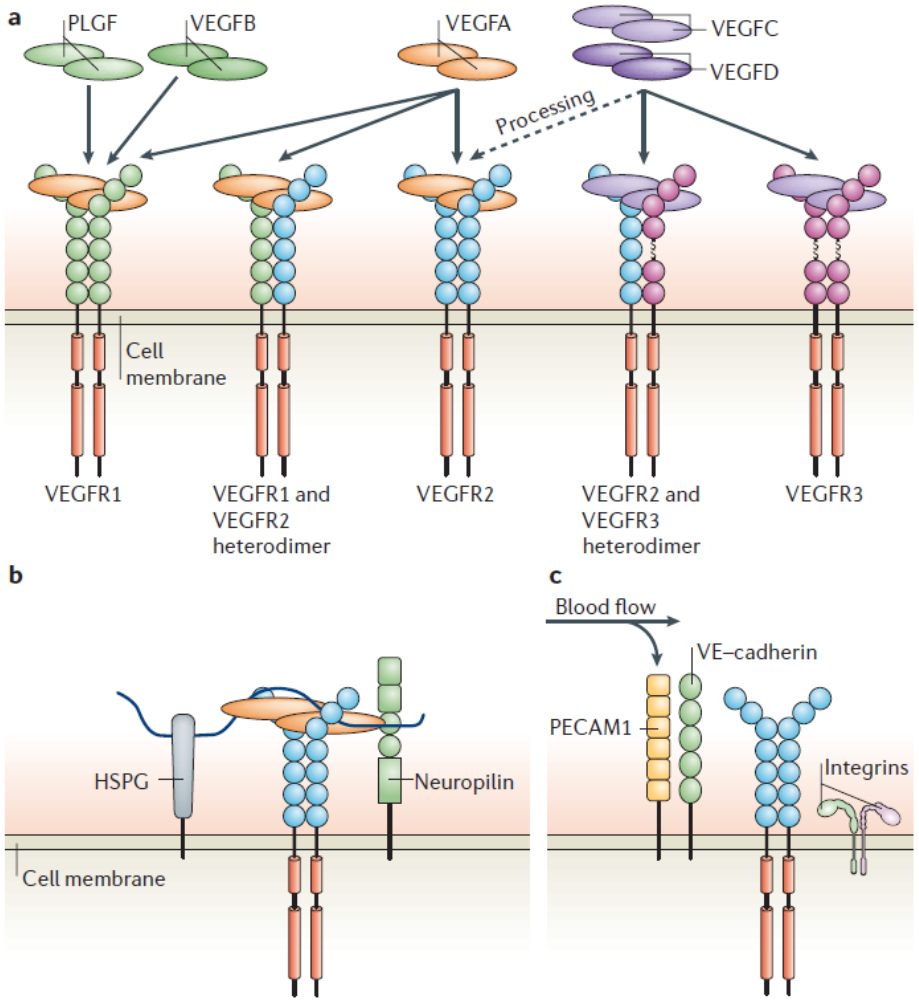

Figure 2.3.1 - VEGF receptor-binding properties and signalling complexes: a) Mammalian VEGFs bind to the three VEGFR tyrosine kinases, leading to the formation of VEGFR homodimers and heterodimers. Proteolytic processing of VEGF-C and D allows for binding to VEGFR-2. b) VEGFR signalling is modulated by different co-receptors. VEGFs as well as VEGFRs bind to co-receptors such as heparan sulphate proteoglycans (HSPGs) and neuropilins. These interactions can influence VEGFR-mediated responses, for example, affecting the half-life of the receptor complex. c) Mechanosensory complex formation. Blood flow might activate VEGFRs in a ligand-independent manner, by the formation of mechanosensory complexes that consist of platelet-endothelial-cell adhesion molecule-1 (PECAM1), vascular endothelial (VE)–cadherin, VEGFRs and integrins. PlGF, placenta growth factor.

Structurally, the VEGFs are related to the PDGF family of growth factors, with intrachain and interchain disulfide bonds between eight cysteine residues in conserved positions. The crystal structure of VEGFA revealed two monomers that are organized in

an anti-parallel fashion to form a dimer, with the receptor-binding sites located at each pole of the dimer.[57] The VEGFs preferentially form homodimers, although VEGFA and PLGF heterodimers have been identified. Alternative splicing of several of the VEGF family members gives rise to isoforms with different biological activities. The human isoforms are denoted $VEGFA_{121}$, $VEGFA_{145}$, $VEGFA_{165}$, $VEGFA_{189}$ and $VEGFA_{206}$. The mouse isoforms are one amino-acid residue shorter than the corresponding human isoform, and they are denoted $VEGFA_{120}$ and so forth. The activities of the VEGFA isoforms are dictated by their different abilities to interact with VEGFR co-receptors, such as neuropilins and HSPGs. The bioactivity of VEGF family members is also regulated by proteolytic processing. This mechanism might enable specific interactions with different types of receptor. For example, in humans, processed VEGFC and D bind to VEGFR2, as well as to VEGFR3.

The VEGFRs are members of the RTK superfamily and they belong to the same subclass as receptors for PDGFs and fibroblast growth factors (FGFs). The VEGFRs are equipped with an approximately 750-amino-acid-residue extracellular domain, which is organized into seven immunoglobulin (Ig)-like folds. Structural and functional studies have yielded insights into how the distinct domains contribute to VEGFR activity. The crystal structure of part of the extracellular domain of VEGFR1, alone and in complex with ligand, shows that the Ig domain-2 constitutes the ligand-binding site on the receptor.[58] In addition, biochemical analyses showed that the Ig domain-3 in VEGFR2 is important for the determination of ligand-binding specificity.[59] Alternative splicing or proteolytic processing of VEGFRs give rise to secreted variants of VEGFR1 and VEGFR2, and in humans, to a C-terminal truncated VEGFR3.[60]

2.3.1.2 Anti-angiogenic therapy via suppression of the VEGF/VEGFR system

Tumor angiogenesis is an attractive target for the treatment of cancer: solid tumors often become hypoxic due to a rapid growth of tumor cells. The VEGFRs, particularly VEGFR-2, are also up-regulated to some extent under hypoxia.

A VEGF-neutralizing antibody (Bevacizumab, Avastin™ by Genentech Inc., San Francisco, CA) was developed for the treatment of solid tumours, including colorectal, lung (non-epithelial, NSCLC) and breast cancers as well as glioblastomas. In the USA, the FDA approved Bevacizumab in 2008 for the treatment of breast cancer because of a statistically significant efficacy in improving overall survival; however, it was withdrawn in late 2011 due to a lack of clear efficacy data in recent large-scale phase III studies. On the other hand, other countries such as EU and Japan approved Bevacizumab for breast cancer treatment based on a statistically significant improvement in progression-free survival . Other anti-VEGF-VEGFR drugs, such as

VEGF-Trap (a VEGFR-1-VEGFR-2 fusion protein) and VEGFR-neutralizing antibodies, have been developed and are now under clinical trials.[61]

Papo and co-workers created a dual-specific therapeutic protein (scVEGF "fusion-protein", Figure 2.3.2 left) that does not rely on associating domains or physical linkage, but rather is based on a naturally occurring ligand (VEGF) into which an additional high affinity receptor binding epitope (RGD) has been introduced without disrupting the original function.[62] Authors showed that dual-specific scVEGF variants can simultaneously bind to both VEGFR and $\alpha_v\beta_3$ integrin, leading to antagonism of immediate signalling events (VEGFR-2 phosphorylation) and downstream processes (proliferation), particularly in the presence of vitronectin. A specific scVEGF variant exhibited increased binding to HUVECs and was a more potent inhibitor of biological activity compared to its mono-specific counterparts, highlighting the effects of the dual functionality engineered into this protein: remarkably, the dual-specific mutant scVEGF (variant 7I), but not the mono-specific variants scVEGFmut or scVEGF m27I (Figure 2.3.2, left), exhibited nearly complete inhibition of VEGF-mediated murine blood vessel formation within implanted Matrigel plugs. (Figure 2.3.2, right).

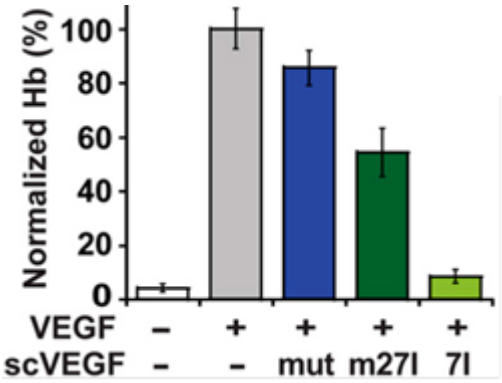

Hemoglobin (Hb) content within Matrigel plugs was quantified and depicted as the percent of Hb compared to VEGF165 / heparin (gray bar).

Figure 2.3.2 – Dual-specific "fusion protein" scVEGF (left) and its anti-angiogenic activity *in vivo* (right)

This inhibition could be due to biological effects mediated by blocking both VEGFR2 and $\alpha_v\beta_3$ integrin, or through blocking receptor cross-talk (see Paragraph 2.3.2). These results provide a basis for further clinical development of dual-specific VEGFR-2/$\alpha_v\beta_3$ integrin antagonists (see Paragraph 2.4).

VEGF function can also be inhibited by small molecules that block or prevent activation of VEGF-A receptor tyrosine kinases (receptor intracellular segments) and consequently interfere with the VEGF signal transduction pathway.[63] Sunitinib (**98,** Figure 2.3.2, Sutent™ by Sugen-Pfizer), is a multikinase indol-2-one inhibitor targeting VEGFR-1 and

VEGFR-2, PDGFRβ, and other kinases, including FLT3, which has been shown to be involved, especially in mutated forms, in acute leukemia.[64] Sunitinib was approved in 2006 by the FDA for the treatment of RCC and of GIST.[65] Sorafenib (**99,** Figure 2.3.2, Nexavar™ by Bayer and Onyx Pharmaceuticals), is a biarylurea multitargeted kinase inhibitor. It inhibits VEGFR-2 ,VEGFR-3 and PDGFRβ. Sorafenib was approved by U.S. FDA in 2005 for the treatment of advanced renal cell carcinoma (RCC) and in 2007 for the treatment of hepatocellular carcinoma (HCC).[66]

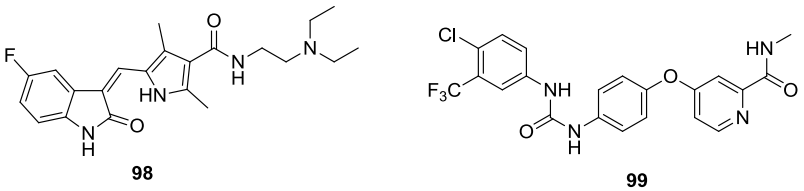

Figure 2.3.3

Another class of small molecules that can effectively block the VEGF receptors is represented by peptides or peptidic derivatives that bind to the VEGFR extracellular segment. Among the successful ligands, the VEGFR2-binding peptoids **100** and **101**,[67] the helical peptides **102, 103** derived from VEGF and Vammin hotspots,[68] the 17-amino acid cyclopeptide **104**[69] and α/β-peptide **105** by Gellman[70] can be mentioned (Figure 2.3.2).

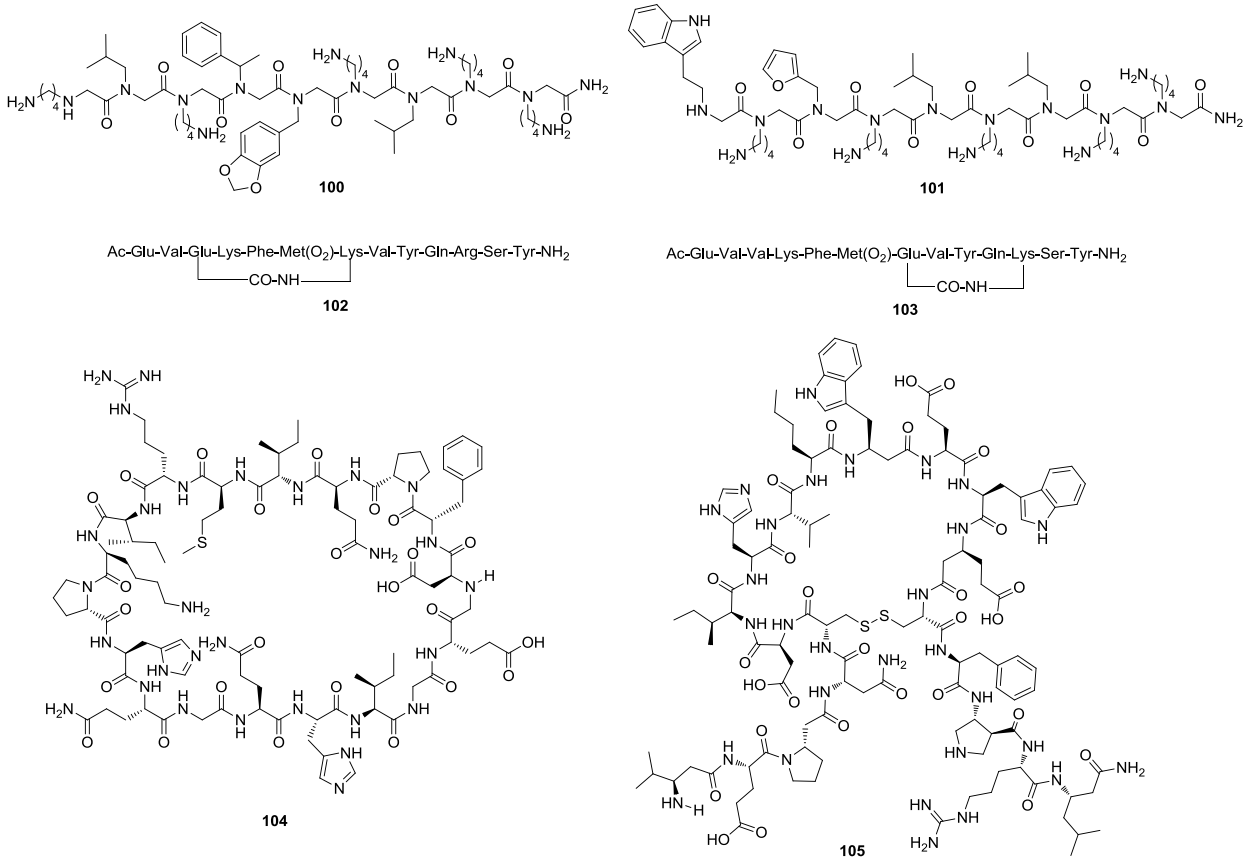

Figure 2.3.4

In 2005 D'Andrea and co-workers published synthesis, structural characterization and biological evaluations of **QK** (**106**), a 15-mer peptide reproducing the VEGF 17–25 helix region (Figure 2.3.3). The α-helix conformation of peptide **106** was stabilized introducing N- and C-capping sequences (amino acids with intrinsic helix propensity and favorable electrostatic interactions). The results demonstrated that **106** binds to VEGF receptors *in vitro* and showed that, quite surprisingly, it promotes capillary formation and organization in in vitro assais on matrigel, thus revealing to be a potent agonist for angiogenesis.[71]

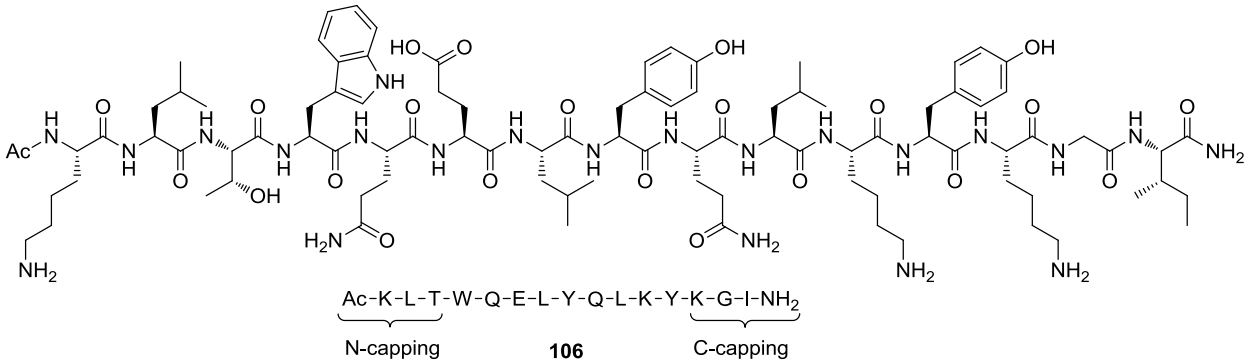

Figure 2.3.5

Moving from the **QK** sequence, D'Andrea and co-workers designed a novel peptide, called **MA** (Figure 2.3.3).[72] Authors showed that **MA** assumes in water a well-defined α-helical conformation, binds to VEGF receptors, and inhibits the VEGF biological activity on ECs. Furthermore, *in vivo* experiments showed that **MA** inhibits VEGF-induced capillary formation and tumor growth.

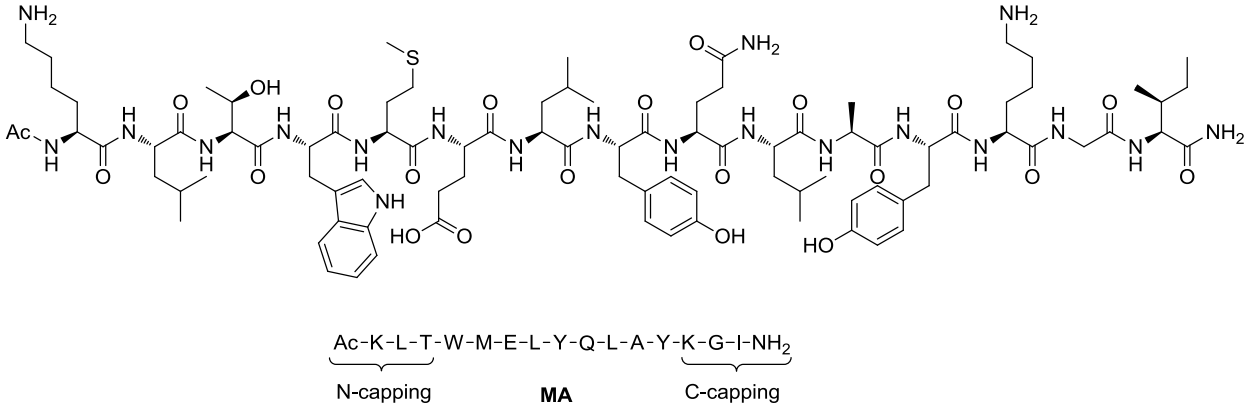

Figure 2.3.6

The peptides **106** and **MA** differ only for two amino acids: Met5 and Ala11 residues in **MA** and Gln5 and Lys11 residues in **106**. It is noteworthy that a two amino acid change in a 15-mer VEGFR binder peptide induces so different biological responses. A

structural approach was adopted to verify if the two different amino acids induce a diverse peptide conformation. Superposition of **MA** and **106** representative structures (Figure 2.3.4) indicates that the two peptides fold very similarly but nonetheless exhibit structural differences at the N-terminus. This small difference affects the conformation and probably the orientation of the Trp4 side chain that together with Met5, Tyr8, Gln9, and Tyr12 is likely involved in the interaction with VEGF receptor. It is possible that this different peptide arrangement could effectively affect the receptor molecular recognition or receptor activation, but this hypothesis needs further computational and/or experimental proof. Furthermore, it is possible to speculate that a different conformational arrangement of the bound receptor, ending up in an opposite receptor activation state, could be induced by a direct role of the two different amino acids.

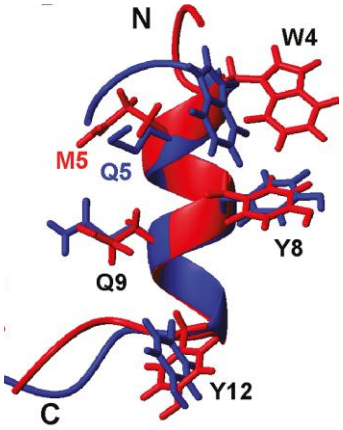

Figure 2.3.7 - NMR structure of MA: superposition of **106** (blue) and **MA** (red) representative structures. The residues potentially involved in the interaction with VEGF are shown.[72a]

This simple 15-mer peptide (**MA**) represents a good candidate for the treatment of diseases associated with excessive VEGF dependent angiogenesis. Among the all other examples found in literature, the VEGFR ligand **MA** proved to be the most accessible, from a synthetic point of view, also for further structure modifications, aiming at designing a novel dual-action conjugate to target both integrin (RGD motif) and VEGF receptors (**MA** sequence) (Chapter 2.4).
The rationale behind the VEGFR/integrin multi-target system project will be deeply explained in the next Paragraph (2.3.2)

2.3.2 Integrin-VEGFR cross-talk

Cross-talk between integrins and growth factor or cytokine receptors on both tumor and host cell types is vital for many aspects of tumor progression. Mechanisms of cross-talk include both direct and indirect association of integrins with growth factor or cytokine receptors, which affects the expression, ligand affinity and signalling of the

receptors. Tumor growth and invasion probably depend on integrin cross-talk with growth factor receptors or oncogenes in both tumor cells and tumor associated cells. Recent studies have demonstrated that some growth factors and oncogenes require specific integrins for tumor initiation and progression. These studies highlight the importance of understanding cross-talk mechanisms, as they could influence the tumor response to inhibitors of growth factor or integrin signalling. Growing evidence supports a central role for cooperative signalling between integrins, growth factor receptors and cytokine receptors in many aspects of tumour progression (Figure 2.3.5).[73]

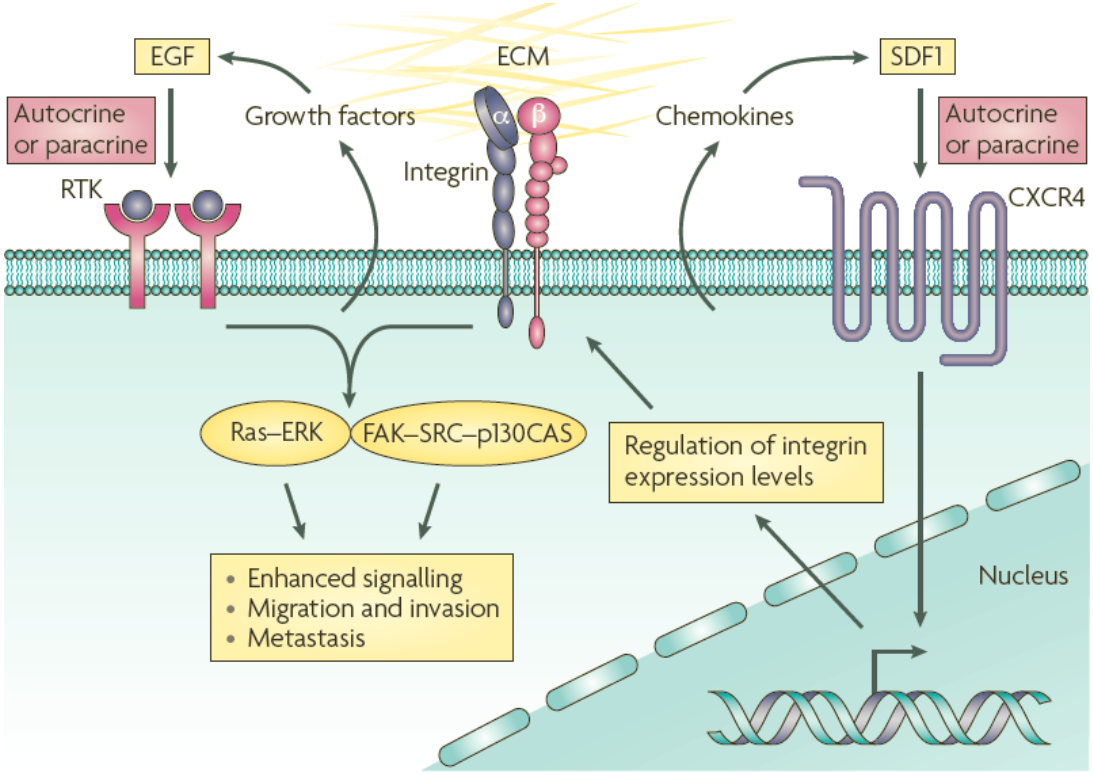

Figure 2.3.8 - *Integrin–growth factor and integrin–cytokine receptor cross-talk.* Cooperation between integrin and growth factor signalling or integrin and cytokine signalling is crucial to tumour progression. Several cross-talk mechanisms have so far been elucidated. Integrin ligation may lead directly to the increased secretion of growth factors and/or cytokines, which can then bind to their receptors in an autocrine or paracrine manner to further induce signalling. In addition, signalling induced by either integrin ligation or growth factor binding may activate common downstream pathways resulting in enhanced signalling overall compared with the activation of either receptor alone. This signalling seems to most commonly converge on kinases such as Src family kinases (SFKs), scaffolding proteins such as p130 CRK-associated substrate (p130CAS), and GTPases, such as the Ras family. Alternatively, both chemokine and growth factor signalling may regulate integrin function by directly controlling integrin expression levels. ECM, extracellular matrix; EGF, epidermal growth factor; FAK, focal adhesion kinase; SDF1, stromal cell-derived factor 1; RTK, receptor tyrosine kinase.

Integrin cross-talk not only regulates tumour cell adhesion, migration, invasion and survival, but also affects many aspects of the host response to cancer, particularly in the angiogenic endothelium. Another mechanism by which VEGF influences integrin $\alpha_v\beta_3$ signalling is through regulating the affinity state, or activation of the integrin: the activation of integrin $\alpha_v\beta_3$ can in turn increase tumour cell secretion of VEGF, providing a feedback loop resulting in increased tumour growth. Therefore, signalling through distinct integrin–growth factor receptor pairs has crucial roles in tumour angiogenesis.[74]

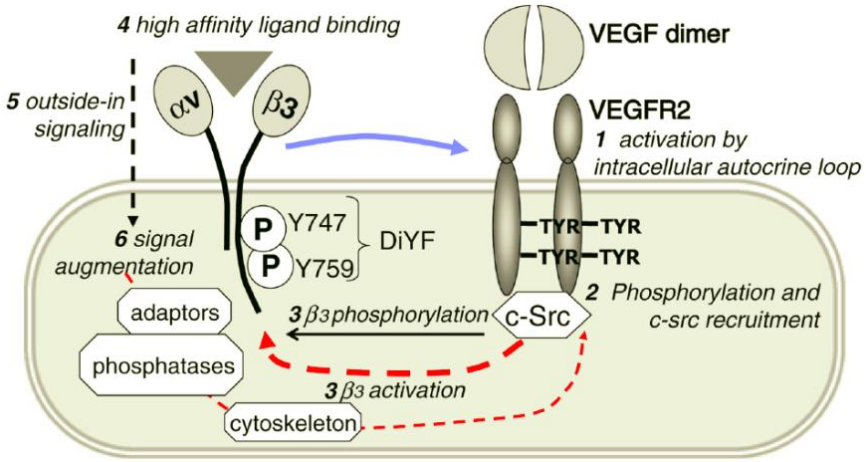

Figure 2.3.9 - Four possible mechanisms responsible for the complex formation between VEGFR-2 and $\alpha_v\beta_3$ on the surface of endothelial cells and the functional consequences of this cross-talk.

In a pioneer study published by Roushlati and coworkers, their main goal was to localize the sites of the αvβ3 integrin that interact with PDGFRb and VEGFR2.[75] The main new finding in this work is that both PDGFRb and VEGFR2 associate with the extracellular domain of the β3 integrin subunit. Ligand binding and phosphorylation of the RTKs do not seem to be required for the integrin interaction. The exact nature of the complex containing αvβ3 and the RTKs is unclear: both direct interaction and binding mediated by a third component are viable possibilities. This result strongly suggests that the integrin RTK extracellular domain interactions described in this work are the physical basis of the functional cooperativity between αvβ3 and RTKs.

The research group of Byzova and coworkers deeply investigated the integrin/VEGFR cross talk system.[76] In a paper published in 2008, they showed that EC stimulation by VEGF induced formation of the high affinity (activated) state of αvβ3 in a monolayer and activated αvβ3 was co-localized with VEGF receptor-2 (VEGFR-2).[76d] Most importantly, activated αvβ3 was detected on endothelial cells of tumor vasculature (Figure 2.3.7).

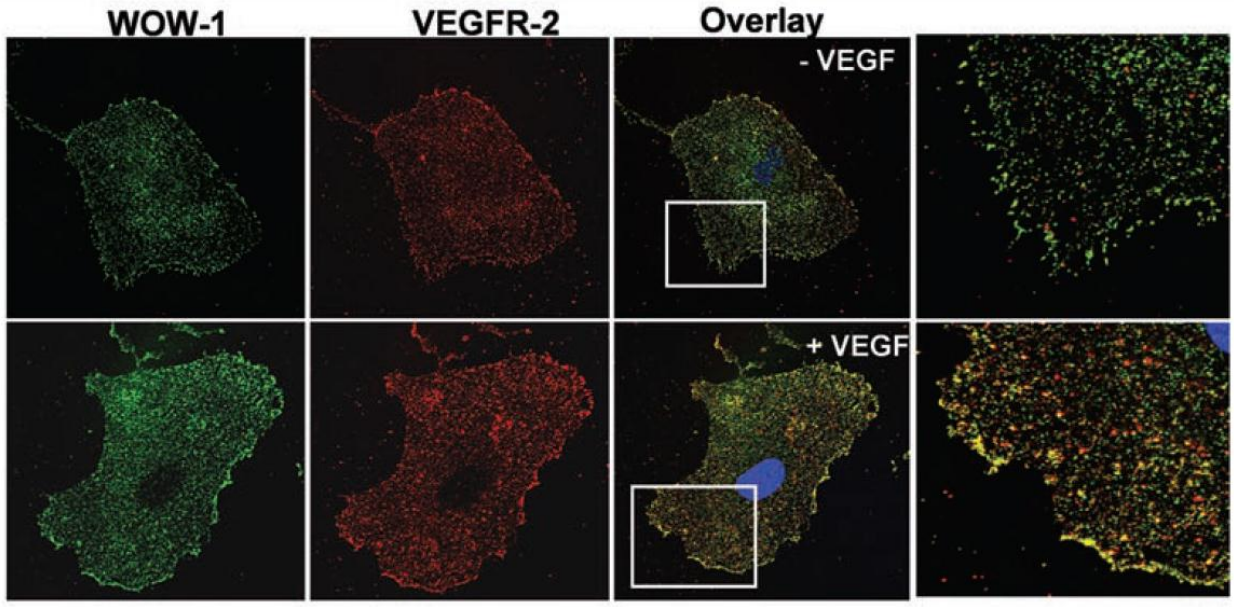

Figure 2.3.10 - αvβ3 integrin and VEGFR-2 co-localize on endothelial cells. HUVECs were serum-starved overnight then stimulated with 20 ng/mL VEGF for 5 minutes. These cells were stained with WOW-1 (a genetically engineered antibody used as a probe to detect αvβ3 in its high affinity state on the cell surface) and anti-VEGFR-2 antibodies, followed by the incubation with goat anti-mouse IgG labeled with Alexa Fluor 488 and goat anti-rabbit IgG conjugated with Alexa Fluor 594. Without a stimulatory signal (upper), very little co-localization of αvβ3 integrin and VEGFR-2 was observed. Upon VEGF stimulation (lower), the affinity of αvβ3 increases and co-localizes with VEGFR-2.

Activation of αvβ3 was substantially increased in highly-vascularized tumors as compared to normal tissues. Activated αvβ3 was co-localized with VEGFR-2 on endothelial cells of proliferating blood vessels. Together, these results show the unique role of αvβ3 integrin in cross-talk with VEGFR-2 in the context of pathological angiogenesis.

2.4 Dual-Action Conjugates Targeting Integrin $\alpha_V\beta_3$ and VEGFR

As suggested from the experimental evidences reported above (Paragraph 2.3), a dual integrin-VEGFR ligand could significantly improve the anti-angiogenic activity associated to the simultaneous inhibition of these extracellular receptors and at the same time elucidate the intracellular signalling deriving from the inhibition of this cross-talk.

We decided to investigate this field designing a novel class of small-molecule dual action conjugates capable of binding both to the $\alpha_v\beta_3$ integrin receptor and to VEGF receptors. So far, the only example known in literature is the already mentioned dual specific fusion protein scVEGFmut (see Paragraph 2.3.1.2).

We decided to use our potent $\alpha_v\beta_3$ integrin ligand **c[DKP-*f*3-RGD]** (see Paragraph 1.2.2) and the recently reported VEGFR1 ligand **MA** (see Paragraph 2.3.1.2) to develop an efficient synthesis of constructs **MA-RGD** and **Ac-MA-RGD** (Figure 2.4.1).

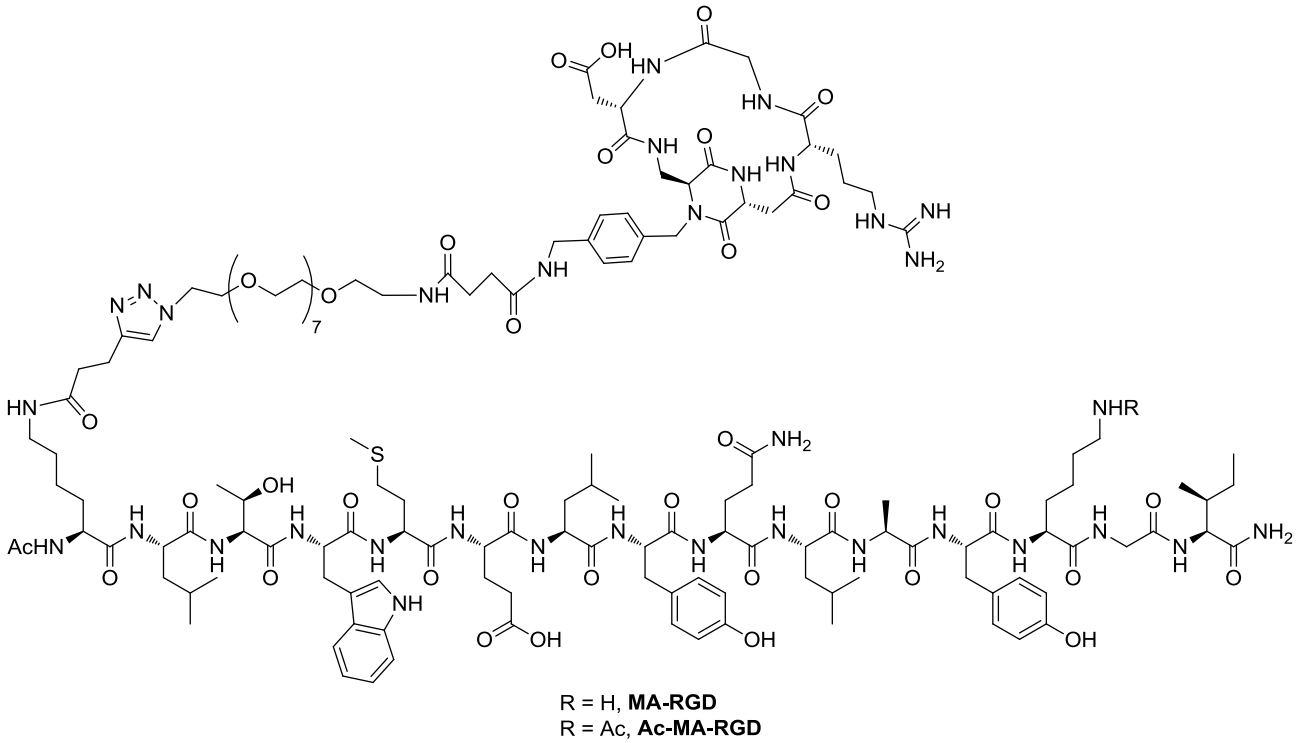

Figure 2.4.1

The retrosynthetic analysis of **MA-RGD** and **Ac-MA-RGD** is illustrated in Figure 2.4.2 and shown in Scheme 2.4.1:

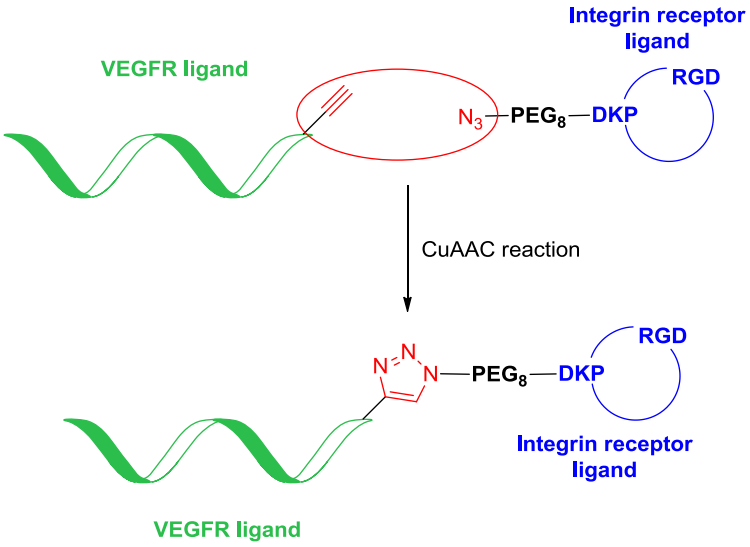

Figure 2.4.2

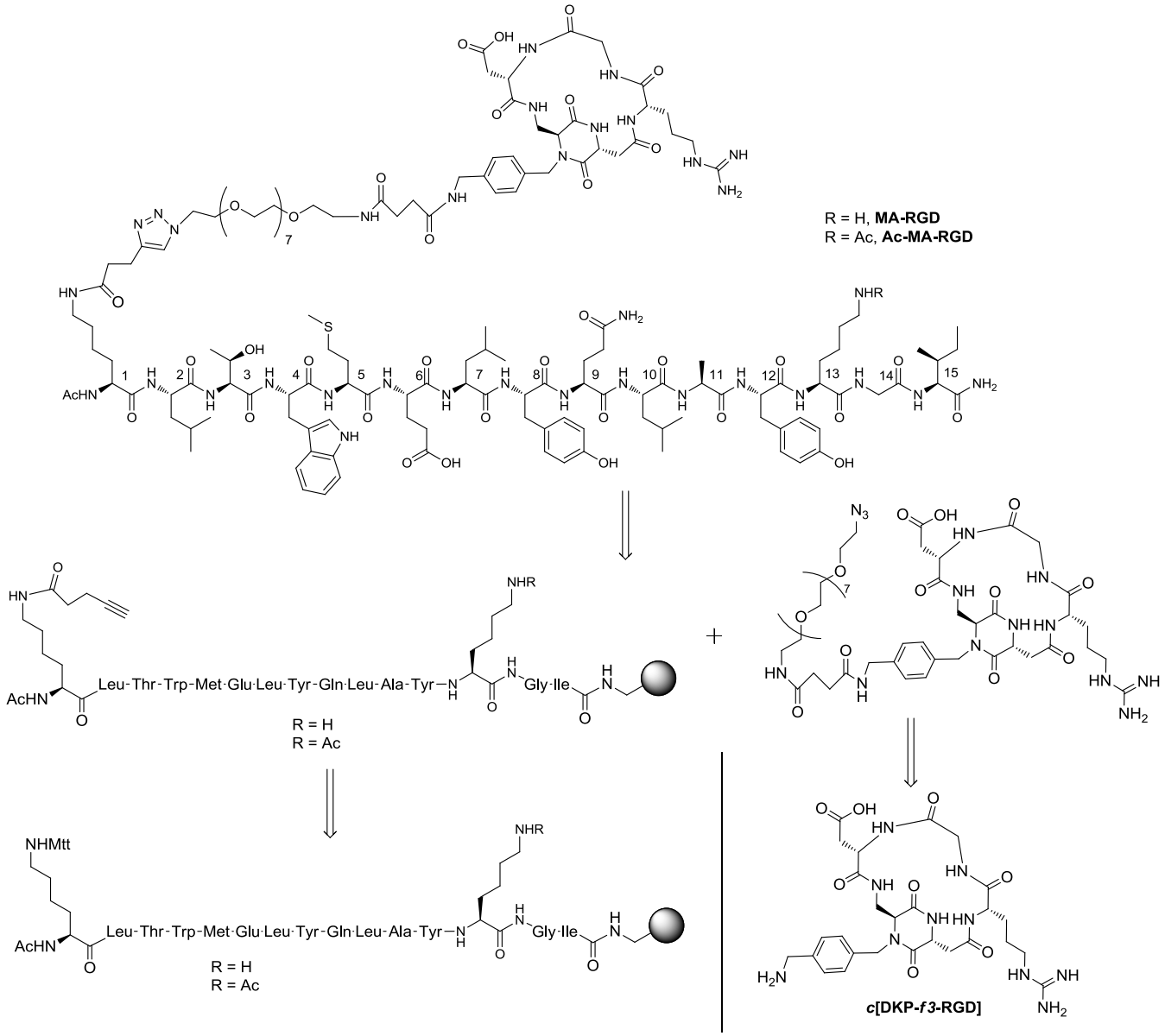

Scheme 2.4.1

First of all, we modified the **MA** peptide (Figure 2.4.3) introducing the alkyne moiety necessary for the CuAAC reaction strategy (see Figure 2.4.2 and Scheme 2.4.1):

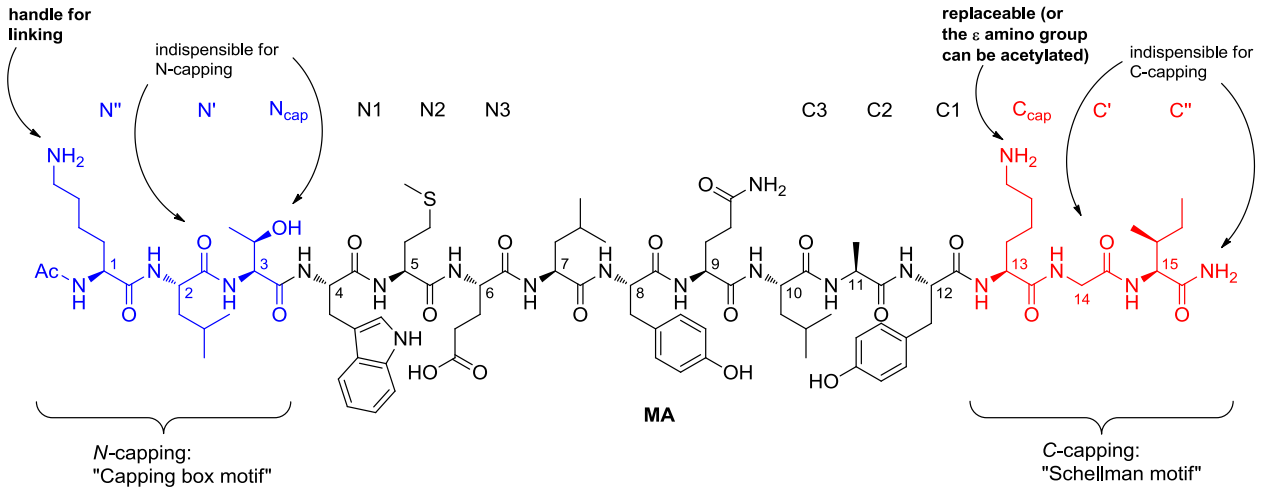

Figure 2.4.3

The N- and C-capping motifs (see also Paragraph 2.3.1.2) were chosen to introduce the modifications needed, as these amino acid residues do not participate in the binding epitopes of the **MA** peptide (Figure 2.4.3). We decided to introduce a variation (acetylation) on the Lys13 residue (affording thus **Ac-MA** peptide) in order to prevent the possible electrostatic interactions that a free charged amine might create with the RGD-ligand counterpart. Indeed these interactions could perturb the interaction with the integrin receptor that is based on an electrostatic clamp (see Chapter 1.1). Then we chose the side chain of Lys1 as the anchorage point for further derivatization and conjugation to the **c[DKP-*f*3-RGD]** counterpart (Figure 2.4.3), and we elongated it with but-3-ynoic acid (see Paragraph 2.4.1.1 for further details).

On the other hand, in order to perform the CuAAC reaction, the RGD ligand **c[DKP-*f*3-RGD]** must bear an azide moiety (Scheme 2.4.1). We decided to introduce the azide through a bi-functional PEG-8 linker (see Paragraph 2.4.1.2 for further details). A critical aspect was the choice of the polyethylene glycol chain length: the PEG-8 linker has a medium length, hopefully able to exploit the proximity of VEGFR and integrin receptors, due to cross-talk induced physical clustering of these receptors (see Chapter 2.3.2). In addition, the chosen PEG-8 linker presents a mono-dispersed structure profile (the longest mono-dispersed bi-functional linker sold by major chemicals suppliers). Mono-dispersion is a fundamental property for the linker because it allows to have a precise structure of the product (necessary for HPLC purifications and mass analysis) rather than a statistical mixture of products differing only for the PEG chain length.

2.4.1 Synthesis

2.4.1.1 Synthesis of VEGFR ligand counterparts

The **MA** and **Ac-MA** peptides were synthesized as reference compounds by microwave-assisted solid phase peptide synthesis (MW SPPS) with Biotage Initiator™ Microwave Synthesizer, using Rink Amide MHBA Resin and the Fmoc strategy (Scheme 2.4.2).

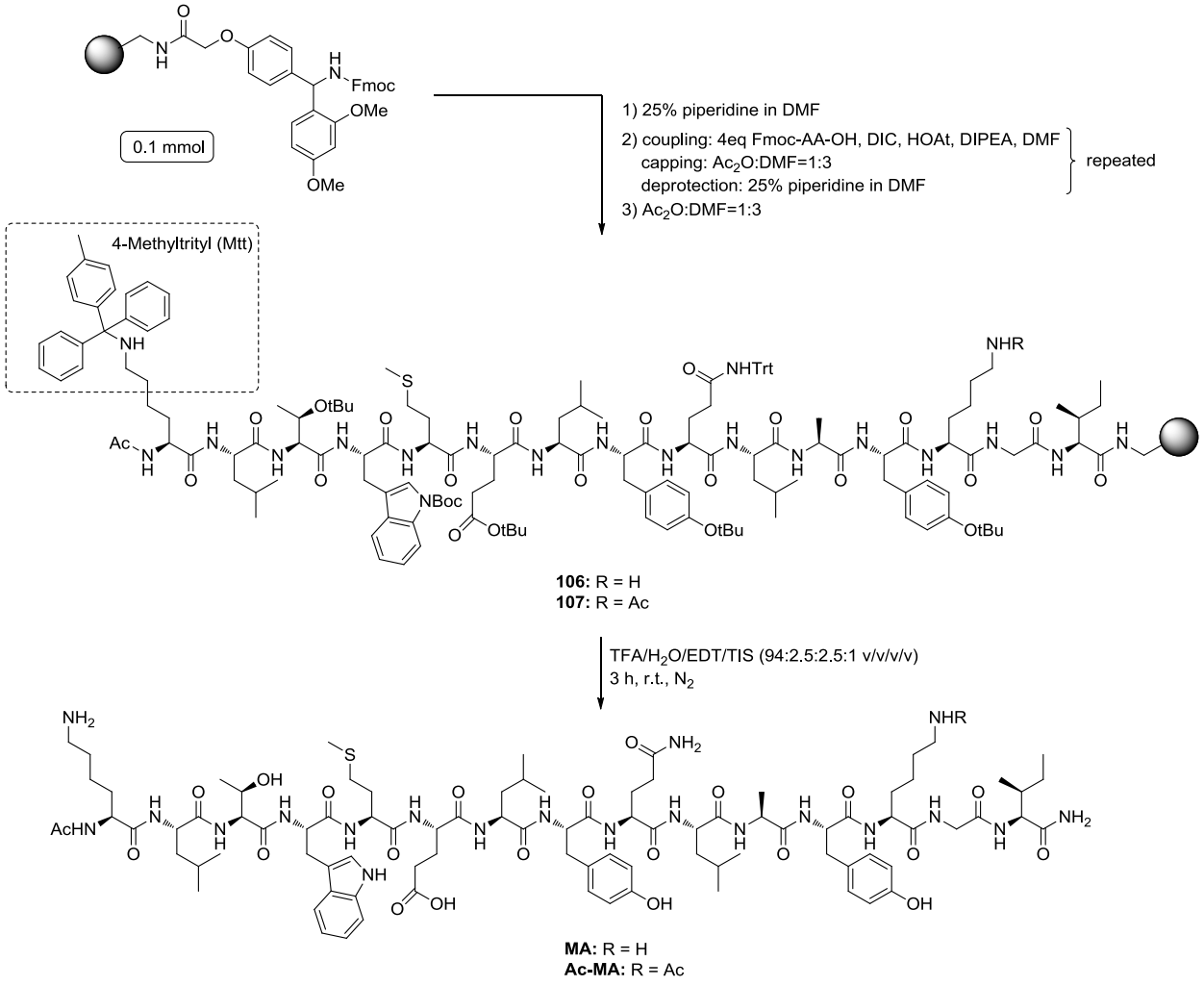

Scheme 2.4.2

Fmoc-Lys(Ac)-H (Novabiochem Ltd.) was used to synthesize on bead-peptide **107** and fully cleaved peptide **Ac-MA**. Each coupling step was carried out under N_2 atmosphere and at 70 °C under microwave irradiation. The use of microwaves allowed to speed up the coupling reactions on solid phase: decapentapeptides **106** and **107** were synthesized in only three days. The power curve maintained by the Biotage Initiator™

Microwave Synthesizer for desired temperature (70 °C) during the coupling step is reported in Figure 2.4.4 .

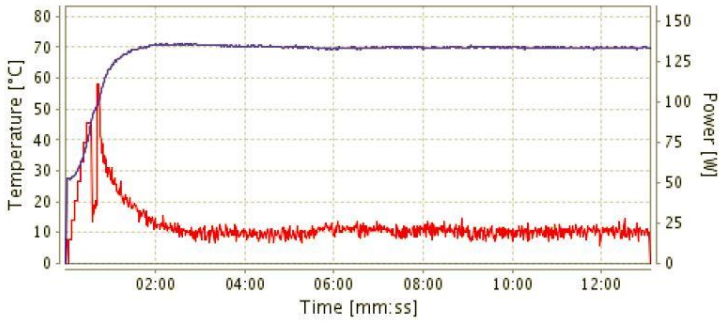

Figure 2.4.4 - *Temperature-power curve*. The temperature curve (°C) is reported in blue, the power curve (W) is reported in red.

The Mtt protecting group on the Lys1 (Scheme 2.4.2) was chosen to perform its selective removal with respect to the other protective groups present in **106** and **107**. Indeed, a single batch of on bead-peptides **106** and **107** was synthesized, and each batch was then split into two portions that were treated differently (Scheme 2.4.3). In particular, as already shown in Scheme 2.4.2, full side chains deprotection and cleavage from resin were accomplished to obtain the reference peptides **MA** and **Ac-MA** (see Scheme 2.4.3). Alternatively, the on bead-peptides **106** and **107** were selectively Mtt-deprotected (and maintained on resin) in order to allow their conjugation with but-3-ynoic acid (see Scheme 2.4.3 and discussion above).

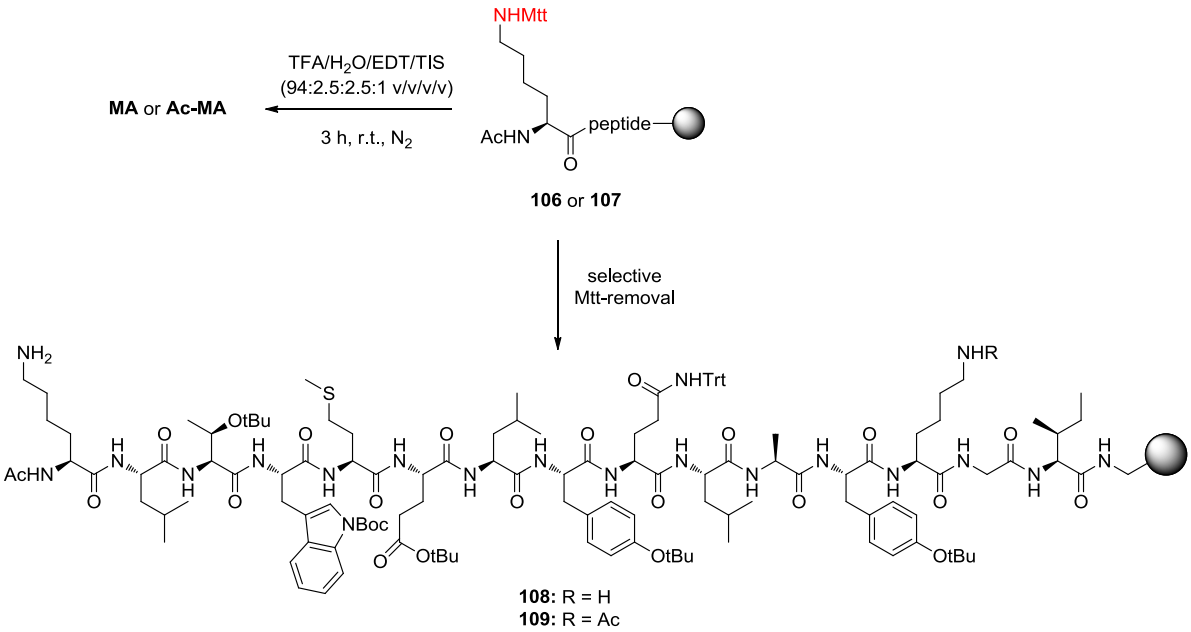

Scheme 2.4.3

The selective Mtt-removal on the on bead-peptides **106** and **107** was not easy and required optimization: it was necessary to establish a procedure to confirm the correct outcome of the selective deprotection reaction. The optimization was performed on petide **106**: as shown in Scheme 2.4.4, **106** was treated with the cleavage cocktail TFA/TIS/DCM (1:2:97 v/v/v, 2.3 mL for 0.05 mmol of resin) and subsequently with a solution of Ac_2O in DMF (1:3, 3.0 mL) to effect the acetylation of the ε-amino moiety of Lys1. The acetylation step was performed in order to verify whether the selective removal (and selective acetylation) of the Mtt group had taken place. Indeed, at this point only the Lys1 side chain $–NH_2$ should be deprotected, whereas all the others side chain functional groups should be still protected (and thus impossible to be acetylated). The last step was the full cleavage of the peptide from the resin, removing all the protecting groups still present on the residues side chains. MS analysis on the fully deprotected peptide gave no evidence of the desired product. Instead it revealed the ineffectiveness of the selective Mtt-removal: the MS spectrum showed the *m*/*z* value of the **MA** peptide, without the Ac group on the Lys1 side chain expected in the case of successful selective cleavage of Mtt. Moreover also a Kaiser test on some beads (after the expected selective cleavage) gave a negative result, i.e. no presence of free amine moieties, thus demonstrating the ineffectiveness of the Mtt-selective cleavage procedure.

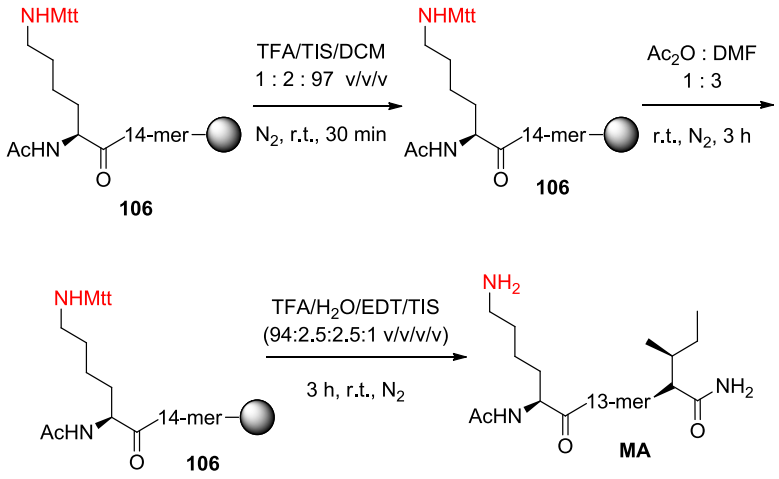

Scheme 2.4.4 – First attempt (failed) to selectively remove the Lys1 Mtt-protecting group.

To overcome this problem, a different selective procedure for the Mtt-removal was followed: **106** was treated with cocktail TFA/TIS/DCM (1:5:94 v/v/v) 12 times, 2 min and 3 mL for each time. Final full cleavage gave **110**, whose MS analysis confirmed the presence of acetylated Lys1 and thus the effectiveness of this procedure (Scheme 2.4.5). Moreover, a Kaiser test, just after the selective cleavage, gave a qualitative evidence of the presence of free amino groups.

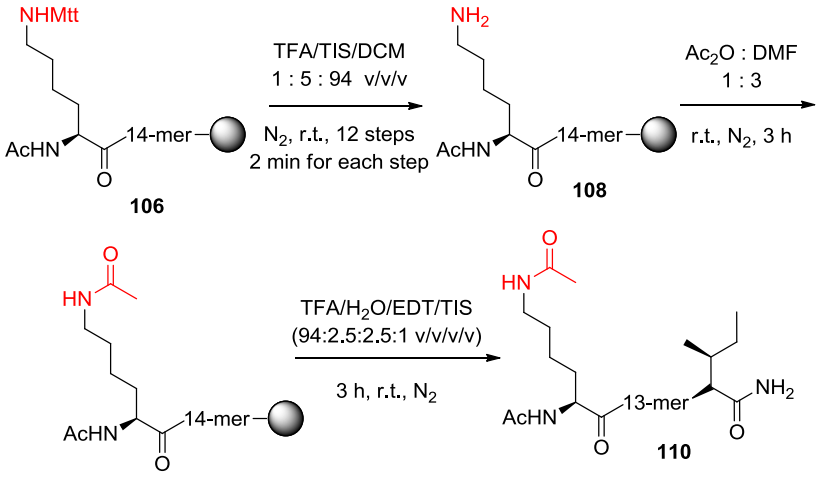

Scheme 2.4.5 – Optimized procedure to selectively remove the Lys1 Mtt-protecting group.

The efficacy of the new procedure is probably due to the repeated additions of fresh cleavage cocktail every 2 minutes, instead of a single passage lasting 30 minutes, as in the first Mtt-removal attempt.

Once established an effective procedure for the selective Mtt group removal, we synthesized the Lys1-deprotected peptides **108** and **109** (Scheme 2.4.6), that will be employed in the synthesis of the dual action conjugates described in Paragraph 2.4.1.3.

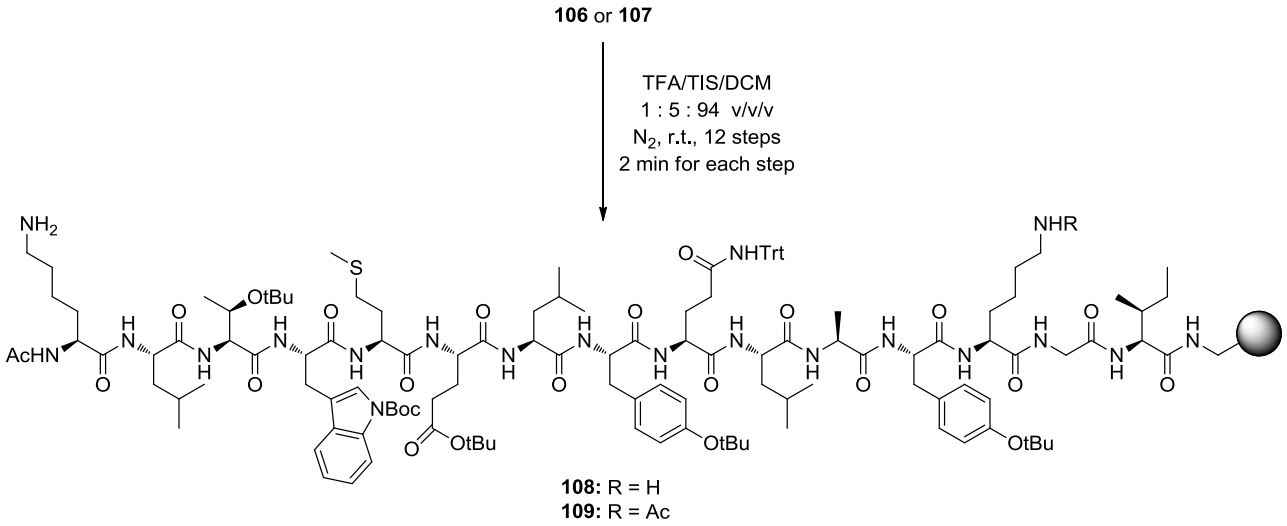

Scheme 2.4.6

2.4.1.2 Synthesis of RGD ligand counterpart

The functionalization of RGD-ligand counterpart **c[DKP-*f*3-RGD]** started with the amino-PEG-8-azide **111** (Sigma-Aldrich) elongation through reaction with succinic anhydride: azide **112** was purified by RP-HPLC and isolated in 96% yield. The next steps consisted in the activation of the carboxylic acid **112** with DIC and *N*-hydroxysuccinimide and subsequent coupling of the activated ester with **c[DKP-*f*3-RGD]** (see Paragraph 1.4.2 for further details). The desired product **113** was purified via RP-HPLC (Scheme 2.4.7).

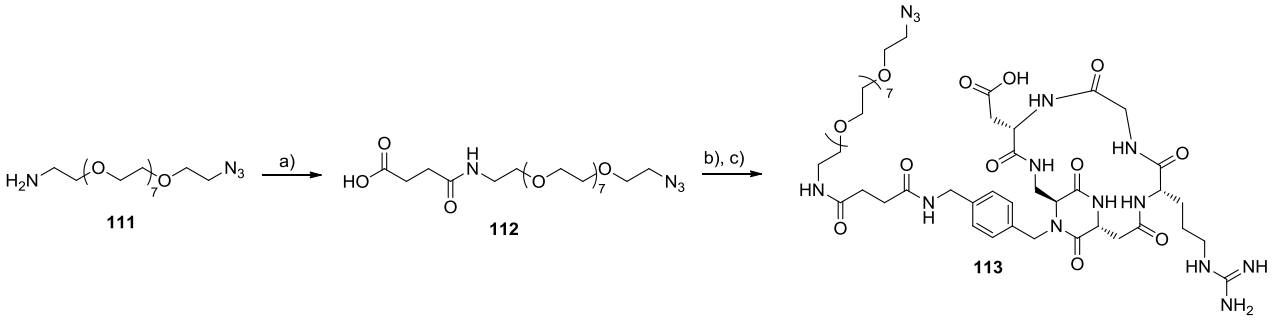

Scheme 2.4.7 - a) succinic anhydride, DMAP, DIPEA, CH_2Cl_2, r.t., 18h, 96%; b) *N*-hydroxysuccinimide, DIC, DMF, r.t., 2h; c) **c[DKP-*f*3-RGD]**, CH_3CN, phosphate buffer, pH 7.5, 0°C, 18h, 65% over 2 steps.

*2.4.1.3 Synthesis of **MA-RGD** and **Ac-MA-RGD***

As described at the beginning of Paragraph 2.4, the dual action conjugates bearing and integrin and VEGFR recognition motifs were synthesized by CuAAC reaction. This kind of reaction has been widely adopted to conjugate complex molecules and to obtain highly branched and elaborate products.[77] Some CuAAC reactions performed with solid supported substrates were also reported in literature.[78]

Regarding the synthesis of **Ac-MA-**RGD, the CuAAC reaction was planned to be performed on solid phase: we decided to set up a reaction model for the optimization of the on-bead click reaction, in order to avoid to waste the valuable azide **113**. The on-bead peptide **109** (Scheme 2.4.6) was used for the optimization: first of all, alkyne **114** was coupled to Lys1-free peptide **109**, thus affording the on-bead alkyne-bearing peptide **115**. Then model-azide **116** was synthesized starting from cinnamyl alcohol (Scheme 2.4.8).

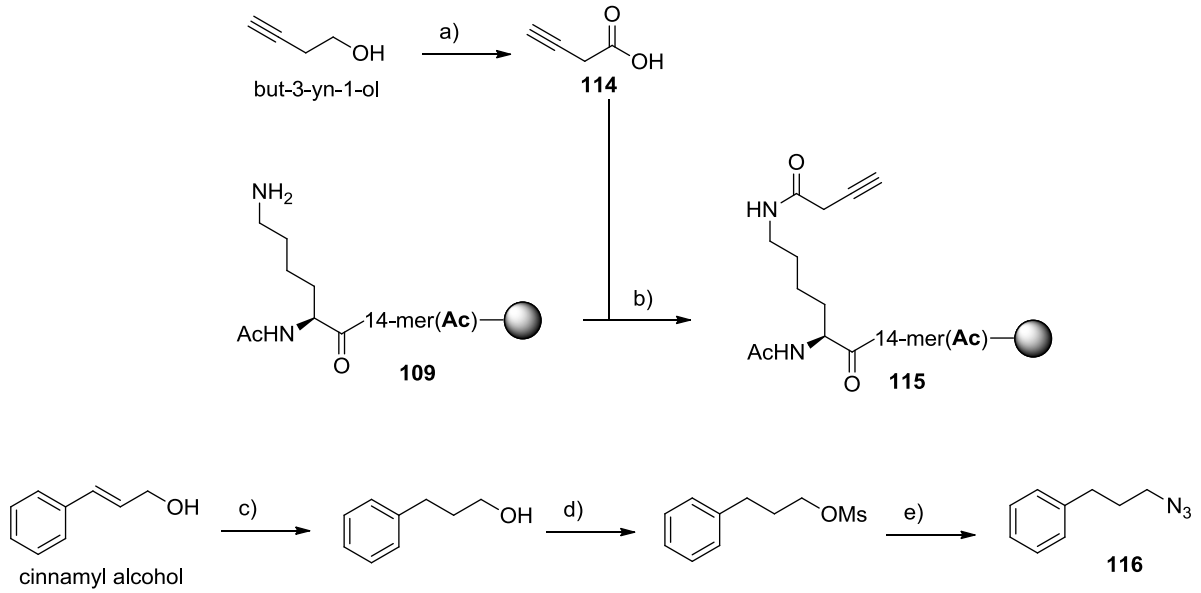

Scheme 2.4.8 - a) CrO_3, H_2SO_4 conc., acetone/H_2O 1:5, 0°C, 3.5h, 26%; b) HATU, HOAt, DIPEA, DMF, r.t., 18h; c) Pd/C 10%, H_2, CH_3OH, r.t., 18h, 96%; d) MsCl, DIPEA, CH_2Cl_2, 0°C, r.t.; e) NaN_3, DMF, 30°C, 24h, 80% over 2 steps.

A Kaiser test on some beads of **115** was carried out, and the negative result confirmed the absence of free amino moiety on the resin, and the effectiveness of the coupling reaction. Then, alkyne **115** was reacted with the model azide **116,** performing the CuAAC reaction on solid phase. The expected peptide **117** was then cleaved from the resin and purified by RP-HPLC (Scheme 2.4.9).

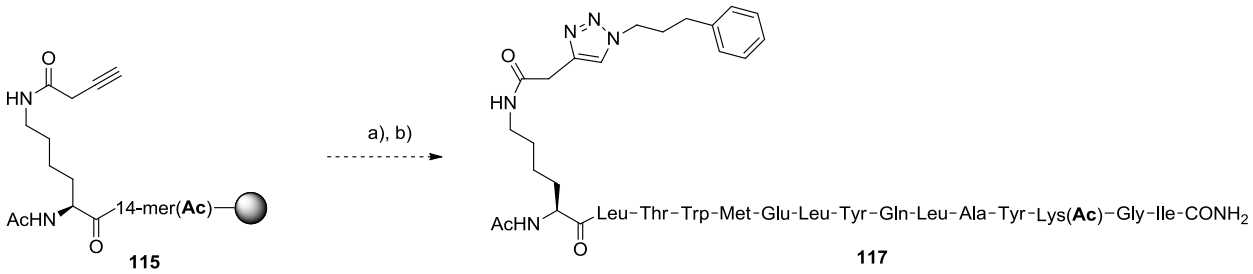

Scheme 2.4.9 - a) **116**, Cu(I), sodium ascorbate, DMF/piperidine 4:1, r.t., 42h; b) TFA/EDT/H_2O/TIS (94:2.5:2.5:1 v/v/v/v), 3 h, r.t.

The HPLC chromatogram of the crude CuAAC reaction to give **117** was upsetting and full of unexpected peaks (Figure 2.4.5).

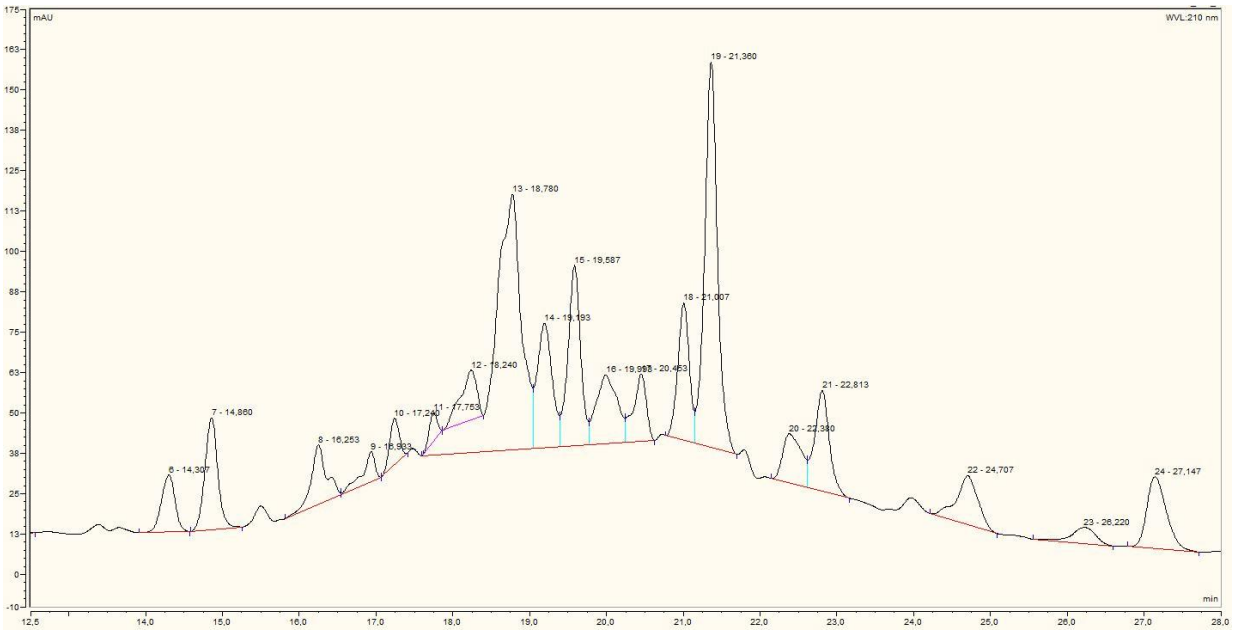

Figure 2.4.5 - HPLC chromatogram of the crude reaction CuAAC for the model conjugate **17**.

The formation of so many by-products could be related to the high reactivity of the acid **114**, which is prone to give the corresponding allene. The allene formation can be due to a base (piperidine, present in the reaction mixture) or a metal (copper, present in a catalytic amount) which coordinates the triple bond and guides the addition of a proton to the terminal alkyne –CH (Scheme 2.4.10).[79]

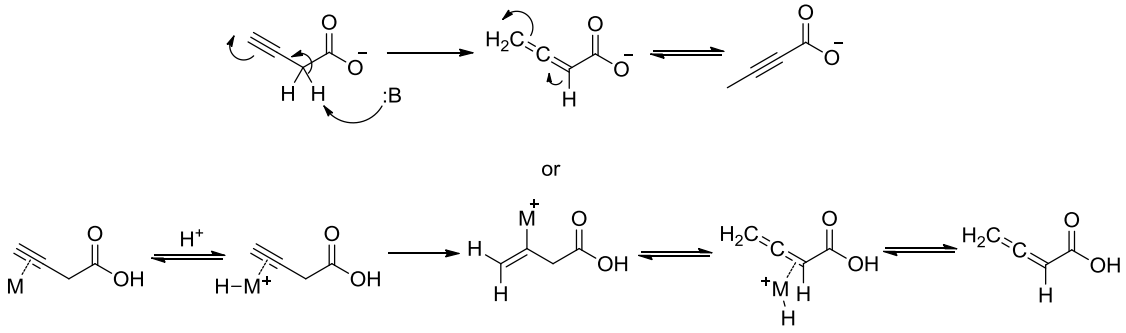

Scheme 2.4.10

To overcome this problem, we decided to use the homologous pent-4-ynoic acid **118** (Sigma-Aldrich), which has an extra carbon between the alkyne and the carboxylic acid moieties, compared to **114**. The reaction conditions for the new alkyne coupling and CuAAC reaction are described in Scheme 2.4.11.

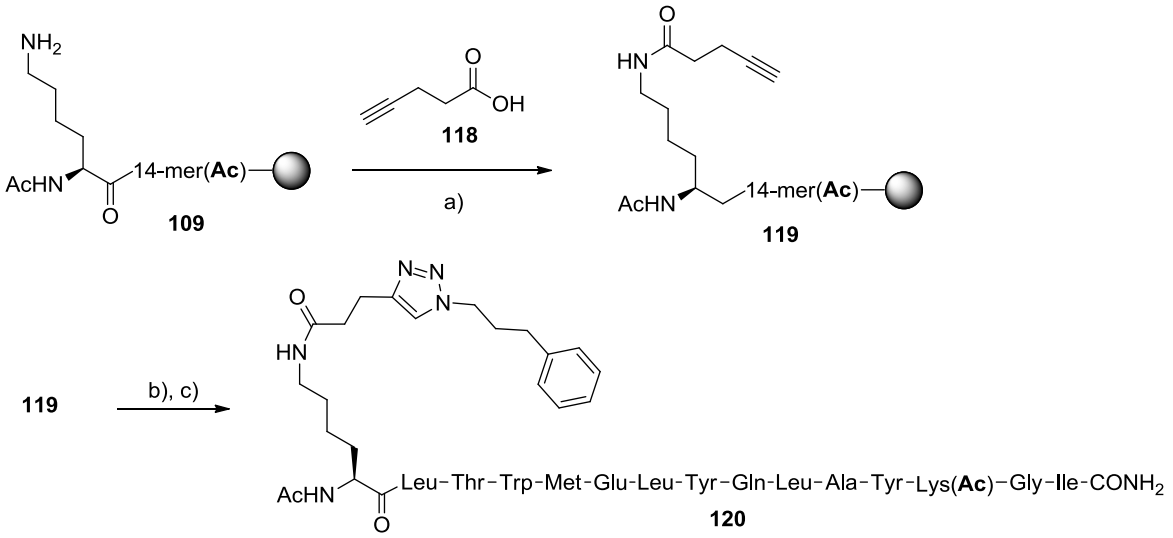

Scheme 2.4.11 – a) HATU, HOAt, DIPEA, DMF, r.t., 18h; b) **116**, CuI, sodium ascorbate, DMF/piperidine 4:1, r.t., 72h; c) TFA/EDT/H_2O/TIS (94:2.5:2.5:1 v/v/v/v), 3 h, r.t.

The HPLC chromatogram of the crude reaction to give the model-peptide **120** is reported in Figure 2.4.6. The main peak was confirmed, by MS analysis, to be the desired product **120**.

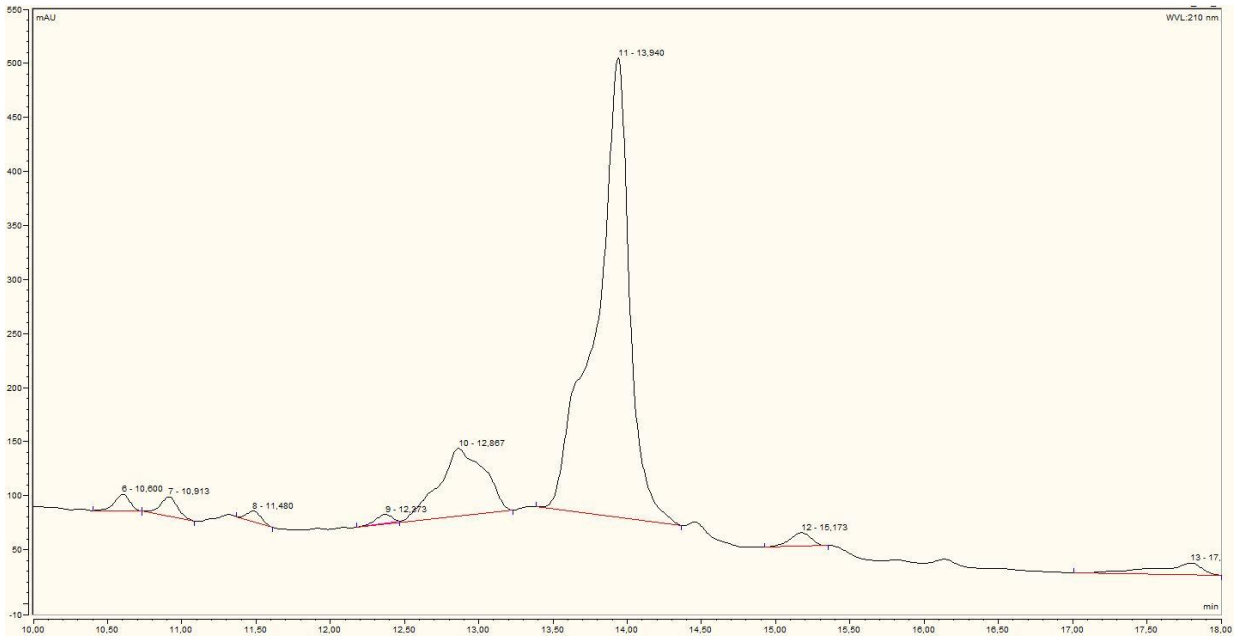

Figure 2.4.6 - HPLC chromatogram of the crude reaction affording to **120**.The main peak corresponds to compound **120**

Having optimized the reaction conditions, the CuAAC reaction was performed between azide **113** (Scheme 2.4.7) and alkyne **119** (Scheme 2.4.12).

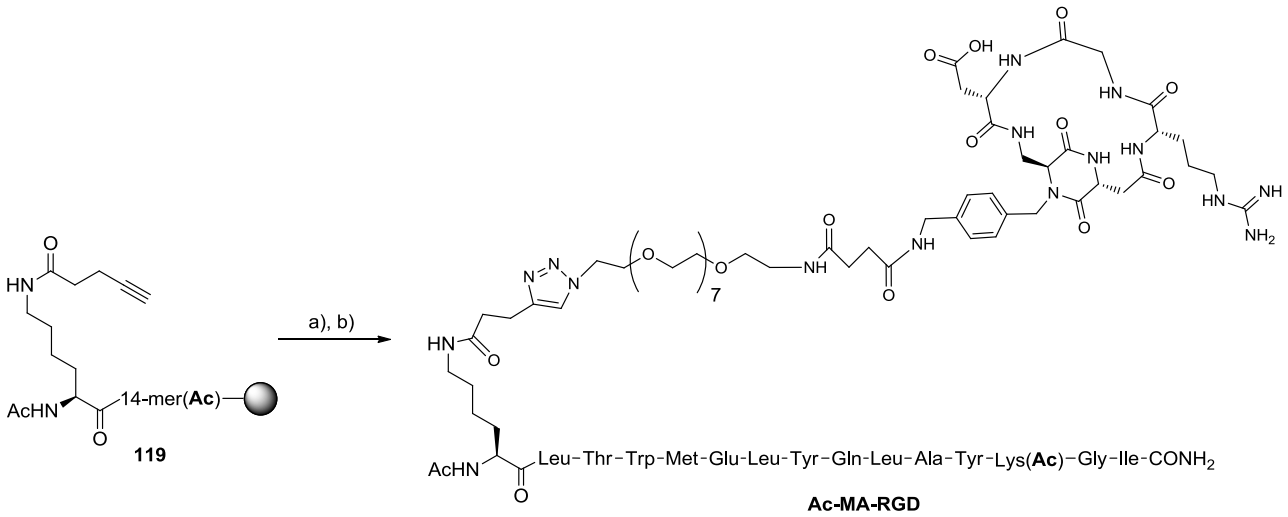

Scheme 2.4.12 - a) **113**, CuI, sodium ascorbate, DMF/piperidine 4:1, r.t., 18h; b) TFA/EDT/H_2O/TIS (94:2.5:2.5:1 v/v/v/v), 3 h, r.t.

The HPLC chromatogram showed the presence of two peaks in a 6:1 ratio. The major peak was assigned to the desired product **Ac-MA-RGD** by MALDI-TOF-MS analysis (Figure 2.4.7)

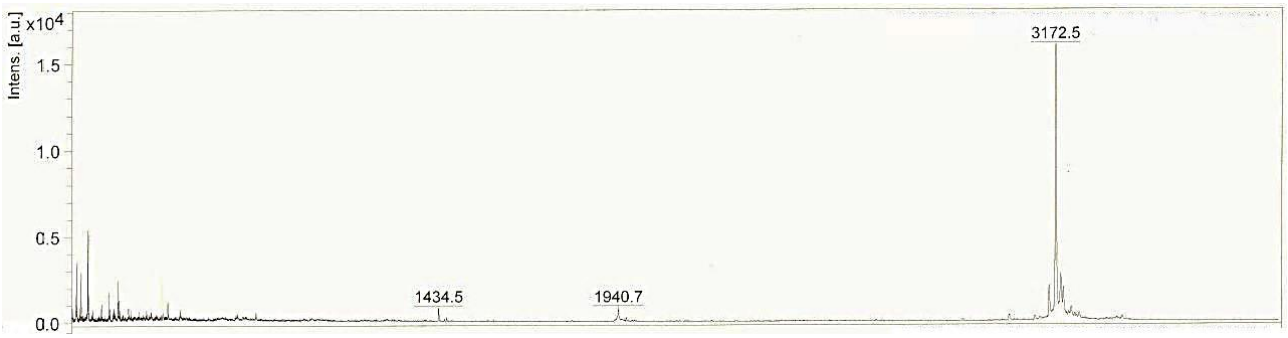

Figure 2.4.7 - MS spectrum of the conjugate product **Ac-MA-RGD** (MALDI-TOF-MS analysis, HCCA matrix). The spectrum shows the *m*/*z* value corresponding to the $[M+H]^+$ ion: the experimental value [3172.5 amu] corresponded to the calculated value [3171.63 amu].

The MS analysis on the minor peak showed a higher *m*/*z* value (3346.6 amu) with respect to that expected for the desired product. It can be hypothesized that this is a by-product deriving from the addition of dehydroascorbate, the oxidised form of ascorbate, to the already formed **Ac-MA-RGD,** leading to **Ac-MA-RGD-Asc** (Scheme 2.4.13). It is reasonable to assume that the dehydroascorbate (deriving from the reduction of Cu(II) to Cu(I)) could be prone to participate to the main click reaction as an electrophile. This probably happens in the last step of the catalytic cycle, when an electrophile (E^+) is required (Scheme 2.4.13). Although this explanation is reasonable, no

studies on this side reaction pathway were conducted to deeply investigate why the by-product formed.

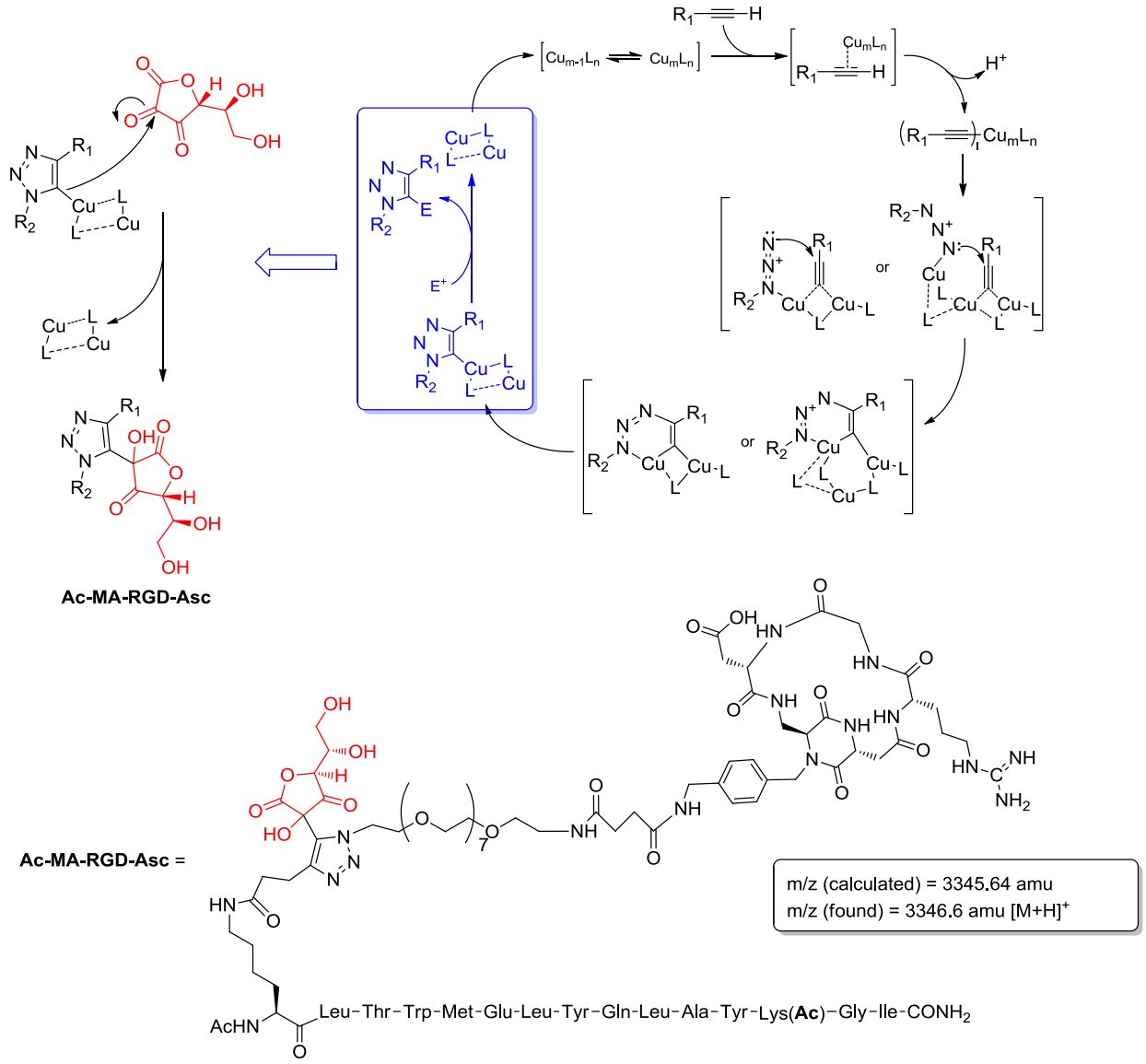

Scheme 2.4.13

Considering the problems found performing the CuAAC reaction on solid phase, it was decided to carry out the synthesis of the other dual action ligand **MA-RGD** in solution phase, also to have better control on the stoichiometry and to compare the outcome of the reactions, if conducted in solution or on solid phase. Moreover, since reaction was conducted in solution phase, the excess of azide **113** was no longer necessary, and it was also easier to control the undesired addition of ascorbate to the final product. To avoid this side reaction it was also decided to use $CuSO_4$ as copper source, in order to have the reduction of Cu(II) to Cu(I) *in situ* by ascorbate.

Peptide **108** (Scheme 2.4.6) was coupled to alkyne **118** and alkyne-bearing peptide **121** was removed from resin (fully deprotection of side chain groups) and purified by RP-

HPLC, affording alkyne **122**. This compound was coupled to azide **113** by Cu(II) click reaction, affording, after RP-HPLC purification, the dual action ligand **MA-RGD** in 25% yield (Scheme 2.4.14).

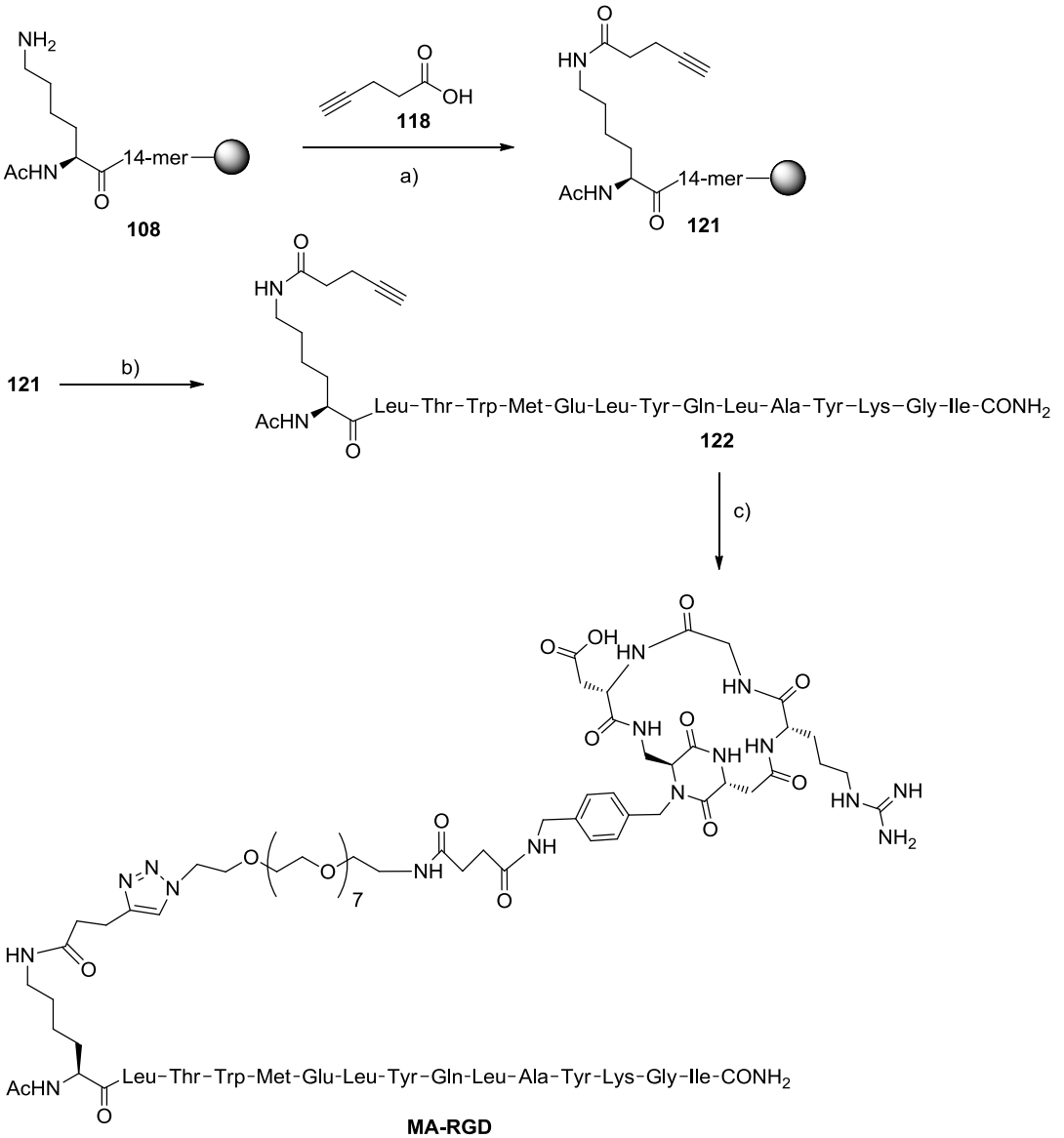

Scheme 2.4.14 - a) HATU, HOAt, DIPEA, DMF, r.t., 18h; b) TFA/EDT/H_2O/TIS (94:2.5:2.5:1 v/v/v/v), 3 h, r.t; c) **113**, $CuSO_4$, sodium ascorbate, DIPEA, DMF, r.t., 48h, 25%.

MALDI-TOF-MS analysis confirmed the mass value for the desired product **MA-RGD** (Figure 2.4.8).

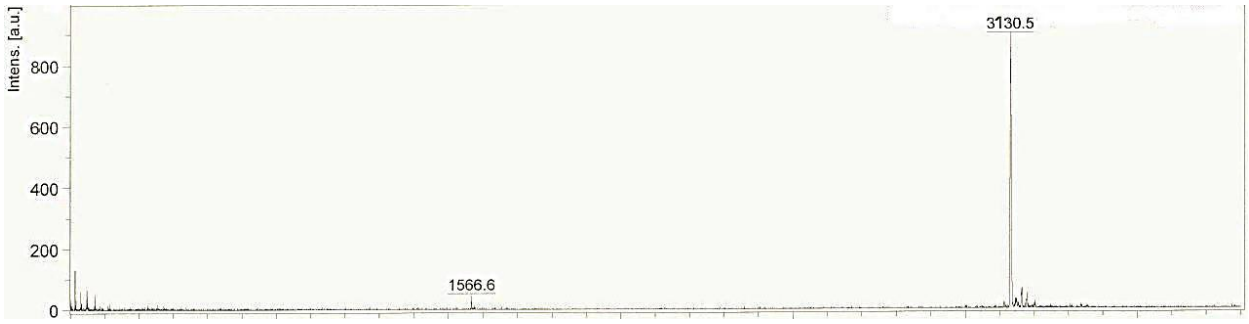

Figure 2.4.8 - MS spectrum of **MA-RGD** (MALDI-TOF-MS analysis, SIN matrix). The spectrum shows the *m*/*z* value corresponding to the $[M+H]^+$ ion: the experimental value [3130.5 amu] corresponded to the calculated value [3129.62 amu].

2.4.2 Circular dichroism analysis [80]

The CD spectroscopy was used to investigate the structural properties of the synthesized compounds and to have a more general view of their behaviour in relation with their biological activity.

The CD spectrum arises from the sum of the dichroic contributes of each amide moiety present in the peptide. When a peptide folds into a helical conformation, the spatial distribution and orientation of its chromophores generate a CD spectrum which usually consists of two major bands, corresponding to the $\pi \rightarrow \pi^*$ and $n \rightarrow \pi^*$ electronic transitions, located at about 208 and 220 nm (the wavelength values can be different due to the helix type, α-helix or 3_{10} helix). The ellipticity sign (positive or negative) in correspondence of these focal wavelengths depends on the rotatory direction of the helix: in the presence of a right-handed helical structure the ellipticity assumes negative values and positive values for the left-handed ones.

The ratio between the two maxima intensities at 220 and 208 nm is defined as **R** and its value is usually used to evaluate the alpha-helix content in the sample: the higher the **R** value is, the bigger is the fraction of the sample which folds into a α-helix conformation.

First the CD spectra of reference compounds **MA** and **Ac-MA** peptides (Chapter 2.4.1.1) were registered in methanol and in trifluoroethanol (TFE), solvents which were expected to better solubilize the two compounds (Figure 2.4.9): in Table 2.4.1 the experimental data obtained are shown.

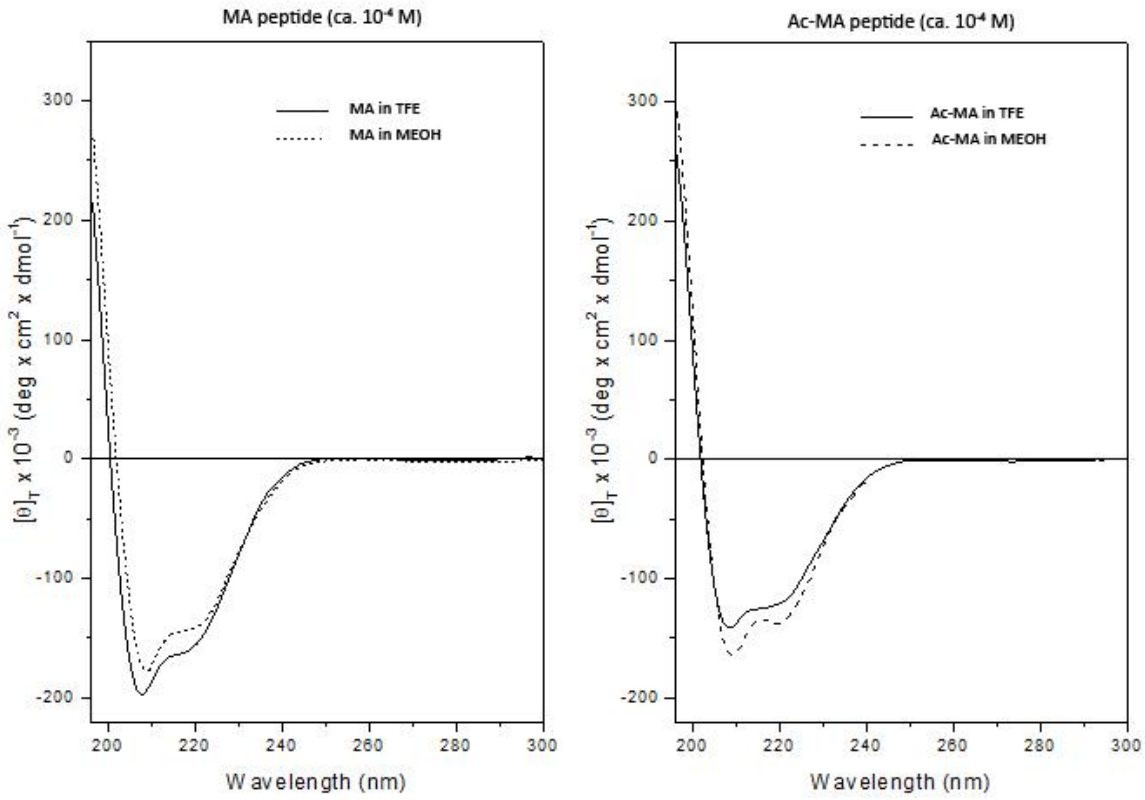

Figure 2.4.9 - MA and **Ac-MA** CD spectra in MeOH and TFE.

Table 2.4.1 - Experimental data for **MA** and **Ac-MA** CD spectra in MeOH and TFE.

Peptide	Solvent	$[\theta]_T$ x 10^{-3} (208 nm)	$[\theta]_T$ x 10^{-3} (220 nm)	R $[\theta]_{220}/[\theta]_{208}$
MA	MeOH	-175.30	-139.38	0.80
	TFE	-196.45	-162.81	0.83
Ac-MA	MeOH	-162.50	-136.33	0.84
	TFE	-141.13	-124.07	0.88

Since the CD spectrum derives from a sum of various contributes, the data reported above can be used to determine the secondary structure of the compounds only when two conditions are fulfilled:

1 the peptide contains a sufficient number of amide bonds, so that they generate a reliable CD spectrum;

2 the peptide has no other chromophores, different from the amide moiety, which absorb the radiation in absorption range of the amide bonds, so that their contribute does not alter the spectrum making it unreliable.

For **MA** and **Ac-MA** it is possible to consider reliable the corresponding values of **R** indicating that the α-helix content in the structures of these two peptides is high.

The CD spectra of **MA** and **Ac-MA** were registered also in water for two main reasons:

1. the cell environment is aqueous, thus it is more useful study the synthesized compounds in water;
2. methanol and TFE are solvents with a well-known ability to induce the helical conformation and this effect could invalidate the experimental results.

In Figure 2.4.10 the CD spectra in water of **MA** and **Ac-MA** are shown. The two spectra are very similar, but in the **MA** spectrum a slightly higher helical content is shown: the **MA** peptide seems to assume a more ordered helical conformation. For the **Ac-MA** peptide, this helical content decrease can be attributed to a greater population of unordered structure.

The only difference between the two sequences is the non-acetylated Lys13 in **MA**: the positive charge of its free amino group could form a salt bridge with the Glu6 residue. In fact, the two amino acids are at the right distance (seven residues, corresponding to two helix turns) to be on the same side of the α-helix, thus stabilizing the secondary structure. The distance between these two residues is about 11 Å, corresponding to two helix turns: Lys and Glu have long side chains and they could get close enough to maintain the stabilizing electrostatic interaction. In Table 2.4.2 the experimental data obtained are reported.

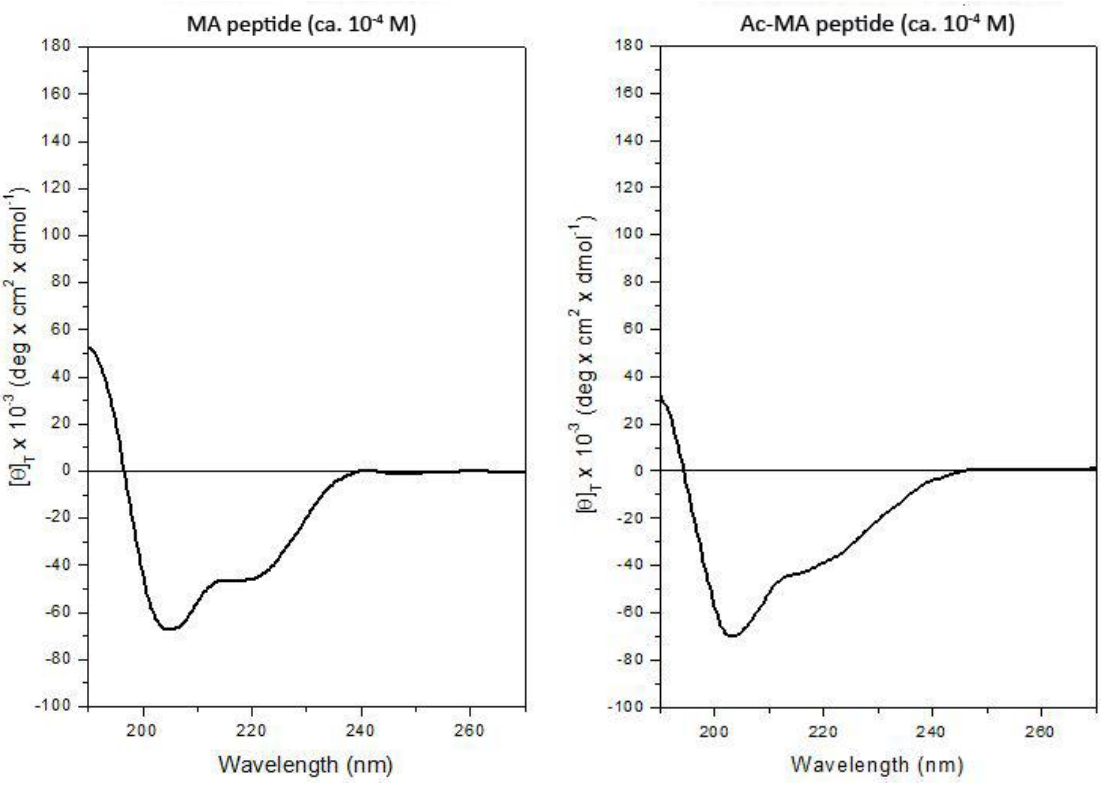

Figure 2.4.10 - MA and **Ac-MA** CD spectra in H_2O.

Table 2.4.2 - Experimental data for **MA** and **Ac-MA** CD spectra in H_2O.

Peptide	Solvent	$[\theta]_T \times 10^{-3}$ (208 nm)	$[\theta]_T \times 10^{-3}$ (220 nm)	R $[\theta]_{220}/[\theta]_{208}$
MA	H_2O	-67.55	-46.58	0.69
Ac-MA	H_2O	-71.28	-38.94	0.55

In the **MA** CD spectrum the negative maximum of the $\pi \rightarrow \pi^*$ transition for the amidic cromophore (parallel component) is centred at 205 nm, but in the **Ac-MA** spectrum this transition slides down to 203 nm. The classic right-handed α-helix is characterized by two negative maxima of roughly equivalent intensity, centred at 208 nm (parallel component of the transition $\pi \rightarrow \pi^*$ for the amidic chromophore) and at 222 nm (transition $n \rightarrow \pi^*$). Therefore, the position of the two negative maxima in the spectrum of **Ac-MA** and their intensities indicate the predominant presence of a helical structure of type α, with a significant participation of disordered structures, also called "polyproline type-II", which move the left band at about 203 nm and determine the intensity decrease of the right band.

The CD spectra in water of **c[DKP-*f*3-RGD]** and **113** (Chapter 2.4.1.2) are reported in Figure 2.4.11. The two curves have the form usually attributed to type β folding, in particular β-turn type II, characterized by two maxima: a positive maximum at ≈203 nm and a negative one at ≈226 nm. In fact, this kind of spectra was observed in cyclic tri-peptides that form β-turn structures. Notably, the modest differences, consisting of variations in the sign and position of the two maxima between the two curves suggest that the PEG-8 moiety does not alter significantly the structure of compound **113**.

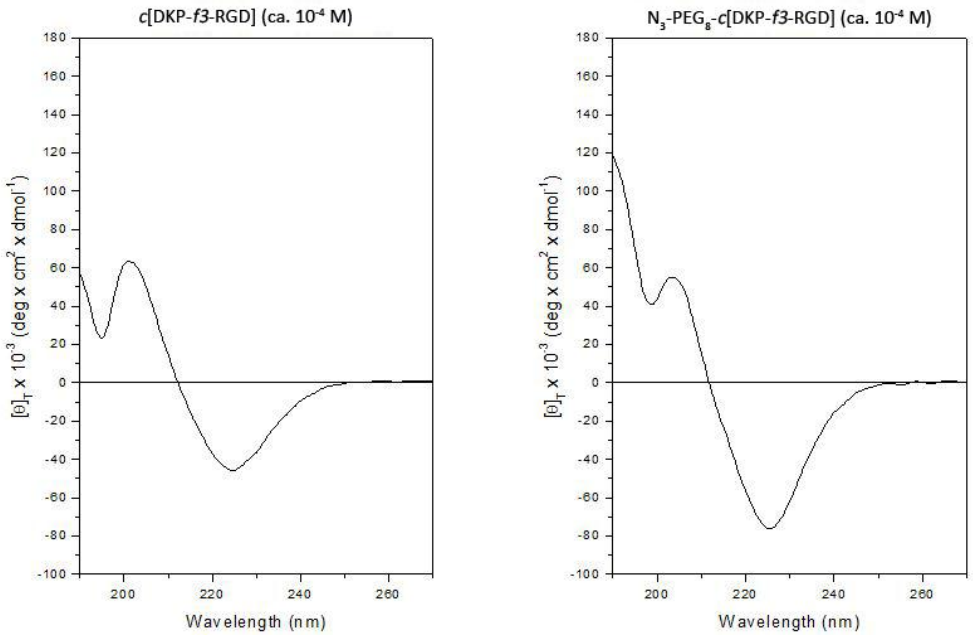

Figure 2.4.11 - c[DKP-f3-RGD] and **N_3-PEG_8-c[DKP-f3-RGD]** CD spectra in H_2O.

In these two compounds the cyclic peptide RGD is too short to assume a well-defined secondary structure: the **R** values are not meaningful in these cases.
In Paragraph 1.5.3 has been already demonstrated, via NMR and computational studies, that **c[DKP-3-RGD]** forms pseudo-β-turn structures.

Figure 2.4.12 shows the superimposed CD spectra of **MA**, **Ac-MA** and **Ac-MA-RGD** in TFE and in MeOH. In Table 2.4.3 the experimental data for these CD spectra are reported.

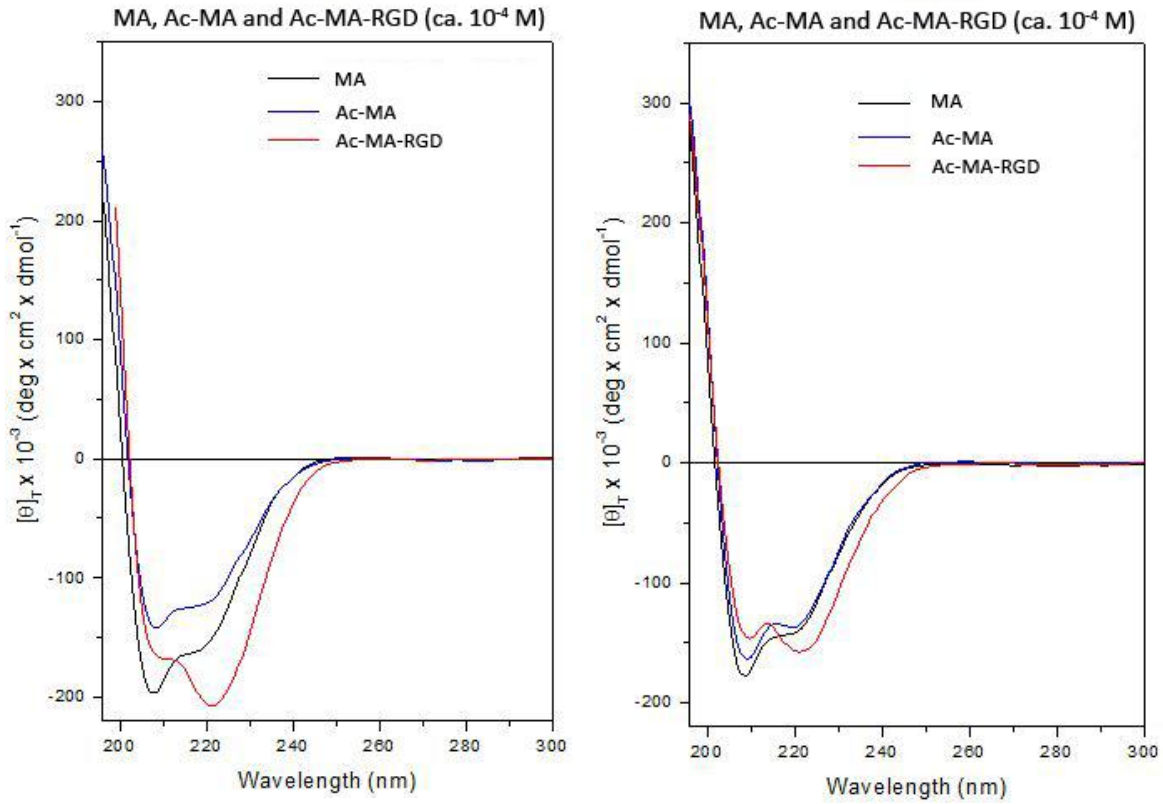

Figure 2.4.12 - MA, **Ac-MA** and **Ac-MA-RGD** stacked CD spectra in TFE (on the left) and in MeOH (on the right).

Table 2.4.3 - Experimental data for **MA**, **Ac-MA** and **Ac-MA-RGD** CD spectra in TFE and in MeOH.

Peptide	Solvent	$[\theta]_T$ x 10^{-3} (208 nm)	$[\theta]_T$ x 10^{-3} (220 nm)	R $[\theta]_{220}/[\theta]_{208}$
MA	MeOH	-175.30	-139.38	0.80
	TFE	-196.45	-162.81	0.83
Ac-MA	MeOH	-162.50	-136.33	0.84
	TFE	-141.13	-124.07	0.88
Ac-MA-RGD	MeOH	-168.07	-207.57	1.23
	TFE	-146.35	-157.61	1.08

In TFE and MeOH the **Ac-MA-RGD** conjugate presents a high helical content, as demonstrated by the **R** values. However, as explained before, these two solvents have a well-known ability to induce the helical conformation, for this reason the **Ac-MA-RGD** CD spectrum was recorded also in water (Figure 2.4.13 left).

The sum CD spectrum of **Ac-MA** + **113** superimposed to the **Ac-MA-RGD** CD spectrum is reported in Figure 2.4.13 (right). The sum spectrum is obtained by summing the molar ellipticities **[θ]** of the two spectra, i.e. it consisted in the sum of the experimental data at the various wavelengths.

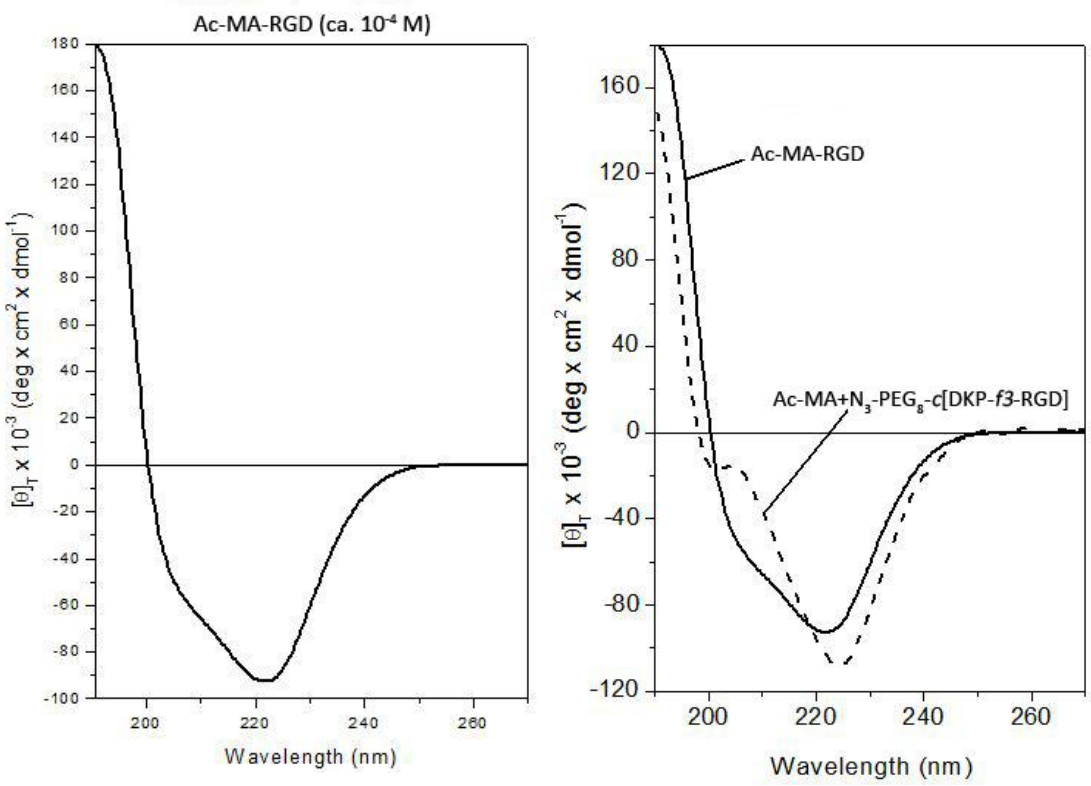

Figure 2.4.13 - Ac-MA-RGD CD spectrum in H_2O. (on the right) Sum CD spectrum **Ac-MA+N_3-PEG_8-c[DKP-f3-RGD]** stacked to the **Ac-MA-RGD** CD spectrum.

Also for the other dual-action conjugate, the CD spectrum of **MA-RGD** in water is shown in Figure 2.4.14; on the right the sum spectrum of **MA+113** superimposed to the **MA-RGD** CD spectrum is reported.

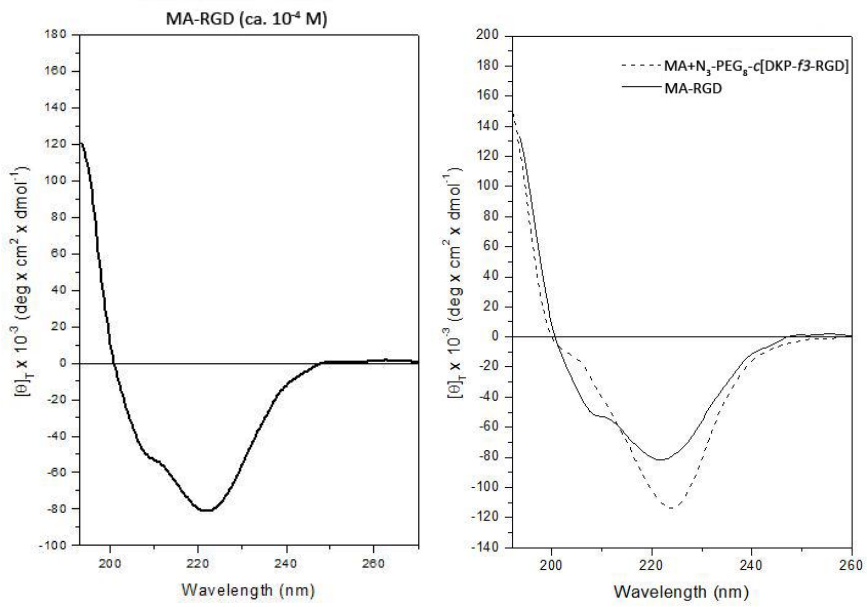

Figure 2.4.14 - MA-RGD CD spectrum in H_2O. (on the right) Sum CD spectrum **MA+N_3-PEG_8-c[DKP-f3-RGD]** stacked to the **MA-RGD** CD spectrum.

The experimental data for the CD spectra of **MA**, **Ac-MA**, **MA-RGD** and **Ac-MA-RGD** in water are summarized in Table 2.4.4

Table 2.4.4 - Experimental data for **MA**, **Ac-MA**, **MA-RGD** and **Ac-MA-RGD** CD spectra in H_2O.

Compound	Solvent	$[\theta]_T$ x 10^{-3} (208 nm)	$[\theta]_T$ x 10^{-3} (220 nm)	R $[\theta]_{220}/[\theta]_{208}$
MA	H_2O	-67.55	-46.58	0.69
Ac-MA	H_2O	-71.28	-38.94	0.55
MA-RGD	H_2O	-51.41	-81.38	1.58
Ac-MA-RGD	H_2O	-53.52	-92.71	1.73

Regarding the **MA-RGD** and **Ac-MA-RGD** final products, the presence of the PEG-8-RGD branch makes the **R** values meaningless because of its contribute to the CD spectra: indeed, in both the two sum spectra reported in Figure 2.4.13 and 2.4.14 (for **Ac-MA-RGD** and **MA-RGD** respectively), it is possible to observe the contributions of the PEG-8-RGD counterpart to the negative maxima at about 220 nm. The dotted lines (which refer to the CD spectra given by the sums of the two parts, the peptide and the DKP-RGD moieties) have a maximum more negative with respect to the curves of the relative conjugates **Ac-MA-RGD** and **MA-RGD**: in this wavelength region the character of the CD spectrum curve is dominated by some contributions deriving from the **113** counterpart (see also Figure 2.4.11, in which the negative maximum at about 220 nm is clearly visible).

2.4.3 Binding assays on isolated receptors [50]

Since the dual action conjugates **MA-RGD** and **Ac-MA-RGD** should exert their function on both integrin and VEGF receptors, two separate binding assays on isolated receptors were planned.

The ability of the new compounds to inhibit (IC_{50}) vitronectin binding to the isolated $\alpha_v\beta_3$ and $\alpha_v\beta_5$ receptors is shown in Table 2.4.5, compared also to other conjugated and unconjugated integrin ligands.

Table 2.4.5 - Inhibition of biotinylated vitronectin binding to $\alpha_v\beta_3$ and $\alpha_v\beta_5$ receptors.

Ligand	$\alpha_v\beta_3$ IC_{50} [nM][a]	$\alpha_v\beta_5$ IC_{50} [nM][a]
MA-RGD	50.2 ± 6.2	1700 ± 100
Ac-MA-RGD	97.5 ± 30.8	4100 ± 1800
c[DKP-3-RGD][b]	4.5 ± 1.1	149 ± 25
c[DKP-*f*3-RGD]-PTX[c]	5.2 ± 2.3	219 ± 124
c[DKP-RGD]-N-SMAC[d]	36.5 ± 0.6	1500 ± 700
c[RGDfV] [e]	3.2 ± 1.3	7.5 ± 4.8

[a] IC_{50} values were calculated as the concentration of compound required for 50% inhibition of biotinylated vitronectin binding as estimated by GraphPad Prism software; all values are the arithmetic mean ± SD of triplicate determinations; [b] see Chapter 1.2.2; [c] see Chapter 2.1.2; [d] see Chapter 2.2.2.1; [e] see Chapter 1.1.3.1

Although the affinity of **MA-RGD** and **Ac-MA-RGD** dual-action conjugates for the $\alpha_v\beta_3$ integrin receptor is reduced compared to the reference compounds **c[DKP-*f*3-RGD]** and **c[DKP-3-RGD]** and to other dual-action conjugates (**c[DKP-*f*3-RGD]-PTX** and **c[DKP-RGD]-N-SMAC**), their residual binding strength (still nanomolar !) is surely sufficient to target them towards integrin receptors. It was thought that the free ε-amino moiety present on Lys13 in the **MA-RGD** could have affected negatively the results, due to a destabilizing interaction of the positive charge on the electrostatic clamp that steers the RGD action mechanism. In order to avoid this problem, the **Ac-MA-RGD** conjugate was synthesized with the ε-amine acetylated: the lower IC_{50} values for **MA-RGD** indicates that, against our expectation, this positive charge does not affect the electrostatic clamp.

The chemiluminescent assays relying on competition between tested compounds and biotinylated $VEGF_{165}$ for binding to the extracellular domain of recombinant VEGFR-1 (isolated receptor D1–D7, full ECD) are still on-going. As a reference for these assays it will be possible to use the K_d value reported by D'Andrea and co-workers: they performed a NMR titration using the second domain of VEGFR-1 ($VEGFR\text{-}1_{D2}$) and the K_d of the MA/$VEGFR\text{-}1_{D2}$ complex was estimated to be in the micromolar range (≈46 ± 13 μM) after an analysis of the NMR titration curves of selected $VEGFR\text{-}1_{D2}$ residues.[72b]
We decided to test our compounds on the isolated VEGFR-1 through the competitive binding assay reported in Figure 2.4.15.[81] The compounds are tested for their ability to compete with biotinylated $VEGF_{165}$ ($btVEGF_{165}$), an endogenous ligand of VEGFR-1. The compound to test and $btVEGF_{165}$ are added to VEGFR-1 and left in incubation to allow equilibration. First Streptavidin-HRP (Horseradish Peroxidase) and then the substrate for HRP are added: the chemiluminescence deriving from the subsequent reaction is read. The competition between the tested compound and $btVEGF_{165}$ affects the chemiluminesce extent: less chemiluminescence is observed in the presence of a better VEGFR-1 ligand respect to $btVEGF_{165}$.

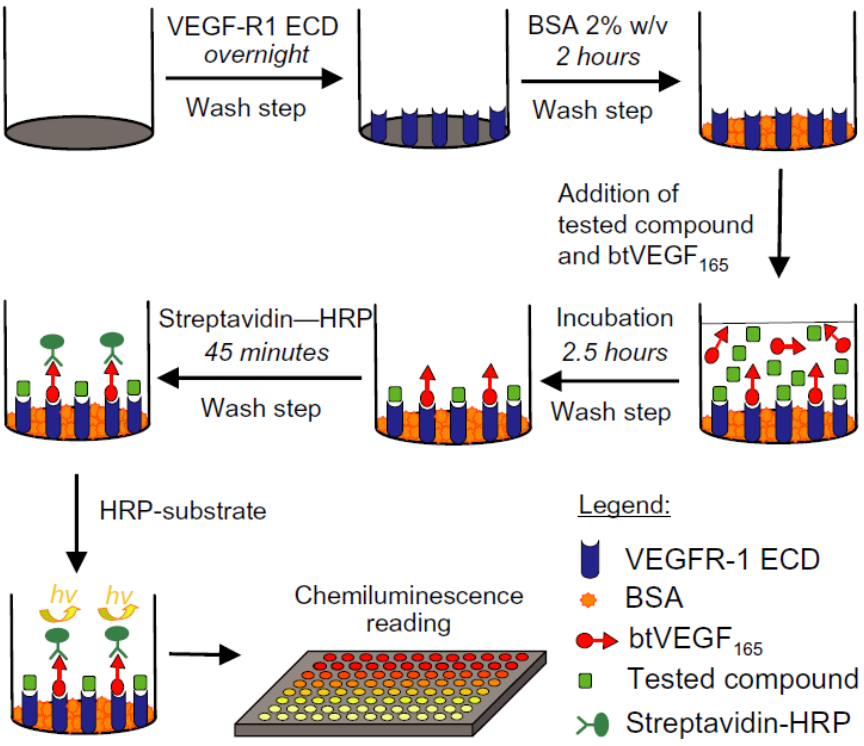

Figure 2.4.15 - In vitro binding assay on isolated VEGFR-1. This is a competition assay between the tested compound and biotynilated $VEGF_{165}$ ($btVEGF_{165}$) on the extracellular domain of recombinant VEGFR-1 (D1–D7 full ECD). The inhibition is read via chemiluminescence.

2.4.4 In vitro tube formation assays [82]

The synthesized compounds were tested for their capacity to block angiogenesis with *in vitro* morphogenesis assays. One of the most specific tests for angiogenesis is the measurement of the ability of endothelial cells to form three-dimensional structures (tube formation). Endothelial cells of all origins appear able to form tubules spontaneously, when enough time is left in order to allow the appropriate extracellular matrix components to lay down. Tube formation can be enhanced by use of collagen or fibrin clots to coat plastic culture dishes. Tube formation on these clots reflects the *in vivo* situation, and the formation of tight junctions can be confirmed by electron microscopy. With the discovery that Matrigel (a matrix-rich product prepared from Engelbreth–Holm–Swarm –EHS- tumour cells whose primary component is laminin) can evoke endothelial cell tube formation within 24 h, tube formation assays have achieved a prominent place in the array of angiogenesis measures (Figure 2.4.16). However, one word of caution is that cultured cells of non-endothelial origin, such as fibroblasts, may also exhibit a response to Matrigel. It is also critical to control the protein concentration of the Matrigel used, because not all commercial preparations of Matrigel promote tube formation *in vitro*.[83]

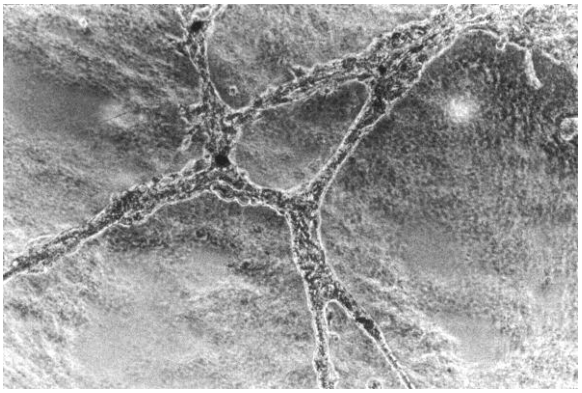

Figure 2.4.16 - Tube formation on Matrigel. Murine myocardium-derived endothelial cells were seeded on Matrigel. Tube formation was observed within 24 h.

The less the tube extent is formed, the more the anti-angiogenic activity of the tested compound is high. So, the quantification in this kind of assay is carried out by an operator, which counts manually the number of formed tubes, or by special software. The qualitative result is very easy to see and understand, evaluating the thickness of the tubes network. Figure 2.4.17 reports three pictures taken during the *in vitro* Matrigel assays of the tested compounds. In the picture on the left, where only VEGF was added, the three-dimensional network is clearly visible. In the central picture, also the **c[DKP-3-RGD]** and **Ac-MA** were added (co-administration) together with VEGF: the tube network is less developed with respect to the photo on the left. On the right the picture

corresponding to the addition of **Ac-MA-RGD** and VEGF to HUVE cells is reported: as in the central photo the network is poorly formed, qualitatively less than the other two assays.

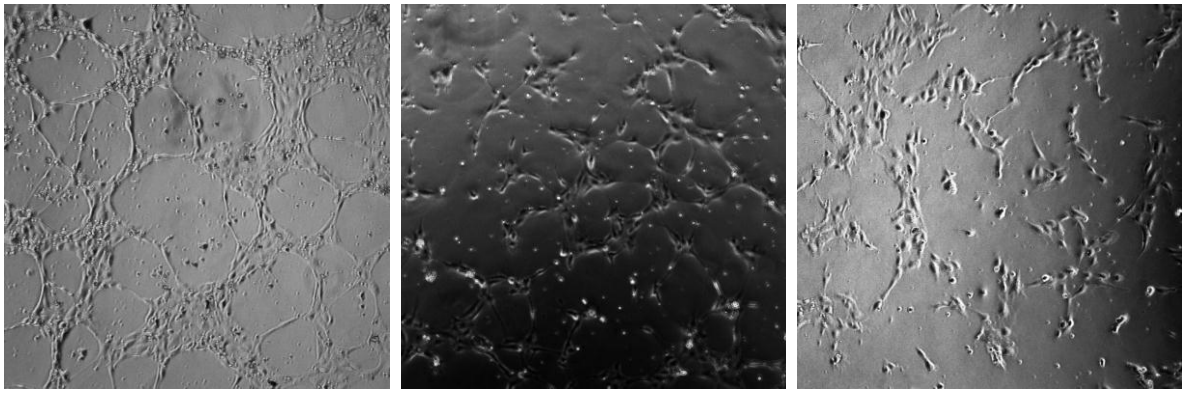

Figure 2.4.17 - In vitro Matrigel angiogenesis assays. On the left: HUVEC+VEGF (10^{-8} M). In the middle: HUVEC+VEGF (10^{-8} M) + **c[DKP-3-RGD]** (10^{-9} M) + **Ac-MA** (10^{-9} M). On the right: HUVEC+VEGF (10^{-8} M) + **Ac-MA-RGD** (10^{-9} M). To assess angiogenic activity, HUVEC 2.5x104 cells were seeded in a 24-well plate coated with 100 µL/well of BD-Matrigel previously polymerized for 1 h at 37 °C. Cells were treated with the reported compounds and incubated for 5 h at 37 °C in a moist atmosphere of 5% CO_2. Tube-like structure formation was evaluated by phase-contrast microscopy using a fluorescence microscope (Axiovert 40CFL, Carl Zeiss S.p.A. Milan, Italy). The total tube length (pixels) was quantified using Adobe Photoshop CS4 (Adobe).

In Figure 2.4.18, *in vitro* tube formation assay results are reported: all the tested compounds (**MA**, **Ac-MA**, **c[DKP-3-RGD]**, **Ac-MA-RGD**) showed a potent anti-angiogenic activity, giving comparable results in terms of total tubule length. HUVEC+BM (EndoGRO Basal Medium) was used as control. The assays on the **MA-RGD** compound are still on-going.

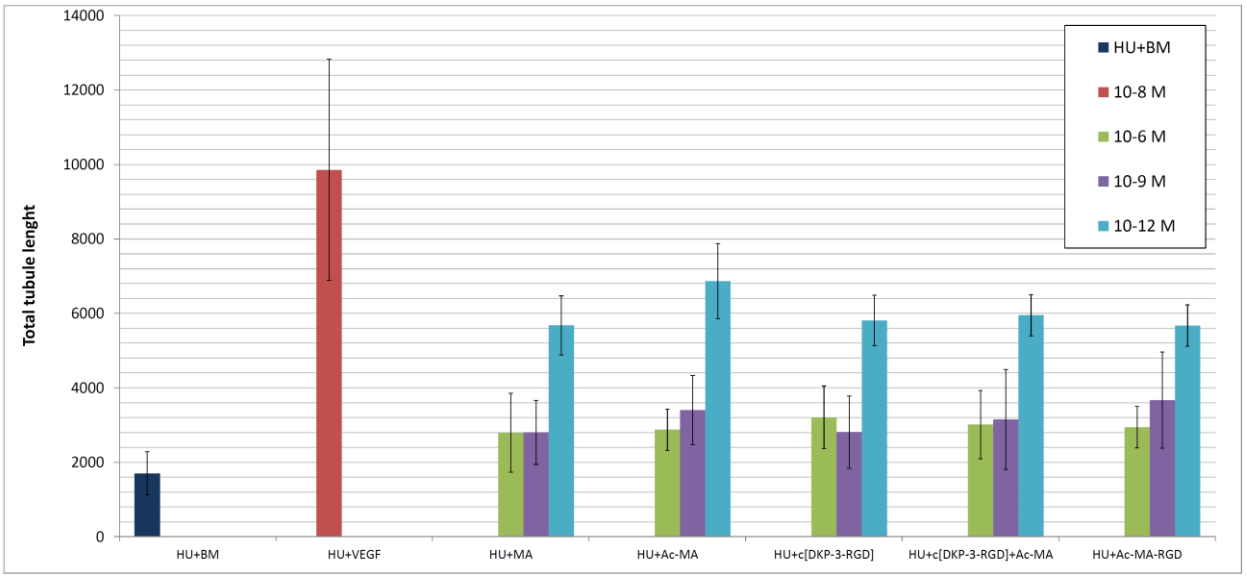

Figure 2.4.19 - In vitro angiogenesis assays on Matrigel. HUVEC+BM (EndoGRO Basal Medium) was taken as control. The assays on **MA-RGD** compound are still on-going.

These similar results underline a very complex angiogenesis regulation system in the examined cell biology. Indeed the integrin ligand **c[DKP-3-RGD]** showed a very high anti-angiogenic activity, as well as the **MA** peptide, known to be a potent VEGF antagonist and its derivative **Ac-MA**. The **c[DKP-3-RGD]** compound is an integrin ligand and it could block angiogenesis by a pathway involving also the VEGFR signalling system (see Paragraph 2.3.2). The dual action conjugate **Ac-MA-RGD** blocks angiogenesis with similar efficacy respect to: (i) the co-administered ligands **Ac-MA** and **c[DKP-3-RGD]**; (ii) the single administration of integrin ligand **c[DKP-3-RGD]** and VGFR ligand **Ac-MA**. Thus it appears that the covalently linked dual action conjugate **Ac-MA-RGD** could not improve, in this kind of assay, the anti-angiogenic effects of its precursors. Moreover, the marked anti-angiogenic activity of the integrin ligand **c[DKP-3-RGD]** was quite unexpected: this strong biological activity could be due to a $\alpha_V\beta_3$/VEGFR-1 cross-talk which disables the VEGFR signalling system when integrin receptors are blocked. It is noteworthy to say that, in *in vivo* experiments, Cilengitide, at very low concentrations (10^{-9} -10^{-10} M) exhibited a marked pro-angiogenic effect (see also Chapter 2.1.1).[12] In this kind of assay (*in vitro* Matrigel study), the integrin ligand **c[DKP-3-RGD]** showed always an anti-angiogenic effect (up to 10^{-12} M).

It is clear that further studies are necessary to have a more detailed picture of the behaviour of these integrin/VEGFR ligands .

2.5 Conclusions

In conclusion, I have started to explore two new classes of dual-action conjugates.

We reported the synthesis and biological characterization of a new class of dual-action SMAC/RGD conjugates, aiming at both targeting cell surface receptors overexpressed on tumor cells (integrins) and interfering with cellular proliferation through the action of a pro-apoptotic unit (SMAC mimetic). We have successfully confirmed their affinity for the molecular target of each monomeric unit ($\alpha_v\beta_3/\alpha_v\beta_5$ receptors and BIR domains), and we have ascertained that the moderate cytotoxicity of their monomeric precursors can be maintained, even if these results indicates that influences of linker composition, its steric hindrance and of overall physico-chemical (e.g., lipophilicity) and electronic properties (e.g., substituents on the SMAC mimetic unit) should be taken in account to develop potent cytotoxic SMAC-based dual-action conjugates. In addition, some preliminary results (e.g., the cytotoxic activity of one dual-action conjugate on IGROV-1 cells) indicate that the combination of a tumor targeting cyclic RGD unit with a pro-apoptotic SMAC mimetic unit may lead to synergistic anticancer effects.

The second class of dual-action conjugates targets simultaneously two different extracellular receptors (integrin $\alpha_v\beta_3$ and VEGFR), both involved, through a cross-talk mechanism, in tumor growth and angiogenesis. The synthesis of the two dual-action conjugates **MA-RGD** and **Ac-MA-RGD** was accomplished after the optimization of the CuAAC reaction on solid phase and in solution. The two final conjugates were characterized with mass spectrometry, and their secondary structures were investigated with circular dichroism spectroscopy: the biologically active α-helical conformation was maintained, despite the conjugation of the 15-mer peptides to the integrin ligand. The biological activities of both the two compounds were evaluated *in vitro* with binding assays on the isolated receptors $\alpha_v\beta_3/\alpha_v\beta_5$: the affinity for the integrin $\alpha_v\beta_3$ was maintained. The anti-angiogenic activity of these compounds and their precursors was tested *in vitro* with morphogenesis assays on Matrigel (HUVEC); similar results were obtained, underlining a very complex angiogenesis regulation system. $\alpha_v\beta_3$/VEGFR dual-action conjugates can be considered a promising tool to further elucidate the cross-talk regulation mechanism in the examined cell biology.

In summary, promising results were obtained in both cases, highlighting the potential of dual-action conjugates capable of tumor targeting or inhibiting two intertwined receptors at the same time.

References:

[1] H. J. Broxterman, J. Lankelma, K. Hoekman. *Drug Resist. Updates.* **2003**, *6*, 111-127.

[2] J. Siepmann, R. A. Siegel, M. J. Rathbone. Fundamentals and applications of controlled release drug delivery. Springer: New York, **2012**; pp 493-516.

[3] (a) T. Lammers, F. Kiessling, W. E. Hennink G. Storm. *J. Controlled Release* **2012**, *161*, 175-187. (b) F. Kratz, I. A. Müller, C. Ryppa, A. Warnecke. *ChemMedChem*. **2008**, *3*, 20–53.

[4] (a) P. S. Low. *Mol. Pharmacol.* **2007**, *4*, 629-630. (b) O. H. Aina, R. W. Liu; J. L. Sutcliffe, J. Marik, C. X. Pan, K. S. Lam. *Mol. Pharmacol*. **2007**, *4*, 631-651.

[5] X. Lu, D. Lu, M. Scully, V. Kakkar. *Perspect. Med. Chem.* **2008**, *2*, 57-73.

[6] R. O. Hynes. *Cell* **2002**, *110*, 673-687.

[7] (a) M. Shimaoka, T. A. Springer. *Nature Rev. Drug Discov*. **2003**, *2*, 703-716. (b) R. Rathinam, S. K. Alahari. *Cancer Metastasis Rev*. **2010**, *29*, 223–237.

[8] E. F. Plow, T. A. Haas, L. Zhang, J. Loftus, J. W. Smith. *J. Biol. Chem.* **2000**, *275*, 21785-21788.

[9] M. A. Dechantsreiter, E. Planker, B. Mathä, E. Lohof, G. Hölzemann, A. Jonczyk, S. L. Goodman, H. Kessler. *J. Med. Chem.* **1999**, *42*, 3033-3040.

[10] E. K. Gottschalk, H. Kessler. *Angew. Chem. Int. Ed.* **2002**, *41*, 3967-3774.

[11] Merck KGaA News Release, 25/02/2013.

[12] (a) A. R. Reynolds, I. R. Hart, A. R. Watson, J. C. Welti, R. G. Silva, S. D. Robinson, G. Da Violante, M. Gourlaouen, M. Salih, M. C. Jones, D. T. Jones, G. Saunders, V. Kostourou, F. Perron-Sierra, J. C. Norman, J. C. Tucker, K. M. Hodivala-Dilke. *Nat. Med.* **2009**, 15, 392-400. (b) S. M. Weis, D. G. Stupack, D. A. Cheresh. *Cancer Cell* **2009**, *15*, 359-361. (c) S. H. Shabbir, J. L. Eisenberg, M. Mrksich. *Angew. Chem. Int. Ed.* **2010**, *49*, 7706-7709. (d) S. D. Robinson, K. M. Hodivala-Dilke. *Curr. Opin. Cell Biol.* **2011**, *23*, 630-637.

[13] D. Cox, M. Brennan, N. Moran. *Nat. Rev. Drug Discov*. 2010, 9, 804–820

[14] K. Chen, X. Chen. *Theranostics* **2011**, *1*, 189-200.

[15] (a) W. Arap, R. Pasqualini, E. Ruoslahti. *Science* **1998**, *279*, 377–80. (b) J. W. Kim, H. S. Lee. *Int. J. Mol. Med.* **2004**,*14*, 529-535.

[16] P. De, N. Dey, B. Terakedis, P. L. Bergsagel, Z. H. Li, D. Mahadevan, J. R. Garlich, S. Trudel, M. T. Makale and D. L. Durden, *Cancer Chemother. Pharmacol.* **2013**, *71*, 867.

[17] D. J. Burkhart, B. T. Kalet, M. P. Coleman, G. C. Post and T. H. Koch, *Mol. Cancer Ther.* **2004**, *3*, 1593.

[18] (a) E. Ruoslahti, S. N. Bhatia, M. J. Sailor. *J. Cell Biol.* **2010**, *188*, 759–768. (b) R. Mahato, W. Tai, K. Cheng. *Adv. Drug Delivery. Rev.* **2011**, *63*, 659-670.

[19] (a) R. Colombo, M. Mingozzi, L. Belvisi, D. Arosio, U. Piarulli, N. Carenini, P. Perego, N. Zaffaroni, M. De Cesare, V. Castiglioni, E. Scanziani, C. Gennari, J. Med. Chem. 2012, 55, 10460−10474; (b) Gennari, C.; Belvisi, L.; Potenza, D.; Colombo, R.; Mingozzi, M.; Marchini, M.; Manzoni, L.; Arosio, D.; Perego, P. M. C.; Zaffaroni, N.; De Cesare, M.; Piarulli, U. Italian Patent - Application **31/01/2012**, N. MI2012A000121; PCT Int. Appl. IB2013/000116, **30/01/2013**.

[20] C. Burz, I. Berindana-Nagoe, O. Balacescu and A. Irimiu, *Acta Oncol.* **2009**, *48*, 811.

[21] A. Strasser, L. O'Connor and V. M. Dixit, *Annu. Rev. Biochem.* **2000**, *69*, 217.

[22] S. Fulda and K.M. Debatin, *Oncogenem* **2006**, *25*, 4798.

[23] T. J. Sayers, *Cancer Immunol. Immunother.* **2011**, *60*, 1173.

[24] S. Danson, E. Dean, C. Dive and M. Ranson, Curr. *Cancer Drug Targets* **2007**, *7*, 785.

[25] X. Wen, Z.-Q Lin, B. Liu and Y.-Q. Wei, *Cell Proliferation* **2012**, *45*, 217.

[26] C. Du, M. Fang, Y. Li and X. Wang, *Cell* **2000**, *102*, 33.

[27] A. M. Verhagen, P. G. Ekert, M. Pakusch, J. Silke, L. M. Connolly, G. E. Reid, R. L. Moritz, R. J. Simpson and D. L. Vaux, Cell **2000**, *102*, 43.

[28] S. M. Srinivasula, R. Hedge, A. Saleh, P. Datta, E. Shiozaki, J. Chai, A. R. Lee, P. D. Robbins and Y. Shi, *Nature* **2001**, *410*, 112.

[29] J. Chai, C. Du, J. W. Wu, S. Kyin, X. Wang and Y. Shi, *Nature* **2000**, *406*, 855.

[30] Z. Liu, C. Sun, E. T. Olejniczak, R. P. Meadows, S. F. Betz, T. Oost, J. Herrmann, J. C. Wu, S. W. Fesik, *Nature* **2000**, *408*, 1004.

[31] D. Potenza, L. Belvisi, F. Vasile, E. Moroni, F. Cossu and P. Seneci, *Org. Biomol. Chem.* **2012**, *10*, 3278.

[32] J. Chai, C. Du, J. W. Wu, S. Kyin, X. Wang and Y. Shi *Nature* **2000**, *406*, 855.

[33] S. J. Riedl, M. Renatus, R. Schwarzenbacher, Q. Zhou, C. Sun, S. W. Fesik, R. C. Liddington, G. S. Salvesen, *Cell* **2001**, *104*, 791.

[34] Z. Shi, Y. J. Liang, Z. S. Chen, X. H. Wang, Y. Ding, L. M. L. Chen, W. Fu, *Oncol. Rep.* **2007**, *17*, 969.

[35] Y. Mizutani, H. Nakanishi, Y. N. Li, H. Matsubara, K. Yamamoto, N. Sato, T. Shiraishi, T. Nakamura, K. Mikami, K. Okihara, N. Takaha, O. Ukimura, A. Kawauchi, N. Nonomura, B. Bonavida, T. Miki, *Int. J. Oncol.* **2007**, *30*, 919.

[36] M. Holcik, H. Gibson, R. G. Korneluk, *Apoptosis* **2001**, *6*, 253.

[37] J. A. Flygare, M. Beresini, N. Budha, H. Chan, I.T. Chan, S. Cheeti, F. Cohen, K. Deshayes, K. Doerner, S. G. Eckhardt, L. O. Elliott, B. Feng, M. C. Franklin, S. Frankovitz Reisner, L. Gazzard, J. Halladay, S. G. Hymowitz, H. La, P. LoRusso, B. Maurer, L. Murray, E. Plise, C. Quan, J.-P. Stephan, S. G. Young, J. Tom, V. Tsui, J. Um, E. Varfolomeev, D. Vucic, A. J. Wagner, H. J. A. Wallweber, L. Wang, J. Ware, Z. Wen, H. Wong, J. M. Wong, M. Wong, S. Wong, R. Yu, K. Zobel and W. J. Fairbrother, *J. Med. Chem.* **2012**, *55*, 4101.

[38] P. Seneci, A. Bianchi, C. Battaglia, L. Belvisi, M. Bolognesi, A. Caprini, F. Cossu, E. De Franco, M. De Matteo, D. Delia, C. Drago, A. Khaled, D. Lecis, L. Manzoni, M. Marizzoni, E. Mastrangelo, M. Milani, I. Motto, D. Potenza, V. Rizzo, F. Servida, E. Turlizzi, M. Varrone, F. Vasile and C. Scolastico, *Bioorg. Med. Chem.* **2009**, *17*, 5834.

[39] A. Bianchi, M. Ugazzi, L Ferrante, D. Lecis, C. Scavullo, E. Mastrangelo and P. Seneci, *Bioorg. Med. Chem. Lett.* **2012**, *22*, 2204.

[40] J. Lu, L. Bai, H. Sun, Z. Nikolovska-Coleska, D. McEachern, S. Qiu, R. S.; Miller, H. Yi, S. Shangary, Y. Sun, J. L. Meagher, J. A. Stuckey and S. Wang, *Cancer Res.* **2008**, *68*, 9384.

[41] L. Manzoni, L. Belvisi, A. Bianchi, A. Conti, C. Drago, M. de Matteo, L. Ferrante, E. Mastrangelo, P. Perego, D. Potenza, C. Scolastico, F. Servida, G. Timpano, F. Vasile, V. Rizzo and P. Seneci, *Bioorg. Med. Chem.* **2012**, *20*, 6687.

[42] D. Lecis, E. Mastrangelo, L. Belvisi, M. Bolognesi, M. Civera, F. Cossu, M. De Cesare, D. Delia, C. Drago, G. Manenti, L. Manzoni, M. Milani, E. Moroni, P. Perego, D. Potenza, V. Rizzo, C. Scavullo, C. Scolastico, F. Servida, F. Vasile and P. Seneci, *Bioorg. Med. Chem.* **2012**, *20*, 6709.

[43] P. Seneci, A. Bianchi, C. Battaglia, L. Belvisi, M. Bolognesi, A. Caprini, F. Cossu, E. De Franco, M. De Matteo, D. Delia, C. Drago, A. Khaled, D. Lecis, L. Manzoni, M. Marizzoni, E. Mastrangelo, M. Milani, I. Motto, D. Potenza, V. Rizzo, F. Servida, E. Turlizzi, M. Varrone, F. Vasile and C. Scolastico, *Bioorg. Med. Chem.* **2009**, *17*, 5834.

[44] D. Lecis, E. Mastrangelo, L. Belvisi, M. Bolognesi, M. Civera, F. Cossu, M. De Cesare, D. Delia, C. Drago, G. Manenti, L. Manzoni, M. Milani, E. Moroni, P. Perego, D. Potenza, V. Rizzo, C. Scavullo, C. Scolastico, F. Servida, F. Vasile and P. Seneci, *Bioorg. Med. Chem.* **2012**, *20*, 6709.

[45] E. Mastrangelo, F. Cossu, M. Milani, G. Sorrentino, D. Lecis, D. Delia, L. Manzoni, C. Drago, P. Seneci, C. Scolastico, V. Rizzo and M. Bolognesi, *J. Mol. Biol.* **2008**, *384*, 673.

[46] M. Couturier, J. L. Tucker, B. M. Andresen, P. Dubé, J. T. Negri *Org. Lett.* **2001** *3*, 465-467

[47] The isolated receptor (IAP) binding assays and the cytotoxicity experiments were carried out by Dr. Daniele Lecis from Fondazione IRCCS Istituto Nazionale dei Tumori, who I sincerely acknowledge for the kind collaboration.

[48] Z. Nikolovska-Coleska, R. Wang, X. Fang, H. Pan, Y. Tomita, P. Li, P. P. Roller, K. Krajewski, N. G. Saito, J. A. Stuckey and S. Wang, *Anal. Biochem.* **2004**, *332*, 261.

[49] Z. Nikolovska-Coleska, J. L. Meagher, S. Jiang, S. A. Kawamoto, W. Gao, H. Yi, D. Qin, P. P. Roller, J. A. Stuckey and S. Wang, *Anal. Biochem.* **2008**, *374*, 87.

[50] The isolated receptor binding assays in this section were carried out by Dr. Daniela Arosio from the CNR-ISTM, who I sincerely acknowledge for the kind collaboration.

[51] D. Alloatti, G. Giannini, L. Vesci, M. Castorina, C. Pisano, E. Badaloni, W. Cabri *Bioorg. Med. Chem. Lett.* **2012**, *22*, 6509–6512

[52] M. Pilkington-Miksa, D. Arosio, L. Battistini, L. Belvisi, M. De Matteo, F. Vasile, P. Burreddu, P. Carta, G. Rassu, P. Perego, N. Carenini, F. Zunino, M. De Cesare, V. Castiglioni, E. Scanziani, C. Scolastico, C. Casiraghi, F. Zanardi and L Manzoni, *Bioconjugate Chem.* **2012**, *23*, 1610.

[53] P. Seneci, unpublished data.

[54] A. K. Olsson, A. Dimberg, J. Kreuger, L. Claesson-Welsh, *Nat. Rev. Mol. Cell Biol.* **2006**, *7*, 359.

[55] K. Suto, Y. Yamazaki, T. Morita, H. Mizuno, *J. Biol. Chem.* **2005**, *280*, 2126–2131.

[56] H. Takahashi, M. Shibuya, *Clin. Sci.* **2005**, *109*, 227–241.

[57] Y. A. Muller, et al. *Proc. Natl Acad. Sci. USA* **1997**, *94*, 7192–7197.

[58] H. W. Christinger, G. Fuh, A. M. de Vos, C. Wiesmann, *J. Biol. Chem.* **2004**, *279*, 10382–10388.

[59] G.Fuh, B. Li, C. Crowley, B. Cunningham, J. A. Wells, *J. Biol. Chem.* **1998**, *273*, 11197–11204.

[60] D. C. Hughes, *J. Mol. Evol.* **2001**, *53*, 77–99.

[61] M. J.Shibuya, *Biochem.* **2013**, *153*, 13.

[62] N. Papo, A. P. Silverman, J. L. Lahti, J. R. Cochran, *PNAS* **2011**, *108*, 14067-14072.

[63] F. Musumeci, M. Radi, C. Brullo, S. Schenone, *J. Med. Chem.* **2012**, *55*, 10797−10822.

[64] S. Schenone, C. Brullo, M. Botta, *Curr. Med. Chem.* **2008**, *15*, 3113−3132.

[65] R. Roskoski, *Jr Biochem. Biophys. Res. Commun.* **2007**, *356*, 323−328.

[66] H. Y. Woo, J. Heo, *Exp. Opin. Pharmacother.* **2012**, *13*, 1059−1067.

[67] D. G. Udugamasooriya, S. P. Dineen, R. A. Brekken, T. Kodadek, *J. Am. Chem. Soc.* **2008**, *130*, 5744.

[68] M. I. García-Aranda, S. González-López,; C. M. Santiveri, N. Gagey-Eilstein, M. Reille-Seroussi, M. Martín-Martínez, N. Inguimbert, M. Vidal, M. T. García-López, M. A. Jiménez, R. González-Muñiza, M. Pérez de Vega, *J. Org. Biomol. Chem.* **2013**, *11*, 1896.

[69] L. Zilberberg, S. Shinkaruk, O. Lequin, B. Rousseau, M. Hagedorn, F. Costa, D. Caronzolo, M. Balke, X. Canron, O. Convert, G. Laïn, K. Gionnet, M. Gonçalvès, M. Bayle, L. Bello, G. Chassaing, G. Deleris, A. Bikfalvi, *J. Biol. Chem.* **2003**, *278*, 35564–35573.

[70] H. S. Haase, K. J. Peterson-Kaufman, S. K. Lan Levengood, J. W. Checco, W. L. Murphy, S. H. Gellman *J. Am. Chem. Soc.* **2012**, *134*, 7652−7655.

[71] L. D. D'Andrea, G. Iaccarino, R. Fattorusso, D. Sorriento, C. Carannante, D. Capasso, B. Trimarco, C. Pedone, *PNAS* **2005**, *102*, 14215.

[72] (a) A. Basile, A. Del Gatto, D. Diana, R. Di Stasi, A. Falco, M. Festa, A. Rosati, A. Barbieri, R. Franco, C. Arra, C. Pedone, R. Fattorusso, M. C. Turco, L. D. D'Andrea, *J. Med. Chem.* **2011**, *54*, 1391; (b) D. Diana, R. Di Stasi, L. De Rosa, C. Isernia, L. D'Andrea, R. Fattorusso, *J. Pept. Sci.* **2013**, *19*, 214.

[73] P. R. Somanath, N. L. Malinin, T. V. Byzova *Angiogenesis* **2009**, *12*, 177–185.

[74] J. S. Desgrosellier, D. A. Cheresh, *Nature Reviews Cancer* **2010**, *10*, 9.

[75] E. Borges, Y. Jan, E. Ruoslahti *J. Biol. Chem.* **2000,** *275*, 39867–39873.

[76] (a) S. De, J. Chen, N. V. Narizhneva, W. Heston, J. Brainard, E. H. Sage, T. V. Byzova *J. Biol. Chem.* **2003,** *278*, 39044–39050; (b) G. H. Mahabeleshwar, W. Feng, D. R. Phillips, T. V. Byzova *J. Exp. Med.* **2006,** *203*, 2495–2507; (c) G. H. Mahabeleshwar, W. Feng, K. Reddy, E. F. Plow, T. V. Byzova *Circ Res.* **2007**, *101*, 570-580; (d) G. H. Mahabeleshwar, J. Chen, W. Feng, P. R. Somanath, O. V. Razorenova, T. V. Byzova *Cell Cycle* **2008**, *7*, 335-347; (e) X. Z. West1, N. Meller, N. L. Malinin, L. Deshmukh, J. Meller, G. H. Mahabeleshwar, M. E. Weber, B. A. Kerr, O. Vinogradova, T. V. Byzova *PLOS One* **2012,** *7*, e31071.

[77] M. Meldal, C. W. Tornøe, *Chem. Rev.* **2008**, *108*, 2952.

[78] (a) R. I. Jølck, R. H. Berg, T. L. Andresen *Bioconjugate Chem.* **2010**, *21*, 807–810; (b) B. B. Metaferia, M. Rittler, J. S. Gheeya, A. Lee, H. Hempel, A. Plaza, W. G. Stetler-Stevenson, C. A. Bewley, J. Khan *Bioorg. & Med. Chem. Lett.* **2010**, *20*, 7337–7340.

[79] (a) S. Maggini, F. Girardi, K. Müller, R. Di Maggio, *J. App. Pol. Sci.* **2012**, *124*, 2110; (b) G. Eglinton, E. R. H. Jones, G. H. Mansfield, M. C. Whiting, *J. Chem. Soc.* **1954**, 3197.

[80] The circular dichroism analysis in this section was carried out by Prof. Fernando Formaggio and Dr. Marta De Zotti from University of Padua, who I sincerely acknowledge for the kind collaboration.

[81] V.Goncalves, B. Gautier, C. Garbay, M. Vidal, N. Inguimbert, *Anal. Biochem.* **2007**, *366*, 108.

[82] The in vitro tube formation assays in this section were carried out by Dr. Roberto Fanelli from University of Insubria, who I sincerely acknowledge for the kind collaboration.

[83] R. Auerbach, R. Lewis, B. Shinners, L. Kubai, N. Akhtar, *Clinical Chemistry* **2013**, *49*, 32.

3 Experimental Section

3.1 CHEMISTRY

3.1.1 - General remarks and procedures

MATERIALS AND METHODS: All manipulations requiring anhydrous conditions were carried out in flame-dried glassware, with magnetic stirring and under a nitrogen atmosphere. All commercially available reagents were used as received. Anhydrous solvents were purchased from commercial sources and withdrawn from the container by syringe, under a slight positive pressure of nitrogen. (*S*)-and-(*R*)-serine methyl ester hydrochloride,[1] (*S*)- and (*R*)-serine methyl ester hydrochloride,[2] (2*R*)- and (2*S*)-aspartic acid β-allyl ester hydrochloride,[3] *N*-(*tert*-butoxycarbonyl)-(2*R*)-aspartic acid β-allyl ester,3 (*S*)- and (*R*)-*N*-Boc-serine methyl ester,[4] (*S*)- and (*R*)-methyl 3-azido-2-(tert-butoxycarbonylamino)propanoate,[5] (*S*)- and (*R*)-3-azido-2-(tert-butoxycarbonylamino) propanoic acid,5 (*S*)- and (*R*)-dimethyl aspartate hydrochloride,[6] (*S*)- and (*R*)-*N*-benzyl-dimethyl aspartate,[7] γ-methyl glutamate hydrochloride,[8] *N*-Boc-glycine benzyl ester,[9] 4-((4-methoxy-2,3,6-trimethylphenylsulfonyl)aminomethyl)benzaldehyde **27**,[10] N_3-(3*R*,6*S*)-DKP-COOAllyl or N_3-(3*S*,6*R*)-DKP-COOAllyl,[11] **81**[12], **c[DKP-*f*3-RGD]**[10] were already synthesized in our laboratory or were prepared according to literature procedures and their analytical data were in agreement with those already published; **83** was kindly provided by Prof. P. Seneci and its synthesis was previously scaled up on 100g scale by Chorisis S.r.l. (Gerenzano, Italy). Reactions were monitored by analytical thin layer chromatography using 0.25 mm pre-coated silica gel glass plates (DURASIL-25 UV254) and compounds visualized using UV fluorescence, aqueous potassium permanganate or ninhydrin. Flash column chromatography was performed according to the method of Still and co-workers[13] using Chromagel 60 ACC (40-63 μm) silica gel. Melting points were obtained in an open capillary apparatus and are uncorrected. Infrared spectra were recorded on a standard FT-IR and peaks are reported in cm^{-}. Optical rotation values were measured on an automatic polarimeter with a 1 dm cell at the sodium D line and are given in units of 10^{-1} deg cm^2 g^{-1}.

NUCLEAR MAGNETIC RESONANCE (NMR)

^{1}H-NMR spectra were recorded on a spectrometer operating at 400.16 MHz. Proton chemical shifts are reported in ppm (δ) with the solvent reference relative to tetramethylsilane (TMS) employed as the internal standard. The following abbreviations are used to describe spin multiplicity: s = singlet, d = doublet, t = triplet, q = quartet, m = multiplet, br = broad signal, dd = doublet of doublet. ^{13}C-NMR spectra were recorded on a spectrometer operating at 100.63 MHz, with complete proton

decoupling. Carbon chemical shifts are reported in ppm (δ) relative to TMS with the respective solvent resonance as the internal standard.

HPLC PURIFICATION

The HPLC purifications were performed on a Dionex Ultimate 3000 instrument equipped with a Dionex RS Variable Wavelenght Detector (column: Atlantis® Prep T3 OBD™ 5 μm 19 x 100 mm). The crude reaction mixture was dissolved in H_2O or, if compounds were insoluble in water, adding first DMF, then diluting slowly with H_2O until reaching at least a 1:1 mixture DMF/H_2O (ultrasonic sonicator was used to assist the dissolution). The solution so obtained was filtered (polypropylene, 0.45 μm, 13 mm ø, PK/100) and injected in the HPLC, affording purified products.

HPLC ANALYSIS

Purity analysis for each of the compounds was carried out on a Waters Acquity™ UPLC-MS (ESI ion source) instrument (column: Waters Acquity™ UPLC HSS T3 2.1 x 50mm; C_{18} 1.8μm). All the described compounds showed a purity ≥ 98%, as determined by UPLC-MS (UV and MS detectors). Alternatively, purity analysis was carried on a Dionex Ultimate 3000 instrument equipped with a Dionex RS Variable Wavelenght detector (column: Atlantis® Prep T3 OBD™ 5 μm 19 x 100 mm). 1 mg of purified product was dissolved in 1 ml of H_2O and was injected using the same gradient used in the purification step. The analysis of the integrals and the relative percentage of purity was performed with the software Cromeleon 6.80 SR11 Build 3161. Each isolated product showed a purity ≥ 98%.

FREEZE-DRYING

Products were freeze-dried after HPLC purification. The desired compound was dissolved in a proper solvent (H_2O, H_2O + 0.1% TFA, glacial acetic acid or a mixture of them, on the base of product solubility), then it was frozen with dry ice for 1h and freeze-dried for 48 h at -50 °C and $5 \cdot 10^{-3}$ mbar, through the 5Pascal Lio5P DGT instrument.

MASS ANALYSIS

High resolution mass spectra (HRMS) were performed on a Fourier Transform Ion Cyclotron Resonance (FT-ICR) Mass Spectrometer APEX II & Xmass software (Bruker Daltonics) – 4.7 T Magnet (Magnex) equipped with ESI source, available at CIGA (Centro Interdipartimentale Grandi Apparecchiature) c/o Università degli Studi di Milano.

Low resolution mass spectra (MS) were measured on a Waters Acquity™ UPLC-MS (ESI ion source). Alternatively, ESI-MS spectra were recorded on the ion trap mass

spectrometer Finnigan LCQ Advantage analysing a solution H_2O/CH_3CN 1:1 + 0,1% TFA.

MALDI-TOF-MS spectra were recorded on the instrument Bruker Microflex™ LT, supporting the sample on the 2,5-dihydroxybenzoic acid (DHB), α-cyano-4-hydroxycinnamic acid (HCCA) and sinapinic acid (SIN) matrices. The peptide calibration standard (300-3000 Da range), which consisted of Angiotensin II, Angiotensin I, Substance P, Bombesin; ACTH clip 1-17, ACTH clip 18-39, Somatostatin 28, was purchased from Bruker Daltonics® and used to calibrate the MALDI-TOF-MS instrument. The sample was mixed in equal volumes with the matrix solution: a small amount (1 μL) of this mixture was spotted on the target surface. The target matrix was dried at room temperature and then analyzed.

GENERAL PROCEDURES FOR SOLUTION PHASE SYNTHESIS:

GENERAL PROCEDURE FOR Boc-DEPROTECTION REACTIONS:

GP1: To a solution of the *N*-Boc-protected amino acid or peptide in CH_2Cl_2 (0.13 M) was added half volume of TFA. The reaction mixture was stirred at for 2 h r.t. and then concentrated at reduced pressure. The excess TFA was azeotropically removed from the residue with toluene. Diethyl ether was added to the residue and the resulting suspension was evaporated under reduced pressure to afford the corresponding TFA salt.

GENERAL PROCEDURE FOR COUPLING REACTIONS:

GP2: To a solution of the *N*-protected amino acid in DMF, under nitrogen atmosphere and at 0 ºC, HATU (1.2 eq.), HOAt (1.2 eq.) and DIPEA (4 eq.) were added successively. After 30 min, a solution of the *N*-deprotected TFA salt of the peptide in DMF was added and the reaction mixture was stirred at 0 ºC for 1 h and at r.t. overnight. The mixture was afterwards diluted with EtOAc and consecutively washed with 1 M $KHSO_4$ (2×), aqueous $NaHCO_3$ (2×) and brine (2×), and dried over Na_2SO_4. Volatiles were evaporated under reduced pressure to afford the crude product.

GENERAL PROCEDURE FOR Cbz AND OBn HYDROGENOLYTIC CLEAVAGE:

GP3: protected compound (1 eq.) was dissolved in a mixture of THF/H_2O (1:1) and Pd/C 10% (0.1 eq.) was added. The reaction mixtures were subjected to three vacuum/hydrogen cycles and then left stirring overnight at room temperature under 1 bar of hydrogen. The mixture was filtered through Celite, and the cake thus obtained was washed thoroughly with THF/H_2O (1:1). The filtrate was concentrated and dried to give the crude product as white solid.

GENERAL PROCEDURE FOR MACROLACTAMIZATION:

GP4: to a 1.4 mM solution of deprotected linear compound (1 eq.) in DMF, under nitrogen atmosphere and at 0 ºC, HATU (4 eq.), HOAt (4 eq.) and DIPEA (6 eq.) were added successively. After stirring the reaction mixture at 0 ºC for 1 h, it was allowed to reach r.t., and stirred overnight. DMF was then removed under reduced pressure and the residue was purified by flash chromatography on silica gel to afford the product as white foam.

GENERAL PROCEDURE FOR Mtr AND O*t*Bu ESTER REMOVAL:

GP5: protected macrolactams was treated with TFA (0.01 M solution), in the presence of ion scavengers: thioanisole (5%), ethanedithiol (3%), anisole (2%). After TFA removal, under reduced pressure, the residue was dissolved in a 1:1 mixture of diisopropyl ether/water. Phases were separated and the aqueous layer was washed several times with diisopropyl ether. The aqueous phase was concentrated under reduced pressure to give the crude product, which was purified by HPLC to give the desired compound as white solid.

GENERAL PROCEDURES FOR MANUAL SPPS:

GENERAL PROCEDURE FOR CAPPING:

GP6: A 2 M solution of acetic anhydride in DMF was added to the previously washed peptidyl resin, and the reaction vessel was shaken for 20 min at room temperature. The solution was sucked away, and the resin was washed in the order with DMF (4x) and *i*PrOH (3x). Kaiser test was performed before proceeding to the next step.

GENERAL PROCEDURE FOR KAISER TEST:

GP7: Phenol (80% solution in ethanol), ninhydrin (6% solution in ethanol) and pyridine (two drops) were added to a small sample of the resin and then heated in a boiling water bath for 60 sec. If the color of the solution maintained yellow, quantitative coupling was achieved. In the case of a slight blue color, the coupling step was not fully completed and had to be repeated.

GENERAL PROCEDURES FOR Fmoc DEPROTECTION:

GP8: The washed and swollen resin was treated twice with a solution of piperidine (2%) and DBU (2%) in DMF (v/v) or with a solution of piperidine (20%) in DMF (v/v), for 5 min and 15 min respectively and then washed with DMF (5x), DCM (5x), and again DMF (4x).

GENERAL PROCEDURE FOR AZIDE REDUCTION:

GP9: Azidopeptidyl resin (1 eq.) was suspended in a 4:1 mixture of dioxane/water. Trimethylphosphine (1 M solution in toluene, 6 eq.) was added and the reaction vessel was shaken for 40 min. The resin was then washed with dioxane (3x).

GENERAL PROCEDURES FOR SEMI-AUTOMATIC SPPS:

The semi-automatic SPPS was accomplished through the Biotage® Initiator™ synthesizer, assisted by microwaves (MW) irradiations; Fmoc/*t*Bu strategy and Rink Amide MHBA Resin (100-200 mesh; loading: 0.5 mmol/g) were used. Each coupling step consisted in: (i) manual activation (solution phase) of the Fmoc-protected amino acid, (ii) addition of the activated amino acid to the resin in the synthesizer vial and perform the automated tasks (coupling reaction, capping, deprotection and washing).

SOLUTIONS AND SOLVENTS

In order to execute the programs set, the synthesizer required the following solutions: 25% Ac_2O in DMF (v/v) (capping solution), 25% piperidine in DMF (v/v) (deprotection solution), methanol (washing solvent) and DMF (washing solvent).

RESIN PREPARATION

The resin was weighted in a 10 ml Teflon-vial (Biotage) and processed with the swelling task and the swelling-Fmoc deprotection task. At the end of these operations the resin was ready for the SPPS.

ACTIVATION OF FMOC-AA-OH

To a solution of the desired Fmoc-AA-OH (0.4 mmol, 4.0 eq with respect to the resin [1 eq.]) in DMF (3.5 mL) DIC (63 μL, 0.4 mmol, 4.0 eq), HOAt (54.4 mg, 0.4 mmol, 4.0 eq) and DIPEA (139 μL, 0.8 mmol, 8.0 eq) were added at 0 °C, under stirring and inert atmosphere. After 25 min, the reaction mixture was added to the resin in the vial inside the synthesizer and a cycle of coupling-capping-deprotection-washing steps was effected. At the end of this cycle it is possible to add another residue or effect a capping-washing cycle if the peptide sequence was completed.

The Biotage® Initiator™ programs "Tasks" used for the semi-automatic SPPS are reported below. Each task can be modified in every of its parameters and it is performed under mechanical stirring at 1000 rpm.

SWELLING TASK

DMF (3.0 mL) was added to the resin: the swelling was accomplished at r.t. in 30 min. At the end of the swelling step, the vial was empty.

SWELLING-FMOC DEPROTECTION TASK

DMF (3.5 mL) was added to the resin and the swelling was performed at r.t. for 15 min. Then two deprotection steps [25% piperidine in DMF (3.0 mL for each step)] were carried out: the reaction was performed at r.t. under inert atmosphere for 5 min and 15 min for the first and the second deprotection step respectively. The resin was washed 8 times with DMF (3 mL × 30 s for every wash). At the end of each step, the vial was empty.

COUPLING-CAPPING-FMOC DEPROTECTION TASK

The activated Fmoc-AA was added to the resin inside the vial and the coupling reaction assisted by microwaves was carried out at 70 °C under inert atmosphere for 12 min. The beads were washed six times with DMF (2.5 mL × 20 s for every wash). The capping solution (3 mL) was added to the resin: the capping step was performed at r.t. under inert atmosphere for 15 min. The beads were washed six times with DMF (2.5 mL × 20 s for every wash). Two deprotection steps were carried out adding the deptotection solution (3.0 mL for each step) to the beads: the reaction was performed at r.t. under inert atmosphere for 5 min and 7 min for the first and the second deprotection step respectively. The beads were washed twice with DMF, MeOH, DMF, MeOH and DMF (3.0 mL × 20 s for every wash; 3.0 mL × 20 s for the last washes in MeOH and DMF). At the end of each step, the vial was empty.

COUPLING-CAPPING TASK

The activated Fmoc-AA was added to the beads and the coupling reaction assisted by microwaves was carried out at 70 °C under inert atmosphere for 12 min. The beads were washed six times with DMF (2.5 mL × 20 s for every wash). The capping solution (3 mL) was added to the resin: the capping step was performed at r.t. under inert atmosphere for 15 min. The beads were washed six times with DMF (2.5 mL × 20 s for every wash). The beads were washed twice with DMF, MeOH, DMF, MeOH (3.0 mL × 20 s for every wash). Eventually, the beads were washed eight times with DMF (3.0 mL × 30 s). At the end of each step, the vial was empty.

CAPPING TASK

The capping solution (3 mL) was added to the resin: the capping step was performed at r.t. under inert atmosphere for 15 min. The beads were washed six times with DMF (2.5 mL × 20 s for every wash). The beads were washed twice with DMF, MeOH, DMF (3.0 mL × 20 s for every wash). Eventually, the beads were washed twice with MeOH (3.0 mL × 30 s) and eight times with DMF (3.0 mL × 30 s). At the end of each step, the vial was empty.

RESIN STORAGE

The on bead-peptides were stored at 4 °C in a small volume of DMF, with the last amino acid of the sequence still Fmoc-protected. The next SPPS cycle restarted with a swelling-deprotection step before continuing the peptide sequence.

PEPTIDE CLEAVAGE

All the cleavage reactions from the resin were performed manually, under inert atmosphere and with mechanical stirring. Under stirring and inert atmosphere, in a round bottom flask the cleavage cocktail was prepared adding TIS (1%$_{v/v}$), EDT (2.5%$_{v/v}$), H_2O (2.5%$_{v/v}$) and TFA (94%$_{v/v}$) in a ratio of 3.0 mL of cleavage cocktail per 0.1 mmol of resin. The cleavage procedure was formed by three cleavage cycles. The on resin-peptide, stored in a vial, was swollen first with DMF (3.5 mL), then with DCM (3.5 mL). The resin was put under inert atmosphere and the cleavage cocktail (3.0 mL per 0.1 mmol of resin to treat) was added: the reaction was carried out at r.t. under mechanical stirring and inert atmosphere. After 1 h, the solution was filtered off under nitrogen flow and collected in a round bottom flask, where neat TFA (1.0 mL) used for washing the beads was collected too: the filtered mixture was then concentrated. Another aliquot of cleavage cocktail was added to the beads and the same procedure described above was accomplished: the cleavage was completed after three cycles. All the filtered, combined fractions were concentrated and poured into cold Et_2O, to provoke peptide precipitation. Ether was removed through suction-filtration with a syringe. The white solid so obtained was purified with RP-HPLC and freeze-dried.

3.1.2 - Synthesis of diketopiperazine (DKP) scaffolds

Preparation of hydrazoic acid

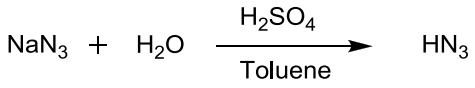

In a three-necked flask, NaN_3 (3 g) was dissolved in H_2O (3 mL). Once completely dissolved, toluene (20 mL) was added and the reaction mixture was cooled to 0 °C under vigorous stirring. Concentrated H_2SO_4 (1.2 mL) was added extremely slowly, so that the solution temperature did not exceed 10 °C. The reaction was stirred for one hour at 0 °C and then filtered on cotton wool. The residue was washed twice with toluene. The toluene solution was titrated by diluting 1 mL in distilled water (50 mL), and addition of NaOH (0.1 M) with phenolphthalein as indicator.

3.1.2.1 DKP-4, DKP-6

(*S*)-dimethyl 2-((*R*)-N-benzyl-3-tert-butoxy-2-(tert- butoxycarbonylamino) propanamido) succinate (30a)
(*R*)-dimethyl 2-((*S*)-N-benzyl-3-tert-butoxy-2-(tert- butoxycarbonylamino) propanamido) succinate (30b)

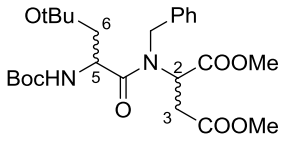

30a: 2*S*, 5*R*
30b: 2*R*, 5*S*

DCC (604 mg, 2.93 mmol, 1 eq.) was added to a solution of *N*-Boc-Ser(O*t*Bu)-OH (Fluorochem™) (1.53g, 5.86 mmol, 2 eq.) in 15 ml of CH_2Cl_2, in one portion. A white precipitate (DCU) formed and stirring continued for 1h at r.t.. The mixture was then filtered on a cotton wool to remove DCU. The white DCU residue was washed twice with cold CH_2Cl_2. The filtrate was concentrated under reduced pressure at r.t., and dried under high vacuum to afford symmetric anhydride as a white foam, which was used without further purification. *N*-Bn-Asp(OMe)-OMe **29** (515.4 mg, 2.05 mmol, 0.7 eq.) was dissolved in CH_2Cl_2 (15 ml) and at 0°C was added dropwise a solution of symmetric anhydride (1.5 g, 2.93 mmol , 1 eq.) in 20 ml of CH_2Cl_2. Reaction was left to warm to r.t. and stirred for 3 days. Then EtOAc was added (60 ml) and the solution was extracted with aqueous 1 M $KHSO_4$ (2x30 ml), aqueous $NaHCO_3$ (2x30 ml) and brine (1x30 ml), dried over Na_2SO_4, and volatiles were removed under reduced pressure. The

residue was purified by flash chromatography on silica gel (Petroleum ether/EtOAc, 7:3) to afford the desired product **30** as a transparent viscous oil (810 mg, 75% yield).
R_f = 0.40 (Hex/EtOAc, 7:3); ^{1}H NMR (400 MHz, CD_2Cl_2) (two rotamers) δ 7.48 – 7.18 (m, 5H), 5.27 (br, 1H), 4.95 (d, 1H, J = 16.7 Hz), 4.83 – 4.46 (m, 3H), 3.69 – 3.58 (m, 6H), 3.51 (d, 2H, J = 6.6 Hz), 3.27 (dd, 1H, J = 16.8, 8.1 Hz), 2.46 (dd, 1H, J = 16.7, 4.6 Hz), 1.46 (s, 9H), 1.20 (s, 9H); ^{13}C NMR (101 MHz, CD_2Cl_2) δ 172.1, 171.2, 170.1, 136.2, 128.6, 128.1, 127.8, 127.7, 127.4, 73.4, 62.9, 56.7, 52.4, 52.0, 51.6, 51.1, 34.3, 28.0, 27.1; MS (ESI) m/z calcd for $[C_{25}H_{39}N_2O_8]^+$: 495.27 $[M+H]^+$; found: 495.4.

OH-DKP-4-CO_2Me (31a);
OH-DKP-6-CO_2Me (31b)

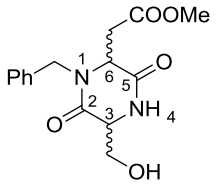

31a: 3*R*, 6*S*
31b: 3*S*, 6*R*

To a solution of **30** (179 mg, 0.36 mmol, 1 eq.) in CH_2Cl_2 (1.8 ml) was added trifluoroacetic acid (1.8 ml, 5 ml/mmol). The reaction mixture was stirred for 3 h at r.t. and then concentrated at reduced pressure. The excess of TFA was azeotropically removed from the residue with toluene. Diethyl ether was added to the residue and the resulting suspension was evaporated under reduced pressure to give the TFA salt of 17 as a white foamy solid in quantitative yield. The TFA salt was dissolved in MeOH (5 ml) and *i*Pr$_2$EtN (247 µl, 1.44 mmol, 4 eq.) was added at r.t. The reaction was stirred for 40 h at r.t., monitoring the formation of DKP by TLC (AcOEt/Hexane: 8/2). The solution was then concentrated under reduced pressure and the residue was purified by flash chromatography on silica gel (Petroleum ether/AcOEt, 75:25) to afford the desired product 18 as a transparent foam (93.7 mg, 85% yield).
R_f = 0.1 (AcOEt/Hexane: 8/2); ^{1}H NMR (400 MHz, CD_2Cl_2) δ 7.40 – 7.22 (m, 5H), 6.55 (br, 1H), 5.08 (d, J = 15.3 Hz, 1H), 4.38 (t, J = 5.2 Hz, 1H), 4.25 (d, J = 15.4 Hz, 1H), 4.10 (t, J = 3.9 Hz, 1H), 4.03 – 3.87 (m, 2H), 3.64 (s, 3H), 3.03 (dd, J = 17.3, 3.7 Hz, 1H), 2.99 – 2.92 (br, 1H), 2.85 (dd, J = 17.3, 5.1 Hz, 1H); ^{13}C NMR (101 MHz, CD_2Cl_2) δ 170.3, 167.5, 166.3, 135.7, 128.8, 127.8, 127.7, 56.0, 55.6, 52.0, 47.3, 34.8; ESI+: m/z calcd for $[C_{15}H_{19}N_2O_5]^+$: 307.13 $[M+H]^+$; found: 307.4.

_N_-benzyl-dimethyl aspartate (29) [6,7]

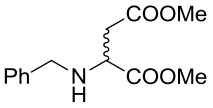

29a: (*S*)
29b: (*R*)

At 0 °C to 50 ml of anhydrous methanol, 3.75 ml (47.5 mmol) of thionly chloride was added dropwise. The solution was stirred at 0 °C for 30 min and then 6.332 g (47.5 mmol) of Asp was added. The reaction mixture was stirred at r.t. for 24 h and TLC (CH_3Cl/CH_3OH, 9:1) indicated complete disappearance of Asp. The reaction mixture was evaporated under reduced pressure and the residue was triturated with petroleum ether repeatedly to provide 7.495 mg (98%) of HCl·Asp-$(OCH_3)_2$ as a white solid which was directly used for the next reaction.

To a vigorously stirred solution of 500 mg (2.54 mmol) of dimethyl aspartate hydrochloride and 160 mg (2.54 mmol) of sodium cyanoborohydride in 12 ml of methanol at rt was added 265 mg (2.54 mmol) of benzaldehyde in one portion. After being stirred for 4 h, the mixture was cooled in an ice bath, and the pH was lowered to ca. 1 with 37% HCl. The mixture was then allowed to warm to r.t. for 2 h, and the methanol was removed under reduced pressure at r.t.. The white residue was dissolved into a minimum volume of water, and the pH was raised to ca. 10 with saturated aqueous Na_2CO_3. After three ethyl acetate extractions, combined organic portions were washed with brine, dried over Na_2CO_3, and evaporated to give **29** (425 mg, 67%) as a pale yellow oil.

Methyl 3-azido-2-(tert-butoxycarbonylamino)propanoate (35) [5]

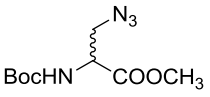

35a: (*S*)
35b: (*R*)

In a round bottom flask were solved (10.0 g, 64.3 mmol, 1 eq.) of serine methyl ester hydrochloride[1] in 232 mL of THF/water 1:1 solution. The reaction flask was lowered into an ice bath and 27 ml (193 mmol, 3 eq.) of triethylamine were added. Then, 16.8 g (77.1 mmol, 1.2 eq.) of Boc_2O were added and the reaction was stirred at room temperature for 24 h. The reaction mixture was then diluted with 200 ml of EtOAc and washed with aqueous $KHSO_4$ 1M until pH = 3 and brine. The organic phase was dried over Na_2SO_4, filtered and concentrated under reduced pressure. The product was then dried under high vacuum for a few hours affording 12.3 g (90 %) of pure Boc-Ser-OMe **34** as viscous transparent oil, which was used in the next step without purification.

To triphenyl phosphine (1.45 g, 5.54 mmol, 1.2 eq.) in THF (11 ml) at -78 °C was added DIAD (1 ml, 5.54 mmol, 1.2 eq.) in THF (10 ml) followed by the HN_3 solution (1.8 M in toluene, 3.1 ml, 5.54 mmol, 1.2 eq.) and Boc-serine methyl ester **34** (1.00 g, 4.62 mmol) in THF (10 ml). After the mixture stirred at -78 °C for 30 min and then allowed to slowly reach 0 °C (within 3 h). The solvent was evaporated and the residue was chromatographed with hexane/EtOAc 9:1 to provide 839 mg (74%) of the azide **35** as a mobile oil which crystallizes upon standing in the refrigerator.

3-azido-2-(tert-butoxycarbonylamino)propanoic acid (36) [5]

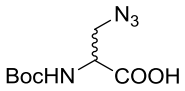

36a: (*S*)
36b: (*R*)

Compound **35** (350.0 mg, 1.433 mmol) dissolved in THF (6 ml) at 0 °C was treated with LiOH monohydrate (84.0 mg, 2.00 mmol) in water (4 ml). After 1 h, the mixture was concentrated, diluted with water, washed with ether, acidified with 1 M $KHSO_4$, and extracted into DCM, which was dried and evaporated to provide 329.2 mg (quant.) of a colorless oil.

(*R*)-dimethyl-2-((*S*)-3-azido-*N*-benzyl-2-(*tert*-butoxycarbonylamino)propanamido)succinate (38a);
(*S*)-dimethyl-2-((*R*)-3-azido-*N*-benzyl-2-(*tert*-butoxycarbonylamino)propanamido)succinate (38b)

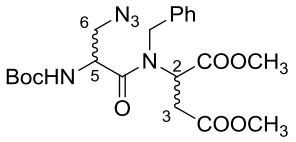

38a: 2*S*, 5*R*
38b: 2*R*, 5*S*

DCC (1.77 g, 8.56 mmol, 1 eq.) was added to a solution of *N*-Boc-Ser(N_3)-OH (**36**) (3.94g, 17.11 mmol, 2 eq.) 60 ml of CH_2Cl_2, in one portion. A white precipitate (DCU) formed and stirring continued for 1h at r.t.. The mixture was then filtered on a cotton wool to remove DCU. The white DCU residue was washed twice with cold CH_2Cl_2. The filtrate was concentrated under reduced pressure at r.t., and dried under high vacuum to afford symmetric anhydride **37** as a pale yellow foam, which was used without further purification. *N*-benzyl-aspartic acid dimethylester **29** (1.51 g, 6.01 mmol, 0.7 eq.) was dissolved in CH_2Cl_2 (50 ml) and the mixture was cooled to 0°C. To this mixture, a solution of symmetric anhydride in 50 ml of CH_2Cl_2 was then added dropwise, very slowly. The reaction mixture was let to reach r.t. and stirred overnight. The solvent was afterwards removed under reduced pressure and the residue was purified by flash

chromatography on silica gel (Hexane/EtOAc, 8:2) to afford the desired product **38** as a viscous transparent oil (2.22 g, 80%).

R_f = 0.37 (Hexane/EtOAc, 7:3); $[\alpha]_D^{20}$=-38.6 (**38a**, *c*=1.0 in $CHCl_3$); ^1H NMR (400 MHz, CD_2Cl_2) (rotamers ratio in CD_2Cl_2 A/B = 4:1) δ 7.51 – 7.11 (m, 5H), 5.61 – 5.50 (m, $1H_B$), 5.40 – 5.28 (m, $1H_B$, overlapping with solvent signal), 5.17 (t, $1H_B$, *J* = 7.1 Hz), 5.07 – 4.99 (m, $1H_B$), 4.86 – 4.69 (m, $3H_A$, $1H_B$), 4.54 – 4.38 (m, $1H_A$, $1H_B$), 3.74 (dd, $1H_B$, *J* = 12.3, 5.4 Hz), 3.69 – 3.65 (m, $3H_A$, $1H_B$), 3.63 (s, $3H_A$), 3.52 (dd, $1H_A$, *J* = 12.4, 6.3 Hz), 3.41 (dd, $1H_A$, *J* = 12.3, 6.0 Hz), 3.28 (dd, $1H_A$, *J* = 16.9, 7.4 Hz), 3.05 (dd, $1H_B$, *J* = 17.1, 7.0 Hz), 2.71 (dd, $1H_B$, *J* = 17.2, 7.3 Hz), 2.55 (dd, $1H_A$, *J* = 16.1, 6.1 Hz), 1.45 (s, 9H); ^{13}C NMR (101 MHz, CD_2Cl_2) δ 171.9, 171.3, 170.4, 155.5, 136.3, 129.5, 129.3, 129.2, 129.1, 129.0, 128.8, 128.2, 128.0, 127.9, 80.9, 58.0, 56.9, 56.6, 53.4, 53.1, 53.0, 52.6, 52.4, 51.4, 48.1, 35.3, 34.9, 28.6; IR (neat): ν_{max} 3343, 2979, 2953, 2106, 1739, 1712, 1651, 1497, 1438, 1367, 1289, 1250, 1166; MS (ESI) *m*/*z* calcd for $[C_{21}H_{29}N_5NaO_7]^+$: 486.20 $[M+Na]^+$; found: 486.3.

N_3-DKP-4-CO_2Me (39a);
N_3-DKP-6-CO_2Me (39b)

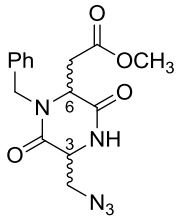

39a: (3*R*, 6*S*)
39b: (3*S*, 6*R*)

Dipeptide **38** (1.44 g, 3.11 mmol, 1 eq.) was deprotected according to general procedure **GP1**, with the addition of Et_3SiH (1.24 ml, 7.78 mmol, 2.5 eq.) as an ion scavenger. The corresponding trifluoroacetate salt was dissolved in *i*PrOH (40 ml) and *i*Pr_2EtN (2.13 ml, 12.44 mmol, 4 eq.) was added at r.t.. The reaction was stirred for 5 h at r.t., then the solution was concentrated under reduced pressure and the residue was purified by flash chromatography on silica gel (EtOAc/Hexane, 8:2) to afford the desired product as a white foam (927.4 mg, 90%).

R_f = 0.33 (Hexane/EtOAc 2:8); $[\alpha]_D^{20}$=+32.2 (**39a**, *c*=1 in $CHCl_3$); ^1H NMR (400 MHz, CD_2Cl_2) δ 7.45 – 7.24 (m, 5H), 6.83 (s, 1H), 5.13 (d, 1H, *J* = 15.3 Hz), 4.53 – 4.47 (m, 1H), 4.24 (d, 1H, *J* = 15.3 Hz), 4.12 (t, 1H, *J* = 4.7 Hz), 3.91 (dd, 1H, *J* = 12.5, 5.8 Hz), 3.85 (dd, 1H, *J* = 12.5, 3.6 Hz), 3.65 (s, 3H), 3.07 (dd, 1H, *J* = 17.5, 3.3 Hz), 2.88 (dd, 1H, *J* = 17.5, 5.0 Hz); ^{13}C NMR (101 MHz, CD_2Cl_2) δ 170.4, 167.6, 164.5, 135.6, 128.9, 127.9, 127.8, 56.0, 54.3, 52.0, 47.4, 34.6; IR (neat): ν_{max} 3249, 3066, 3030, 3007, 2953, 2924, 2852, 2362, 2342, 2117, 1736, 1558, 1496, 1449, 1372, 1332, 1281, 1204, 1180, 1138; MS (ESI) *m*/*z* calcd for $[C_{15}H_{18}N_5O_4]^+$: 332.14 $[M+H]^+$; found: 332.3.

NH_2-DKP-4-CO_2Me (40a);
NH_2-DKP-6-CO_2Me (40b)

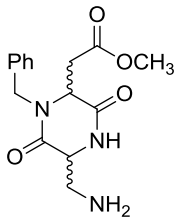

40a: (3*R*,6*S*)
40b: (3*S*,6*R*)

Compound **39** (737 mg, 2.22 mmol, 1 eq.) was dissolved in THF (45 ml) and Pd/C (237 mg, 0.22 mmol, 0.1 eq.) was added. The flask was thoroughly purged with H_2, and the system was closed. The reaction mixture was stirred at r.t. for 4 h, and then filtered through a Celite pad. The cake thus obtained was washed thoroughly with THF. The filtrate was concentrated and dried to give the crude product as a transparent paste (643.9 mg, 95%) which was used without further purification.
R_f = 0.13 (CH_2Cl_2/MeOH 95:5); $[\alpha]_D^{20}$=+83.2 (**40a**, *c*=1 in $CHCl_3$); ^{1}H NMR (400 MHz, CD_2Cl_2) δ 7.30 – 7.09 (m, 5H), 6.75 (br s, 1H), 4.99 (d, 1H, *J* = 15.3 Hz), 4.15 – 4.04 (m, 2H), 4.00 (br s, 1H), 3.53 (s, 3H), 3.18 (dd, 1H, *J* = 13.1, 3.6 Hz), 2.99 – 2.84 (m, 2H), 2.73 (dd, 1H, *J* = 17.0, 5.1 Hz), 1.33 (s, 2H); ^{13}C NMR (101 MHz, CD_2Cl_2) δ 170.3, 167.4, 166.2, 136.1, 128.8, 127.7, 56.3, 55.9, 51.9, 47.2, 44.2, 35.0; IR (neat): ν_{max} 1736, 1685, 1659, 1496, 1449, 1371, 1318, 1254, 1203, 1179, 1109; MS (ESI) *m*/*z* calcd for $[C_{15}H_{20}N_3O_4]^+$: 306.14 $[M+H]^+$; found: 306.3.

NHBoc-DKP-4-CO_2Me (41a);
NHBoc-DKP-6-CO_2Me (41b)

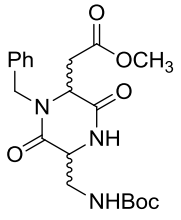

41a: (3*R*,6*S*)
41b: (3*S*,6*R*)

To a solution of **40** (586 mg, 1.92 mmol, 1 eq.) in THF (35 ml), Boc_2O (461 mg, 2.11 mmol, 1.1 eq.) was added in one portion. After stirring the mixture at r. t. overnight, EtOAc (60 ml) was added. The solution was washed with 1 M $KHSO_4$ (4x) and brine (1x). The organic phase was dried over Na_2SO_4 and volatiles were removed under reduced pressure, to afford the desired product as a white foam (739.5 mg, 95%), which was used without further purification.

R_f = 0.23 (EtOAc/Hex 7:3); $[\alpha]_D^{20}$ =+82.2 (**41a**, *c*=1 in $CHCl_3$); ^1H NMR (400 MHz, CD_2Cl_2) δ 7.33 – 7.06 (m, 5H), 6.69 (br s, 1H), 5.12 (br s, 1H), 4.96 (d, 1H, *J* = 15.2 Hz), 4.26 (s, 1H), 4.14 (d, 1H, *J* = 15.3 Hz), 4.00 (s, 1H), 3.68 – 3.57 (m, 3H), 3.56 – 3.45 (m, 4H), 2.86 (d, 1H, *J* = 16.9 Hz), 2.72 (dd, 1H, *J* = 17.1, 4.9 Hz), 1.35 (s, 9H); ^{13}C NMR (101 MHz, CD_2Cl_2) δ 170.3, 167.3, 166.0, 146.7, 135.9, 128.8, 127.8, 127.6, 79.9, 56.6, 55.9, 51.9, 47.7, 42.2, 35.1, 28.0; IR (neat): ν_{max} 3328, 3004, 2979, 2953, 2934, 1809, 1737, 1690, 1586, 1508, 1497, 1450, 1393, 1368, 1333, 1250, 1208, 1168, 1119; MS (ESI) *m*/*z* calcd for $[C_{20}H_{28}N_3O_6]^+$: 406.20 $[M+H]^+$; found: 406.3.

NHBoc-DKP-4-COOH (DKP-4);
NHBoc-DKP-6-COOH (DKP-6)

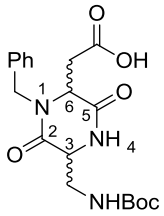

DKP-4: (3*R*,6*S*)
DKP-6: (3*S*,6*R*)

Compound **41** (710 mg, 1.75 mmol, 1 eq.) was dissolved in THF (60 ml) and the mixture was cooled to 0 °C. A solution of $LiOH{\cdot}H_2O$ (183.7 mg, 4.38 mmol, 2.5 eq.) in H_2O (30 ml) was added dropwise. The resulting solution was let reacting for 1 h at 0 °C. Then, maintaining the temperature at 0 °C, the mixture was acidified with HCl 1M to pH = 1-2, and extracted with CH_2Cl_2 (4x). The collected organic phases were dried over Na_2SO_4 and volatiles removed under reduced pressure. Either **DKP-4** or **DKP-6** were afforded as a white foam (685 mg, 100%), which was used in subsequent steps without further purification.

3.1.2.2 DKP-f4, DKP-f6

(*S*)-dimethyl-2-(4-((4-methoxy-2,3,6-trimethylphenylsulfonamido)methyl)benzylamino) succinate 109
(*R*)-dimethyl-2-(4-((4-methoxy-2,3,6-trimethylphenylsulfonamido)methyl)benzylamino) succinate 110

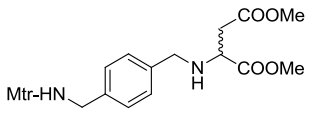

42a: (*S*)
42b: (*R*)

To a vigorously stirred solution of (*S*)- or (*R*)-dimethylaspartate hydrochloride (490 mg, 2.5 mmol, 1 equiv) and sodium cyanoborohydride (160 mg, 2.5 mmol, 1 equiv) in methanol (12 mL), aldehyde **27**[10] (870 mg, 2.5 mmol, 1 equiv) was added in one portion at rt under N_2. After being stirred for 4 h, the mixture was cooled to 0 °C and the pH was lowered to approximately 1 with a few drops of 37% aqueous HCl (v/v). The mixture was allowed to warm and stirred at rt for 2 h. The solvent was removed under reduced pressure at rt, the residue was suspended in a small volume of water and the pH was adjusted to 7 with an aqueous $NaHCO_3$ solution. AcOEt was added and the mixture was stirred for a few minutes. Then, the emulsion was filtered over a small pad of celite to afford a separable mixture. The aqueous phase was extracted 3 times with AcOEt and the organic phases were collected, dried with Na_2SO_4 and the solvent was evaporated to afford a clear oil.

This oil was dissolved in THF (50 mL) and treated with an excess of activated MnO_2: in this way, the small amount (ca. 10%) of benzyl-alcoholic byproduct [*i.e. N*-(4-(hydroxymethyl)benzyl)-4-methoxy-2,3,6-trimethylbenzenesulfonamide] was re-oxidized to aldehyde **27**, which is less polar with respect to the alcohol (which co-eluted with the desired product). The mixture was stirred for 4 h, filtered over a pad of celite and the solvent was evaporated under reduced pressure. The brown oil was purified by column chromatography on silica gel (Hexane/AcOEt, 1:1) to afford the desired product **42** as a viscous transparent oil (800 mg, 66% yield).

R_f = 0.45 (Hexane/AcOEt, 1:1); $[\alpha]_D^{20}$ = -20.5 (**42a,** *c*=1.0 in CH_3OH); ^{1}H NMR (400 MHz, CD_2Cl_2) δ 7.18 (AB system, 4H), 6.66 (s, 1H), 4.88 (t, 1H, *J* = 5.6 Hz), 4.06 (d, 2H, *J* = 6.3 Hz), 3.90 (s, 3H), 3.85 (d, 1H, *J* = 13.9 Hz), 3.75 (s, 3H), 3.69-3.61 (m, 5H), 2.77-2.64 (m, 5H), 2.56 (s, 3H), 2.16 (s, 3H); ^{13}C NMR (101 MHz, CD_2Cl_2) δ 174.2, 171.5, 159.7, 139.9, 139.2, 139.0, 135.9, 129.2, 128.6, 128.2, 125.6, 112.5, 57.4, 55.9, 52.3, 52.0, 51.8, 46.9, 38.3, 24.4, 18.1, 12.1; IR (film) 3356, 2940, 2847, 1736, 1585, 1562, 1308, 1141 cm^{-1}; MS (ESI) *m*/*z* calcd for. $[C_{24}H_{33}N_2O_7S]^+$: 493.20 $[M+H]^+$; found: 493.2.

(*S*)-dimethyl-2-((*R*)-3-azido-2-(*tert*-butoxycarbonylamino)-*N*-(4-((4-methoxy-2,3,6-trimethylphenylsulfonamido)methyl)benzyl)propanamido)succinate (43a);
(*R*)-dimethyl-2-((*S*)-3-azido-2-(*tert*-butoxycarbonylamino)-*N*-(4-((4-methoxy-2,3,6-trimethylphenylsulfonamido)methyl)benzyl)propanamido)succinate (43b)

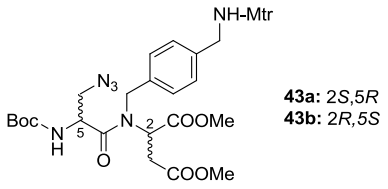

43a: 2*S*,5*R*
43b: 2*R*,5*S*

(*S*)- or (*R*)-3-azido-2-(*tert*-butoxycarbonylamino) propanoic acid **36** (1.84 g, 8.0 mmol, 5 equiv) was dissolved in CH_2Cl_2 (12 ml) and then DCC (826 g, 4 mmol, 2.5 equiv) was added in one portion. A white precipitate (DCU) was formed and stirring was continued for 1h at rt. The mixture was then filtered on cotton funnel to remove DCU, which was washed with cold CH_2Cl_2. The filtrate and the washings were concentrated under reduced pressure at rt, to afford symmetric anhydride **37** as a pale yellow foam, which was immediately used without further purification.

(*S*)- or (*R*)-*N*-(*N*-Mtr-aminomethylbenzyl)-Asp(OMe)-OMe **42** (780 mg, 1.59 mmol, 1 equiv) was dissolved in CH_2Cl_2 (12 ml) and cooled to 0 °C. A solution of symmetric anhydride in CH_2Cl_2 (8 ml) was added dropwise and very slowly. The reaction was warmed up to rt and stirred overnight. Then solvent was removed under reduced pressure and the residue was purified by flash chromatography on silica gel (Hexane/AcOEt, 6:4) to afford the desired product **43** as a viscous transparent oil (440 mg, 40% yield).

R_f = 0.43 (Hex/AcOEt 1:1); $[\alpha]_D^{20}$ = -31.6 (**43a,** *c*=0.5 in CH_2Cl_2); ^{1}H NMR (400 MHz, CD_2Cl_2) (rotamers ratio in CD_2Cl_2 A/B = 4:1) δ 7.34 – 7.17 (m, 4H$_A$), 7.12 – 7.01 (m, 4H$_B$), 6.66 – 6.60 (m, 1H$_A$ + 1H$_B$), 5.49 (d, 1H$_B$, *J* = 8.2 Hz), 5.26 (d, 1H$_A$, *J* = 8.5 Hz), 5.14 – 5.07 (m, 1H$_B$), 4.99 – 4.92 (m, 1H$_B$), 4.78 (t, 1H$_A$, *J* = 6.3 Hz), 4.74 – 4.60 (m, 3H$_A$ + 1H$_B$), 4.36 (t, 1H$_A$, *J* = 6.4 Hz), 4.29 (d, 1H$_B$, *J* = 15.9 Hz), 4.05 – 3.96 (m, 2H$_A$ + 2H$_B$), 3.85 (s, 3H$_A$ + 3H$_B$), 3.71 – 3.53 (m, 6H$_A$ + 8H$_B$), 3.45 (dd, 1H$_A$, *J* = 12.3, 6.3 Hz), 3.34 (dd, 1H$_A$, *J* = 12.3, 6.1 Hz), 3.22 (dd, 1H$_A$, *J* = 16.9, 7.3 Hz), 2.98 (dd, 1H$_B$, *J* = 17.3, 7.0 Hz), 2.72 – 2.61 (m, 3H$_A$ + 4H$_B$), 2.60 – 2.45 (m, 4H$_A$ + 3H$_B$), 2.14 (s, 3H$_A$ + 3H$_B$), 1.50 – 1.35 (m, 9H$_A$ + 9H$_B$); ^{13}C NMR (101 MHz, CD_2Cl_2) δ 171.6, 171.0, 170.0, 159.8, 155.2, 139.3, 139.0, 137.3, 135.6, 129.4, 128.8, 128.2, 127.8, 125.7, 112.5, 80.7, 57.8, 56.7, 55.9, 53.1, 52.8, 52.4, 52.2, 51.1, 50.7, 47.5, 46.7, 35.0, 34.6, 28.3, 24.4, 18.1, 12.1; IR (film) 3301, 2933, 2112, 1736, 1691, 1670, 1585, 1561, 1307, 1140 cm^{-1}; MS (ESI) m/z calcd for $[C_{32}H_{45}N_6O_{10}S]^+$: 705.29 $[M+H]^+$; found: 705.4.

N$_3$-DKP-*f*4-COOMe (44a)
N$_3$-DKP-*f*6-COOMe (44b)

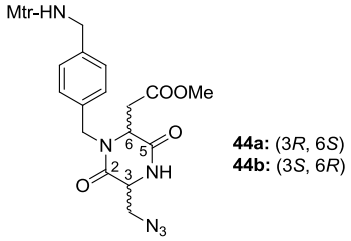

Dipeptide-N$_3$ **43** (400 mg, 0.57 mmol, 1 equiv) was deprotected according to general procedure **GP1**, with the addition of Et$_3$SiH (0.23 ml, 1.43 mmol, 2.5 equiv) as ion

scavenger. The corresponding trifluoroacetate salt was dissolved in *i*PrOH (8 ml) and *i*Pr$_2$EtN (0.4 ml, 2.28 mmol, 4 equiv) was added at rt. The reaction was stirred for 5 h at rt, then the solution was concentrated under reduced pressure and the residue was purified by flash chromatography on silica gel (AcOEt/Hexane, 8:2) to afford the desired product **44** as a white foam (300 mg, 92% yield).

R_f = 0.49 (AcOEt); $[\alpha]_D^{20}$ = +15.6 (**44a**, *c*=0.5 in CH_2Cl_2); ^{1}H NMR (400 MHz, CD_2Cl_2) δ 7.17 – 7.10 (m, 4H), 6.62 (s, 1H), 6.59 (s, 1H), 5.08 (d, 1H, *J* = 15.3 Hz), 4.92 (t, 1H, *J* = 6.3 Hz), 4.46 – 4.40 (m, 1H), 4.08 (d, 1H, *J* = 15.3 Hz), 4.04 – 3.97 (m, 3H), 3.90 – 3.82 (m, 4H), 3.79 (dd, 1H, *J* = 12.6, 3.5 Hz), 3.60 (s, 3H), 3.00 (dd, 1H, *J* = 17.5, 3.4 Hz), 2.80 (dd, 1H, *J* = 17.5, 5.0 Hz), 2.64 (s, 3H), 2.52 (s, 3H), 2.12 (s, 3H); ^{13}C NMR (101 MHz, CD_2Cl_2) δ 170.7, 167.7, 164.9, 159.8, 139.3, 139.0, 137.1, 135.5, 128.8, 128.3, 125.7, 112.5, 56.2, 55.9, 54.6, 53.7, 52.4, 47.3, 46.7, 34.9, 24.4, 18.1, 12.1; IR (film) 3265, 2933, 2110, 1735, 1690, 1671, 1586, 1559, 1308, 1141 cm^{-1}; MS (ESI) m/z calcd for $[C_{26}H_{33}N_6O_7S]^+$: 573.21 $[M+H]^+$; found: 573.5.

Boc-DKP-*f*4-COOMe (45a)
Boc-DKP-*f*6-COOMe (45b)

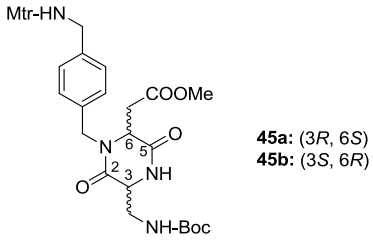

45a: (3*R*, 6*S*)
45b: (3*S*, 6*R*)

A solution of azide **44** (300 mg, 0.52 mmol, 1 equiv) in THF (45 ml) was treated with 10% Pd/C (56 mg, 0.052 mmol, 0.1 equiv), and the flask was purged three times with vacuum/H_2. The mixture was stirred at rt for 4 h under H_2 atmosphere, then filtered through a pad of Celite and the Celite cake was washed thoroughly with THF. The solvent was removed under vacuum to give the crude amine as a white foam (280 mg, 99% yield), which was used without further purification.

To a solution of the crude amine (280 mg, 0.52 mmol, 1 equiv) in DCM (40 ml) at 0 °C, *i*-Pr$_2$NEt (0.17 ml, 1.0 mmol, 2 equiv) and Boc$_2$O (132 mg, 0.6 mmol, 1.2 equiv) were added. The mixture was stirred at rt for 6 h, the solvent was evaporated and the crude compound was purified over a small pad of silica gel with AcOEt as eluent, to afford the desired product **45** as a white foam (320 mg, 96% yield).

R_f = 0.59 (AcOEt); $[\alpha]_D^{20}$ =+60.0 (**45a,** *c*=1.00 in CH_2Cl_2); ^{1}H NMR (400 MHz, CD_2Cl_2) δ 7.17 – 7.06 (m, 5H), 6.62 (s, 1H), 5.39 (t, 1H, *J* = 6.0 Hz), 5.27 (t, 1H, *J* = 5.9 Hz), 4.97 (d, 1H, *J* = 15.3 Hz), 4.29 (t, 1H, *J* = 4.4 Hz), 4.14 (d, 1H, *J* = 15.3 Hz), 4.03 – 3.96 (m, 3H, *J* = 6.1 Hz), 3.85 (s, 3H), 3.66 (ddd, 1H, *J* = 14.2, 6.6, 4.3 Hz), 3.59 (s, 3H), 3.57 – 3.48 (m, 1H), 2.92 (dd,

1H, *J* = 17.1, 4.1 Hz), 2.76 (dd, 1H, *J* = 17.1, 5.1 Hz), 2.63 (s, 3H), 2.52 (s, 3H), 2.11 (s, 3H), 1.41 (s, 9H); ^{13}C NMR (101 MHz, CD_2Cl_2) δ 170.7, 167.8, 166.5, 159.7, 157.2, 139.3, 139.1, 137.1, 135.7, 128.7, 128.1, 125.6, 112.5, 80.1, 56.8, 56.0, 55.9, 52.4, 47.6, 46.6, 42.7, 35.3, 28.4, 24.4, 18.1, 12.1; IR (film) 3340, 2971, 2937, 1741, 1681, 1650, 1586, 1554, 1455, 1307, 1141 cm^{-1}; MS (ESI) m/z calcd for $[C_{31}H_{43}N_4O_9S]^+$: 647.27 $[M+H]^+$; found: 647.4

Boc-DKP-*f*4-COOH (DKP-*f*4)
Boc-DKP-*f*6-COOH (DKP-*f*6)

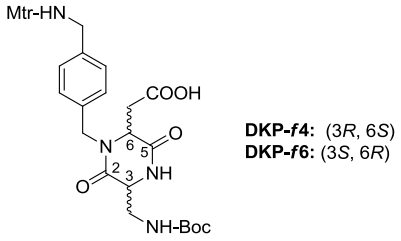

A solution of compound **45** (320 mg, 0.5 mmol, 1 equiv) in THF (20 mL) was cooled to 0 °C and treated dropwise with a solution of $LiOH{\cdot}H_2O$ (52 mg, 1.24 mmol, 2.5 equiv) in H_2O (10 mL). The resulting solution was stirred for 1 h at 0 °C, then acidified with a 1M $KHSO_4$ solution to pH 1-2. The mixture was extracted with CH_2Cl_2 (4x), and the collected organic extracts were dried over Na_2SO_4 and evaporated under reduced pressure, to afford **DKP-*f*4** or **DKP-*f*6** as a white foam (310 mg, 100% yield), which was used without further purification.

3.1.2.3 DKP-5, DKP-7

N_3-DKP-5-CO_2Me (46a);
N_3-DKP-7-CO_2Me (46b)

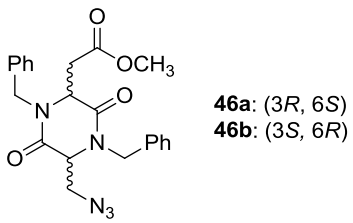

A flame-dried flask under N_2 was charged with a solution of **39** (640 mg, 1.93 mmol, 1 eq.) in dry THF (32 ml). The temperature was lowered to -78°C and KHMDS (4.25 ml of a 0.5 M solution in toluene, 2.12 mmol, 1.1 eq.) was added dropwise. After 30 min benzyl bromide (1.18 ml, 9.65 mmol, 5 eq.) was added, and a final solvent ratio

THF/DMF 7:3 was reached by adding DMF (13.6 ml). The mixture was allowed to reach -40°C and stirred for 3 h. Then aqueous NH_4Cl was slowly added and the mixture was extracted with EtOAc (3x). Organic phases were washed with brine and dried over Na_2SO_4. Volatiles were removed under reduced pressure and the residue was purified by flash chromatography on silica gel (Hex/EtOAc, 7:3) to afford the desired product as a viscous transparent oil (761 mg, 86%).

R_f=0.20 (Hexane/EtOAc 6:4); $[\alpha]_D^{20}$=+14.8 (**46b**, *c*=1 in $CHCl_3$); ^{1}H NMR (400 MHz, CD_2Cl_2) δ 7.46 – 7.27 (m, 10H), 5.42 – 5.34 (m, 1H, overlapping with solvent signal), 5.29 (d, 1H, *J* = 15.5 Hz), 4.31 – 4.25 (m, 1H), 4.23 – 4.14 (m, 3H), 4.11 (dd, 1H, *J* = 12.9, 2.0 Hz), 3.82 (dd, 1H, *J* = 12.8, 3.2 Hz), 3.61 (s, 3H), 3.26 (dd, 1H, *J* = 17.5, 2.9 Hz), 2.93 (dd, 1H, *J* = 17.5, 5.1 Hz); ^{13}C NMR (101 MHz, CD_2Cl_2) δ 170.9, 166.7, 165.6, 136.0, 129.5, 128.8, 128.4, 127.3, 104.3, 59.0, 55.7, 52.5, 52.1, 47.8, 47.6, 35.4; IR (neat): ν_{max} 2117, 1735, 1660, 1449, 1439, 1362, 1329, 1267, 1216, 1174; MS (ESI) *m*/*z* calcd for $[C_{22}H_{24}N_5O_4]^+$: 422.18 $[M+H]^+$; found: 422.3.

NHBoc-DKP-5-CO_2Me (47a);
NHBoc-DKP-7-CO_2Me (47b)

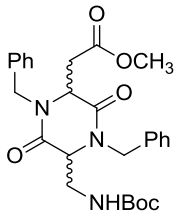

47a: (3*R*, 6*S*)
47b: (3*S*, 6*R*)

To a solution of azide **46** (751 mg, 1.78 mmol, 1 eq.) in THF (48 ml), under a nitrogen atmosphere and at -20 ºC, 2-(*t*-butoxycarbonyloxyimino)-2-phenylacetonitrile (Boc-ON, 964 mg, 3.92 mmol, 2.2 eq.) and Me_3P (3.57 ml of 1 M solution in toluene, 3.56 mmol, 2 equiv) were added successively. After stirring for 6 h at r.t., the solution was diluted with CH_2Cl_2 and washed with H_2O (3x) and brine. The organic phase was dried over Na_2SO_4 and volatiles were removed under reduced pressure. The residue was purified by flash chromatography on silica gel (CH_2Cl_2/EtOAc, 8:2) to afford the desired product as a white foam (716 mg, 87%).

R_f = 0.39 (CH_2Cl_2/EtOAc, 9:1); $[\alpha]_D^{20}$=-103.6 (**47b**, *c*=1.5 in $CHCl_3$); ^{1}H NMR (400 MHz, CD_2Cl_2) δ 7.48 – 7.24 (m, 10H), 5.56 (d, 1H, *J* = 15.3 Hz), 5.12 (d, 1H, *J* = 15.1 Hz), 4.98 (br s, 1H), 4.36 – 4.18 (m, 3H), 4.05 (s, 1H), 3.87 – 3.63 (m, 2H), 3.57 (s, 3H), 3.23 (dd, 1H, *J* = 17.3, 2.7 Hz), 2.92 (dd, 1H, *J* = 17.3, 4.9 Hz), 1.47 (s, 9H); ^{13}C NMR (101 MHz, CD_2Cl_2) δ 170.8, 166.7, 166.4, 156.5, 136.5, 136.3, 129.6, 129.4, 129.2, 128.5, 128.4, 80.3, 59.4, 56.0, 52.5, 48.0, 47.1, 41.5, 35.7, 28.8; IR (neat): ν_{max} 3323, 2978, 1738, 1714, 1658, 1497, 1450,

1366, 1330, 1252, 1202, 1168; MS (ESI) *m*/*z* calcd for $[C_{27}H_{34}N_3O_6]^+$: 496.24 $[M+H]^+$; found: 496.3.

NHBoc-DKP-5-CO_2H (DKP-5);
NHBoc-DKP-7-CO_2H (DKP-7)

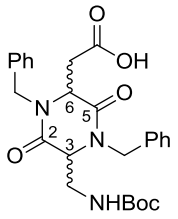

DKP-5: 3*R*,6*S*
DKP-7: 3*S*,6*R*

Compound **47** (370 mg, 0.75 mmol, 1 eq.) was dissolved in THF (30 ml) and the mixture was cooled to 0 °C. A solution of LiOH·H_2O (78.3 mg, 1.86 mmol, 2.5 eq.) in H_2O (15 ml) was added dropwise. The resulting solution was let reacting for 1 h at 0 °C. Then, maintaining the temperature at 0 °C, the mixture was acidified with HCl 1M to pH = 1-2, and extracted with CH_2Cl_2 (4x). The collected organic phases were dried over Na_2SO_4 and volatiles removed under reduced pressure. Either **DKP-5** or **DKP-7** were afforded as a white foam (361 mg, 100%), which was used in subsequent steps without further purification.

3.1.2.4 DKP-8

(*R*)-*N*-(tert-butoxycarbonyl)glutamic acid γ-methyl ester (48) [8]

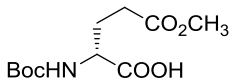

48

To a flask containing MeOH (4,6 ml) and cooled to -14 °C was slowly added Acetyl chloride (1.3ml, 18.4 mmol, 2.7 eq) followed by D-glutamic acid (1g, 6.8 mmol, 1eq). Cooling bath was removed, and the solution was stirred for 30 min at r.t. and then poured into Et_2O (330 ml). The precipitate was filtered off and washed well with Et_2O (50 ml) to give (*R*)- glutamic acid γ-methyl ester hydrochloride (1.25 g, 93%) as a white solid, which was used without further purification.
In a round bottom flask was solved 1 g (5.06 mmol, 1 eq) of (*R*)- glutamic acid γ-methyl ester hydrochloride in 20 ml of THF/water 1:1 solution. The reaction flask was lowered into an ice bath, and triethylamine (2.12 ml, 15.2 mmol, 3 eq.) and Boc_2O (1.21 g, 5.56 mmol, 1.1 eq) were added. After stirring at r.t. for 24 h. The reaction mixture was

diluted with 60 ml of EtOAc and washed with aqueous $KHSO_4$ 1M until pH = 3 and brine. The organic phase was dried over Na_2SO_4, filtered and concentrated under reduced pressure. The product was then dried under high vacuum for a few hours affording 1.3 g (98%) of the pure expected product as viscous transparent oil.

(*R*)-1-((*S*)-2-(benzylamino)-3-methoxy-3-oxopropyl)5-methyl2-(tert-butoxycarbonylamino)pentanedioate (49)

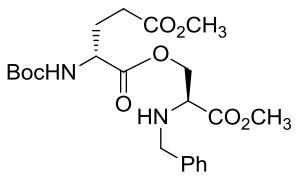

49

(*R*)-*N*-(tert-butoxycarbonyl)glutamic acid γ-methyl ester **48** (1.0 g, 3.8 mmol, 1.3 eq.) was coupled with (*S*)-*N*-benzylserine methyl ester **47** (607 mg, 2.9 mmol, 1 eq.) according to general procedure **GP2**. The crude product was purified by flash chromatography on silica gel (Hexane/EtOAc, 7:3) to afford the desired product as a transparent oil (774 mg, 59%).

R_f = 0.35 (Hexane/EtOAc 7:3); $[\alpha]_D^{20}$=-4 (*c*=1.00 in $CHCl_3$); ^{1}H NMR (400 MHz, $CDCl_3$) δ 7.31 (m, 5H), 5.12 (m, 1H), 4.47 (dd, *J* = 11.0, 4.9 Hz, 1H), 4.40 (m, 1H); 4.30 (dd, *J* = 11.0, 4.9 Hz, 1H), 3.90 (d, *J* = 13.1 Hz, 1H), 3.79 (s, 3H), 3.71 (d, *J* = 10.3 Hz, 1H), 3.68 (s, 3H), 3.56 (t, *J* = 4.9 Hz, 1H), 2.49 – 2.34 (m, 2H), 2.17 (dt, *J* = 13.3, 7.4 Hz, 1H), 1.95 (dt, *J* = 14.8, 7.9 Hz, 1H), 1.45 (s, 9H); ^{13}C NMR (101 MHz, CD_2Cl_2) δ 173.7, 173.1, 172.5, 155.8, 140.3, 129.0, 128.8, 127.7, 80.3, 66.2, 59.8, 53.5, 52.7, 52.4, 52.2, 30.5, 28.6, 28.2; IR (neat): ν_{max} 3368, 2976, 2953, 1739, 1716, 1509, 1454, 1367, 1249, 1201, 1166, 1051; MS (ESI) *m*/*z* calcd for $[C_{22}H_{33}N_2O_8]^+$: 453,22 $[M+H]^+$; found: 453.6.

HO-DKP-8-CO_2Me (50)

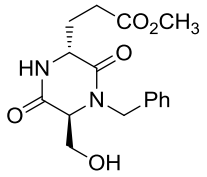

50

Isopeptide **49** (440 mg, 0.97 mmol, 1 eq.) was deprotected according to general procedure **GP1**. The corresponding trifluoroacetate salt was dissolved in *i*PrOH (12 ml) and *i*Pr$_2$EtN (0.7 ml, 3.9 mmol, 4 eq.) was added at r.t. The reaction was stirred for 18 h at r.t., monitoring the formation of DKP by TLC (EtOAc). The solution was then concentrated under reduced pressure and the residue was purified by flash

chromatography on silica gel (EtOAc) to afford the desired product as a white foam (289 mg, 93%).

R_f = 0.12 (EtOAc); $[\alpha]_D^{20}$ =+29.5 (*c*=1.00 in $CHCl_3$); ^1H NMR (400 MHz, $CDCl_3$) δ 7.41 – 7.25 (m, 5H), 5.32 (d, *J* = 15.1 Hz, 1H), 4.43 (t, *J* = 4.4 Hz, 1H), 4.13 (d, *J* = 15.1 Hz, 1H), 3.95 (dd, *J* = 11.7, 2.4 Hz, 2H), 3.80 (t, *J* = 2.1 Hz, 1H), 3.67 (s, 3H), 2.53 – 2.26 (m, 3H), 2.23 – 2.10 (m, 1H); ^{13}C NMR (101 MHz, CD_3OD) δ 174.35, 169.95, 168.69, 136.75, 129.19, 128.77, 128.25, 128.17, 62.82, 61.46, 53.77, 51.51, 47.41, 29.05, 27.25; IR (neat): ν_{max} 3420, 2952, 1732, 1682, 1653, 1496, 1449, 1328, 1259, 1175, 1122, 1070; MS (ESI) *m*/*z* calcd for $[C_{16}H_{21}N_2O_5]^+$: 321,14 $[M+H]^+$; found: 321.4.

N_3-DKP-8-CO_2Me (51)

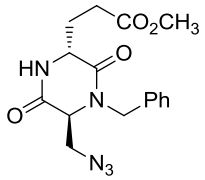

51

To a solution of diketopiperazine **50** (104 mg, 0.32 mmol, 1 eq.) in CH_2Cl_2/toluene/DMF (3 ml/2.5 ml/1 ml), under nitrogen atmosphere and at -20 ºC, PPh_3 (128 mg, 0.49 mmol, 1.5 eq.) was added and the mixture was stirred until a solution was obtained. Hydrazoic acid (1.9 M in toluene, 0.51 ml, 0.97 mmol, 3 eq.) was added followed by dropwise addition of DIAD (0.096 ml, 0.49 mmol, 1.5 eq.) and the reaction was stirred at -20ºC overnight. The reaction mixture was loaded onto a silica gel column (EtOAc/Hexane 8:2) to afford the desired product as a white foam (72 mg, 65%).

R_f = 0.52 (EtOAc); $[\alpha]_D^{20}$ =+57.9 (*c*=1.00 in $CHCl_3$); ^1H NMR (400 MHz, $CDCl_3$) δ 7.44 – 7.30 (m, 3H), 7.30 – 7.23 (m, 2H), 5.15 (d, *J* = 15.0 Hz, 1H), 4.43 (t, *J* = 4.7 Hz, 1H), 4.25 (d, *J* = 15.0 Hz, 1H), 3.94 (d, *J* = 2.7 Hz, 1H), 3.88 (dd, *J* = 12.8, 2.4 Hz, 1H), 3.71 (s, 3H), 3.64 (dd, *J* = 12.7, 3.4 Hz, 1H), 2.61 – 2.46 (m, 2H), 2.34 (dd, *J* = 9.1, 3.7 Hz, 2H); ^{13}C NMR (101 MHz, $CDCl_3$) δ 174.58, 167.72, 167.37, 136.06, 129.82, 128.97, 128.71, 78.02, 77.70, 59.99, 54.39, 52.71, 52.42, 48.51, 30.24, 27.73; IR (neat): ν_{max} 2116, 1733, 1686, 1654, 1437, 1327, 1289, 1258, 1174; MS (ESI) *m*/*z* calcd for $[C_{16}H_{20}N_5O_4]^+$: 346,15 $[M+H]^+$; found: 346.3.

NHBoc-DKP-8-CO_2Me (53)

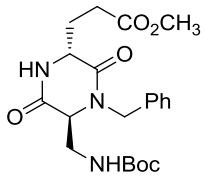

53

Azide **51** (192 mg, 0.55 mmol, 1 eq.) was dissolved in 12 ml of THF. After addition of 59 mg of Pd/C 10% (0.05 mmol, 0.1 eq.), the mixture was hydrogenated under vigorous stirring over 3 h. Pd/C was then filtered off on a celite pad, which was thoroughly washed with THF. The filtrate was concentrated to dryness, obtaining amine **52** as a white solid, which was, without further purification, dissolved in THF. The mixture was cooled to 0 °C before adding Boc anhydride (132 mg, 0.6 mmol, 1.1 eq.) and *i*Pr$_2$EtN (0.19 ml, 1.1 mmol, 2 eq.). The mixture was afterwards let to reach r.t. and stirred for 18 h. Volatiles were then removed under reduced pressure, and the residue was purified by flash chromatography on silica gel (EtOAc/Hexane, 1:1) to afford the desired product as a white foam (201 mg, 87%).

R_f = 0.34 (EtOAc); [*a*]D20=-4.4 (*c*=1.00 in $CHCl_3$); ^{1}H NMR (400 MHz, $CDCl_3$) δ 7.44 (d, *J* = 9.9 Hz, 1H), 7.39 – 7.14 (m, 5H), 5.48 (d, *J* = 15.1 Hz, 1H), 5.29 (s, 1H), 4.25 (t, *J* = 4.4 Hz, 1H), 4.06 (d, *J* = 15.0 Hz, 1H), 3.80 (s, 1H), 3.77 – 3.57 (m, 4H), 3.57 – 3.43 (m, 1H), 2.60 – 2.42 (m, 2H), 2.38 – 2.19 (m, *J* = 6.1 Hz, 2H), 1.43 (s, 9H); ^{13}C NMR (101 MHz, $CDCl_3$) δ 174.56, 168.93, 166.59, 156.62, 136.35, 129.64, 128.92, 128.66, 80.80, 60.21, 53.98, 52.59, 47.78, 41.22, 29.96, 28.96, 28.28; IR (neat): ν_{max} 3298, 2978, 2952, 1689, 1523, 1448, 1393, 1366, 1329, 1253, 1169, 1059; MS (ESI) *m*/*z* calcd for $[C_{21}H_{30}N_3O_6]^+$: 420.21 $[M+H]^+$; found: 420.3.

NHBoc-DKP-8-CO$_2$H (DKP-8)

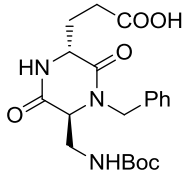

DKP-8

Compound **53** (117 mg, 0.28 mmol, 1 eq.) was dissolved in THF (7 ml). The mixture was cooled to 0°C and a 2.7 M solution of LiOOH in H_2O_2 (453 mg of LiOH in 7 ml of H_2O_2 35%) was added dropwise. The mixture was stirred for additional 30 min at 0°C, then warmed up to r.t. and stirred for 7h. After the addition of Na_2SO_3 (30.6 mg, 0.24 mmol, 6 eq.) the reaction mixture was diluted with 8 ml of THF/H_2O 1:1. $KHSO_4$ 1M was added to reach pH = 1-2, and the mixture was extracted with DCM (4x). The collected organic phases were dried over Na_2SO_4 and volatiles removed under reduced pressure, to afford crude **DKP-8** as a yellowish solid. Crude product was dissolved in EtOAc and extracted with $NaHCO_3$ sat.; collected aqueous layers were acidified with $KHSO_4$ 1M to reach pH 1-2, and extracted with DCM (4x). Collected organic phases were dried over Na_2SO_4 and volatiles removed under reduced pressure, to afford **DKP-8** as a white foam (100 mg, 90%), which was used without further purification.

3.1.3 - Synthesis of c[DKP-RGD] integrin ligands

Boc-Arg(Mtr)-Gly-OBn (54)

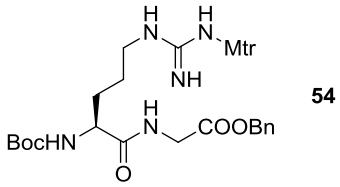

54

N-Boc glycine benzylester[9] (1.6 mg, 6 mmol, 1.2 eq.) was deprotected according to general procedure **GP1**. The corresponding trifluoroacetate salt was then coupled with Boc-Arg(Mtr)-OH (Sigma-Aldrich) (2.5g, 5.14 mmol, 1 eq.) according to general procedure **GP2**. The residue was purified by flash chromatography on silica gel (CH_2Cl_2/MeOH; 97:3) to afford the desired product as white foam (2.9 g, 90%).
R_f = 0.21 (CH_2Cl_2/MeOH 97:3); $[\alpha]_D^{20}$=-6.0 (*c*=0.5 in $CHCl_3$); ^{1}H NMR (400 MHz, CD_2Cl_2) δ 7.40 - 7.31 (m, 5H), 7.27 (br, 1H), 6.58 (s, 1H), 6.19 (s, 2H), 6.00 (br, 1H), 5.50 (d, 1H, *J* = 6.6), 5.15 (s, 2H), 4.24 (m, 1H), 4.09 (dd, 1H, *J* = 17.5, 6.4), 3.99 (dd, 1H, *J* = 17.9, 5.7), 3.84 (s, 3H), 3.25 (m, 2H), 2.67 (s, 3H), 2.60 (s, 3H), 2.14 (s, 3H), 1.84 (m, 2H), 1.61 (m, 2H), 1.43 (s, 9H); ^{13}C NMR (101 MHz, CD_2Cl_2) δ 172.9, 170.0, 158.5, 156.5, 156.0, 138.4, 136.5, 135.4, 133.4, 128.5, 128.4, 128.2, 124.8, 111.7, 80.1, 67.1, 55.4, 50.5, 41.2, 40.4, 30.0, 28.0, 25.1, 23.8, 18.1, 11.6; IR (neat): ν_{max} 3343, 2937, 1669, 1621, 1555, 1455, 1366, 1307, 1251, 1171, 1120; MS (ESI) *m*/*z* calcd for $[C_{30}H_{44}N_5O_8S]^+$: 634.29 $[M+H]^+$; found: 634.3.

***N*-Boc-DKP-Arg(Mtr)-Gly-OBn (55)**

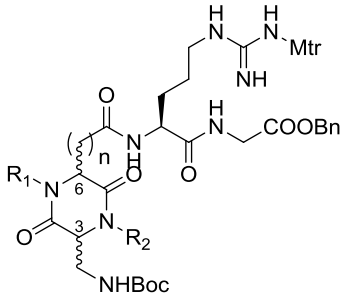

55a: (3*R*,6*S*), R_1 = Bn, R_2 = H, n = 1
55b: (3*R*,6*S*), R_1 = Bn, R_2 = Bn, n = 1
55c: (3*S*,6*R*), R_1 = Bn, R_2 = H, n = 1
55d: (3*S*,6*R*), R_1 = Bn, R_2 = Bn, n = 1
55e: (3*S*,6*R*), R_1 = H, R_2 = Bn, n = 2

a) *N*-Boc-DKP-4-Arg(Mtr)-Gly-OBn (55a)

Compound **54** (973.5 mg, 1.54 mmol, 1.2 eq.) was deprotected according to general procedure **GP1**. The corresponding trifluoroacetate salt was then coupled with **DKP-4** (500 mg, 1.28 mmol, 1 eq.) according to general procedure **GP2**. The residue was

purified by flash chromatography on silica gel (CH_2Cl_2/MeOH, 93:7) to afford the desired product as white foam (811 mg, 70%).

R_f = 0.36 (CH_2Cl_2/MeOH 9:1); $[\alpha]_D^{20}$=+21.7 (*c*=1 in $CHCl_3$); ^{1}H NMR (400 MHz, Acetone-d_6) δ 7.85 (t, 1H, *J* = 5.8 Hz), 7.61 (d, 1H, *J* = 7.7 Hz), 7.44 – 7.23 (m, 10H), 6.69 (s, 1H), 6.54 (br s, 2H), 6.19 (br s, 1H), 5.24 (d, 1H, *J* = 15.2 Hz), 5.17 (s, 2H), 4.56 – 4.47 (m, 1H, *J* = 8.1 Hz), 4.35 (t, 1H, *J* = 4.8 Hz), 4.17 (d, 1H, *J* = 15.2 Hz), 4.10 (t, 1H, *J* = 5.4 Hz,), 4.00 (d, 2H, *J* = 5.9 Hz), 3.85 (s, 3H), 3.77 – 3.68 (m, 1H), 3.62 – 3.50 (m, 1H), 3.34 – 3.11 (m, 2H), 2.92 (d, 2H, *J* = 5.4 Hz), 2.69 (s, 3H), 2.64 (s, 3H), 2.12 (s, 3H), 1.97 – 1.79 (m, 1H), 1.69 – 1.49 (m, 3H), 1.43 (s, 9H); ^{13}C NMR (101 MHz, Acetone-d_6) δ 138.9, 137.4, 136.9, 135.6, 129.3, 129.1, 128.7, 128.5, 128.2, 124.6, 112.3, 79.3, 66.8, 57.6, 55.9, 55.6, 53.1, 47.4, 42.9, 41.5, 40.8, 37.3, 28.4, 26.1, 24.0, 18.5, 11.9; IR (neat): ν_{max} 3331, 2936, 1681, 1555, 1454, 1392, 1366, 1333, 1306, 1249, 1172, 1120; MS (ESI) *m*/*z* calcd for $[C_{44}H_{59}N_8O_{11}S]^+$: 907.40 $[M+H]^+$; found: 907.5.

b) *N*-Boc-DKP-5-Arg(Mtr)-Gly-OBn (55b)

Compound **54** (410 mg, 0.65 mmol, 1.2 eq.) was deprotected according to general procedure **GP1**. The corresponding trifluoroacetate salt was then coupled with **DKP-5** (260 mg, 0.54 mmol, 1 eq.) according to general procedure **GP2**. The residue was purified by flash chromatography on silica gel (CH_2Cl_2/MeOH, 97:3) to afford the desired product as white foam (323 mg, 60% yield).

R_f=0.44 (CH_2Cl_2/MeOH, 9:1); $[\alpha]_D^{20}$=-51.2 (*c*=0.6 in $CHCl_3$); ^{1}H NMR (400 MHz, CD_2Cl_2) δ 7.69 (br s, 1H), 7.41 (br s, 1H), 7.38 – 7.22 (m, 15H), 6.57 (s, 1H), 6.26 (br s, 2H), 5.33 (d, 1H, *J* = 15.6 Hz), 5.24 (d, 1H, *J* = 15.3 Hz), 5.12 (s, 2H), 4.77 (br s, 1H), 4.51 – 4.41 (m, 1H), 4.36 (br s, 1H), 4.28 (d, 1H, *J* = 15.5 Hz), 4.17 (d, 1H, *J* = 15.4 Hz), 4.08 – 3.95 (m, 3H), 3.84 (s, 3H), 3.76 – 3.65 (m, 1H), 3.64 – 3.53 (m, 1H), 3.34 – 3.13 (m, 2H), 3.07 (d, 1H, *J* = 13.3 Hz), 2.93 (dd, 1H, *J* = 15.8, 6.6 Hz), 2.66 (s, 3H), 2.58 (s, 3H), 2.11 (s, 3H), 2.01 – 1.88 (m, 1H), 1.75 – 1.48 (m, 3H), 1.42 (s, 9H); ^{13}C NMR (101 MHz, CD_2Cl_2) δ 172.9, 170.6, 170.3, 167.8, 166.7, 159.1, 157.1, 139.1, 137.1, 136.5, 136.1, 134.0, 129.6, 129.5, 129.2, 128.9, 128.9, 128.6, 128.5, 128.4, 125.4, 112.4, 67.7, 59.8, 56.3, 56.1, 47.6, 41.9, 41.6, 41.1, 37.2, 30.3, 29.5, 28.7, 26.2, 24.5, 18.8, 12.3; IR (neat): ν_{max} 3329, 2938, 2357, 2341, 1750, 1719, 1660, 1652, 1557, 1455, 1369, 1301, 1257, 1176, 1121; MS (ESI) *m*/*z* calcd for $[C_{51}H_{65}N_8O_{11}S]^+$: 997.45 $[M+H]^+$; found: 997.5.

c) *N*-Boc-DKP-6-Arg(Mtr)-Gly-OBn (55c)

Compound **54** (973 mg, 1.54 mmol, 1.2 eq.) was deprotected according to general procedure **GP1**. The corresponding trifluoroacetate salt was then coupled with **DKP-6** (500 mg, 1.28 mmol, 1 eq.) according to general procedure **GP2**. The residue was

purified by flash chromatography on silica gel (CH_2Cl_2/MeOH, 93:7) to afford the desired product as white foam (811 mg, 70%).

R_f=0.38 (CH_2Cl_2/MeOH 9:1); $[\alpha]_D^{20}$=+23.4 (c=1 in $CHCl_3$); ^{1}H NMR (400 MHz, Acetone-d_6) δ 7.93 (t, 1H, J = 5.8 Hz), 7.73 (d, 1H, J = 8.1 Hz,), 7.45 – 7.24 (m, 10H), 6.69 (s, 1H), 6.59 (br s, 2H), 6.24 (br s, 1H), 5.34 (d, 1H, J = 15.2 Hz,), 5.16 (s, 2H), 4.68 – 4.58 (m, 1H), 4.34 (t, 1H, J = 4.6 Hz), 4.17 (d, 1H, J = 15.1 Hz), 4.11 – 3.93 (m, 3H), 3.85 (s, 3H), 3.75 – 3.65 (m, 1H), 3.65 – 3.54 (m, 1H), 3.32 – 3.11 (m, 2H), 3.07 (dd, 1H, J = 15.2, 5.8 Hz), 2.97 – 2.85 (m, 1H, overlapping with water signal), 2.70 (s, 3H), 2.65 (s, 3H), 2.11 (s, 3H), 1.92 – 1.80 (m, 1H), 1.67 – 1.47 (m, 3H), 1.42 (s, 9H); ^{13}C NMR (101 MHz, Acetone-d_6) δ 172.5, 170.2, 169.7, 168.7, 167.2, 158.7, 157.4, 157.3, 138.9, 137.1, 136.9, 136.8, 135.6, 129.4, 129.1, 128.8, 128.6, 128.2, 124.6, 112.3, 79.3, 66.9, 57.3, 56.1, 55.7, 52.7, 47.0, 43.1, 41.5, 40.8, 37.1, 30.5, 28.4, 25.7, 24.1, 18.5, 11.9; ; IR (neat): ν_{max} 3329, 2932, 1687, 1560, 1451, 1387, 1361, 1338, 1310, 1243, 1177, 1121; MS (ESI) m/z calcd for $[C_{44}H_{59}N_8O_{11}S]^+$: 907.40 $[M+H]^+$; found: 907.5.

d) *N*-Boc-DKP-7-Arg(Mtr)-Gly-OBn (55d)

Compound **54** (327 mg, 0.52 mmol, 1.1 eq.) was deprotected according to general procedure **GP1**. The corresponding trifluoroacetate salt was then coupled with DKP-7 (227 mg, 0.47 mmol, 1 eq.) according to general procedure **GP2**. The residue was purified by flash chromatography on silica gel (CH_2Cl_2/MeOH, 95:5) to afford the desired product as white foam (286 mg, 61%).

R_f=0.45 (CH_2Cl_2/MeOH 9:1); $[\alpha]_D^{20}$=-55.6 (c=0.7 in $CHCl_3$); ^{1}H NMR (400 MHz, Acetone-d_6) δ 7.85 (t, 1H, J = 5.7 Hz), 7.55 (d, 1H, J = 8.2 Hz), 7.51 – 7.22 (m, 15H), 6.68 (s, 1H), 6.54 (br s, 2H), 6.26 (br s, 1H), 5.92 (br s, 1H), 5.50 (d, 1H, J = 15.6 Hz), 5.29 (d, 1H, J = 15.3 Hz), 5.16 (s, 2H), 4.68 – 4.56 (m, 1H), 4.32 (d, 2H, J = 15.2 Hz), 4.26 – 4.20 (m, 1H), 4.06 (t, 1H, J = 3.3 Hz), 4.03 – 3.92 (m, 2H), 3.84 (s, 3H), 3.79 – 3.65 (m, 2H), 3.40 – 3.22 (m, 1H), 3.22 – 2.99 (m, 3H), 2.69 (s, 3H), 2.64 (s, 3H), 2.10 (s, 3H), 1.96 – 1.79 (m, 1H), 1.68 – 1.48 (m, 3H), 1.43 (s, 9H); ^{13}C NMR (101 MHz, Acetone-d_6) δ 171.7, 169.4, 169.1, 166.8, 166.4, 158.0, 156.7, 155.9, 138.3, 136.3, 128.7, 128.5, 128.3, 128.1, 127.6, 127.3, 123.9, 111.6, 78.5, 66.1, 58.9, 55.5, 54.9, 51.8, 46.5, 46.2, 40.8, 40.5, 39.9, 36.1, 27.7, 25.1, 23.4, 17.8, 11.2; IR (neat): ν_{max} 3326, 2936, 2361, 2343, 1748, 1714, 1659, 1650, 1555, 1453, 1366, 1306, 1253, 1172, 1120; MS (ESI) m/z calcd for $[C_{51}H_{65}N_8O_{11}S]^+$: 997.45 $[M+H]^+$; found: 997.6.

e) *N*-Boc-DKP-8-Arg(Mtr)-Gly-OBn (55e)

Compound **54** (200 mg, 0.31 mmol, 1.1 eq.) was deprotected according to general procedure **GP1**. The corresponding trifluoroacetate salt was then coupled with **DKP-8** (116 mg, 0.29 mmol, 1 eq.) according to general procedure **GP2**. The residue was

purified by flash chromatography on silica gel (CH_2Cl_2/MeOH, 95:5) to afford the desired product as white foam (163 mg, 61%).

R_f=0.4 (CH_2Cl_2/MeOH 9:1); $[\alpha]_D^{20}$=-2.0 (c=0.2 in $CHCl_3$); ^{1}H NMR (400 MHz, CD_3OD) δ 7.42 – 7.26 (m, 10H), 6.67 (s, 1H), 5.39 (d, 1H, J = 15.3 Hz), 5.16 (s, 2H), 4.43 – 4.36 (m, 1H), 4.30 (t, 1H, J = 3.7 Hz), 4.09 – 4.00 (m, 2H), 3.93 (d, 1H, J = 17.6 Hz), 3.84 (s, 3H), 3.82 – 3.73 (m, 2H), 3.45 (d, 1H, J = 13.2 Hz), 3.25 – 3.09 (m, 2H), 2.69 (s, 3H), 2.63 (s, 3H), 2.46 – 2.22 (m, 3H), 2.22 – 2.16 (m, 1H), 2.14 (s, 3H), 1.87 – 1.76 (m, 1H), 1.68 – 1.52 (m, 3H), 1.44 (s, 9H); ^{13}C NMR (101 MHz, CD_2Cl_2) δ 173.7, 173.1, 170.3, 168.8, 167.0, 158.8, 157.0, 156.5, 138.8, 136.8, 136.5, 135.8, 133.9, 129.2, 128.9, 128.7, 128.5, 128.3, 125.1, 112.1, 80.0, 67.4, 60.6, 55.8, 53.9, 53.0, 48.0, 41.6, 41.1, 40.8, 31.6, 30.3, 28.4, 28.0, 25.6, 24.2, 18.5, 12.1; IR (neat): ν_{max} 3328, 3066, 3007, 2974, 2937, 1747, 1660, 1550, 1455, 1392, 1366, 1306, 1254, 1173, 1120; MS (ESI) m/z calcd for $[C_{45}H_{61}N_8O_{11}S]^+$: 921.42 $[M+H]^+$; found: 921.7.

Cbz-Asp(O*t*Bu)-DKP-Arg(Mtr)-Gly-OBn (56)

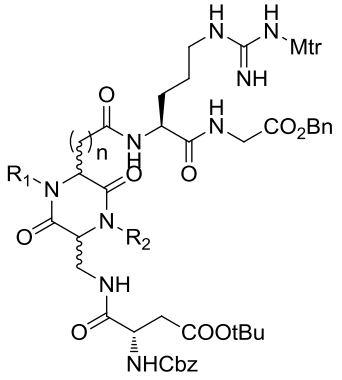

56a: (3*R*,6*S*), R_1 = Bn, R_2 = H, n = 1
56b: (3*R*,6*S*), R_1 = Bn, R_2 = Bn, n = 1
56c: (3*S*,6*R*), R_1 = Bn, R_2 = H, n = 1
56d: (3*S*,6*R*), R_1 = Bn, R_2 = Bn, n = 1
56e: (3*S*,6*R*), R_1 = H, R_2 = Bn, n = 2

a) Cbz-Asp(O*t*Bu)-DKP4-Arg(Mtr)-Gly-OBn (56a)

Compound **55a** (290 mg, 0.32 mmol, 1 eq.) was deprotected according to general procedure **GP1**. The corresponding trifluoroacetate salt was then coupled with Cbz-L-Asp(O*t*Bu)-OH (124 mg, 0.38 mmol, 1.2 eq.) according to general procedure **GP2**. The residue was purified by flash chromatography on silica gel (CH_2Cl_2/MeOH, 9:1) to afford the desired product as white foam (327 mg, 92%).

R_f=0.45 (CH_2Cl_2/MeOH 9:1); $[\alpha]_D^{20}$=+22.1 (c=1 in $CHCl_3$); ^{1}H NMR (400 MHz, Acetone-d_6) δ 7.84 (t, 1H, J = 5.8 Hz), 7.77 (t, 1H, J = 5.9 Hz), 7.60 (d, 1H, J = 8.0 Hz), 7.46 – 7.21 (m, 16H), 6.77 (d, 1H, J = 8.2 Hz), 6.69 (s, 1H), 6.54 (br s, 2H), 6.43 – 6.17 (br, 1H), 5.23 (d, 1H, J = 15.2 Hz), 5.19 – 5.10 (m, 3H), 5.06 (d, 1H, J = 12.5 Hz), 4.58 (td, 1H, J = 7.8, 5.6 Hz), 4.53 – 4.46 (m, 1H), 4.43 (t, 1H, J = 5.3 Hz), 4.18 (d, 1H, J = 15.2 Hz), 4.12 (t, 1H, J = 5.3 Hz), 4.06 – 3.93 (m, 2H), 3.93 – 3.81 (m, 4H), 3.70 – 3.59 (m, 1H), 3.31 – 3.11 (m, 2H), 2.97 – 2.89 (m, 2H), 2.87 – 2.77 (m, 1H, overlapping with water signal), 2.76 –

2.58 (m, 7H), 2.12 (s, 3H), 1.97 – 1.77 (m, 1H), 1.70 – 1.48 (m, 3H), 1.42 (s, 9H).; ^{13}C NMR (101 MHz, Acetone-d_6) δ 172.3, 172.0, 170.2, 169.8, 169.4, 168.5, 166.4, 158.4, 157.1, 156.5, 138.7, 137.4, 137.1, 136.6, 135.4, 129.1, 128.8, 128.7, 128.4, 128.2, 127.9, 124.3, 112.0, 80.9, 66.7, 66.6, 57.4, 55.4, 54.7, 47.1, 41.7, 41.3, 40.6, 37.9, 36.9, 29.9, 29.7, 29.6, 29.4, 29.2, 29.0, 28.8, 27.7, 25.8, 23.8, 18.2, 11.6; IR (neat): ν_{max} 3317, 2937, 1726, 1667, 1548, 1454, 1367, 1306, 1254, 1190, 1156, 1120; MS (ESI) *m*/*z* calcd for $[C_{55}H_{70}N_9O_{14}S]^+$: 1112.48 $[M+H]^+$; found: 1112.5.

b) Cbz-Asp(O*t*Bu)-DKP5-Arg(Mtr)-Gly-OBn (56b)

Compound **55b** (147 mg, 0.15 mmol, 1 eq.) was deprotected according to general procedure **GP1**. The corresponding trifluoroacetate salt was then coupled with Cbz-L-Asp(O*t*Bu)-OH (58 mg, 0.18 mmol, 1.2 eq.) according to general procedure **GP2**. The residue was purified by flash chromatography on silica gel (CH_2Cl_2/MeOH, 95:5) to afford the desired product as white foam (172 mg, 96%).

R_f=0.43 (CH_2Cl_2/MeOH 95:5); $[\alpha]_D^{20}$=-23.6 (*c*=0.7 in $CHCl_3$); ^{1}H NMR (400 MHz, Acetone-d_6) δ 7.89 (t, 1H, *J* = 5.9 Hz), 7.51 – 7.19 (m, 20H), 6.75 – 6.65 (m, 2H), 6.55 (br s, 2H), 6.33 (br s, 1H), 5.39 (d, 1H, *J* = 15.4 Hz), 5.16 (s, 2H), 5.10 (d, 1H, *J* = 13.8 Hz), 5.04 (d, 1H, *J* = 15.5 Hz), 4.59 – 4.49 (m, 3H), 4.46 (d, 1H, *J* = 15.6 Hz), 4.28 (d, 1H, *J* = 15.5 Hz), 4.20 – 4.15 (m, 1H), 4.08 – 3.91 (m, 3H), 3.84 (s, 3H), 3.81 – 3.73 (m, 1H), 3.39 – 3.24 (m, 1H), 3.22 – 3.11 (m, 1H), 3.08 (dd, 1H, *J* = 15.9, 3.5 Hz), 2.92 (dd, 1H, *J* = 15.9, 6.4 Hz), 2.87 – 2.77 (m, 4H), 2.73 – 2.60 (m, 4H), 2.08 (s, 3H, overlapping with solvent signal), 1.95 – 1.81 (m, 1H), 1.69 – 1.50 (m, 3H), 1.42 (s, 9H); ^{13}C NMR (101 MHz, Acetone-d_6) δ 171.7, 171.2, 169.8, 169.4, 166.1, 162.8, 158.0, 156.7, 147.4, 136.9, 136.5, 128.7, 128.6, 128.3, 128.1, 128.0, 127.8, 127.6, 127.3, 111.6, 80.4, 66.3, 66.1, 58.5, 55.9, 54.9, 52.2, 52.0, 46.8, 46.6, 40.9, 40.1, 39.3, 37.2, 35.9, 27.3, 25.6, 23.4, 17.8, 11.2; IR (neat): ν_{max} 3324, 2938, 1731, 1660, 1654, 1546, 1451, 1368, 1310, 1253, 1160, 1122; MS (ESI) *m*/*z* calcd for $[C_{62}H_{76}N_9O_{14}S]^+$: 1202.52 $[M+H]^+$; found: 1202.5.

c) Cbz-Asp(O*t*Bu)-DKP6-Arg(Mtr)-Gly-OBn (56c)

Compound **55c** (400 mg, 0.44 mmol, 1 eq.) was deprotected according to general procedure **GP1**. The corresponding trifluoroacetate salt was then coupled with Cbz-L-Asp(O*t*Bu)-OH (171 mg, 0.52 mmol, 1.2 eq.) according to general procedure **GP2**. The residue was purified by flash chromatography on silica gel (CH_2Cl_2/MeOH, 9:1) to afford the desired product as white foam (451 mg, 92%).

R_f=0.46 (CH_2Cl_2/MeOH 9:1); $[\alpha]_D^{20}$=+25.1 (*c*=1 in $CHCl_3$); ^{1}H NMR (400 MHz, Acetone-d_6) δ 7.92 (br s, 1H), 7.82 (br s, 1H), 7.70 (br s, 1H), 7.43 – 7.22 (m, 15H), 6.81 (d, 1H, *J* = 8.1 Hz), 6.68 (s, 1H), 6.58 (br s, 2H), 5.31 (d, 1H, *J* = 15.1 Hz), 5.19 – 5.10 (m, 3H), 5.05 (d, 1H, *J* = 12.6 Hz), 4.60 (m, 2H), 4.41 (t, 1H, *J* = 5.1 Hz), 4.17 (d, 1H, *J* = 15.1 Hz), 4.10

– 3.91 (m, 3H), 3.89 – 3.80 (m, 4H), 3.80 – 3.68 (m, 1H), 3.31 – 3.11 (m, 2H), 3.04 (dd, 1H, *J* = 15.3, 5.7 Hz), 2.98 – 2.86 (m, 1H, overlapping with water signal), 2.82 (dd, 1H, *J* = 16.2, 5.4 Hz), 2.70 (s, 3H), 2.65 (s, 3H), 2.11 (s, 3H), 1.92 – 1.79 (m, 1H), 1.70 – 1.46 (m, 3H), 1.41 (s, 9H); ^{13}C NMR (101 MHz, Acetone-d_6) δ 172.7, 172.5, 170.4, 170.2, 169.7, 168.7, 167.0, 158.7, 157.4, 156.9, 138.9, 137.7, 137.1, 136.9, 136.8, 135.6, 129.4, 129.3, 129.1, 129.0, 128.8, 128.7, 128.5, 128.2, 124.6, 112.3, 81.1, 66.9, 57.3, 55.7, 55.3, 52.8, 52.7, 47.1, 44.0, 43.7, 41.9, 41.5, 40.8, 38.6, 38.3, 37.0, 30.5, 28.0, 25.8, 24.1, 18.5, 11.9; IR (neat): ν_{max} 3312, 2943, 1729, 1672, 1553, 1453, 1369, 1309, 1259, 1186, 1161, 1124; MS (ESI) *m*/*z* calcd for $[C_{55}H_{70}N_9O_{14}S]^+$: 1112.48 $[M+H]^+$; found: 1112.5.

d) Cbz-Asp(O*t*Bu)-DKP7-Arg(Mtr)-Gly-OBn (56d)

Compound **55d** (210 mg, 0.21 mmol, 1 eq.) was deprotected according to general procedure **GP1**. The corresponding trifluoroacetate salt was then coupled with Cbz-L-Asp(O*t*Bu)-OH (82 mg, 0.25 mmol, 1.2 eq.) according to general procedure **GP2**. The residue was purified by flash chromatography on silica gel (CH_2Cl_2/MeOH, 97:3) to afford the desired product as white foam (226 mg, 90%).

R_f=0.45 (CH_2Cl_2/MeOH 95:5); $[\alpha]_D^{20}$=-28.9 (*c*=0.8 in $CHCl_3$); ^{1}H NMR (400 MHz, Acetone-d_6) δ 7.85 (t, 1H, *J* = 5.8 Hz), 7.53 (d, 1H, *J* = 8.1 Hz), 7.50 – 7.21 (m, 21H), 6.71 (d, 1H, *J* = 8.3 Hz), 6.67 (s, 1H), 6.53 (br s, 2H), 6.24 (br s, 1H), 5.44 (d, 1H, *J* = 15.5 Hz), 5.24 (d, 1H, *J* = 15.2 Hz), 5.18 – 5.10 (m, 3H), 5.07 (d, 1H, *J* = 12.6 Hz), 4.64 – 4.50 (m, 2H), 4.39 – 4.30 (m, 2H), 4.27 (s, 1H), 4.14 (t, 1H, *J* = 3.5 Hz), 4.06 – 3.94 (m, 2H), 3.94 – 3.77 (m, 5H), 3.38 – 3.22 (m, 1H), 3.20 – 3.01 (m, 3H), 2.84 – 2.78 (m, 1H, overlapping with water signal), 2.69 (s, 3H), 2.66 – 2.56 (m, 4H), 2.09 (s, 3H), 1.94 – 1.78 (m, 1H), 1.66 – 1.45 (m, 3H), 1.41 (s, 9H); ^{13}C NMR (101 MHz, Acetone-d_6) δ 172.1, 171.5, 170.0, 169.8, 169.5, 167.5, 166.7, 158.4, 157.1, 138.6, 136.7, 136.6, 129.2, 128.9, 128.8, 128.7, 128.6, 128.5, 128.4, 128.2, 127.9, 127.6, 124.3, 111.9, 80.7, 66.6, 66.5, 58.7, 55.9, 55.4, 52.3, 52.2, 47.0, 46.6, 41.2, 40.3, 39.5, 37.7, 36.4, 30.2, 27.7, 25.6, 23.8, 18.2, 11.6; IR (neat): ν_{max} 3322, 2936, 1729, 1659, 1651, 1549, 1454, 1367, 1306, 1256, 1161, 1120; MS (ESI) *m*/*z* calcd for $[C_{62}H_{76}N_9O_{14}S]^+$: 1202.52 $[M+H]^+$; found: 1202.5.

e) Cbz-Asp(O*t*Bu)-DKP8-Arg(Mtr)-Gly-OBn (56e)

Compound **55e** (143 mg, 0.16 mmol, 1 eq.) was deprotected according to general procedure **GP1**. The corresponding trifluoroacetate salt was then coupled with Cbz-L-Asp(O*t*Bu)-OH (62 mg, 0.19 mmol, 1.2 eq.) according to general procedure **GP2**. The residue was purified by flash chromatography on silica gel (CH_2Cl_2/EtOH, 95:5) to afford the desired product as white foam (155 mg, 86%).

R_f=0.5 (CH_2Cl_2/MeOH 9:1); $[\alpha]_D^{20}$=-3.0 (*c*=0.35 in $CHCl_3$); ^{1}H NMR (400 MHz, Acetone-d_6) δ 8.02 (s, 1H), 7.97 – 7.89 (m, 2H), 7.58 (d, 1H, *J* = 7.9 Hz), 7.39 – 7.21 (m, 15H), 6.87

(d, 1H, *J* = 8.6 Hz), 6.66 (s, 1H), 6.54 (br s, 2H), 5.31 (d, 1H, *J* = 15.2 Hz), 5.16 – 5.09 (m, 3H), 5.01 (d, 1H, *J* = 12.5 Hz), 4.61 – 4.52 (m, 2H), 4.41 (br s, 1H), 4.14 (d, 1H, *J* = 15.2 Hz), 4.04 (dd, 1H, *J* = 17.6, 6.0 Hz), 3.95 (dd, 1H, *J* = 17.6, 5.8 Hz), 3.90 – 3.86 (m, 1H), 3.85 – 3.76 (m, 4H), 3.76 – 3.66 (m, 1H), 3.28 – 3.10 (m, 2H), 2.81 (dd, 1H, *J* = 16.3, 5.3 Hz), 2.70 – 2.59 (m, 7H), 2.56 – 2.40 (m, 2H), 2.36 – 2.24 (m, 1H), 2.23 – 2.11 (m, 1H), 2.08 (s, 3H), 1.89 – 1.78 (m, 1H), 1.70 – 1.49 (m, 3H), 1.38 (s, 9H); ^{13}C NMR (101 MHz, Acetone-d_6) δ 174.0, 173.2, 172.7, 170.7, 170.5, 168.5, 167.6, 158.9, 157.6, 157.2, 139.1, 137.8, 137.1, 137.0, 135.8, 129.6, 129.3, 129.2, 129.0, 128.8, 128.7, 128.4, 124.9, 112.5, 81.3, 67.3, 67.2, 60.6, 55.9, 54.2, 53.3, 53.0, 48.0, 41.8, 41.1, 40.4, 38.3, 31.9, 30.5, 28.2, 28.0, 26.3, 24.3, 18.7, 12.1; IR (neat): ν_{max} 3309, 2932, 2359, 1731, 1652, 1541, 1455, 1258, 1120; MS (ESI) *m*/*z* calcd for $[C_{56}H_{72}N_9O_{14}S]^+$: 1126.49 $[M+H]^+$; found: 1126.7.

H-Asp(O*t*Bu)-DKP-Arg(Mtr)-Gly-OH (57)

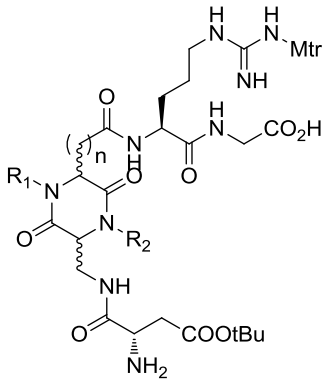

57a: (3*R*,6*S*), R_1 = Bn, R_2 = H, n = 1
57b: (3*R*,6*S*), R_1 = Bn, R_2 = Bn, n = 1
57c: (3*S*,6*R*), R_1 = Bn, R_2 = H, n = 1
57d: (3*S*,6*R*), R_1 = Bn, R_2 = Bn, n = 1
57e: (3*S*,6*R*), R_1 = H, R_2 = Bn, n = 2

a) H-Asp(O*t*Bu)-DKP4-Arg(Mtr)-Gly-OH (57a)

Compound **56a** (307 mg, 0.28 mmol, 1 eq.) was treated with Pd/C 10% (29.3 mg, 0.03 mmol, 0.1 eq.) in the conditions described in general procedure **GP3**. The crude product was obtaine as white solid (248 mg, 100%) that was used without further purification.

b) H-Asp(OtBu)-DKP5-Arg(Mtr)-Gly-OH (57b)

Compound **56b** (170 mg, 0.14 mmol, 1 eq.) was treated with Pd/C 10% (14.9 mg, 0.014 mmol, 0.1 eq.) in the conditions described in general procedure **GP3**. The crude product was obtained as white solid (137 mg, 100%) that was used without further purification.

c) H-Asp(O*t*Bu)-DKP6-Arg(Mtr)-Gly-OH (57c)

Compound **56c** (400 mg, 0.36 mmol, 1 eq.) was treated with Pd/C 10% (38.1 mg, 0.04 mmol, 0.1 eq.) in the conditions described in general procedure **GP3**. The crude product was obtained as white solid (322 mg, 100%) that was used without further purification.

d) H-Asp(O*t*Bu)-DKP7-Arg(Mtr)-Gly-OH (57d)

Compound **56d** (218 mg, 0.18 mmol, 1 eq.) was treated with Pd/C 10% (19.3 mg, 0.018 mmol, 0.1 eq.) in the conditions described in general procedure **GP3**. The crude product was obtained as white solid (176 mg, 100%) that was used without further purification.

e) H-Asp(O*t*Bu)-DKP8-Arg(Mtr)-Gly-OH (57e)

Compound **56e** (148 mg, 0.13 mmol, 1 eq.) was treated with Pd/C 10% (13.8 mg, 0.013 mmol, 0.1 eq.) in the conditions described in general procedure **GP3**. The crude product was obtained as white solid (124 mg, 100%) that was used without further purification.

***Cyclo*[Arg(Mtr)-Gly-Asp(O*t*Bu)-DKP] (58)**

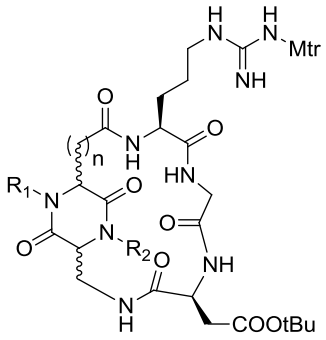

58a: (3*R*,6*S*), R_1 = Bn, R_2 = H, n = 1
58b: (3*R*,6*S*), R_1 = Bn, R_2 = Bn, n = 1
58c: (3*S*,6*R*), R_1 = Bn, R_2 = H, n = 1
58d: (3*S*,6*R*), R_1 = Bn, R_2 = Bn, n = 1
58e: (3*S*,6*R*), R_1 = H, R_2 = Bn, n = 2

a) *Cyclo*[Arg(Mtr)-Gly-Asp(O*t*Bu)-DKP4] (58a)

Compound **57a** (224 mg, 0.25 mmol, 1 eq.) was cyclized in the conditions described in general procedure **GP4**, in presence of HATU (380.2 mg, 1 mmol, 4 eq.), HOAt (136.1 mg, 1 mmol, 4 eq.) and DIPEA (0.26 ml, 1.5 mmol, 6 eq). The crude product was purified by flash chromatography on silica gel (CH_2Cl_2/MeOH, 95:5) to afford yellowish solid that was further purified by Biotage (gradient: 95% H_2O / 5% acetonitrile to 5% H_2O / 95% acetonitrile), to obtain the product as white foam (133 mg, 61%).

R_f=0.45 (CH_2Cl_2/MeOH 9:1); ^{1}H NMR (400 MHz, CD_3OD) δ 7.41 – 7.21 (m, 5H), 6.68 (s, 1H), 5.36 (br s, 1H), 4.53 – 4.41 (m, 1H), 4.39 – 4.28 (m, 1H), 4.24 – 3.89 (m, 3H), 3.85 (s, 1H), 3.78 (d, 1H, *J* = 10.6 Hz,), 3.68 – 3.48 (m, 1H), 3.31 – 3.26 (m, 1H) 3.20 (t, 2H, *J* = 5.7

Hz), 2.98 – 2.86 (m, 1H), 2.83 – 2.72 (m, 2H), 2.72 – 2.56 (m, 7H), 2.14 (s, 3H), 1.89 – 1.75 (m, 1H), 1.74 – 1.52 (m, 3H), 1.49 (s, 9H); ^{13}C NMR (101 MHz, CD_3OD) δ 172.3, 172.1, 169.9, 169.4, 168.4, 166.9, 158.5, 138.1, 136.5, 128.6, 127.5, 124.3, 111.4, 81.3, 56.8, 54.6, 53.2, 41.9, 40.7, 40.1, 35.8, 30.7, 27.8, 26.9, 22.8, 17.3, 10.7; MS (ESI) *m*/*z* calcd for $[C_{40}H_{56}N_9O_{11}S]^+$: 870.38 $[M+H]^+$; found: 870.4.

b) *Cyclo*[Arg(Mtr)-Gly-Asp(O*t*Bu)-DKP5] (58b)

Compound **57b** (224 mg, 0.25 mmol, 1 eq.) was cyclized in the conditions described in general procedure **GP4**, in presence of HATU (103.4 mg, 0.27 mmol, 4 eq.), HOAt (37.3 mg, 0.27 mmol, 4 eq.) and DIPEA (54 µl, 0.41 mmol, 6 eq). The crude product was purified by flash chromatography on silica gel (CH_2Cl_2/MeOH, 95:5) to afford yellowish solid that was further purified by Biotage (gradient: 95% H_2O / 5% acetonitrile to 5% H_2O / 95% acetonitrile), to obtain the product as white foam (20 mg, 31%).

R_f=0.33 (CH_2Cl_2/MeOH 9:1); ^{1}H NMR (400 MHz, Acetone-d_6) δ 8.00 (d, 1H, *J* = 6.9 Hz), 7.84 (d, 1H, *J* = 6.7 Hz), 7.79 – 7.70 (m, 1H), 7.58 (d, 1H, *J* = 7.7 Hz), 7.48 – 7.17 (m, 10H), 6.69 – 6.62 (m, 2H), 6.52 (br s, 2H), 6.38 (br s, 2H), 5.30 (d, 1H, *J* = 15.4 Hz), 5.24 (d, 1H, *J* = 16.0 Hz), 5.02 (d, 1H, *J* = 8.2 Hz), 4.65 – 4.38 (m, 2H), 4.38 – 3.89 (m, 5H), 3.82 (s, 3H), 3.52 (dd, 1H, *J* = 15.6, 2.3 Hz), 3.42 (dd, 1H, *J* = 13.9, 4.4 Hz), 3.28 – 3.13 (m, 2H), 2.87 (dd, 1H, *J* = 16.2, 8.2 Hz), 2.72 – 2.54 (m, 9H), 2.08 (s, 3H), 1.91 – 1.78 (m, 1H), 1.73 – 1.48 (m, 3H), 1.40 (s, 9H); ^{13}C NMR (101 MHz, Acetone-d_6) δ 172.1, 171.7, 171.6, 169.4, 169.1, 166.9, 158.0, 156.6, 138.5, 138.2, 136.3, 136.1, 128.9, 128.5, 127.9, 127.7, 127.0, 123.9, 111.6, 80.4, 58.9, 58.7, 54.9, 50.8, 49.3, 46.7, 41.9, 40.3, 39.4, 39.2, 36.8, 27.7, 27.3, 26.2, 23.3, 17.7, 11.2; MS (ESI) *m*/*z* calcd for $[C_{47}H_{62}N_9O_{11}S]^+$: 960.43 $[M+H]^+$; found: 960.7.

c) *Cyclo*[Arg(Mtr)-Gly-Asp(O*t*Bu)-DKP6] (58c)

Compound **57c** (322 mg, 0.36 mmol, 1 eq.) was cyclized in the conditions described in general procedure **GP4**, in presence of HATU (547.2 mg, 1.44 mmol, 4 eq.), HOAt (195.8 mg, 1.44 mmol, 4 eq.) and DIPEA (0.37 ml, 2.2 mmol, 6 eq). The crude product was purified by flash chromatography on silica gel (CH_2Cl_2/MeOH, 95:5) to afford yellowish solid that was further purified by Biotage (gradient: 95% H_2O / 5% acetonitrile to 5% H_2O / 95% acetonitrile), to obtain the product as white foam (180 mg, 58%).

R_f=0.47 (CH_2Cl_2/MeOH 9:1); ^{1}H NMR (400 MHz, DMSO-d_6) δ 9.08 – 8.95 (m, 1H), 8.37 (d, 1H, *J* = 8.2 Hz), 7.95 (br s, 1H), 7.71 – 7.61 (m, 1H), 7.46 (br s, 1H, *J* = 7.6 Hz), 7.39 – 7.22 (m, 5H), 6.88 – 6.64 (m, 2H), 6.55 – 6.25 (m, 1H), 5.14 (d, 1H, *J* = 14.9 Hz), 4.21 (br s, 2H), 4.05 (d, 1H, *J* = 16.0 Hz), 3.99 – 3.92 (m, 1H), 3.90 – 3.75 (m, 5H), 3.63 – 3.43 (m,

3H), 3.01 (m, 2H), 2.88 (dd, 1H, *J* = 16.2, 7.4 Hz), 2.78 – 2.48 (m, 8H, overlapping with solvent signal), 2.44 (dd, 1H, *J* = 16.3, 7.0 Hz), 2.06 (s, 3H), 1.74 – 1.58 (m, 1H), 1.56 – 1.26 (m, 12H); ^{13}C NMR (101 MHz, DMSO-d_6) δ 172.3, 171.6, 170.9, 169.8, 167.4, 166.7, 158.6, 157.2, 138.8, 137.8, 136.7, 135.7, 129.8, 128.8, 128.5, 124.7, 112.9, 81.2, 58.5, 56.6, 55.6, 53.4, 51.5, 47.2, 43.6, 42.1, 36.6, 35.5, 32.4, 29.9, 28.8, 26.8, 24.7, 19.1, 12.9; MS (ESI) *m*/*z* calcd for $[C_{40}H_{56}N_9O_{11}S]^+$: 870.38 $[M+H]^+$; found: 870.4.

d) *Cyclo*[Arg(Mtr)-Gly-Asp(O*t*Bu)-DKP7] (58d)

Compound **57d** (167 mg, 0.17 mmol, 1 eq.) was cyclized in the conditions described in general procedure **GP4**, in presence of HATU (259.7 mg, 0.68 mmol, 4 eq.), HOAt (93 mg, 0.68 mmol, 4 eq.) and DIPEA (0.17 ml, 1.02 mmol, 6 eq). The crude product was purified by flash chromatography on silica gel (CH_2Cl_2/MeOH, 95:5) to afford yellowish solid that was further purified by Biotage (gradient: 95% H_2O / 5% acetonitrile to 5% H_2O / 95% acetonitrile), to obtain the product (75 mg, 46%) as a 2:1 mixture of two inseparable diastereomers.

R_f=0.32 (CH_2Cl_2/MeOH 9:1); ^{1}H NMR (400 MHz, CD_3OD) δ (two diastereomers A and B; A/B = 2:1) 7.47 – 7.19 (m, 10H$_A$+ 10H$_B$), 6.70 – 6.65 (m, 1H$_A$ + 1H$_B$), 5.40 (d, 1H$_B$, *J* = 15.2 Hz), 5.35 (d, 1H$_B$, *J* = 16.6 Hz), 5.19 (d, 1H$_A$, *J* = 14.9 Hz), 5.05 – 4.94 (m, 2H$_A$), 4.78 (dd, 1H$_A$, *J* = 11.5, 2.1 Hz), 4.57 (t, 1H$_B$, *J* = 6.7 Hz), 4.52 (d, 1H$_B$, *J* = 16.7 Hz), 4.46 (d, 1H$_A$, *J* = 17.4 Hz), 4.43 – 4.39 (m, 1H$_B$), 4.34 (d, 1H$_B$, *J* = 16.5 Hz), 4.29 – 4.19 (m, 1H$_A$ + 2H$_B$), 4.13 (d, 1H$_A$, *J* = 15.1 Hz), 4.08 – 3.96 (m, 2H$_A$), 3.91 (d, 1H$_B$, *J* = 15.3 Hz), 3.88 – 3.78 (m, 3H$_A$ + 4H$_B$), 3.70 (dd, 1H$_A$, *J* = 10.4, 4.1 Hz), 3.66 – 3.56 (m, 1H$_A$ + 1H$_B$), 3.53 – 3.42 (m, 1H$_A$ + 1H$_B$), 3.28 – 3.09 (m, 2H$_A$ + 2H$_B$), 3.03 – 2.80 (m, 2H$_A$ + 1H$_B$), 2.78 – 2.65 (m, 4H$_A$ + 4H$_B$), 2.63 (s, 3H$_B$), 2.60 (s, 3H$_A$), 2.58 – 2.43 (m, 1H$_A$ + 2H$_B$), 2.15 (s, 3H$_B$), 2.13 (s, 3H$_A$), 2.11 – 2.00 (m, 1H$_A$), 1.94 – 1.81 (m, 1H$_A$ + 1H$_B$), 1.80 – 1.70 (m, 1H$_B$), 1.66 – 1.52 (m, 2H$_A$ + 2H$_B$), 1.49 – 1.44 (m, 9H$_A$ + 9H$_B$); ^{13}C NMR (101 MHz, CD_3OD) δ (two rotamers) 173.2, 172.2, 171.7, 171.1, 170.7, 170.4, 169.8, 168.5, 167.5, 158.5, 156.7, 138.1, 136.9, 136.5, 135.8, 135.5, 133.5, 128.7, 128.6, 128.5, 128.3, 127.9, 127.8, 127.0, 126.9, 126.1, 124.3, 111.4, 80.9, 59.7, 58.4, 56.9, 56.8, 54.6, 53.8, 50.2, 48.7, 43.2, 42.2, 39.7, 38.2, 35.9, 35.6, 35.1, 28.3, 26.9, 26.0, 25.5, 22.9, 17.4, 13.0, 10.7; MS (ESI) *m*/*z* calcd for $[C_{47}H_{62}N_9O_{11}S]^+$: 960.43 $[M+H]^+$; found: 960.5.

e) *Cyclo*[DKP-8-Arg(Mtr)-Gly-Asp(O*t*Bu)] (58e)

Compound **57e** (124 mg, 0.13 mmol, 1 eq.) was cyclized in the conditions described in general procedure **GP4**, in presence of HATU (197 mg, 0.52 mmol, 4 eq.), HOAt (70 mg, 0.52 mmol, 4 eq.), and DIPEA (137 µl, 0.8 mmol, 6 eq.). The crude product was purified by flash chromatography on silica gel (CH_2Cl_2/MeOH, 93:7) to afford the desired product as white foam (85 mg, 74%).

R_f=0.4 (CH_2Cl_2/MeOH, 9:1); ^{1}H NMR (400 MHz, CD_3OD) δ 7.41 – 7.22 (m, 5H), 6.66 (s, 1H), 5.31 (d, 1H, *J* = 15.3 Hz), 4.47 (dd, 1H, *J* = 8.4, 4.9 Hz), 4.27 (dd, 1H, *J* = 8.7, 5.8 Hz), 4.18 – 4.08 (m, 2H), 4.05 (d, 1H, *J* = 15.3 Hz), 3.97 (d, 1H, *J* = 16.8 Hz), 3.88 – 3.79 (m, 4H), 3.67 (d, 1H, *J* = 16.8 Hz), 3.55 (d, 1H, *J* = 13.7 Hz), 3.26 – 3.14 (m, 2H), 2.91 (dd, 1H, *J* = 16.6, 4.9 Hz), 2.76 (dd, 1H, *J* = 16.6, 8.4 Hz), 2.71 – 2.56 (m, 7H), 2.56 – 2.42 (m, 2H), 2.12 (s, 3H), 1.86 – 1.52 (m, 5H), 1.44 (s, 9H); ^{13}C NMR (101 MHz, CD_3OD) δ 176.4, 175.9, 175.0, 173.9, 171.6, 171.6, 169.6, 169.5, 159.9, 158.2, 139.5, 138.0, 137.4, 134.8, 130.0, 129.0, 125.7, 112.8, 82.4, 60.4, 56.0, 54.9, 53.0, 52.4, 48.2, 44.0, 41.1, 40.2, 37.5, 31.8, 30.7, 29.0, 28.3, 27.4, 24.4, 18.9, 12.1**;** MS (ESI) *m*/*z* calcd for $[C_{41}H_{58}N_9O_{11}S]^+$: 884.40 $[M+H]^+$; found: 884.46.

***Cyclo*[Arg-Gly-Asp-DKP] – c[DKP-RGD]**

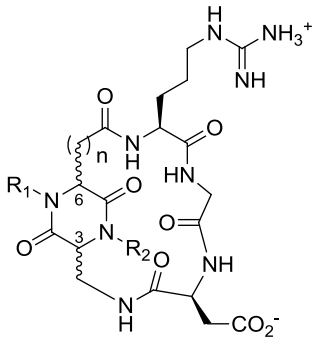

c[DKP-4-RGD]: (3*R*,6*S*), R_1 = Bn, R_2 = H, n = 1
c[DKP-5-RGD]: (3*R*,6*S*), R_1 = Bn, R_2 = Bn, n = 1
c[DKP-6-RGD]: (3*S*,6*R*), R_1 = Bn, R_2 = H, n = 1
c[DKP-7-RGD]-A: (3*S*,6*R*), R_1 = Bn, R_2 = Bn, n = 1
c[DKP-7-RGD]-B: (3*S*,6*R*), R_1 = Bn, R_2 = Bn, n = 1
c[DKP-8-RGD]: (3*S*,6*R*), R_1 = H, R_2 = Bn, n = 2

***Cyclo*[Arg-Gly-Asp-DKP4] - c[DKP-4-RGD]**

Compound **58a** (93.7 mg, 0.11 mmol) was fully deprotected in the conditions described in general procedure **GP5**. The crude product was purified by HPLC (Water's Atlantis 21 mm x 10 cm column, gradient: 90% H_2O / 10% acetonitrile to 70% H_2O / 30% acetonitrile) to give the desired compound as white solid (62 mg, 80%).

^{1}H NMR (400 MHz, H_2O/D_2O 9:1, T= 298K) δ 8.88 (br s, 1H, Asp-NH), 8.37 – 8.23 (m, 2H, Arg-NH + Gly-NH), 8.20 (m, 1H, DKP-NH4), 7.59 (m, 1H, DKP-NH10), 7.35 – 7.19 (m, 5H, H-Ar), 7.11 (t, 1H, *J* = 6.1 Hz, NH-guan), 5.08 (m, 1H, $\underline{CH_2}$-Ph), 4.35 (m, 1H, αH-Asp), 4.29 – 4.14 (m, 2H, αH-Arg + DKP-H6), 4.01 – 3.82 (m, 2H, αH-Gly + DKP-H3), 3.77 – 3.58 (m, 2H, αH-Gly + DKP-H9), 3.34 (m, 1H, DKP-H9), 3.12 (m, 2H, δH-Arg), 3.01 – 2.67 (m, 4H, DKP-H7 + βH-Asp), 1.85 – 1.43 (m, 4H, βH-Arg + γH-Arg); ^{13}C NMR (101 MHz, D_2O, T= 298K) δ 173.8, 172.8, 170.8, 168.5, 156.8, 135.3, 128.7, 127.6, 57.5, 53.5, 53.3, 52.0, 47.3, 42.3, 40.7, 40.6, 35.7, 34.3, 28.0, 24.4; HRMS (ESI) *m*/*z* calcd for $[C_{26}H_{35}N_9O_8Na]^+$: 624.25008 $[M+Na]^+$; found: 624.24942.

***Cyclo*[Arg-Gly-Asp-DKP5] - c[DKP-5-RGD]**

Compound **58b** (20 mg, 0.02 mmol) was fully deprotected in the conditions described in general procedure **GP5**. The crude product was purified by HPLC (Water's Atlantis 21 mm x 10 cm column, gradient: 90% H_2O / 10% acetonitrile to 30% H_2O / 70% acetonitrile) to give the desired compound (as trifluoroacetate salt) as white solid (9.5 mg, 60%).

^{1}H NMR (400 MHz, H_2O/D_2O 9:1, T= 298K) δ 8.61 – 8.53 (m, 1H, DKP-NH10), 8.48 (d, 1H, *J* = 6.6 Hz, Arg-NH), 8.42 (d, 1H, *J* = 8.3 Hz, Asp-NH), 8.23 (d, 1H, *J* = 9.6 Hz, Gly-NH), 7.44 – 7.19 (m, 10H, H-Ar), 7.11 – 7.03 (m, 1H, NH-guan), 5.10 (m, 1H, CH_2-Ph), 5.00 (m, 1H, CH_2-Ph), 4.62 (m, 1H, αH-Asp), 4.41 (m, 1H, DKP-H6), 4.37 (m, 1H, CH_2-Ph), 4.33 (m, 1H, DKP-H3), 4.32 (m, 1H, DKP-H9), 4.23 (m, 1H, αH-Gly), 4.15 (d, 1H, *J* = 15.4 Hz, CH_2-Ph), 4.11 (m, 1H, αH-Arg), 3.42 (d, 1H, *J* = 17.3 Hz, αH-Gly), 3.34 (m, 1H, DKP-H9), 3.10 (dd, 2H, *J* = 12.6, 6.6 Hz, δH-Arg), 2.86 (dd, 1H, *J* = 16.8, 7.8 Hz, βH-Asp), 2.70 (dd, 1H, *J* = 17.0, 7.2 Hz, βH-Asp), 2.55 (m, 2H, DKP-H7), 1.82 – 1.50 (m, 4H, βH-Arg + γH-Arg); ^{13}C NMR (101 MHz, D_2O, T= 298K) δ 175.0, 174.8, 174.4, 173.7, 173.3, 169.7, 167.8, 136.5, 135.5, 129.1, 129.0, 128.7, 128.5, 127.6, 126.2, 59.5, 55.1, 51.5, 50.1, 48.3, 48.1, 41.9, 40.3, 39.7, 39.4, 38.6, 26.8, 24.3; HRMS (ESI) *m*/*z* calcd for $[C_{33}H_{41}N_9O_8Na]^+$: 714.29703 $[M+Na]^+$; found: 714.29588.

***Cyclo*[Arg-Gly-Asp-DKP6] - c[DKP-6-RGD]**

Compound **58c** (80.2 mg, 0.09 mmol) was fully deprotected in the conditions described in general procedure **GP5**. The crude product was purified by (Water's Atlantis 21 mm x 10 cm column, gradient: 90% H_2O / 10% acetonitrile to 70% H_2O / 30% acetonitrile) to give the desired compound (as trifluoroacetate salt) as white solid (54 mg, 82%).

^{1}H NMR (400 MHz, H_2O/D_2O 9:1, T= 298K) δ 8.80 (d, 1H, *J* = 6.4 Hz, Asp-NH), 8.40 – 8.26 (m, 2H, Gly-NH + Arg-NH), 8.07 (s, 1H, DKP-NH4), 7.89 (t, 1H, *J* = 6.1 Hz, DKP-NH10), 7.40 – 7.22 (m, 5H, H-Ar), 7.10 (t, 1H, *J* = 5.7 Hz, NH-guan), 5.06 (d, 1H, *J* = 17.9 Hz, CH_2-Ph), 4.35 (m, 1H, αH-Asp), 4.29 (m, 1H, αH-Arg), 4.26 – 4.19 (m, 2H, DKP-H6 + CH_2-Ph), 3.96 – 3.89 (m, 1H, DKP-H3), 3.90 – 3.75 (m, 2H, αH-Gly + DKP-H9), 3.67 (dd, 1H, *J* = 15.6, 6.1 Hz, αH-Gly), 3.58 – 3.43 (m, 1H, DKP-H9), 3.13 (dd, 2H, *J* = 12.9, 6.9 Hz, δH-Arg), 2.81 – 2.67 (m, 3H, DKP-H7 + βH-Asp), 2.56 (dd, 1H, *J* = 16.1, 8.3 Hz, βH-Asp), 1.84 – 1.48 (m, 4H, βH-Arg + γH-Arg); ^{13}C NMR (101 MHz, D_2O, T= 298K) δ 174.6, 173.3, 172.7, 171.9, 171.0, 168.3, 166.7, 135.3, 129.1, 128.6, 127.6, 57.6, 54.9, 53.1, 51.3, 47.7, 47.1, 42.8, 40.4, 35.4, 35.0, 27.8, 24.2; HRMS (ESI) *m*/*z* calcd for $[C_{26}H_{35}N_9O_8Na]^+$: 624.25008 $[M+Na]^+$; found: 624.24929.

***Cyclo*[Arg-Gly-Asp-DKP7] - c[DKP-7-RGD]**

Compound **58d** (65 mg, 0.068 mmol) was fully deprotected in the conditions described in general procedure **GP5**. The crude product was purified by HPLC (Water's Atlantis 21 mm x 10 cm column, gradient: 90% H_2O / 10% acetonitrile to 40% H_2O / 60% acetonitrile) to give **c[DKP-7-RGD]-A** (as trifluoroacetate salt) (21.3 mg) and **c[DKP-7-RGD]-B** (as trifluoroacetate salt) (10.6 mg) as white solids (60% overall).

A: ^{1}H NMR (400 MHz, H_2O/D_2O 9:1, T= 298K) δ 8.66 (d, 1H, *J* = 7.7 Hz, Arg-NH), 8.04 (t, 1H, *J* = 6.6 Hz, DKP-NH10), 7.95 – 7.89 (m, 1H, Gly-NH), 7.77 – 7.70 (m, 1H, Asp-NH), 7.44 – 7.16 (m, 10H, H-Ar), 7.10 – 7.04 (m, 1H, NH-guan), 5.06 – 4.99 (m, 1H, $\underline{CH_2}$-Ph), 4.89 (m, 1H, αH-Asp), 4.80 (m, 1H, $\underline{CH_2}$-Ph), 4.69 (m, 1H, DKP-H6), 4.57 (m, 1H, $\underline{CH_2}$-Ph), 4.39 – 4.33 (m, 2H, αH-Gly, DKP-H3), 4.14 – 4.07 (m, 1H, αH-Arg), 4.04 (d, 1H, *J* = 14.8 Hz, $\underline{CH_2}$-Ph), 3.91 (dd, 1H, *J* = 15.4, 7.1 Hz, DKP-H9), 3.71 – 3.61 (m, 1H, DKP-H9), 3.60 – 3.52 (m, 1H, αH-Gly), 3.10 (dd, 2H, *J* = 12.9, 6.9 Hz, δH-Arg), 2.90 – 2.76 (m, 2H, DKP-H7, βH-Asp), 2.62 (dd, 1H, *J* = 17.1, 6.3 Hz, βH-Asp), 2.58 – 2.49 (m, 1H, DKP-H7), 2.01 – 1.87 (m, 1H, βH-Arg), 1.73 – 1.58 (m, 1H, βH-Arg), 1.55 – 1.42 (m, 2H, γH-Arg); ^{13}C NMR (101 MHz, D_2O, T= 298K) δ 174.3, 173.4, 173.0, 172.4, 171.2, 170.6, 169.4, 156.8, 129.3, 129.1, 128.5, 127.8, 126.5, 58.7, 56.9, 53.7, 48.9, 48.3, 47.6, 43.2, 40.9, 39.7, 37.7, 36.9, 25.4, 24.4; HRMS (ESI) *m*/*z* calcd for $[C_{33}H_{41}N_9O_8Na]^+$: 714.29703 $[M+Na]^+$; found: 714.29618.

B: ^{1}H NMR (400 MHz, H_2O/D_2O 9:1, T= 298K) δ 8.55 (d, 1H, *J* = 8.1 Hz, Asp-NH), 8.45 (t, 1H, *J* = 5.8 Hz, Gly-NH), 8.34 (d, 1H, *J* = 5.9 Hz, Arg-NH), 7.73 (d, 1H, *J* = 8.4 Hz, DKP-NH10), 7.46 – 7.16 (m, 10H, H-Ar), 7.16 – 7.10 (m, 1H, NH-guan), 5.27 – 5.15 (m, 2H, $\underline{CH_2}$-Ph), 4.52 (m, 1H, αH-Asp), 4.44 (m, 1H, DKP-H6), 4.36 – 4.29 (m, 1H, $\underline{CH_2}$-Ph), 4.20 (d, 1H, *J* = 14.8 Hz, $\underline{CH_2}$-Ph), 4.16 – 4.07 (m, 2H, αH-Arg, DKP-H3), 3.80 (dd, 1H, *J* = 15.2, 4.1 Hz, αH-Gly), 3.76 – 3.63 (m, 2H, αH-Gly, DKP-H9), 3.38 – 3.28 (m, 1H, DKP-H9), 3.16 (dd, 2H, *J* = 13.6, 7.1 Hz, δH-Arg), 2.94 (dd, 1H, *J* = 14.9, 6.1 Hz, DKP-H7), 2.87 – 2.72 (m, 2H, DKP-H7, βH-Asp), 2.60 (dd, 1H, *J* = 16.6, 7.2 Hz, βH-Asp), 1.77 (dd, 2H, *J* = 15.6, 8.3 Hz, βH-Arg), 1.69 – 1.52 (m, 2H, γH-Arg);^{13}C NMR (101 MHz, D_2O, T= 298K) δ 174.5, 174.1, 171.9, 171.6, 170.8, 169.0, 168.3, 136.8, 135.4, 129.2, 129.0, 128.3, 127.8, 127.6, 125.9, 60.7, 56.8, 53.6, 51.4, 49.6, 47.5, 43.5, 40.6, 39.3, 36.7, 35.6, 27.8, 24.7; HRMS (ESI) *m*/*z* calcd for $[C_{33}H_{41}N_9O_8Na]^+$: 714.29703 $[M+Na]^+$; found: 714.29676.

***Cyclo*[Arg-Gly-Asp-DKP8] - c[DKP-8-RGD]**

Compound **58e** (50 mg, 0.06 mmol) was fully deprotected in the conditions described in general procedure **GP5**. The crude product was purified by HPLC HPLC (Water's Atlantis 21 mm x 10 cm column, gradient: 95% H_2O / 5% acetonitrile

to 80% H_2O / 20% acetonitrile) to give the desired compound (as trifluoroacetate salt) as white solid (34 mg, 80%).

^{1}H NMR (600 MHz, H_2O/D_2O 9:1, T= 298K) δ 8.42 (d, 1H, *J* = 7.3 Hz, Arg-NH), 8.27 (t, 1H, *J* = 6.6 Hz, Gly-NH), 8.16 – 8.14 (m, 2H, Asp-NH, DKP-NH10), 7.75 (s, 1H, DKP-NH1), 7.26 – 7.14 (m, 5H, H-Ar), 7.05 (t, 1H, *J* = 5.9 Hz, NH-guan), 5.03 (d, 1H, *J* = 17.6 Hz, $\underline{CH_2}$-Ph), 4.42 (m, 1H, αH-Asp), 4.16 (q, 1H, *J* = 7.8 Hz, αH-Arg), 4.02 (d, 1H, *J* = 15.9, $\underline{CH_2}$-Ph), 4.05 – 3.96 (m, 2H, DKP-H3, DKP-H6), 3.90 – 3.75 (m, 3H, αH-Gly, DKP-H9), 3.65 (dd, 1H, *J* = 15.0, 6.2 Hz, DKP-H9), 3.10 (q, 2H, *J* = 7.1 Hz, δH-Arg), 2.76 – 2.71 (m, 2H, βH-Asp), 2.50 – 2.30 (m, 3H, DKP-H7, DKP-H8), 1.75 – 1.45 (m, 5H, DKP-H8, βH-Arg, γH-Arg); ^{13}C NMR (151 MHz, D_2O, T= 298K) δ 174.9, 174.5, 174.3, 173.8, 171.1, 168.6, 168.2, 157.1, 135.4, 129.1, 128.1, 127.6, 59.3, 53.6, 51.9, 50.9, 47.6, 42.3, 40.6, 39.4, 35.3, 30.3, 29.6, 27.1, 24.5; HRMS (ESI) *m*/*z* calcd for $[C_{27}H_{37}N_9O_8Na]^+$: 638.26573 $[M+Na]^+$; found: 638.26512.

3.1.4 - Synthesis of c[DKP-*f*-RGD] integrin ligands

***N*-Boc-DKP-*f*-Arg(Mtr)-Gly-OBn (59)**

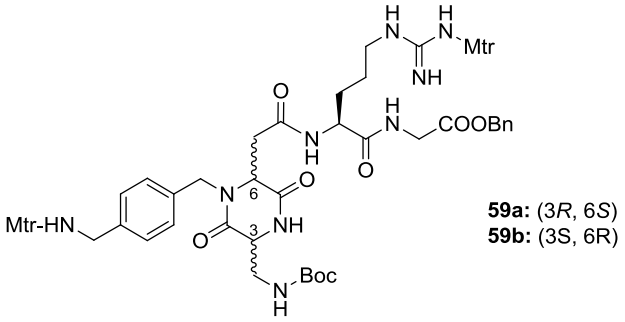

a) Boc-DKP-*f*4-Arg(Mtr)-Gly-OBn (59a)

Dipeptide Boc-Arg(Mtr)-Gly-OBn **54** (280 mg, 0.44 mmol, 1.2 equiv) was deprotected according to general procedure **GP1**. The corresponding trifluoroacetate salt was then coupled with **DKP-*f*4** (230 mg, 0.37 mmol, 1 equiv), according to general procedure **GP2**. The residue was purified by flash chromatography on silica gel (CH_2Cl_2/MeOH, 93:7) to afford the desired product as a white foam (350 mg, 83%).

R_f=0.36 (CH_2Cl_2/MeOH 9:1); $[\alpha]_D^{20}$=+29.7 (*c*=1.0 in CH_2Cl_2); ^{1}H NMR (400 MHz, acetone-d_6) δ 7.84 (t, 1H, *J* = 5.9 Hz), 7.49 (d, 1H, *J* = 7.3 Hz), 7.40-7.32 (m, 5H), 7.19-7.15 (A2 system, 4H), 6.76 (s, 1H), 6.71-6.67 (m, 2H), 6.51 (br s, 2H), 6.16 (t, 1H, *J* = 4.7 Hz), 5.15 (s, 2H), 5.06 (d, 1H, *J* = 15.2 Hz), 4.52-4.47 (m, 1H), 4.33 (t, 1H, *J* = 4.9 Hz), 4.20 (d, 1H, *J* = 15.2 Hz), 4.07-4.02 (m, 3H), 4.00 (d, 2H, *J* = 6.8 Hz), 3.88 (s, 3H), 3.84 (s, 3H), 3.70 (ddd, 1H, *J* = 14.0, 5.9, 4.6 Hz), 3.57-3.51 (m, 1H), 3.27-3.11 (m, 2H), 2.92-2.82 (m overlapped with

water signal, 2H), 2.67 (s, 3H), 2.63 (s, 3H), 2.62 (s 3H), 2.57 (s, 3H), 2.10 (s, 6H), 1.87-1.82 (m, 1H), 1.63-1.52 (m, 4H), 1.41 (s, 9H); ^{13}C NMR (101 MHz, acetone-d_6) δ 172.6, 170.3, 169.9, 169.1, 167.0, 160.0, 159.0, 157.57, 157.53, 139.51, 139.32, 139.17, 138.2, 137.12, 137.08, 136.7, 135.8, 131.2, 129.3, 129.12, 128.99, 128.97, 128.6, 125.5, 124.9, 113.0, 112.5, 79.6, 67.1, 58.0, 56.14, 56.10, 55.91, 53.3, 47.6, 46.8, 43.2, 41.8, 41.1, 37.5, 30.2, 28.6, 26.3, 24.42, 24.28, 18.7, 18.2, 12.1; IR (film) 3343, 2972, 2939, 1741, 1680, 1656, 1586, 1557, 1455, 1306, 1140 cm^{-1}; MS (ESI) *m/z* calcd for $[C_{55}H_{74}N_9O_{14}S_2]^+$: 1148.48 $[M+H]^+$; found: 1148.6.

a) Boc-DKP-*f*6-Arg(Mtr)-Gly-OBn (59b)

Dipeptide Boc-Arg(Mtr)-Gly-OBn **54** (460 mg, 0.73 mmol, 1.1 equiv) was deprotected according to general procedure **GP1**. The corresponding trifluoroacetate salt was then coupled with **DKP-*f*6** (420 mg, 0.66 mmol, 1 equiv), according to general procedure **GP2**. The residue was purified by flash chromatography on silica gel (CH_2Cl_2/MeOH, 93:7) to afford the desired product as a white foam (630 mg, 83%).

R_f=0.47 (DCM/MeOH 9:1); $[\alpha]_D^{20}$=-34.8 (*c*=1.0 in CH_2Cl_2); ^{1}H NMR (400 MHz, acetone-d_6) δ 7.97 (br s, 1H , *J* = 5.3 Hz), 7.73 (d, 1H, *J* = 7.4 Hz), 7.49 (s, 1H), 7.40 – 7.27 (m, 5H), 7.23 – 7.13 (m, 4H), 6.80 – 6.73 (m, 2H), 6.67 (s, 1H), 6.58 (br s, 2H), 6.25 (t, 1H, *J* = 5.0 Hz), 5.25 (d, 1H, *J* = 15.1 Hz), 5.13 (s, 2H), 4.68 – 4.58 (m, 1H, *J* = 4.4 Hz), 4.31 (br s, 1H, *J* = 3.8 Hz), 4.14 – 3.91 (m, 6H), 3.87 (s, 3H), 3.82 (s, 3H), 3.74 – 3.63 (m, 1H), 3.62 – 3.52 (m, 1H), 3.15 (m, 2H), 3.02 (dd, 2H), 2.89 (d, 1H, *J* = 12.7 Hz), 2.68 (s, 3H), 2.66 – 2.60 (m, 6H), 2.55 (s, 3H), 2.09 (s, 6H), 1.89 – 1.77 (m, 1H), 1.66 – 1.46 (m, 3H), 1.40 (s, 9H); ^{13}C NMR (101 MHz, acetone-d_6) δ 172.9, 170.4, 170.0, 169.0, 167.3, 159.9, 158.9, 157.6, 157.4, 139.4, 139.3, 139.2, 138.3, 137.1, 136.9, 136.1, 135.6, 131.0, 129.3, 129.1, 129.0, 128.8, 125.4, 124.9, 113.0, 112.5, 79.6, 67.2, 57.4, 56.2, 56.1, 55.9, 52.9, 46.9, 46.6, 43.3, 41.7, 40.9, 37.3, 30.7, 28.6, 25.9, 24.4, 24.3, 18.7, 18.2, 12.1; IR (film) 3340, 2971, 2937, 1740, 1684, 1660, 1584, 1558, 1456, 1307, 1141 cm^{-1}; MS (ESI) m/z calcd for $[C_{55}H_{74}N_9O_{14}S_2]^+$: 1148.48 $[M+H]^+$; found: 1148.7

Cbz-Asp(O*t*Bu)-DKP-*f*-Arg(Mtr)-Gly-OBn (60)

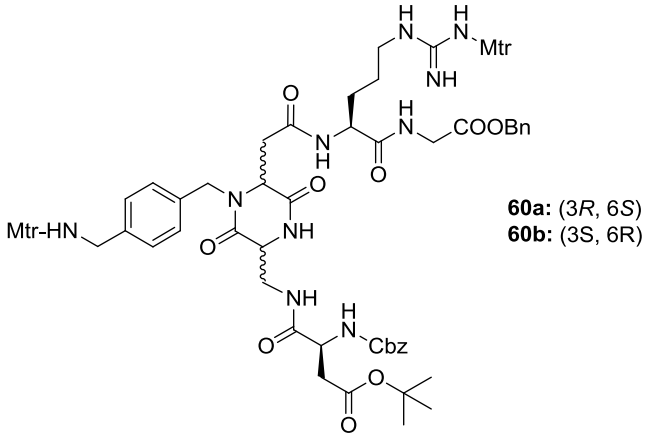

a) Cbz-Asp(O*t*Bu)-DKP-*f*4-Arg(Mtr)-Gly-OBn (60a)

Boc-DKP-*f*4-Arg(Mtr)-Gly-OBn **59a** (270 mg, 0.235 mmol, 1 equiv) was deprotected according to general procedure **GP1**. The corresponding trifluoroacetate salt was then coupled with Cbz-L-Asp(O*t*Bu)-OH (91 mg, 0.28 mmol, 1.2 equiv), according to general procedure **GP2**. The residue was purified by flash chromatography on silica gel (CH_2Cl_2/MeOH, 9:1) to afford the desired product as a white foam (280 mg, 88%).

R_f=0.45 (CH_2Cl_2/MeOH 9:1); $[\alpha]_D^{20}$=+22.1 (*c*=1.0 in CH_2Cl_2); ^{1}H NMR (400 MHz, acetone-d_6) δ 7.85 (t, 1H, *J* = 5.5 Hz), 7.74 (t, 1H, *J* = 5.8 Hz), 7.47 (d, 1H, *J* = 7.9 Hz), 7.40-7.28 (m, 10H), 7.17 (A2 system, 4H), 6.76 (m, 2H), 6.68 (m, 2H), 6.51 (br s, 2H), 5.14-5.01 (m, 5H), 4.54 (td, 1H, *J* = 7.8, 6.0 Hz), 4.47 (m, 1H), 4.41 (t, 1H, *J* = 5.4 Hz), 4.22 (d, 1H, *J* = 15.1 Hz), 4.06 (t, 1H, *J* = 5.3 Hz), 4.02 (d, 2H, *J* = 6.3), 3.99 (d, 2H, *J* = 6.6), 3.90-3.84 (m, 4H), 3.83 (s, 3H), 3.61 (dt, *J* = 14.0, 6.6 Hz, 1H), 3.25-3.12 (m, 2H), 2.91-2.85 (m, 2H), 2.81-2.79 (m overlapped with water signal, 1H), 2.69-2.65 (m, 4H), 2.64 (s, 3H), 2.62 (s, 3H), 2.55 (s, 3H), 2.10 (s, 6H), 1.87-1.81 (m, 1H), 1.62-1.51 (m, 3H), 1.40 (s, 9H); ^{13}C NMR (101 MHz, acetone-d_6) δ 172.8, 172.5, 170.7, 170.3, 169.8, 169.0, 166.9, 160.0, 158.9, 157.5, 157.0, 139.51, 139.34, 139.17, 138.07, 137.88, 137.12, 137.08, 136.8, 135.8, 129.32, 129.23, 129.14, 129.09, 128.99, 128.95, 128.7, 125.5, 124.8, 113.0, 112.5, 81.4, 67.21, 67.11, 58.1, 56.08, 55.88, 55.2, 53.3, 52.9, 47.6, 46.8, 42.3, 41.8, 38.4, 37.5, 30.3, 28.2, 26.2, 24.43, 24.29, 18.7, 18.2, 12.1; IR (film) 3343, 3291, 2927, 1718, 1685, 1655, 1554, 1456, 1308, 1141 cm^{-1}; MS (ESI) *m*/*z* calcd for $[C_{66}H_{85}N_{10}O_{17}S_2]^+$: 1353.56 $[M+H]^+$; found: 1353.6.

b) Cbz-Asp(O*t*Bu)-DKP-*f*4-Arg(Mtr)-Gly-OBn (60b)

Boc-DKP-*f*6-Arg(Mtr)-Gly-OBn **59b** (420 mg, 0.37 mmol, 1 equiv) was deprotected according to general procedure **GP1**. The corresponding trifluoroacetate salt was then coupled with Cbz-L-Asp(O*t*Bu)-OH (141.6 mg, 0.44 mmol, 1.2 equiv), according to general procedure **GP2**. The residue was purified by flash chromatography on silica gel (CH_2Cl_2/MeOH, 9:1) to afford the desired product as a white foam (428 mg, 86%).

R_f=0.49 (DCM/MeOH 9:1); $[\alpha]_D^{20}$=-27.6 (*c*=0.5 in MeOH); ^{1}H NMR (400 MHz, acetone-d_6) δ 7.97 (t, 1H, *J* = 5.5 Hz), 7.83 (br s, 1H), 7.70 (d, 1H, *J* = 6.8 Hz), 7.48 (s, 1H), 7.40 – 7.24 (m, 10H), 7.24 – 7.14 (m, 4H), 6.84 (d, 1H, *J* = 8.2 Hz), 6.79 – 6.71 (m, 2H), 6.66 (s, 1H), 6.58 (br s, 2H), 5.21 (d, 1H, *J* = 15.0 Hz), 5.16 – 5.06 (m, 3H), 5.00 (d, 1H, *J* = 12.5 Hz), 4.65 – 4.55 (m, 2H), 4.38 (t, 1H, *J* = 4.8 Hz), 4.17 – 3.92 (m, 6H), 3.90 – 3.77 (m, 7H), 3.75 – 3.65 (m, 1H), 3.28 – 3.09 (m, 2H), 3.04 – 2.95 (m, 1H), 2.94 – 2.86 (m, 1H), 2.85 – 2.76 (m, 1H), 2.75 – 2.59 (m, 10H), 2.55 (s, 3H), 2.17 – 2.05 (m, 6H), 1.88 – 1.76 (m, 1H), 1.66 – 1.46 (m, 3H), 1.38 (s, 9H); ^{13}C NMR (101 MHz, acetone-d_6) δ 172.9, 170.7, 170.4, 170.0, 168.9, 167.1, 159.9, 158.9, 157.6, 157.1, 139.3, 139.2, 138.2, 137.8, 137.1, 136.9, 136.2, 135.7, 131.0, 129.2,

129.0, 128.7, 125.4, 124.9, 113.0, 112.5, 81.4, 67.2, 57.5, 56.1, 55.9, 55.4, 53.0, 52.9, 47.1, 46.7, 42.3, 41.8, 41.0, 38.4, 37.3, 30.7, 28.2, 26.1, 24.4, 18.7, 18.2, 12.1; IR (film) 3342, 3299, 2927, 1718, 1683, 1658, 1557, 1453, 1307, 1141 cm^{-1}; MS (ESI) m/z calcd for $[C_{66}H_{85}N_{10}O_{17}S_2]^+$: 1353.55 $[M+H]^+$; found: 1353.8.

H-Asp(O*t*Bu)-DKP-*f*-Arg(Mtr)-Gly-OH (61)

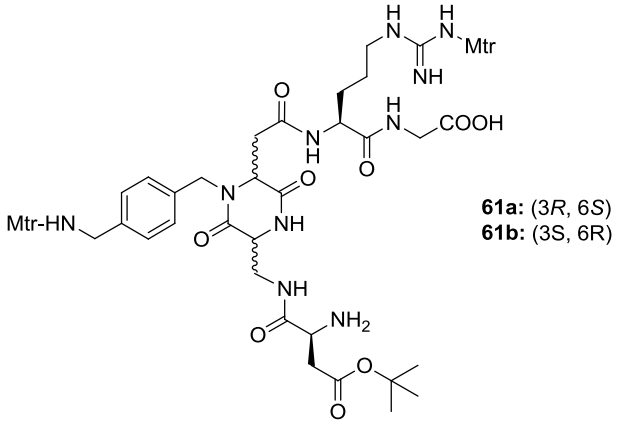

a) H-Asp(O*t*Bu)-DKP-*f*4-Arg(Mtr)-Gly-OH (61a)

A solution of Cbz-Asp(O*t*Bu)-DKP-*f*4-Arg(Mtr)-Gly-OBn **60a** (200 mg, 0.148 mmol, 1 equiv) in THF/H_2O 1:1 (50 mL) was treated with 10% Pd/C (16 mg, 0.015 mmol, 0.1 equiv), and the flask was purged three times with vacuum/H_2. The mixture was stirred at rt overnight under H_2 atmosphere, then filtered through a pad of Celite and the Celite cake was washed thoroughly with THF/H_2O 1:1. The solvents were removed under vacuum to give the crude product as a white solid (166 mg, 100%), which was used without further purification.

b) H-Asp(O*t*Bu)-DKP-*f*6-Arg(Mtr)-Gly-OH (61b)

A solution of Cbz-Asp(O*t*Bu)-DKP-*f*6-Arg(Mtr)-Gly-OBn **60b** (317 mg, 0.23 mmol, 1 equiv) in THF/H_2O 1:1 (80 mL) was treated with 10% Pd/C (25 mg, 0.023 mmol, 0.1 equiv), and the flask was purged three times with vacuum/H_2. The mixture was stirred at rt overnight under H_2 atmosphere, then filtered through a pad of Celite and the Celite cake was washed thoroughly with THF/H_2O 1:1. The solvents were removed under vacuum to give the crude product **138** as a white solid (260 mg, 100%), which was used without further purification.

***Cyclo*[DKP-*f*-Arg(Mtr)-Gly-Asp(O*t*Bu)] (62)**

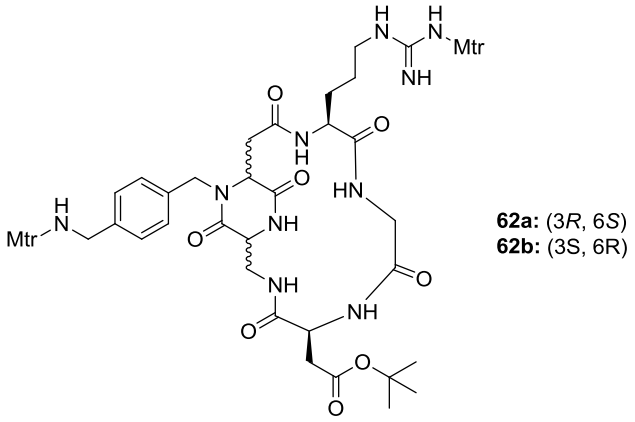

a) *Cyclo*[DKP-*f*4-Arg(Mtr)-Gly-Asp(O*t*Bu)] (62a)

To a solution of H-Asp(O*t*Bu)-DKP-*f*4-Arg(Mtr)-Gly-OH **61a** (166 mg, 0.148 mmol, 1 equiv) in DMF (110 mL), under nitrogen atmosphere and at 0 ºC, HATU (224 mg, 0.593 mmol, 4 equiv), HOAt (81 mg, 0.592 mmol, 4 equiv) and *i*-Pr$_2$NEt (0.160 mL, 0.89 mmol, 6 equiv) were added. The reaction was warmed up to rt and stirred overnight. DMF was then removed under reduced pressure to afford a yellowish solid. The solid was dissolved in AcOEt (150 mL) and the resulting solution was washed with 1 M aqueous KHSO$_4$ (2×20 mL), saturated aqueous NaHCO$_3$ (2×20 mL) and brine (2×32 mL), dried over Na$_2$SO$_4$ and the solvent evaporated under reduced pressure to afford the crude product. The crude was purified by flash-chromatography on silica gel (CH$_2$Cl$_2$/MeOH, 9:1) to afford the desired product as a fluffy solid (110 mg, 67%).

R_f=0.4 (CH$_2$Cl$_2$/MeOH 9:1); $[\alpha]_D^{20}$=-42.0 (*c*=1.0 in DMSO); ^{1}H NMR (400 MHz, DMSO-*d*$_6$) δ 8.88 (br s, 1H), 8.25 (m, 2H), 8.03 (br s, 1H), 7.85 (t, 1H, *J* = 6.2 Hz), 7.41 (br s, 1H), 7.12 (AB system, 4H), 6.75 (s, 1H), 6.68 (s, 1H), 6.41 (br s, 1H), 5.18 (d, 1H, *J* = 14.1 Hz), 4.26-4.18 (m, 2H), 4.02-3.97 (m, 1H), 3.92-3.87 (m, 3H), 3.82 (s, 3H), 3.80-3.74 (m, 4H), 3.70-3.56 (m, 2H), 3.34 (m overlapped with water signal, 1H), 3.08-2.95 (m, 3H), 2.93-2.83 (m, 1H), 2.64-2.60 (m, 4H), 2.54 (m, 7H), 2.50 (m overlapped with solvent signal, 1H), 2.44 (s, 3H), 2.05 (s, 3H), 2.04 (s, 3H), 1.73-1.61 (m, 1H), 1.55-1.40 (m, 12H); ^{13}C NMR (101 MHz, DMSO-*d*$_6$) δ 171.2, 170.3, 169.8, 169.1, 168.4, 167.6, 158.5, 157.5, 156.1, 138.2, 137.79, 137.65, 137.3, 135.6, 135.0, 130.0, 128.0, 127.5, 124.0, 123.5, 112.2, 111.7, 80.5, 55.67, 55.50, 52.19, 52.05, 51.98, 45.10, 45.00, 42.1, 39.9, 39.7, 36.1, 35.6, 28.1, 27.7, 25.8, 23.81, 23.64, 18.0, 17.7, 11.8; IR (film) 3436, 3309, 3055, 2927, 2857, 1720, 1674, 1656, 1584, 1557, 1458, 1306 cm^{-1}; MS (ESI) *m*/*z* calcd for [C$_{51}$H$_{71}$N$_{10}$O$_{14}$S$_2$]$^+$: 1111.46 [M+H]$^+$; found: 1111.7.

b) *Cyclo*[DKP-*f*6-Arg(Mtr)-Gly-Asp(O*t*Bu)] (62b)

To a solution of H-Asp(O*t*Bu)-DKP-*f*6-Arg(Mtr)-Gly-OH **61b** (260 mg, 0.23 mmol, 1 equiv) in DMF (165 mL), under nitrogen atmosphere and at 0 ºC, HATU (350 mg, 0.92 mmol, 4 equiv), HOAt (125 mg, 0. 92 mmol, 4 equiv) and *i*-Pr_2NEt (0.236 mL, 1.38 mmol, 6 equiv) were added. The reaction was warmed up to rt and stirred overnight. DMF was then removed under reduced pressure to afford a yellowish solid. The solid was dissolved in AcOEt (200 mL) and the resulting solution was washed with 1 M aqueous $KHSO_4$ (2×20 mL), saturated aqueous $NaHCO_3$ (2×20 mL) and brine (2×32 mL), dried over Na_2SO_4 and the solvent evaporated under reduced pressure to afford the crude product. The crude was purified by flash-chromatography on silica gel (CH_2Cl_2/MeOH, 9:1) to afford the desired product as a fluffy solid (170 mg, 68%).

R_f=0.35 (DCM/MeOH 9:1); $[\alpha]_D^{20}$=-38.0 (*c*=0.5 in DMSO); ^{1}H NMR (400 MHz, CD_3OD) δ 7.19 – 7.06 (m, 4H), 6.67 (s, 1H), 6.65 (s, 1H), 5.18 (d, 1H, *J* = 14.7 Hz), 4.50 – 4.39 (m, 2H), 4.12 – 3.95 (m, 5H), 3.92 – 3.81 (m, 7H), 3.78 – 3.65 (m, 2H), 3.61 (dd, 1H, *J* = 13.7, 3.6 Hz), 3.29 – 3.08 (m, 2H), 2.99 (dd, 1H, *J* = 16.6, 7.0 Hz), 2.75 – 2.69 (m, 2H), 2.66 (s, 3H), 2.64 – 2.56 (m, 7H), 2.47 (s, 3H), 2.11 (s, 3H), 2.07 (s, 3H), 1.83 – 1.71 (m, 1H), 1.69 – 1.49 (m, 3H), 1.45 (s, 9H); ^{13}C NMR (101 MHz, CD_3OD) δ 174.2, 174.0, 173.1, 172.3, 171.8, 171.3, 160.7, 159.9, 158.2, 139.9, 139.5, 138.6, 137.9, 136.3, 134.7, 131.0, 129.5, 129.0, 126.1, 125.7, 113.2, 112.8, 82.3, 56.2, 56.0, 54.5, 52.2, 47.8, 46.9, 44.0, 42.5, 36.6, 36.1, 28.3, 24.5, 24.4, 18.9, 18.2, 12.1; IR (film) 3304, 3060, 2927, 2855, 1719, 1674, 1654, 1584, 1559, 1456, 1307 cm^{-1}; MS (ESI) m/z calcd for $[C_{51}H_{71}N_{10}O_{14}S_2]^+$: 1111.46 $[M+H]^+$; found: 1111.6

***Cyclo*[DKP-*f*-Arg-Gly-Asp] - c[DKP-*f*-RGD]**

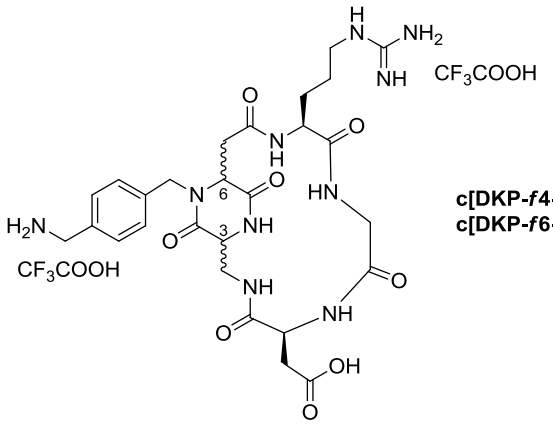

c[DKP-*f*4-RGD]: (3*R*, 6*S*)
c[DKP-*f*6-RGD]: (3*S*, 6*R*)

a) *Cyclo*[DKP-*f*4-Arg-Gly-Asp] - c[DKP-*f*4-RGD]

Cyclo[DKP-*f*4-Arg(Mtr)-Gly-Asp(O*t*Bu)] **62a** (90 mg, 0.081 mmol) was treated with TFA (10 mL), in the presence of ion scavengers thioanisole (1.5 mL), ethanedithiol (0.75 mL) and phenol (150 mg). The mixture was cooled to 0 °C and flushed with N_2.

Trimethylsilylbromide (2 mL) was then added, the flask was open and the mixture warmed up to rt and stirred for 2 h. All volatiles were then evaporated and the crude was dissolved in a mixture of water and diisopropyl ether 1:1 (30 mL). The aqueous phase was washed several time with diisopropyl ether and then concentrated under reduced pressure to give the crude compound, which was purified by semipreparative-HPLC (Water's Atlantis 21 mm x 10 cm column, gradient: 95% H_2O / 5% acetonitrile to 80% H_2O / 20% acetonitrile) to give the desired compound (as trifluoroacetate salt) as a white solid (49 mg, 70% yield).

^{1}H NMR (400 MHz, D_2O) δ 7.40 (AB system, 4H), 5.35-5.18 (m, 1H), 4.44 (br s, 1H), 4.35 (dd, 1H, J = 9.1, 5.0 Hz), 4.28 (br s, 1H), 4.22-4.12 (m, 3H), 4.08-3.94 (m, 2H), 3.78-3.63 (m, 2H), 3.43 (br s, 1H), 3.22 (t, 2H, J = 6.6 Hz), 3.10-3.00 (m, 1H), 2.96-2.83 (m, 3H), 1.93-1.76 (m, 2H), 1.73-1.61 (m, 2H); ^{13}C NMR (101 MHz, D_2O,) δ 174.5, 173.9, 173.4, 171.3, 169.1, 157.4, 136.7, 132.9, 130.0, 128.6, 58.2, 54.2, 53.6, 53.0, 47.3, 43.3, 43.1, 41.05, 41.02, 36.9, 35.2, 28.3, 25.2; IR (film) 3258, 3063, 2942, 1671, 1545, 1425, 1202, 1133 cm^{-1} MS (ESI) *m*/*z* calcd for $[C_{27}H_{39}N_{10}O_8]^+$: 631.30 $[M+H]^+$; found: 631.4

b) *Cyclo*[DKP-*f*6-Arg-Gly-Asp] - c[DKP-*f*6-RGD]

Cyclo[DKP-*f*6-Arg(Mtr)-Gly-Asp(O*t*Bu)] **62b** (90 mg, 0.081 mmol) was treated with TFA (10 mL), in the presence of ion scavengers thioanisole (1.5 mL), ethanedithiol (0.75 mL) and phenol (150 mg). The mixture was cooled to 0 °C and flushed with N_2. Trimethylsilylbromide (2 mL) was then added, the flask was open and the mixture warmed up to rt and stirred for 2 h. All volatiles were then evaporated and the crude was dissolved in a mixture of water and diisopropyl ether 1:1 (30 mL). The aqueous phase was washed several time with diisopropyl ether and then concentrated under reduced pressure to give the crude compound, which was purified by semipreparative-HPLC (Water's Atlantis 21 mm x 10 cm column, gradient: 95% H_2O / 5% acetonitrile to 80% H_2O / 20% acetonitrile) to give the desired compound (as trifluoroacetate salt) as a white solid (50 mg, 71% yield).

^{1}H NMR (400 MHz, D_2O) δ 8.06 (t, 1H, J = 6.1 Hz), 7.43 (AB system, 4H), 5.16 (d, 1H, J = 15.7 Hz), 4.53 (t, 1H, J = 7.1 Hz), 4.39 (dd, 1H, J = 9.3, 5.7 Hz), 4.36 – 4.29 (m, 2H), 4.20 (s, 2H), 4.05 (t, 1H, J = 6.2 Hz), 3.89 (d, 1H, J = 15.4 Hz), 3.82 (d, 1H, J = 15.4 Hz), 3.77 – 3.71 (m, 2H), 3.21 (t, 2H, J = 6.8 Hz), 3.11 (dd, 1H, J = 17.0, 6.8 Hz), 2.92 – 2.76 (m, 3H), 1.92 – 1.54 (m, 4H); ^{13}C NMR (101 MHz, D_2O) δ 175.2, 173.9, 173.3, 172.5, 171.6, 168.8, 167.4, 157.4, 136.9, 132.9, 130.0, 128.8, 58.9, 55.4, 54.2, 51.6, 48.3, 43.4, 43.4, 41.7, 41.0, 35.9, 34.4, 28.4, 25.1; IR (film) 3254, 3062, 2942, 1671, 1545, 1423, 1202, 1134 cm^{-1}; MS (ESI) m/z calcd for $[C_{27}H_{39}N_{10}O_8]^+$: 631.29 $[M+H]^+$; found: 631.5

3.1.5 - Synthesis of c[DKP-*iso*DGR] integrin ligands

N_3-(3*R*,6*S*)-DKP-COOH (63a)
N_3-(3*S*,6*R*)-DKP-COOH (63b)

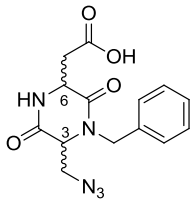

63a: (3*R*, 6*S*)
63b: (3*S*, 6*R*)

N_3-(3*R*,6*S*)-DKP-COOAllyl[11] or N_3-(3*S*,6*R*)-DKP-COOAllyl[11] (300 mg, 0.84 mmol, 1 eq.) was dissolved in CH_2Cl_2 (8.0 ml) under a nitrogen atmosphere, and the mixture was cooled to 0°C. [$Pd(PPh_3)_4$] (290 mg, 0.25 mmol, 0.3 eq.) and freshly distilled *N*-methyl aniline (109µl, 1.0 mmol, 1.2 eq.) were added successively. The mixture was then allowed to reach room temperature. After 1 h of stirring, the mixture was diluted with EtOAc (40 ml) and extracted with aqueous $NaHCO_3$ (4 x 20 ml). The combined aqueous phases were acidified to pH 2 by adding $KHSO_4$ (1M solution) and then extracted with CH_2Cl_2 (4 x 20 ml). The resulting organic phase was dried over Na_2SO_4 and the solvent was evaporated to afford the desired product as a slightly yellow solid (241 mg, 90%) which was used without further purification.
R_f=0.40 (CH_2Cl_2/MeOH 8:2); ^{1}H NMR (400 MHz, $CDCl_3$) δ 8.12 (s, 1H, COOH), 7.42 – 7.31 (m, 3H), 7.31 – 7.23 (m, *J* = 7.9 Hz, 2H), 5.18 (d, *J* = 15.1 Hz, 1H), 4.66 (dd, *J* = 9.8, 2.9 Hz, 1H), 4.27 (d, *J* = 15.1 Hz, 1H), 3.96 (t, *J* = 2.4 Hz, 1H), 3.89 (dd, *J* = 12.8, 2.2 Hz, 1H), 3.69 (dd, *J* = 12.8, 3.4 Hz, 1H), 3.38 (dd, *J* = 17.9, 3.2 Hz, 1H), 2.80 (dd, *J* = 17.9, 9.9 Hz, 1H); ^{13}C NMR (101 MHz, $CDCl_3$) δ 173.8, 167.5, 166.3, 129.2, 128.4, 128.2, 77.5, 77.2, 76.8, 59.2, 51.8, 51.1, 48.1, 37.2.

The syntheses of compounds **c[DKP-2-*iso*DGR]** and **c[DKP-3-*iso*DGR]** were carried out by manual coupling using Fmoc/*t*Bu strategy on SASRIN™ resin (200-400 mesh, 1.02 mmol/g) on a 0.1 mmol scale. Swelling of the resin was achieved suspending it in either DCM or DMF for 15 min.
SASRIN™ RESIN LOADING: The first Fmoc protected amino acid (Fmoc-Gly-OH, 119 mg, 0.4 mmol, 4 eq.) residue was dissolved in the minimum amount of DMF, and the solution was cooled to 0° C. DIC (62 µl, 0.4 mmol, 4 eq.) was added dropwise. The mixture was stirred for 20 min at the same temperature before adding it to the resin (98 mg, 0.1 mmol, 1 eq.). DMAP (1.2 mg, 0.01 mmol, 0.1 eq.) was then added in one portion. The reaction vessel was gently shaken for 1 h at r.t.. Resin was thoroughly washed in the order with DMF (4x), DCM (4x), *i*PrOH (3x). Capping was performed (see general procedure **GP6**).
COUPLING REACTIONS: A sample vial equipped with a magnetic stirrer was charged with the appropriate *N*-protected-amino acid (2.5 - 4 eq.), which was dissolved in a 1:1 mixture of DCM/DMF. After cooling the mixture to 0 °C, DIC (2.5 – 4 eq.) and HOAt (2.5 – 4 eq.) were added successively. The mixture was stirred for 20 min at the same

temperature. The solution was then added to the swelled peptidylresin (0.1 mmol, 1 eq.). The resin was gently agitated for 2-18 h and, after sucking off the solution, it was washed in the order with DMF (4x), DCM (4x), *i*PrOH (3x) and/or Et_2O (2x). If a Fmoc-amino acid was coupled, Kaiser test was performed (see general procedure **GP7**). If resin gives a positive color test, coupling procedure was repeated with fresh reagents. After a maximum of 3 coupling cycles, capping was performed (see general procedure **GP6**).
Fmoc DEPROTECTION: After successful coupling, washing and Fmoc deprotecting steps were carried out as described in general procedure **GP8**. This deprotection/coupling strategy was applied for each synthetic step involving N-Fmoc protected α-amino acids.
AZIDE REDUCTION: After successful coupling of DKP building blocks (**63a** and **63b**), washing and azide reduction steps were carried out as described in general procedure **GP9**.

Exact amounts of the amino acids and coupling reagents used for SPPS are reported in Table 3.1.1.

Table 3.1.1

REAGENTS	eq.	mmol	amounts
Fmoc-L-Asp(OH)-O*t*Bu	3	0.3	123 mg
DIC	3	0.3	47 µl
HOAt	3	0.3	41 mg
63a or **63b**	2.5	0.25	79 mg
DIC	2.5	0.25	38 µl
HOAt	2.5	0.25	34 mg
Cbz-L-Arg(Mtr)-OH · CHA	4	0.4	248 mg
DIC	4	0.4	62 µl
HOAt	4	0.4	27 mg

Cbz-Arg(Mtr)-DKP-*iso*Asp(O*t*Bu)-Gly-OH (64)

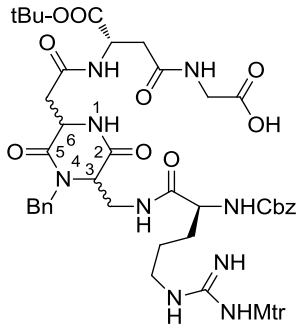

64a: 3*R*, 6*S*
64b: 3*S*, 6*R*

CLEAVAGE FROM SASRIN™ RESIN: The resin was thoroughly washed with DCM (10 times) and then treated with 1% TFA in DCM (2 ml) for 2-5 min. The mixture was filtered off with a N_2 pressure into a vial containing 0.2 ml of 12% of pyridine in MeOH. The filtrate was checked for the presence of peptide by TLC (DCM/MeOH 9:1). Treatment with 1% TFA in DCM was repeated as long as the peptide was being cleaved from the resin (5-8 times). Peptide containing fractions were combined and half of the DCM volume was removed at reduced pressure. The mixture was then diluted with abundant EtOAc and washed with 1M $KHSO_4$ (4x) to remove pyridinium trifluoroacetate and to free the carboxylic acid. The organic layer was dried over Na_2SO_4, filtered and evaporated to afford a white solid which was purified by flash chromatography (DCM/MeOH 8:2) (**64a**: 89 mg, 88%; **64b**: 90 mg, 88%).

64a

R_f=0.55 (CH_2Cl_2/MeOH 8:2); ^{1}H NMR (400 MHz, CD_3OD) δ 8.33 (m, 1H), 8.26 – 8.15 (m, 1H), 7.40 – 7.21 (m, 9H), 7.17 (d, *J* = 7.6 Hz, 1H), 6.63 (s, 1H), 5.36 (d, *J* = 15.4 Hz, 1H), 5.07 (q, *J* = 12.4 Hz, 2H), 4.72 – 4.58 (m, 2H), 4.19 – 4.04 (m, 2H), 3.98 – 3.82 (m, 4H), 3.80 (s, 3H), 3.65 – 3.53 (m, 1H), 3.25 – 3.07 (m, 2H), 3.03 (dd, *J* = 16.3, 4.0 Hz, 1H), 2.81 (dd, *J* = 16.4, 6.8 Hz, 1H), 2.75 (d, *J* = 6.2 Hz, 2H), 2.66 (s, 3H), 2.60 (s, 3H), 2.10 (s, 3H), 1.79 – 1.64 (m, 1H), 1.64 – 1.46 (m, 3H), 1.43 (s, 9H); ^{13}C NMR (101 MHz, CD_3OD) δ 175.7, 173.3, 172.6, 171.6, 171.5, 169.0, 168.4, 159.8, 158.4, 158.2, 139.5, 138.1, 137.9, 137.2, 134.8, 129.9, 129.5, 129.2, 129.0, 128.9, 125.7, 112.8, 83.3, 67.9, 60.6, 56.2, 56.0, 52.2, 51.4, 49.6, 41.9, 40.2, 38.2, 30.2, 28.2, 27.0, 24.4, 18.9, 12.1; MS (ESI) *m*/*z* calcd for $[C_{48}H_{64}N_9O_{14}S]^+$: 1022.43 $[M+H]^+$; found: 1022.8.

64b:

R_f=0.53 (CH_2Cl_2/MeOH 8:2); ^{1}H NMR (400 MHz, CD_3OD) δ 7.40 – 7.20 (m, 9H), 6.65 (s, 1H), 5.36 (d, *J* = 15.3 Hz, 1H), 5.15 – 5.02 (m, 2H), 4.69 (t, *J* = 5.9 Hz, 1H), 4.60 (t, *J* = 5.5 Hz, 1H), 4.15 – 4.06 (m, 2H), 3.98 – 3.83 (m, 4H), 3.81 (s, 3H), 3.65 – 3.55 (m, 1H), 3.28 – 3.07 (m, 2H), 2.95 (dd, *J* = 15.8, 5.4 Hz, 1H), 2.81 (dd, *J* = 16.4, 6.4 Hz, 1H), 2.75 (d, *J* = 5.9 Hz, 2H), 2.67 (s, 3H), 2.60 (s, 3H), 2.11 (s, 3H), 1.80 – 1.69 (m, 1H), 1.64 – 1.48 (m, 3H), 1.45 (s, 9H); ^{13}C NMR (101 MHz, CD_3OD) δ 175.7, 173.2, 172.5, 171.6, 168.9, 168.4, 159.9, 158.5, 158.1, 139.6, 138.1, 138.0, 137.1, 130.0, 129.5, 129.2, 129.1, 128.9, 125.8, 112.8, 83.5, 67.8, 60.5, 56.1, 56.0, 52.4, 51.4, 48.2, 41.8, 40.2, 38.8, 38.3, 30.3, 28.2, 24.4, 18.8, 14.4, 12.1; MS (ESI) *m*/*z* calcd for $[C_{48}H_{64}N_9O_{14}S]^+$: 1022.43 $[M+H]^+$; found: 1022.9.

H-Arg-DKP-*iso*Asp(O*t*Bu)-Gly-OH (65)

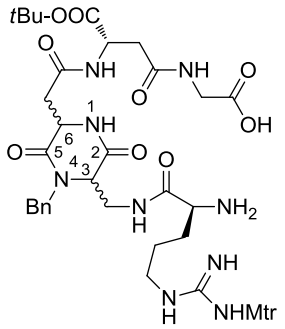

65a: 3*R*, 6*S*
65b: 3*S*, 6*R*

Compound 65a:
Compound **64a** (89 mg, 0.09 mmol, 1 eq.) was treated with 10% Pd/C (9.2 mg, 0.009 mmol, 0.1 eq.) under the conditions described in general procedure **GP3**. The crude product was obtained as a white solid (77 mg, 100%) and was used without further purification.

Compound 65b:
Compound **64b** (90 mg, 0.09 mmol, 1 eq.) was treated with 10% Pd/C (9.3 mg, 0.009 mmol, 0.1 eq.) under the conditions described in general procedure **GP3**. The crude product was obtained as a white solid (78 mg, 100%) and was used without further purification.

***Cyclo*[*iso*Asp(O*t*Bu)-Gly-Arg(Mtr)-DKP] (66)**

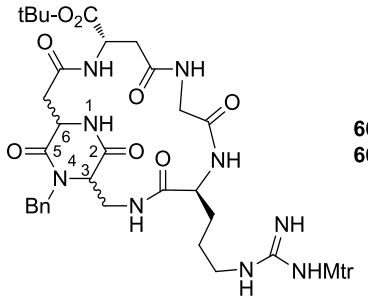

66a: 3*R*, 6*S*
66b: 3*S*, 6*R*

66a:
Compound **65a** (77 mg, 0.09 mmol, 1 eq.) was cyclized in presence of HATU (136 mg, 0.36 mmol, 4 eq.), HOAt (49 mg, 0.36 mmol, 4 eq.) and DIPEA (93 µl, 0.54 mmol, 6 eq) under the conditions described in general procedure **GP2**. The crude product was purified by flash chromatography on silica gel (CH_2Cl_2/MeOH, 95:5) to afford the desired product as a white foam (41 mg, 55%).
R_f=0.83 (CH_2Cl_2/MeOH 8:2); ^{1}H NMR (400 MHz, CD_3OD) δ 7.40 – 7.24 (m, 5H), 6.66 (s, 1H), 5.35 (d, J = 15.3 Hz, 1H), 5.01 (t, J = 6.9 Hz, 1H), 4.74 – 4.68 (m, 1H), 4.24 – 4.04 (m, 4H), 3.87 – 3.76 (m, 5H), 3.40 – 3.33 (m, 1H), 3.17 (t, J = 6.0 Hz, 2H), 2.96 – 2.85 (m, 1H), 2.77 (dd, J = 14.0, 4.5 Hz, 1H), 2.73 – 2.68 (m, 2H), 2.67 (s, 3H), 2.60 (s, 3H), 2.12 (s, 3H), 1.79 – 1.53 (m, 4H), 1.49 (s, 9H); ^{13}C NMR (101 MHz, CD_3OD) δ 175.6, 172.9, 172.1, 171.5,

171.1, 168.5, 168.1, 159.9, 158.2, 139.5, 137.9, 137.0, 130.1, 129.2, 129.1, 112.8, 83.4, 60.5, 56.0, 55.3, 52.2, 47.8, 42.8, 42.8, 41.4, 39.7, 38.7, 29.0, 28.3, 27.0, 24.3, 18.8, 12.1; MS (ESI) *m*/*z* calcd for $[C_{40}H_{56}N_9O_{11}S]^+$: 870.38 $[M+H]^+$; found: 870.8.

66b:

Compound **65b** (78 mg, 0.09 mmol, 1 eq.) was cyclized in presence of HATU (137 mg, 0.36 mmol, 4 eq.), HOAt (49 mg, 0.36 mmol, 4 eq.) and DIPEA (93 µl, 0.54 mmol, 6 eq) under the conditions described in general procedure **GP2**. The crude product was purified by flash chromatography on silica gel (CH_2Cl_2/MeOH, 95:5) to afford the desired product as a white foam (31 mg, 35%).

R_f=0.64 (CH_2Cl_2/MeOH 8:2); ^{1}H NMR (400 MHz, CD_3OD) δ 7.40 – 7.21 (m, 5H), 6.66 (s, 1H), 5.42 (d, *J* = 15.3 Hz, 1H), 5.04 (dd, *J* = 11.8, 3.2 Hz, 1H), 4.59 (d, *J* = 10.1 Hz, 1H), 4.31 – 4.19 (m, 2H), 4.05 (d, *J* = 15.3 Hz, 1H), 3.88 – 3.79 (m, 4H), 3.78 – 3.61 (m, 2H), 3.28 – 3.09 (m, 3H), 2.89 (dd, *J* = 14.7, 3.3 Hz, 1H), 2.73 – 2.57 (m, 7H), 2.31 – 2.21 (m, 1H), 2.12 (s, 3H), 1.86 – 1.73 (m, 1H), 1.72 – 1.52 (m, 3H), 1.48 (s, 9H); ^{13}C NMR (101 MHz, CD_3OD) δ 176.5, 173.3, 172.5, 171.7, 171.2, 169.1, 167.8, 159.9, 158.3, 139.5, 137.9, 137.1, 134.8, 130.0, 129.1, 125.7, 112.8, 83.6, 60.4, 56.0, 55.1, 52.0, 50.9, 47.9, 42.7, 40.9, 40.0, 39.2, 38.5, 29.8, 28.2, 27.2, 24.3, 18.9, 12.1; MS (ESI) *m*/*z* calcd for $[C_{40}H_{56}N_9O_{11}S]^+$: 870.38 $[M+H]^+$; found: 870.8.

***Cyclo*[*iso*Asp-Gly-Arg-DKP] – c[DKP-*iso*DGR]**

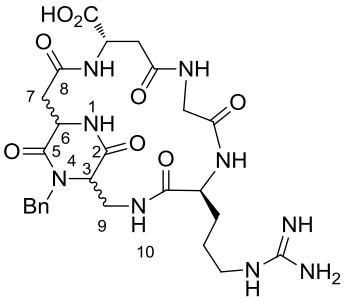

c[DKP-2-*iso*DGR]: 3*R*, 6*S*
c[DKP-3-*iso*DGR]: 3*S*, 6*R*

c[DKP-2-*iso*DGR]:

Compound **66a** (41 mg, 0.05 mmol) was fully deprotected under the conditions described in general procedure **GP5**. The crude product was purified by HPLC (Water's Atlantis™ 21 mm x 10 cm column, gradient: 90% H_2O / 10% acetonitrile to 40% H_2O / 60% acetonitrile) to give the desired compound (as trifluoroacetate salt) as a white solid (7 mg, 24%).

^{1}H NMR (400 MHz, H_2O/D_2O 9:1, T= 298K) δ 8.44 (t, *J* = 6.5 Hz, 1H, DKP-NH10), 8.35 (s, 1H, DKP-NH1), 8.30 – 8.21 (m, 2H, Asp-NH, Arg-NH), 7.89 (t, *J* = 6.2 Hz, 1H, Gly-NH), 7.40 – 7.21 (m, 5H, H-Ar), 7.11 (t, *J* = 5.7 Hz, 1H, NH-guan), 5.09 (d, *J* = 15.8 Hz, 1H, $\underline{CH_2}$-Bn), 4.20 – 4.09 (m, 2H, αH-Arg, $\underline{CH_2}$-Bn), 4.08 – 3.88 (m, 3H, αH-Gly, DKP-H9, DKP-H3), 3.83 (dd, *J* = 17.1, 5.7 Hz, 1H, αH-Gly), 3.53 – 3.41 (m, 1H, DKP-H9), 3.13 (q, *J* = 6.7 Hz, 2H, δH-Arg), 2.83 – 2.71 (m, 3H, βH-Asp, DKP-H7), 2.59 (dd, *J* = 14.8, 10.4 Hz, 1H, DKP-H7), 1.79 – 1.42 (m, 4H, βH-Arg, γH-Arg); ^{13}C NMR (101 MHz, D_2O, T= 298K) δ 175.4, 174.6, 172.6, 171.7, 170.7, 167.5, 167.0, 135.2, 129.2, 128.3,127.9, 59.5, 54.3, 51.3, 47.3,

41.8, 41.3, 40.5, 39.1, 37.6, 27.4, 24.5; MS (ESI) *m*/*z* calcd for $[C_{26}H_{36}N_9O_8]^+$: 602.27 $[M+H]^+$; found: 602.3.

c[DKP-3-*iso*DGR]:
Compound **66b** (31 mg, 0.035 mmol) was fully deprotected under the conditions described in general procedure **GP5**. The crude product was purified by HPLC (Water's Atlantis™ 21 mm x 10 cm column, gradient: 90% H_2O / 10% acetonitrile to 60% H_2O / 40% acetonitrile) to give the desired compound (as trifluoroacetate salt) as a white solid (6 mg, 29%).
^{1}H NMR (400 MHz, H_2O/D_2O 9:1, T= 298K) δ 8.62 (d, *J* = 8.2 Hz, 1H, Asp-NH), 8.45 (t, *J* = 6.7 Hz, 1H, DKP-H10), 8.26 (d, *J* = 6.5 Hz, 1H, Arg-NH), 8.15 (t, *J* = 6.1 Hz, 1H, Gly-NH), 7.60 (s, 1H, DKP-NH1), 7.41 – 7.19 (m, 5H, H-Ar), 7.17 – 7.05 (m, 1H, NH-guan), 5.15 (d, *J* = 15.6 Hz, 1H, $\underline{CH_2}$-Bn), 4.34 (d, *J* = 11.4 Hz, 1H, DKP-H6), 4.23 – 4.07 (m, 3H, αH-Gly, αH-Arg, $\underline{CH_2}$-Bn), 4.06 – 4.00 (m, 1H, DKP-H3), 3.88 (dd, *J* = 13.6, 6.6 Hz, 1H, DKP-H9), 3.71 (dd, *J* = 17.5, 5.0 Hz, 1H, αH-Gly), 3.59 (dd, *J* = 15.5, 6.8 Hz, 1H, DKP-H9), 3.17 – 3.02 (m, 3H, δH-Arg, DKP-H7), 2.94 (dd, *J* = 15.3, 3.8 Hz, 1H, βH-Asp), 2.62 (dd, *J* = 15.4, 11.8 Hz, 1H, βH-Asp), 2.30 (dd, *J* = 14.1, 11.9 Hz, 1H, DKP-H7), 1.82 – 1.43 (m, 4H, βH-Arg, γH-Arg); ^{13}C NMR (101 MHz, D_2O, T= 298K) δ 176.0, 174.5, 172.3, 171.3, 168.0, 167.0, 135.2, 129.2, 128.2, 127.7, 59.5, 54.2, 51.3, 47.8, 41.6, 40.5, 39.3, 38.3, 37.7, 28.1, 24.6; MS (ESI) *m*/*z* calcd for $[C_{26}H_{36}N_9O_8]^+$: 602.27 $[M+H]^+$; found: 602.2.

3.1.6 - Synthesis of SMAC-RGD conjugates

4-(hydroxymethyl)benzaldehyde (86)

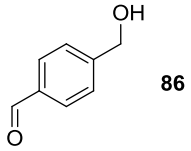

86

Terephthalaldehyde (benzene-1,4-dicarboxaldehyde) (1.0 g, 7.45 mmol, 1 eq.) was dissolved in 12.5 ml of EtOH/H_2O (95:5) and then 17.5 ml of THF were added. To the resulting stirred solution, $NaBH_4$ (70 mg, 1.86 mmol, 0.25 eq.) was added at -5 °C in small portions over 30 min. The mixture was stirred for 6 h, while the temperature was maintained at 0 °C. The reaction mixture was then adjusted to pH = 5 with 2 M HCl. The solvent was evaporated, then H_2O (20 ml) was added and the solution was extracted three times with AcOEt. The resulting organic phase was dried over Na_2SO_4 and the solvent was evaporated. The crude product was purified by flash chromatography on silica gel (Hex/AcOEt, 1:1) to afford the desired product as a white solid (840 mg, 83%).
R_f = 0.5 (Hex/AcOEt, 4:6); ^{1}H NMR (400 MHz, $CDCl_3$) δ 9.82 (s, 1H), 7.71 (d, *J* = 7.8 Hz, 2H), 7.39 (d, *J* = 7.9 Hz, 2H), 4.65 (s, 2H), 2.07 (s, 1H); ^{13}C NMR (101 MHz, CD_2Cl_2) δ 192.6, 148.8, 135.9, 130.2, 127.3, 64.5.

Benzyl 4-formylbenzylcarbamate (87)

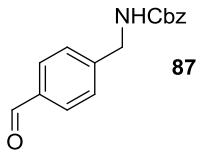

87

(4-(aminomethyl)phenyl)methanol (800 mg, 5.83 mmol, 1 eq.) was dissolved in 60 ml of THF, under N_2 atmosphere. The mixture was cooled to 0 °C and DIPEA (2 ml, 11.66 mmol, 2 eq.) was added dropwise. The resulting mixture was left stirring for 5 min. at 0 °C, then benzyl chloroformate (1.66 ml, 11.66 mmol, 2 eq.) was added dropwise. The reaction was left stirring at 0 °C for 45 min, then it was allowed to reach room temperature. The mixture was left stirring overnight. DIPEA·HCl salts was then removed over celite and the filter was washed with AcOEt. The solution was concentrated, the residue was dissolved in AcOEt and washed with $KHSO_4$ 1M solution. The resulting organic phase was dried over Na_2SO_4 and the solvent was evaporated. The crude product was recrystallized from cold CH_2Cl_2, the desired product (benzyl 4-(hydroxymethyl)benzylcarbamate) was filtered over buckner and washed with cold CH_2Cl_2, affording a white solid that was used without further purification (1.13 g, 71%).
R_f = 0.5 (Hex/AcOEt, 3:7); ^{1}H NMR (400 MHz, CD_3OD) δ 7.46 – 7.18 (m, 9H), 5.11 (s, 2H), 4.59 (s, 2H), 4.30 (s, 2H).

Benzyl 4-(hydroxymethyl)benzylcarbamate (500 mg, 1.84 mmol, 1 eq.) was dissolved in 45 ml of THF, under N_2 atmosphere. MnO_2 (1.76 g, 20.27 mmol, 11 eq.) was added at room temperature and the reaction was left stirring overnight. MnO_2 was then filtered over celite, washing the filter with THF. The solvent was then evaporated affording **87** as a white solid that was used without further purification (480 mg, 97%).
R_f = 0.55 (Hex/AcOEt, 1:1); ^{1}H NMR (400 MHz, $CDCl_3$) δ 9.98 (s, 1H), 7.83 (d, J = 7.8 Hz, 2H), 7.44 (d, J = 7.6 Hz, 2H), 7.36 (m, 5H), 5.30 (br, 1H), 5.14 (s, 2H), 4.46 (d, J = 6.0 Hz, 2H); ^{13}C NMR (101 MHz, CD_2Cl_2) δ 192.2, 157.0, 146.3, 137.1, 136.0, 130.2, 128.9, 128.5, 128.3, 128.0, 67.2, 45.0.

***tert*-butyl ((*S*)-1-(((3*S*,6*S*,7*R*,9a*S*)-3-(benzhydrylcarbamoyl)-7-(2-((4 (hydroxymethyl)benzyl)amino)ethyl)-5-oxooctahydro-1H-pyrrolo[1,2-a]azepin-6-yl)amino)-1-oxobutan-2-yl)(methyl)carbamate (89)**

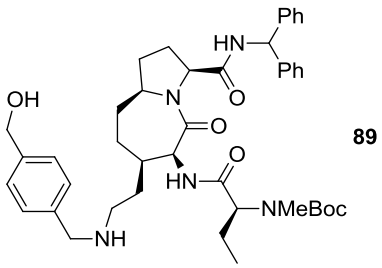

89

A solution of **81**[12] (50 mg, 0.074 mmol, 1.05 eq.), DIPEA (18 μl, 0.105 mmol, 1.5 eq.) in dry MeOH (0.5 ml) was added into a flask containing 4-(hydroxymethyl)benzaldehyde **86** (9.5 mg, 0.074 mmol, 1 eq.) under nitrogen atmosphere. The mixture was let stirring at room temperature for 5 h. $NaBH_4$ (5.3 mg, 0.14 mmol, 2 eq.) was then added stepwise (5 additions within 3 min) and the mixture was let react at room temperature under nitrogen for 30 min. The mixture was then concentrated under vacuum. 5 ml of a saturated solution of $NaHCO_3$ were added, then the mixture was extracted with AcOEt (7 ml, three times). The organic phase was dried over Na_2SO_4 and the solvent was evaporated. The crude product was purified by flash chromatography on silica gel (CH_2Cl_2/MeOH, 9:1) to afford the desired product as a white foam (41 mg, 80% yield).
R_f = 0.3 (CH_2Cl_2/MeOH, 9:1); ^{1}H NMR (400 MHz, THF-d_8) δ 8.27 (bs, 1H), 7.54 (bs, 1H), 7.40 – 7.00 (m, 14H), 6.21 (d, J = 8.81 Hz, 1H) 4.62 (d, J = 6.53 Hz, 1H), 4.60 – 4.35 (m, 4H), 4.00 – 3.70 (m, 4H), 2.84 (bs, 3H), 2.66 (bs, 1H), 2.52 (bs, 1H), 2.15 (m, 4H), 1.91 (m, 2H), 1.85 – 2.57 (m, 4H), 1.46 (s, 9H), 1.47 – 1.31 (m, 4H), 0.87 (t, J = 7.32 Hz, 3H); ^{13}C NMR (400 MHz, THF-d_8) δ172.3, 171.5, 170.6, 157.0, 143.5, 143.3, 142.7, 129.2, 129.0, 128.9, 128.2, 128.1, 127.6, 127.5, 127.0., 80.2, 80.1, 79.7, 67.9, 67.7, 67.4, 67.2, 66.9, 66.7, 66.6, 64.6, 64.4, 53.4, 53.1, 49.3, 48.4, 47.1, 35.0, 34.9, 34.6, 34.4, 34.3, 33.9, 33.7, 33.5, 31.8, 27.7, 27.4, 27.1, 25.5, 25.3, 25.1, 24.9, 24.7, 22.4, 22.2, 22.2; MS (ESI) m/z calcd for $[C_{43}H_{58}N_5O_6]^+$: 740.44 $[M+H]^+$; found: 739.75.

***tert*-butyl ((*S*)-1-(((3*S*,6*S*,7*R*,9a*S*)-3-(benzhydrylcarbamoyl)-7-(2-((tert-butoxycarbonyl)(4-(hydroxymethyl)benzyl)amino)ethyl)-5-oxooctahydro-1H-pyrrolo[1,2-a]azepin-6-yl)amino)-1-oxobutan-2-yl)(methyl)carbamate (90)**

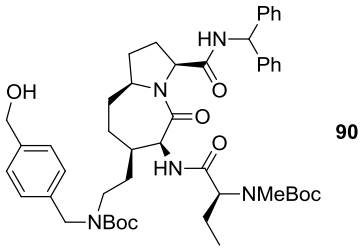

90

A solution of compound **89** (41 mg, 0.056 mmol, 1 eq.) and DIPEA (19 μl, 0.112 mmol, 2 eq.) in dry CH_2Cl_2 (0.6 ml) was put in an ice bath under nitrogen atmosphere. A solution of Boc_2O (17 mg, 0.079 mmol, 1.4 eq.) in dry CH_2Cl_2 (0.2 ml) was added. The mixture was let react at 0°C for 1h under nitrogen atmosphere, then it was let stirring overnight at room temperature. As the starting material was still present, more Boc_2O (6.7 mg, 0.030 mmol, 0.5 eq.) was dissolved in CH_2Cl_2 (0.2 ml) and added to the mixture, which was let react for 4 h. Then the solvent was removed under reduced pressure. The crude product was passed through a plug of silica gel (CH_2Cl_2/MeOH, 95:5) to afford the desired product as a white foam (41 mg, 87% yield).
R_f = 0.7 (CH_2Cl_2/MeOH, 9:1); ^{1}H NMR (400 MHz, acetone-d_6) δ 8.18 (d, J = 8.70 Hz, 1H), 7.40 – 7.08 (m, 14H), 6.19 (d, J = 8.66 Hz, 1H), 4.69 (d, J = 7.92 Hz, 1H), 4.61 (d, J = 5.76 Hz, 2H), 4.58 – 4.30 (m, 4H), 4.13 (t, J = 5.76 Hz, 1H), 3.99 (m, 1H), 3.25 (m, 1H), 2.25 (m,

1H), 2.17 (bs, 1H), 2.00 – 1.58 (m, 7H), 1.50 (s, 18H), 1.46 (m, 4H), 1.32 (m, 2H), 0.90 (t, *J* = 7.38 Hz, 3H); MS (ESI) *m*/*z* calcd for $[C_{48}H_{66}N_5O_8]^+$: 840.49 $[M+H]^+$; found: 840.45.

4-((4-(((2-((3*S*,6*S*,7*R*,9a*S*)-3-(benzhydrylcarbamoyl)-6-((*S*)-2-((tert-butoxycarbonyl)(methyl)amino)butanamido)-5-oxooctahydro-1H-pyrrolo[1,2-a]azepin-7-yl)ethyl)(tert-butoxycarbonyl)amino)methyl)benzyl)oxy)-4-oxobutanoic acid (91)

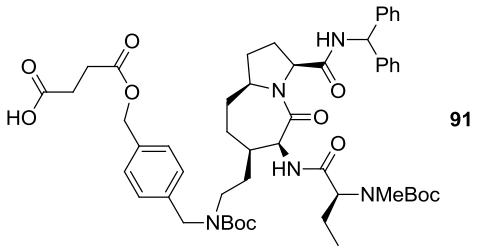

91

Compound **90** (17 mg, 0.020 mmol, 1 eq.) was dissolved in dry CH_2Cl_2 (0.12 ml). Then DIPEA (4.1 μl, 0.024 mmol, 1.2 eq.) was addes and the mixture was put in an ice bath. DMAP (1.46 mg, 0.012 mmol, 0.6 eq.) and succinic anhydride (3.6 mg, 0.036 mmol, 1.8 eq.) were added. The reaction was let stirring at room temperature under nitrogen atmosphere for 2h. CH_2Cl_2 (15 ml) was then added and the solution was washed with a solution of $KHSO_4$ 1M (7 ml, twice). The aqueous phase was extracted with CH_2Cl_2 (7 ml, once), then the collected organic phases were dried over Na_2SO_4 and the solvent was evaporated, to afford a white foam that was used without further purification (17 mg, 90% yield).
R_f = 0.6 (CH_2Cl_2/MeOH, 9:1); ^{1}H NMR (400 MHz, acetone-d_6) δ 10.72 (bs, 1H), 8.19 (d, *J* = 8.4 Hz, 1H), 7.48 – 6.98 (m, 15H), 6.19 (d, *J* = 8.4 Hz, 1H), 5.12 (s, 2H), 4.69 (d, *J* = 7.1 Hz, 1H), 4.63 – 4.26 (m, 3H), 3.99 (d, *J* = 7.1 Hz, 1H), 3.27 (s, 1H), 3.03 – 2.93 (m, 2H), 2.80 (s, 3H), 2.70 – 2.54 (m, 2H), 2.36 – 2.21 (m, 1H), 2.16 (s, 1H), 2.02 – 1.57 (m, 6H), 1.49 (s, 18H), 1.45 – 1.35 (m, 6H), 0.88 (t, J = 7.4 Hz, 3H).^{13}C NMR (400 MHz, acetone-d_6) δ 173.6, 172.7, 170.8, 143.6, 143.3, 139.7, 136.3, 129.4, 129.3, 129.1, 128.1, 128., 127.9, 79.8, 66.3, 62.1, 60.7, 59.2, 57.3, 55.8, 49.6, 45.4, 34.6, 34.0, 33.6, 30.1 (overlapping with solvent signal), 29.8 (overlapping with solvent signal), 29.2, 28.6, 27.3, 22.2, 11.0; MS (ESI) *m*/*z* calcd for $[C_{52}H_{70}N_5O_{11}]^+$: 940.51 $[M+H]^+$; found: 940.33.

2-((1*S*,5*S*,11*S*,15*R*)-18-(4-((4-((4-(((2-((3*S*,6*S*,7*R*,9a*S*)-3-(benzhydrylcarbamoyl)-6-((*S*)-2-((tert-butoxycarbonyl)(methyl)amino)butanamido)-5-oxooctahydro-1H-pyrrolo[1,2-a]azepin-7-yl)ethyl)(tert-butoxycarbonyl)amino)methyl)benzyl)oxy)-4-oxobutanamido)methyl)benzyl)-11-(3-guanidinopropyl)-4,7,10,13,17,19-hexaoxo-3,6,9,12,16,18-hexaazabicyclo[13.2.2]nonadecan-5-yl)acetic acid (92)

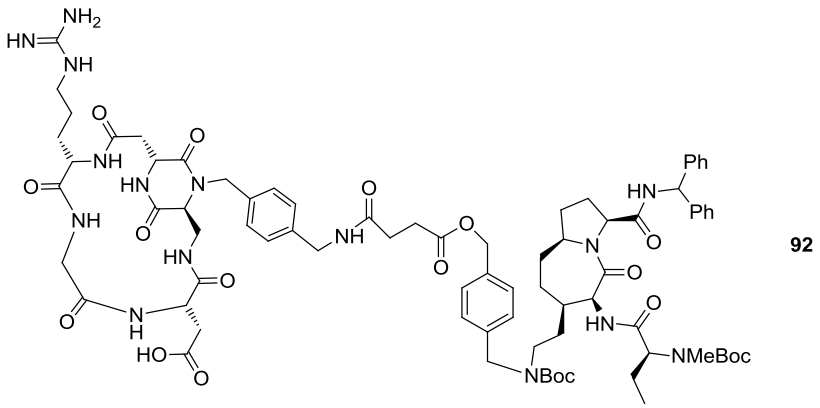

92

Compound **91** (17 mg, 0.018 mmol, 1 eq.) was dissolved under nitrogen atmosphere in a flame dried Schlenk tube with 1 ml of DMF. Then were added, at room temperature and in a single portion, *N*-hydroxysulfosuccinimide (5 mg, 0.023 mmol, 1.24 eq.) and *N*,*N*'-diisopropylcarbodiimide (4.18 µl, 0.027 mmol, 1.52 eq.). The solution was stirred overnight, then DMF was removed under vacuum in the Schlenk tube. The resulting residue was then dissolved, in the same Schlenk tube, with 1.2 ml of CH_3CN. To this solution was added a previously prepared solution of **c[DKP-*f*3-RGD]**[10] (12.4 mg, 0.0144 mmol, 0.8 eq.) dissolved in 1 ml of phosphate buffer solution (the pH was adjusted to 7.5 with 0.2 M NaOH). The resulting mixture was set to 0 °C and pH was adjusted to 7.5 with 0.2M NaOH. The solution was then stirred overnight. The reaction was then concentrated and purified by HPLC (gradient: 90% H_2O + 0.2% HCOOH / 10% acetonitrile + 0.2% HCOOH to 30% H_2O + 0.2% HCOOH / 70% acetonitrile + 0.2% HCOOH in 15 min). The purified product was then freeze dried to give the desired compound **92** as a white foam (9 mg, 40% yield).

t_R = 12.7 min; ^{1}H NMR (400 MHz, CD_3OD) δ 8.80 (d, J = 8.3 Hz, 1H), 8.40 (t, J = 5.5 Hz, 1H), 8.34 – 8.15 (br m, 1H), 7.39 – 7.12 (m, 18H), 6.12 (d, J = 8.3 Hz, 1H), 5.21 – 5.03 (m, 3H), 4.84 – 4.73 (m, 2H), 4.61 (t, J = 5.8 Hz, 1H), 4.58 – 4.27 (m, 7H), 4.24 – 4.15 (m, 1H), 4.07 – 3.91 (m, 3H), 3.88 (d, J = 6.3 Hz, 1H), 3.52 (d, J = 17.2 Hz, 1H), 3.45 (dd, J = 14.7, 6.8 Hz, 1H), 3.29 – 3.14 (m, 3H), 3.14 – 2.89 (m, 1H), 2.80 (s, 3H), 2.74 – 2.57 (m, 6H), 2.54 (t, J = 6.7 Hz, 2H), 2.30 – 2.16 (m, 1H), 2.15 – 1.33 (m, 33H), 0.92 (t, J = 7.2 Hz, 3H).; ^{13}C NMR (101 MHz, CD_3OD) δ 174.2, 174.0, 173.7, 173.6, 173.0, 172.9, 172.3, 172.2, 172.2, 171.3, 171.2, 171.1, 158.6, 143.1, 140.2, 136.7, 135.9, 135.9, 129.7, 129.5, 129.3, 128.7, 128.6, 128.5, 128.3, 81.4, 67.1, 62.8, 62.2, 60.6, 59.7, 58.3, 56.9, 54.3, 53.2, 51.3, 50.6, 48.1, 46.0, 43.9, 43.8, 42.2, 40.1, 40.1, 39.9, 37.8, 34.0, 33.6, 31.4, 31.1, 31.0, 30.8, 30.4, 28.9, 28.8, 27.7, 26.5, 23.0, 11.1; MS (ESI) m/z calcd for $[C_{79}H_{106}N_{15}O_{18}]^+$: 1552.78 $[M+H]^+$; found: 1552.85.

c[DKP-RGD]-O-SMAC

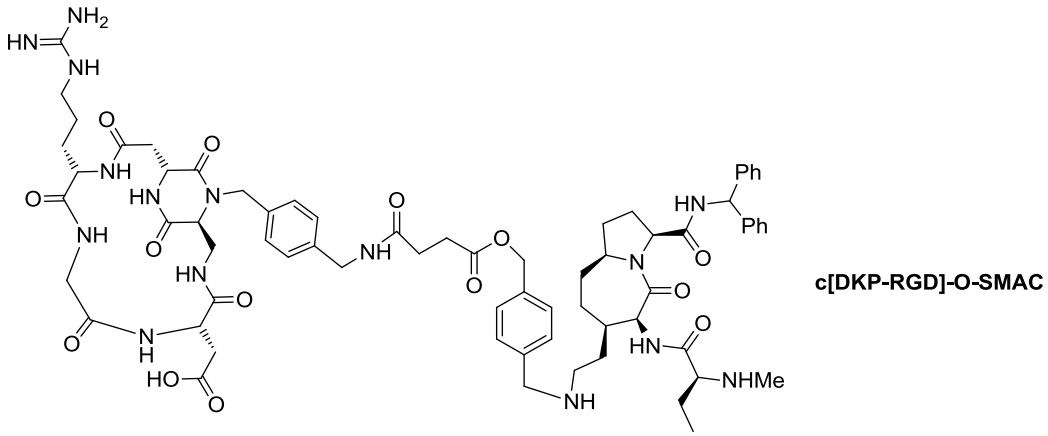

Compound **92** (9 mg, 0.0058 mmol, 1 eq.) was dissolved in CH_2Cl_2 (100 µl) and then was added, at room temperature, TFA (66 µl, 0.87 mmol, 150 eq.). The reaction was stirred at room temperature for 50 min, then the volatiles were removed and the crude product was purified by HPLC (gradient: 90% H_2O + 0.1% CF_3COOH / 10% acetonitrile + 0.1% CF_3COOH to 30% H_2O + 0.1% CF_3COOH / 70% acetonitrile + 0.1% CF_3COOH in 14 min). The purified product was then freeze dried to give the desired compound (as tris-trifluoroacetate salt) as a white foam (9.7 mg, 99% yield).
t_R = 8.7 min;^{1}H NMR (400 MHz, CD_3CN) δ 7.97 (d, J = 8.1 Hz, 1H), 7.86 (dd, J = 8.4, 3.6 Hz, 1H), 7.44 – 7.13 (m, 18H), 6.05 (d, J = 8.1 Hz, 1H), 5.08 (s, 2H), 4.99 (d, J = 15.2 Hz, 1H), 4.75 (t, J = 6.8 Hz, 1H), 4.54 (d, J = 9.4 Hz, 1H), 4.50 (dd, J = 7.9, 4.2 Hz, 1H), 4.45 (dd, J = 9.0, 4.3 Hz, 1H), 4.31 – 4.23 (m, 3H), 4.10 (s, 2H), 4.04 – 3.89 (m, 3H), 3.89 – 3.78 (m, 3H), 3.46 (d, J = 17.1 Hz, 1H), 3.34 (dd, J = 15.0, 6.5 Hz, 1H), 3.12 (t, J = 6.5 Hz, 2H), 3.07 – 2.98 (m, 1H), 2.82 – 2.66 (m, 2H), 2.65 – 2.54 (m, 6H), 2.55 – 2.43 (m, 3H), 2.26 – 2.14 (m, 1H), 2.13 – 1.42 (m, 15H, overlapping with solvent signal), 0.92 (t, J = 7.5 Hz, 3H); ^{13}C NMR (101 MHz, CD_3CN) δ 173.9, 173.2, 173.1, 173.0, 172.2, 171.2, 170.8, 170.6, 170.6, 170.0, 168.6, 168.5, 157.9, 143.1, 142.9, 140.1, 138.7, 135.4, 131.8, 131.2, 129.7, 129.3, 129.1, 128.8, 128.4, 128.3, 128.0, 66.4, 63.2, 62.4, 60.3, 59.2, 58.0, 56.5, 54.9, 52.8, 51.7, 50.0, 48.2, 46.4, 43.4, 43.2, 41.8, 39.8, 38.9, 37.3, 35.5, 33.6, 32.9, 32.5, 32.3, 31.1, 30.2, 29.0, 28.6, 26.9, 26.0, 23.9, 9.1; MS (ESI) *m/z* calcd for $[C_{69}H_{90}N_{15}O_{14}]^+$: 1352.68 $[M+H]^+$; found: 1353.41; HRMS (ESI) *m/z* calcd for $[C_{69}H_{90}N_{15}O_{14}]^+$: 1352.67862 $[M+H]^+$; found: 1352.68112.

***tert*-butyl ((*S*)-1-(((3*S*,6*S*,7*R*,9a*S*)-3-(benzhydrylcarbamoyl)-7-(2-((4-((((benzyloxy)carbonyl)amino)methyl)benzyl)amino)ethyl)-5-oxooctahydro-1H-pyrrolo[1,2-a]azepin-6-yl)amino)-1-oxobutan-2-yl)(methyl)carbamate (93)**

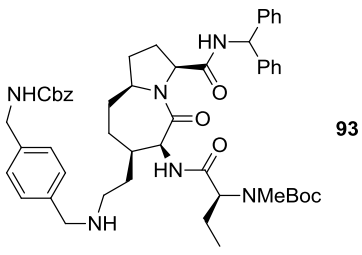

A solution of **81**[12] (20.6 mg, 0.030 mmol, 1.05 eq.), DIPEA (7.42 µl, 0.043 mmol, 1.5 eq.) in dry MeOH (0.2 ml) was put into a flask containing benzyl 4-formylbenzylcarbamate (7.8 mg, 0.029 mmol, 1 eq.) under nitrogen atmosphere. The mixture was let stirring at room temperature for 5 h. $NaBH_4$ (2.2 mg, 0.058 mmol, 2 eq.) was then added stepwise (5 additions within 3 min) and the mixture was let react at room temperature under nitrogen for 30 min. The mixture was then concentrated under vacuum and 5 ml of a saturated solution of $NaHCO_3$ were added, then the mixture was extracted with AcOEt (7 ml, three times). The organic phase was dried over Na_2SO_4 and the solvent was evaporated. The crude product was purified by flash chromatography on silica gel (DCM/MeOH, 9:1) to afford the desired product as a white foam (21 mg, 83%yiled).
R_f = 0.53 (CH_2Cl_2/MeOH, 9:1); ^{1}H NMR (400 MHz, CD_2Cl_2) δ 7.99 (br s, 1H), 7.45 – 7.10 (m, 19H), 7.10 – 6.93 (m, 1H), 6.14 (d, *J* = 8.4 Hz, 1H), 5.41 (s, 1H), 5.10 (s, 2H), 4.68 (d, *J* = 6.8 Hz, 1H), 4.52 (t, *J* = 8.2 Hz, 1H), 4.43 (dd, *J* = 9.6, 5.8 Hz, 1H), 4.32 (d, *J* = 6.0 Hz, 2H), 3.86 (m, 1H), 3.78 (s, 2H), 2.78 (br s, 3H), 2.67 (br s, 1H), 2.48 (s, 1H), 2.35 (s, 1H), 2.28 – 2.14 (m, 1H), 1.99 – 1.57 (m, 7H), 1.56 – 1.30 (m, 12H), 1.14 (s, 1H), 0.88 (t, *J* = 7.4 Hz, 3H); ^{13}C NMR (101 MHz, CD_2Cl_2) δ 172.9, 171.4, 171.0, 170.2, 156.7, 142.7, 142.0, 138.3, 137.9, 137.3, 129.0, 128.9, 128.8, 128.3, 128.3, 127.8, 127.7, 127.6, 127.5, 127.4, 80.5, 66.9, 61.5, 61.1, 60.6, 59.0, 57.2, 55.2, 53.6, 47.3, 45.0, 38.4, 35.0, 34.0, 33.8, 31.9, 30.9, 28.5, 26.1, 21.7, 10.7; MS (ESI) *m*/*z* calcd for $[C_{51}H_{65}N_6O_7]^+$: 873.49 $[M+H]^+$; found: 873.39.

***tert*-butyl ((*S*)-1-(((3*S*,6*S*,7*R*,9a*S*)-3-(benzhydrylcarbamoyl)-7-(2-((4-((((benzyloxy)carbonyl)amino)methyl)benzyl)(tert-butoxycarbonyl)amino)ethyl)-5-oxooctahydro-1H-pyrrolo[1,2-a]azepin-6-yl)amino)-1-oxobutan-2-yl)(methyl)carbamate (94)**

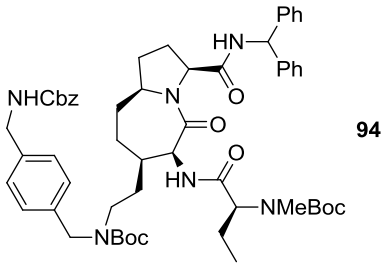

94

A solution of compound **93** (21 mg, 0.024 mmol, 1 eq.) and DIPEA (8.2 µl, 0.048 mmol, 2 eq.) in dry CH_2Cl_2 (0.15 ml) was put in an ice bath under nitrogen atmosphere. A solution of Boc_2O (7.9 mg, 0.036 mmol, 1.5 eq.) in dry CH_2Cl_2 (0.1 ml) was added. The mixture was let react at 0°C for 1h under nitrogen atmosphere, then it was let stirring overnight at room temperature. As the starting material was still present, more Boc_2O (2.1 mg, 0.01 mmol, 0.4 eq.) was dissolved in CH_2Cl_2 (80 µl) and added to the mixture, which was let react for 4 h. Then the solvent was removed under reduced pressure. The crude product was passed through a plug of silica gel (CH_2Cl_2/MeOH 95:5) to afford the desired product as a white foam (23.2 mg, 100% yield).
R_f = 0.62 (CH_2Cl_2/MeOH, 9:1); ^{1}H NMR (400 MHz, acetone-d_6) δ 8.18 (d, *J* = 8.4 Hz, 1H), 7.41 – 7.05 (m, 20H), 6.83 (t, *J* = 5.6 Hz, 1H), 6.19 (d, *J* = 8.7 Hz, 1H), 5.08 (s, 2H), 4.69 (d, *J* = 7.4 Hz, 1H), 4.63 – 4.24 (m, 6H), 4.05 – 3.92 (m, 1H), 3.33 – 3.18 (m, 1H), 3.17 – 2.88 (m,

1H), 2.78 (s, 3H), 2.33 – 2.10 (m, 2H), 2.02 – 1.57 (m, 7H), 1.56 – 1.21 (m, 22H), 0.87 (t, *J* = 7.4 Hz, 3H); MS (ESI) *m*/*z* calcd for $[C_{56}H_{73}N_6O_9]^+$: 973.54 $[M+H]^+$; found: 973.33.

tert-butyl ((*S*)-1-(((3*S*,6*S*,7*R*,9a*S*)-7-(2-((4-(aminomethyl)benzyl)(tert-butoxycarbonyl)amino)ethyl)-3-(benzhydrylcarbamoyl)-5-oxooctahydro-1H-pyrrolo[1,2-a]azepin-6-yl)amino)-1-oxobutan-2-yl)(methyl)carbamate (95)

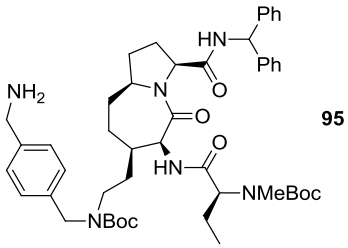

Compound **94** (18.4 mg, 0.019 mmol, 1 eq.) was dissolved in a mixture of THF/H_2O 1:1 (6.4 ml) and Pd/C 10% (2.01 mg, 0.002 mmol, 0.1 eq.) was added. The reaction mixtures were subjected to three vacuum/hydrogen cycles and then left stirring overnight at room temperature under 1 bar of hydrogen. The mixture was filtered through Celite, and the cake thus obtained was washed thoroughly with THF/H_2O 1:1. The filtrate was concentrated and dried to give the crude product as white foam (17 mg, 100% yield) that was used without further purification.
R_f = 0.23 (CH_2Cl_2/MeOH, 9:1); ^{1}H NMR (400 MHz, acetone-d_6) δ 8.20 (d, *J* = 8.4 Hz, 1H), 7.41 – 7.04 (m, 14H), 6.19 (d, *J* = 8.7 Hz, 1H), 4.69 (d, *J* = 7.0 Hz, 1H), 4.64 – 4.25 (m, 5H), 4.06 – 3.93 (m, 1H), 3.78 (s, 1H), 3.29 – 3.19 (m, 1H), 3.19 – 2.91 (m, 2H), 2.79 (s, 3H), 2.28 – 2.20 (m, 1H), 2.21 – 2.11 (m, 1H), 2.02 – 1.31 (m, 29H), 0.88 (t, *J* = 7.4 Hz, 3H); MS (ESI) *m*/*z* calcd for $[C_{48}H_{67}N_6O_7]^+$: 839.51 $[M+H]^+$; found: 839.12.

4-((4-(((2-((3*S*,6*S*,7*R*,9a*S*)-3-(benzhydrylcarbamoyl)-6-((*S*)-2-((tert-butoxycarbonyl)(methyl)amino)butanamido)-5-oxooctahydro-1H-pyrrolo[1,2-a]azepin-7-yl)ethyl)(tert-butoxycarbonyl)amino)methyl)benzyl)amino)-4-oxobutanoic acid (96)

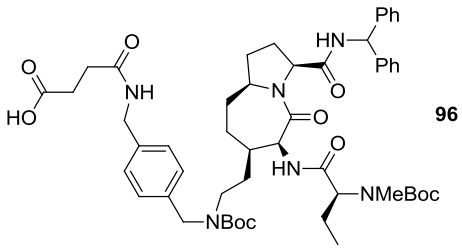

Compound **95** (17 mg, 0.020 mmol, 1 eq.) was dissolved in dry CH_2Cl_2 (0.15 ml). Then DIPEA (3.4 µl, 0.020 mmol, 1 eq.) was added and the mixture was put in an ice bath. DMAP (1.22 mg, 0.010 mmol, 0.5 eq.) and succinic anhydride (3.04 mg, 0.030 mmol, 1.5 eq.) were added. The reaction was let stirring at room temperature under nitrogen atmosphere for 2h. CH_2Cl_2 (15 ml) was then added and the solution was washed with a solution of $KHSO_4$ 1M (7 ml, 2x). The aqueous phase was extracted with CH_2Cl_2 (7 ml, 1x), then the collected organic phases were dried over Na_2SO_4 and the solvent was

evaporated, to afford the crude product. The crude product was purified by HPLC (gradient: 70% H_2O + 0.2% HCOOH / 30% acetonitrile + 0.2% HCOOH to 100% acetonitrile + 0.2% HCOOH in 10 min) to give the desired compound as a white foam (17.6 mg, 99% yield).

t_R = 8.7 min; ^{1}H NMR (400 MHz, acetone-d_6) δ 8.22 (d, J = 7.6 Hz, 1H), 7.65 (s, 1H), 7.39 – 7.01 (m, 15H), 6.19 (d, J = 8.6 Hz, 1H), 4.69 (d, J = 7.1 Hz, 1H), 4.64 – 4.23 (m, 6H), 4.07 – 3.90 (m, 1H), 3.32 – 2.89 (m, 2H), 2.80 (s, 3H), 2.60 (dd, J = 10.3, 4.1 Hz, 2H), 2.51 (dd, J = 10.2, 3.9 Hz, 2H), 2.31 – 2.19 (m, 1H), 2.19 – 2.09 (m, 1H), 2.07 – 1.55 (m, 9H), 1.56 – 1.36 (m, 20H), 0.87 (t, J = 7.4 Hz, 3H); ^{13}C NMR (101 MHz, acetone-d_6) δ 174.2, 172.2, 170.9, 170.8, 156.3, 155.7, 143.5, 143.3, 139.2, 138.6, 129.4, 129.3, 128.6, 128.1, 128.0, 128.0, 79.7, 62.1, 60.6, 59.3, 57.3, 55.8, 50.7, 49.7, 43.4, 38.5, 34.6, 33.9, 33.6, 33.5, 31.1, 28.6, 27.4, 22.2, 11.0; MS (ESI) m/z calcd for $[C_{52}H_{71}N_6O_{10}]^+$: 939.52 $[M+H]^+$; found: 939.45.

2-((1*S*,5*S*,11*S*,15*R*)-18-(4-((4-((4-(((2-((3*S*,6*S*,7*R*,9a*S*)-3-(benzhydrylcarbamoyl)-6-((*S*)-2-((tert-butoxycarbonyl)(methyl)amino)butanamido)-5-oxooctahydro-1H-pyrrolo[1,2-a]azepin-7-yl)ethyl)(tert-butoxycarbonyl)amino)methyl)benzyl)amino)-4-oxobutanamido)methyl)benzyl)-11-(3-guanidinopropyl)-4,7,10,13,17,19-hexaoxo-3,6,9,12,16,18-hexaazabicyclo[13.2.2]nonadecan-5-yl)acetic acid (97)

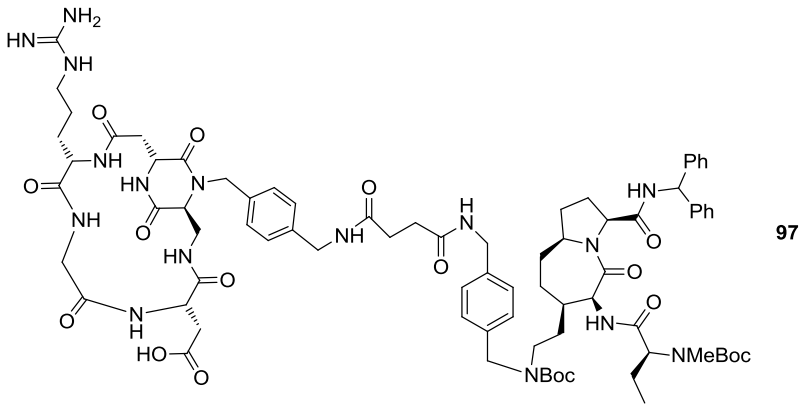

97

Compound **96** (20 mg, 0.021 mmol, 1 eq.) was dissolved under nitrogen atmosphere in a flame dried Schlenk tube with 2 ml of DMF. Then were added, at room temperature and in a single portion, *N*-hydroxysulfosuccinimide (5.7 mg, 0.026 mmol, 1.24 eq.) and *N*,*N*'-diisopropylcarbodiimide (4.94 µl, 0.032 mmol, 1.52 eq.). The solution was stirred overnight, then DMF was removed under vacuum in the Schlenk tube. The resulting residue was then dissolved, in the same Schlenk tube, with 2 ml of CH3CN. To this solution was added a previously prepared solution of **c[DKP-*f*3-RGD]**[10] (11.0 mg, 0.0128 mmol, 0.67 eq.) dissolved in 1 ml of phosphate buffer solution (the pH was adjusted to 7.5 with 0.2M NaOH). The resulting mixture was set to 0 °C and pH was adjusted to 7.5 with 0.2M NaOH. The solution was then stirred overnight. The reaction was then concentrated and purified by HPLC (gradient: 90% H_2O + 0.2% HCOOH / 10% acetonitrile + 0.2% HCOOH to 30% H_2O + 0.2% HCOOH / 70% acetonitrile + 0.2% HCOOH in 15 min). The purified product was then freeze dried to give the desired compound as a white foam (9.7 mg, 49% yield).

t_R = 12.1 min; ^{1}H NMR (400 MHz, CD_3OD) δ 8.44 (s, 1H), 7.38 – 7.12 (m, 18H), 6.13 (s, 1H), 5.15 (d, *J* = 14.9 Hz, 1H), 5.05 (dd, *J* = 10.2, 2.1 Hz, 1H), 4.69 – 4.59 (m, 2H), 4.58 – 4.23 (m, 10H), 4.11 – 4.01 (m, 2H), 3.97 (dd, *J* = 14.6, 7.3 Hz, 1H), 3.85 (d, *J* = 5.7 Hz, 1H), 3.52 (d, *J* = 17.1 Hz, 1H), 3.42 (dd, *J* = 14.3, 5.7 Hz, 1H), 3.28 – 2.92 (m, 4H), 2.88 – 2.72 (m, 5H), 2.60 – 2.51 (m, 4H), 2.45 (dd, *J* = 16.7, 5.5 Hz, 1H), 2.29 – 2.17 (m, 1H), 2.11 – 1.52 (m, 14H), 1.52 – 1.24 (m, 19H), 0.92 (t, *J* = 7.3 Hz, 3H); ^{13}C NMR (101 MHz, CD_3OD) δ 178.0, 174.5, 174.4, 173.8, 173.6, 173.5, 173.0, 172.6, 172.2, 171.5, 171.2, 170.6, 158.7, 143.1, 140.2, 140.0, 139.1, 138.7, 135.9, 129.7, 129.5, 129.3, 128.9, 128.7, 128.6, 128.5, 128.3, 81.7, 81.4, 62.8, 62.0, 60.8, 59.7, 58.3, 56.8, 53.4, 53.2, 51.4, 50.8, 48.1, 46.0, 43.9, 43.8, 42.2, 40.9, 40.1, 37.8, 37.2, 34.1, 33.7, 33.4, 32.3, 31.1, 30.9, 28.8, 27.8, 26.2, 23.0, 11.1; MS (ESI) *m/z* calcd for $[C_{79}H_{107}N_{16}O_{17}]^+$: 1551.80 $[M+H]^+$; found: 1552.30.

c[DKP-RGD]-N-SMAC

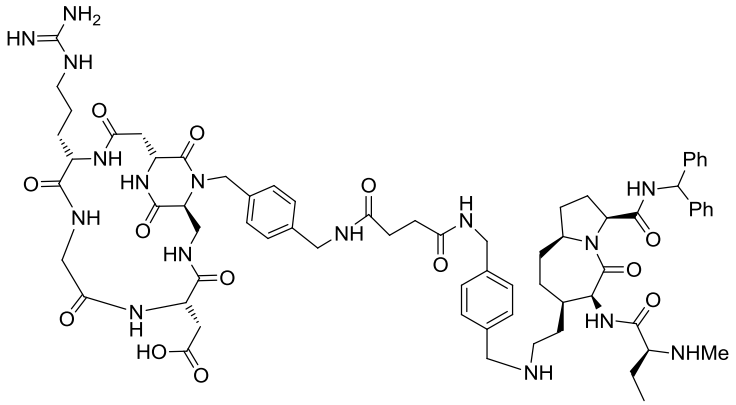

c[DKP-RGD]-N-SMAC

Compound **97** (9 mg, 0.0058 mmol, 1 eq.) was dissolved in CH_2Cl_2 (100 µl) and then was added, at room temperature, TFA (66 µl, 0.87 mmol, 150 eq.). The reaction was stirred at room temperature for 50 min, then the volatiles were removed and the crude product was purified by HPLC (gradient: 90% H_2O + 0.1% CF_3COOH / 10% acetonitrile + 0.1% CF_3COOH to 30% H_2O + 0.1% CF_3COOH / 70% acetonitrile + 0.1% CF_3COOH in 14 min). The purified product was then freeze dried to give the desired compound (as tris-trifluoroacetate salt) as a white foam (9.8 mg, 100% yield).
t_R = 8.3 min;^{1}H NMR (400 MHz, CD_3CN) δ 7.95 (d, *J* = 8.1 Hz, 1H), 7.85 (dd, *J* = 8.2, 3.3 Hz, 1H), 7.40 – 7.14 (m, 18H), 6.05 (d, *J* = 8.1 Hz, 1H), 4.96 (d, *J* = 15.2 Hz, 1H), 4.73 (t, *J* = 6.7 Hz, 1H), 4.58 – 4.42 (m, 3H), 4.36 – 4.20 (m, 5H), 4.14 – 3.80 (m, 7H), 3.45 (d, *J* = 16.9 Hz, 1H), 3.33 (dd, *J* = 14.8, 6.3 Hz, 1H), 3.19 – 3.06 (m, 2H), 3.06 – 2.94 (m, 1H), 2.95 – 2.80 (m, 1H, overlapping with solvent signal), 2.80 – 2.64 (m, 2H), 2.63 – 2.43 (m, 9H), 2.25 – 2.13 (m, 1H), 2.10 – 1.40 (m, 15H), 0.92 (t, *J* = 7.5 Hz, 3H); ^{13}C NMR (101 MHz, CD_3CN) δ 174.0, 173.9, 173.2, 173.1, 172.2, 171.2, 170.8, 170.6, 170.0, 168.6, 158.0, 143.1, 142.9, 141.5, 140.0, 135.5, 131.2, 130.7, 129.7, 129.7, 129.1, 128.8, 128.8, 128.4, 128.3, 128.1, 63.2, 62.5, 60.5, 59.2, 58.0, 56.5, 54.9, 52.9, 51.8, 50.1, 48.3, 46.3, 43.4, 43.3, 41.8, 39.9, 39.0, 37.3, 35.7, 33.7, 32.9, 32.5, 32.3, 32.0, 29.1, 28.6, 27.0, 26.0, 23.9, 9.2; MS (ESI) *m/z* calcd for $[C_{69}H_{91}N_{16}O_{13}]^+$: 1351.69 $[M+H]^+$; found: 1352.40; HRMS (ESI) *m/z* calcd for $[C_{69}H_{90}N_{16}O_{13}Na]^+$: 1373.67655 $[M+Na]^+$; found: 1373.67702.

3.1.7 - Synthesis of $\alpha v\beta_3$ / VEGFR dual action ligands

MA peptide

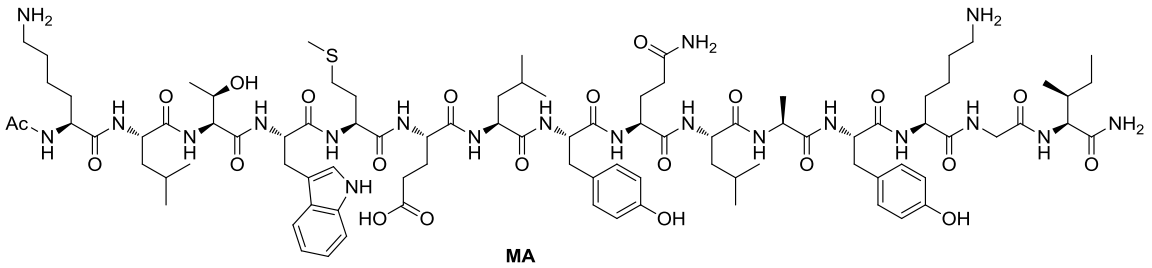

MA

The semi-automatic SPPS was accomplished as described in 3.1.1 on 0.100 mmol of resin (200 mg).

Exact amounts of the amino acids used for SPPS are reported in Table 3.1.2.

Table 3.1.2

Fmoc-AA-OH	M.W. (g/mol)	Mass (mg)
Fmoc-Ile-OH	353.41	141.4
Fmoc-Gly-OH	297.31	118.9
Fmoc-Lys(Boc)-OH	468.54	187.4
Fmoc-Tyr(t-Bu)-OH	459.53	183.8
Fmoc-Ala-OH	311.33	124.5
Fmoc-Leu-OH	353.41	141.4
Fmoc-Gln(Trt)-OH	610.70	244.3
Fmoc-Tyr(t-Bu)-OH	459.53	183.8
Fmoc-Leu-OH	353.41	141.4
Fmoc-Glu(Ot-Bu)-OH	425.47	170.2
Fmoc-Met-OH	371.45	148.6
Fmoc-Trp(Boc)-OH	526.58	210.6
Fmoc-Thr(t-Bu)-OH	397.46	159.0
Fmoc-Leu-OH	353.41	141.4
Fmoc-Lys(Mtt)-OH	624.79	249.9

The on bead-peptide **106** (66 mg of resin, 0.033 mmol) cleavage, RP-HPLC purification and freeze-drying were performed as described in 3.1.1.

RP-HPLC gradient: 80% H_2O + 0.1% CF_3COOH / 20% CH_3CN + 0.1% CF_3COOH to 20% H_2O + 0.1% CF_3COOH / 80% CH_3CN + 0.1% CF_3COOH in 30 min, then 20% H_2O / 80% CH_3CN to 100% CH_3CN in 1 min; flow: 5 mL/min.

The desired compound was obtained (as acetate salt) as a white solid (8 mg, 12%).

t_R = 15.2 min; MS (MALDI-TOF) *m/z* calcd for $[C_{91}H_{141}N_{20}O_{22}S]^+$: 1899.03 amu $[M+H]^+$; found: 1899.1 amu (HCCA matrix).

Ac-MA peptide

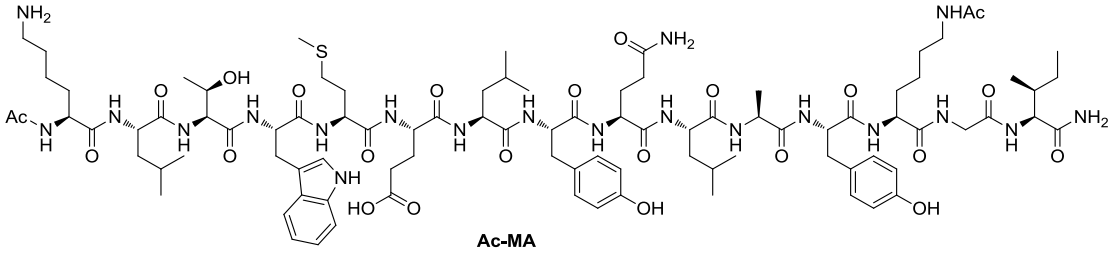

The semi-automatic SPPS was accomplished as described in 3.1.1 on 0.100 mmol of resin (200 mg).
Exact amounts of the amino acids used for SPPS are reported in Table 3.1.3.

Table 3.1.3

Fmoc-AA-OH	M.W. (g/mol)	Mass (mg)
Fmoc-Ile-OH	353.41	141.4
Fmoc-Gly-OH	297.31	118.9
Fmoc-Lys(Ac)-OH	410.50	164.2
Fmoc-Tyr(t-Bu)-OH	459.53	183.8
Fmoc-Ala-OH	311.33	124.5
Fmoc-Leu-OH	353.41	141.4
Fmoc-Gln(Trt)-OH	610.70	244.3
Fmoc-Tyr(t-Bu)-OH	459.53	183.8
Fmoc-Leu-OH	353.41	141.4
Fmoc-Glu(Ot-Bu)-OH	425.47	170.2
Fmoc-Met-OH	371.45	148.6
Fmoc-Trp(Boc)-OH	526.58	210.6
Fmoc-Thr(t-Bu)-OH	397.46	159.0
Fmoc-Leu-OH	353.41	141.4
Fmoc-Lys(Mtt)-OH	624.79	249.9

The on bead-peptide **107** (66 mg of resin, 0.033 mmol) cleavage, RP-HPLC purification and freeze-drying were performed as described in 3.1.1.
RP-HPLC gradient: 80% H_2O + 0.1% CF_3COOH / 20% CH_3CN + 0.1% CF_3COOH to 20% H_2O + 0.1% CF_3COOH / 80% CH_3CN+ 0.1% CF_3COOH in 30 min, then 20% H_2O + 0.1% CF_3COOH / 80% CH_3CN + 0.1% CF_3COOH to 100% CH_3CN + 0.1% CF_3COOH in 1 min; flow: 5 mL/min.
The desired compound was obtained (as acetate salt) as a white solid (3.6 mg, 5%).
t_R = 16.0 min; MS (MALDI-TOF) *m*/*z* calcd for $[C_{93}H_{143}N_{20}O_{23}S]^+$: 1941.04 amu $[M+H]^+$; found: 1941.0 amu (SIN matrix).

Selective removal of Mtt-protecting group (108, 109 and 110)

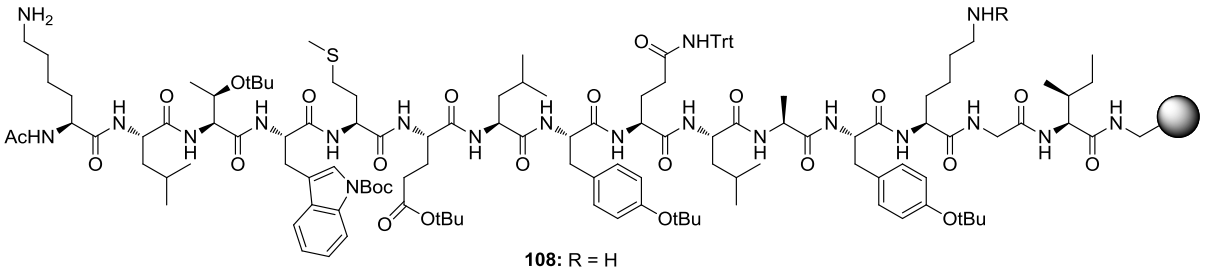

108: R = H
109: R = Ac

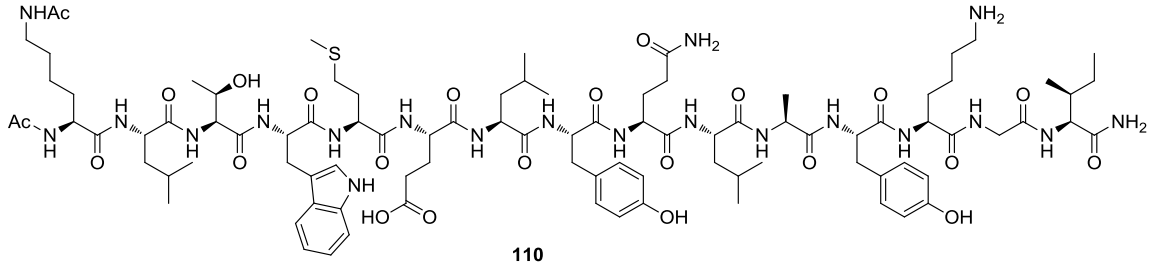

110

108 and 109:

The on bead-MA peptide **106** or **107** (100 mg of resin, 0.05 mmol) was swollen first with DMF, then with DCM (3 mL for each swelling). The Mtt-selective cleavage cocktail was prepared: DCM (33.84 mL, 94%), TIS (1.80 mL, 5%) and TFA (360 μL, 1%) were put in a round bottom flask under stirring and inert atmosphere. The beads were treated with the cleavage cocktail (3 mL per 12 times, 2 minutes each step, 36 mL of cleavage mixture). At the end of the cleavage steps, the the on bead-peptides **108** and **109** were washed twice with DCM, MeOH, DCM, 1% DIPEA in DMF, DMF (3 mL per 5 minutes for each wash).

110:

To a small amount of **108** was added a solution of Ac_2O/DMF 1:3 (3 mL): the reaction was carried out at r.t. under inert atmosphere and mechanical stirring for 3 h. A Kaiser test was performed on a small amount of resin. The full cleavage of the peptide from the resin was effected as reported in 3.1.1. The crude product was purified with RP-HPLC (gradient: 80% H_2O + 0.1% CF_3COOH / 20% CH_3CN + 0.1% CF_3COOH to 20% H_2O + 0.1% CF_3COOH / 80% CH_3CN + 0.1% CF_3COOH in 30 min, then 20% H_2O + 0.1% CF_3COOH / 80% CH_3CN + 0.1% CF_3COOH to 100% CH_3CN + 0.1% CF_3COOH in 1 min; flow: 5 mL/min) and freeze-dried from glacial acetic acid to give the product (as acetate salt) as a white solid (9 mg, 9%).

t_R = 15.9 min; MS (MALDI) *m/z* calcd for $[C_{93}H_{143}N_{20}O_{23}S]^+$: 1941.04 amu $[M+H]^+$; found: 1940.2 amu (SIN matrix).

1-azido-28-oxo-3,6,9,12,15,18,21,24-octaoxa-27-azahentriacontan-31-oic acid (112)

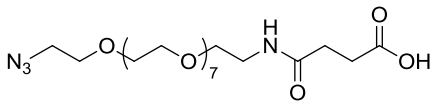

112

Azide **111** (30.0 mg, 0.07 mmol, 1.0 eq) was dissolved in a Schlenk tube with DCM (0.80 mL, dry solvent) under inert atmosphere and stirring. Succinic anhydride (13.7 mg, 0.14 mmol, 2.0 eq) and DIPEA (12 μL, 0.07 mmol, 1.0 eq) were added: the reaction was left at r.t. under stirring and inert atmosphere overnight. The reaction mixture was transferred in a round bottom flask with DCM and acidified with TFA (5 μL, 0.07 mmol). The reaction mixture was concentrated under vacuum and purified with RP-HPLC as described in 3.1.1

RP-HPLC gradient: 100% H_2O + 0.1% CF_3COOH to 70% H_2O + 0.1% CF_3COOH / 30% CH_3CN + 0.1% CF_3COOH in 11 min, then 70% H_2O + 0.1% CF_3COOH / 30% CH_3CN + 0.1% CF_3COOH to 100% CH_3CN + 0.1% CF_3COOH in 2 min; flow: 15 mL/min.

The desired product was obtained as a colourless oil (35 mg, 96%).

t_R = 8.2 min; ^{1}H NMR (400 MHz, Acetone) δ 7.31 (s, 1H), 3.74 – 3.68 (m, 2H), 3.67 – 3.56 (m, 28H), 3.53 (t, J = 5.6 Hz, 2H), 3.45 – 3.32 (m, 4H), 2.59 (dd, J = 10.4, 4.2 Hz, 2H), 2.50 (dd, J = 10.5, 4.0 Hz, 2H).

2-((*1S,5S,11S,15R*)-18-(4-(33-azido-3,6-dioxo-10,13,16,19,22,25,28,31-octaoxa-2,7-diazatritriacontyl)benzyl)-11-(3-guanidinopropyl)-4,7,10,13,17,19-hexaoxo-3,6,9,12,16,18-hexaazabicyclo[13.2.2]nonadecan-5-yl)acetic acid (113)

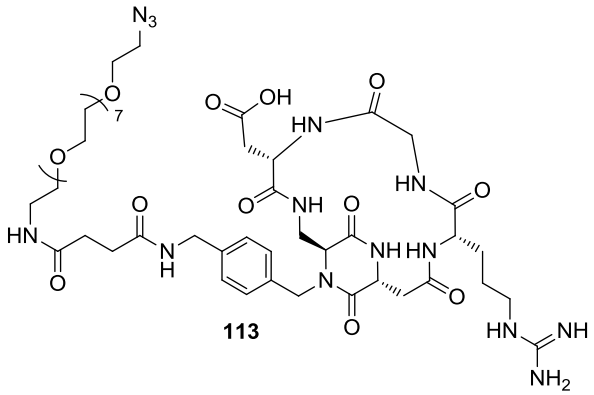

113

122 (35.0 mg, 0.065 mmol, 1.24 eq) was dissolved with DCM (2.8 mL) in a Schlenk tube; *N*-hydroxysuccinimide (9.5 mg, 0.081 mmol, 1.55 eq) and DIC (18 μL, 0.117 mmol, 2.23 eq) were added: the reaction was left at r.t., under stirring and inert atmosphere. After 2 h, the reaction mixture was concentrated under vacuum and the residue was dissolved with CH_3CN (2.8 mL). The previously prepared solution of **c[DKP-*f*3-RGD]**[10] (45.0 mg,

0.052 mmol, 1.0 eq) in phosphate-buffer solution (1.4 mL) was added at 0 °C: pH had to be controlled and maintained in the 7.3-7.6 range, correcting it with some drops of NaOH 0.2 M. pH was monitored for the first 2 h of the reaction, and then the reaction was left at r.t. overnight. The reaction mixture was concentrated, purified with RP-HPLC as described in 3.1.1

RP-HPLC gradient: 100% H_2O + 0.1% CF_3COOH to 55% H_2O + 0.1% CF_3COOH / 45% CH_3CN + 0.1% CF_3COOH in 11 min, then 55% H_2O + 0.1% CF_3COOH / 45% CH_3CN + 0.1% CF_3COOH to 100% CH_3CN + 0.1% CF_3COOH in 1 min; flow: 15 mL/min.

The desired compound was obtained (as trifluoroacetate salt) as a white solid (43.0 mg, 65%).

t_R = 11.7 min; ^{1}H NMR (400 MHz, CD_3OD) δ 8.17 (dd, J = 8.6, 3.1 Hz, 1H), 7.27 (AB system , J = 17.3, 8.2 Hz, 4H), 5.16 (d, J = 15.0 Hz, 1H), 4.99 – 4.83 (m, 1H, overlap with the solvent signal), 4.59 (dd, J = 9.6, 3.8 Hz, 1H), 4.47 – 4.38 (m, 1H), 4.35 (s, 2H), 4.01 – 3.87 (m, 4H), 3.70 – 3.57 (m, 31H), 3.53 (dd, J = 10.8, 5.4 Hz, 4H), 3.40 – 3.32 (m, 4H), 3.22 (t, J = 7.0 Hz, 2H), 3.02 – 2.92 (m, 1H), 2.79 (dd, J = 13.4, 9.8 Hz, 1H), 2.61 – 2.45 (m, 6H), 2.19 – 2.08 (m, 1H), 2.01 – 1.89 (m, 1H), 1.66 (dtt, J = 20.1, 13.3, 6.5 Hz, 2H); ^{13}C NMR (101 MHz, CD_3OD) δ 174.70, 174.55, 173.86, 173.84, 173.54, 171.95, 171.59, 170.90, 158.60, 140.20, 135.79, 129.39, 129.17, 71.52, 71.43, 71.23, 71.07, 70.54, 60.26, 55.96, 53.13, 51.75, 50.28, 48.16, 43.72, 43.59, 42.15, 40.41, 39.68, 38.59, 35.60, 32.23, 32.16, 27.37, 27.05; MS (ESI) m/z calcd for $[C_{49}H_{78}N_{14}NaO_{18}]^+$: 1173.55 amu $[M+Na]^+$; found: 1173.9 amu.

But-3-ynoic acid (114)

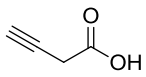

114

In a round bottom flask 3-butyn-1-ol (0.50 g, 7.1 mmol, 1.0 eq) was dissolved in acetone (7.0 mL). In a second round bottom flask CrO_3 (1.39 g, 13.9 mmol, 2.0 eq) was dissolved in H_2O (36 mL) and 97% H_2SO_4 (9.6 mL) was added carefully (exothermic reaction). The solution of 3-butyn-1-ol was added, at 0 °C and dropwise over a period of 1 h, to the solution of CrO_3. The solution was stirred at 0 °C for 3.5 h. The mixture was then extracted three times with Et_2O and the combined organic phases were washed twice with brine, dried with Na_2SO_4 and concentrated. The solid product obtained was dissolved in DCM and extracted three times with sat. aq. $NaHCO_3$: the combined aqueous phases were acidified (pH = 3) with $KHSO_4$ and washed with Et_2O. The final, combined organic phases were dried and concentrated, affording the desired product **114** (156 mg, 26%).

^{1}H NMR (400 MHz, $CDCl_3$) δ 10.97 (s, 1H), 3.37 (d, J = 2.7 Hz, 2H), 2.23 (t, J = 2.7 Hz, 1H); ^{13}C NMR (101 MHz, $CDCl_3$) δ 174.52, 74.86, 72.06, 25.70.

Alkyne-bearing peptide 115

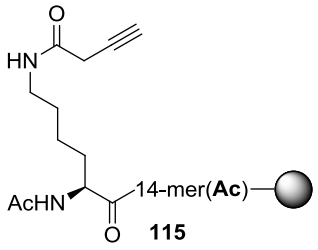

115

On bead-peptide **109** (100 mg of resin, 0.05 mmol, 1.0 eq) was swollen in DMF. But-3-ynoic acid **114** (17 mg, 0.20 mmol, 4.0 eq) was dissolved in DMF (3 mL) and HATU (76 mg, 0.20 mmol, 4.0 eq), HOAt (27 mg, 0.20 mmol, 4.0 eq) and DIPEA (51 μL, 0.30 mmol, 6.0 eq) were added at 0 °C. The reaction was left at 0 °C under stirring for 20 min. The reaction mixture was then added to the on bead-peptide **109**. The reaction was left at r.t. under mechanical stirring and inert atmosphere. After 16 h, the beads were washed twice with DMF, MeOH, Et_2O, MeOH, DMF (3 mL per 5 min for each wash). A Kaiser test was performed on some beads as described in 3.1.1.

(3-azidopropyl)benzene (116)

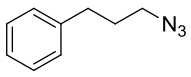

116

Cinnamyl alcohol (500 mg, 3.37 mmol, 1.0 eq) was dissolved in MeOH (37.3 mL) and Pd/C 10 % (39.7 mg, 0.37 mmol, 0.1 eq) was added: the reaction was left overnight at r.t. under stirring and 1 bar of H_2 atmosphere. The reaction mixture was filtered on celite and concentrated affording to the 3-phenylpropan-1-ol as a clear yellow oil (485 mg, 96%), that was directly used in the next step without further purification.
R_f = 0.3 (Hexane/EtOAc, 6:4)

3-phenylpropan-1-ol (485 mg, 3.23 mmol, 1.0 eq) was dissolved in a round bottom flask in DCM (36.4 mL, dry solvent). DIPEA (1.828 mL, 10.68 mmol, 3.3 eq) and MsCl (522 μL, 5.34 mmol, 1.65 eq) were added dropwise under stirring and inert atmosphere at 0 °C. The temperature was let to reach r.t. and the reaction progress was monitored by TLC. After 2 h, the reaction mixture was diluted with DCM and washed twice with 5% aqueous citric acid, once with $NaHCO_3$ and brine. The combined organic phases were dried and concentrated, affording 736 mg (quantitative yield) of 3-phenylpropyl methanesulfonate as a yellow oil, that was directly used in the next step without further purification.

The 3-phenylpropyl methanesulfonate (736 mg, 3.23 mmol, 1.0 eq) was dissolved in a round bottom flask in DMF (16 mL) and NaN_3 (1.05 g, 16.15 mmol, 5.0 eq) was added at 0 °C: the reaction was let to reach r.t. and monitored via TLC. After 24 h, the reaction mixture was diluted with AcOEt, the organic phase was washed twice with brine, dried and concentrated. The crude product was purified by flash chromatography on silica gel (85:15 hexane/EtOAc) to afford the desired product as viscous colourless oil (451.7 mg, 80%).

R_f = 0.56 (Hexane/EtOAc, 85:15); ^{1}H NMR (400 MHz, $CDCl_3$) δ 7.30 (m, 2H), 7.24 – 7.16 (m, 3H), 3.29 (t, J = 6.8 Hz, 2H), 2.76 – 2.68 (m, 2H), 1.92 (dt, J = 14.1, 6.9 Hz, 2H).

CuAAC reaction adduct 117

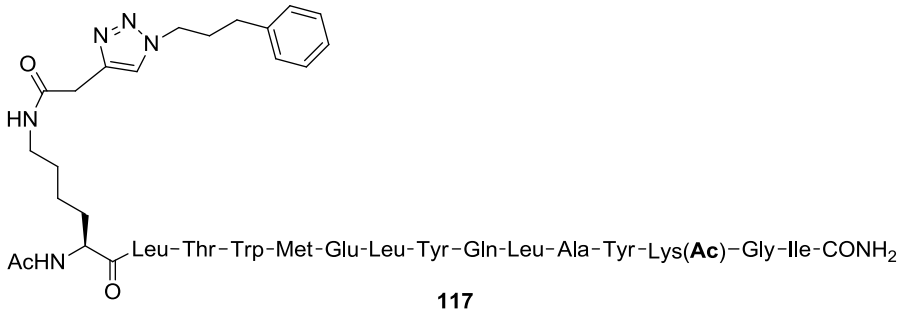

117

On-bead alkyne **115** (50 mg of resin, 0.025 mmol, 1.0 eq) was swollen in DMF (3 mL). Azide **116** (22 mg, 0.125 mmol, 5.0 eq) was dissolved in a DMF/piperidine 4:1 solution (2 mL) and added to the resin. CuI (24 mg, 0.125 mmol, 5.0 eq) and sodium ascorbate (24 mg, 0.125 mmol, 5.0 eq) were added to the mixture: the reaction was carried out at r.t. under mechanical stirring. After 42 h, the beads were washed two times with DMF, MeOH and DCM (3 mL per 5 min for each wash). The product was fully cleaved from the resin and purified with RP-HPLC as described in 3.1.1.

RP-HPLC gradient: from 80% H_2O + 0.1% CF_3COOH / 20% CH_3CN + 0.1% CF_3COOH to 20% H_2O + 0.1% CF_3COOH / 80% CH_3CN + 0.1% CF_3COOH in 30 min, then 20% H_2O + 0.1% CF_3COOH / 80% CH_3CN + 0.1% CF_3COOH to 100% CH_3CN + 0.1% CF_3COOH in 1 min; flow: 5 mL/min.

None of the isolated peaks corresponded to the desired product **117**.

Alkyne-bearing peptide 119

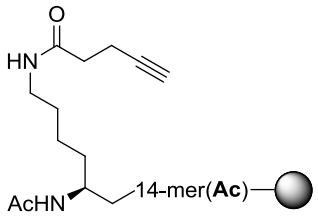

119

On bead-peptide **109** (50 mg of resin, 0.025 mmol, 1.0 eq) was swollen in DMF. Pent-4-ynoic acid **118** (Sigma-Aldrich) (31.8 mg, 0.100 mmol, 4.0 eq) was dissolved in a round bottom flask with DMF (2.00 mL). HATU (24.7 mg, 0.100 mmol, 4.0 eq), HOAt (8.9 mg, 0.100 mmol, 4.0 eq) and DIPEA (39 μL, 0.150 mmol, 6.0 eq) were added under stirring at 0 °C: the reaction was left at 0 °C under stirring and inert atmosphere. After 20 min, the reaction mixture was added to the beads: the reaction was left at r.t. under mechanical stirring. After 16 h, the beads were washed twice with DMF, MeOH, Et_2O, MeOH, DMF (3 mL per 5 min for each wash). A Kaiser test was performed on some beads as described in 3.1.1.

CuAAC reaction adduct 120

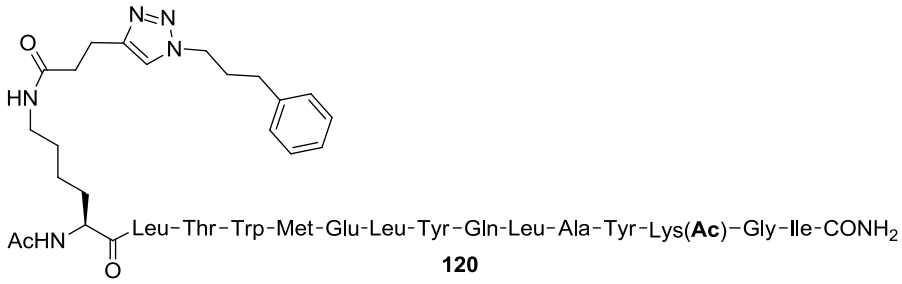

120

On bead-alkyne **119** (50 mg of resin, 0.025 mmol, 1.0 eq) was swollen in DMF and then suspended in DMF (1 mL). Azide **116** (25 mg, 0.125 mmol, 5.0 eq) was dissolved in a round bottom flask in DMF (1 mL) and then added to the beads. CuI (9 mg, 0.125 mmol, 5.0 eq), sodium ascorbate (32 mg, 0.125 mmol, 5.0 eq) and DIPEA (39 μL, 0.125 mmol, 5.0 eq) were added to the solution: the reaction was left under mechanical stirring at r.t. for 72 h. The beads were washed twice with DMF, MeOH, Et_2O, MeOH, DCM, DMF/EDTA (saturated aqueous solution) 1:1, DMF. The product was cleaved from resin and purified by RP-HPLC as described in 3.1.

RP-HPLC gradient: 80% H_2O + 0.1% CF_3COOH / 20% CH_3CN + 0.1% CF_3COOH to 20% H_2O + 0.1% CF_3COOH / 80% CH_3CN + 0.1% CF_3COOH in 15 min, then 20% H_2O + 0.1%

CF_3COOH / 80% CH_3CN + 0.1% CF_3COOH to 100% CH_3CN + 0.1% CF_3COOH in 1 min; flow: 5 mL/min.

The product was obtained as a white solid (3.4 mg, 6%).

t_R = 21.7 min; MS (ESI) *m*/*z* calcd for $[C_{107}H_{159}N_{23}O_{24}S]^{2+}$: 1091.08 amu $[M+2H]^{2+}$; found: 1091.3 amu.

Dual action ligand Ac-MA-RGD

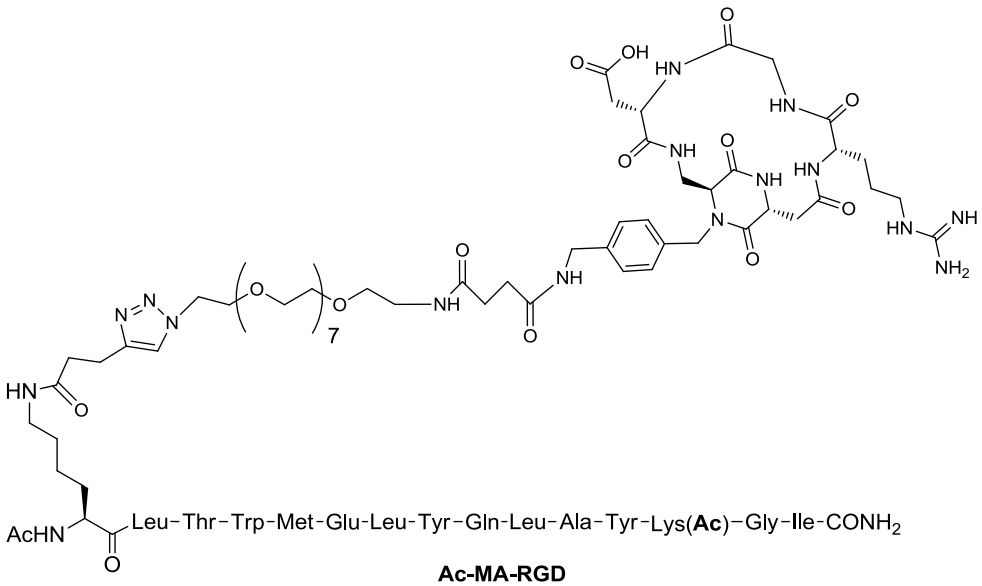

Ac-MA-RGD

On-bead alkyne **119** (36 mg of resin, 0.0183 mmol, 1.0 eq) was swollen in DMF (3 mL). Azide **113** (35 mg, 0.0275 mmol, 1.5 eq) was dissolved in DMF (1.5 mL) under inert atmosphere and added to the resin. CuI (5 mg, 0.0275 mmol, 1.5 eq), sodium ascorbate (5 mg, 0.0275 mmol, 1.5 eq) and DIPEA (9.4 μL, 0.0550 mmol, 3.0 eq) were added to the mixture. The reaction was carried out at r.t. under mechanical stirring and inert atmosphere. After 72 h, the beads were washed two times with DMF, MeOH, DCM, a DMF/EDTA (saturated aqueous solution) 1:1 solution, a 1% TFA in DCM solution and DMF (3 mL per 5 min for each wash). The product was cleaved from the resin and purified by RP-HPLC as described in 3.1.1.

RP-HPLC gradient: 80% H_2O + 0.1% CF_3COOH / 20% CH_3CN + 0.1% CF_3COOH to 55% H_2O + 0.1% CF_3COOH / 45% CH_3CN + 0.1% CF_3COOH in 17 min, then 55% H_2O + 0.1% CF_3COOH / 45% CH_3CN + 0.1% CF_3COOH to 100% CH_3CN + 0.1% CF_3COOH in 1 min; flow: 10 mL/min.

The product was obtained (as acetate salt) as a white solid (3.5 mg, 6%).

t_R = 18.7 min; MS (MALDI-TOF) *m*/*z* calcd for $[C_{147}H_{225}N_{34}O_{42}S]^+$: 3171.63 amu $[M+H]^+$; found: 3172.5 amu (HCCA matrix).

Alkyne-bearing peptide 122

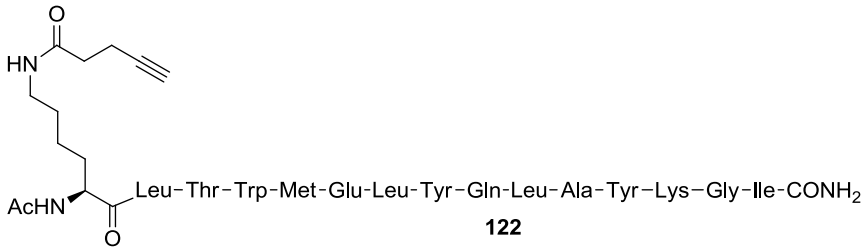

122

Peptide **108** (32 mg of resin, 0.016 mmol, 1.0 eq) was swollen in DMF. Pent-4-ynoic acid **118** (6.3 mg, 0.064 mmol, 4.0 eq) was dissolved in a round bottom flask in DMF (1.00 mL) and HATU (24 mg, 0.064 mmol, 4.0 eq), HOAt (9 mg, 0.064 mmol, 4.0 eq) and DIPEA (16 μL, 0.096 mmol, 6.0 eq) were added under stirring at 0 °C: the reaction was left at 0 °C under inert atmosphere. After 20 min, the reaction mixture was added to the peptide **108**: the reaction was left at r.t. under mechanical stirring. After 16 h, the beads were washed twice with DMF, MeOH, Et_2O, MeOH, DMF (3 mL per 5 min for each wash). A Kaiser test was performed as described in 3.1.1. The product was fully cleaved and purified with RP-HPLC as described in 3.1.1.

RP-HPLC gradient: 80% H_2O + 0.1% CF_3COOH / 20% CH_3CN + 0.1% CF_3COOH to 37% H_2O + 0.1% CF_3COOH / 63% CH_3CN + 0.1% CF_3COOH in 22 min, then 37% H_2O + 0.1% CF_3COOH / 63% CH_3CN + 0.1% CF_3COOH to 100% CH_3CN + 0.1% CF_3COOH in 1 min; flow: 5 mL/min.

The product was obtained (as acetate salt) as a white solid (10.0 mg, 31%).

t_R = 21.7 min; MS (MALDI-TOF) *m/z* calcd for $[C_{96}H_{145}N_{20}O_{23}S]^+$: 1979.05 amu $[M+H]^+$; found: 1979.1 amu (SIN matrix).

Dual action ligand MA-RGD

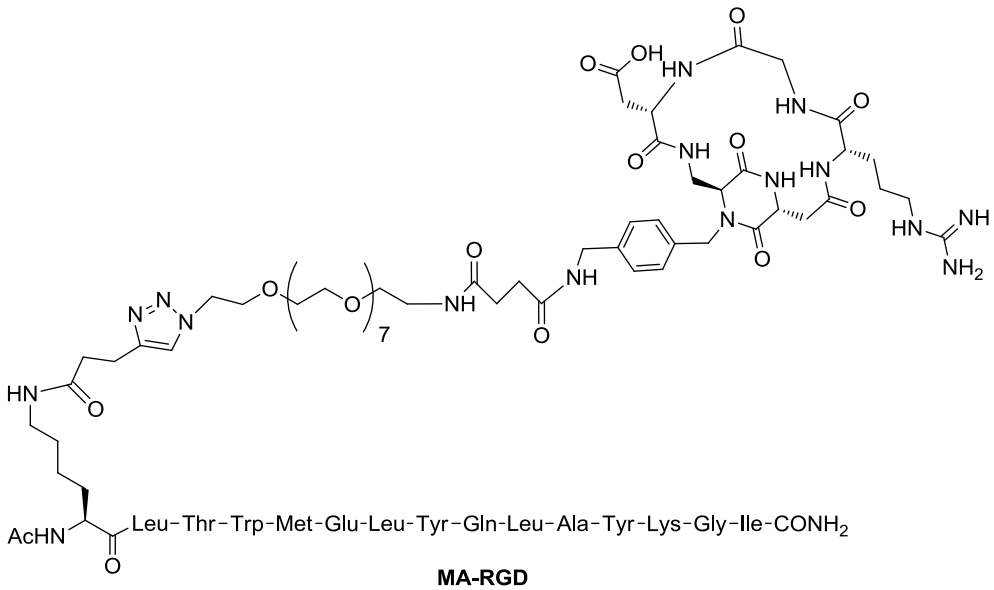

MA-RGD

Alkyne **122** (10.0 mg, 5.0 μmol, 1.05 eq) and azide **113** (6 mg, 4.7 μmol, 1.0 eq) were dissolved in a Schlenk tube in DMF (400 μL). $CuSO_4 \cdot 5H_2O$ (0.24 mg, 0.96 μmol, 0.2 eq), sodium ascorbate (0.30 mg, 1.5 μmol, 0.3 eq) and DIPEA (1.6 μL, 9.4 μmol, 2.0 eq) were added: the reaction was left at r.t. under stirring and inert atmosphere for 48 h. The reaction mixture was diluted with DMF and purified with RP-HPLC as described in 3.1.1.

RP-HPLC gradient: 80% H_2O + 0.1% CF_3COOH / 20% CH_3CN + 0.1% CF_3COOH to 40% H_2O + 0.1% CF_3COOH / + 0.1% CF_3COOH 60% CH_3CN + 0.1% CF_3COOH in 12 min, then 40% H_2O + 0.1% CF_3COOH / 60% CH_3CN + 0.1% CF_3COOH to 100% CH_3CN + 0.1% CF_3COOH in 1 min; flow: 10 mL/min.

The product was obtained (as acetate salt) as a white solid (3.8 mg, 25%).

t_R = 11.7 min; MS (MALDI-TOF) *m*/*z* calcd for $[C_{145}H_{223}N_{34}O_{41}S]^+$: 3129.62 amu $[M+H]^+$; found: 3130.5 amu (SIN matrix).

3.2 NMR, CD, COMPUTATIONAL AND BIOLOGICAL PROCEDURES

3.2.1 NMR studies

NMR experiments were performed at a temperature of 298 K on Bruker Avance 400 and 600 MHz spectrometers. All proton and carbon chemical shifts were assigned unambiguously. The NMR experiments were carried out in a D_2O/H_2O 1:9 mixture in order to observe amide protons. Two-dimensional experiments (TOCSY, NOESY, and HSQC) were carried out on samples of cyclic RGD-peptidomimetics **c[DKP-RGD]** at a concentration in the range 3-6 mM. NOESY experiments were performed at 0.7 or 0.8 s. The water resonance was saturated with the excitation sculpting sequence from the Bruker library. The conformations of the cyclic pentapeptides were analyzed with respect to hydrogen bonding of amide protons (VT-NMR spectroscopy) and NOE contacts.

3.2.2 Circular Dichroism studies

The circular dichroism spectra were registered on a Jasco J-715 CD instrument with Hellma 0.1 cm quarts cell in milliQ H_2O solvent (for the CD spectra recorded in water). The spectra were elaborated with Origin and Jasco instrument associated softwares. The values are reported as total molar ellipticity $[\theta]_T$ (deg × cm^2 × $dmol^{-1}$).

3.2.3 Computational procedures

All calculations were run using the Schrödinger suite of programs (http://www.schrodinger.com) through the Maestro graphical interface. *Conformational analysis*. Conformational preferences of the RGD-peptidomimetics were investigated by Monte Carlo/stochastic dynamics (MC/SD) hybrid simulations using the NMR restraints derived from the experimental NOE contacts (for distance restraints used for each calculation, see the Supporting Information). All the NOE restraints have been set to a distance value of 2±0.5Å with a force constant of 100 kJ/mol·$Å^2$. MC/SD simulations were performed at 300K within the framework of MacroModel version 9.5 employing the OPLS_2001 force field and the implicit water GB/SA solvation model RGD side-chain dihedral angles were defined as internal coordinate degrees of freedom in the Monte Carlo part of the algorithm. A time step of 1 fs was used for the stochastic dynamics (SD) part of the algorithm for 10 ns of simulation time. Samples were taken at 2 ps intervals during each simulation, yielding 5000 conformations for analysis. The

percentages of H-bonds discussed in this thesis have been calculated as percentages of conformations sampled during the simulation in which donor H - acceptor O distance < 2.5 Å (γ-turn) or < 4 Å (β-turn).

3.2.3.1 Molecular docking

The recently solved crystal structure of the extracellular domain of the integrin $\alpha_v\beta_3$ receptor in complex with Cilengitide and in the presence of the proadhesive ion Mn2+ (PDB entry code 1L5G) was used for docking studies. Docking was performed only on the globular head of the integrin because the headgroup of integrin has been identified in the X-ray structure as the ligand-binding region. The protein structure was setup for docking as follows; the protein was truncated to residue sequences 41-342 for chain α and 114-347 for chain β. Due to a lack of parameters, the Mn2+ ions in the experimental protein structure were modelled by replacing them with Ca2+ ions. The resulting structure was prepared using the Protein Preparation Wizard of the graphical user interface Maestro and the OPLSAA force field. The automated docking calculations were performed using Glide (Grid-based Ligand Docking with Energetics). The grid generation step started from the extracellular fragment of X-ray structure of $\alpha_v\beta_3$ complex with Cilengitide, as described in the protein setup section. The center of the grid enclosing box was defined by the center of the bound ligand, as described in the original PDB entry. The enclosing box dimensions, which are automatically deduced from the ligand size, fit the entire active site. For the docking step, the size of the bounding box for placing the ligand center was set to 12 Å. No further modifications were applied to the default settings. The GlideScore function was used to select 20 poses for each ligand. The Glide program was initially tested for its ability to reproduce the crystallized binding geometry of cilengitide. The program was successful in reproducing the experimentally determined binding mode of this compound, as it corresponds to the best-scored pose.

3.2.4 Solid-phase integrin receptor binding assay

Purified $\alpha_v\beta_3$ and $\alpha_v\beta_5$ receptors (Millipore Corporation, Billerica, MA, USA) were diluted to 0.5 μg/mL in coating buffer containing 20 mM Tris-HCl (pH 7.4), 150 mM NaCl, 1 mM $MnCl_2$, 2 mM $CaCl_2$, and 1 mM $MgCl_2$. An aliquot of diluted receptors (100 μL/well) was added to 96-well microtiter plates (NUNC MW 96F Maxisorp Straight) and incubated overnight at 4°C. The plates were then incubated with blocking solution (coating buffer plus 1% bovine serum albumin) for an additional 2 h at room

temperature to block nonspecific binding, followed by 3 h incubation at room temperature with various concentrations (10^{-5}–10^{-12} M) of test compounds in the presence of biotinylated vitronectin (1 μg/mL). Biotinylation was performed using an EZ-Link Sulfo-NHS-Biotinylation kit (Pierce, Rockford, IL, USA). After washing, the plates were incubated for 1 hr at room temperature with biotinylated streptavidin–peroxidase complex (Amersham Biosciences, Uppsala, Sweden) followed by 30 min incubation with 100 μL/well Substrate Reagent Solution (R&D Systems, Minneapolis, MN, USA) before stopping the reaction with the addition of 50 μL/well 2N H_2SO_4. Absorbance at 415 nm was read in a Synergy™ HT Multi-Detection Microplate Reader (BioTek Instruments, Inc.). Each data point represents the average of triplicate wells; data analysis was carried out by nonlinear regression analysis with GraphPad Prism software. Each experiment was repeated in triplicate.

Purified $\alpha_5\beta_1$ receptor (R&D Systems, Minneapolis, MN) was diluted to 0.5 μg/mL in coating buffer containing 20 mM Tris-HCl (pH 7.4), 150 mM NaCl, 1 mM $MnCl_2$, 2 mM $CaCl_2$, and 1 mM $MgCl_2$. An aliquot of diluted receptor (100 μL/well) was added to 96-well microtiter plates (NUNC MW 96F Maxisorp Straight) and incubated overnight at 4°C. The plates were then incubated with blocking solution (coating buffer plus 1% bovine serum albumin) for an additional 2 h at room temperature to block nonspecific binding, followed by 3 h incubation at room temperature with various concentrations (10^{-4}–10^{-11} M) of test compounds in the presence of biotinylated fibronectin (1 μg/mL). Fibronectin was purchased from Sigma. Biotinilation was performed using an EZ-Link Sulfo-NHS-Biotinylation kit (Pierce, Rockford, IL, USA). After washing, the plates were incubated for 1 h at room temperature with biotinylated streptavidin–peroxidase complex (Amersham Biosciences, Uppsala, Sweden) followed by 30 min incubation with 100 μL/well Substrate Reagent Solution (R&D Systems, Minneapolis, MN) before stopping the reaction with the addition of 50 μL/well 2N H_2SO_4. Absorbance at 415 nm was read in a SynergyTM HT Multi-Detection Microplate Reader (BioTek Instruments, Inc.). Each data point represents the average of triplicate wells; data analysis was carried out by nonlinear regression analysis with GraphPad Prism software. Each experiment was repeated in duplicate.

3.2.5 Fluorescence polarization-based BIR/IAP binding assay

Recombinant XIAP (60 nM final concentration) and cIAP2 (25 nM) BIR3, or XIAP BIR23 (3 nM) domains were diluted in the assay buffer containing 100 mM potassium phosphate, pH 7.5, 100 μg/mL bovine γ-globulin and 0.02 % sodium azide. Serial dilutions of each tested compound (concentrations ranging from 2 μM to 0.2 nM) were added to displace a fluorescent probe (FITC-SMAC for BIR3 domains; SMAC-1F for BIR23)[14] and fluorescence polarization was measured with the Ultra plate reader (Tecan), at excitation and emission wavelengths of 485 nm and 530 nm, respectively. All experiments were performed in black, flat-bottom 96 well plates (Greiner Bio-One). Three independent experiments were performed in duplicates. The analyses were performed using Graphpad Prism v.5.02.

3.2.6 Measurement of cytotoxic activity

Human breast MDA-MB231 and ovarian IGROV-1 carcinoma cell lines were cultured *in vitro* with RPMI plus 10% fetal calf serum. For cytotoxic experiments, 10^4 cells were plated in 96 well plates and grown overnight before being treated with serial dilutions of the compounds (concentrations ranging from 25 μM to 10 nM). Cell viability was determined after 72 hours using the CellTiter-Glo (Promega) assay for ATP. Three independent experiments were performed in triplicates.

3.2.7 *In vitro* tube formation assay

Matrigel Basement Membrane Matrix (10 mg/mL) was purchased from BD (Becton Dickinson Italy, Milan, Italy). Human umbilical vein endothelial cells (HUVEC) were obtained from PromoCell (PromoCell Gmbh, Germany). EndoGRO Basal Medium (BM) and rh-VEGF were purchased from Millipore (Millipore S.p.A., MI, Italy). HUVEC 2.5x104 cells were seeded in a 24-well plate coated with 100 μL/well of BD-Matrigel previously polymerized for 1 h at 37 °C. Cells were treated with HUVEC+VEGF (10^{-8} M) and with HUVEC+VEGF (10^{-8} M) + tested compounds (**MA**, **Ac-MA**, **c[DKP-3-RGD]**, **Ac-MA-RGD**) at three different concentrations (10^{-6} M, 10^{-9} M, 10^{-12} M) and incubated for 5 h at 37 °C in a moist atmosphere of 5% CO_2. Tube-like structure formation was evaluated by phase-contrast microscopy using a fluorescence microscope (Axiovert 40CFL, Carl Zeiss S.p.A. Milan, Italy). The total tube length (pixels) was quantified using Adobe Photoshop CS4 (Adobe).

References:

[1] Y. Huang, D. R. Dalton, P. J. Carroll, *J. Org. Chem.* **1997**, *62*, 372-376.

[2] C. M. Thompson, J. A. Frick, D. L. Green, *J. Org. Chem.* **1990**, *55*, 111-116.

[3] K. L.Webster, A. B.Maude, M. E. O'Donnell, A. P. Mehrotra, D. J. Gani, *Chem. Soc. Perkin Trans. 1* **2001**, 1673-1695.

[4] M.C. Pirrung, S.W. Shuey, *J. Org. Chem.* **1994**, *59*, 3890-3897.

[5] S H. Rosenberg, K. P. Spina, K. W. Woods, J. Polakowski, D. L. Martin, Z. Yao, H. H. Stein, J. Cohen, J. L. Barlow, D. A. Egan, K. A. Tricarico, W. R. Baker, H. D. Kleinert, *J. Med. Chem.* **1993**, *36*, 449-459.

[6] K. Gu, L. Bi, M. Zhao, C. Wang, J. Juc, S. Peng, *Bioorg. Med. Chem.* **2007**, *15*, 6273-6290.

[7] J. M. Humphrey, R. J. Bridges, J. A. Hart, A. R. Chamberlin, *J. Org. Chem.* **1994**, *59*, 2467-2472.

[8] V. Bavetsias, A. L. Jackman, R. Kimbell, W. Gibson, F. T. Boyle, G. M. F. Bisset, *J. Med. Chem.* **1996**, *39*, 73-85.

[9] Y. Narukawa, K. N. Juneau, D. Snustad, D. B. Miller, L. S. Hegedus, *J. Org. Chem.* **1992**, *57*, 5453-5462.

[10] R. Colombo (2012). *Synthesis and biological evaluation of potent integrin ligands containing a diketopiperazine scaffold, and of their conjugates with cytotoxic agents.* Ph.D. Thesis. Università degli Studi di Milano: Italy.

[11] M. Marchini (2011). *Peptidomimetics containing new bifunctional 2,5-diketopiperazine scaffolds: synthesis, conformational analysis and use as potent integrin ligands*. Ph.D. Thesis. Università degli Studi di Milano: Italy.

[12] A. Bianchi, M. Ugazzi, L Ferrante, D. Lecis, C. Scavullo, E. Mastrangelo and P. Seneci, *Bioorg. Med. Chem. Lett.* **2012**, *22*, 2204

[13] W. C. Still, M. Kahn, A. Mitra, *J. Org. Chem.* **1978**, *43*, 2923-2925.

[14] D. Lecis, E. Mastrangelo, L. Belvisi, M. Bolognesi, M. Civera, F. Cossu, M. De Cesare, D. Delia, C. Drago, G. Manenti, L. Manzoni, M. Milani, E. Moroni, P. Perego, D. Potenza, V. Rizzo, C. Scavullo, C. Scolastico, F. Servida, F. Vasile and P. Seneci, *Bioorg. Med. Chem.* **2012**, *20*, 6709.

Appendix

^{1}H and ^{13}C NMR Spectra

MS-MALDI-TOF Spectra

Abbreviations

30a:

^{1}H NMR (400 MHz, CD_2Cl_2)

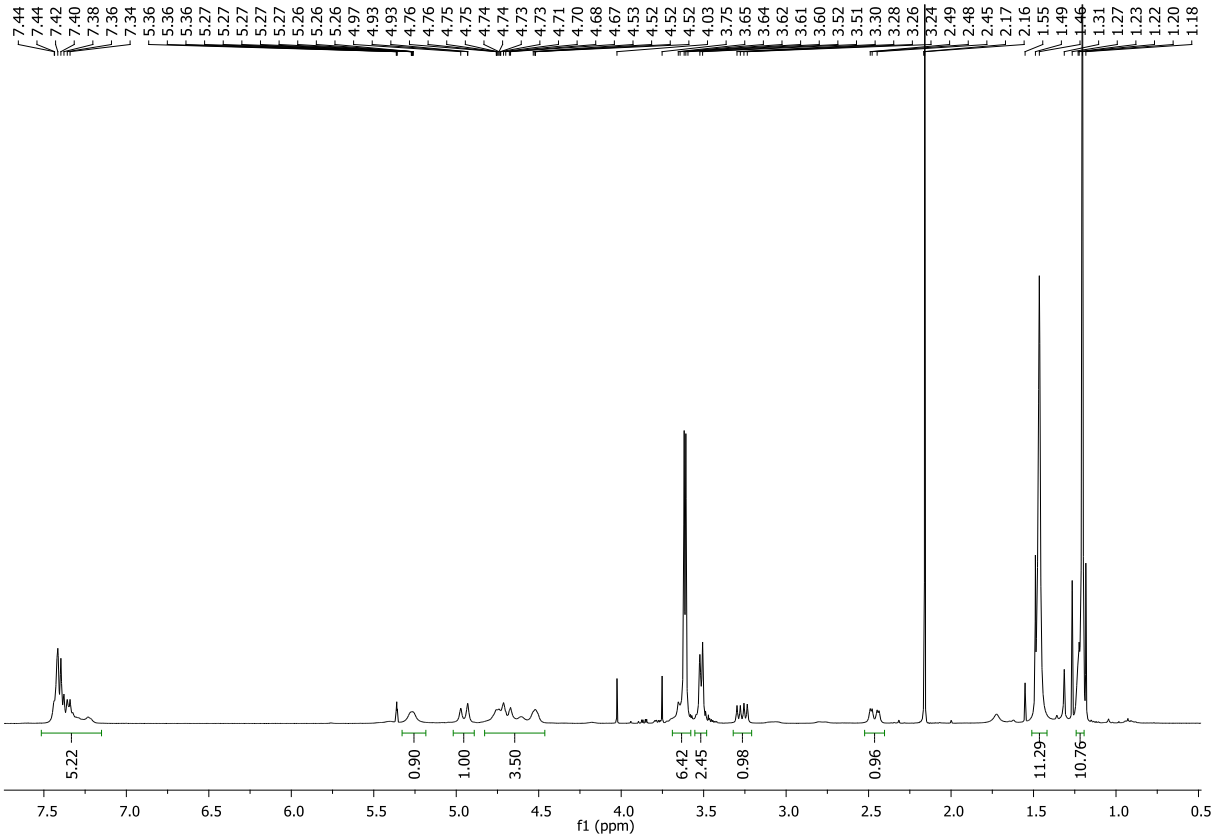

^{13}C NMR (101 MHz, CD_2Cl_2)

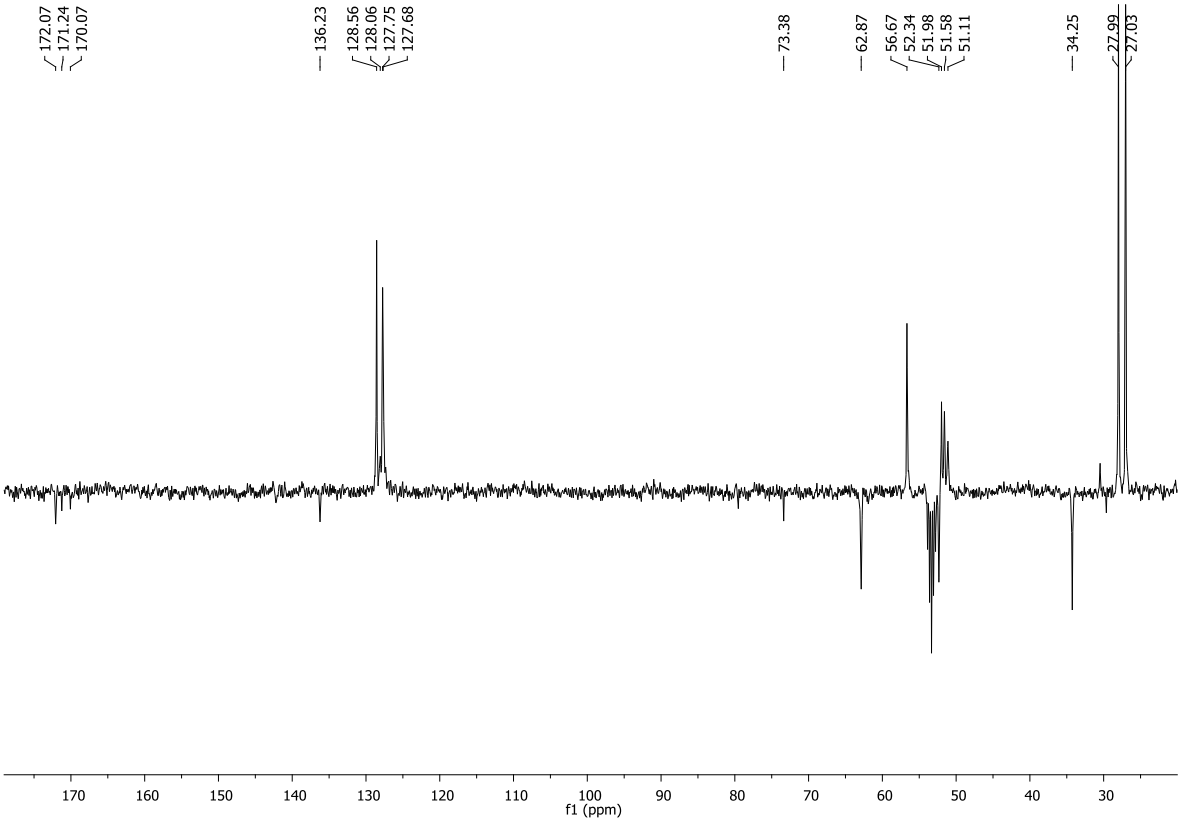

38a:

^{1}H NMR (400 MHz, CD_2Cl_2)

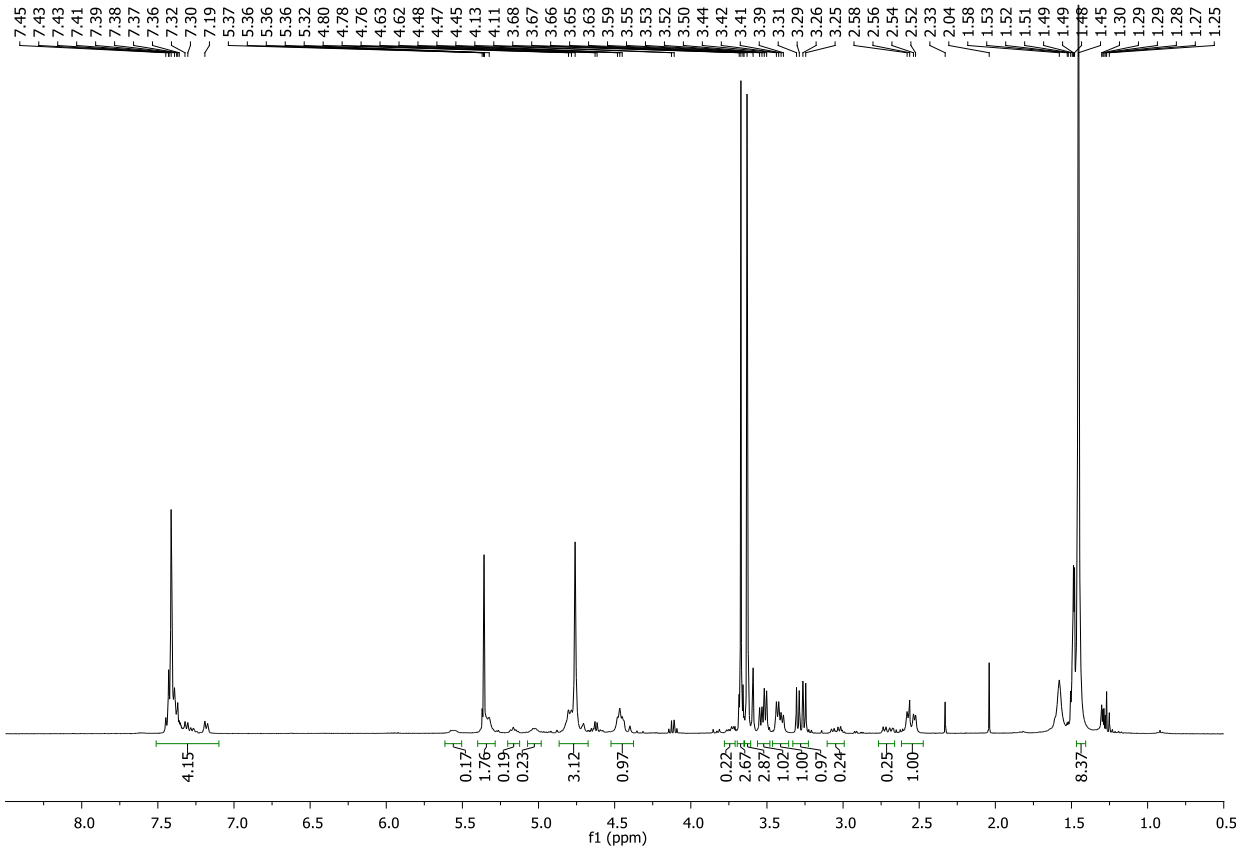

^{13}C NMR (101 MHz, CD_2Cl_2)

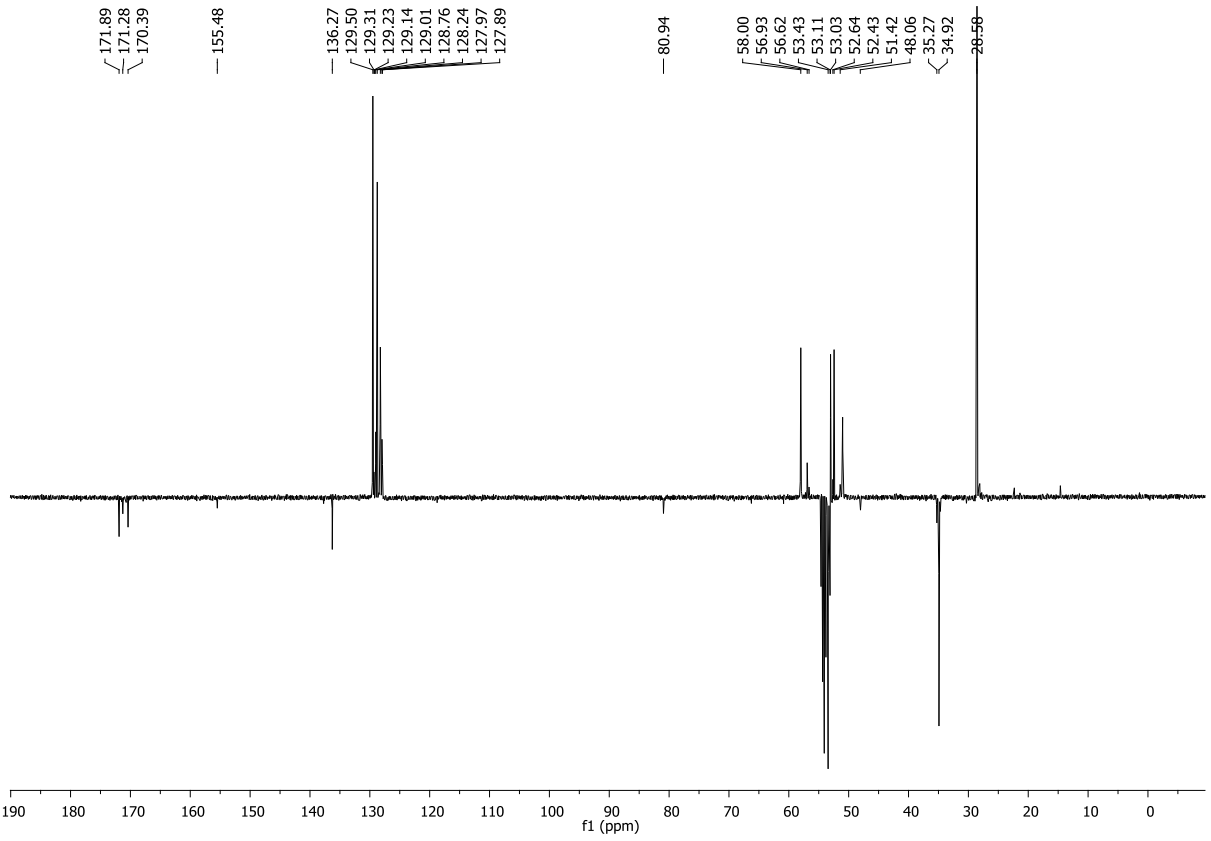

39a:

^{1}H NMR (400 MHz, CD_2Cl_2)

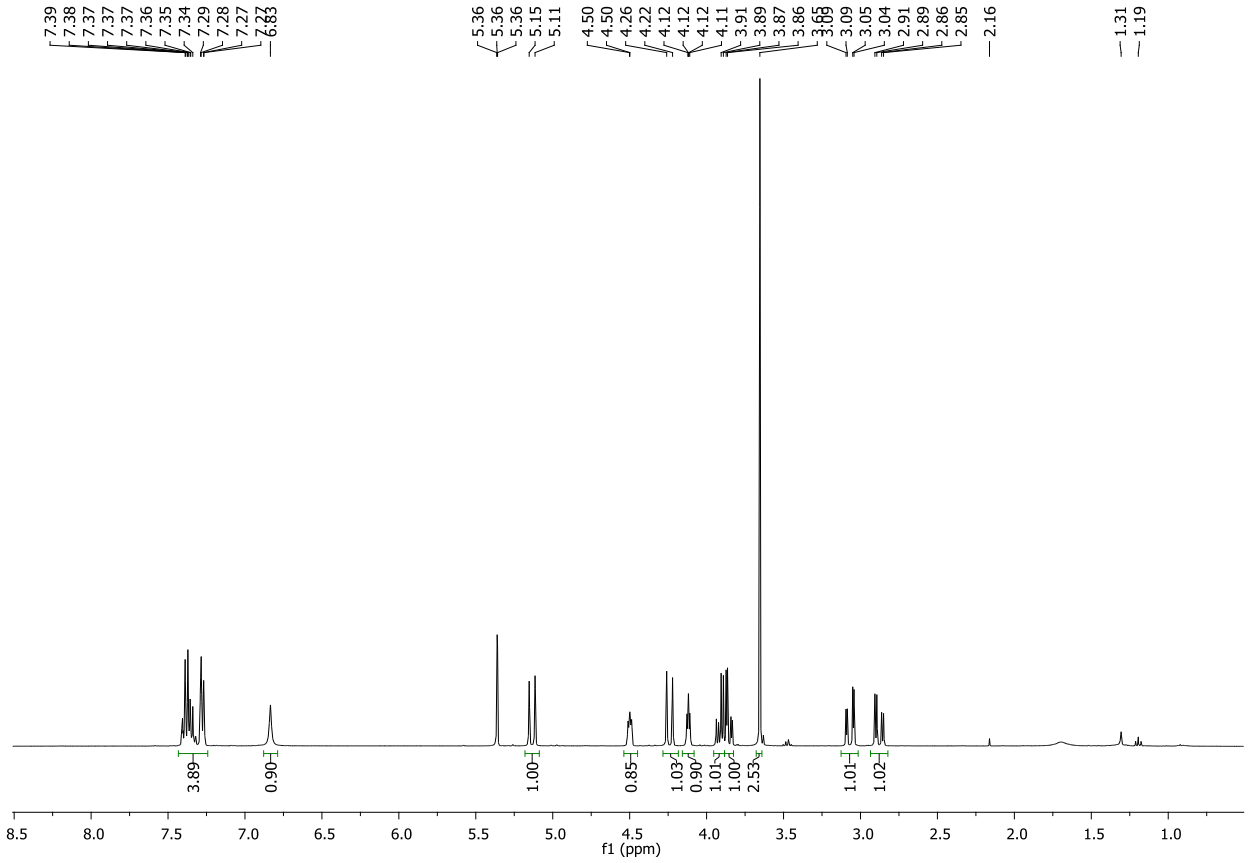

^{13}C NMR (101 MHz, CD_2Cl_2)

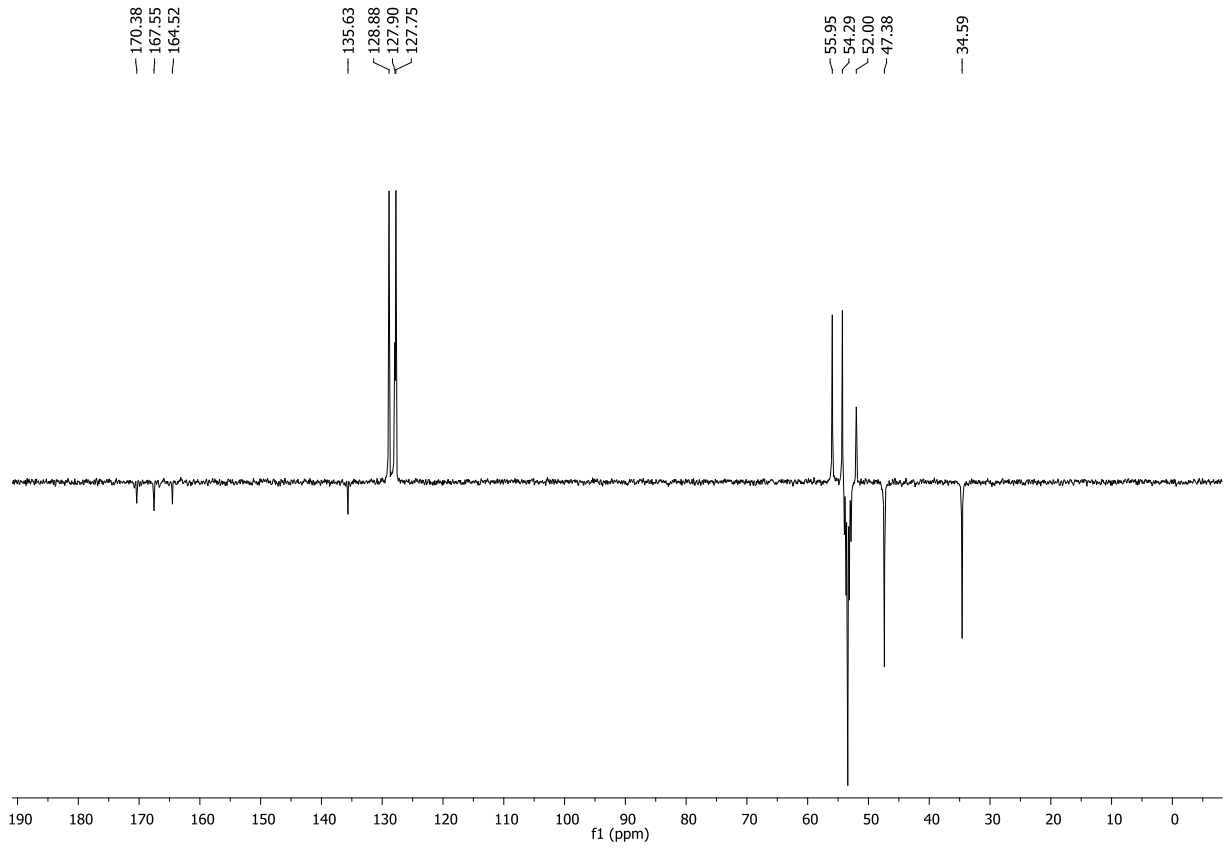

40a:

^{1}H NMR (400 MHz, CD_2Cl_2)

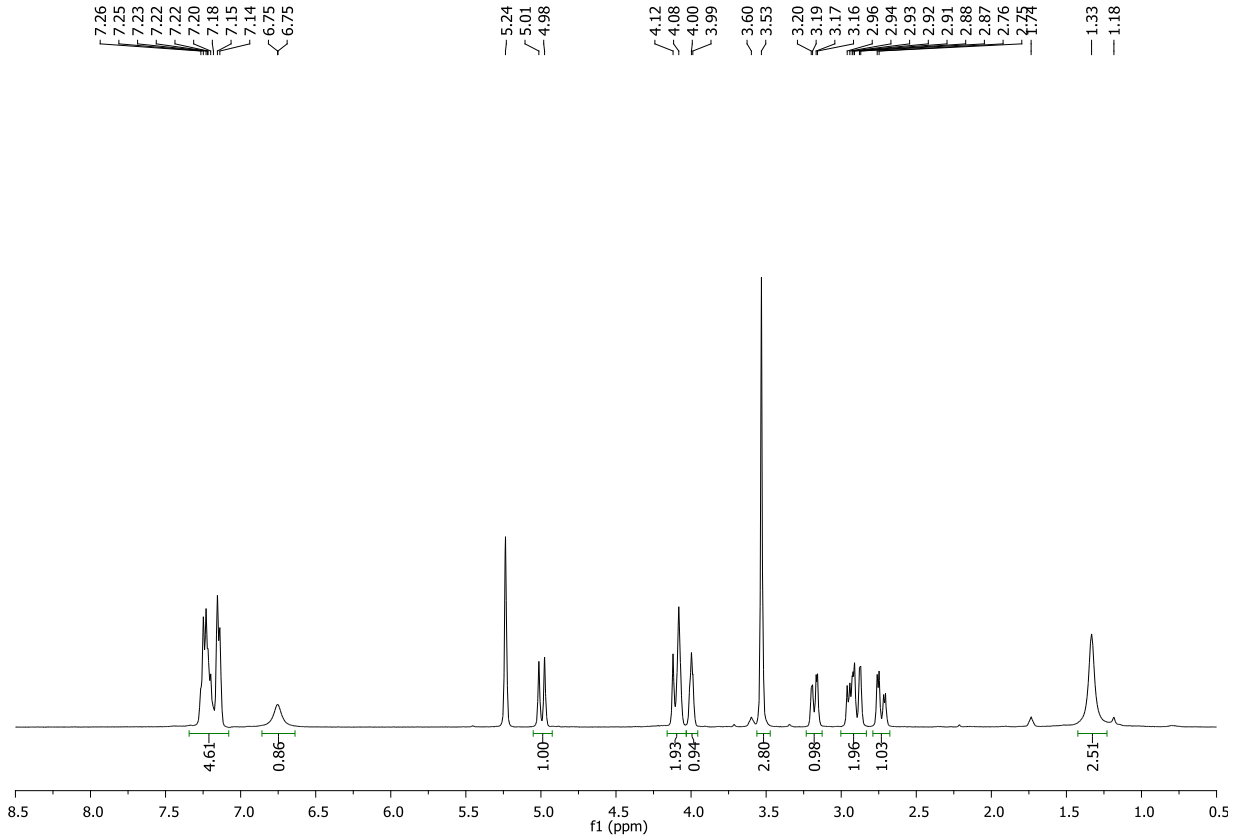

^{13}C NMR (101 MHz, CD_2Cl_2)

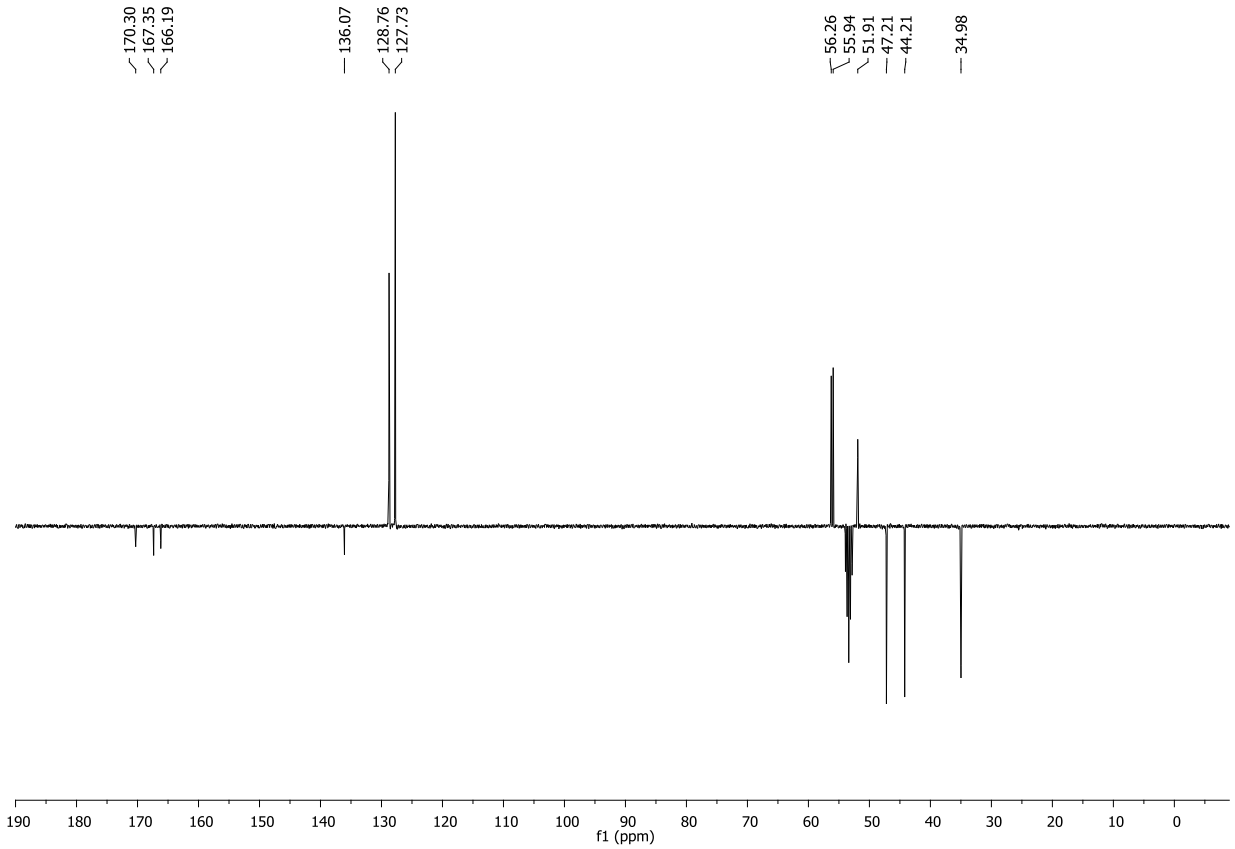

41a:

^{1}H NMR (400 MHz, CD_2Cl_2)

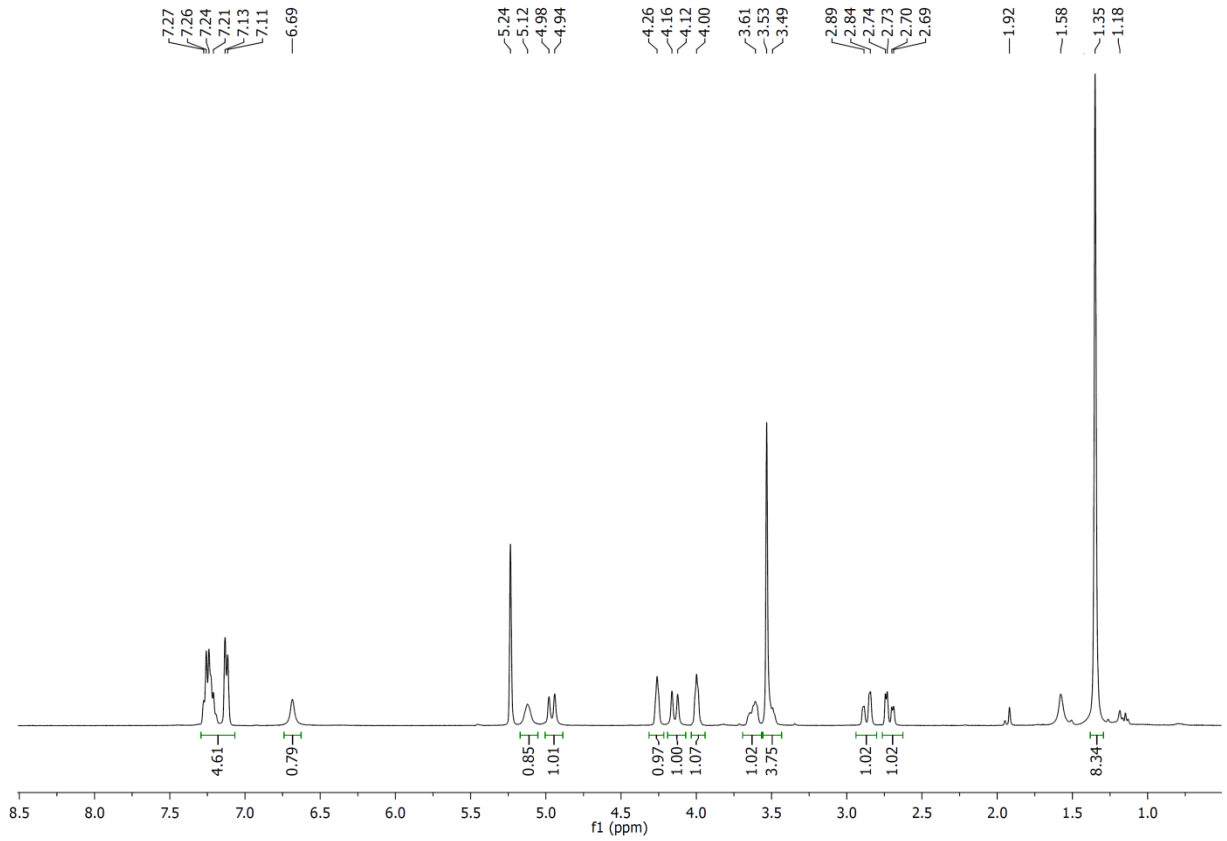

^{13}C NMR (101 MHz, CD_2Cl_2)

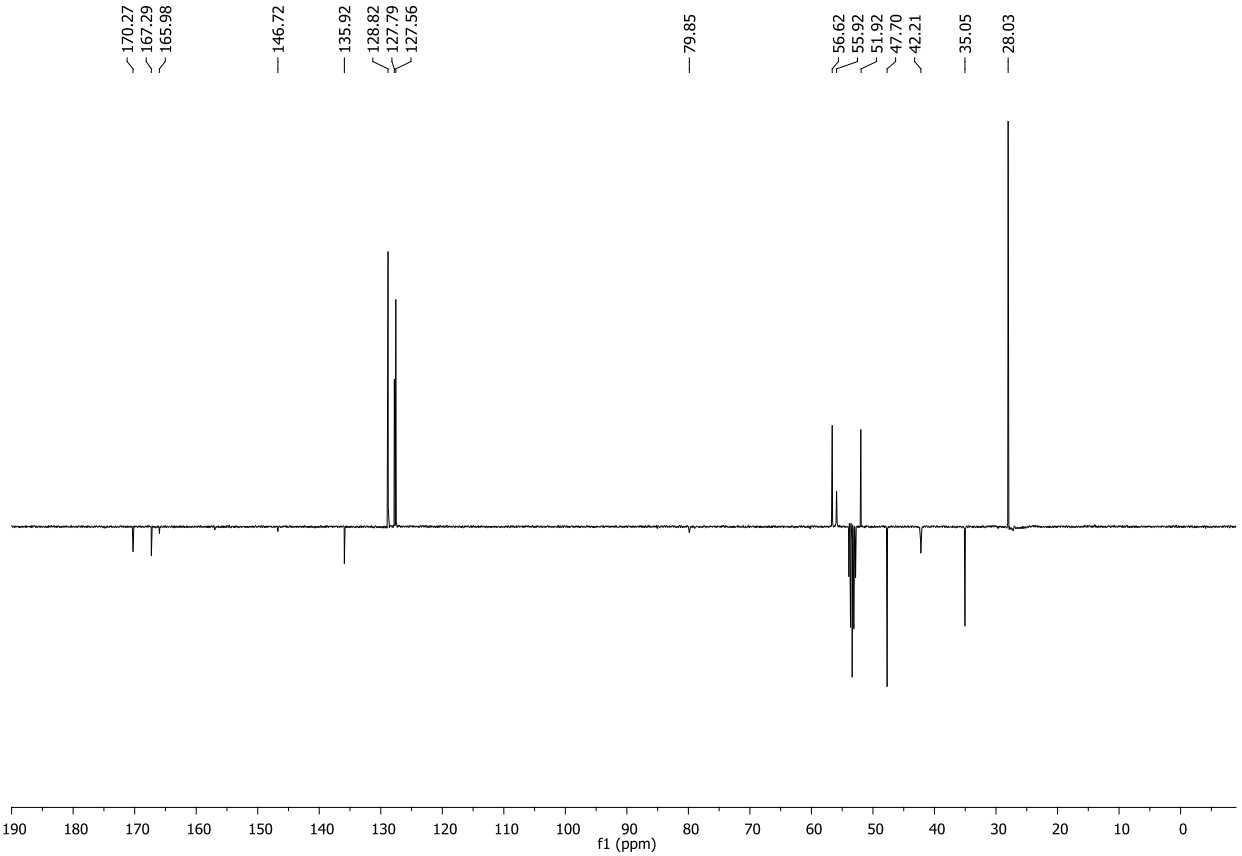

42a:

^{1}H NMR (400 MHz, CD_2Cl_2)

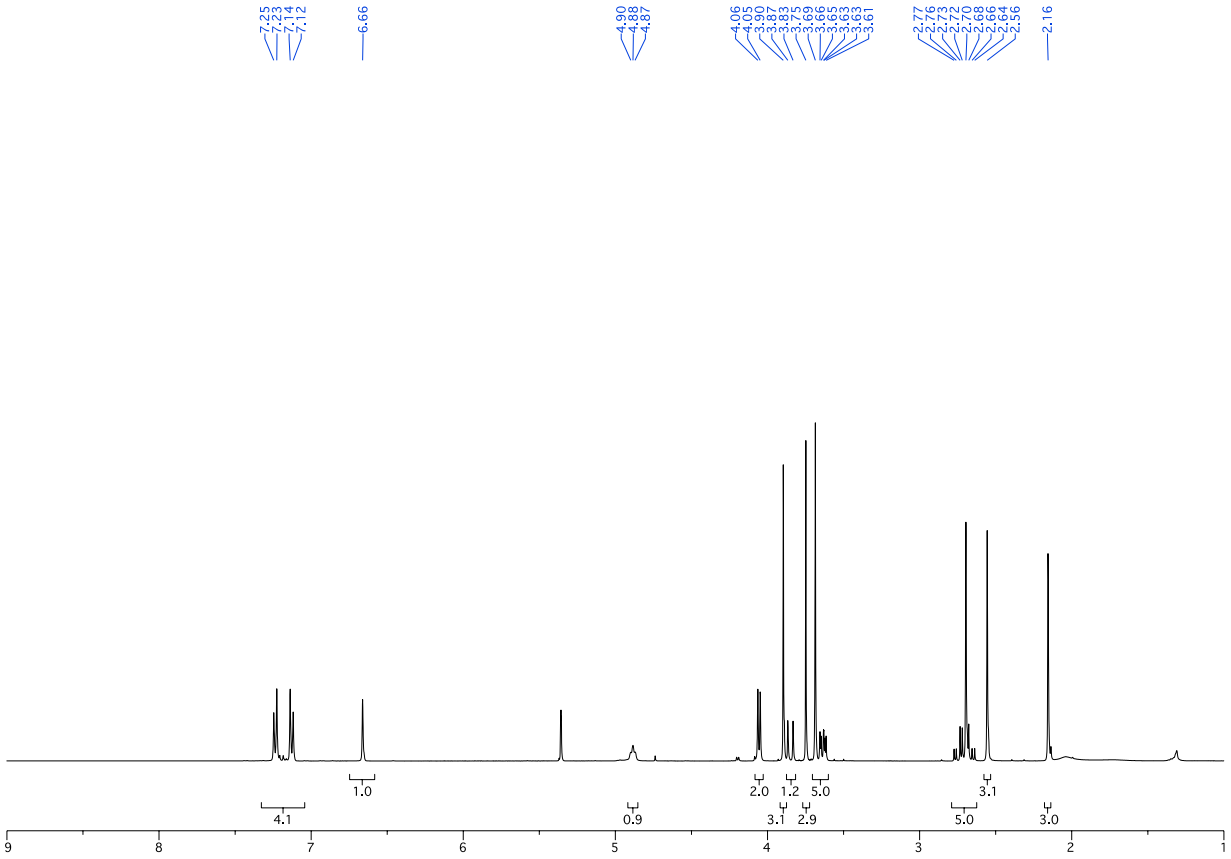

^{13}C NMR (101 MHz, CD_2Cl_2)

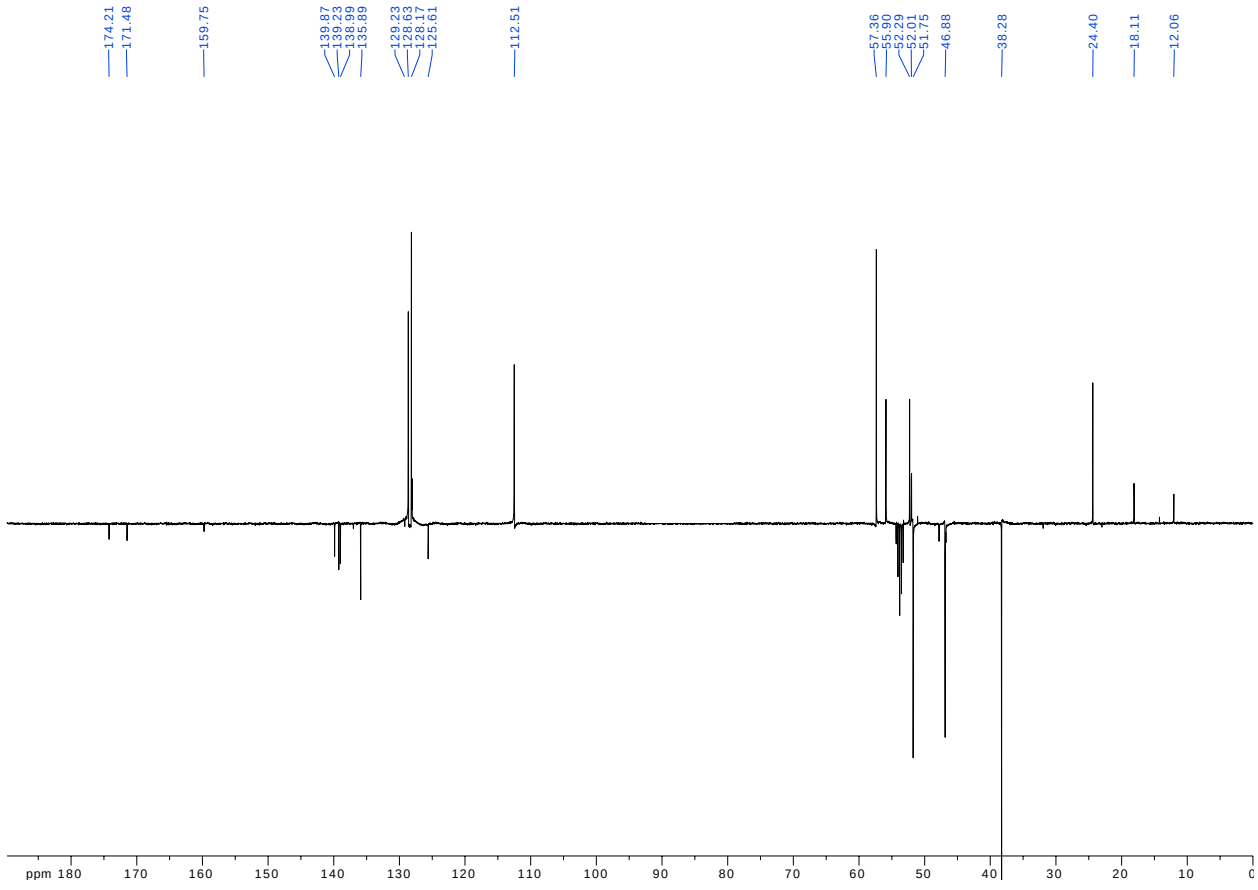

43a:

^{1}H NMR (400 MHz, CD_2Cl_2)

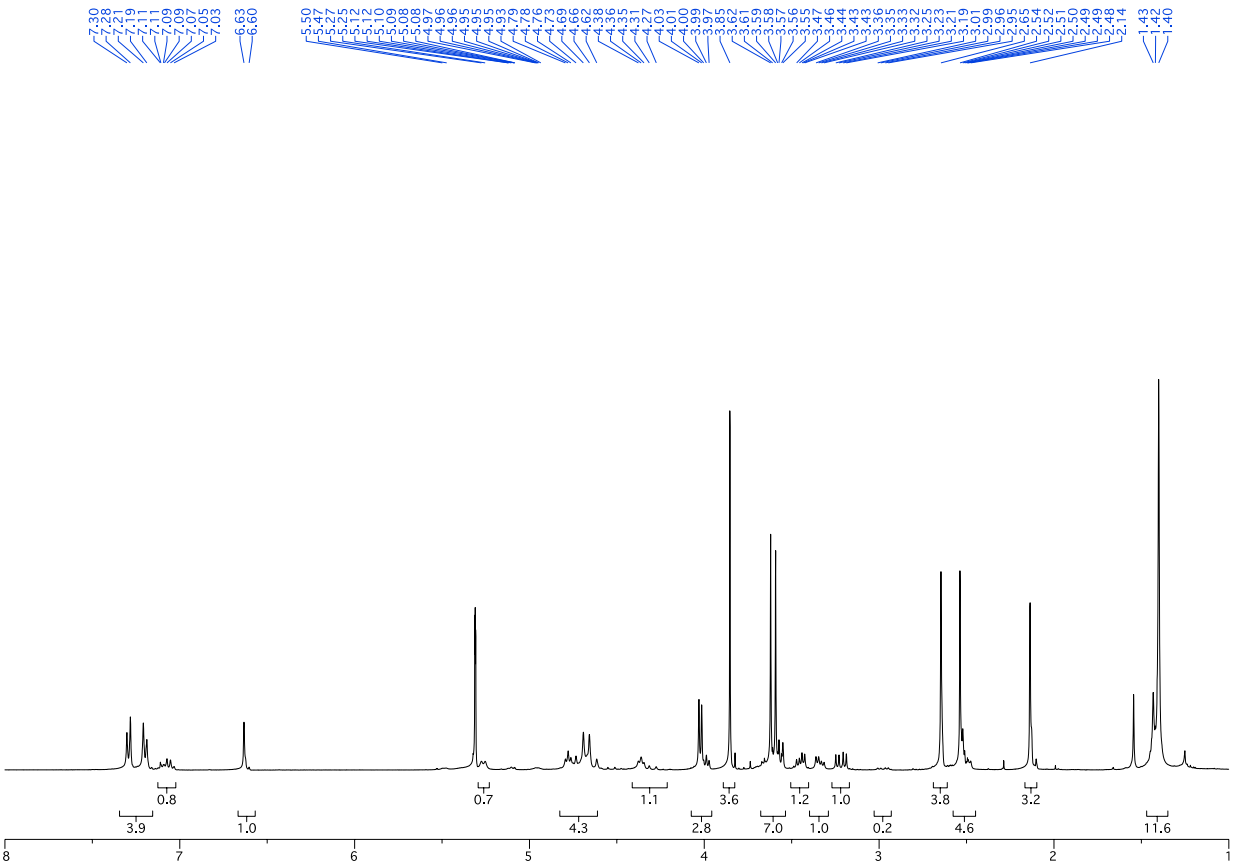

^{13}C NMR (101 MHz, CD_2Cl_2)

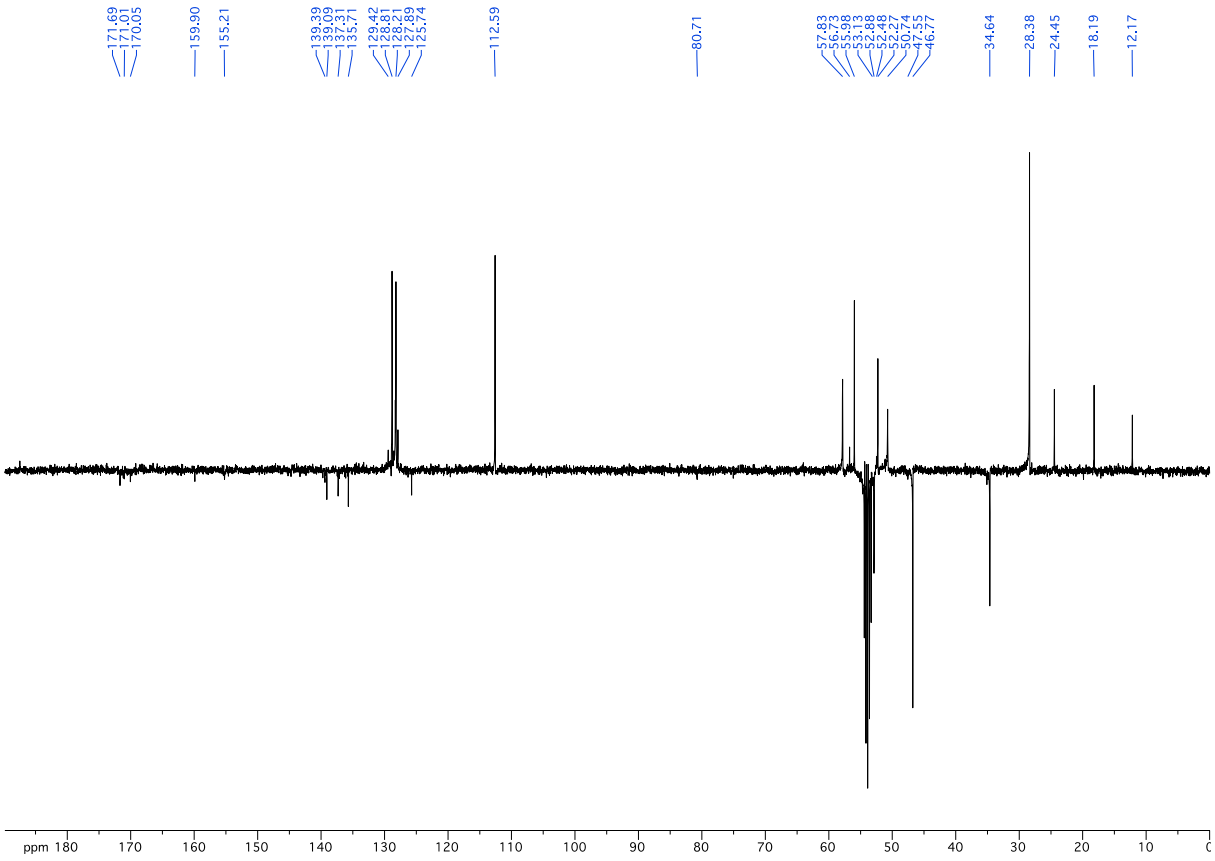

44a:

^{1}H NMR (400 MHz, CD_2Cl_2)

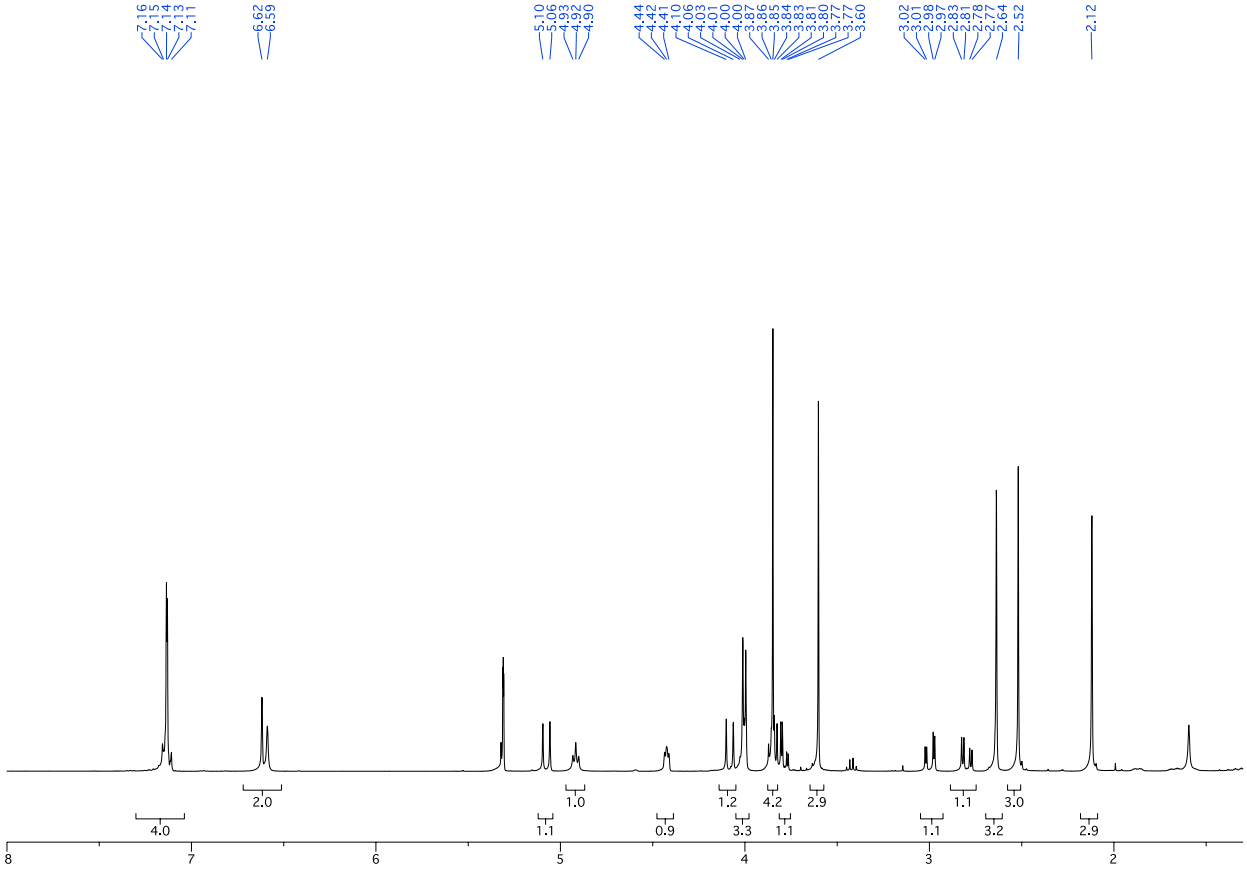

^{13}C NMR (101 MHz, CD_2Cl_2)

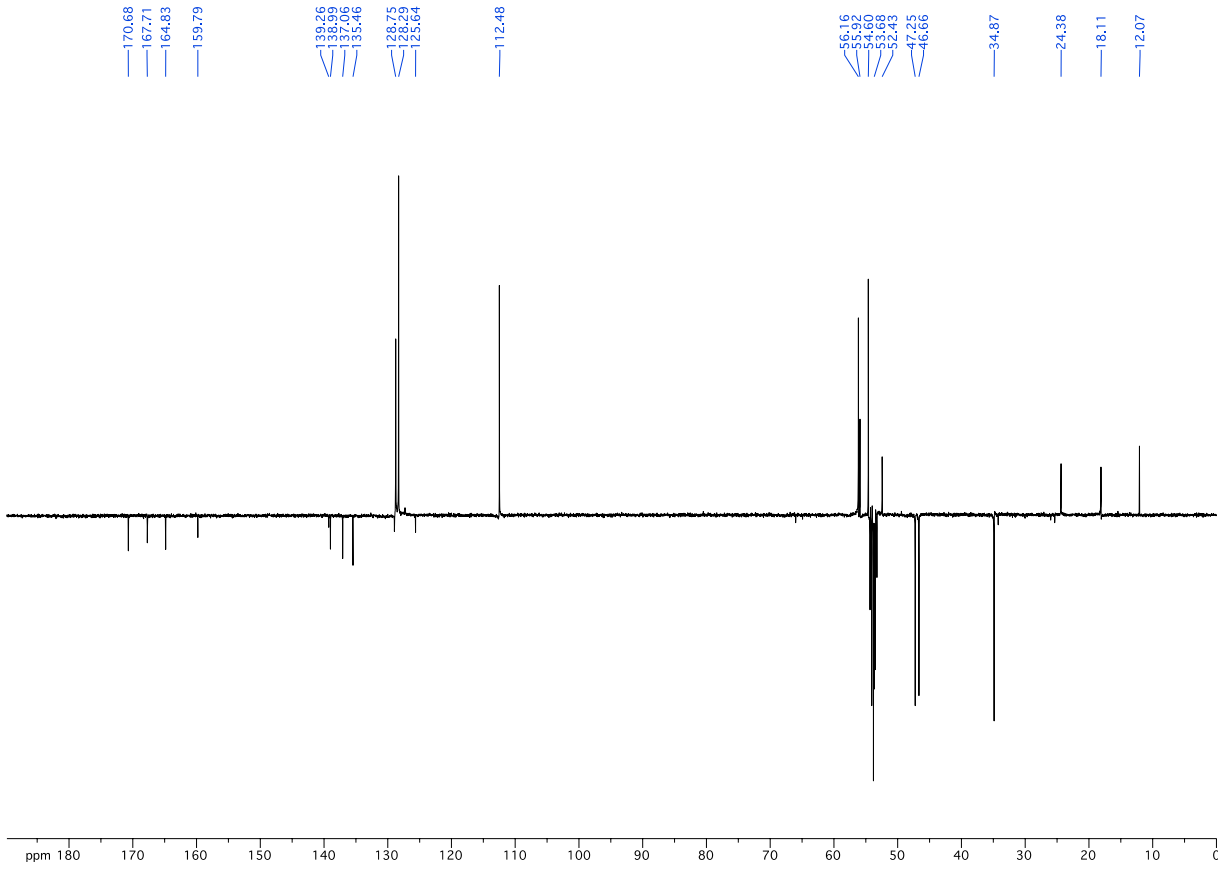

45a:

^{1}H NMR (400 MHz, CD_2Cl_2)

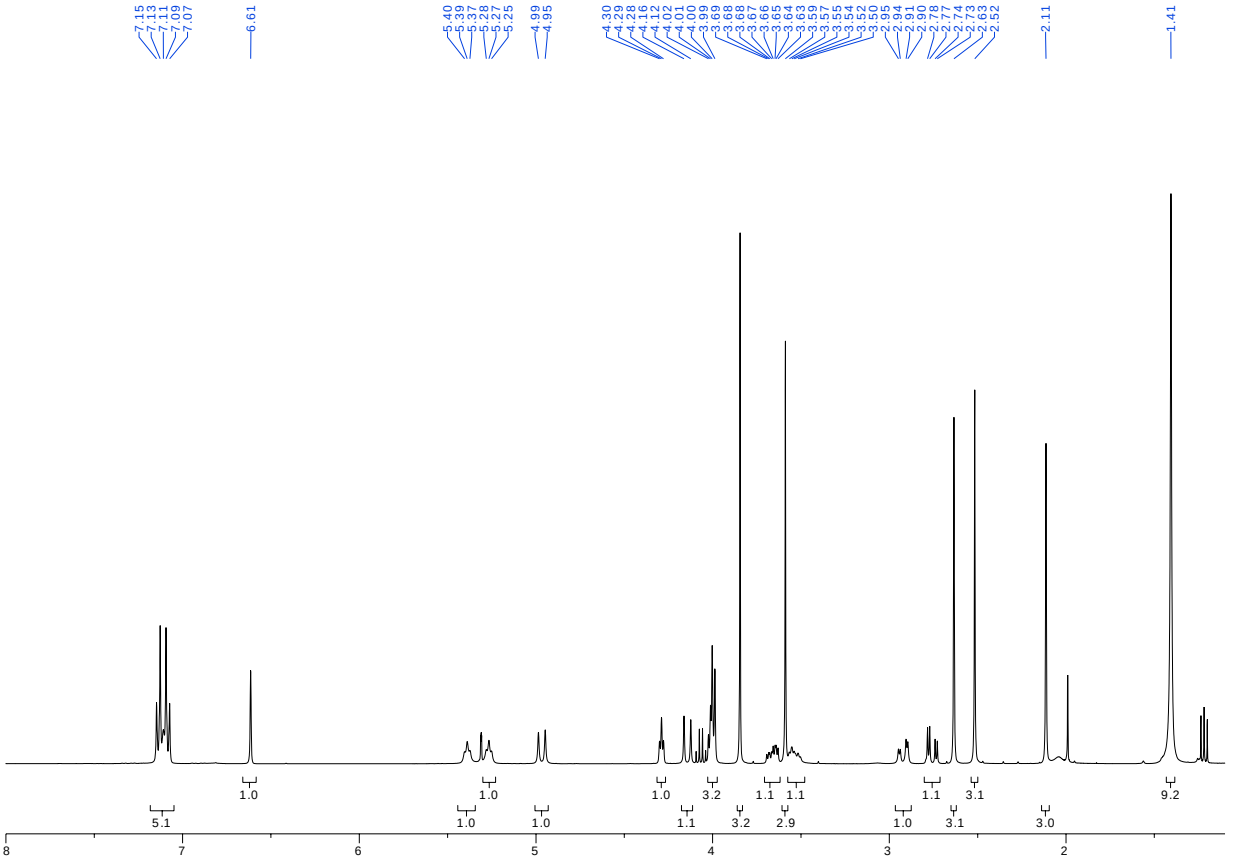

^{13}C NMR (101 MHz, CD_2Cl_2)

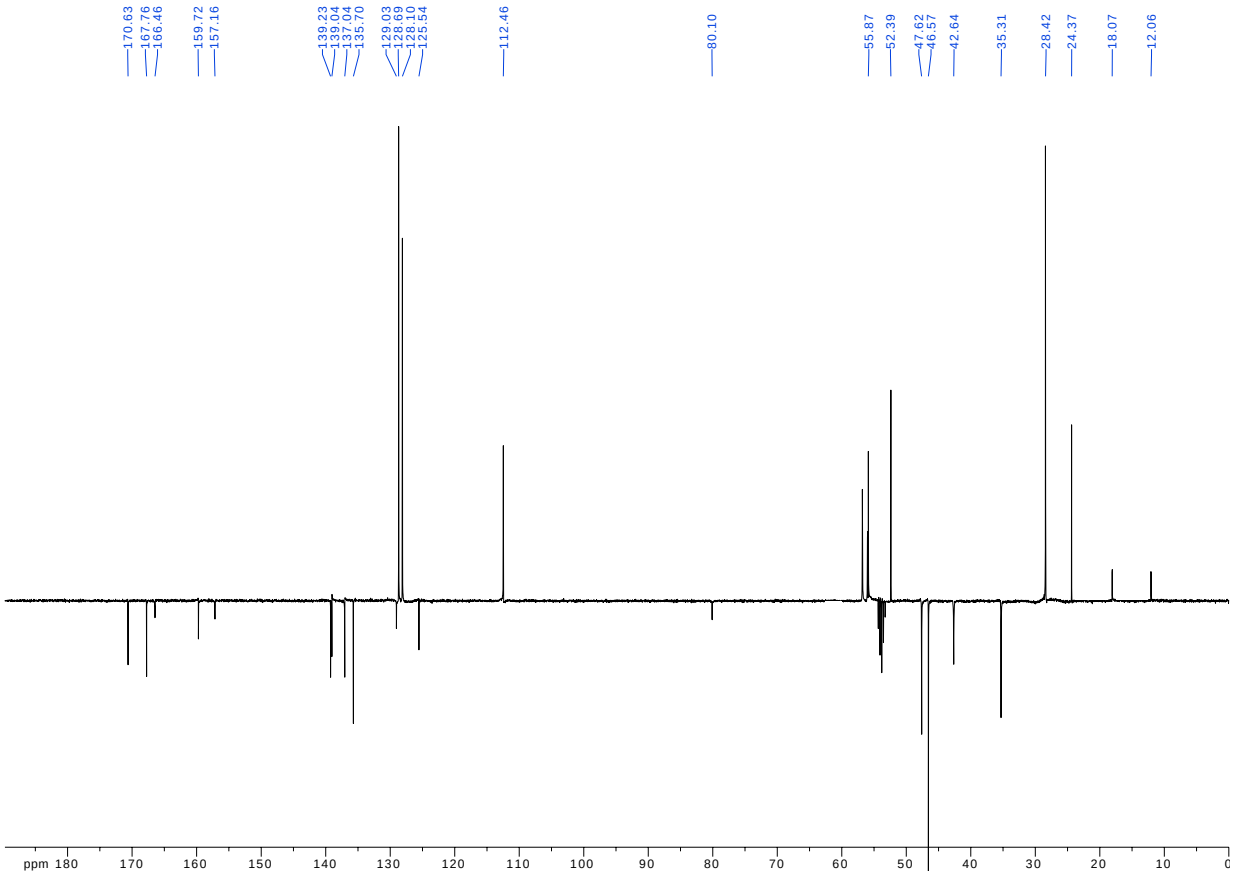

46b:

^{1}H NMR (400 MHz, CD_2Cl_2)

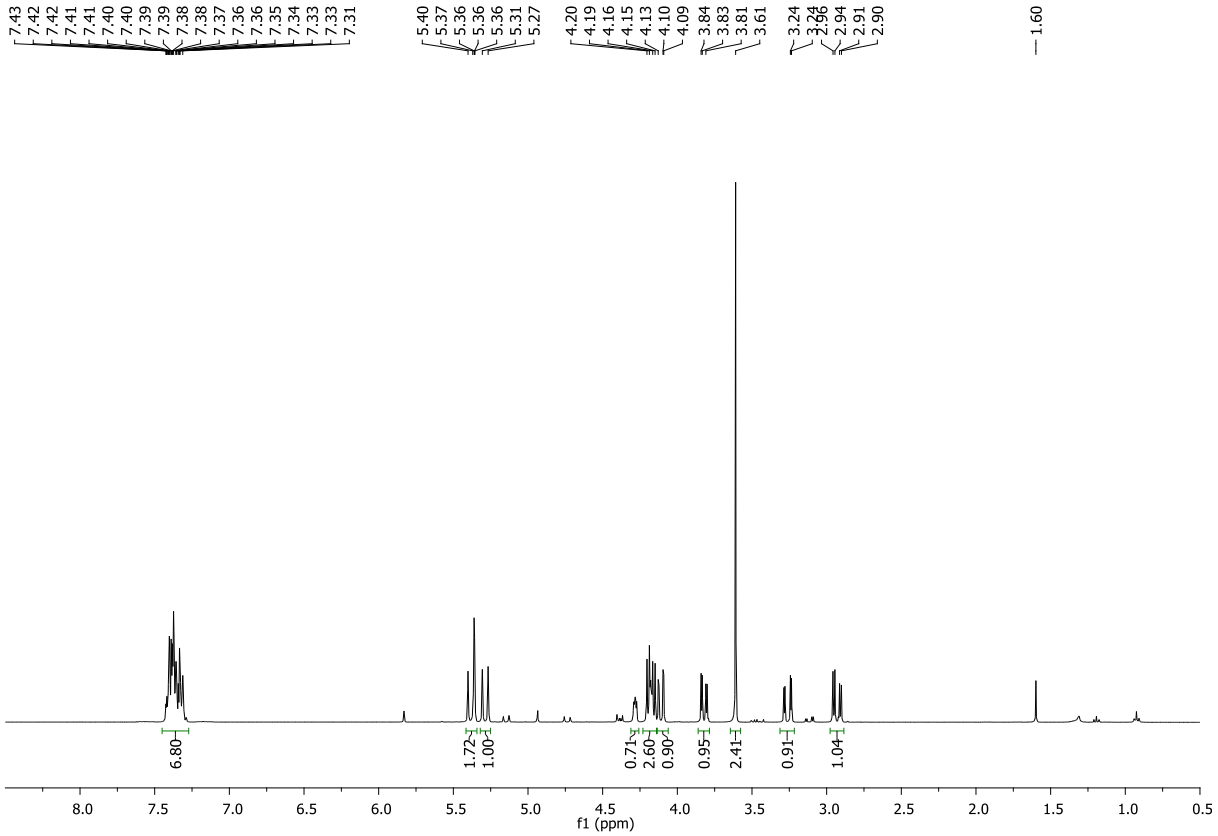

^{13}C NMR (101 MHz, CD_2Cl_2)

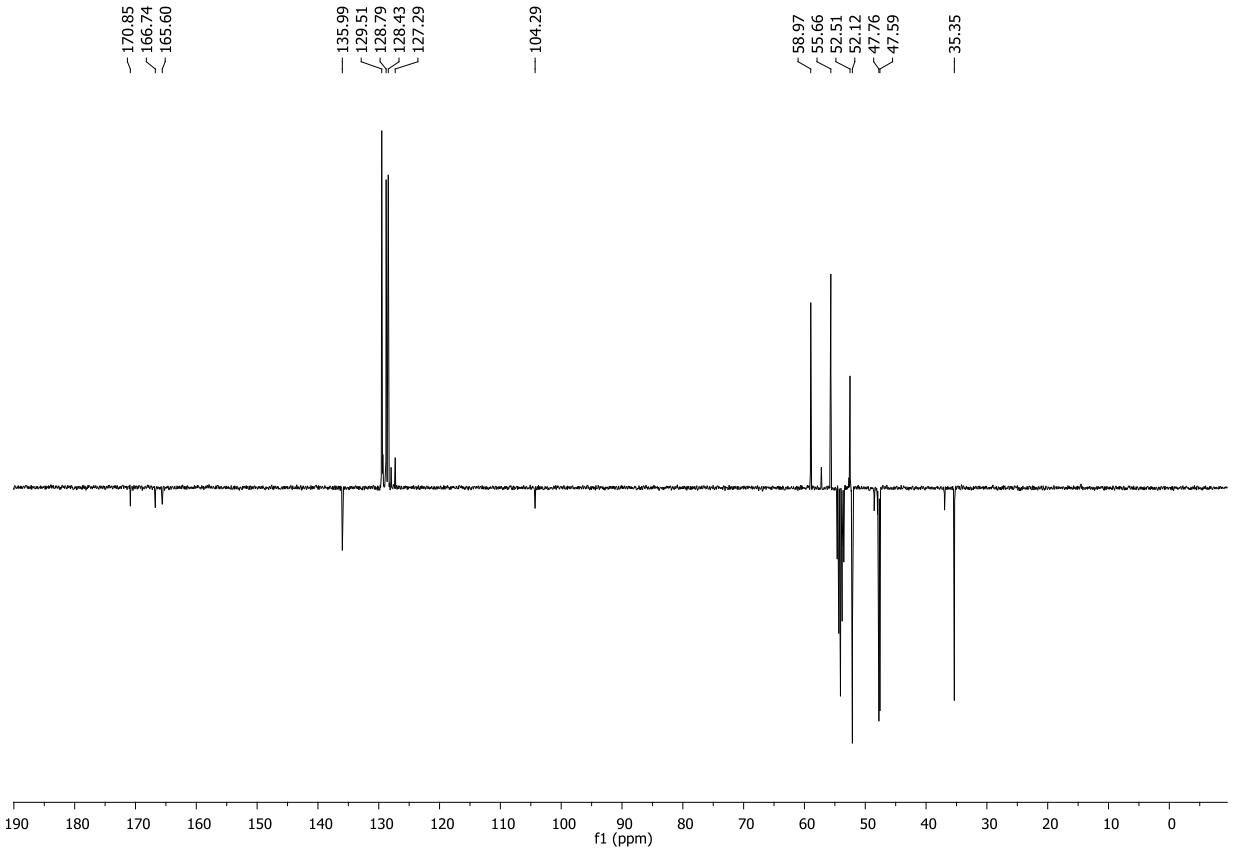

47b:

^{1}H NMR (400 MHz, CD_2Cl_2)

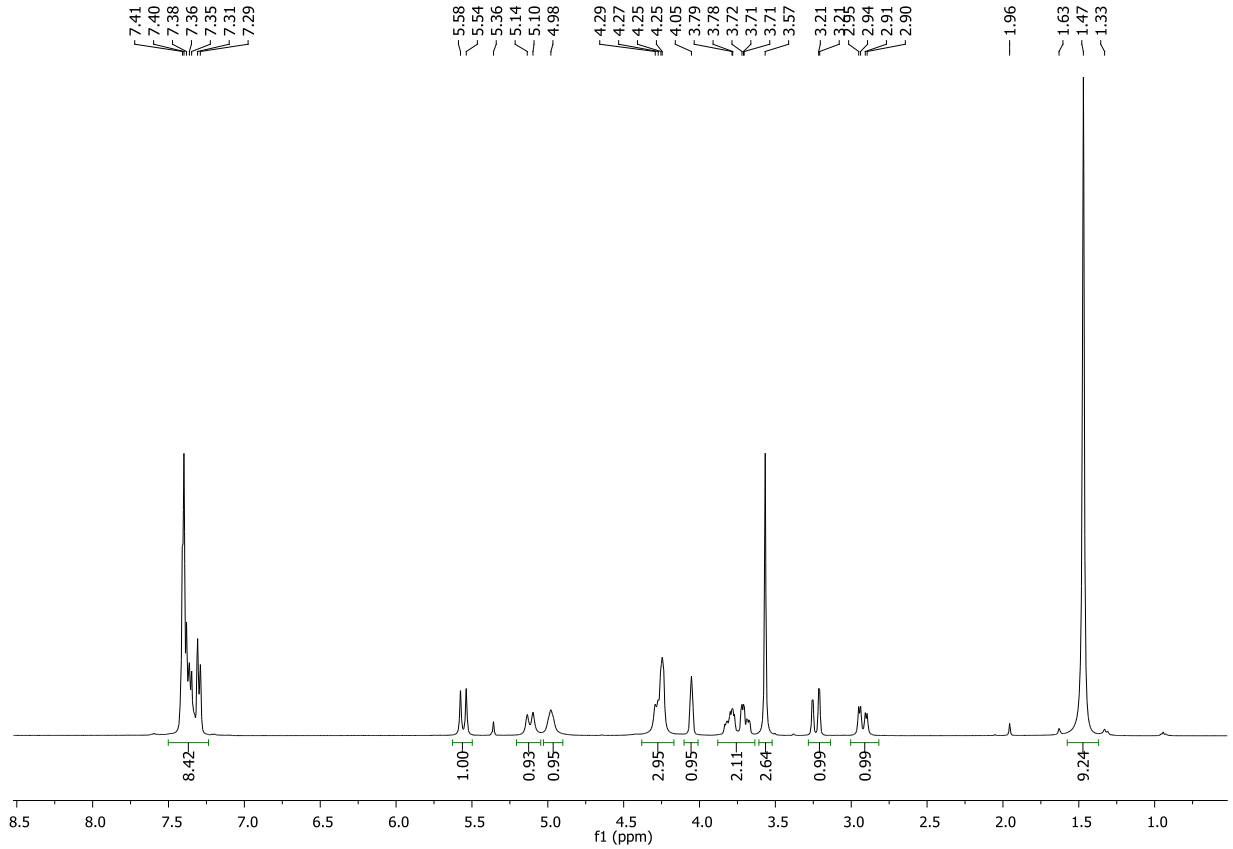

^{13}C NMR (101 MHz, CD_2Cl_2)

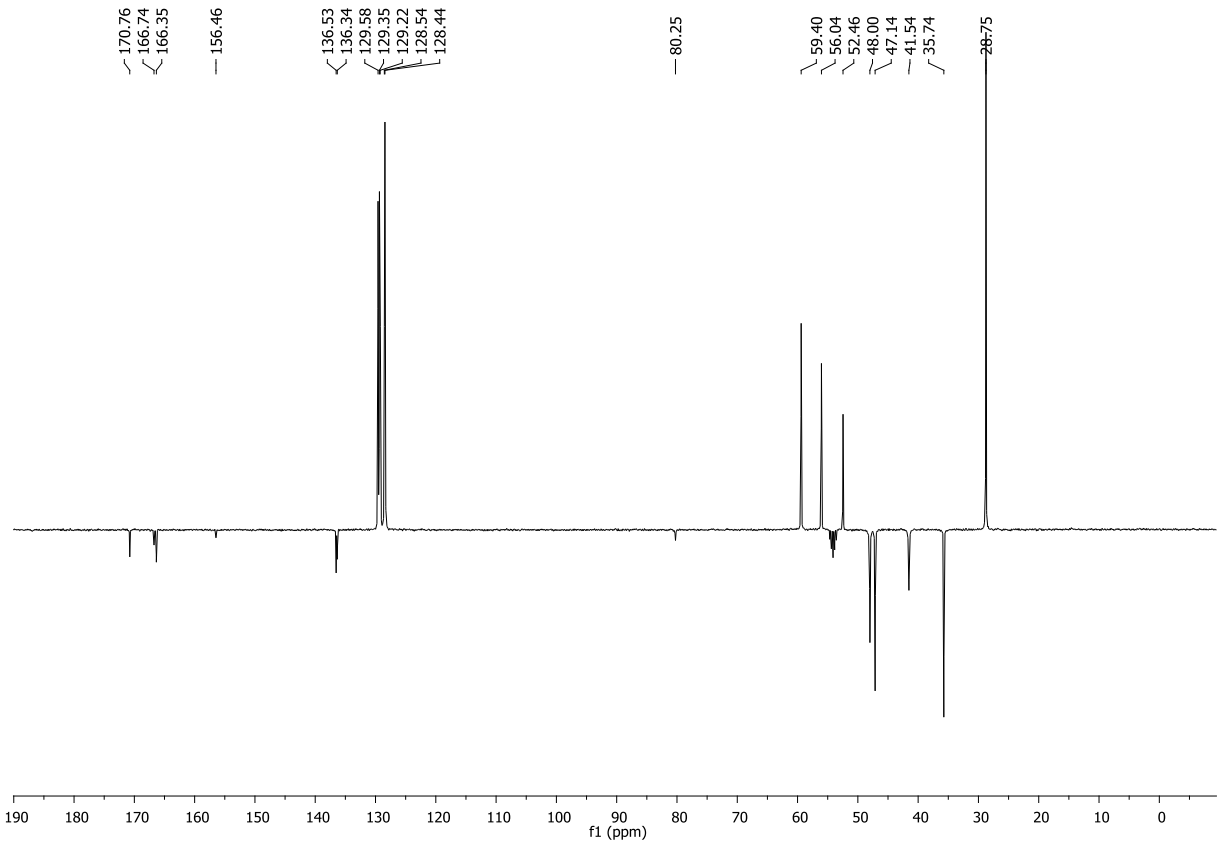

49:

^{1}H-NMR (400 MHz, $CDCl_3$)

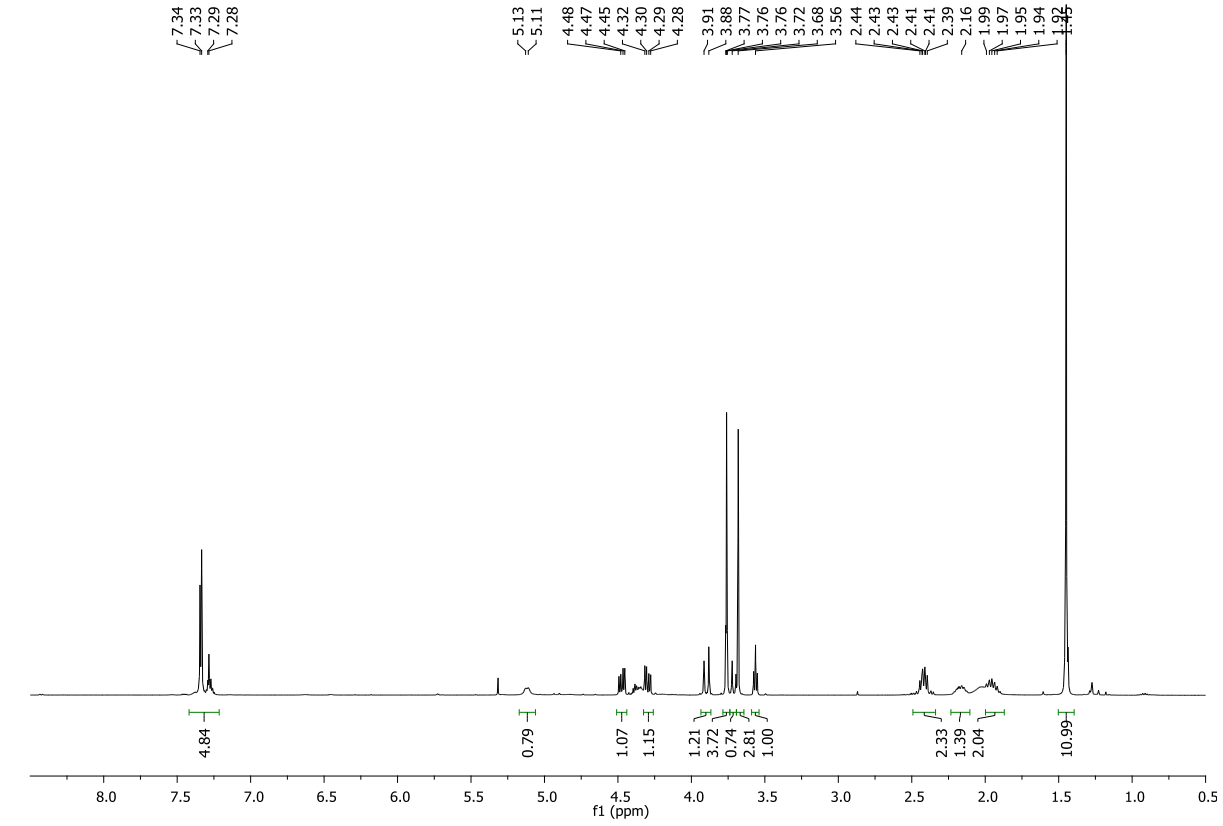

^{13}C-NMR (101 MHz, CD_2Cl_2)

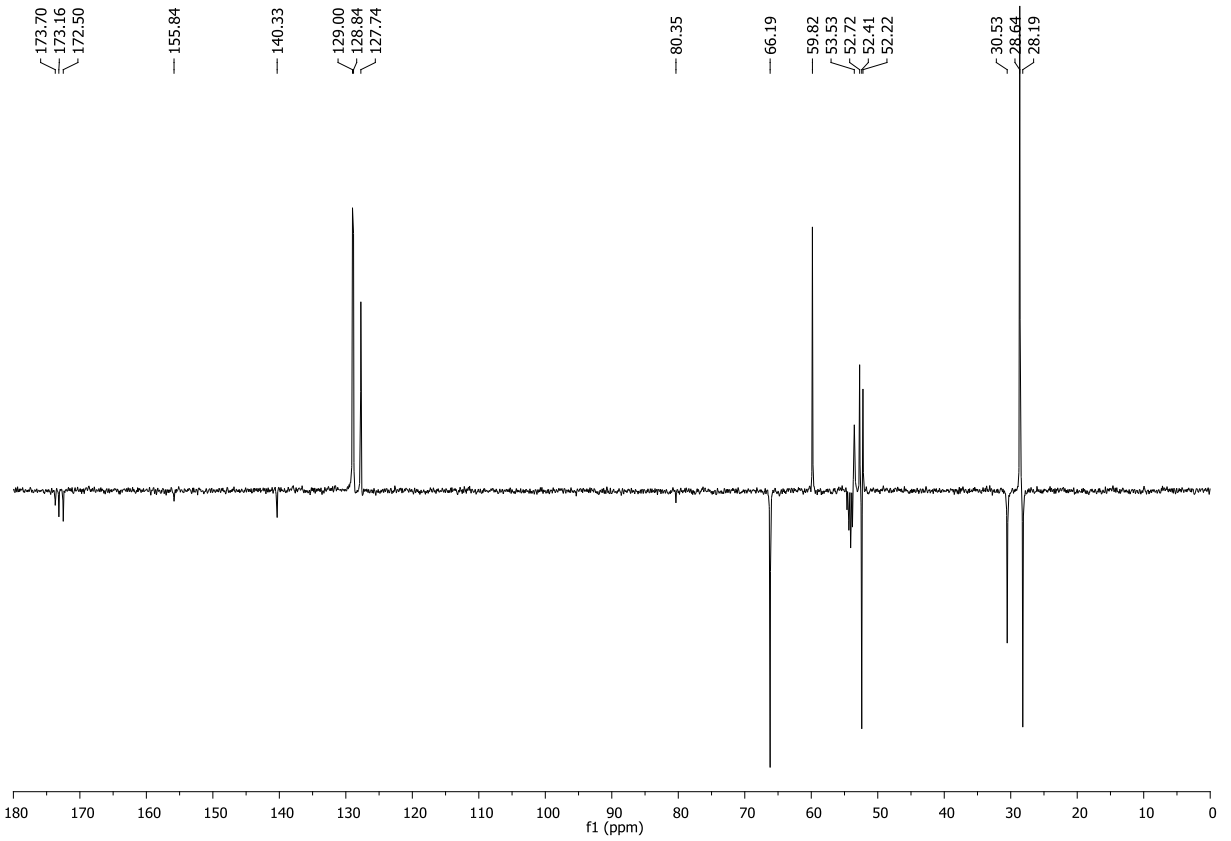

50:

^{1}H-NMR (400 MHz, CD_2Cl_2)

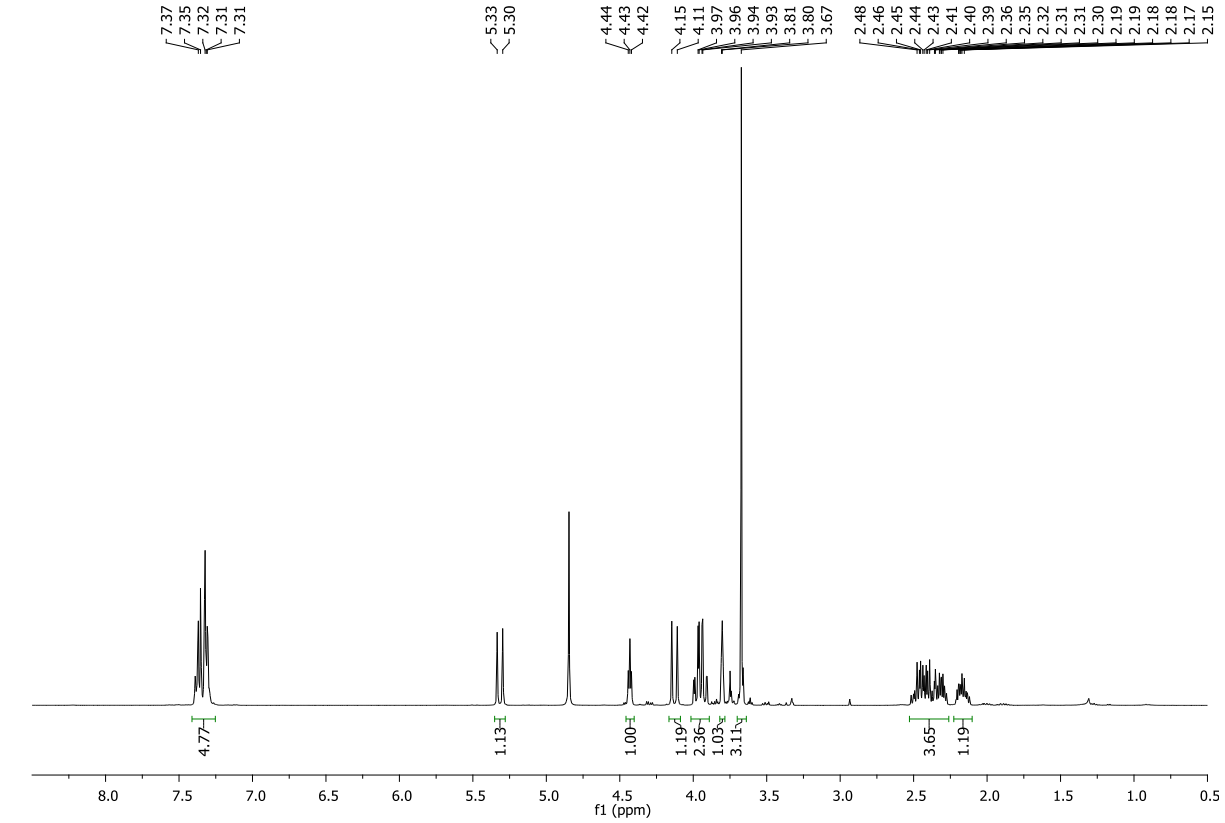

^{13}C-NMR (101 MHz, CD_3OD)

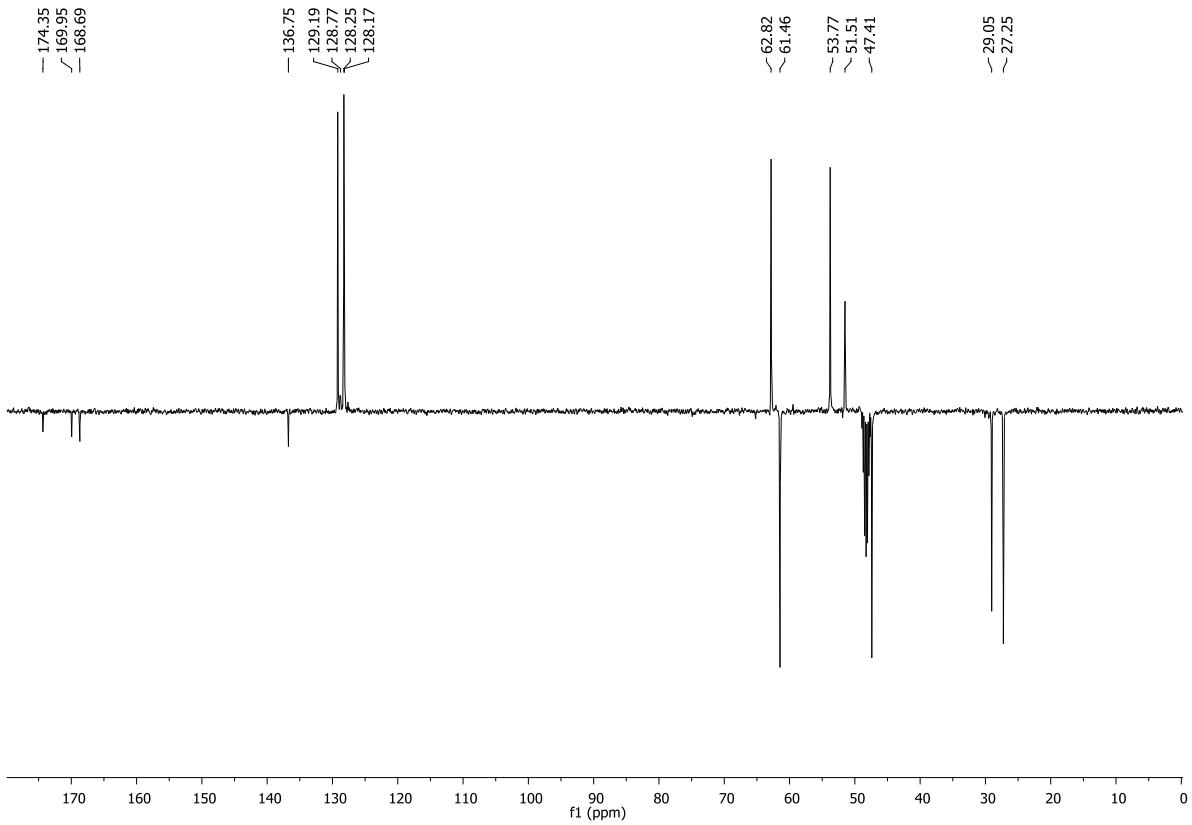

51:

^{1}H-NMR (400 MHz, $CDCl_3$)

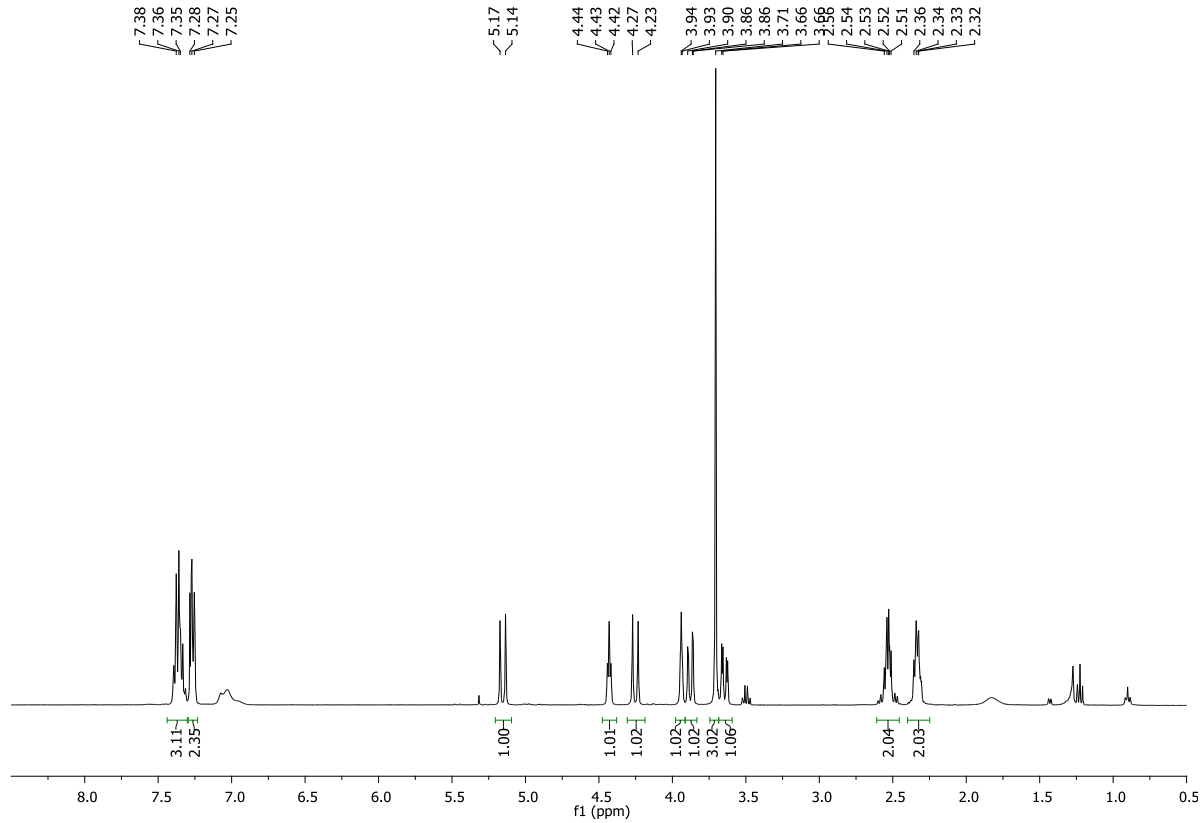

^{13}C-NMR (101 MHz, $CDCl_3$)

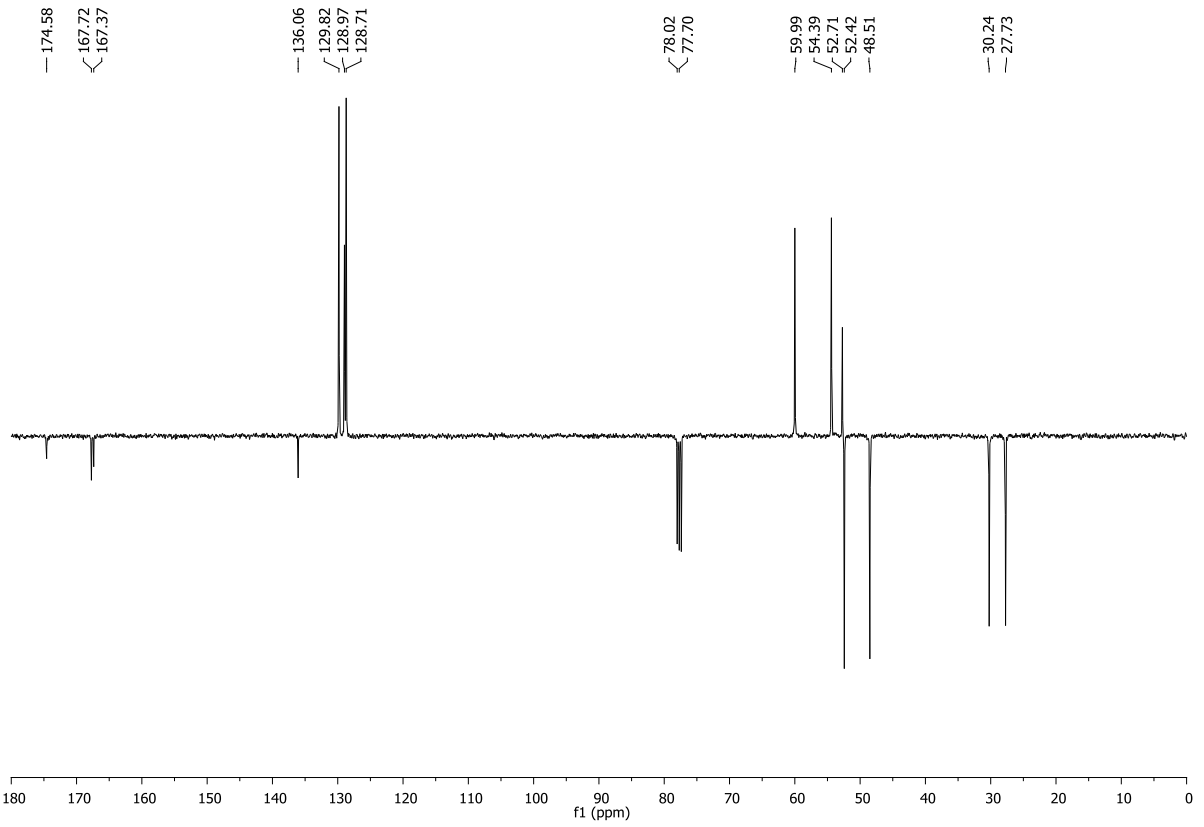

53:

^{1}H-NMR (400 MHz, $CDCl_3$)

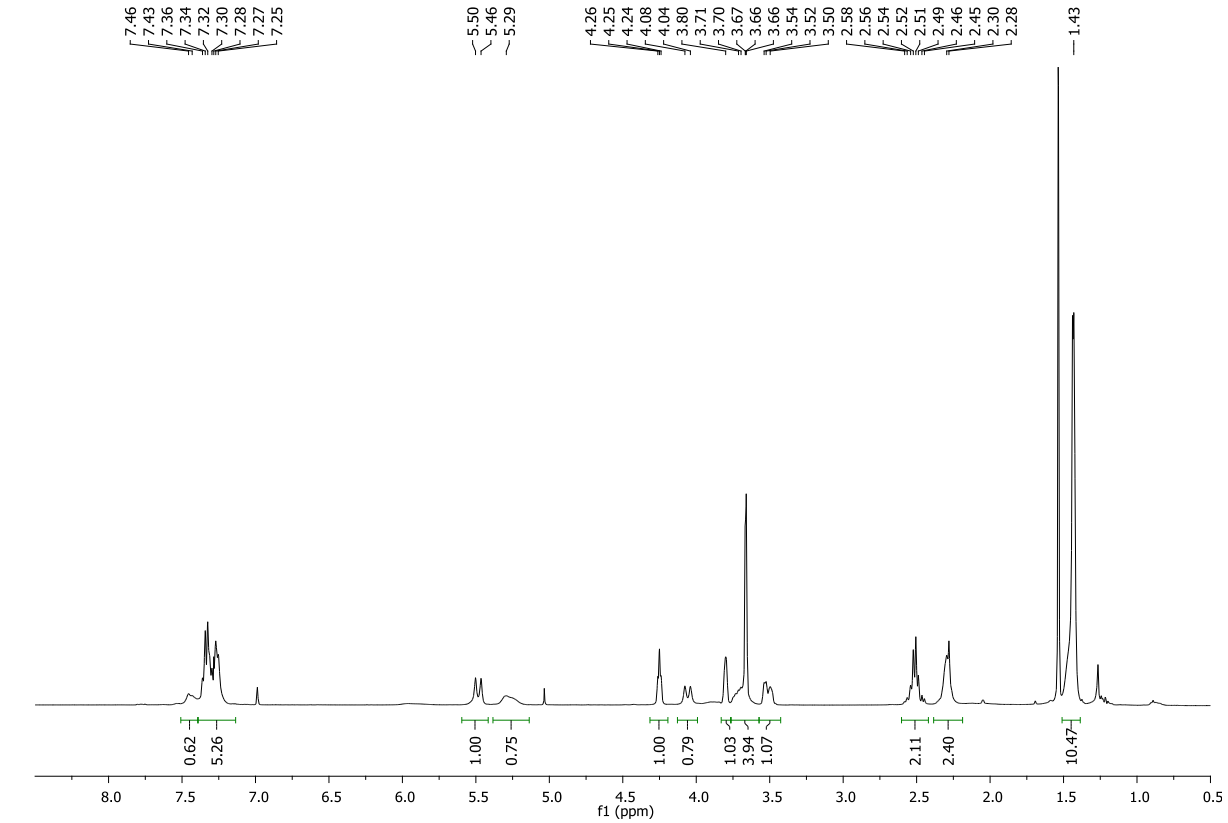

^{13}C-NMR (101 MHz, $CDCl_3$)

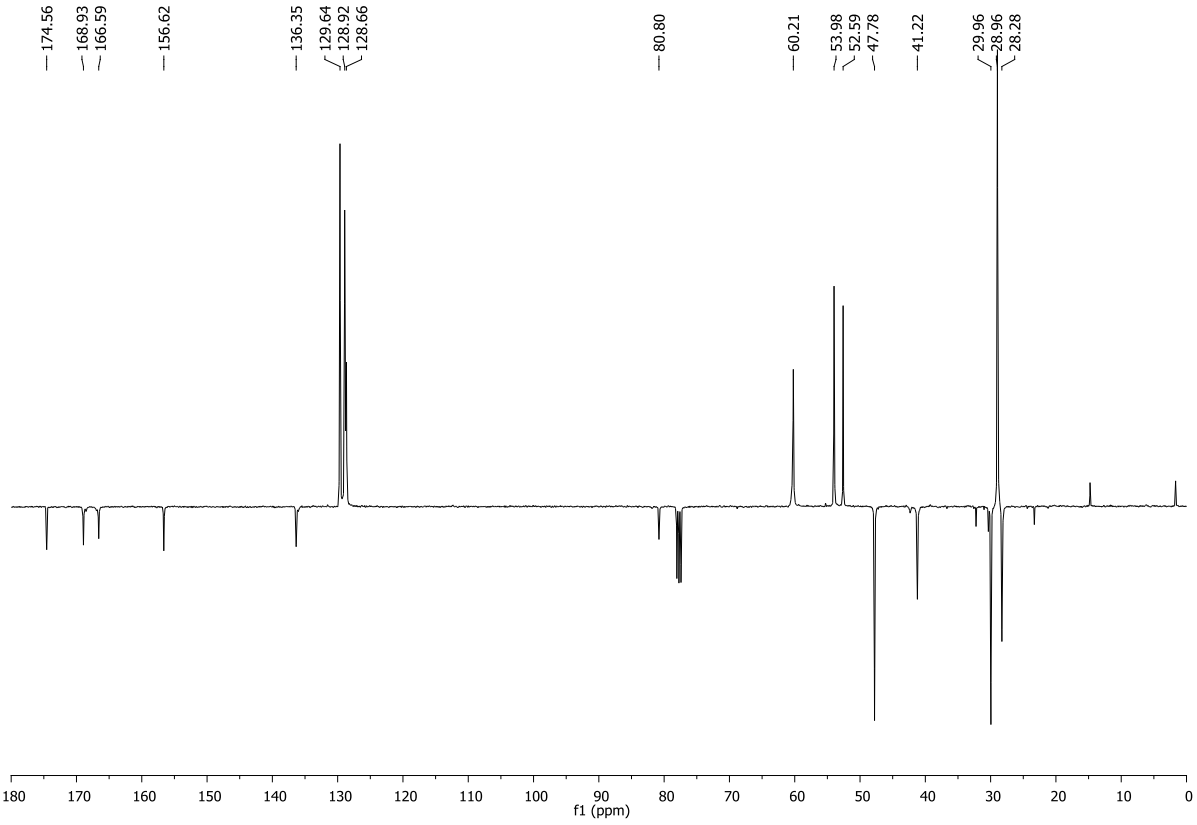

54:

^{1}H NMR (400 MHz, CD_2Cl_2)

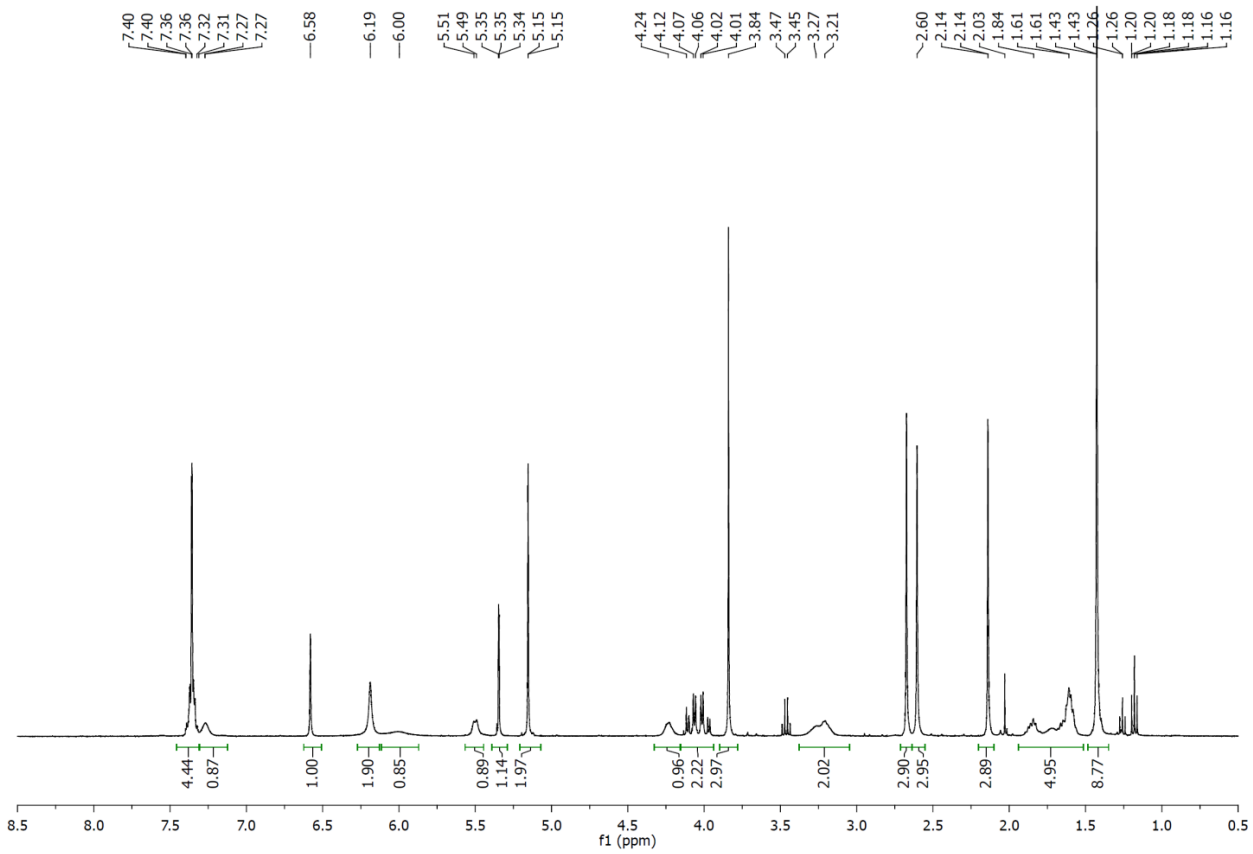

^{13}C NMR (101 MHz, CD_2Cl_2)

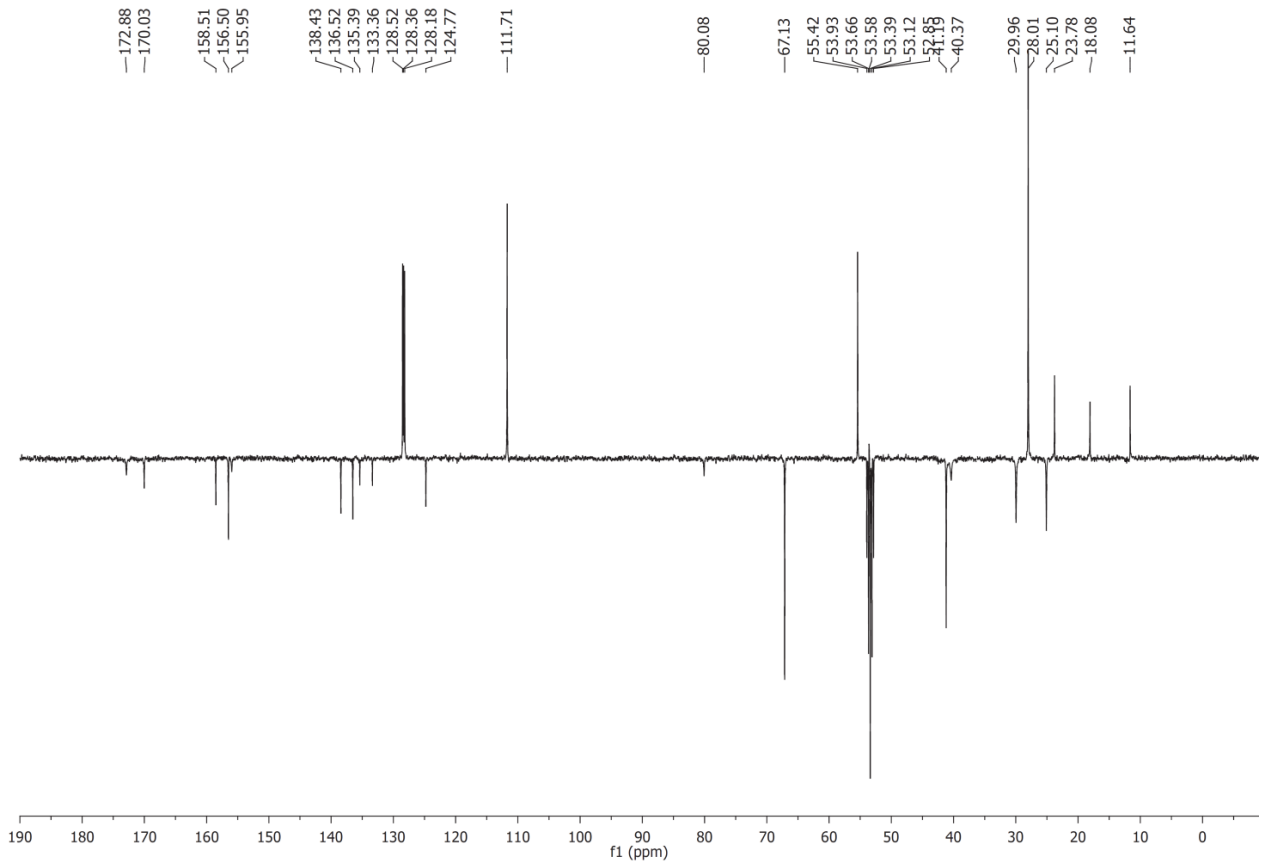

55a:

^{1}H NMR (400 MHz, Acetone-d_6)

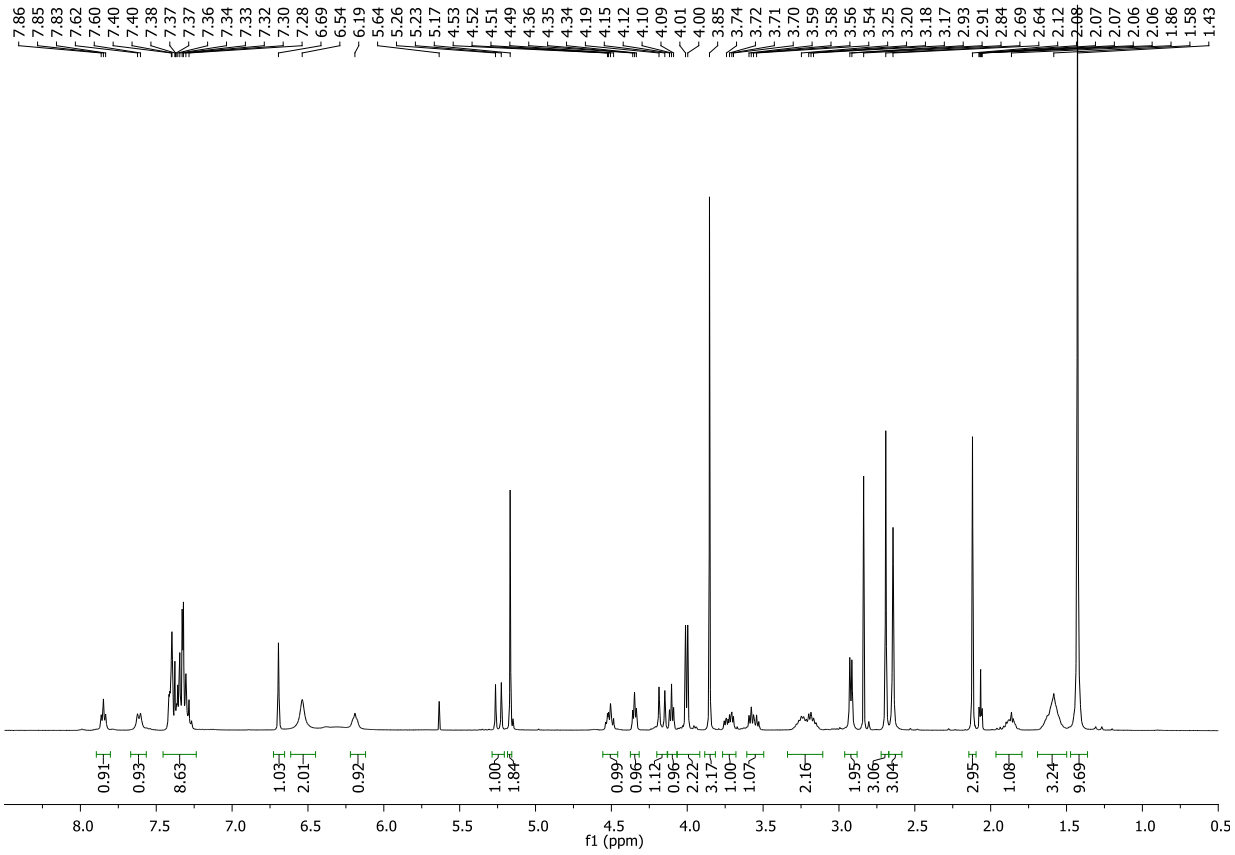

^{13}C NMR (101 MHz, Acetone-d_6)

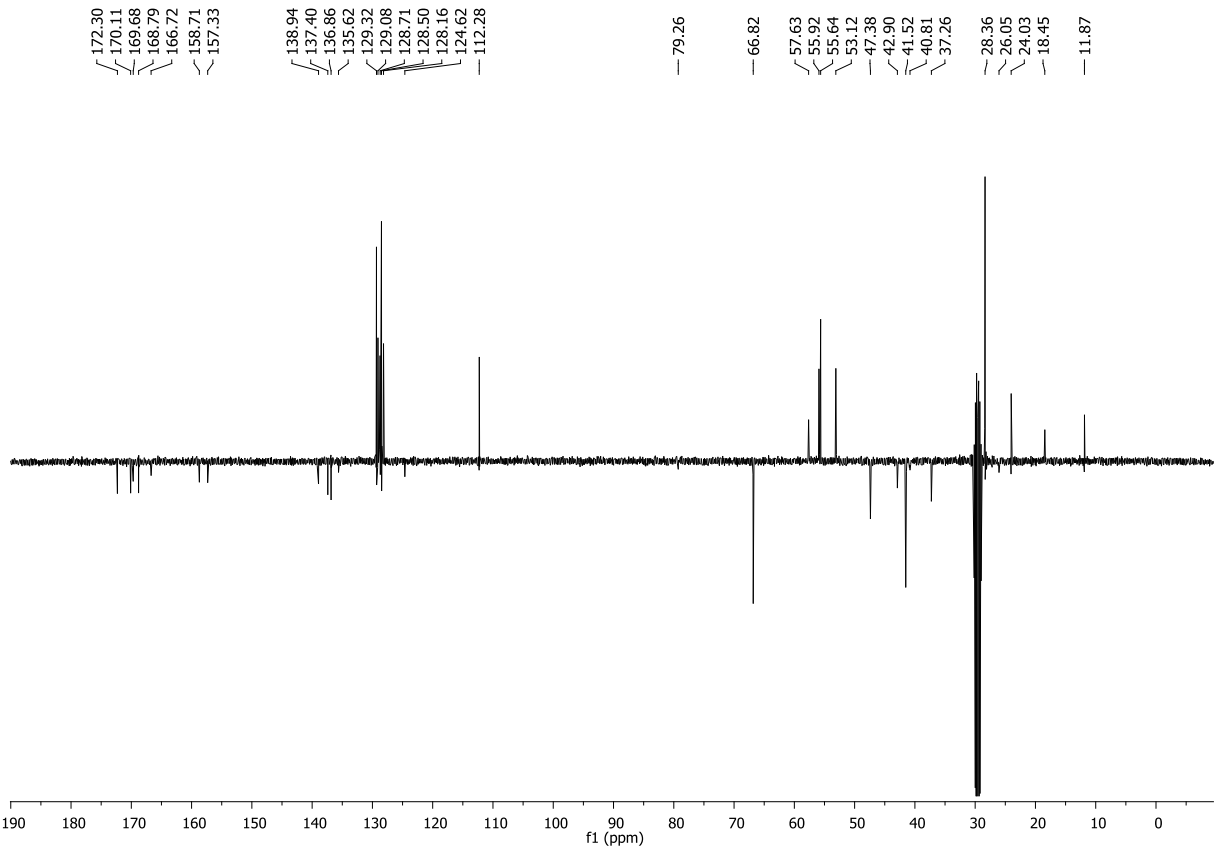

55b:

^{1}H NMR (400 MHz, CD_2Cl_2)

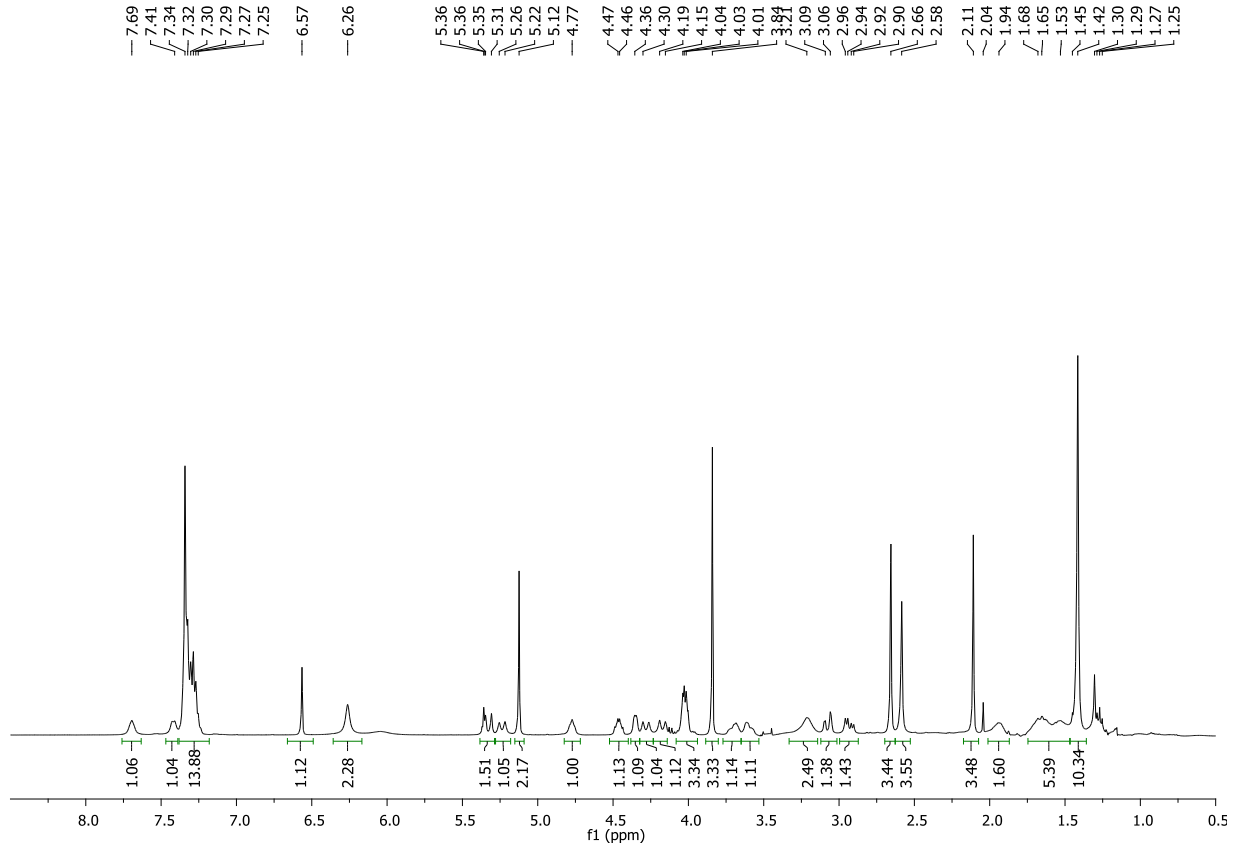

^{13}C NMR (101 MHz, CD_2Cl_2)

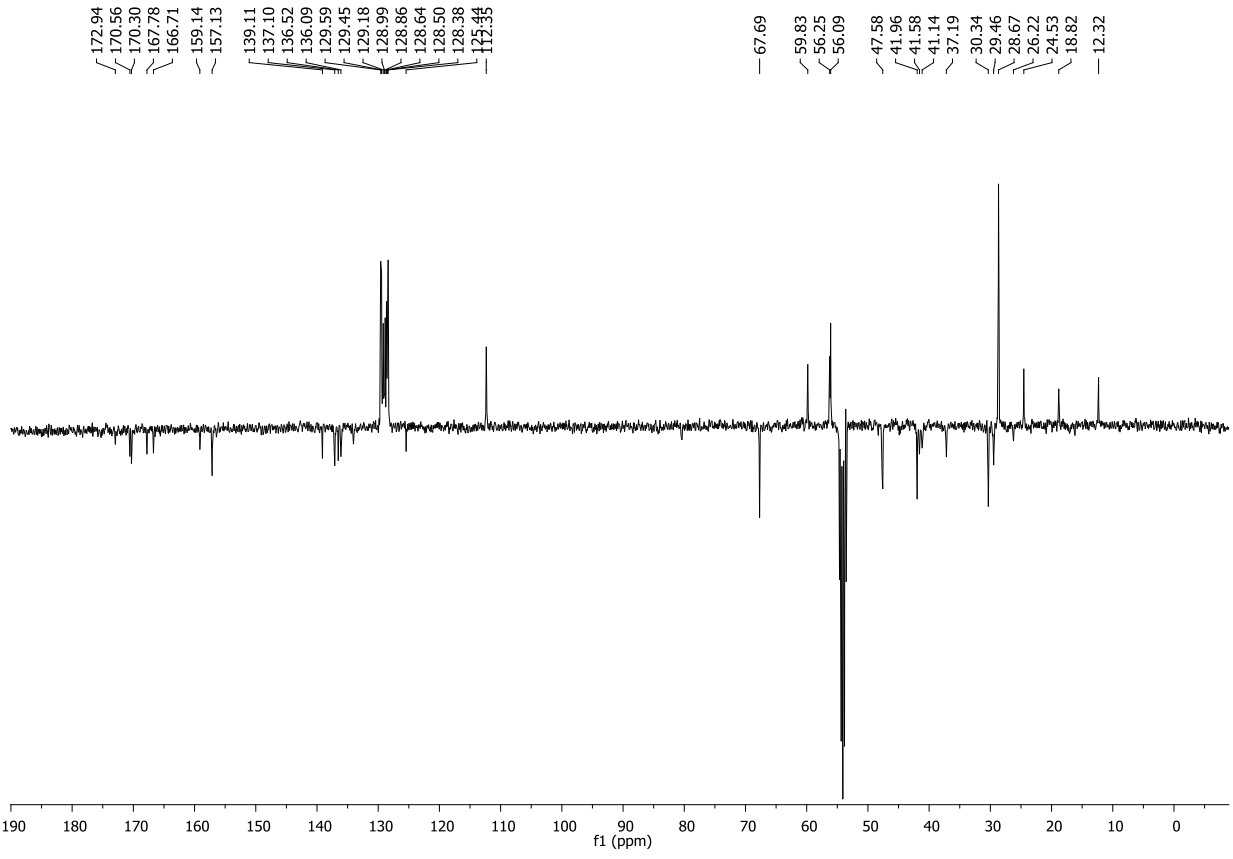

55c:

^{1}H NMR (400 MHz, Acetone-d_6)

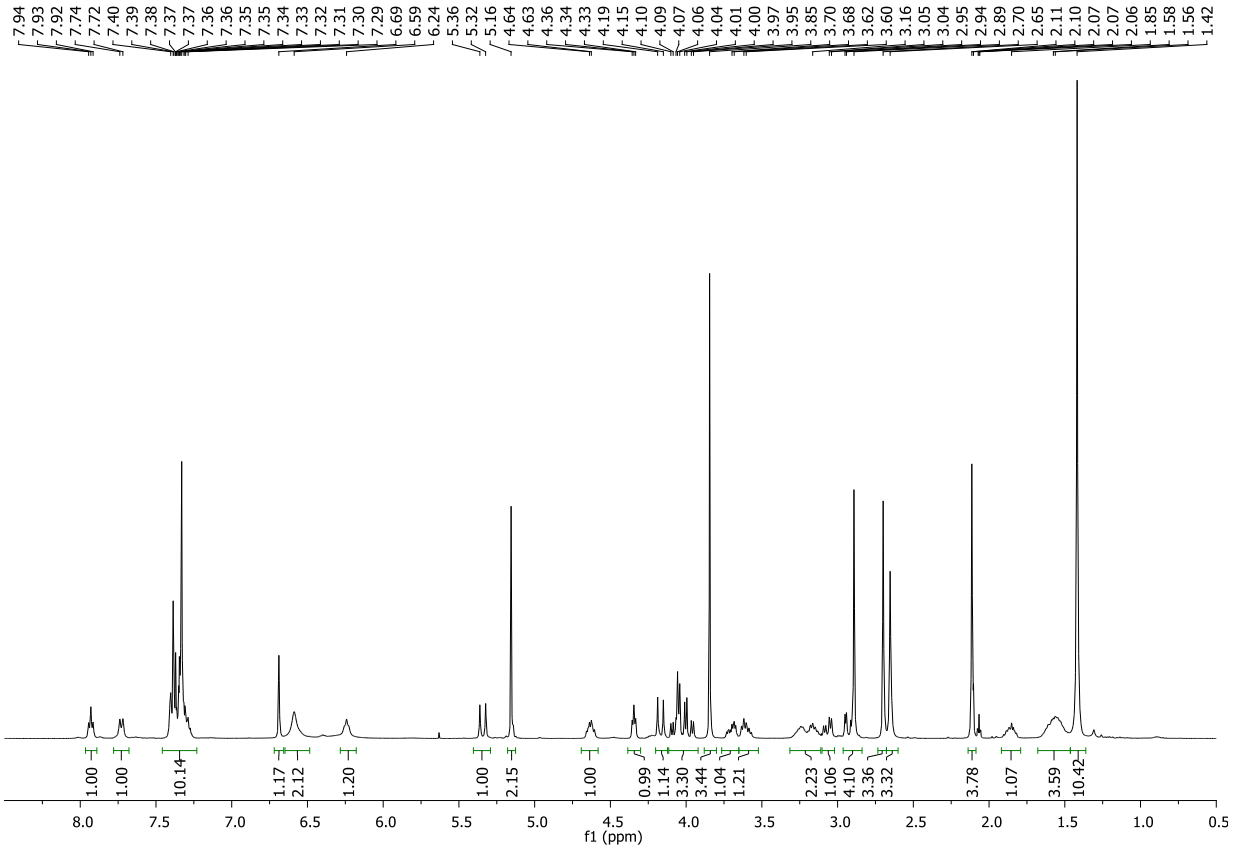

^{13}C NMR (101 MHz, Acetone-d_6)

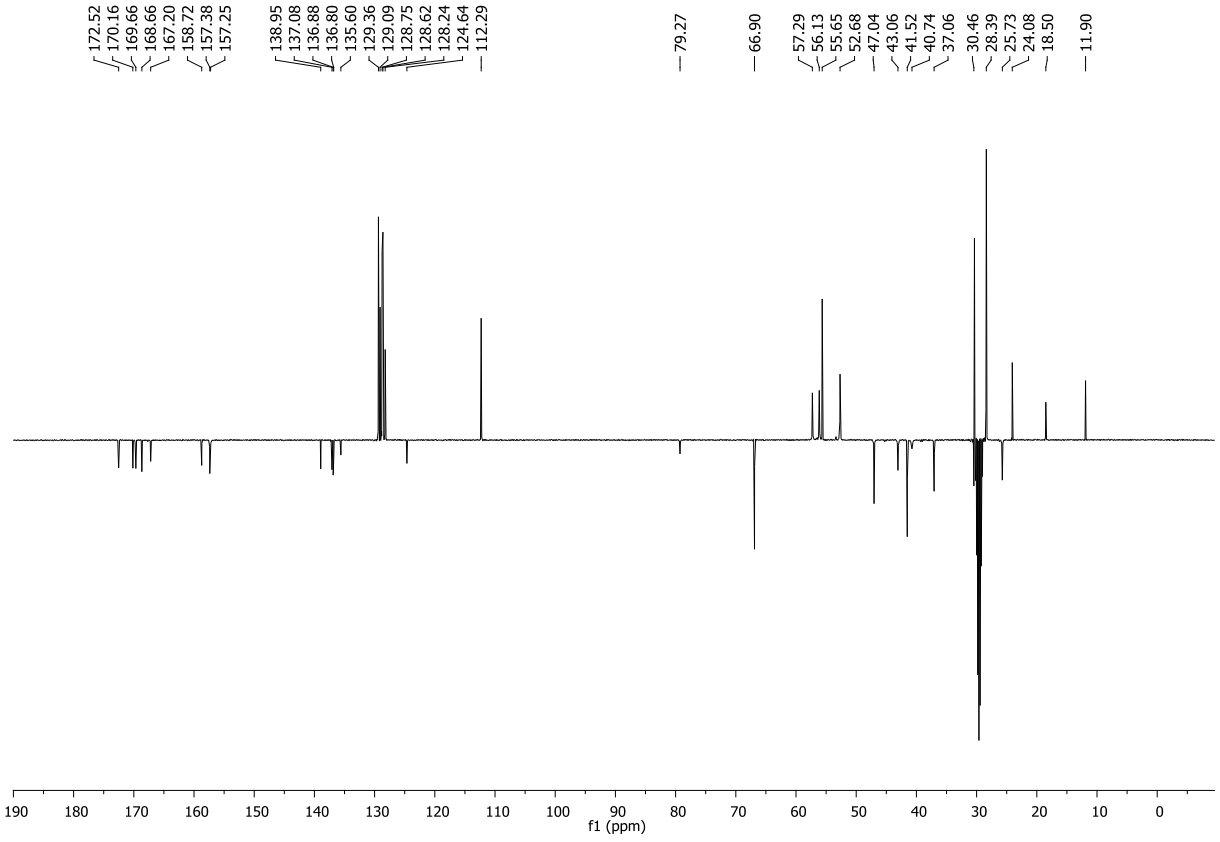

55d:

^{1}H NMR (400 MHz, Acetone-d_6)

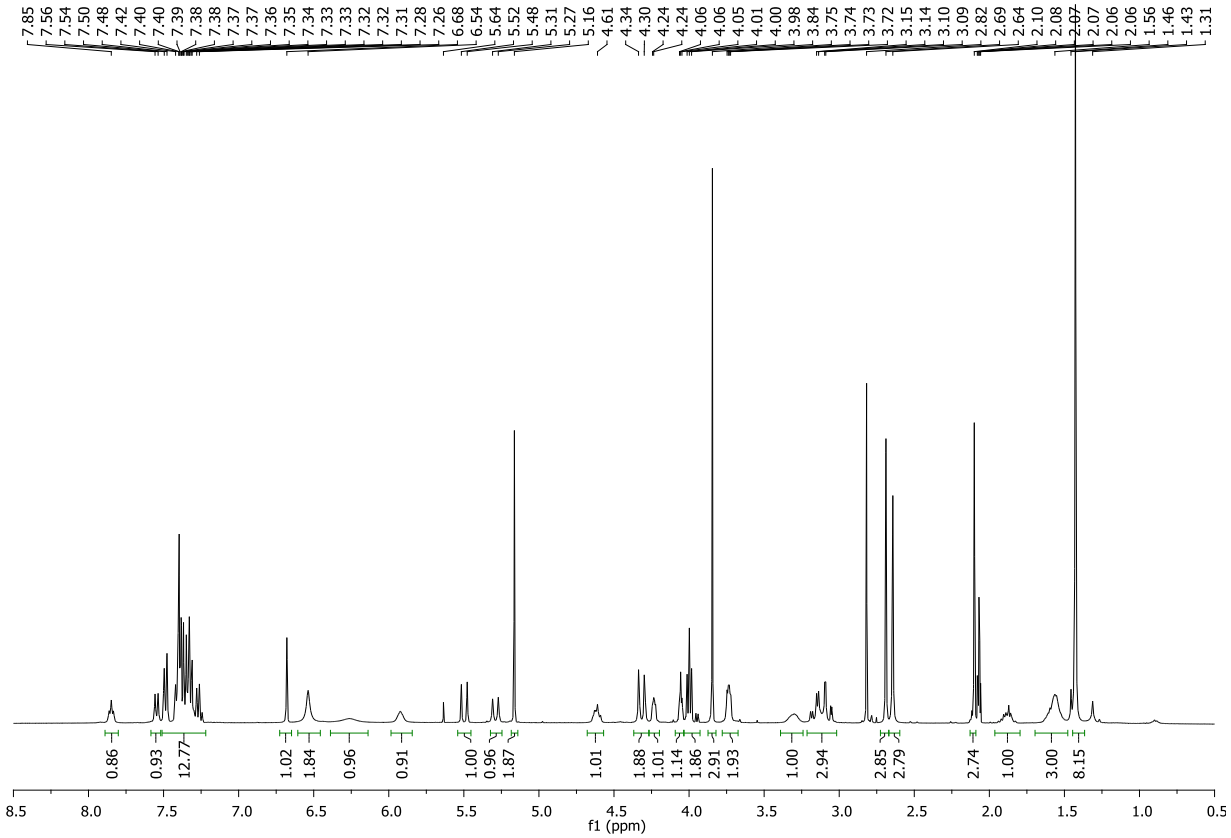

^{13}C NMR (101 MHz, Acetone-d_6)

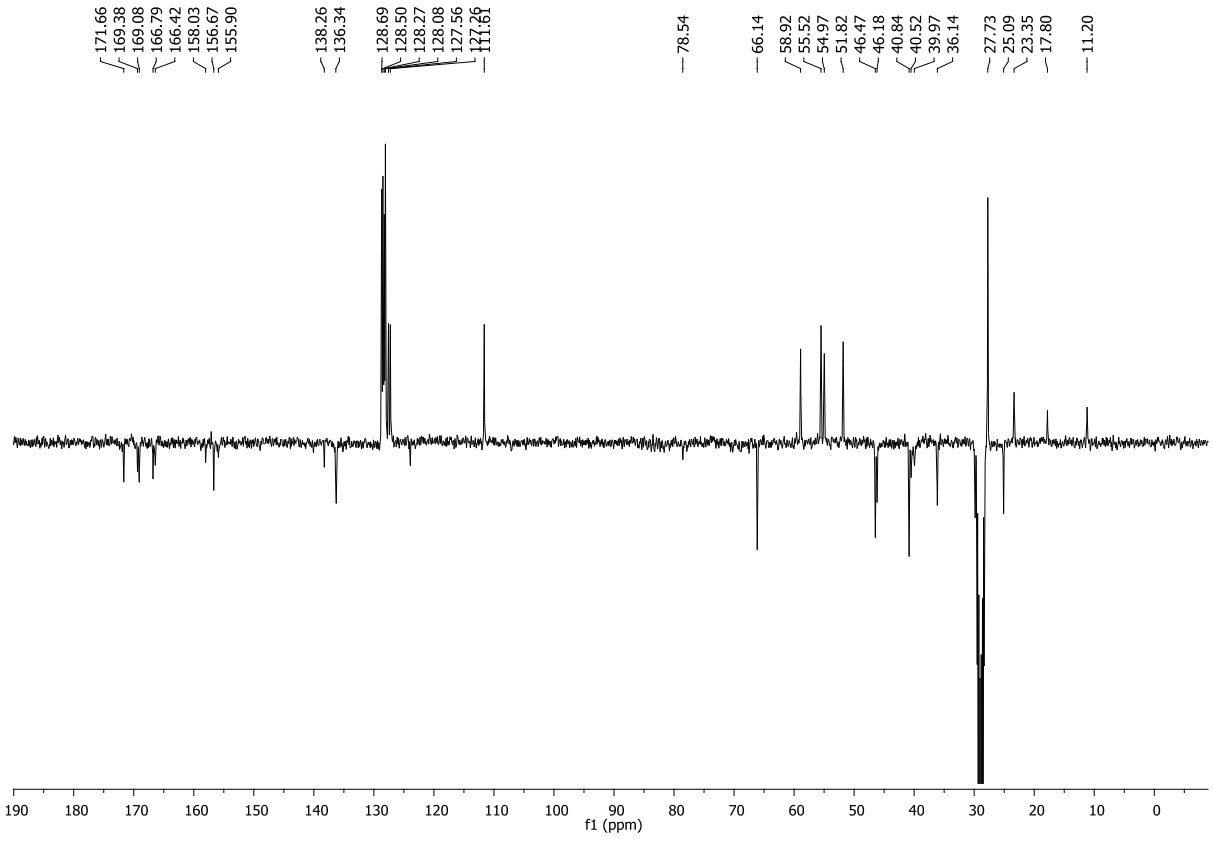

55e:

^{1}H-NMR (400 MHz, CD_3OD)

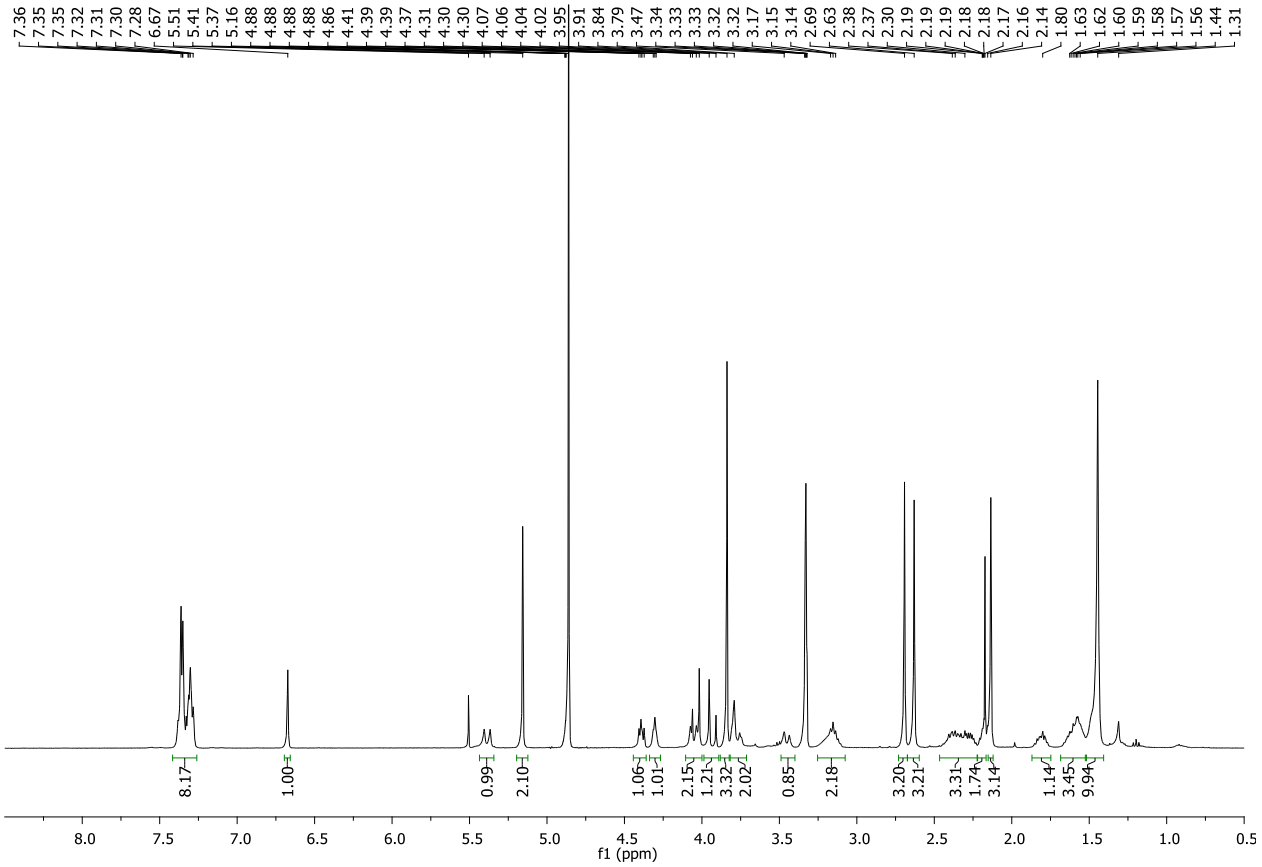

^{13}C-NMR (101 MHz, CD_2Cl_2)

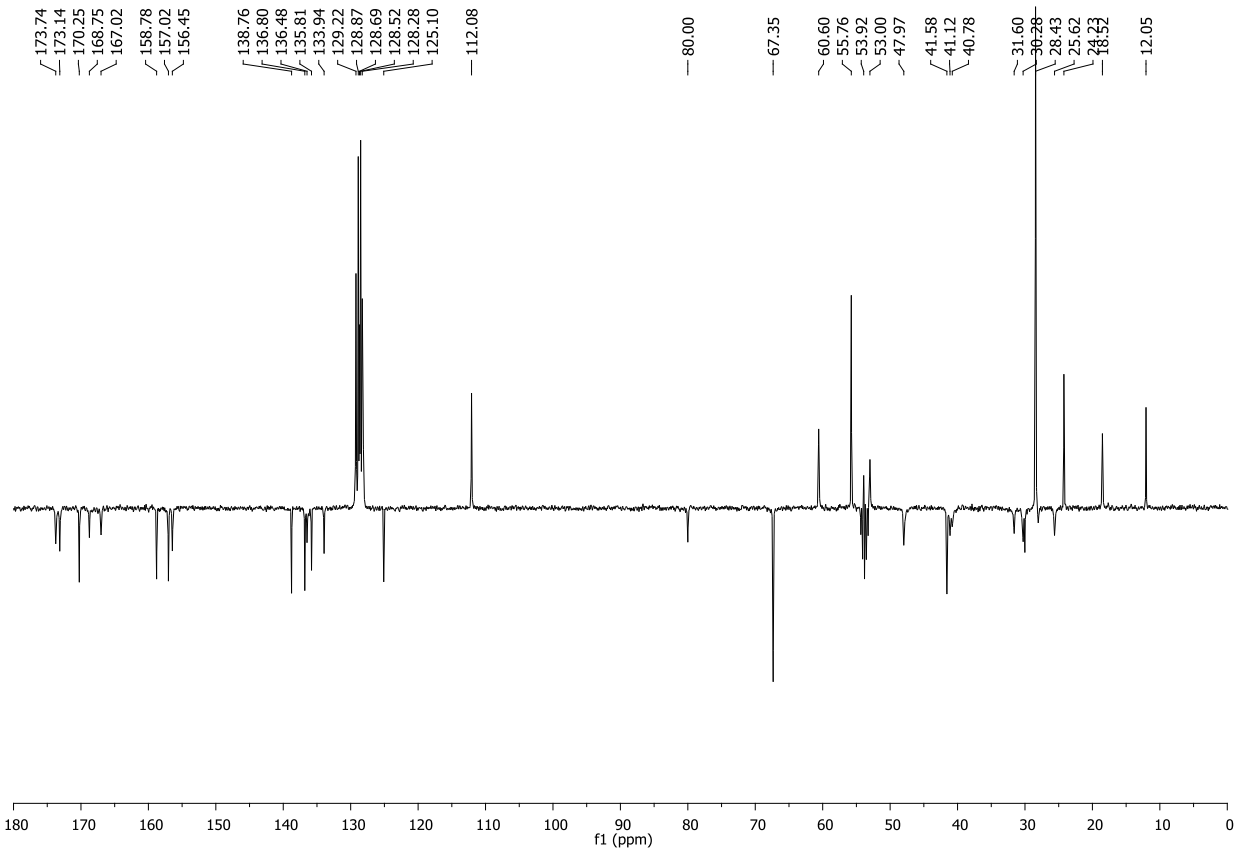

56a:

^{1}H NMR (400 MHz, Acetone-d_6)

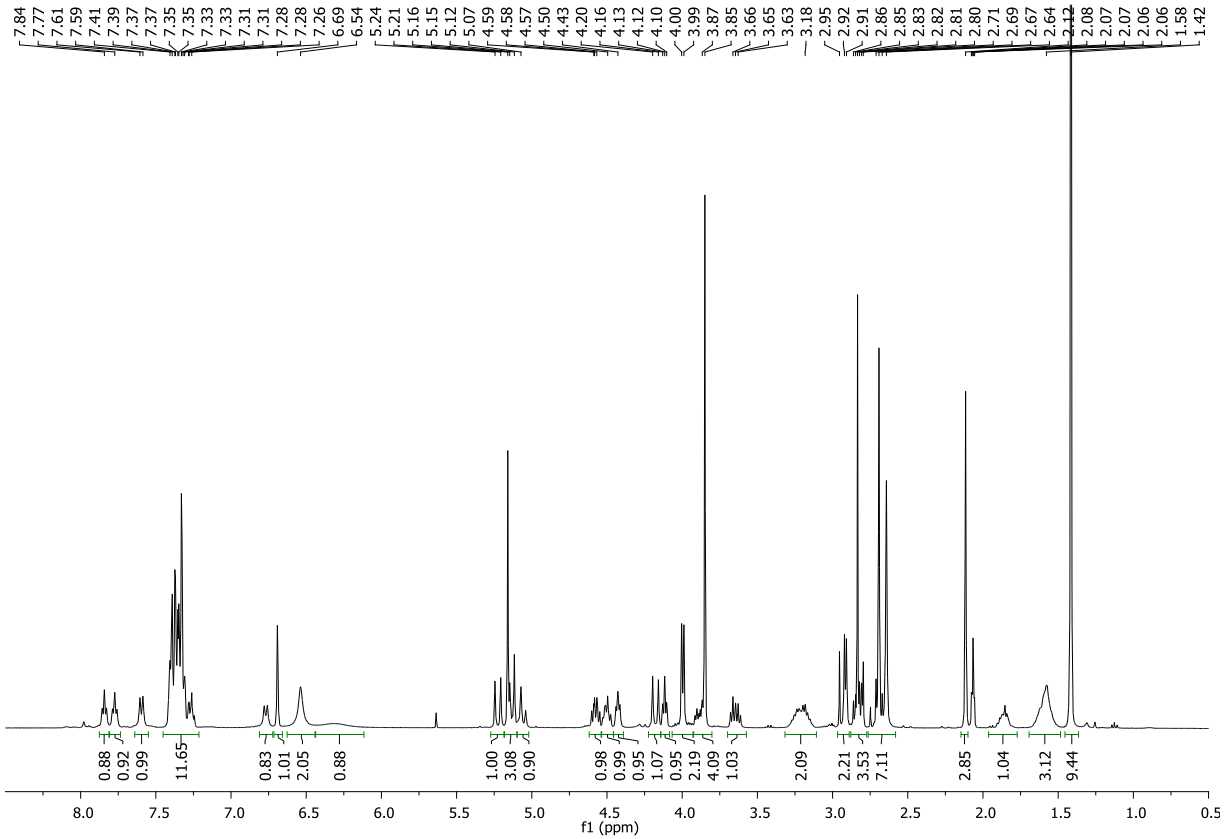

^{13}C NMR (101 MHz, Acetone-d_6)

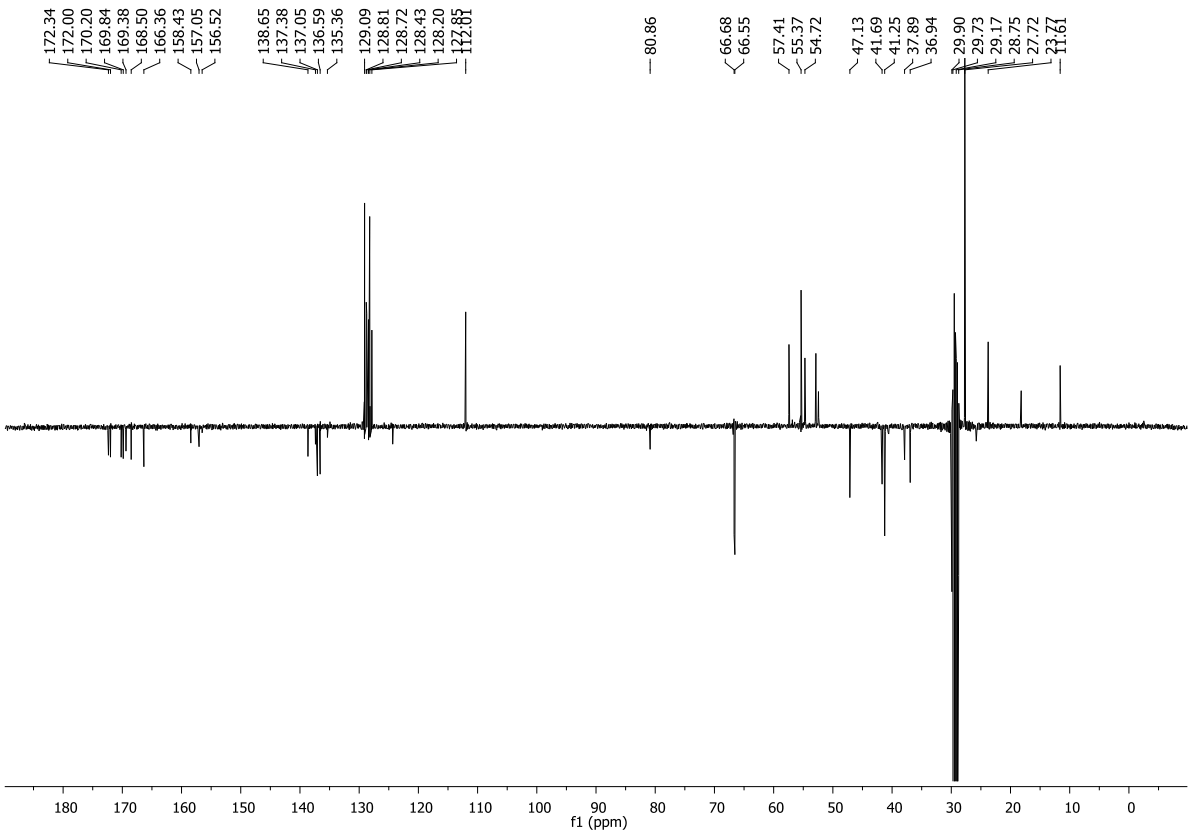

56b:

^{1}H NMR (400 MHz, Acetone-d_6)

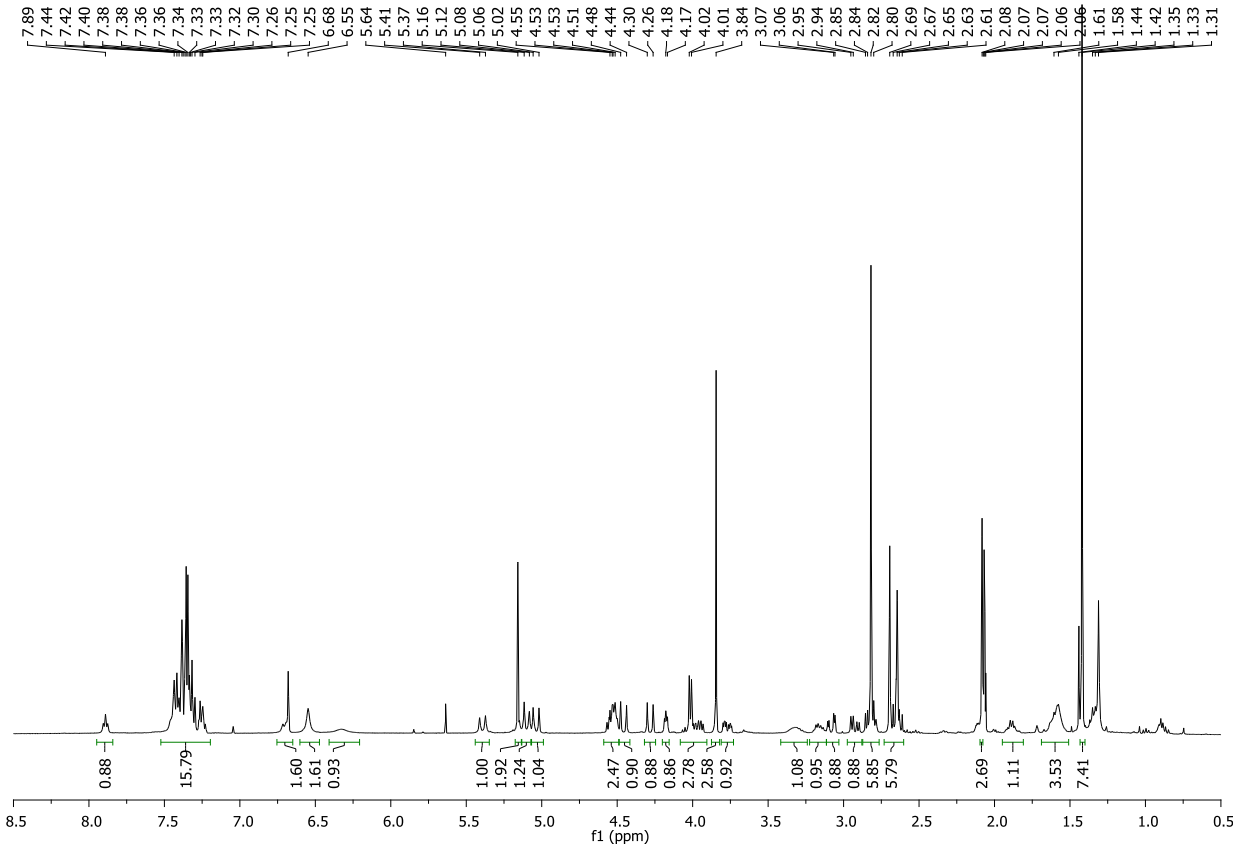

^{13}C NMR (101 MHz, Acetone-d_6)

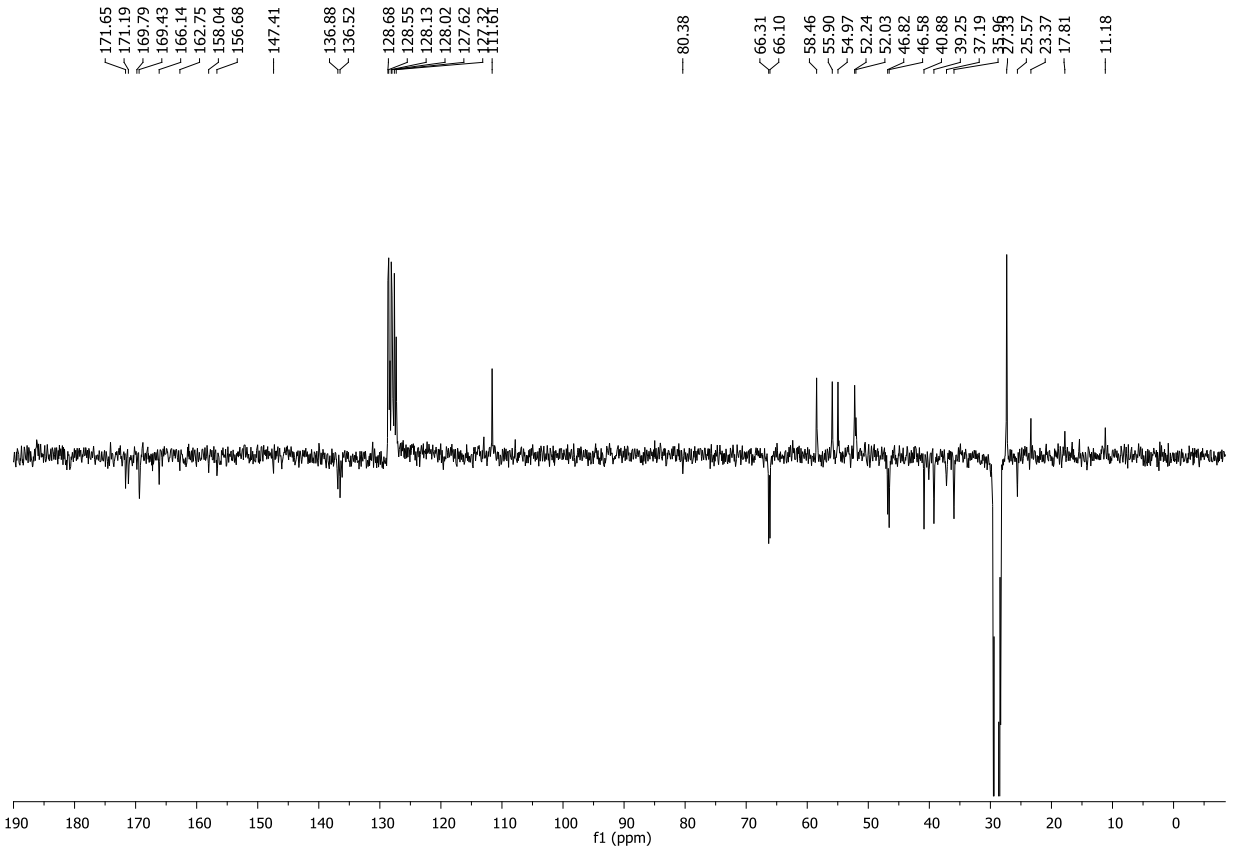

56c:

^{1}H NMR (400 MHz, Acetone-d_6)

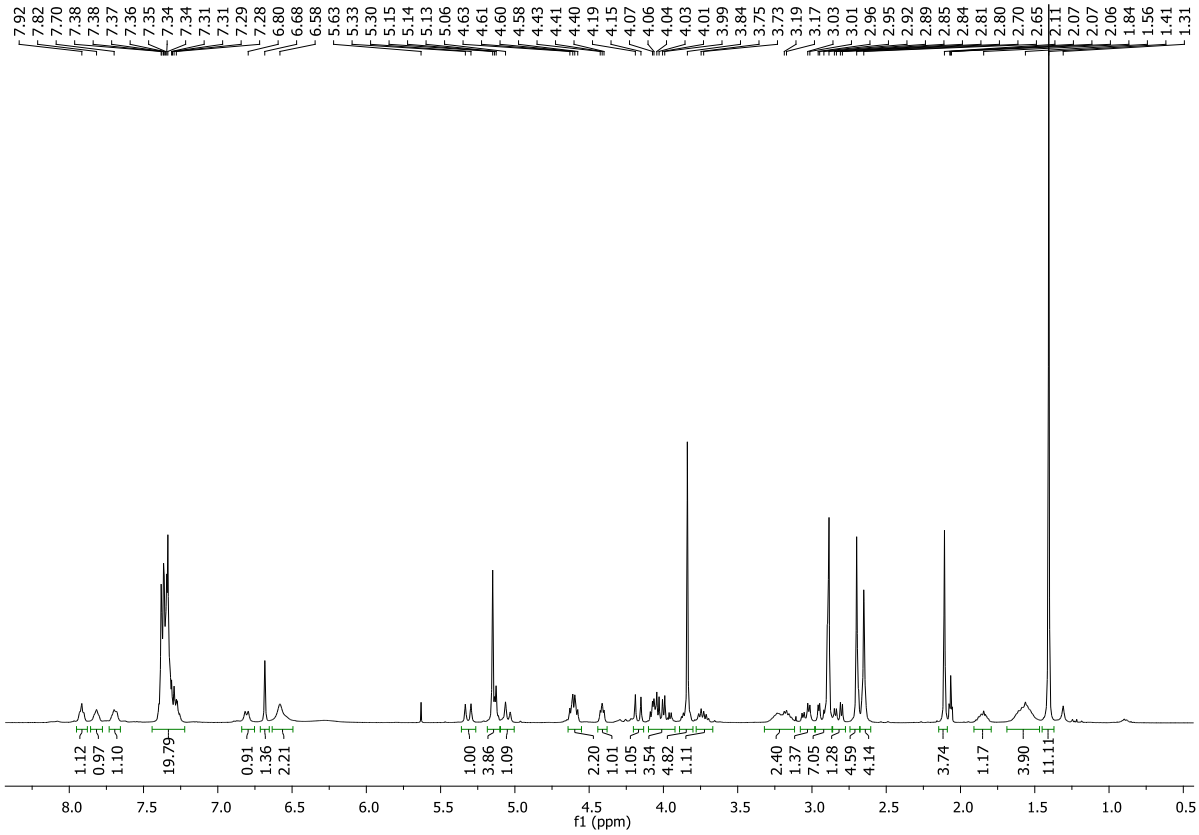

^{13}C NMR (101 MHz, Acetone-d_6)

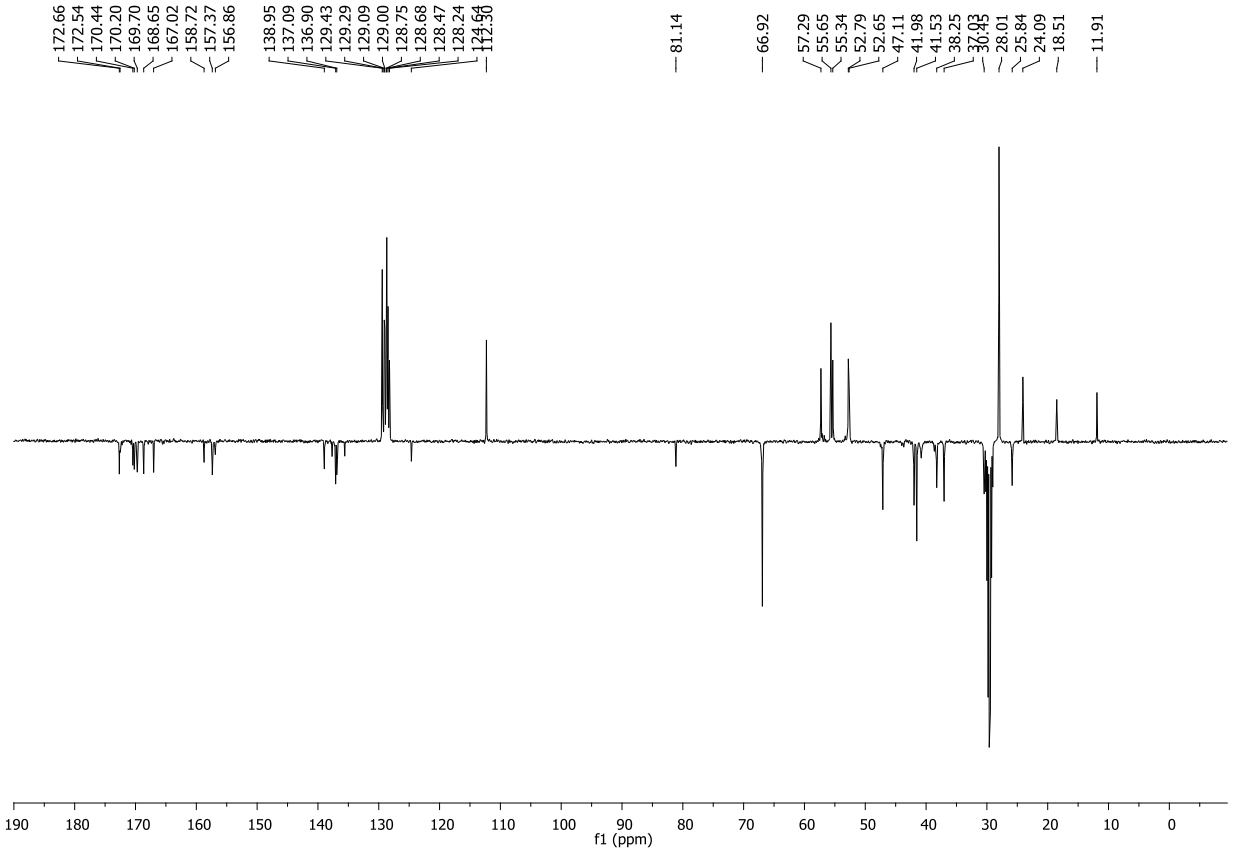

56d:

^{1}H NMR (400 MHz, Acetone-d_6)

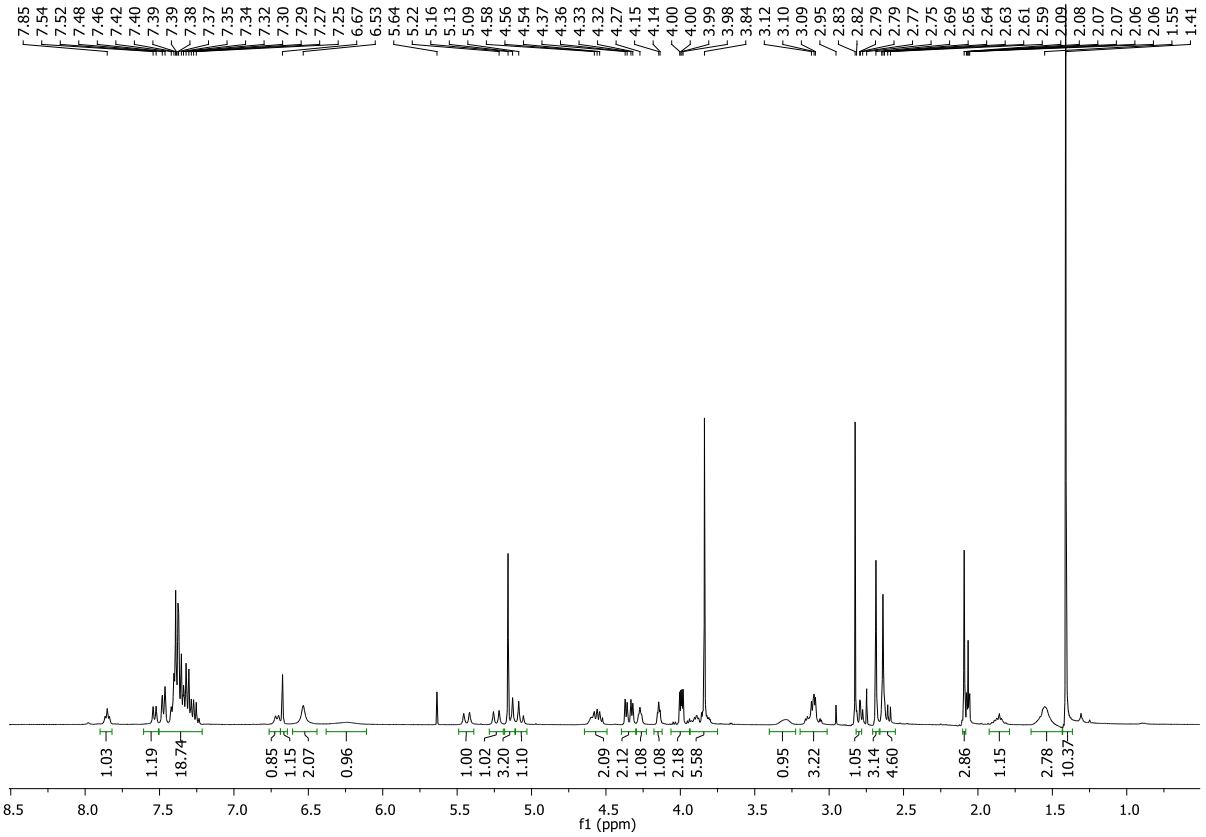

^{13}C NMR (101 MHz, Acetone-d_6)

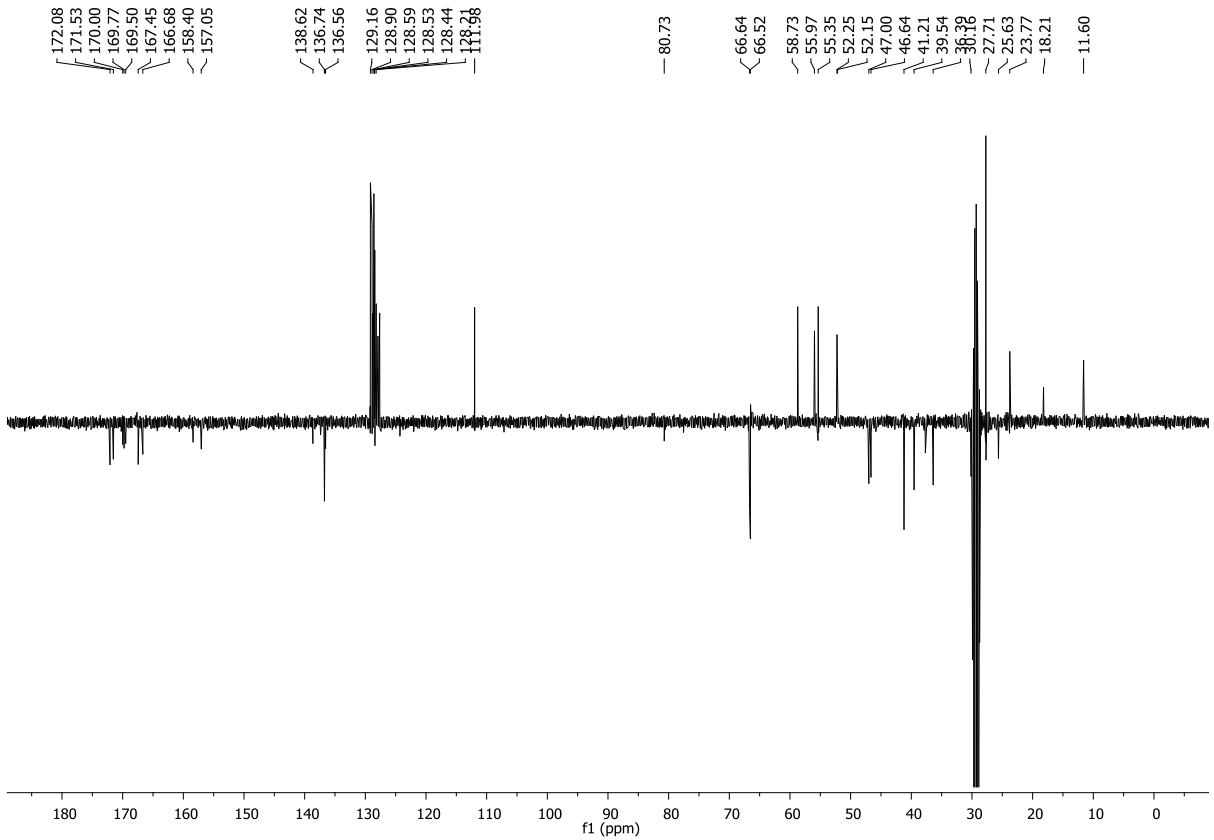

56e:

^{1}H-NMR (400 MHz, Acetone-d_6)

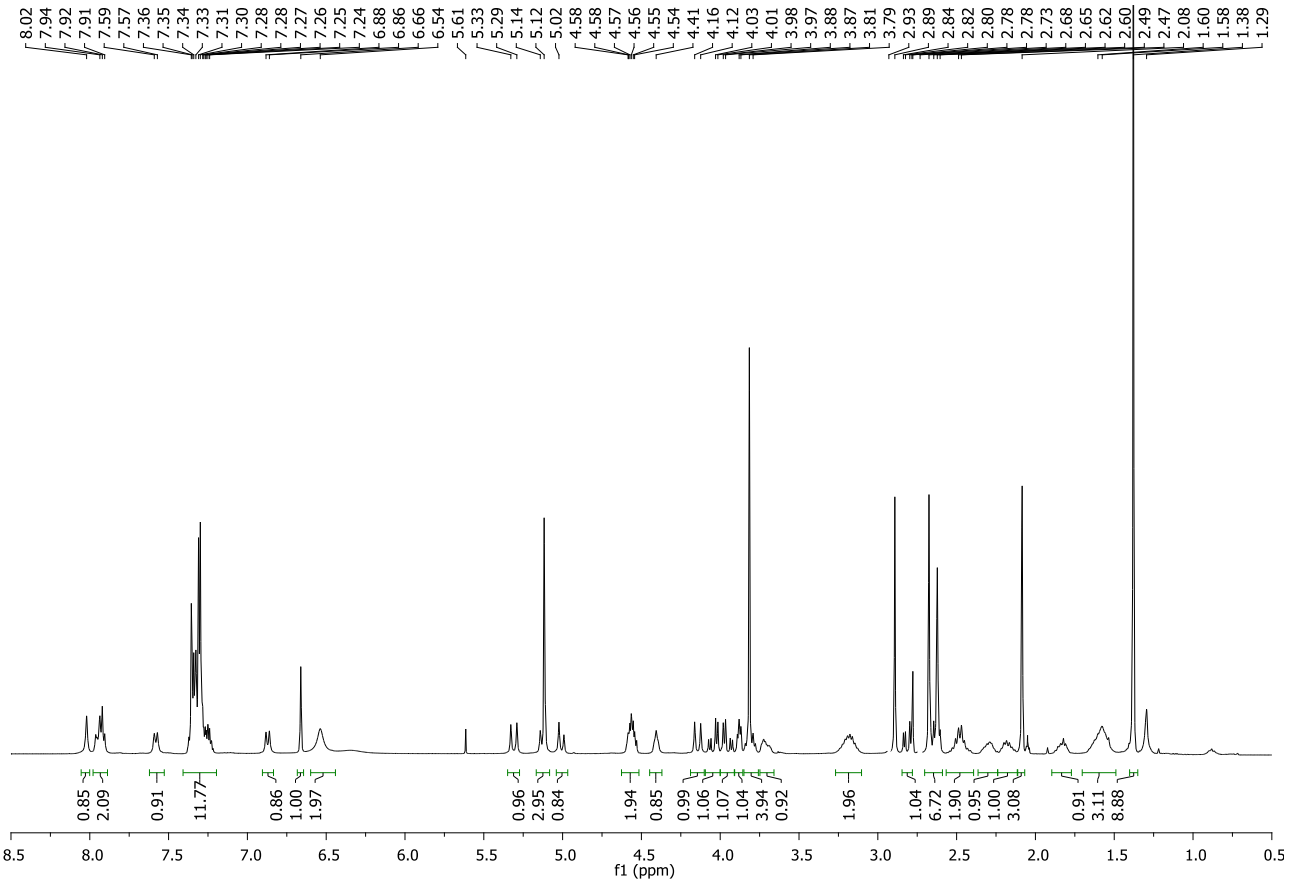

^{13}C-NMR (101 MHz, Acetone-d_6)

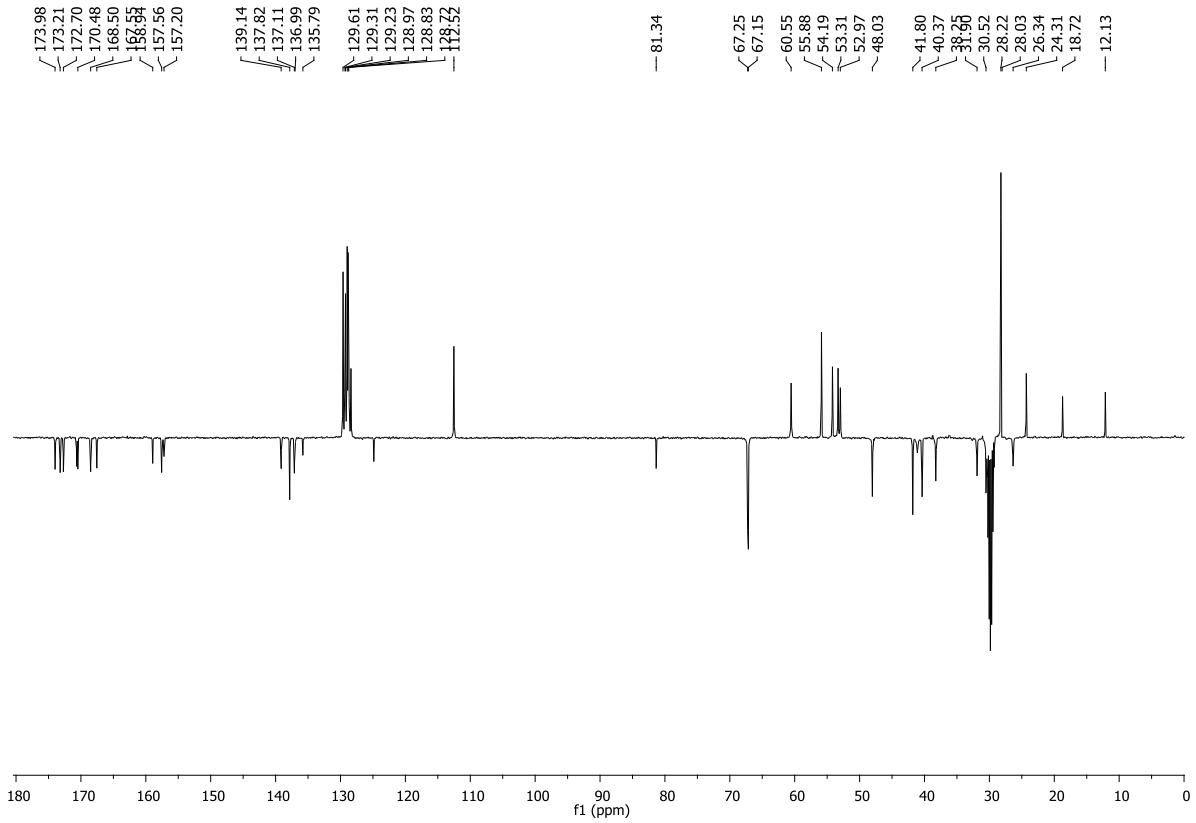

58a:

^{1}H NMR (400 MHz, CD_3OD)

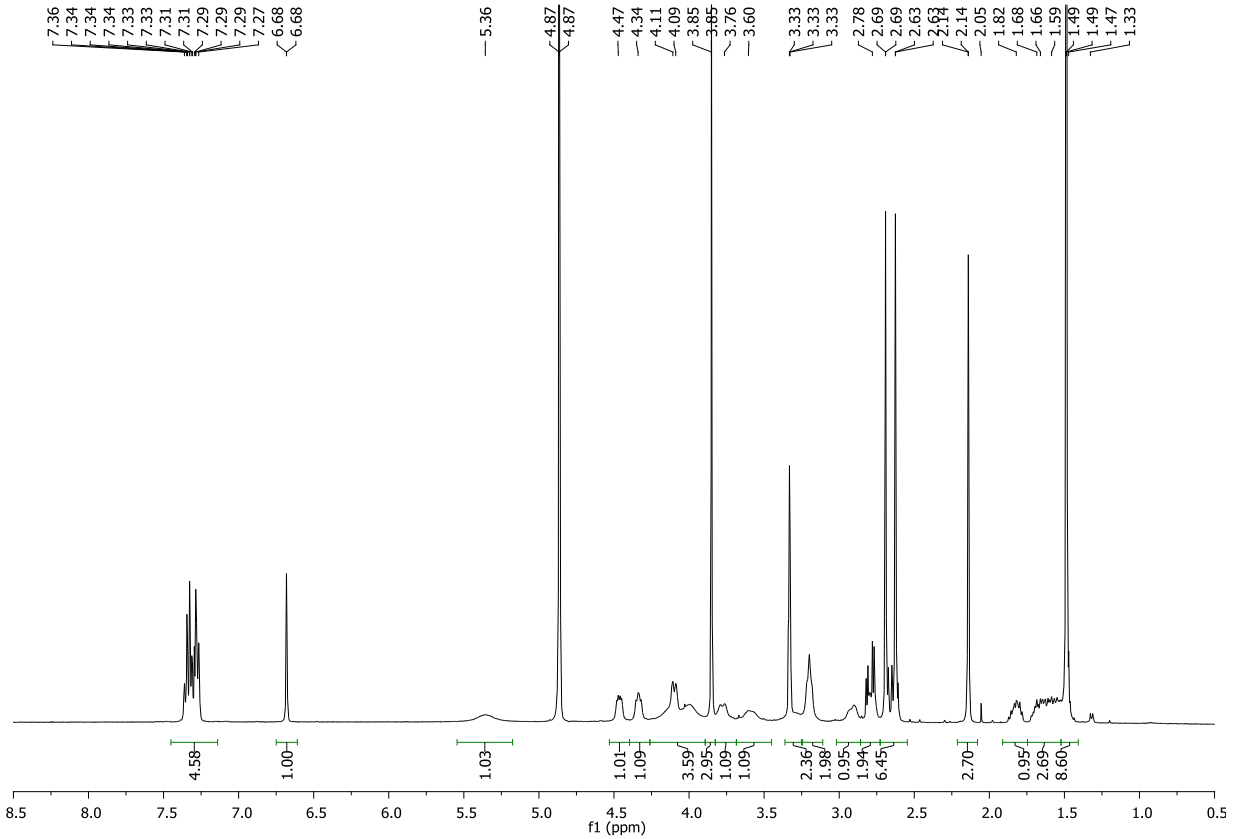

^{13}C NMR (101 MHz, CD_3OD)

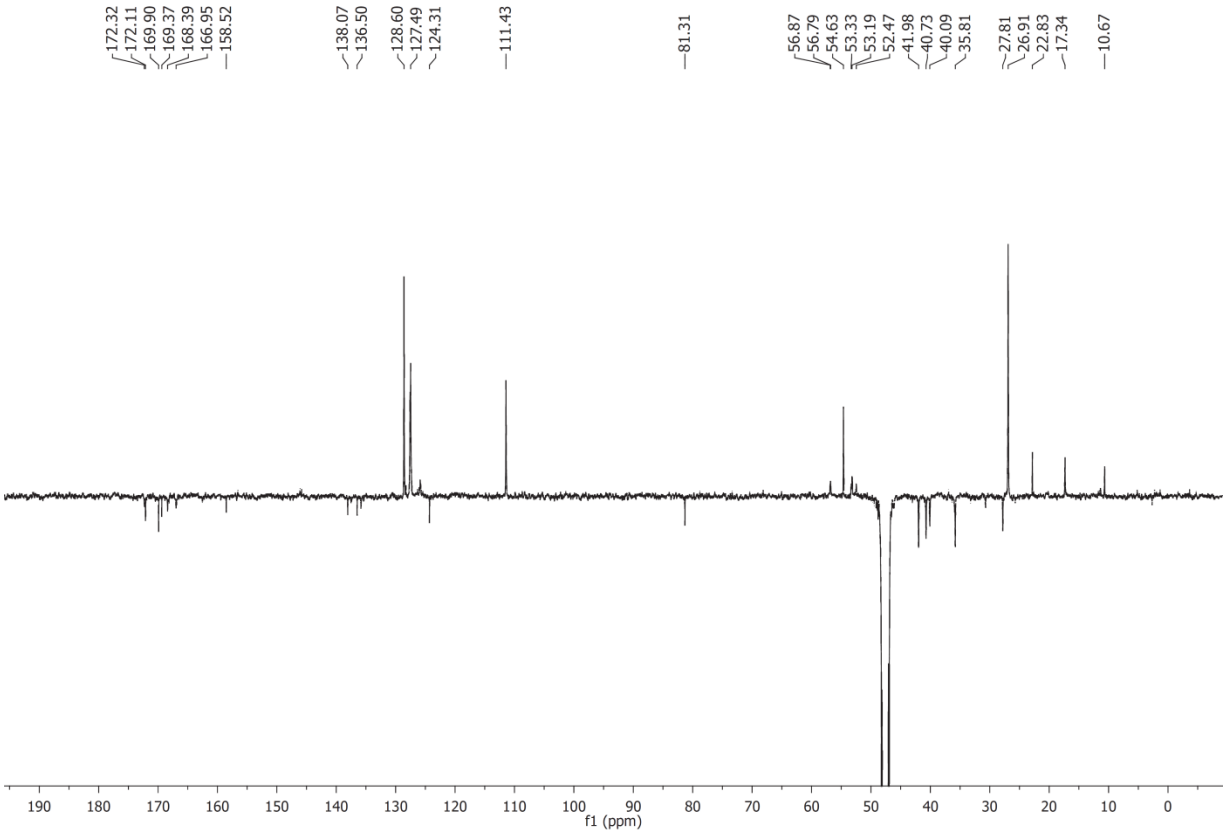

58b:

^{1}H NMR (400 MHz, Acetone-d_6)

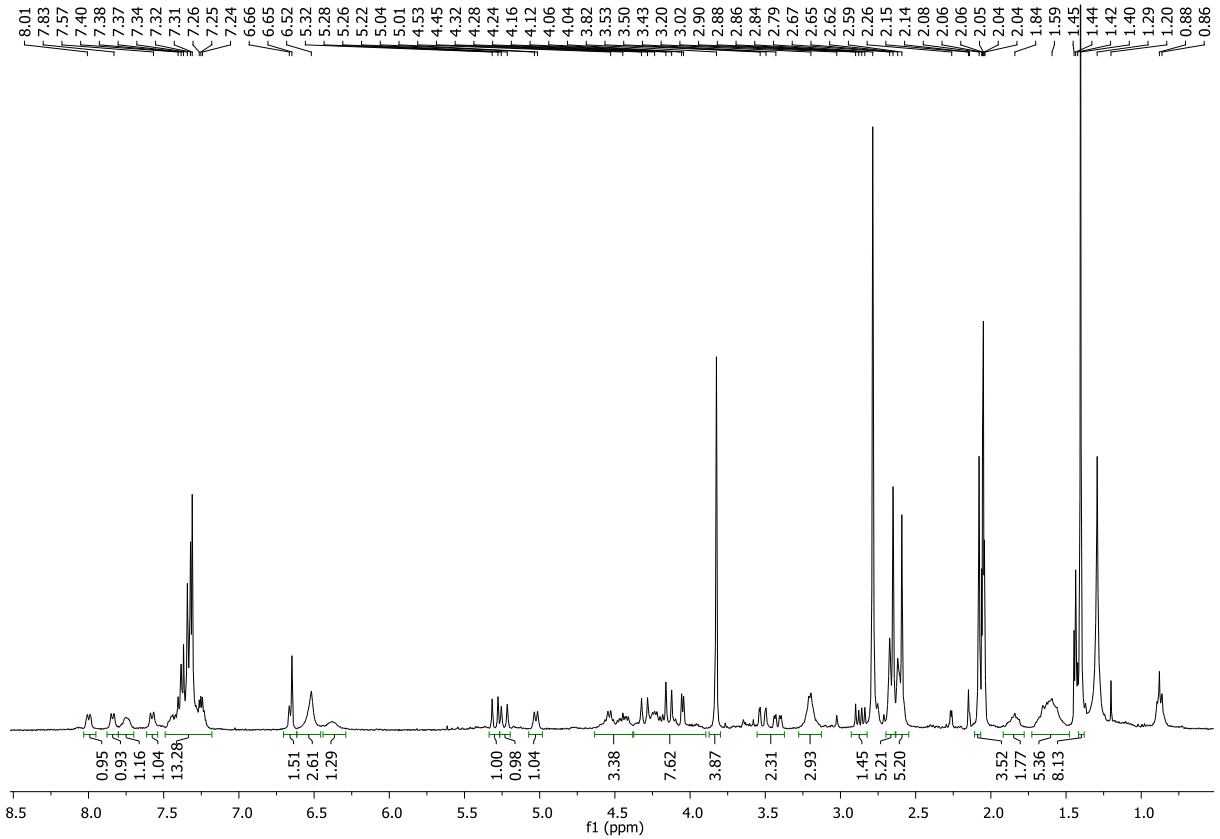

^{13}C NMR (101 MHz, Acetone-d_6)

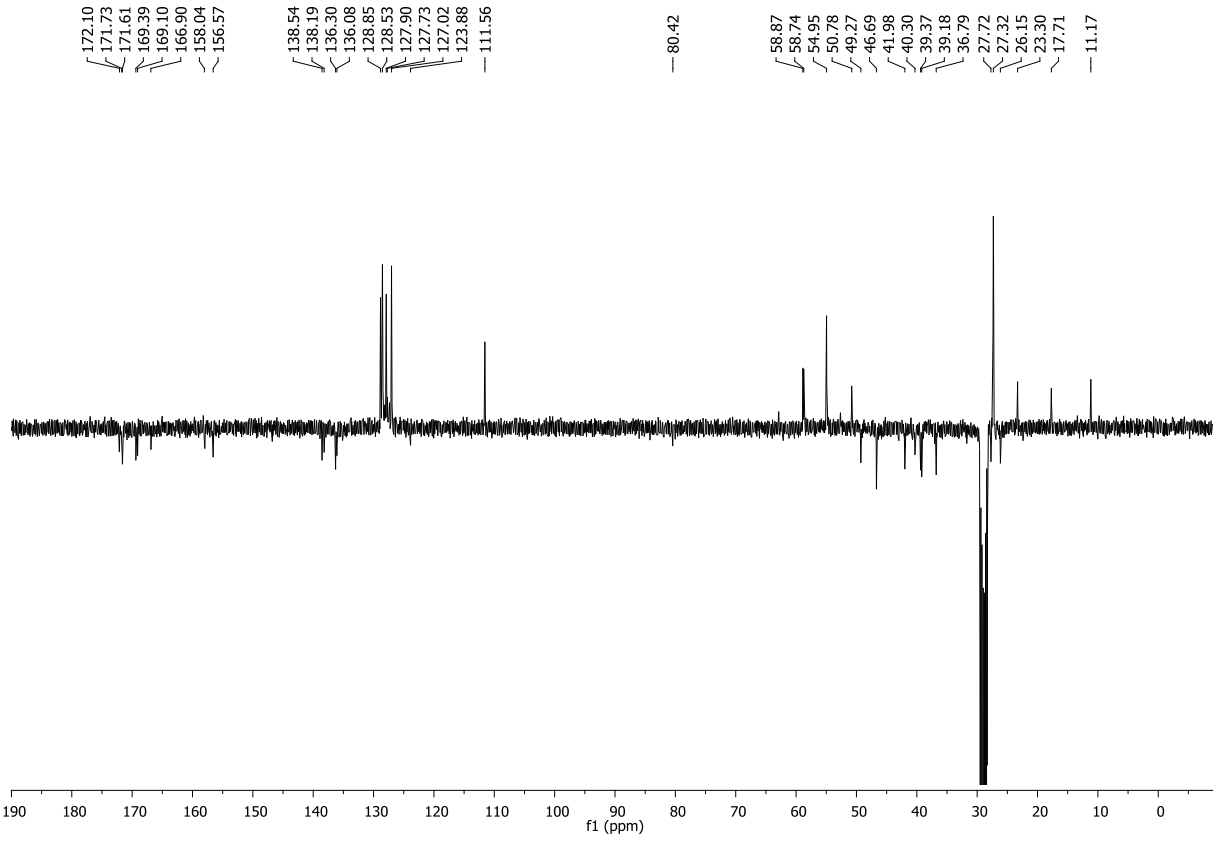

58c:

^{1}H NMR (400 MHz, DMSO-d_6)

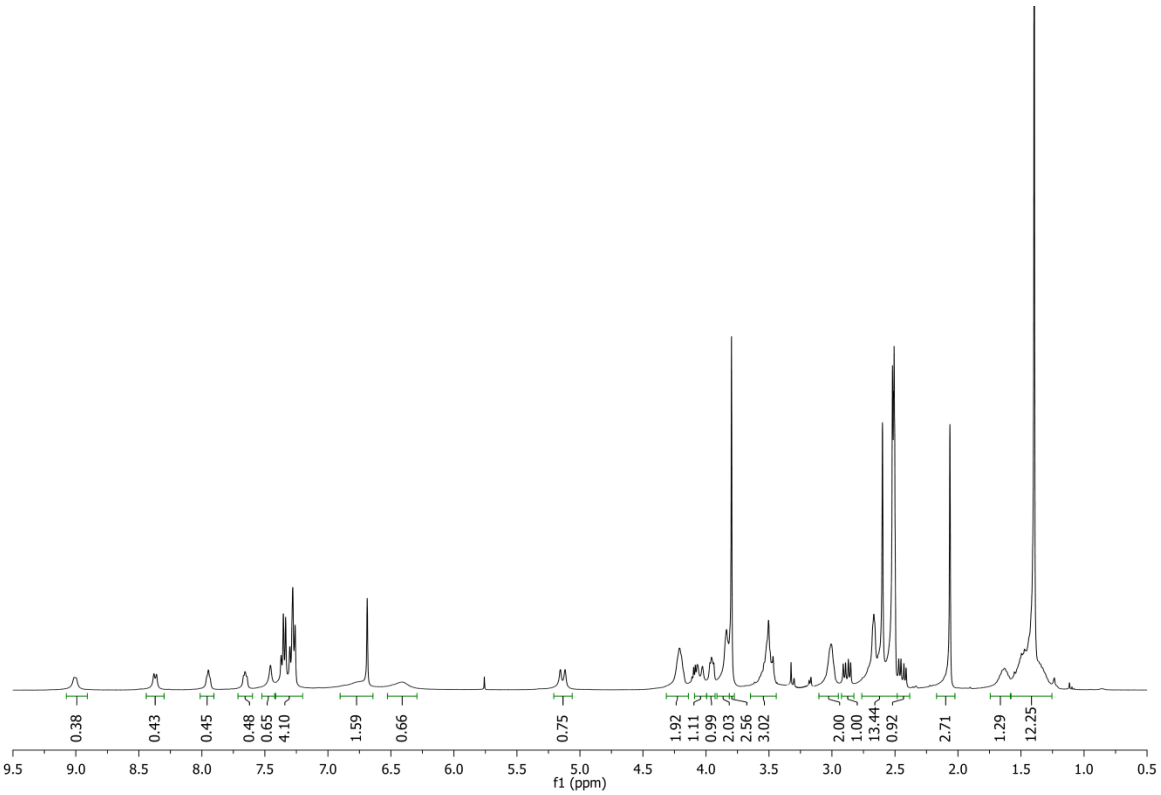

b) ^{13}C NMR (101 MHz, DMSO-d_6)

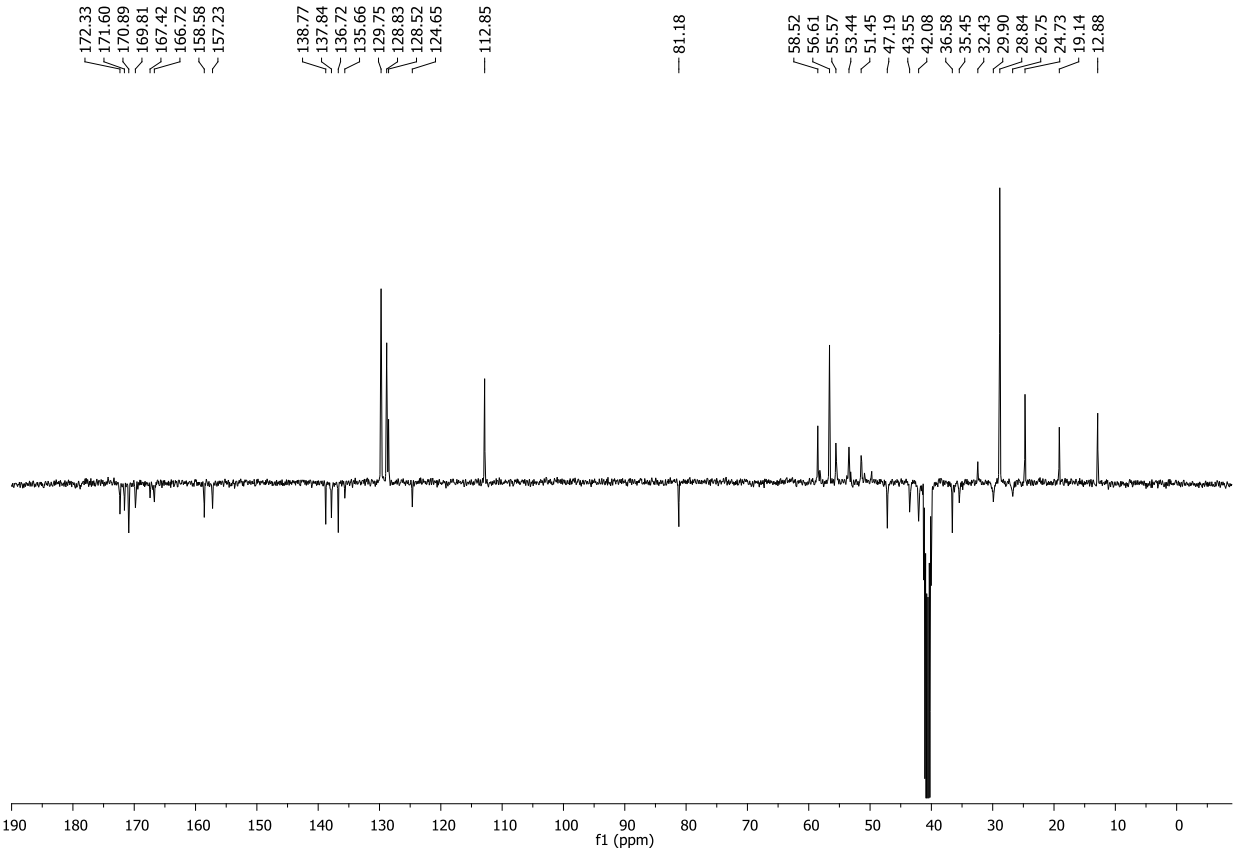

58d:

^{1}H NMR (400 MHz, CD_3OD)

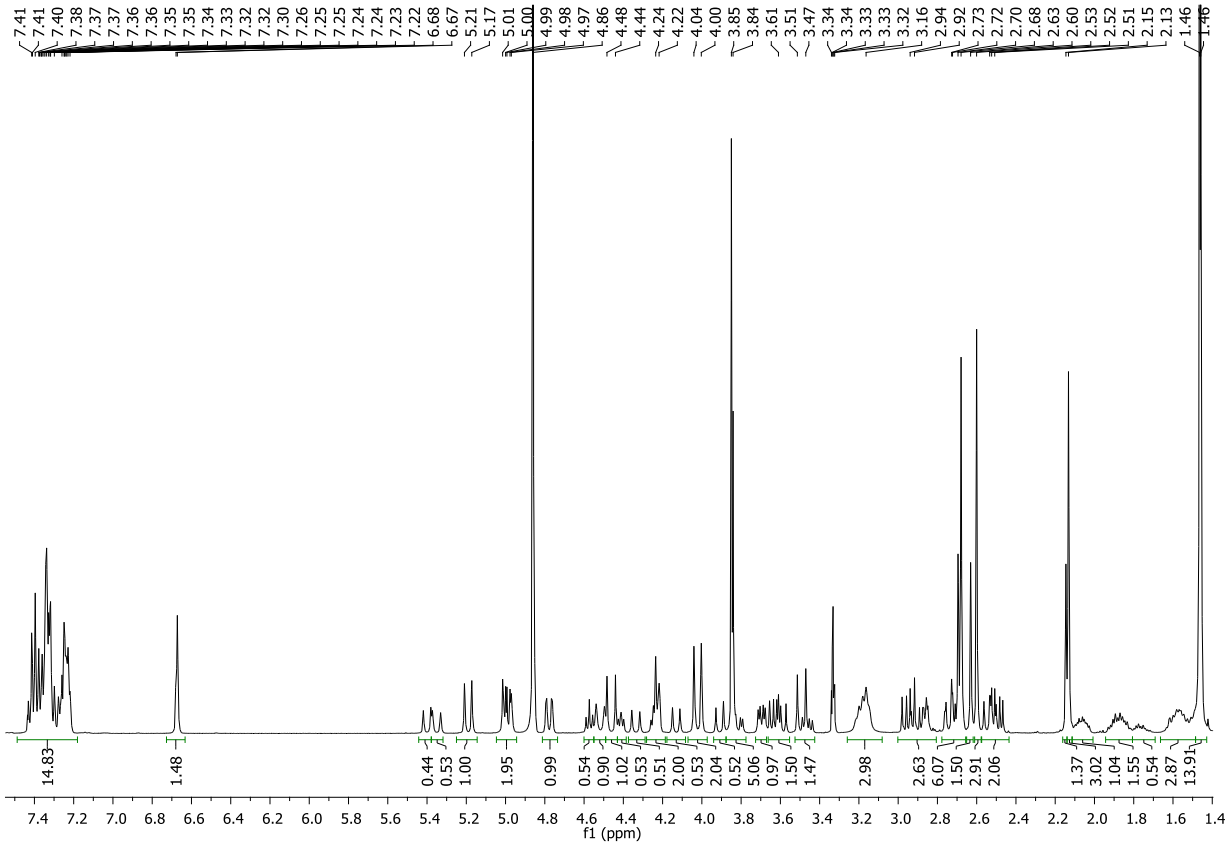

^{13}C NMR (101 MHz, CD_3OD)

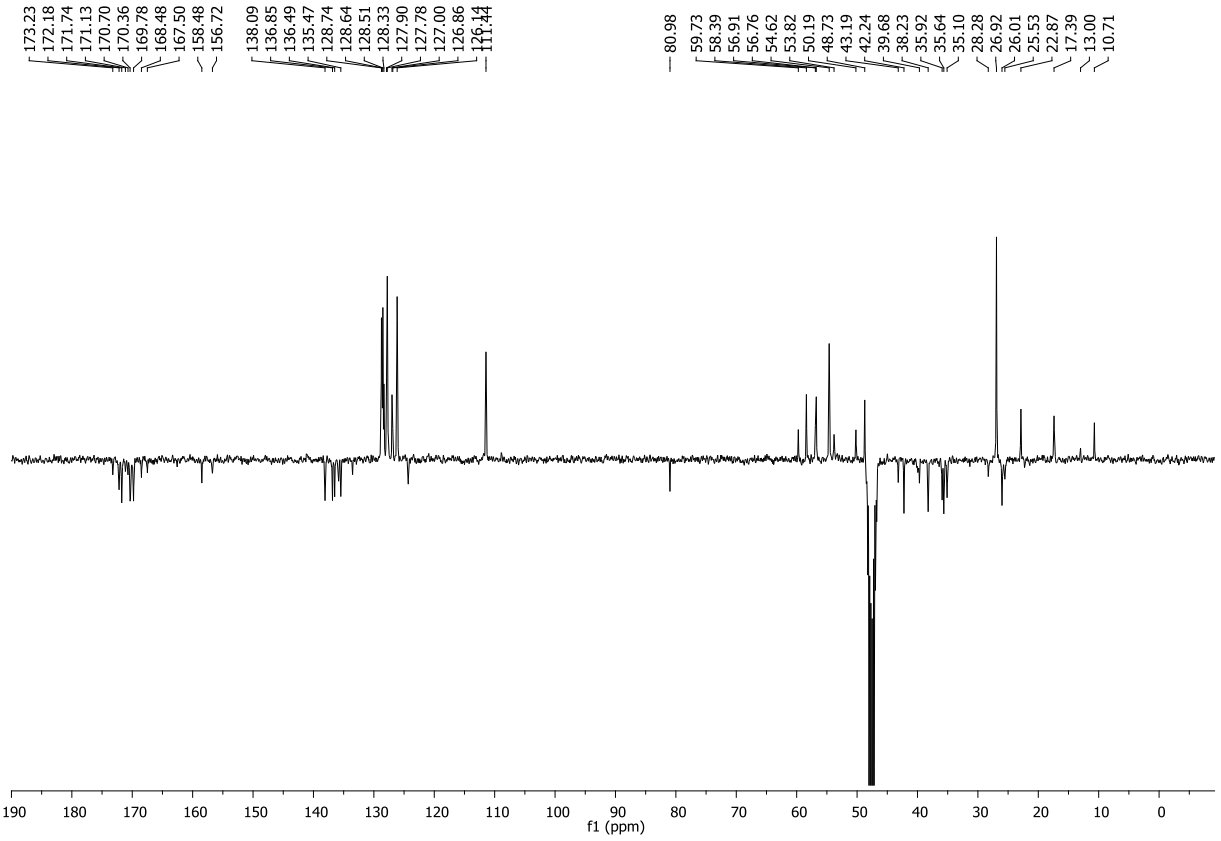

58e:

^{1}H-NMR (400 MHz, CD_3OD)

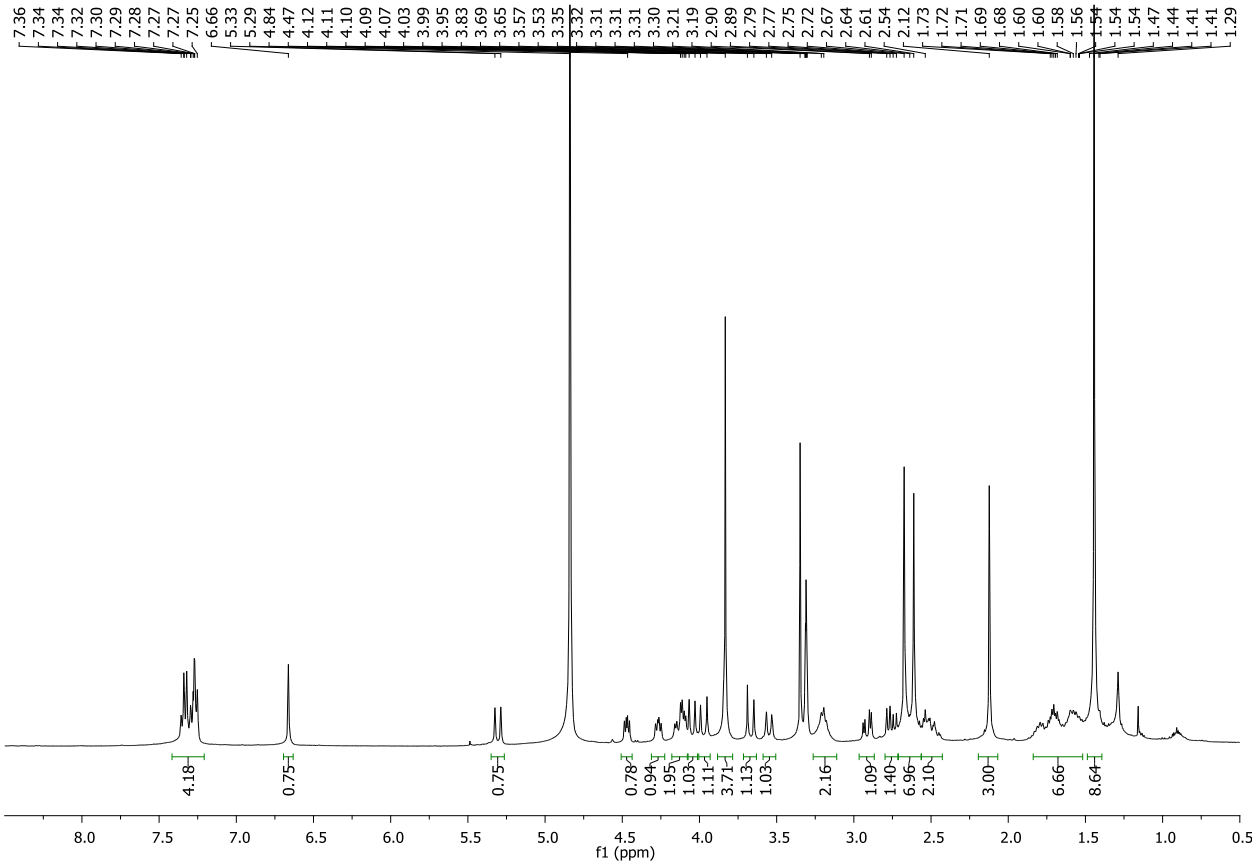

^{13}C-NMR (101 MHz, CD_3OD)

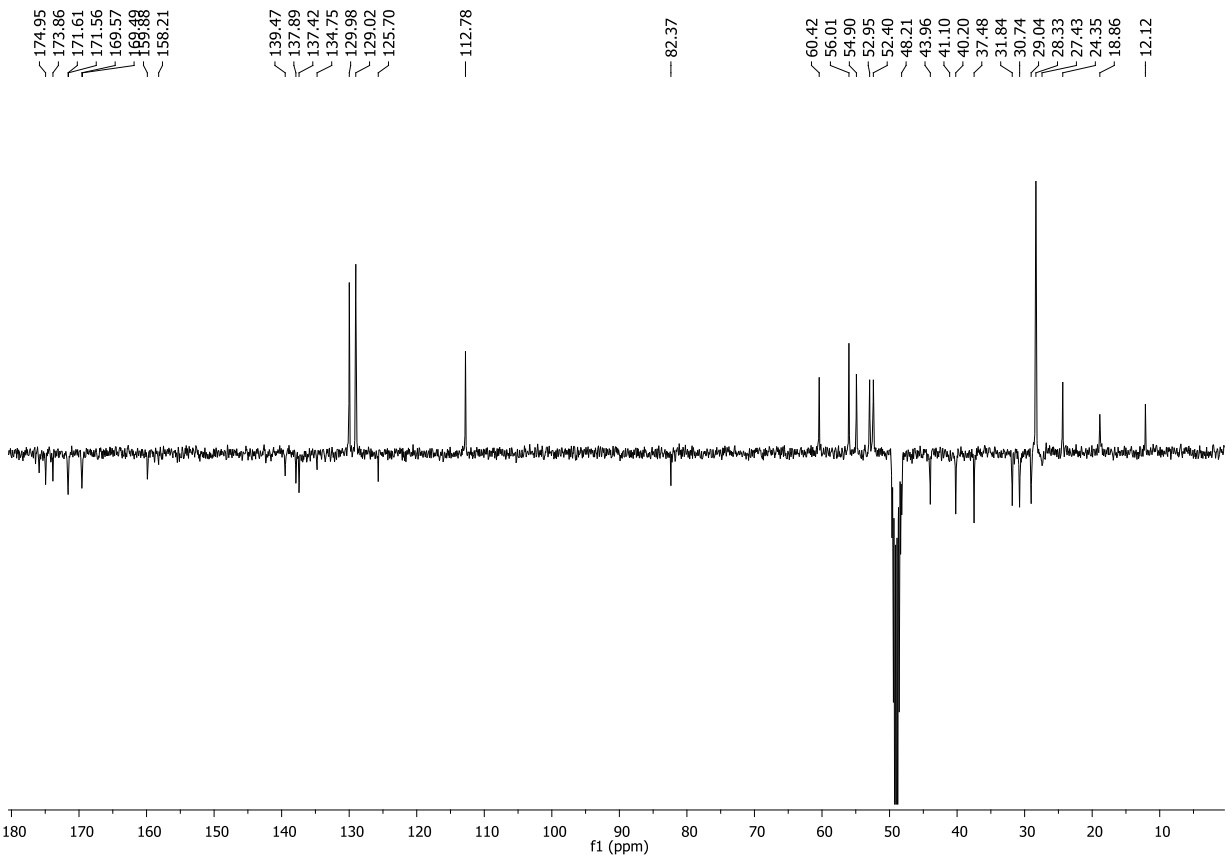

c[DKP-4-RGD]:

^{1}H NMR (400 MHz, H_2O/D_2O 9:1)

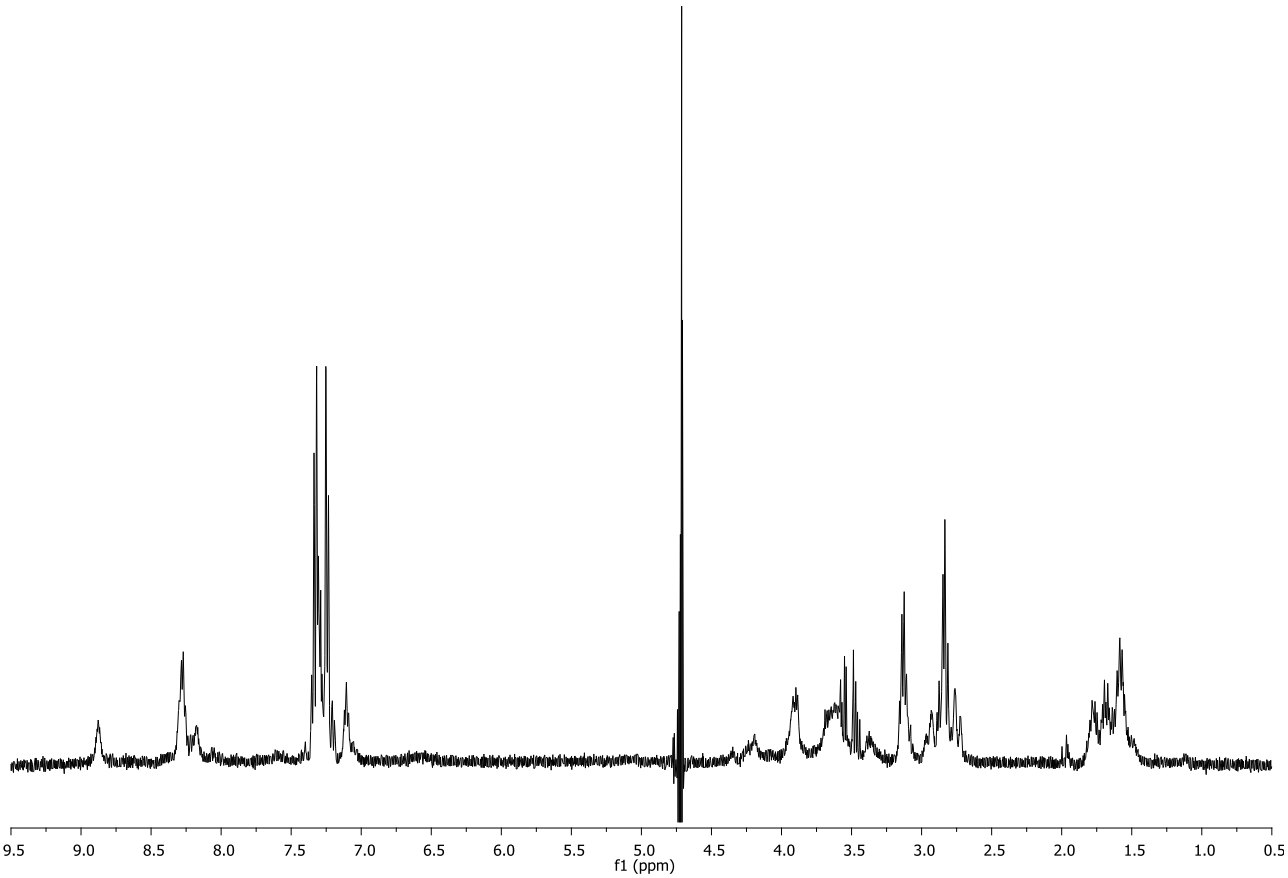

^{13}C NMR (101 MHz, D_2O)

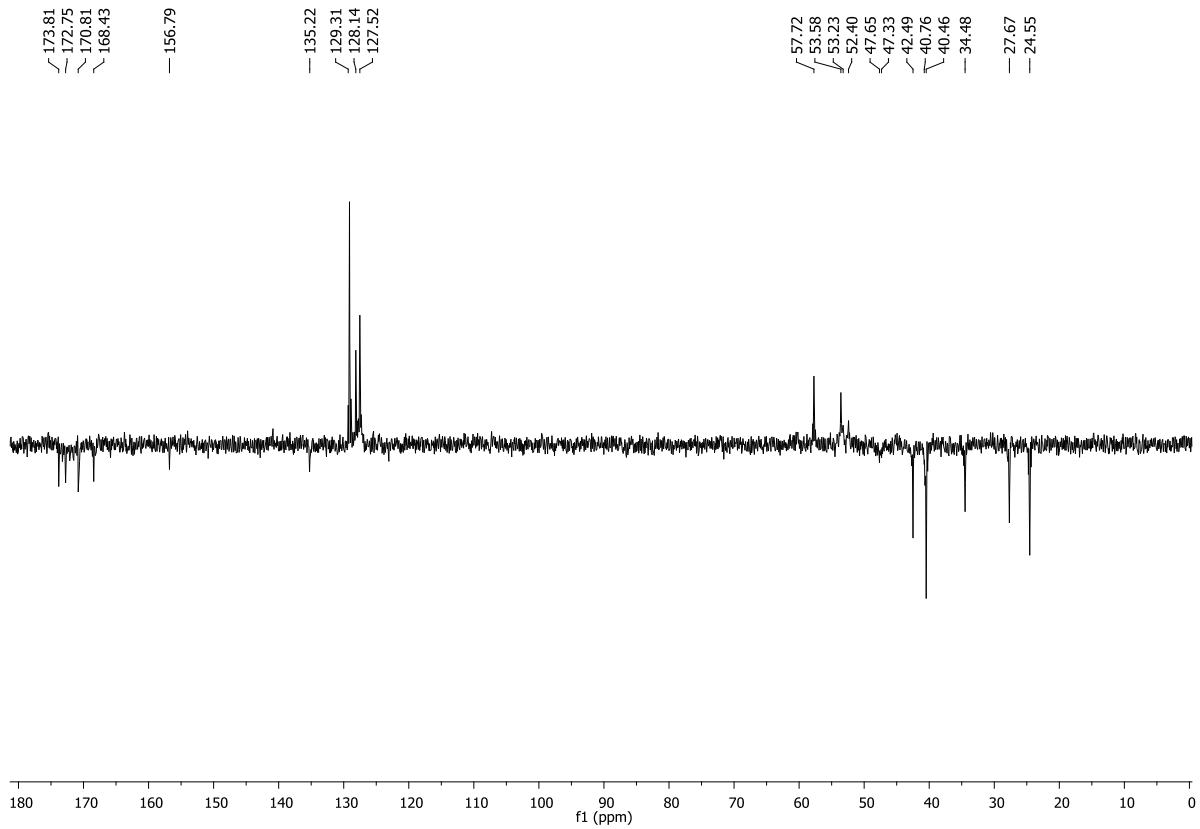

c[DKP-5-RGD]:

^{1}H NMR (400 MHz, H_2O/D_2O 9:1)

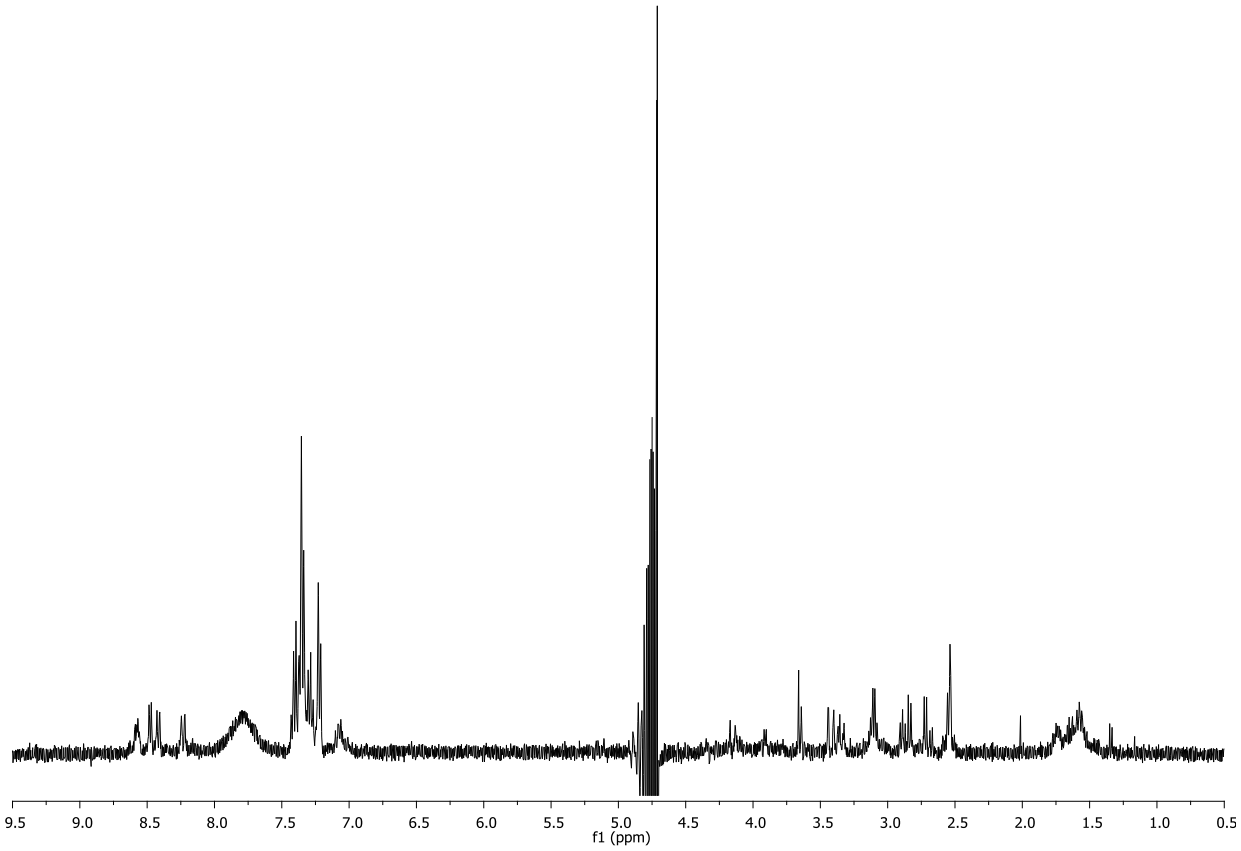

^{13}C NMR (101 MHz, D_2O)

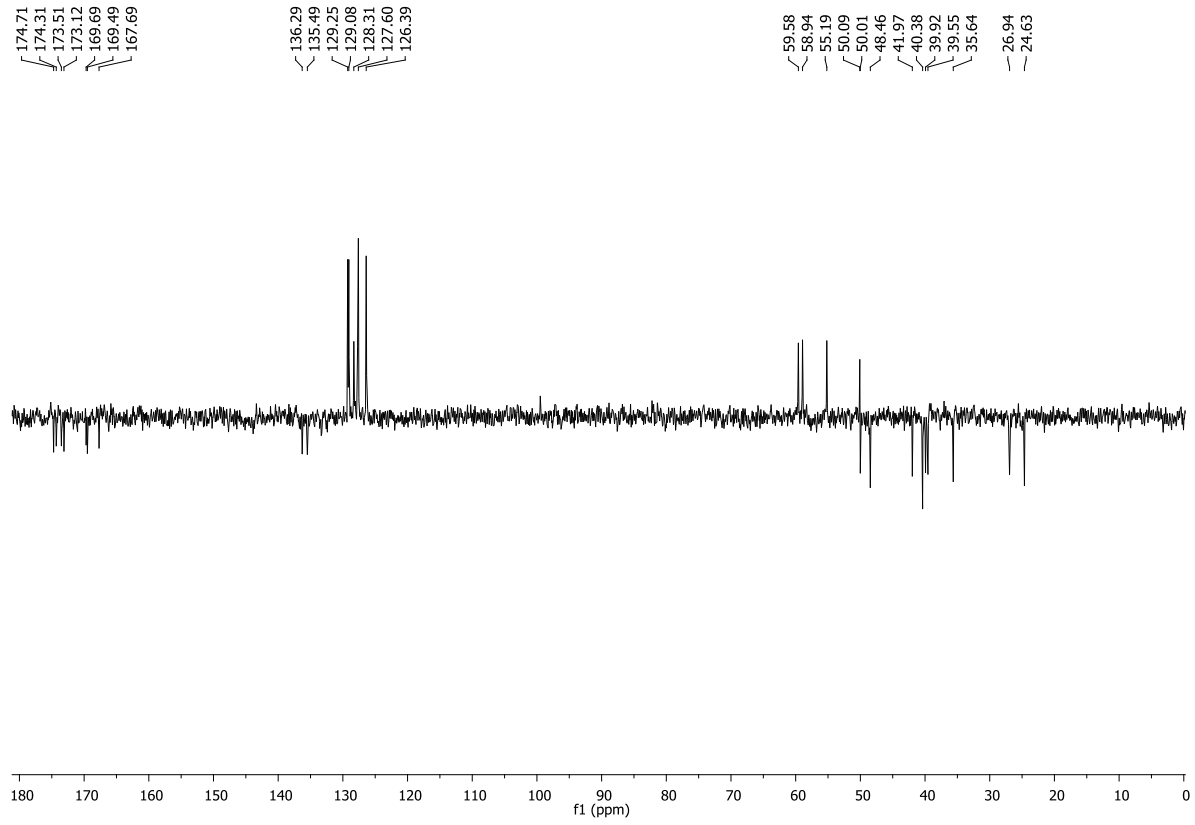

c[DKP-6-RGD]:

^{1}H NMR (400 MHz, H_2O/D_2O 9:1)

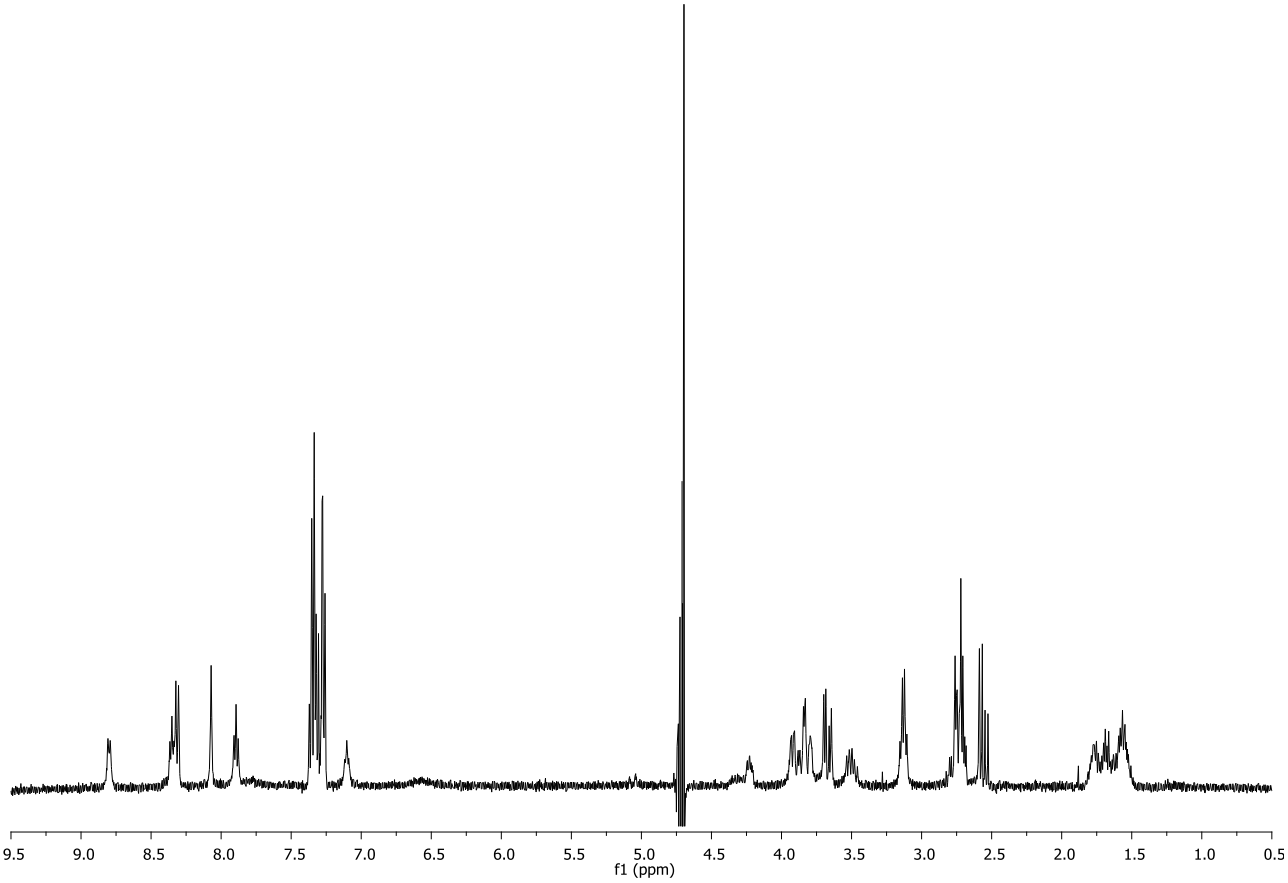

^{13}C NMR (101 MHz, D_2O)

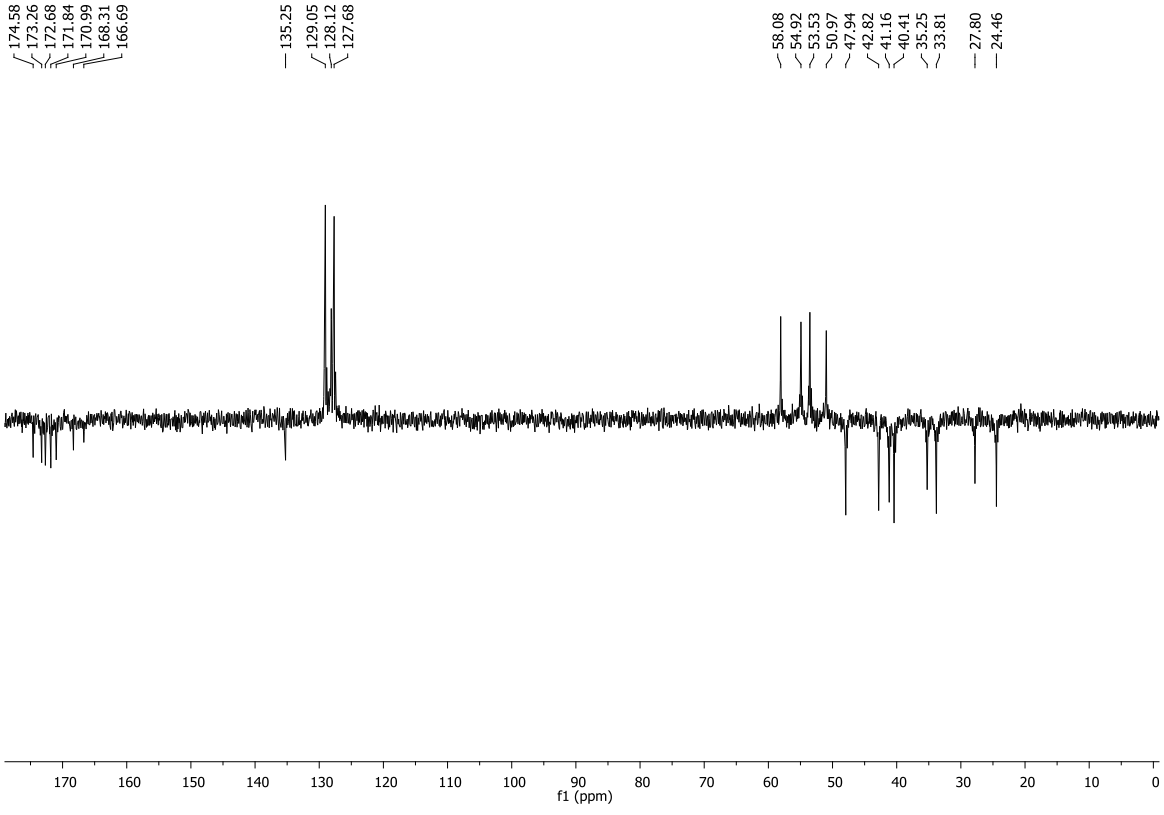

c[DKP-7-RGD]-A:

^{1}H NMR (400 MHz, H_2O/D_2O 9:1)

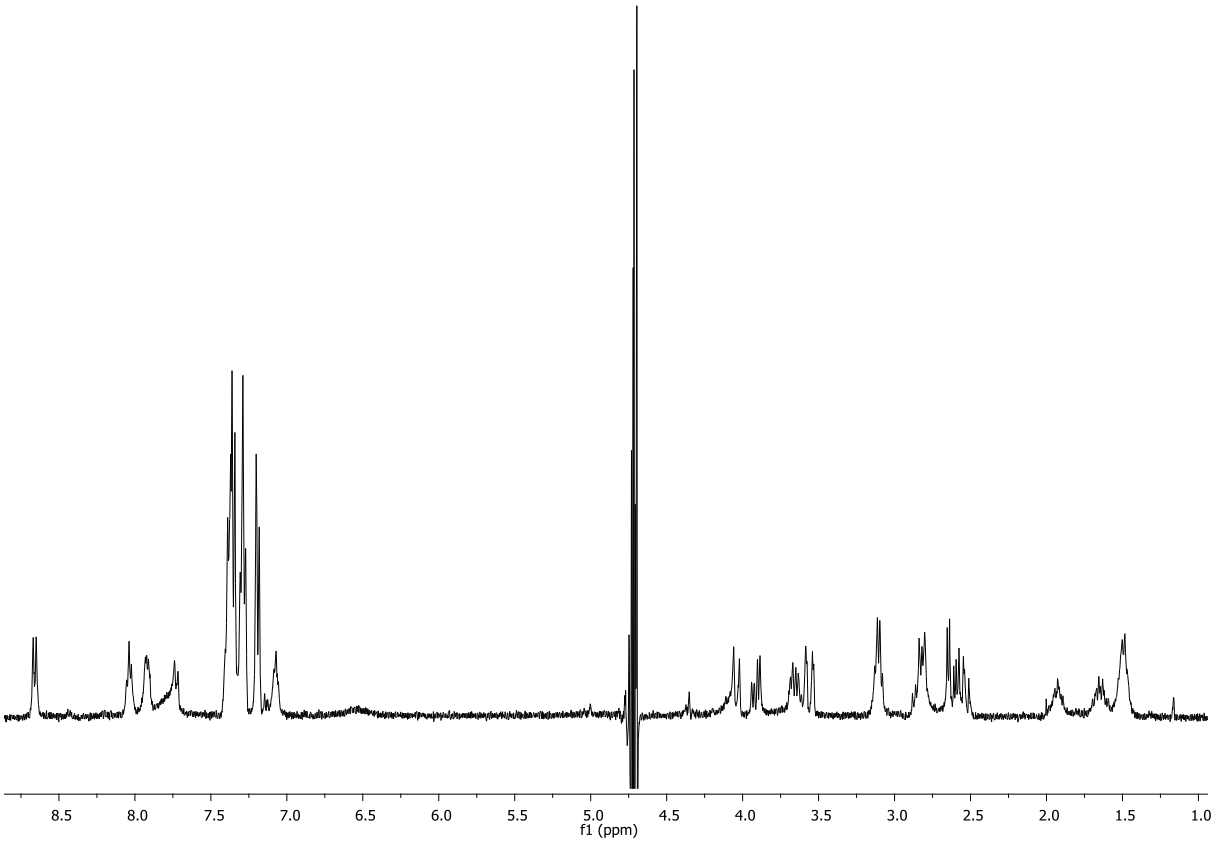

^{13}C NMR (101 MHz, D_2O)

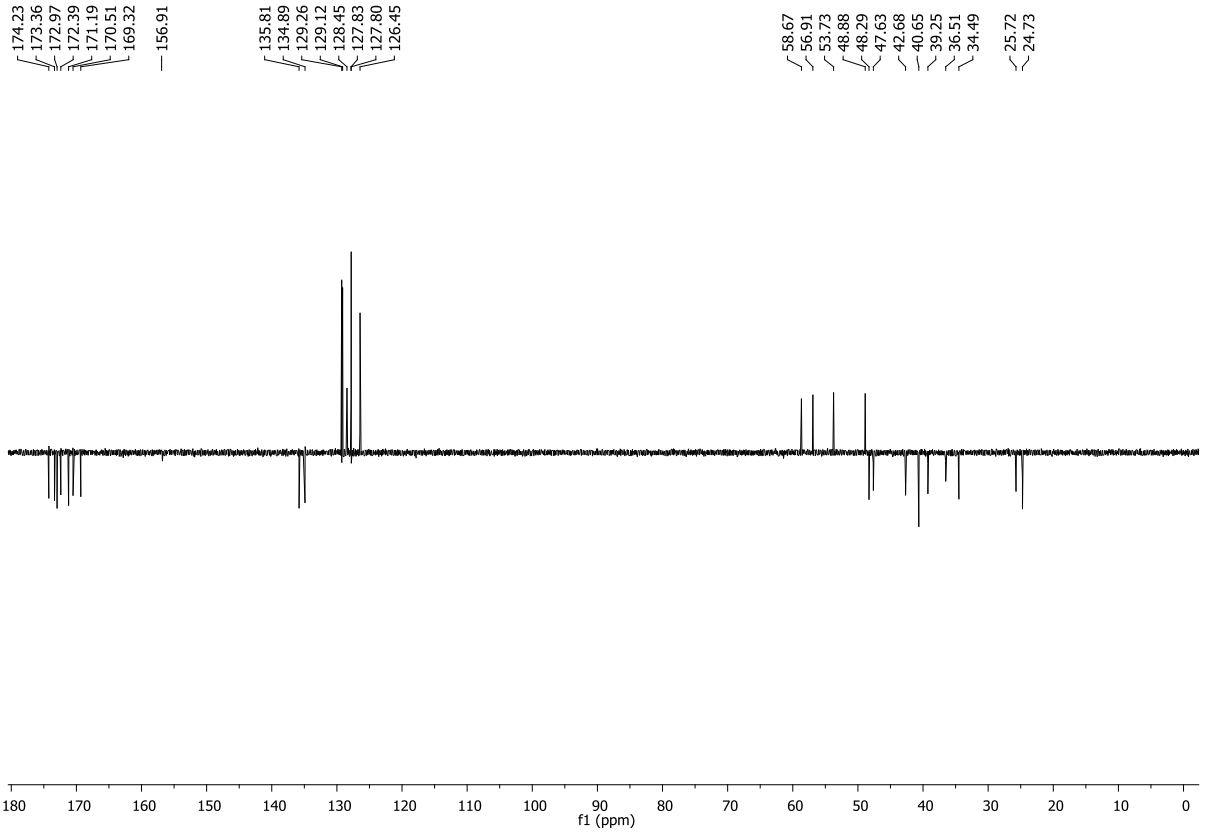

c[DKP-7-RGD]-B:

^{1}H NMR (400 MHz, H_2O/D_2O 9:1)

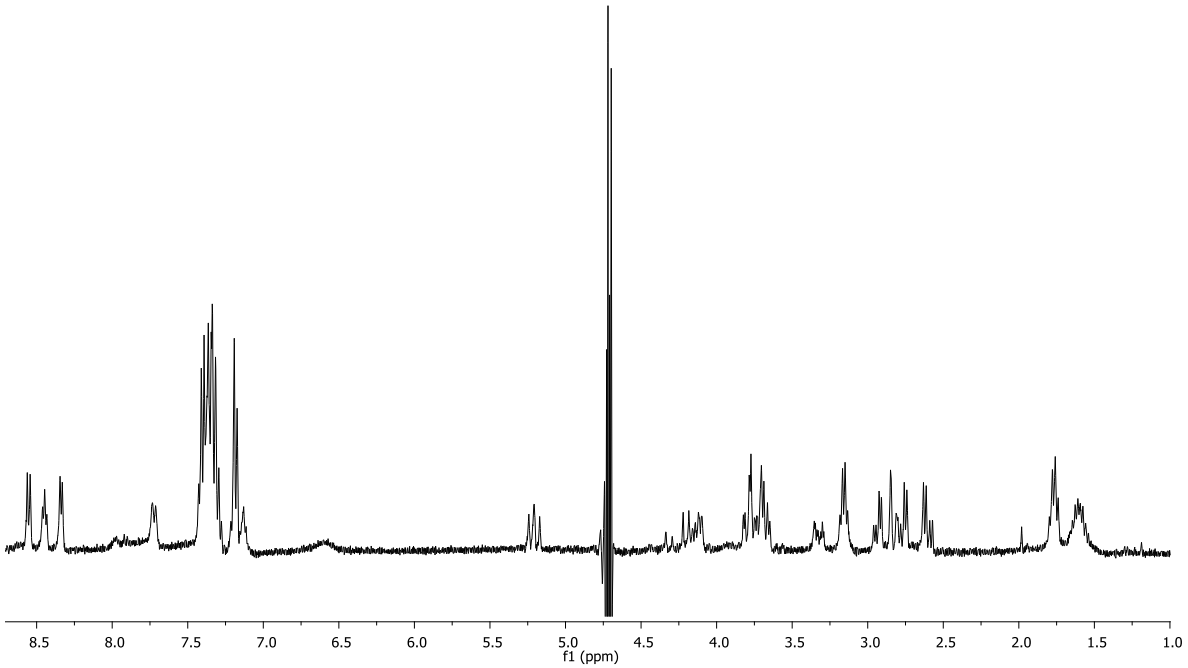

^{13}C NMR (101 MHz, D_2O)

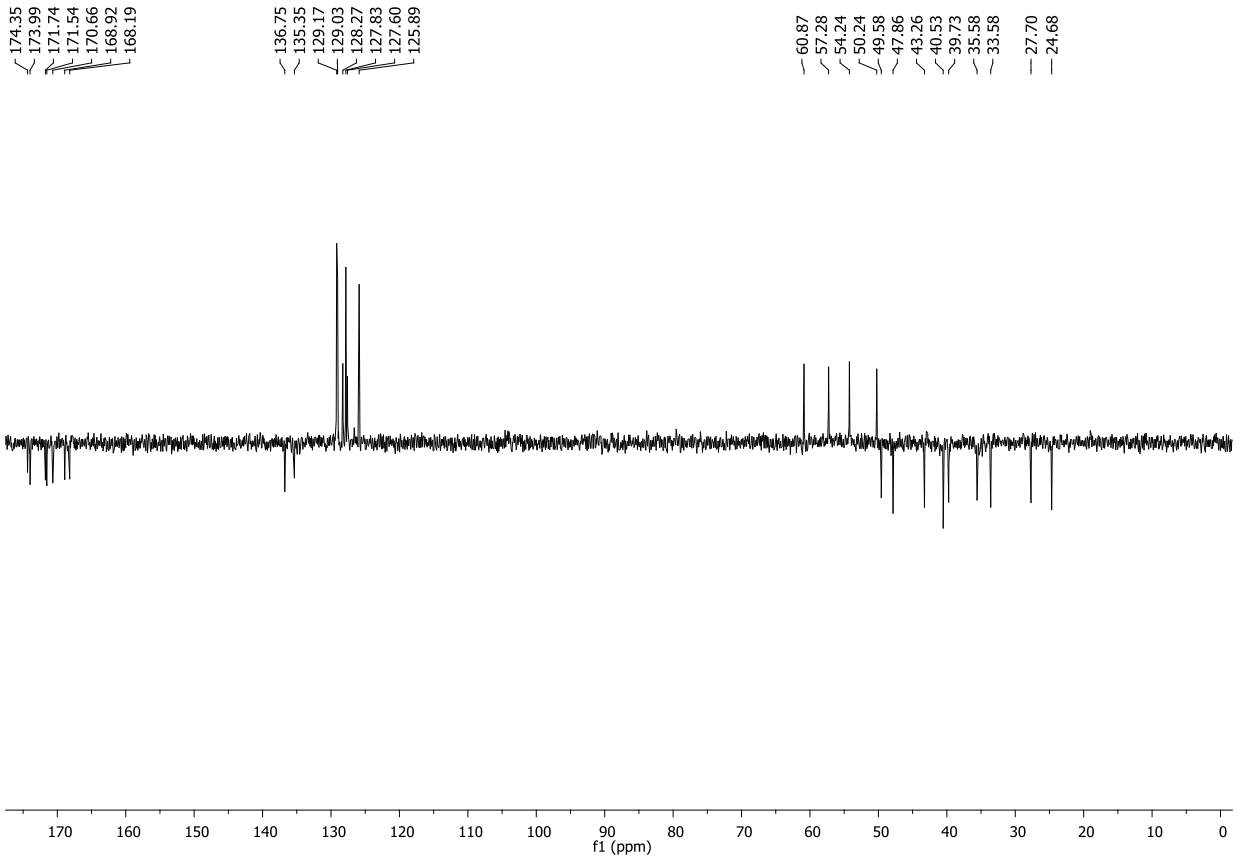

c[DKP-8-RGD]:

^{1}H-NMR (600 MHz, H_2O/D_2O 9:1)

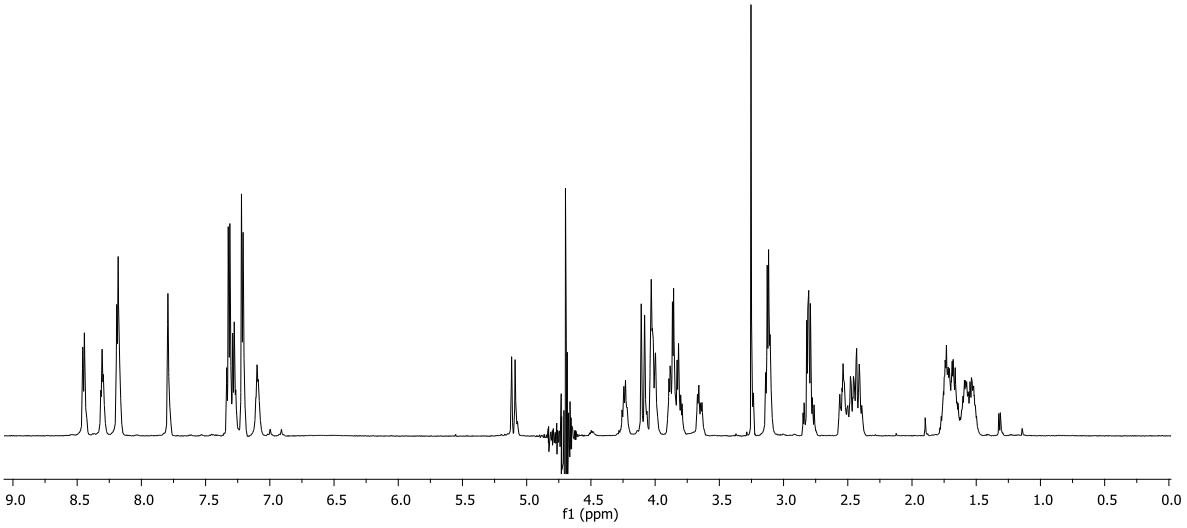

^{13}C-NMR (151 MHz, D_2O)

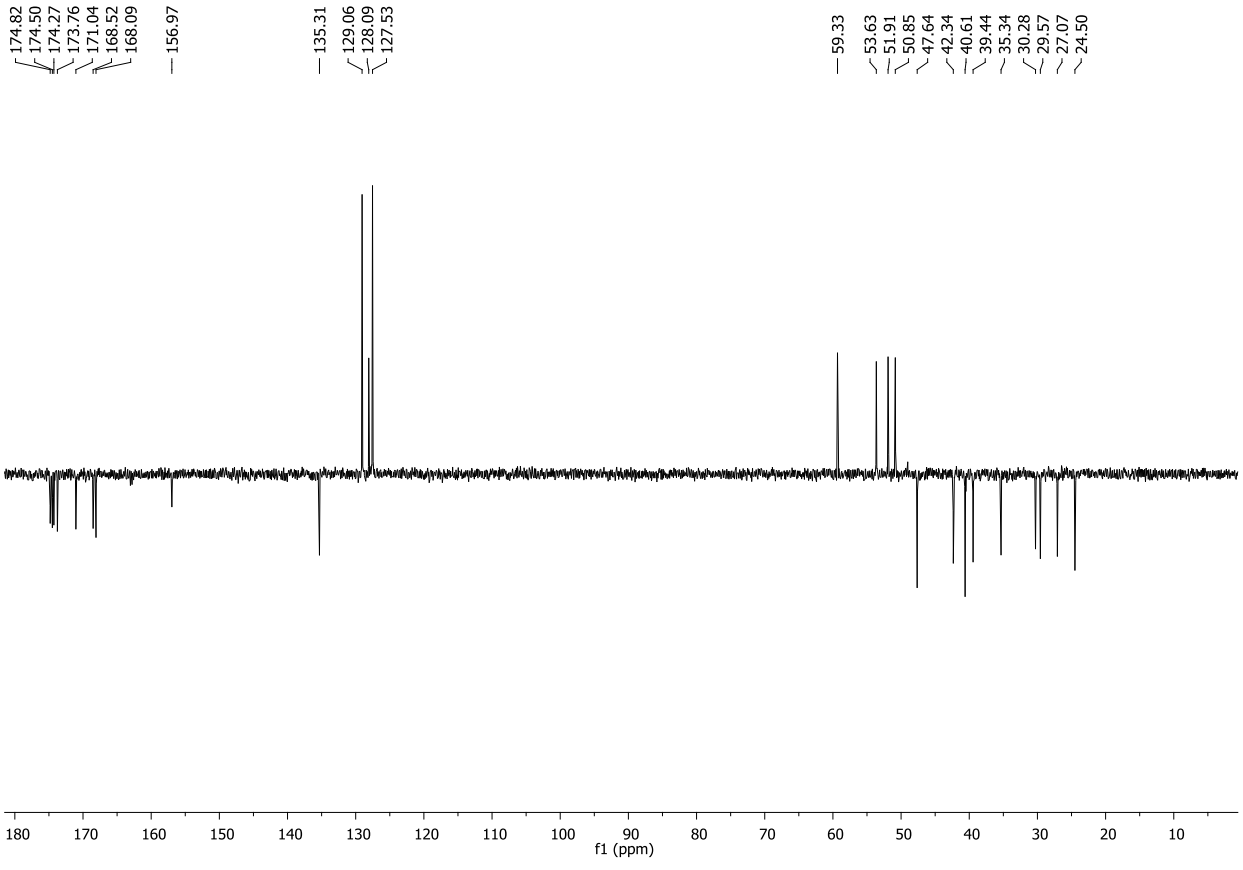

59a:

^{1}H NMR (400 MHz, Acetone-d_6)

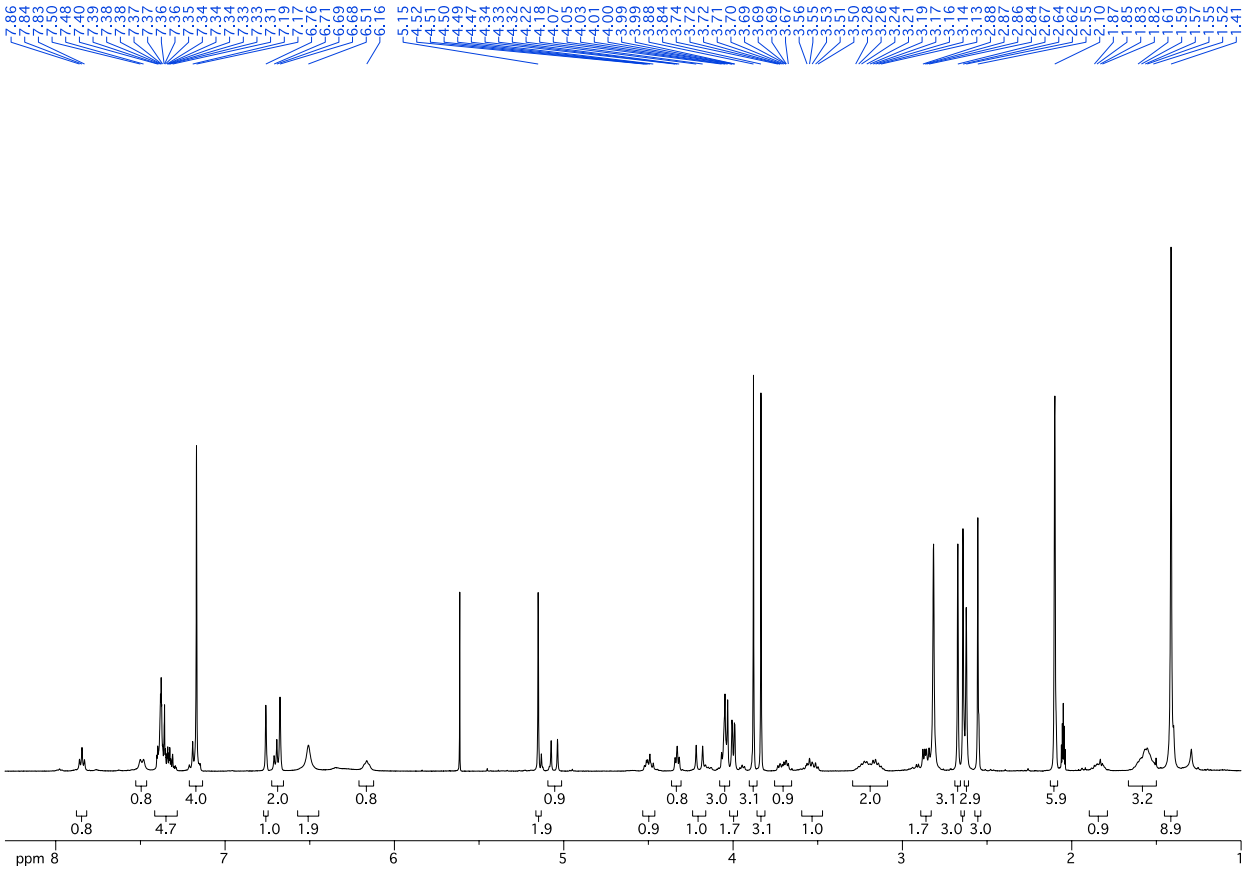

^{13}C NMR (101 MHz, Acetone-d_6)

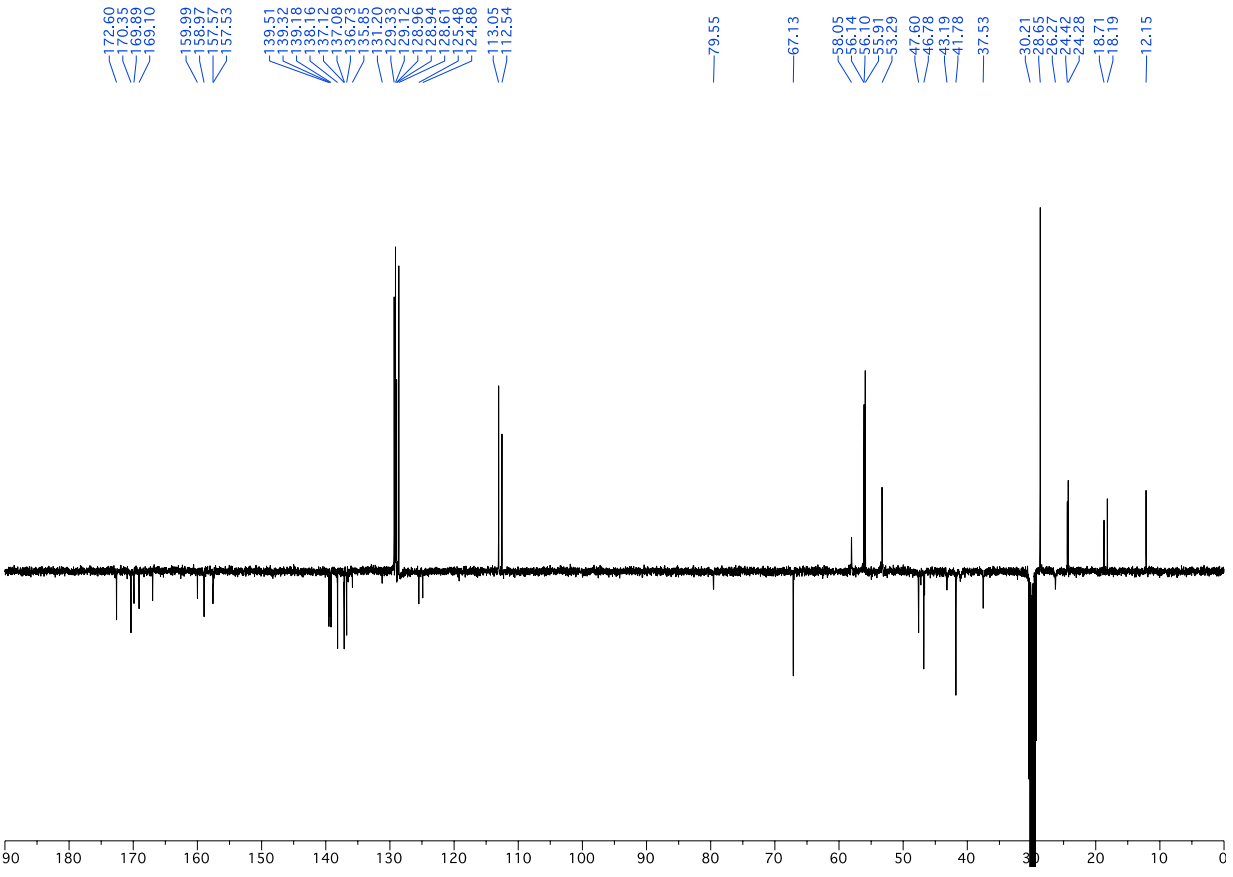

59b:

^{1}H NMR (400 MHz, Acetone-d_6)

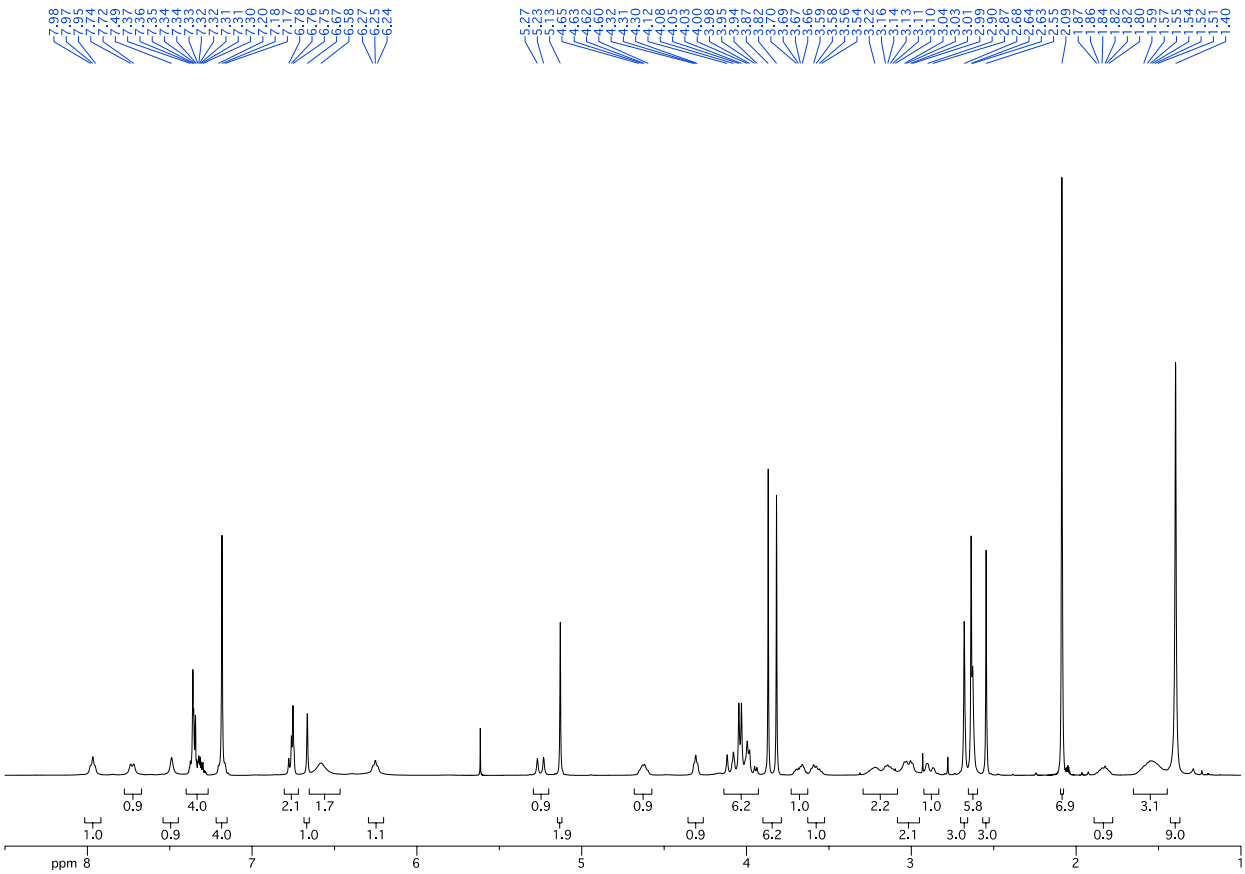

^{13}C NMR (101 MHz, Acetone-d_6)

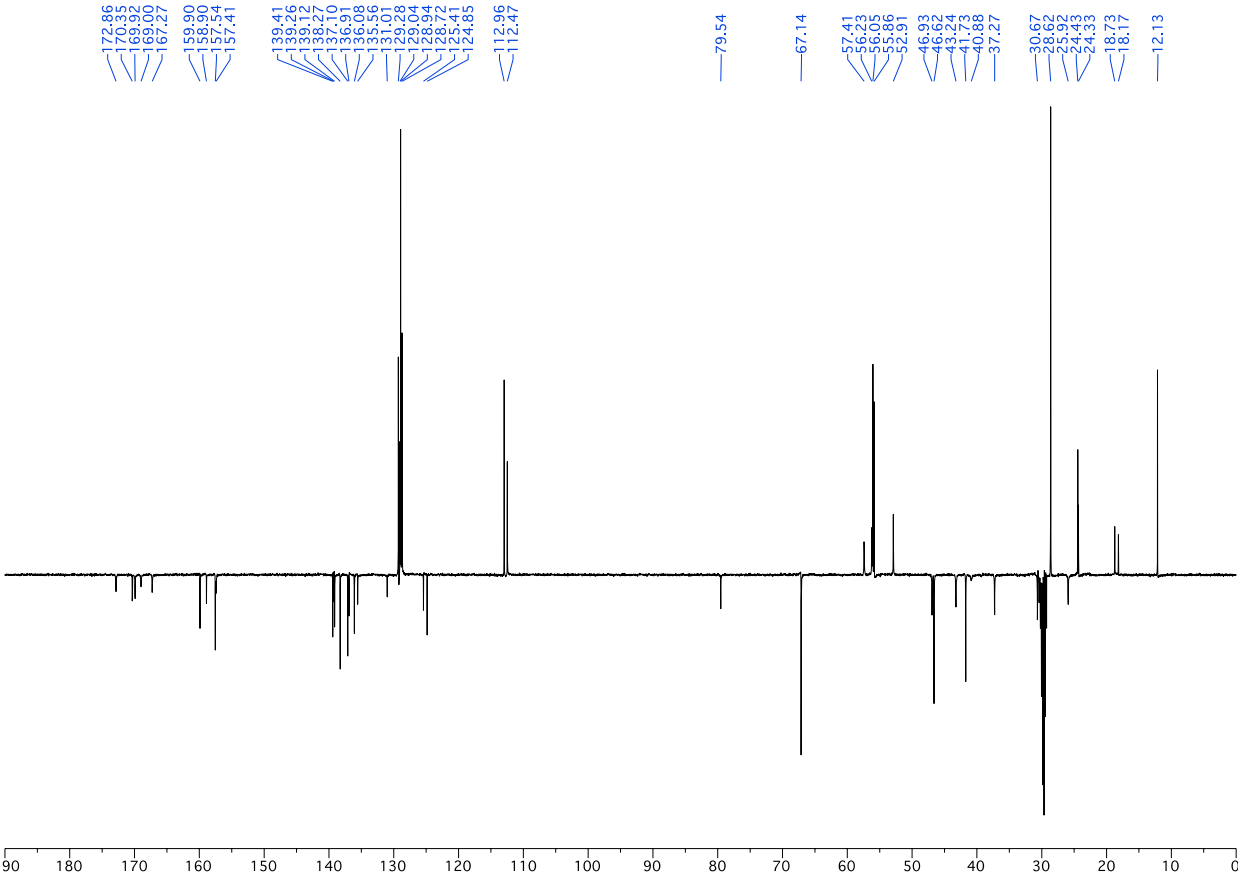

60a:

^{1}H NMR (400 MHz, Acetone-d_6)

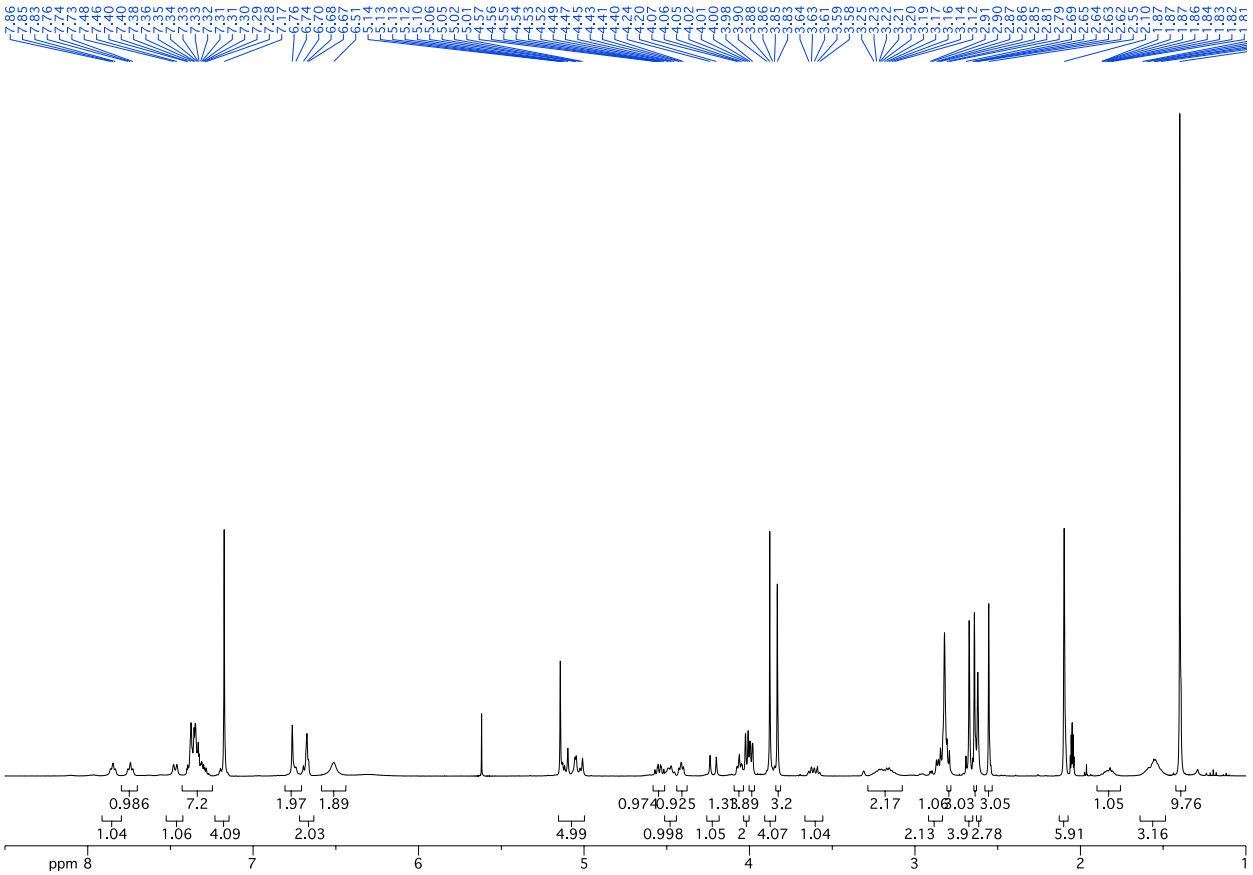

^{13}C NMR (101 MHz, Acetone-d_6)

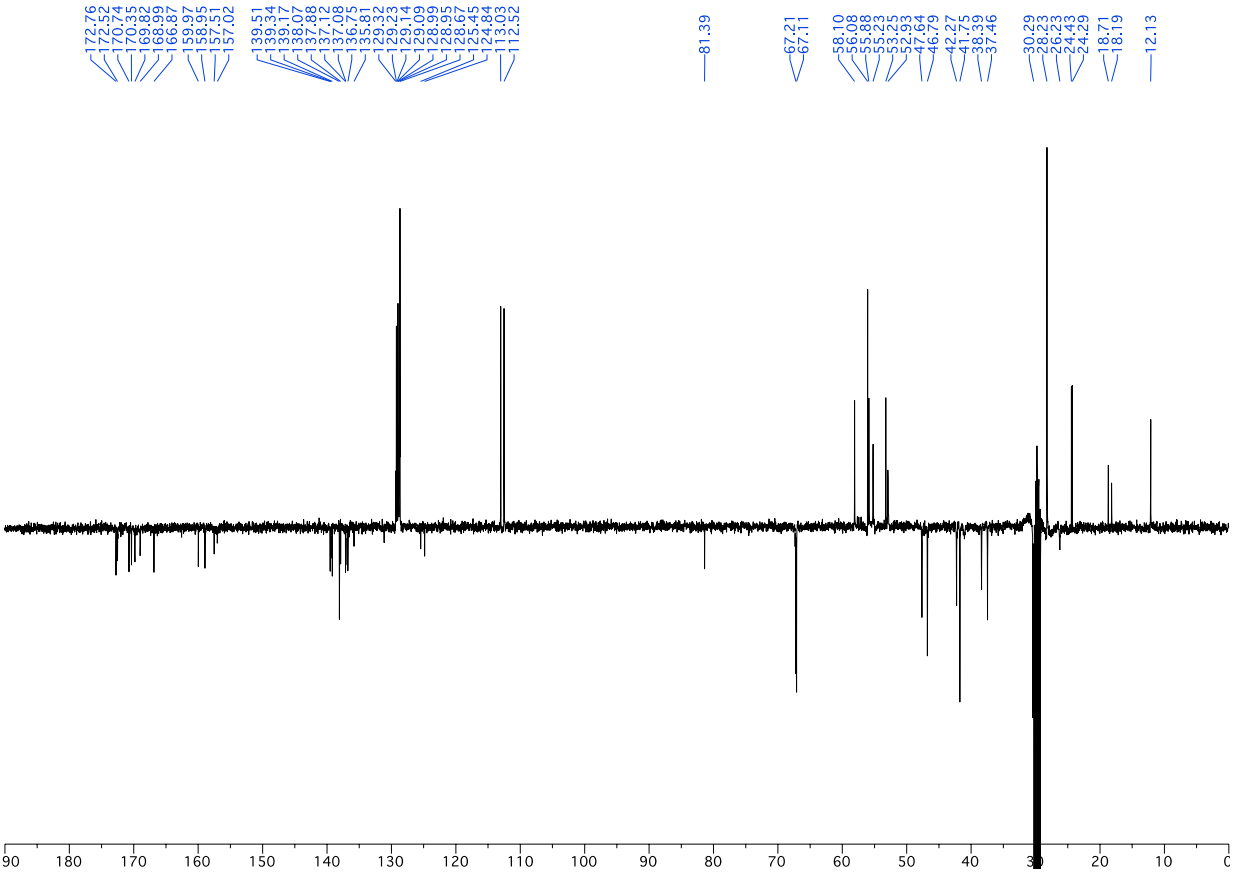

60b:

^{1}H NMR (400 MHz, Acetone-d_6)

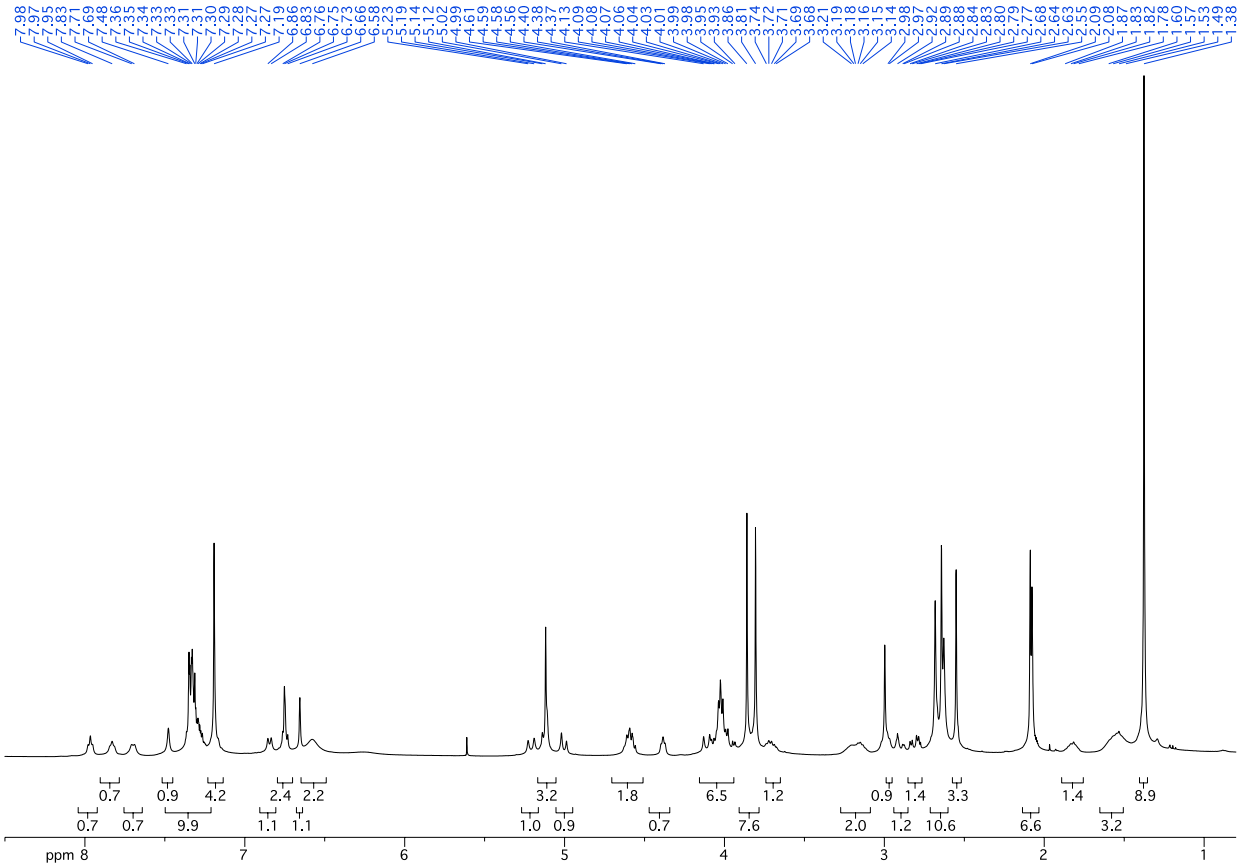

^{13}C NMR (101 MHz, Acetone-d_6)

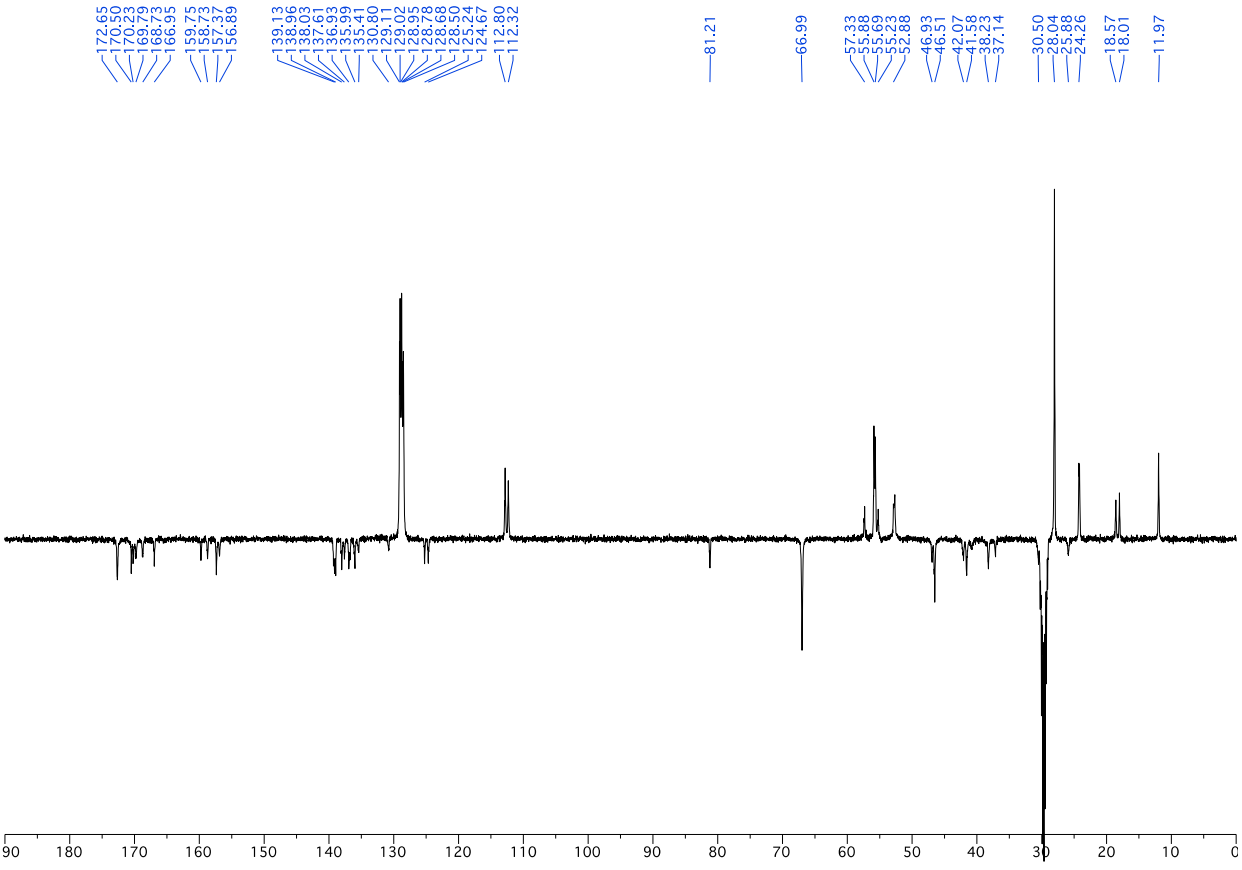

62a:

^{1}H NMR (400 MHz, DMSO-d_6)

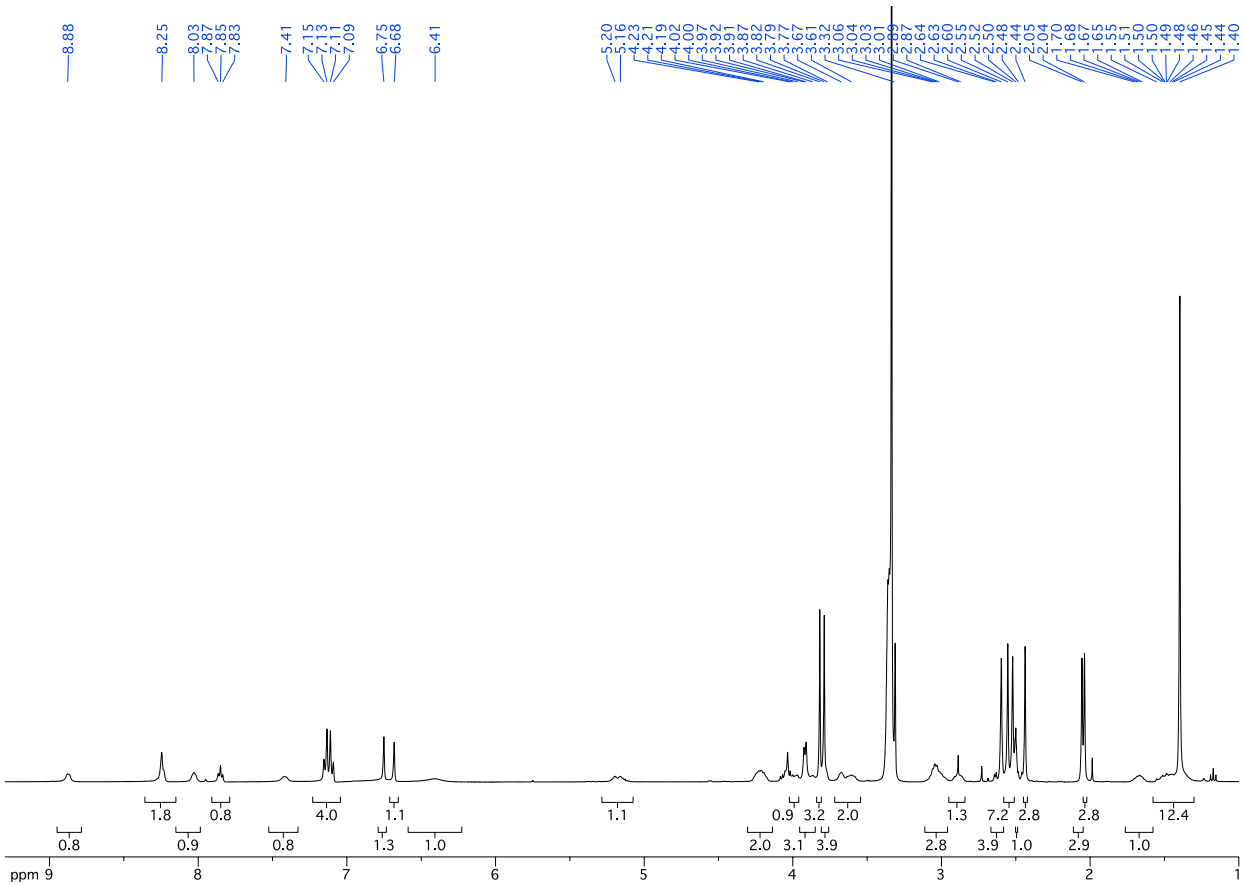

^{13}C NMR (101 MHz, DMSO-d_6)

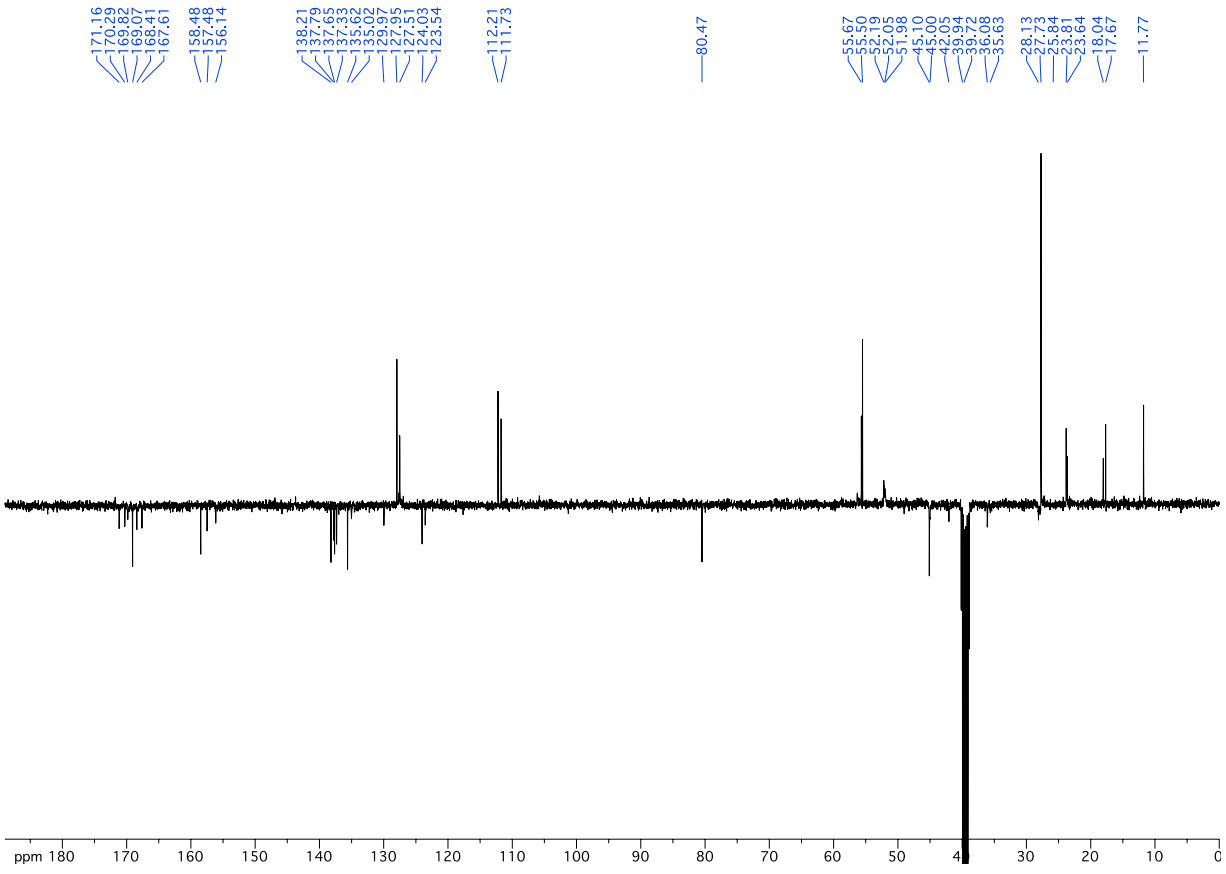

62b:

^{1}H NMR (400 MHz, CD_3OD)

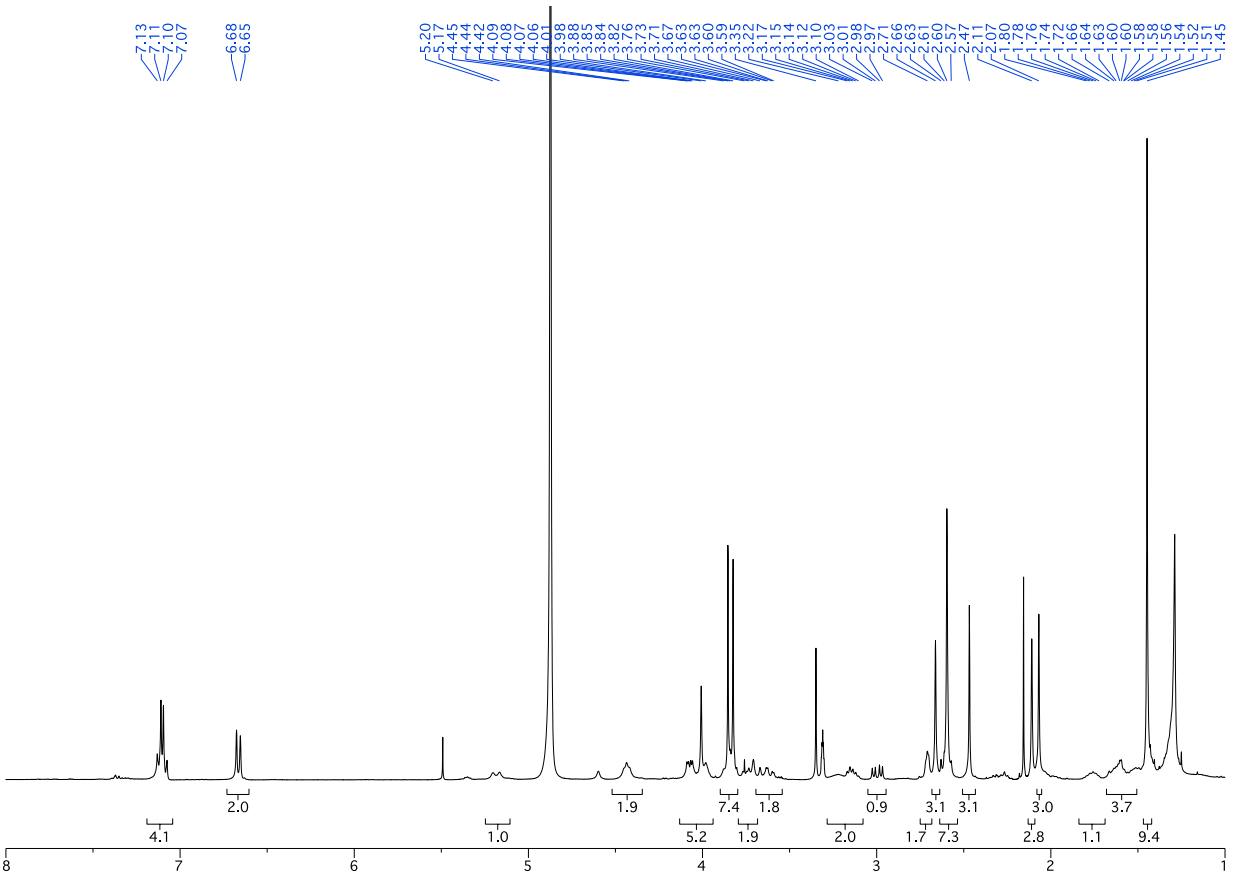

^{13}C NMR (101 MHz, CD_3OD)

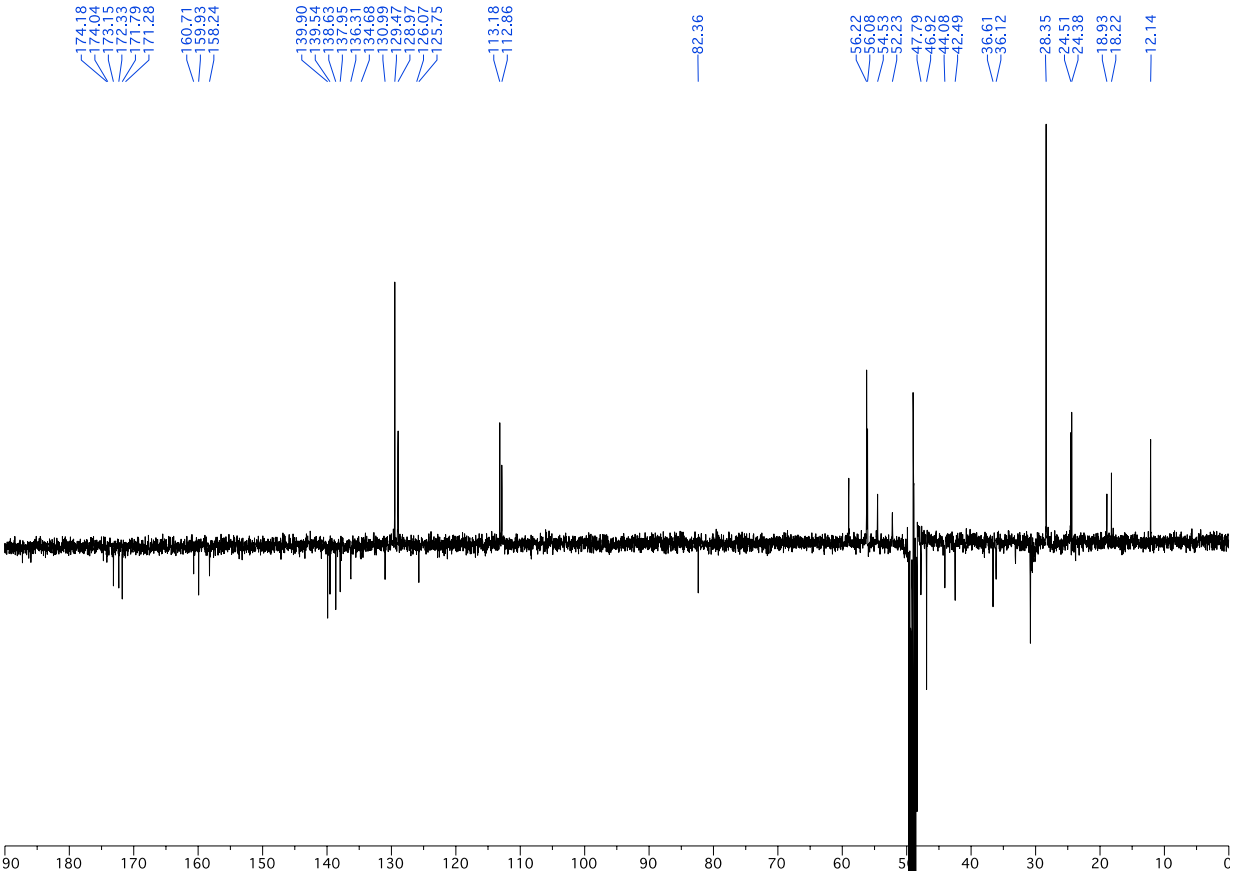

c[DKP-*f*4-RGD]:

^{1}H NMR (400 MHz, D_2O)

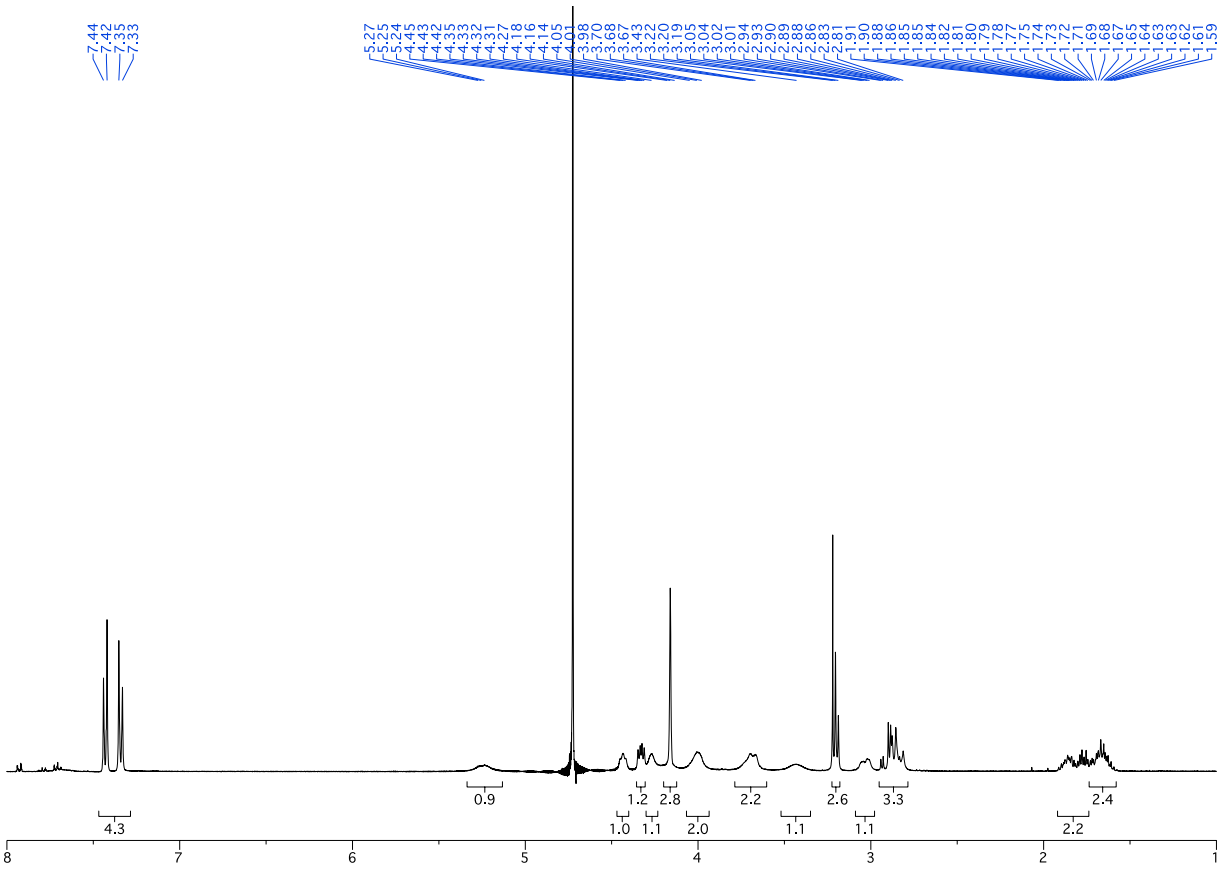

^{13}C NMR (101 MHz, D_2O)

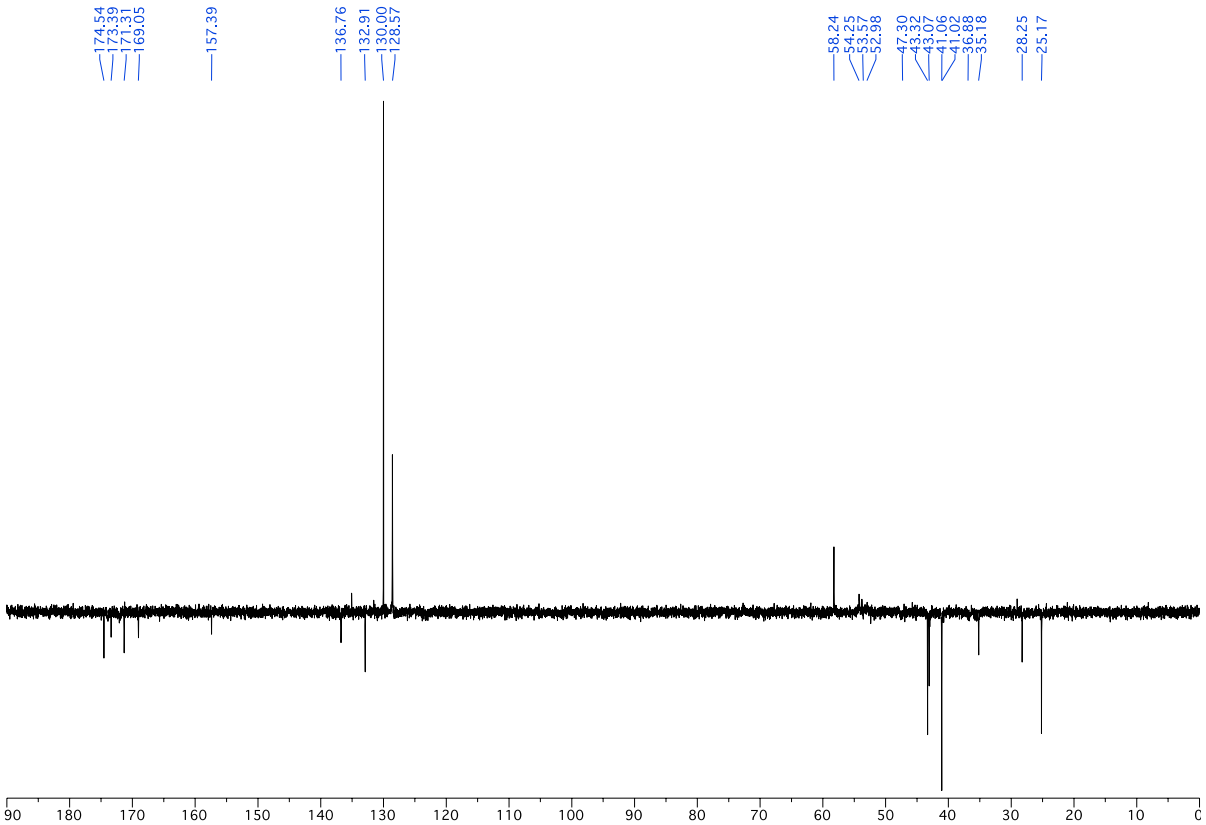

c[DKP-*f*6-RGD]:

^{1}H NMR (400 MHz, D_2O)

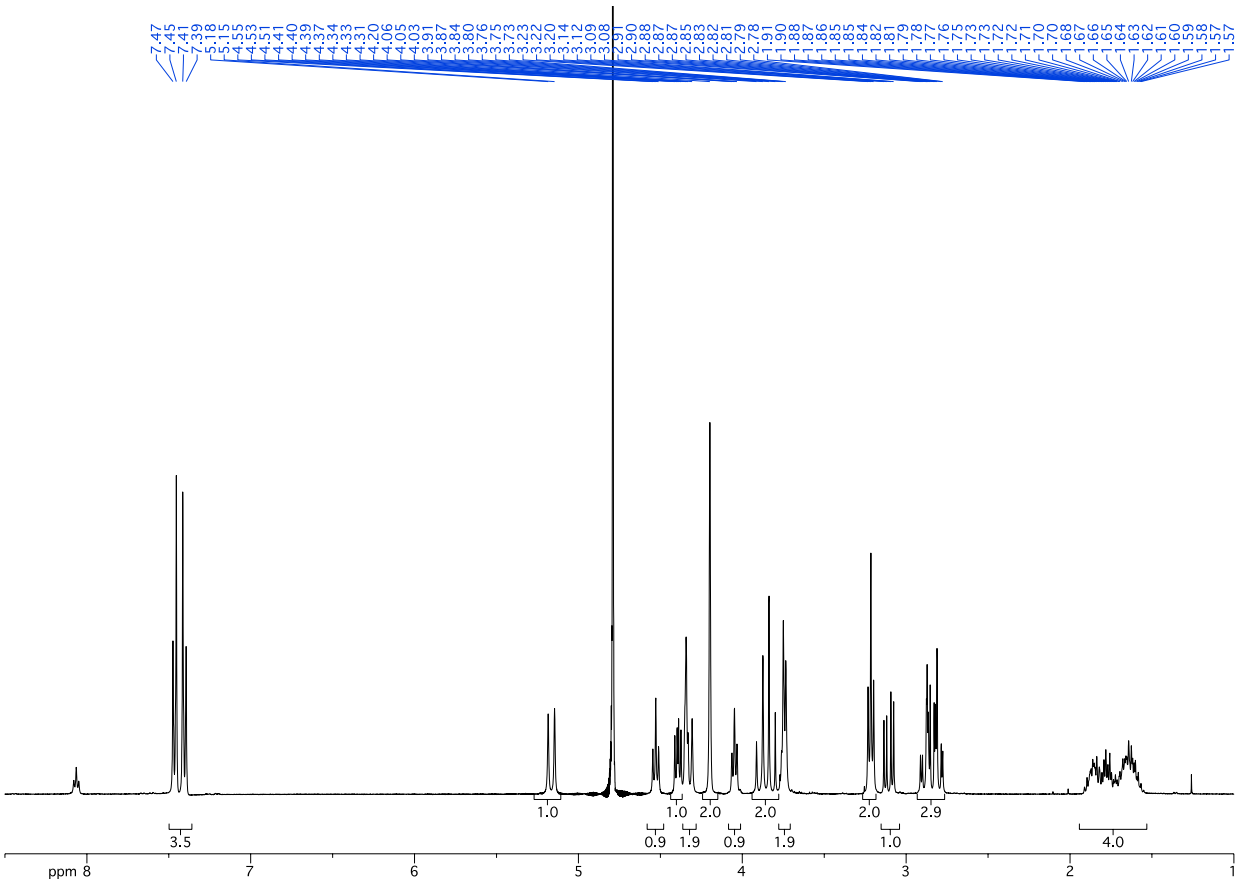

^{13}C NMR (101 MHz, D_2O)

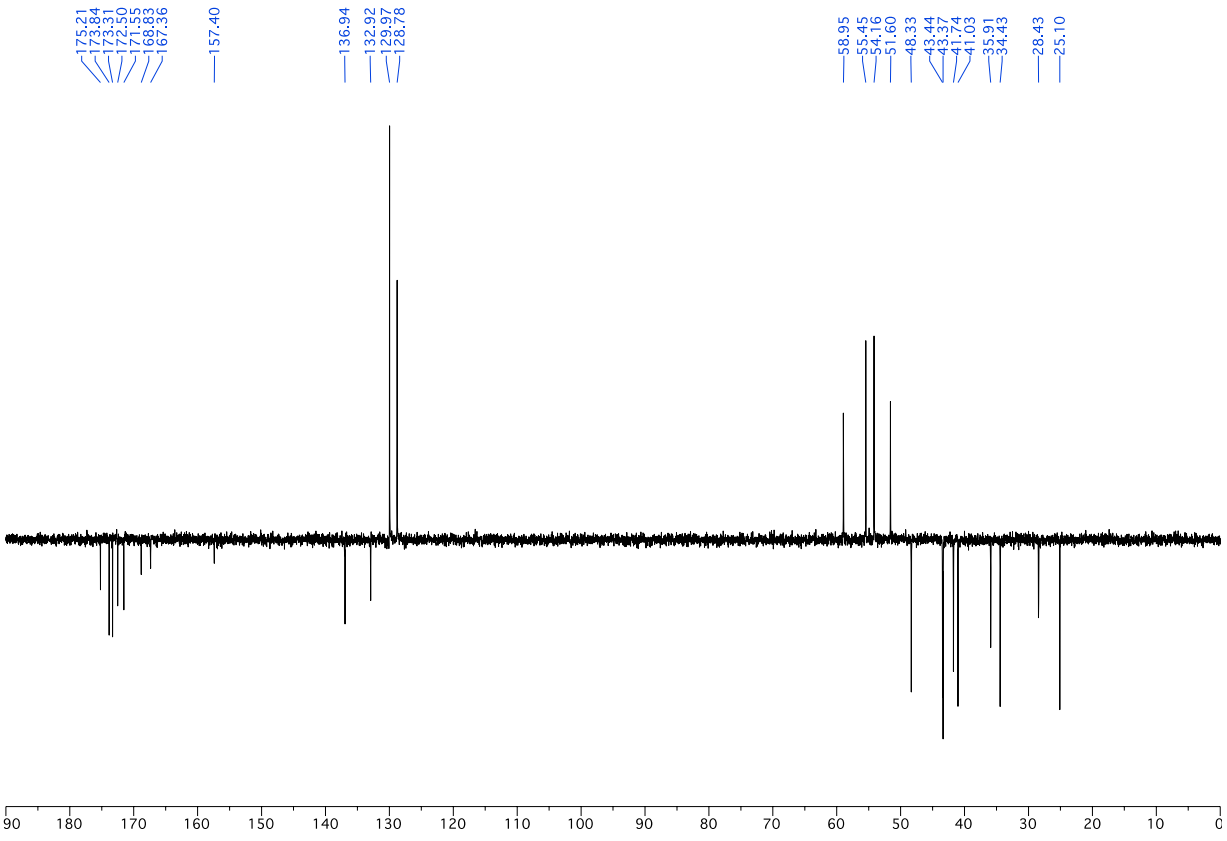

63a:

^{1}H NMR (400 MHz, $CDCl_3$)

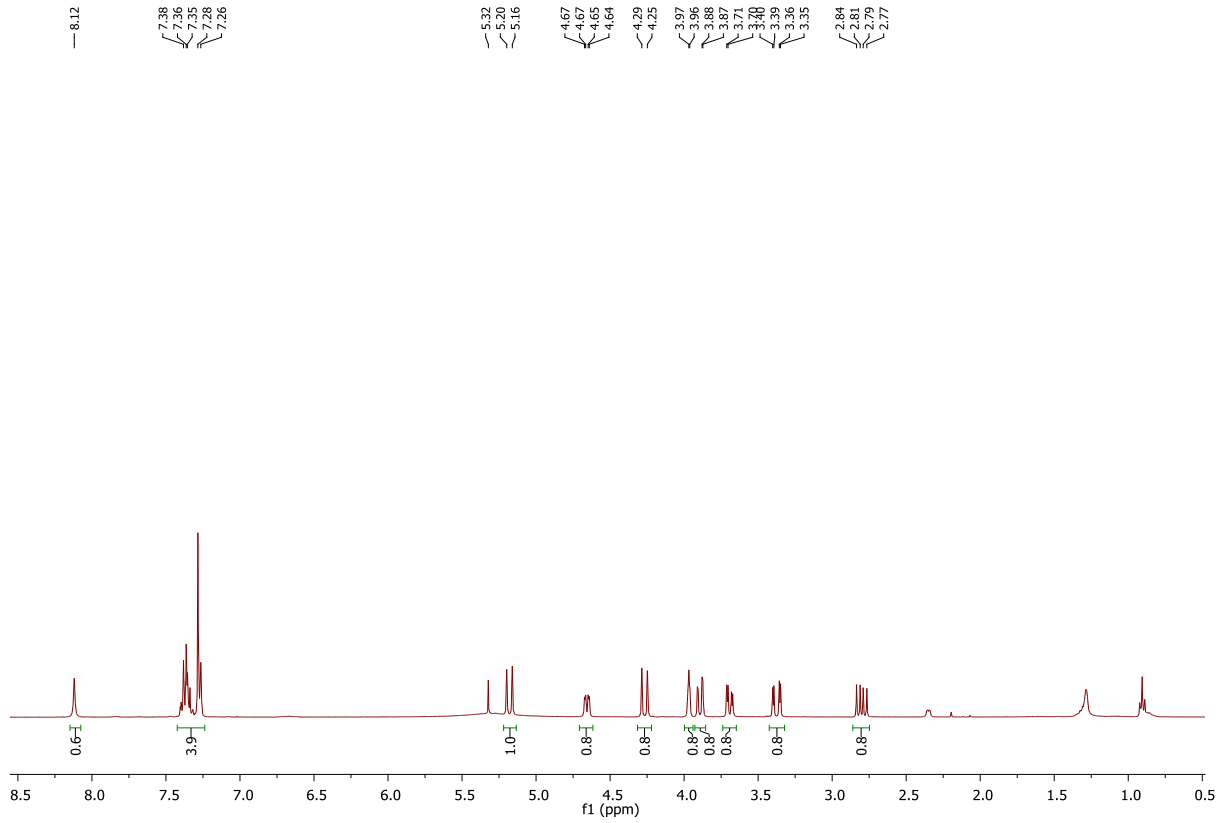

^{13}C NMR (101 MHz, $CDCl_3$)

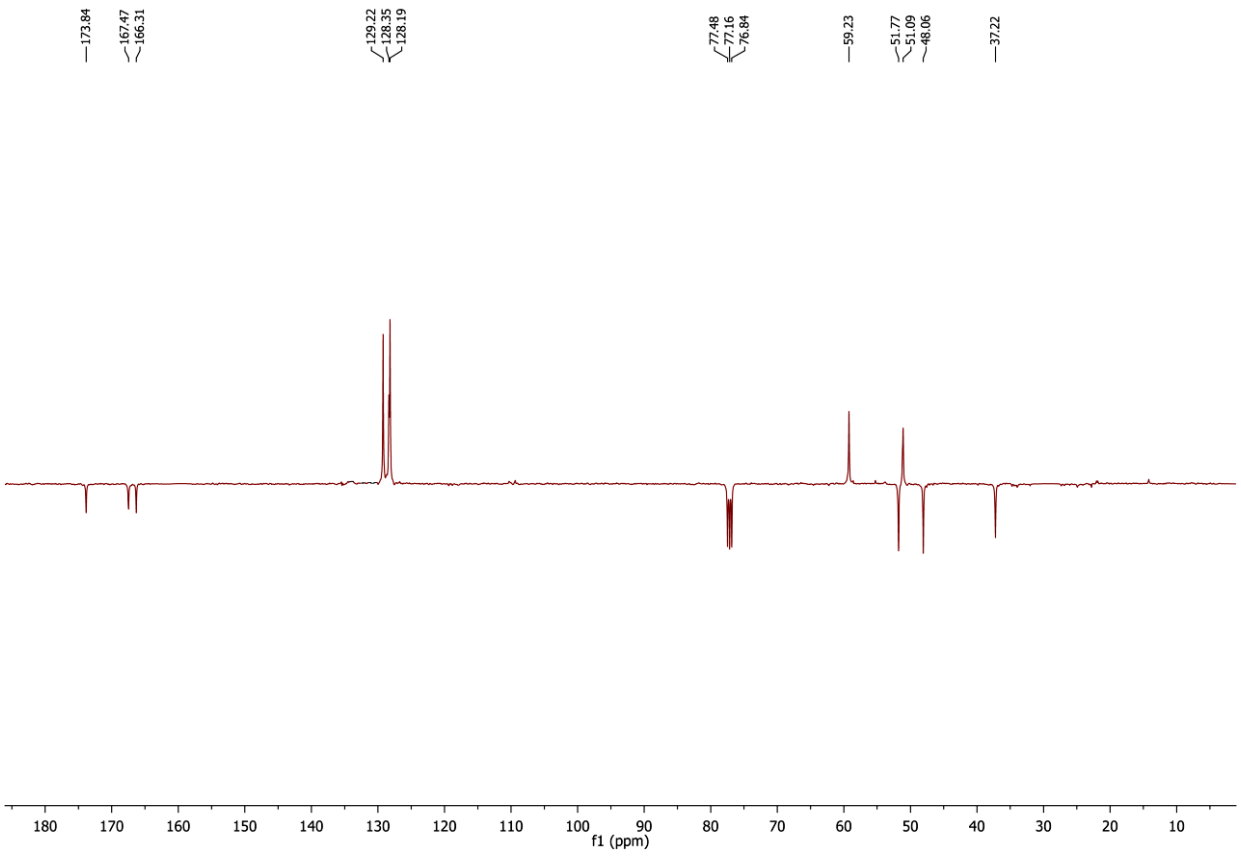

64a:

^{1}H NMR (400 MHz, CD_3OD)

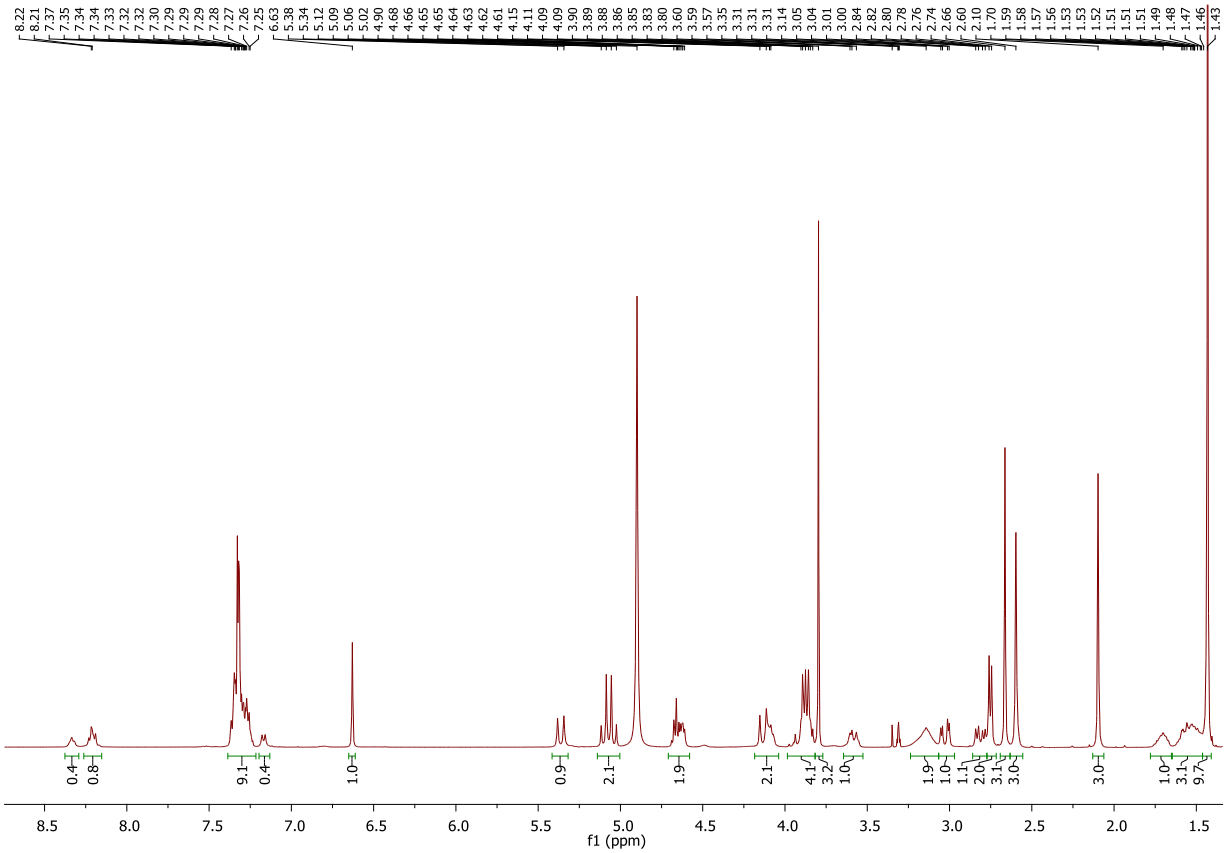

^{13}C NMR (101 MHz, CD_3OD)

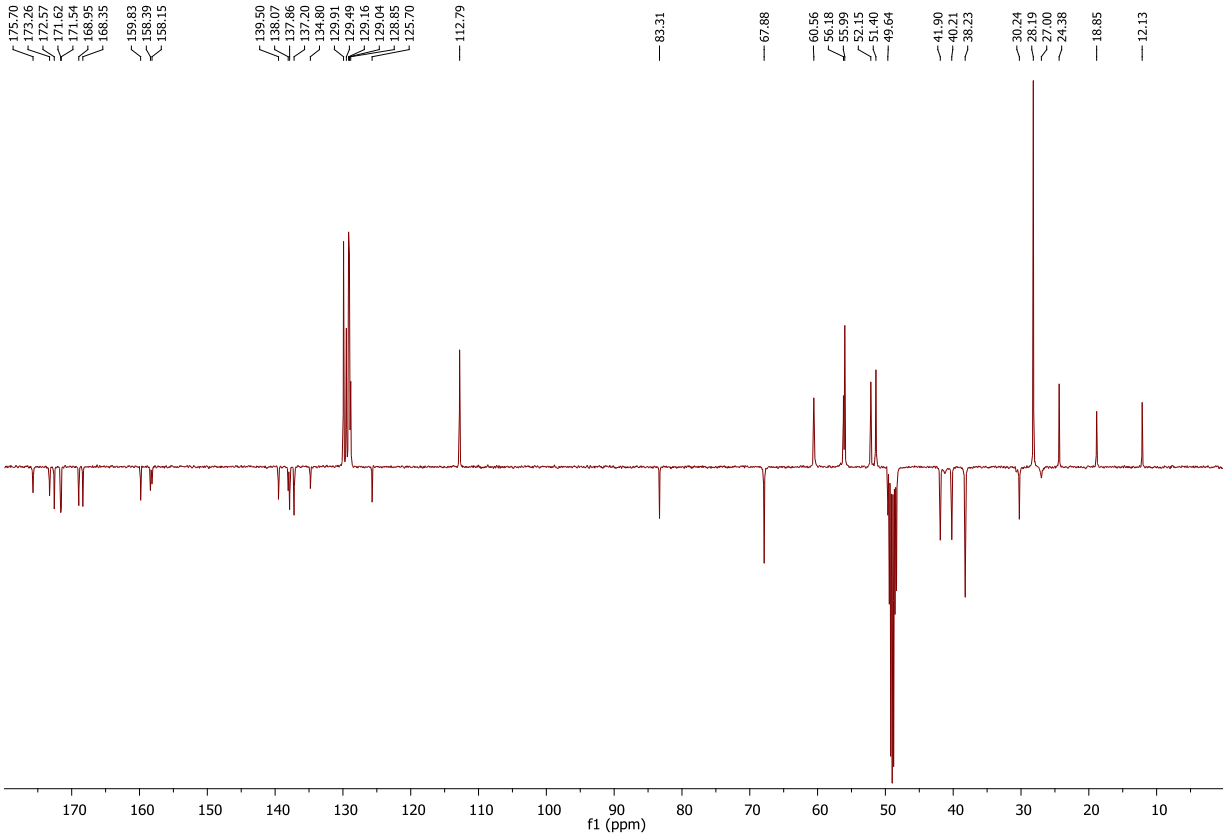

64b:

^{1}H NMR (400 MHz, CD_3OD)

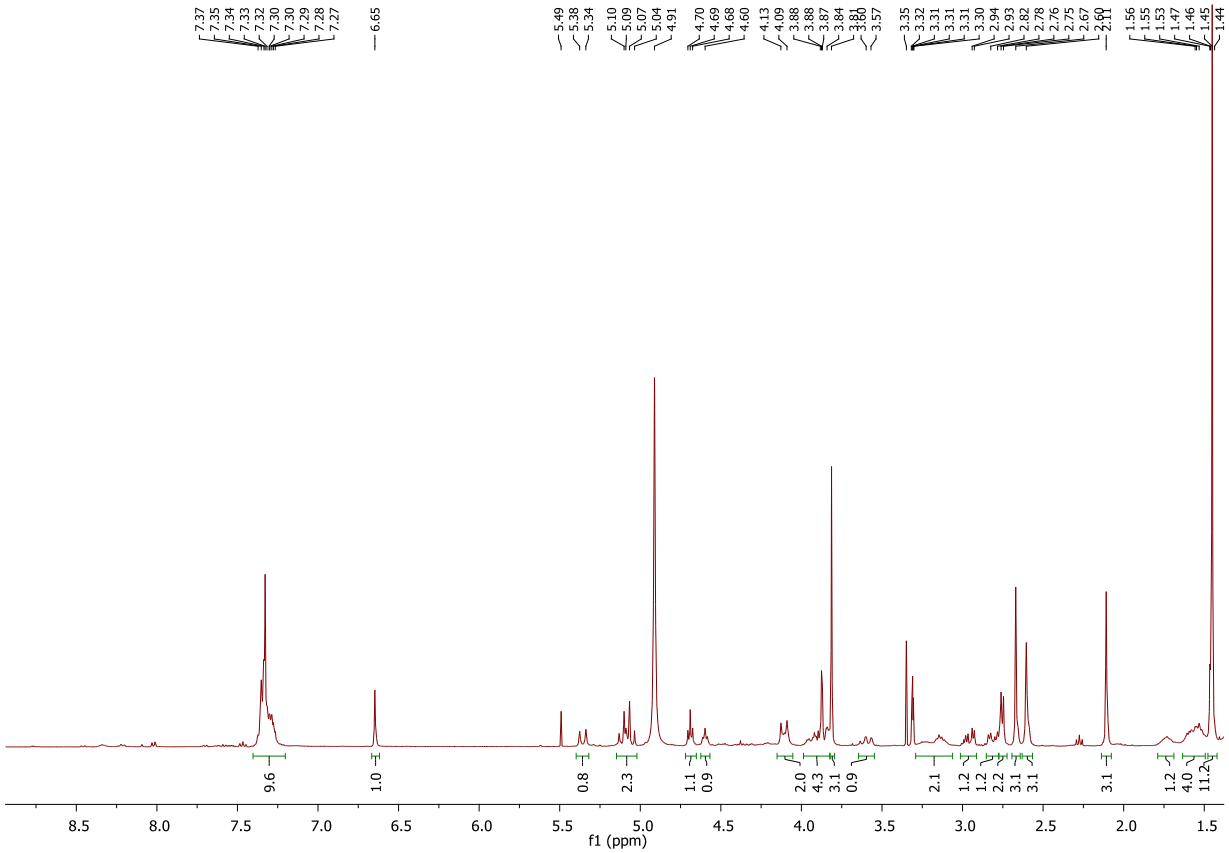

^{13}C NMR (101 MHz, CD_3OD)

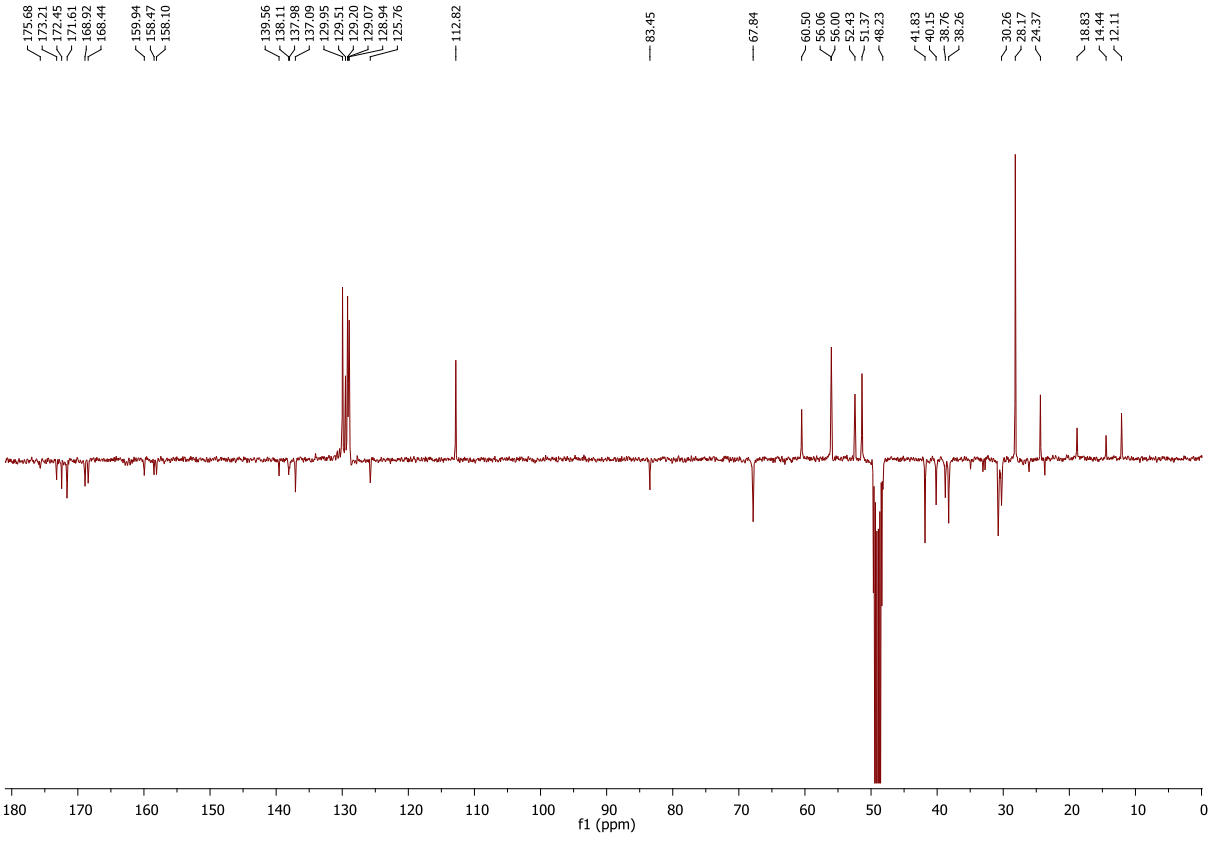

66a:

^{1}H NMR (400 MHz, CD_3OD)

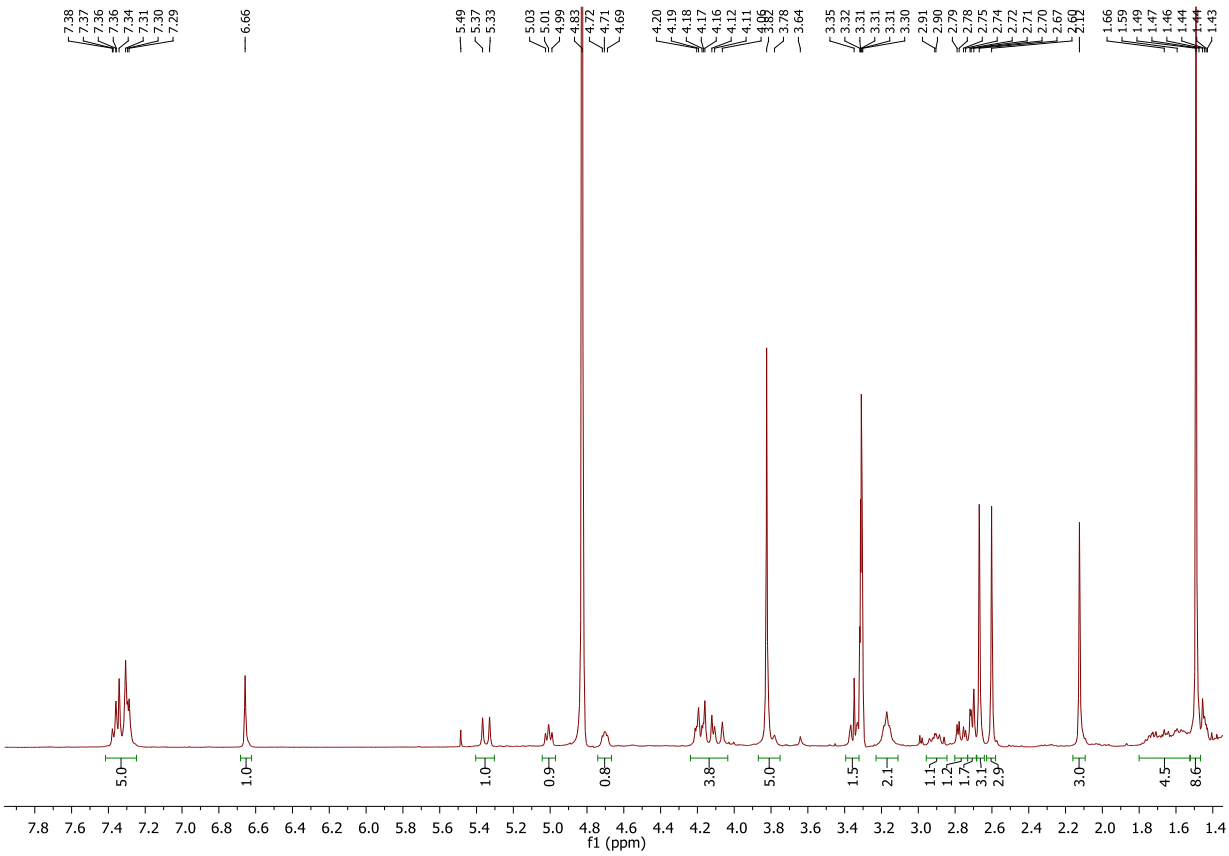

^{13}C NMR (101 MHz, CD_3OD)

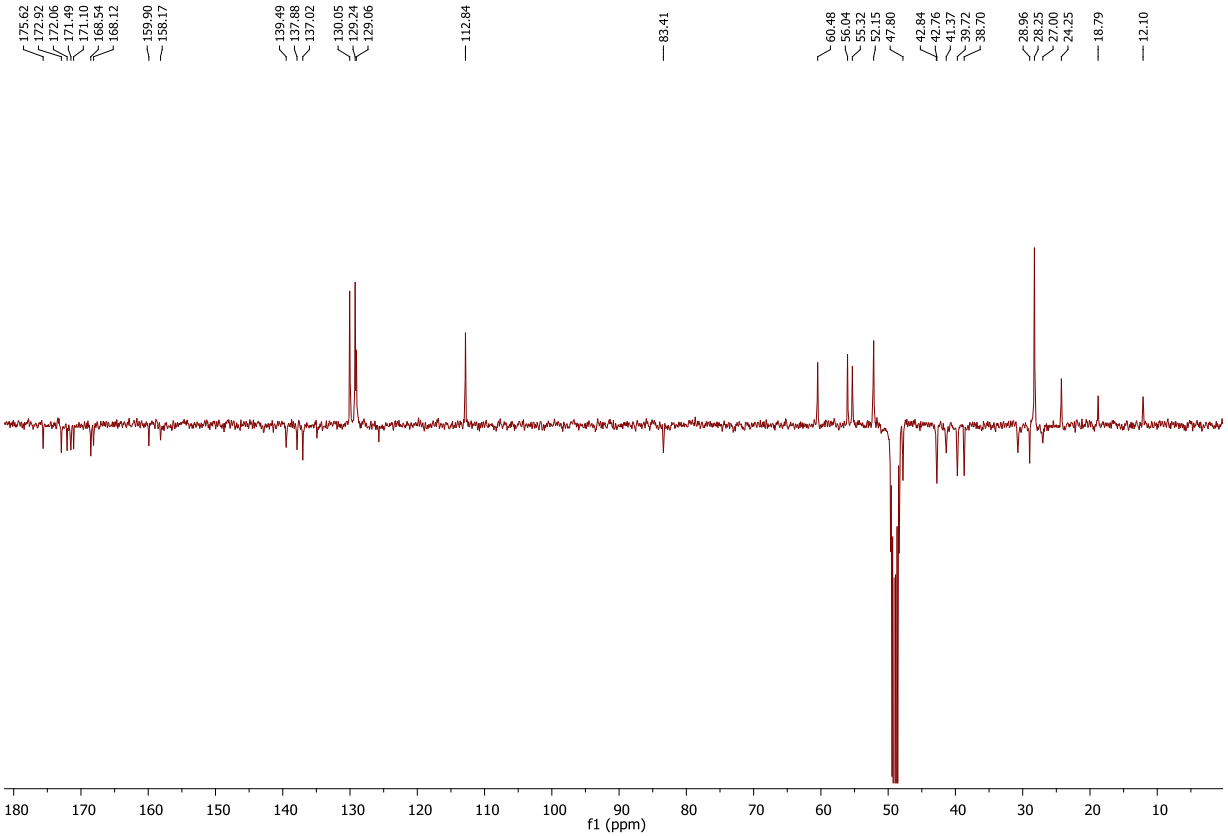

66b:

^{1}H NMR (400 MHz, CD_3OD)

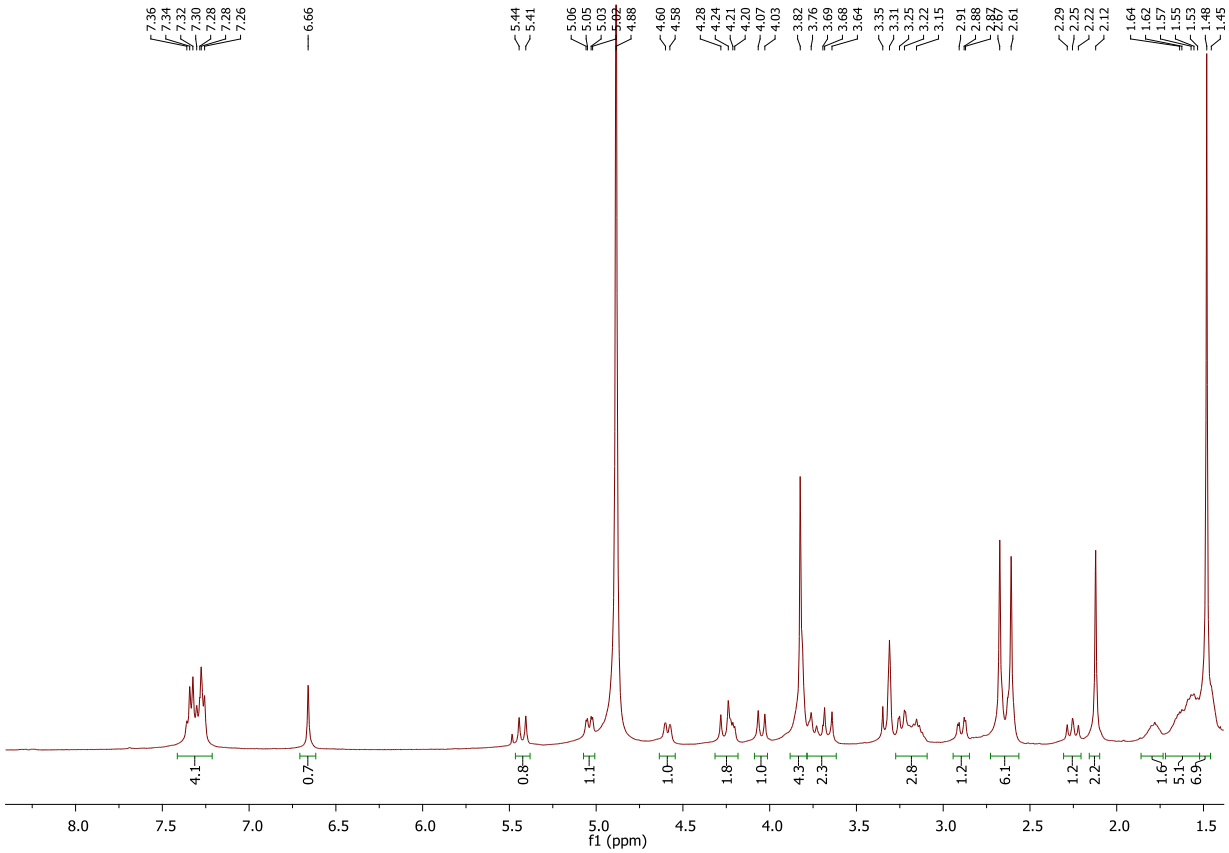

^{13}C NMR (101 MHz, CD_3OD)

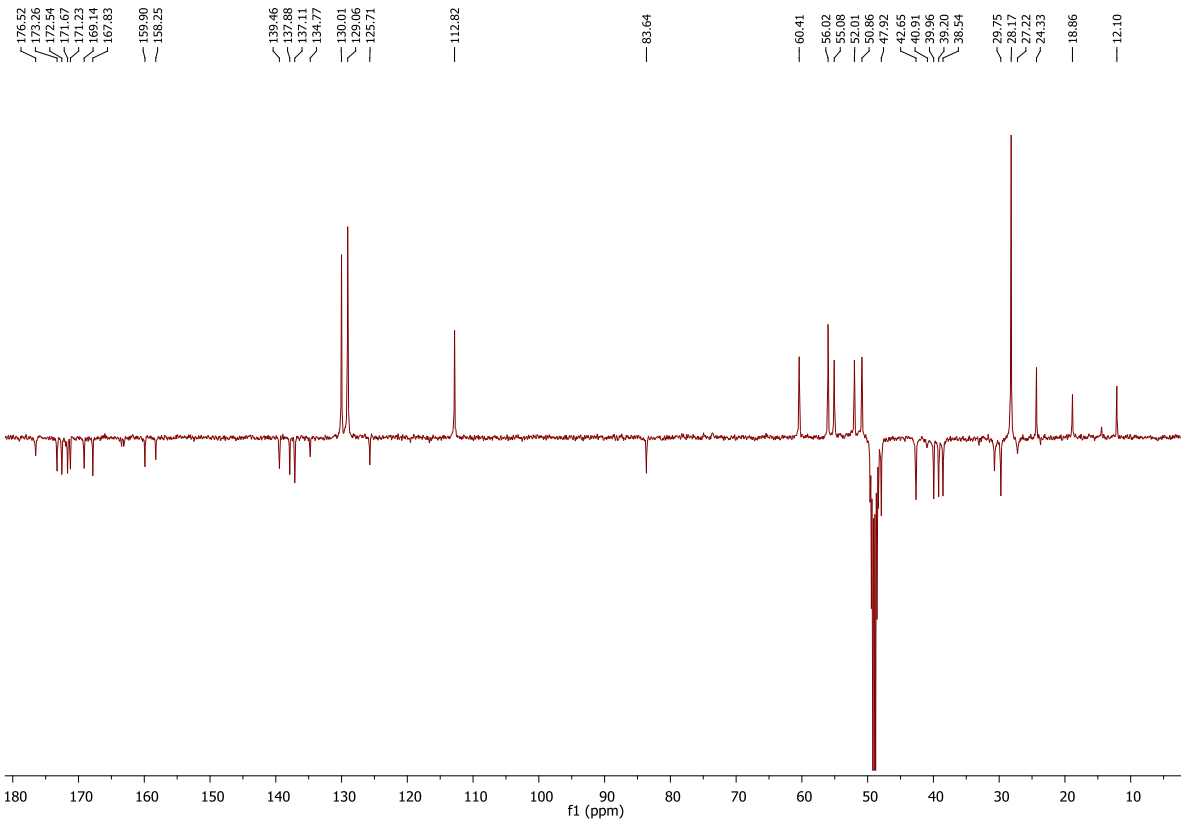

c[DKP-2-*iso*DGR]:

^{1}H NMR (400 MHz, H_2O/D_2O 9:1, T= 298K)

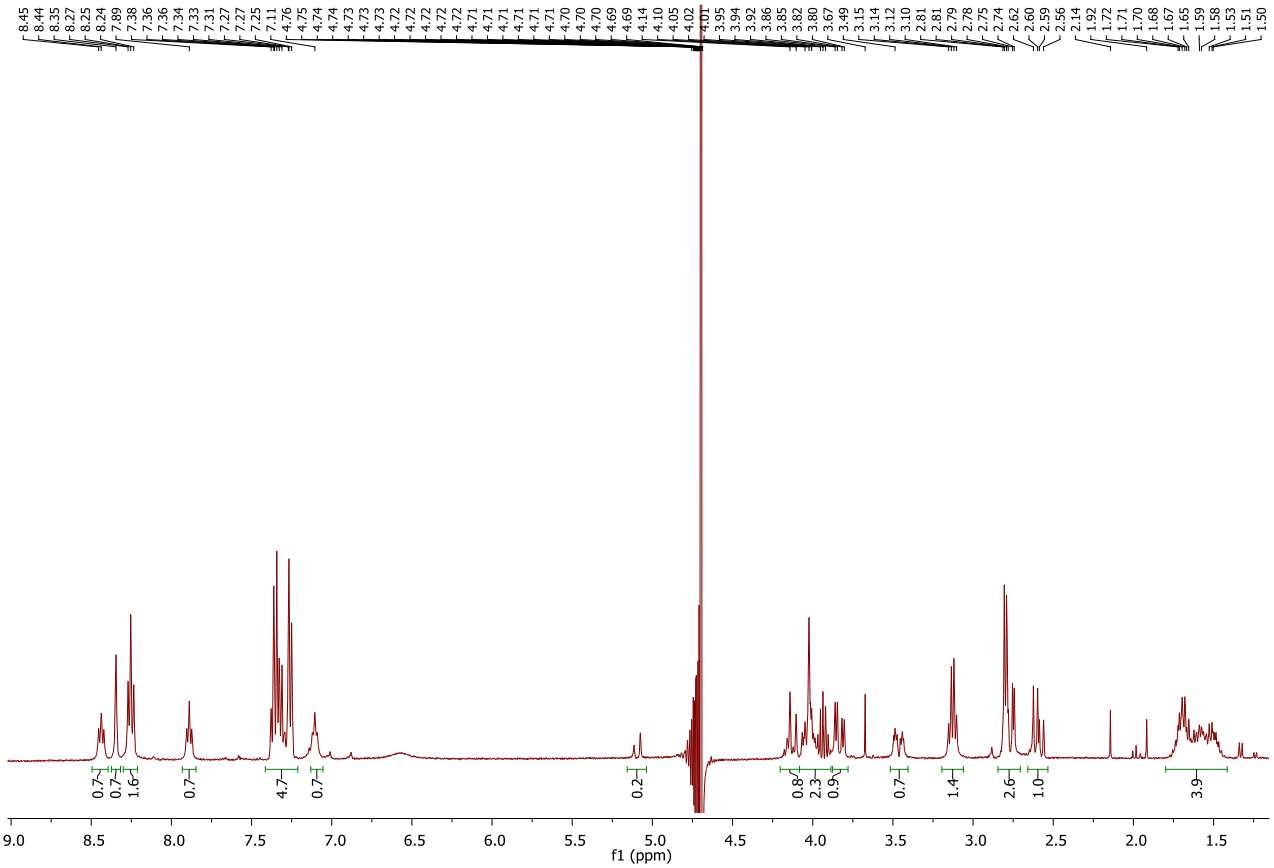

^{13}C NMR (101 MHz, D_2O, T= 298K)

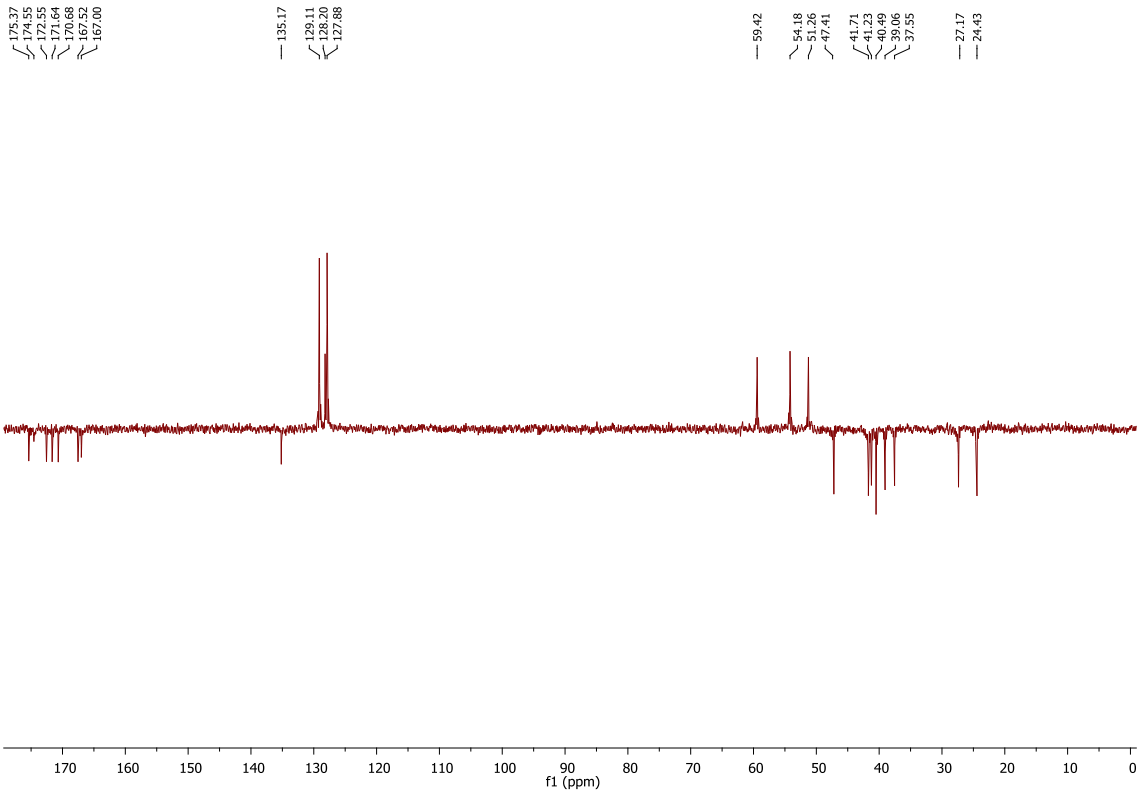

c[DKP-3-*iso*DGR]:

^{1}H NMR (400 MHz, H_2O/D_2O 9:1, T= 298K)

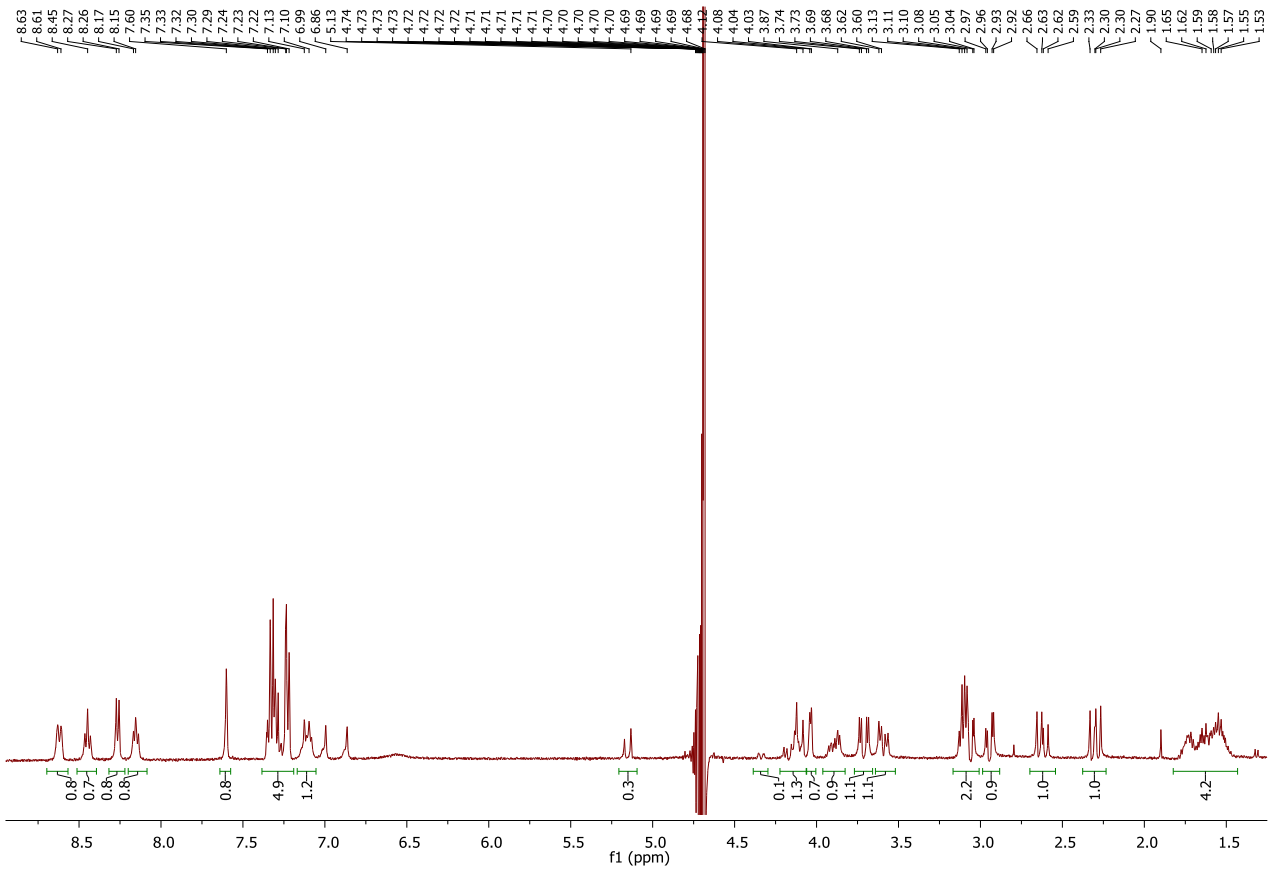

^{13}C NMR (101 MHz, D_2O, T= 298K)

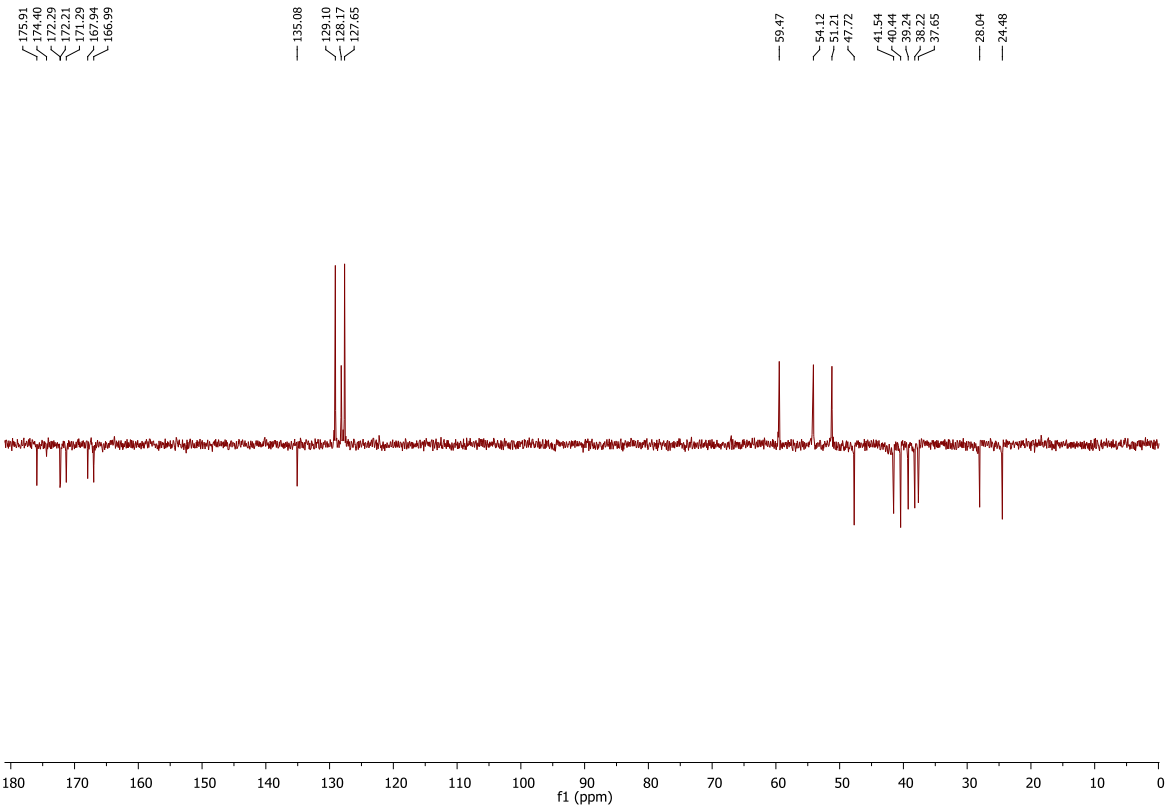

86:

^{1}H NMR (400 MHz, $CDCl_3$)

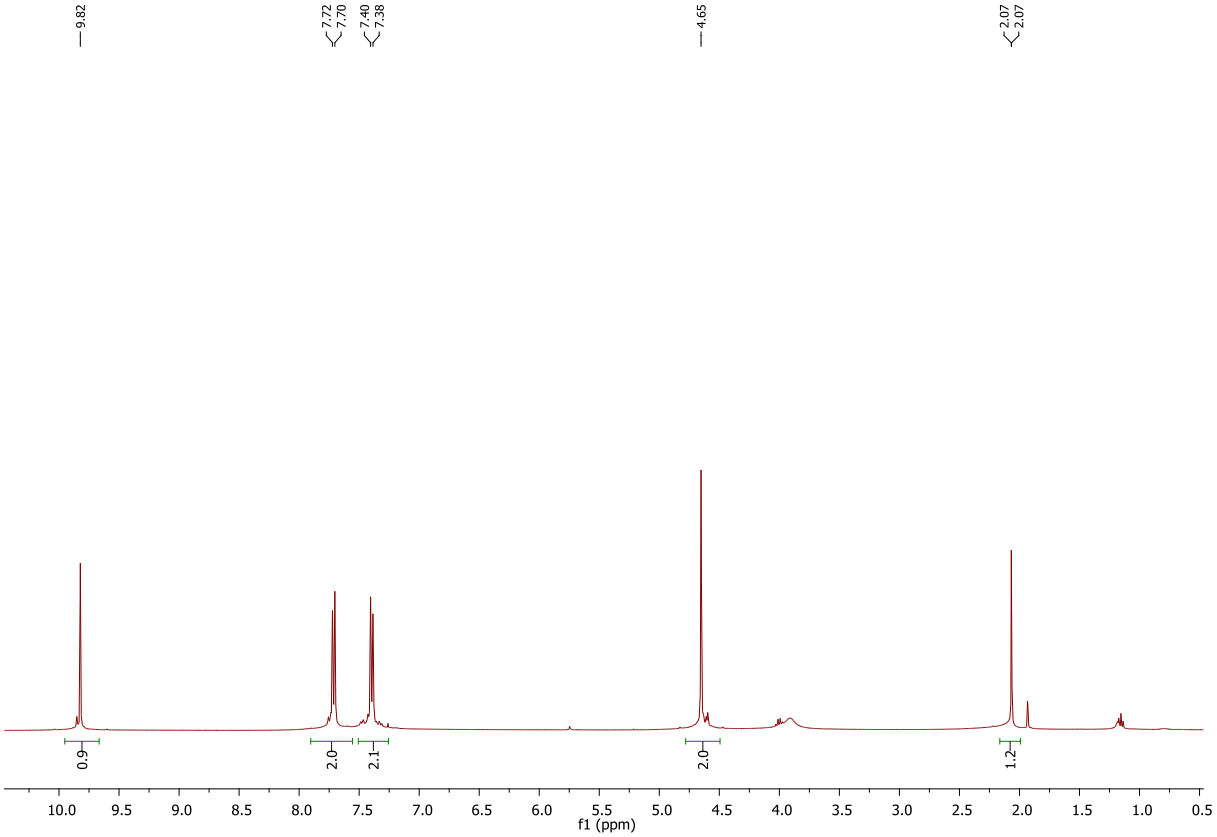

^{13}C NMR (101 MHz, CD_2Cl_2)

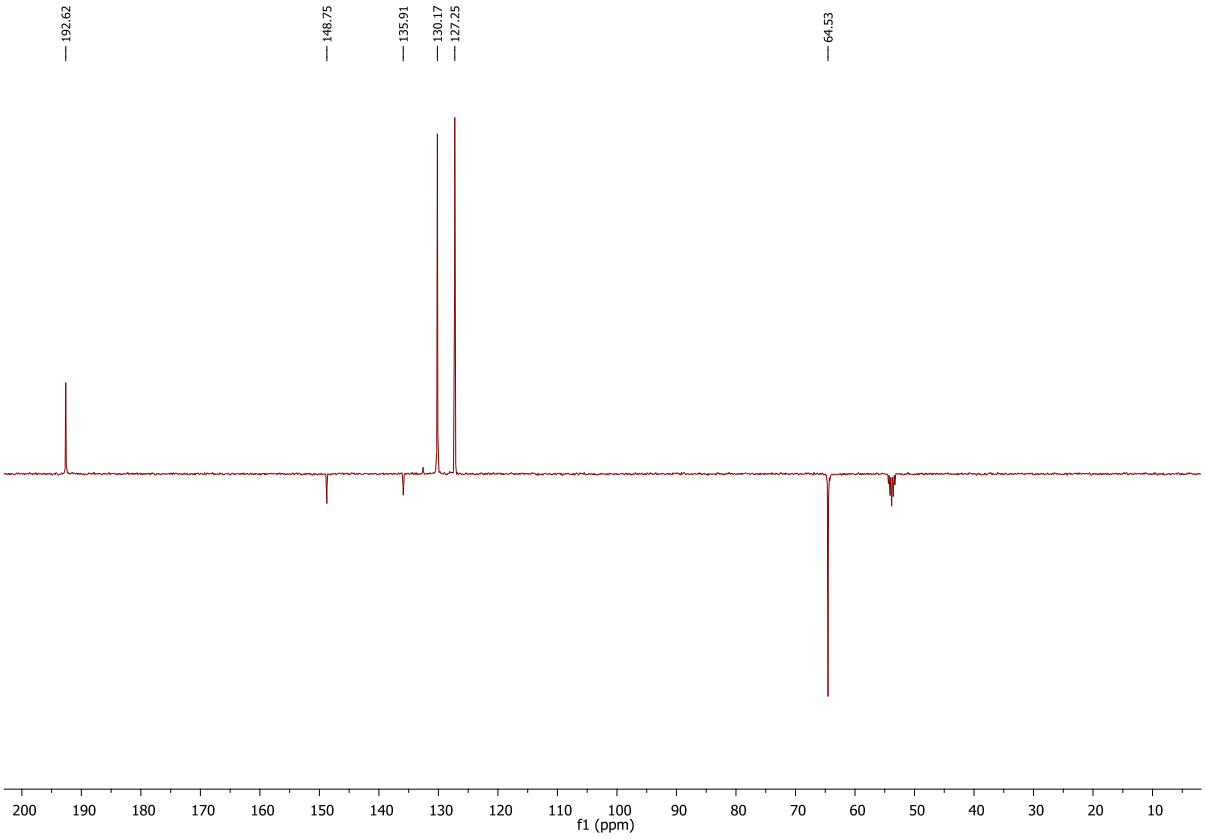

87:

^{1}H NMR (400 MHz, $CDCl_3$)

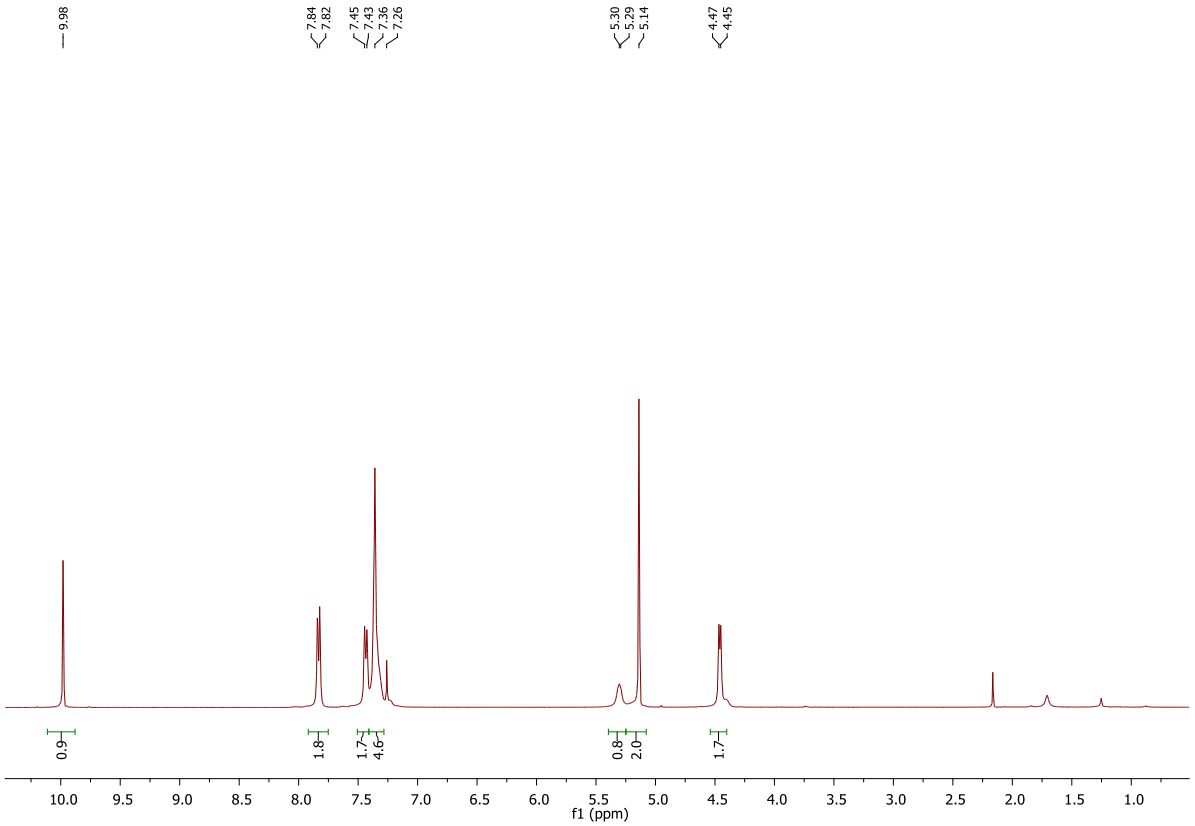

^{13}C NMR (101 MHz, CD_2Cl_2)

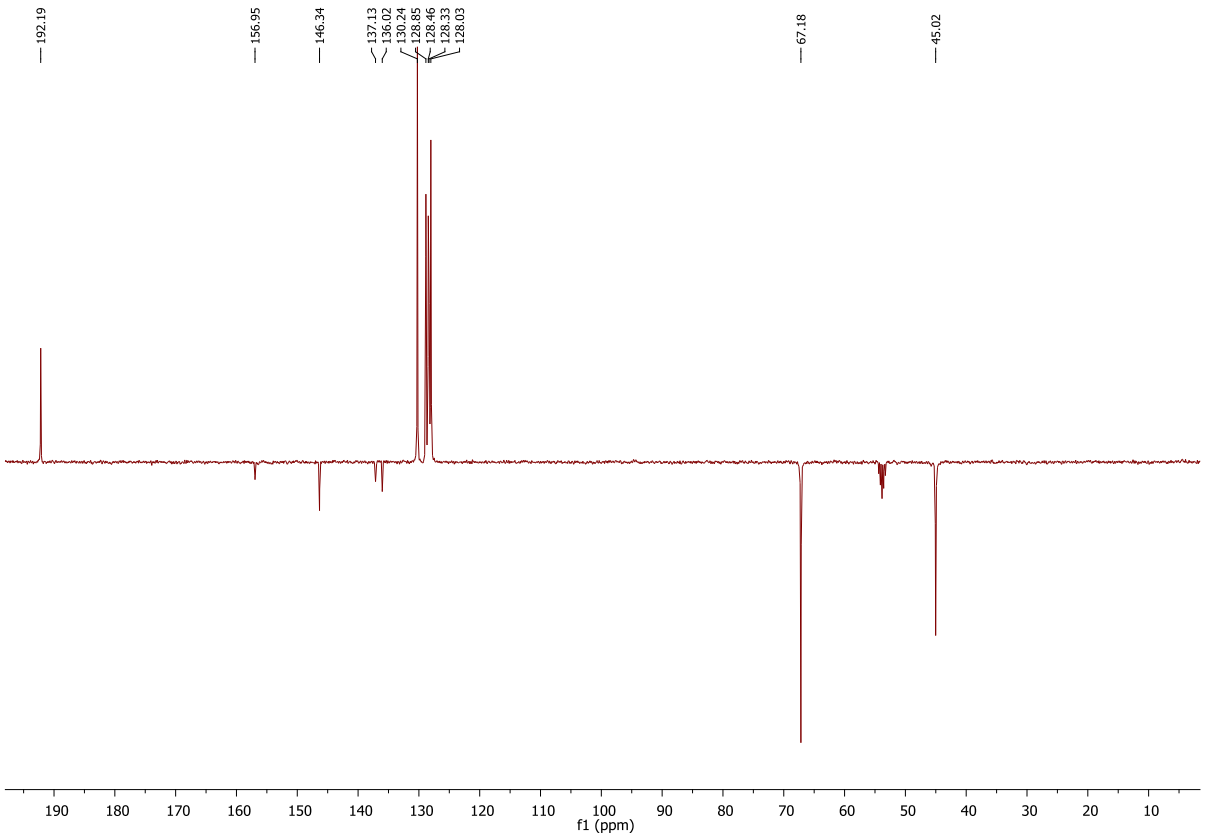

89:

^{1}H NMR (400 MHz, THF-d_8)

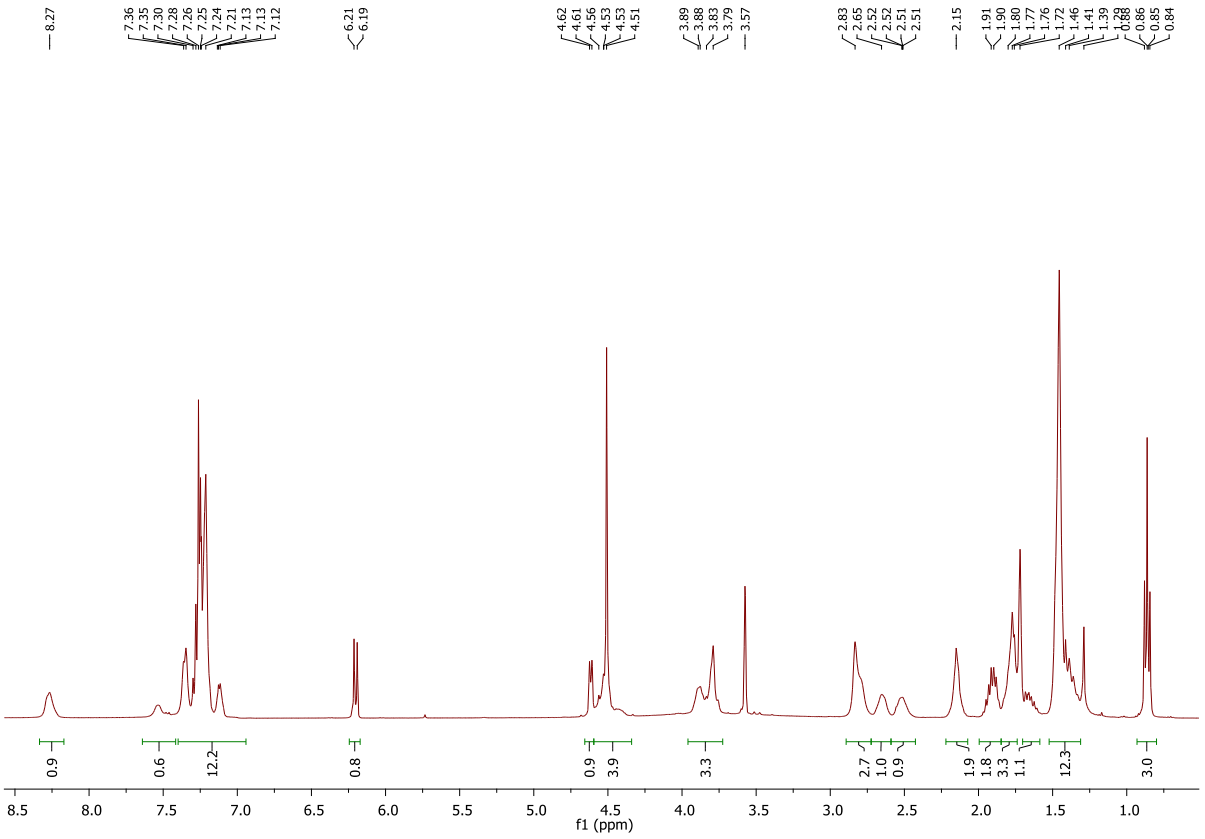

13

C NMR (101 MHz, THF-d_8)

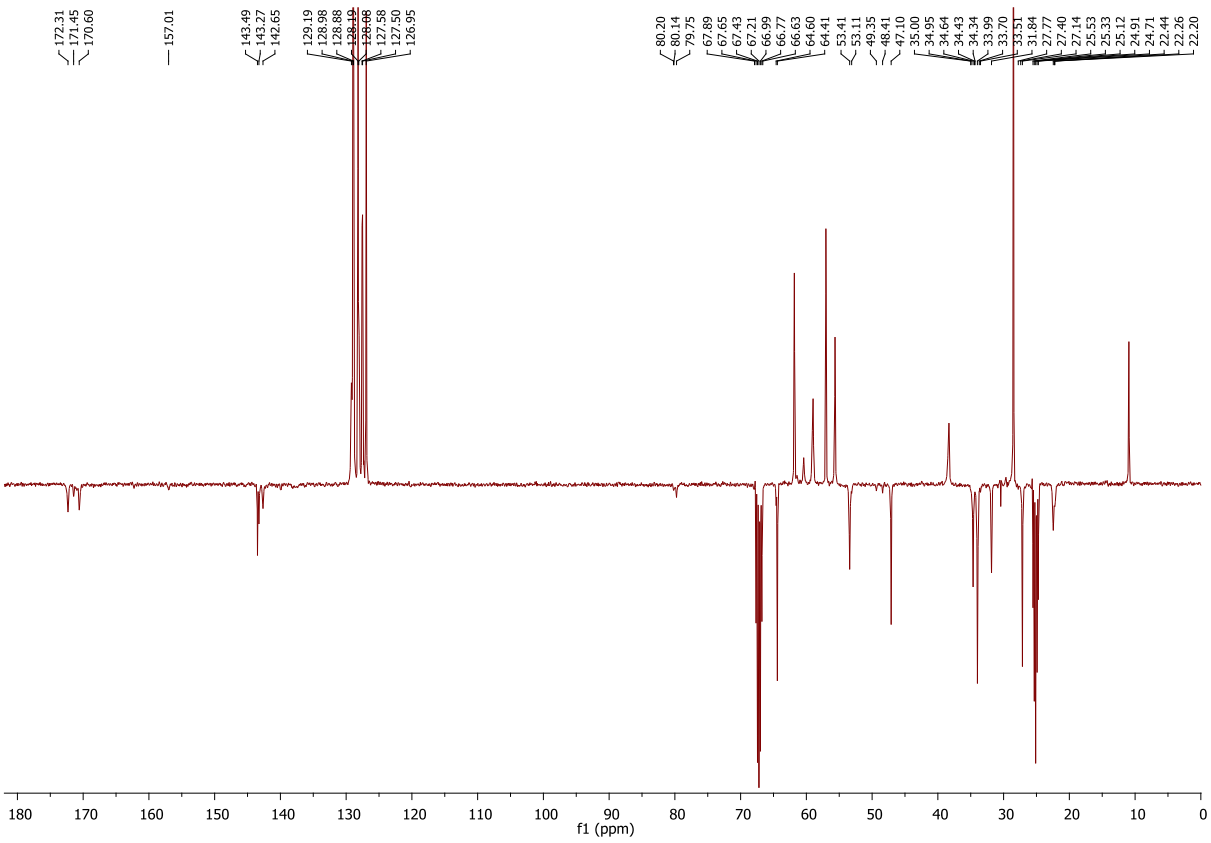

90:

^{1}H NMR (400 MHz, acetone-d_6)

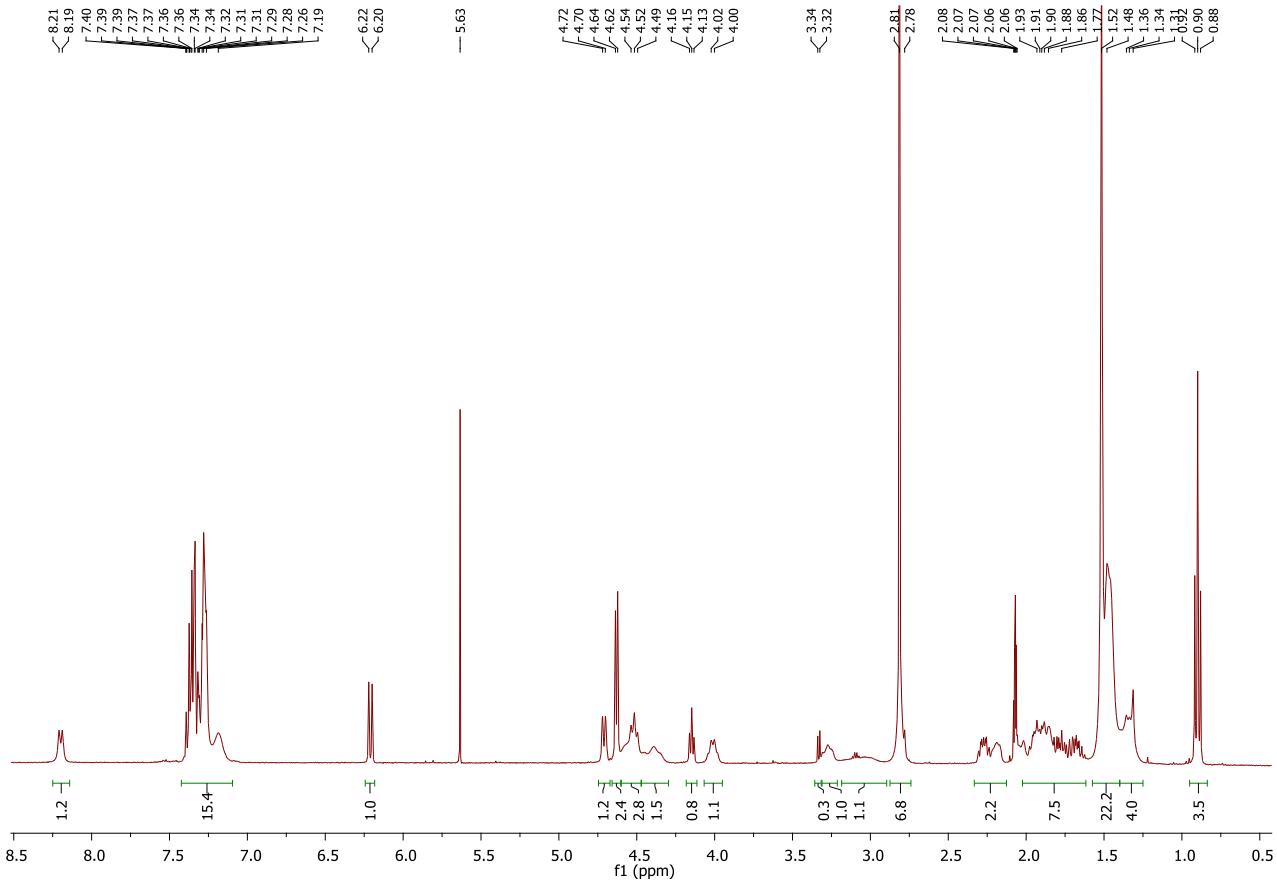

91:

^{1}H NMR (400 MHz, acetone-d_6)

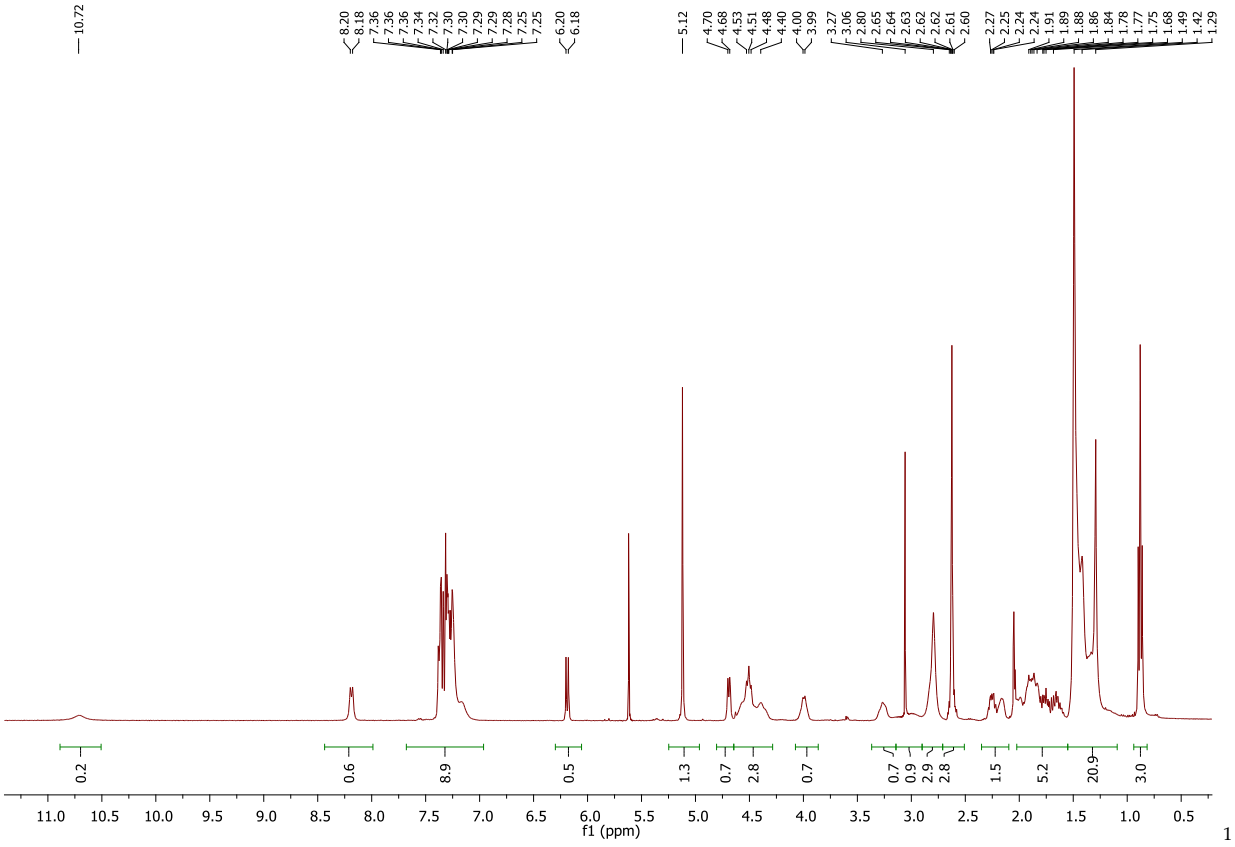

1

^{3}C NMR (101 MHz, acetone-d_6)

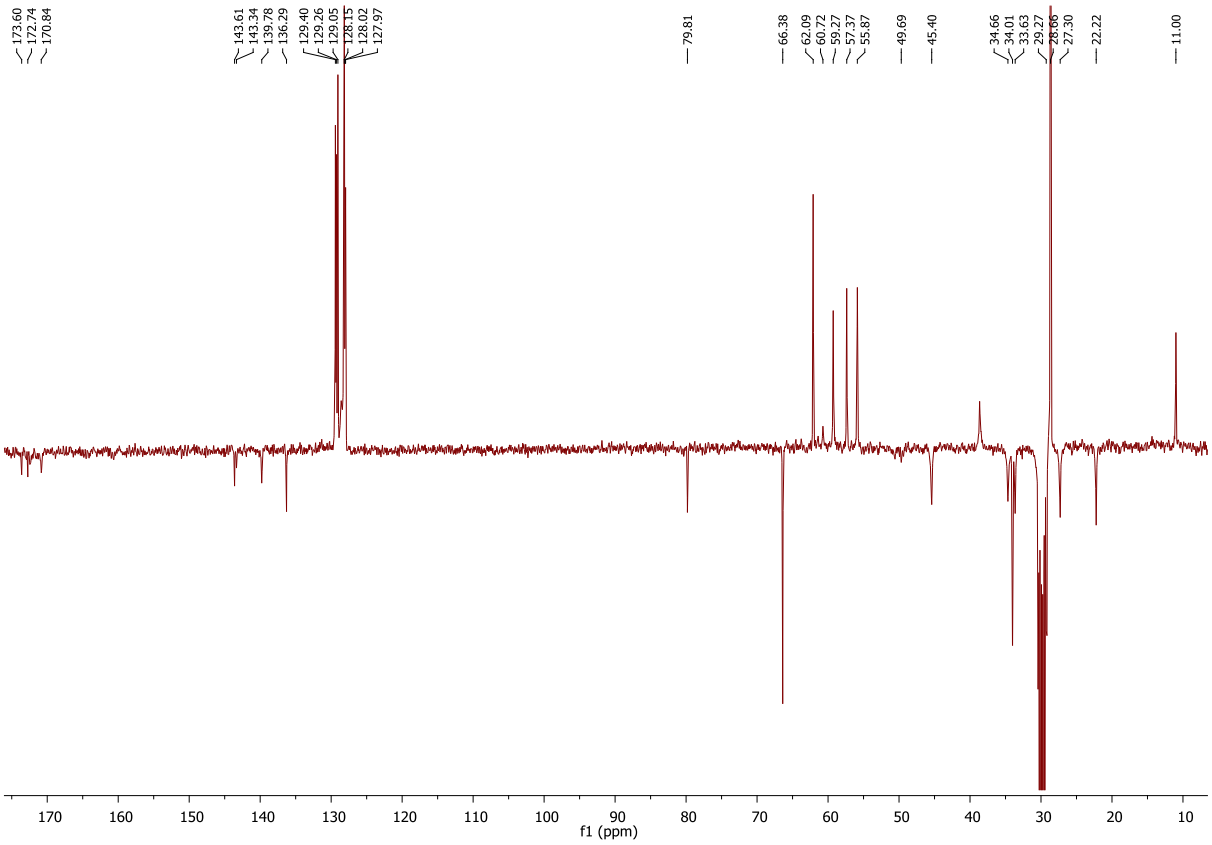

92:

^{1}H NMR (400 MHz, CD_3OD)

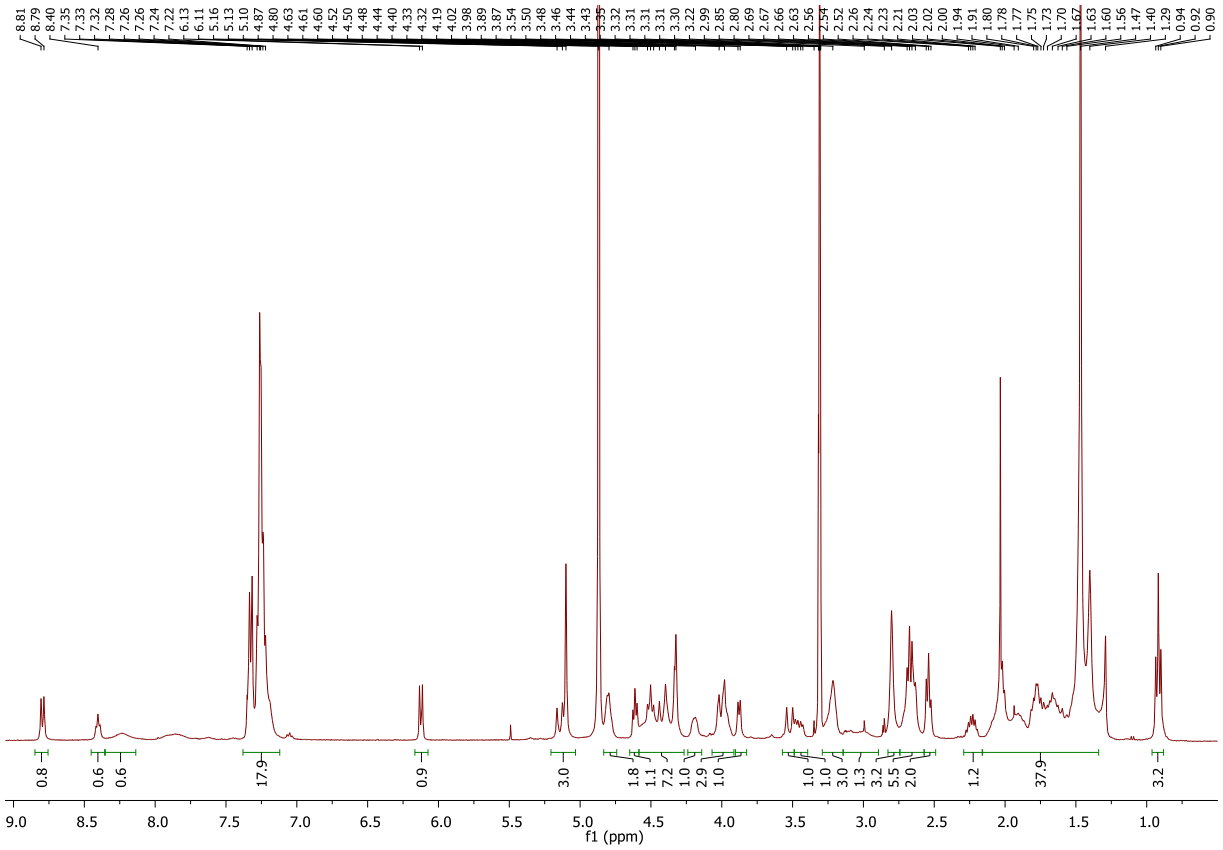

1

^{3}C NMR (101 MHz, CD_3OD)

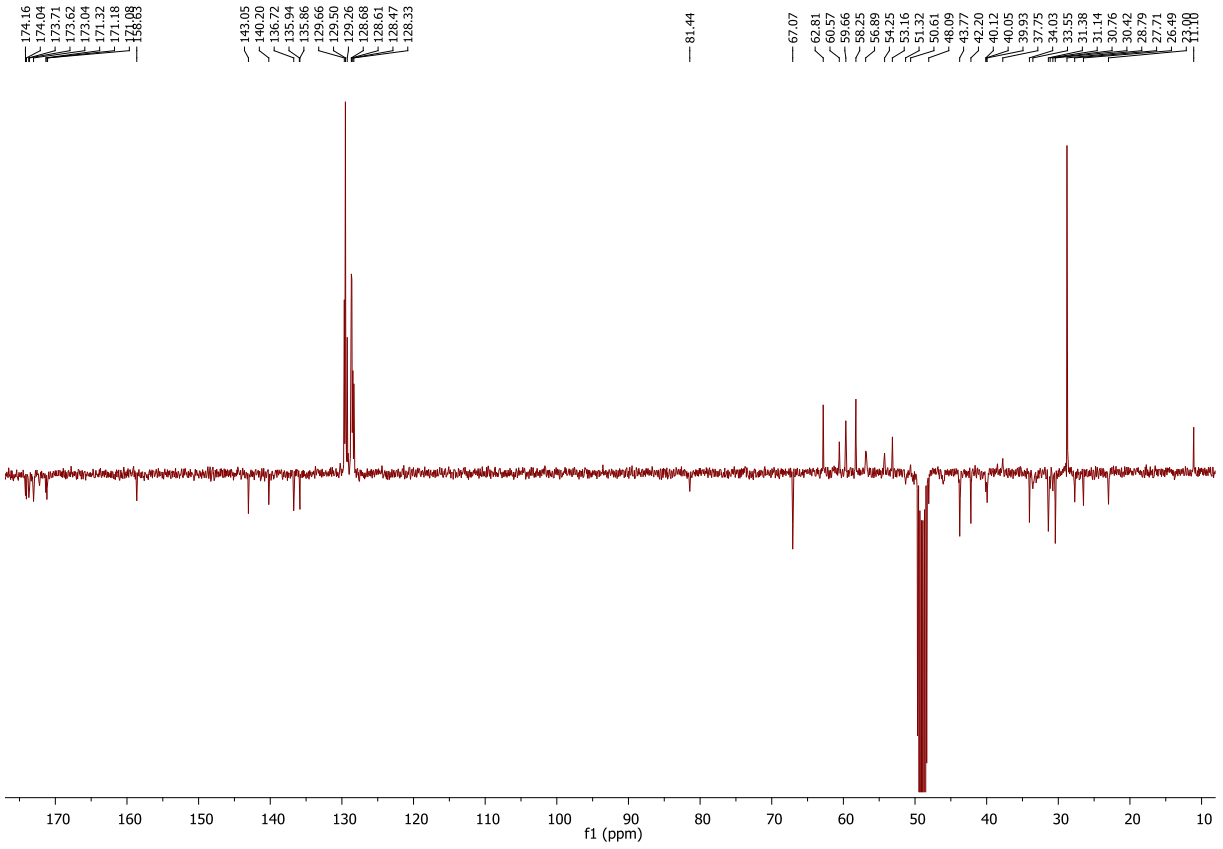

c[DKP-RGD]-O-SMAC:

^{1}H NMR (400 MHz, CD_3CN)

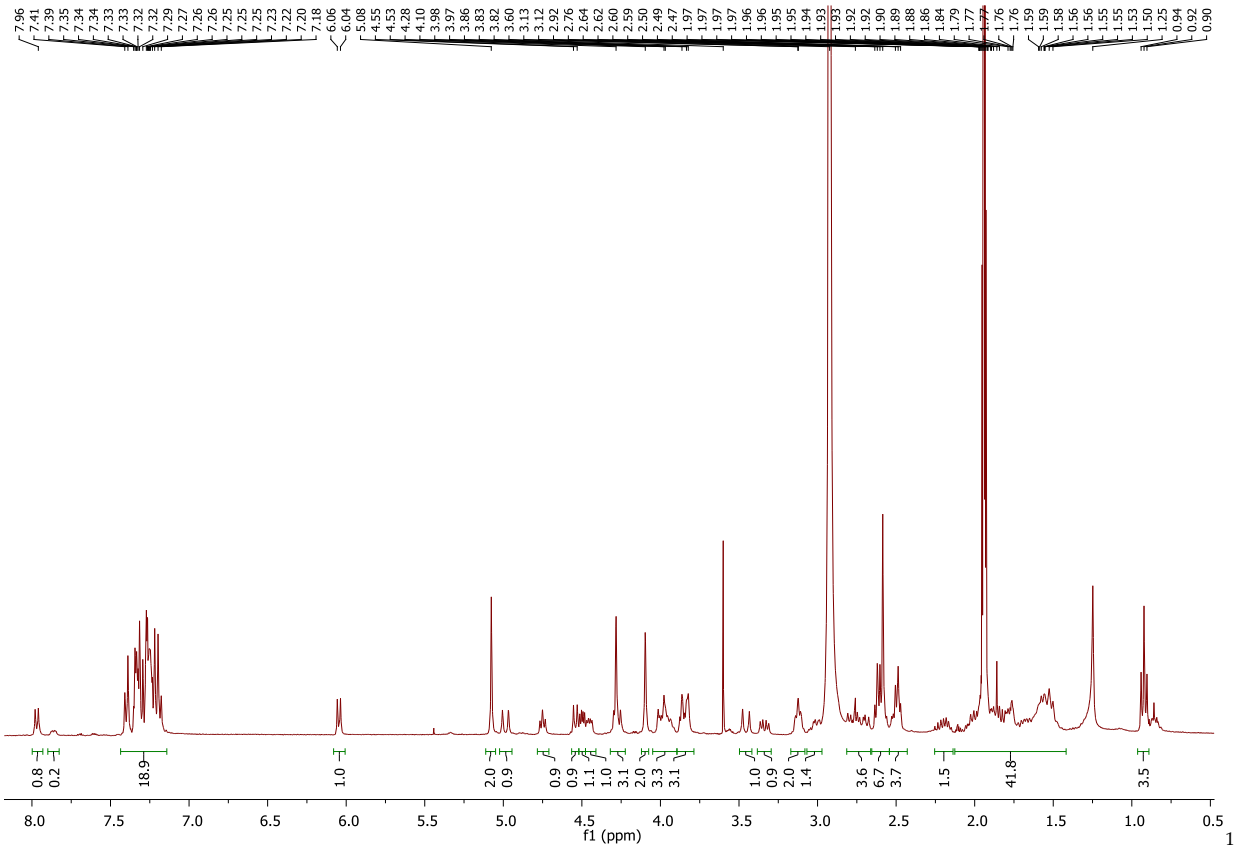

^{3}C NMR (101 MHz, CD_3CN)

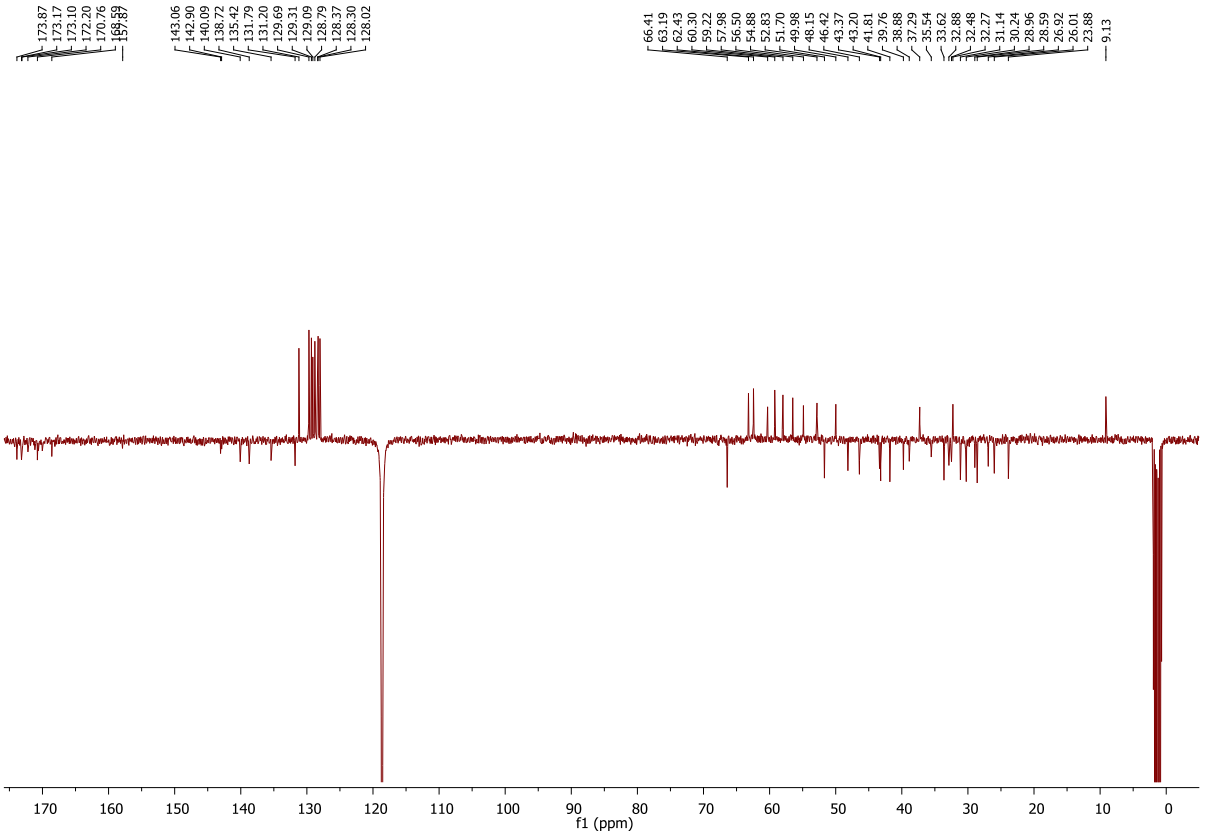

93:

^{1}H NMR (400 MHz, CD_2Cl_2)

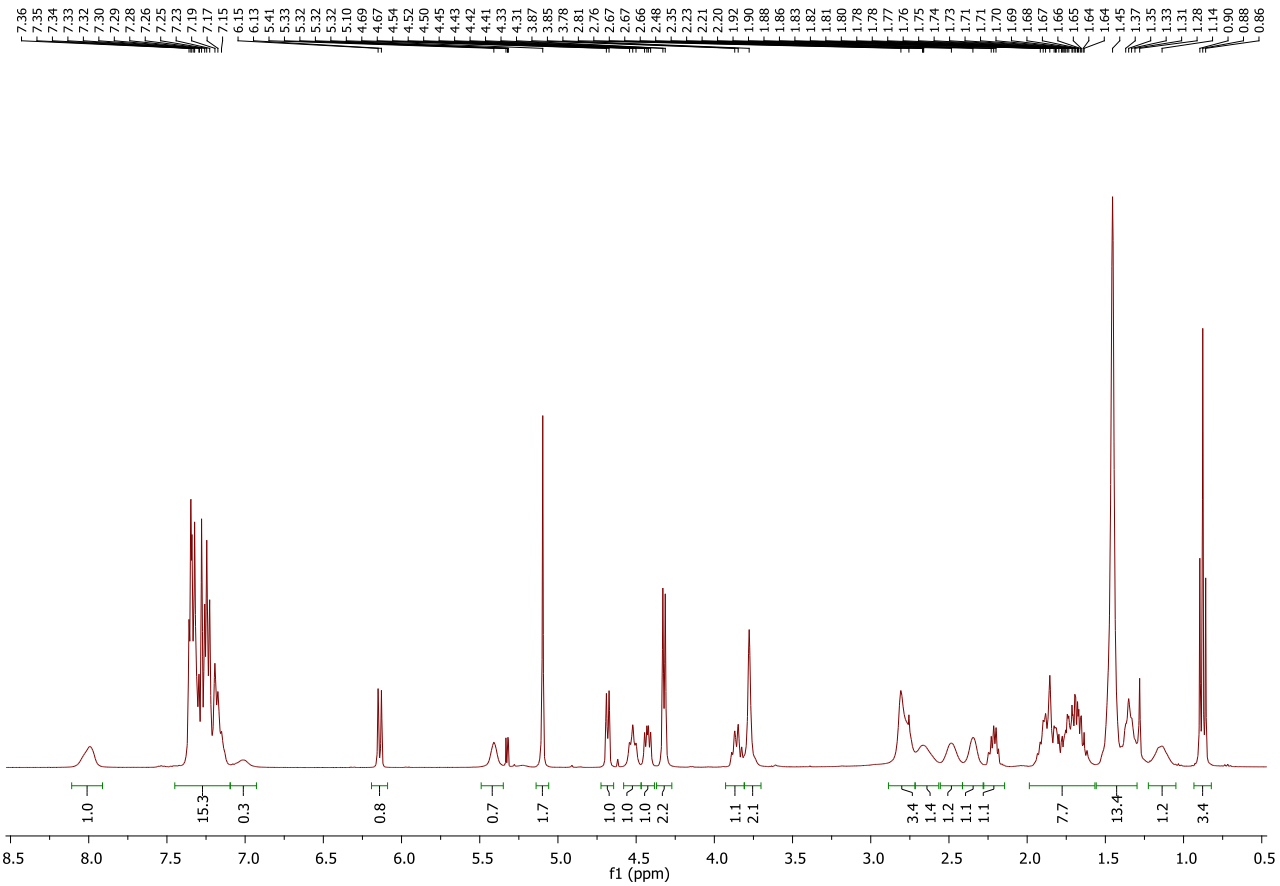

^{13}C NMR (101 MHz, CD_2Cl_2)

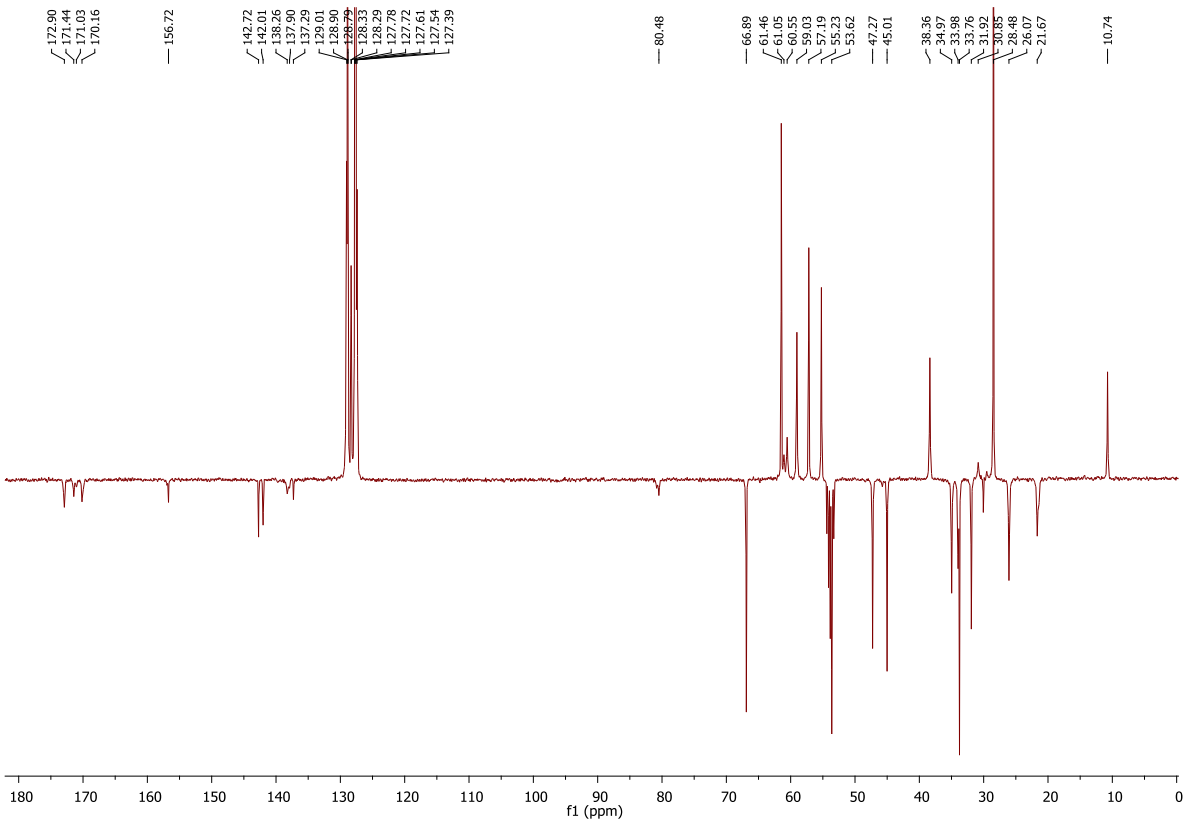

94:

^{1}H NMR (400 MHz, acetone-d_6)

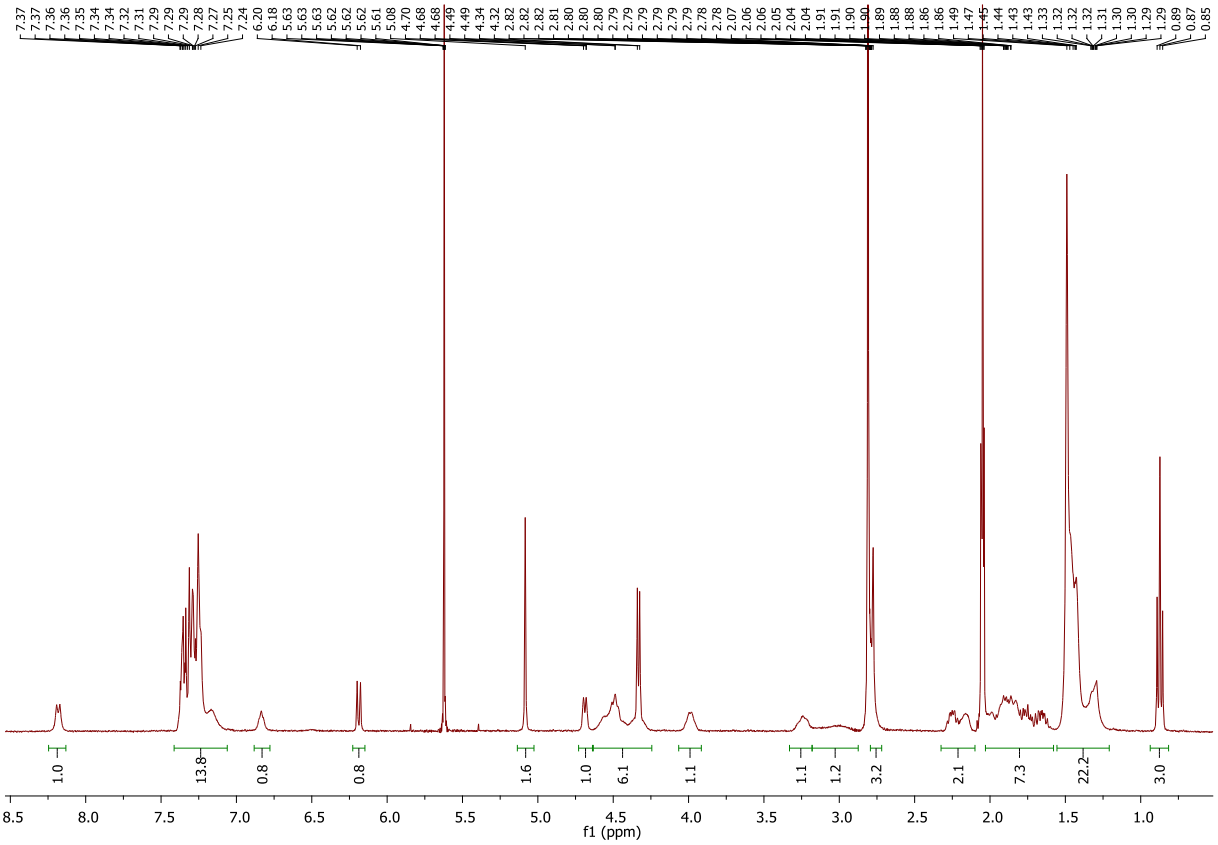

9

5:

^{1}H NMR (400 MHz, acetone-d_6)

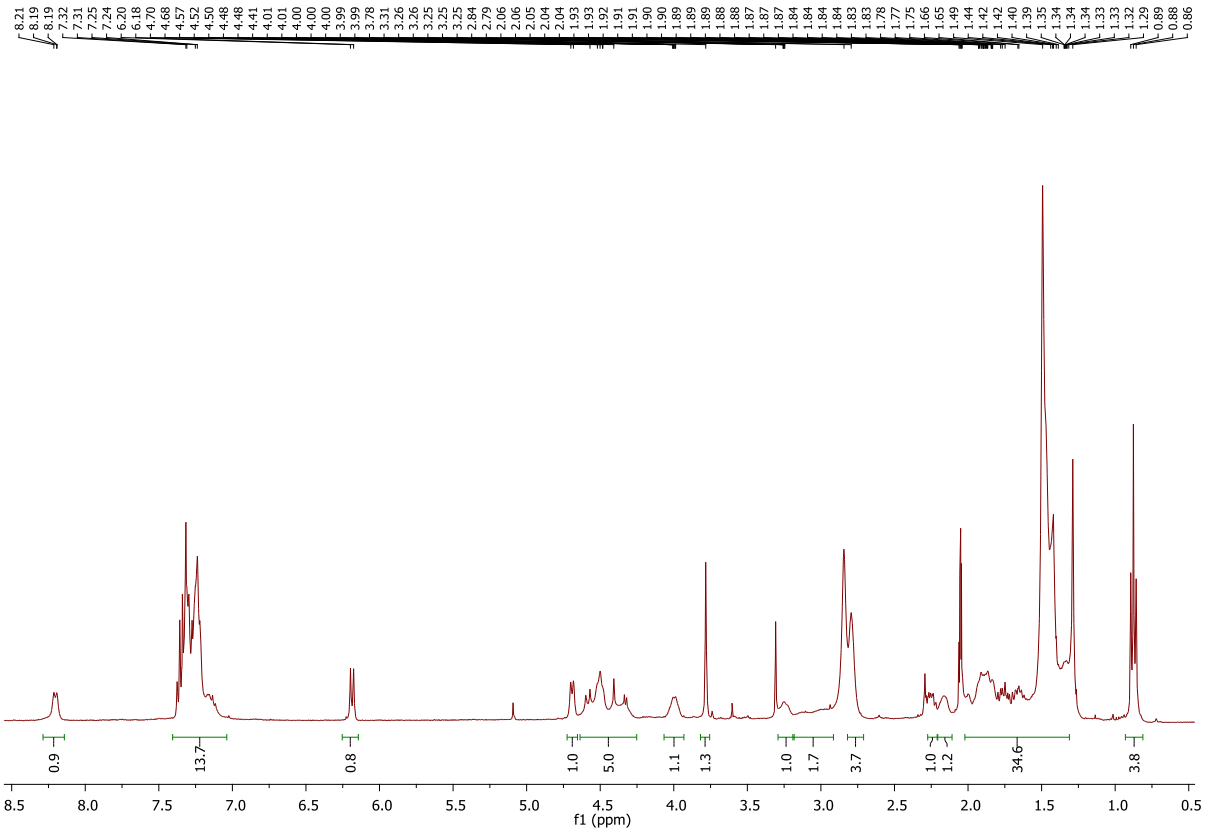

96:

^{1}H NMR (400 MHz, acetone-d_6)

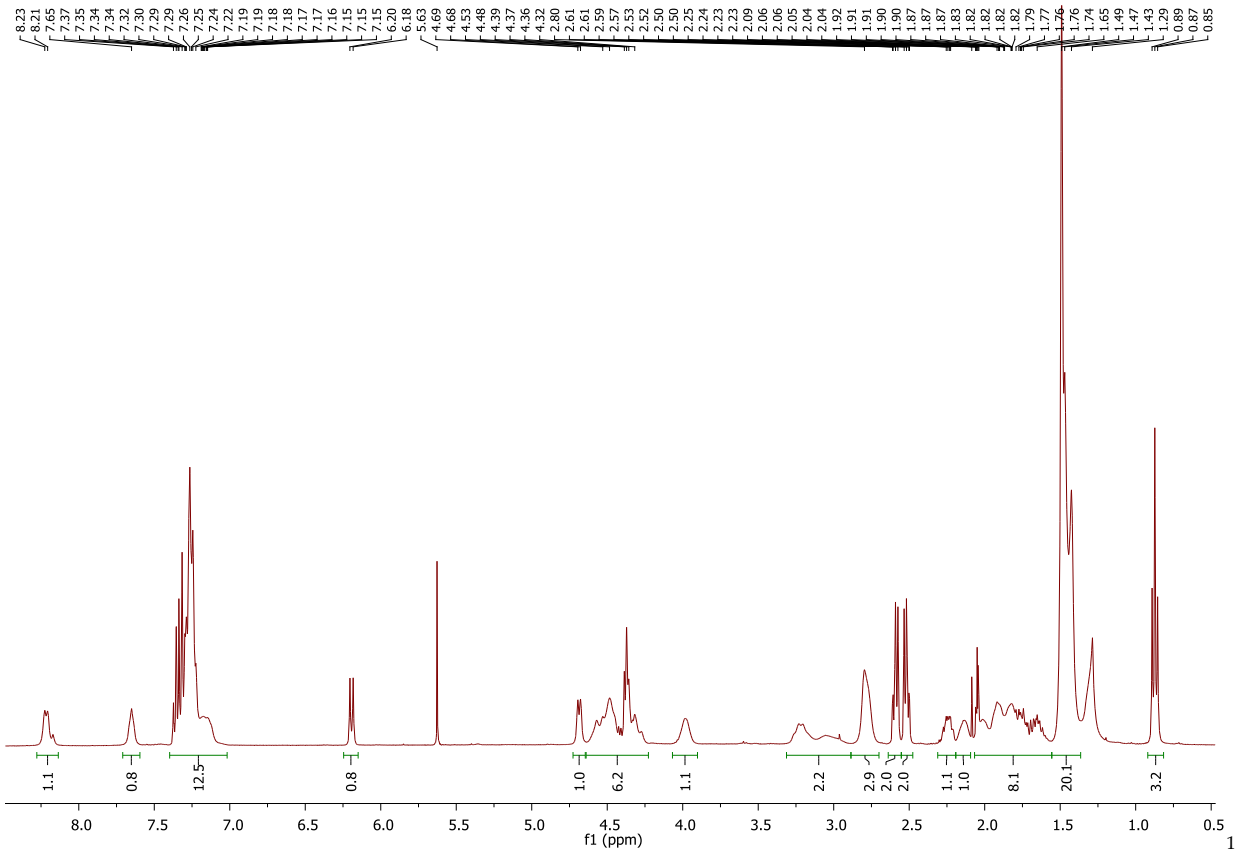

^{3}C NMR (101 MHz, acetone-d_6)

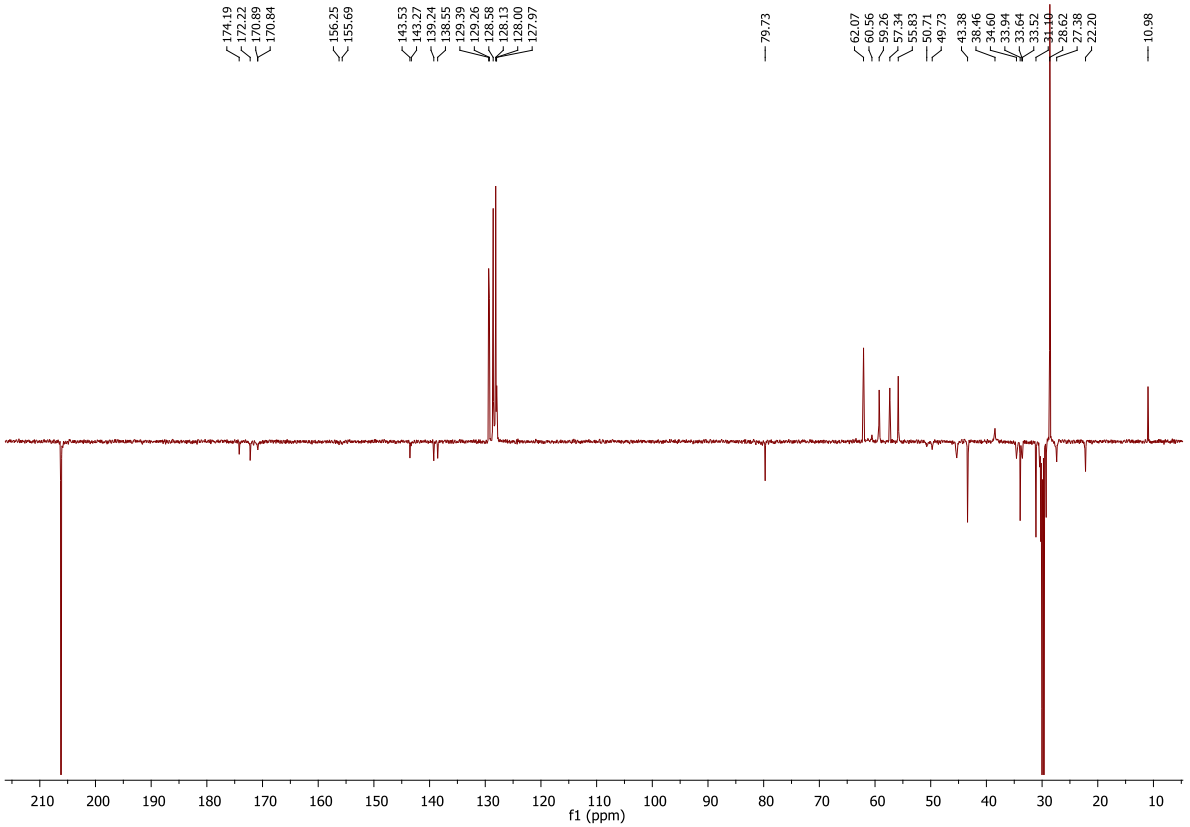

97:

^{1}H NMR (400 MHz, CD_3OD)

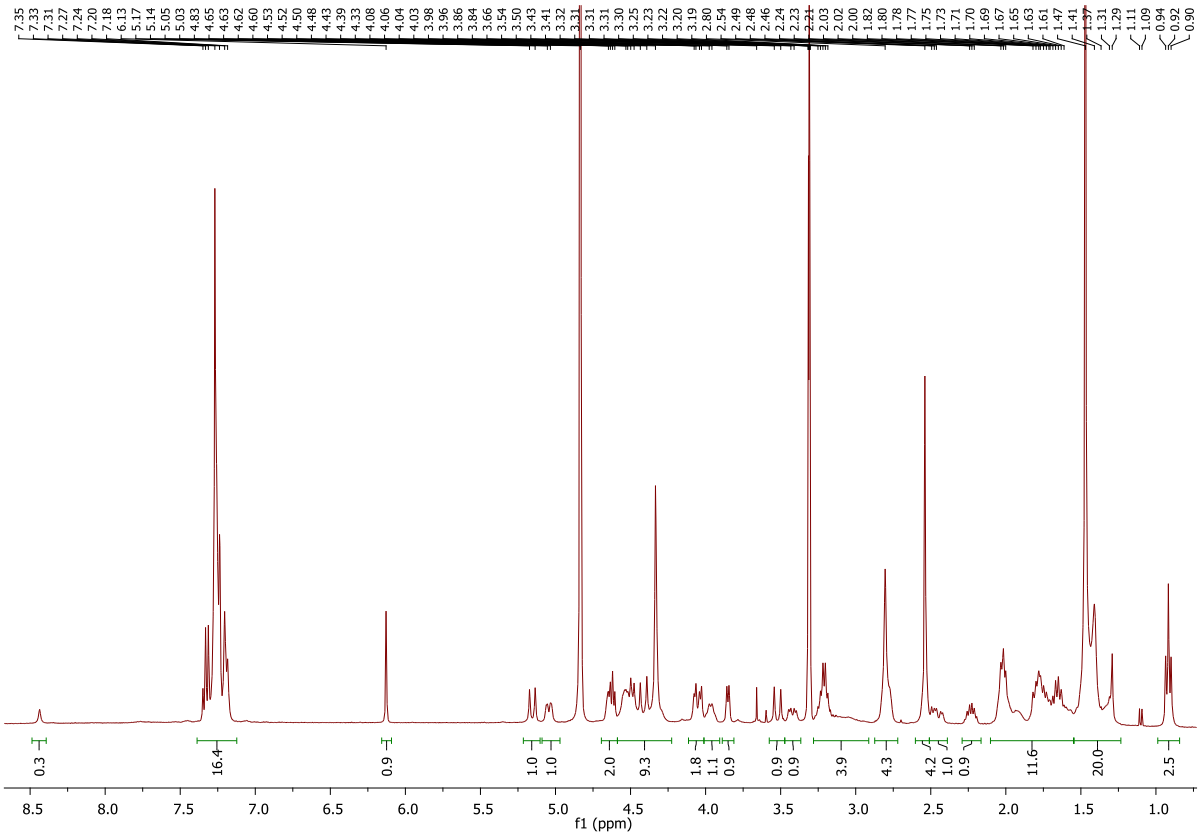

13

C NMR (101 MHz, CD_3OD)

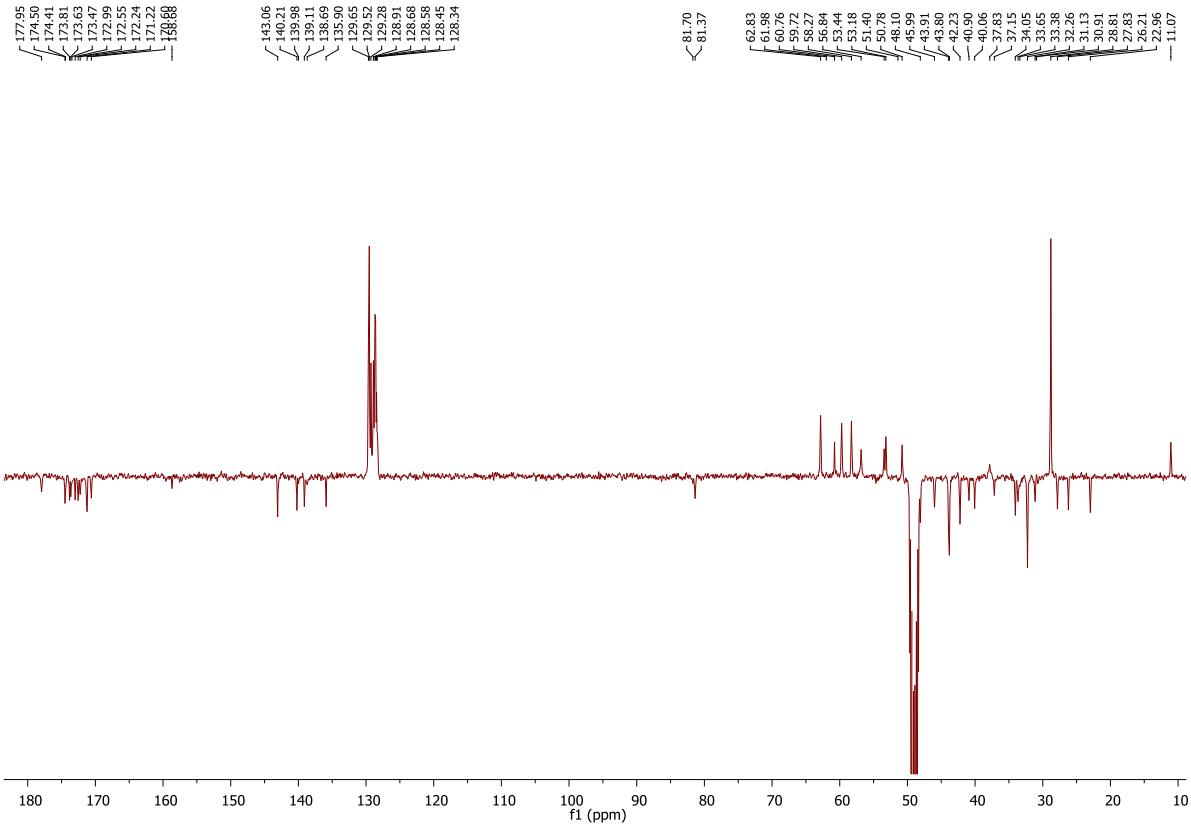

c[DKP-RGD]-N-SMAC:

^{1}H NMR (400 MHz, CD_3CN)

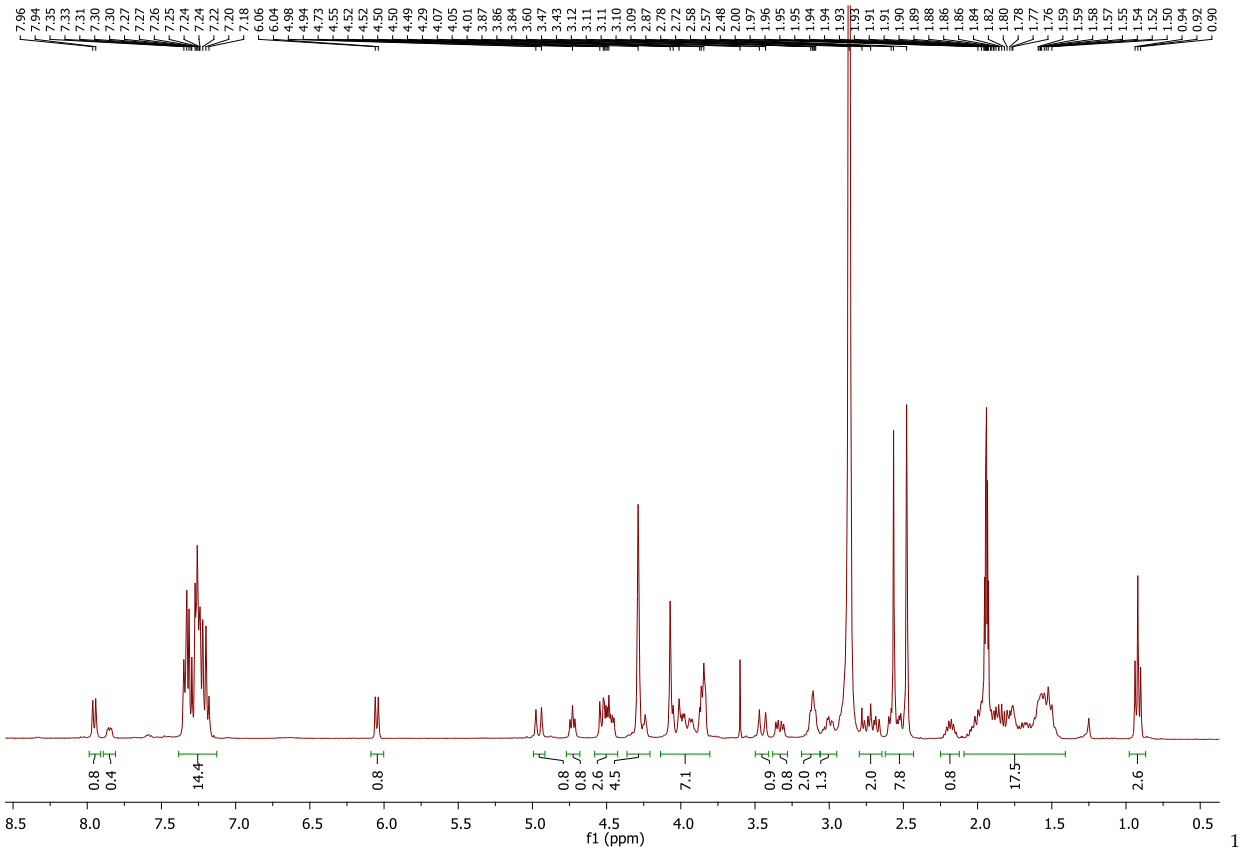

1

^{3}C NMR (101 MHz, CD_3CN)

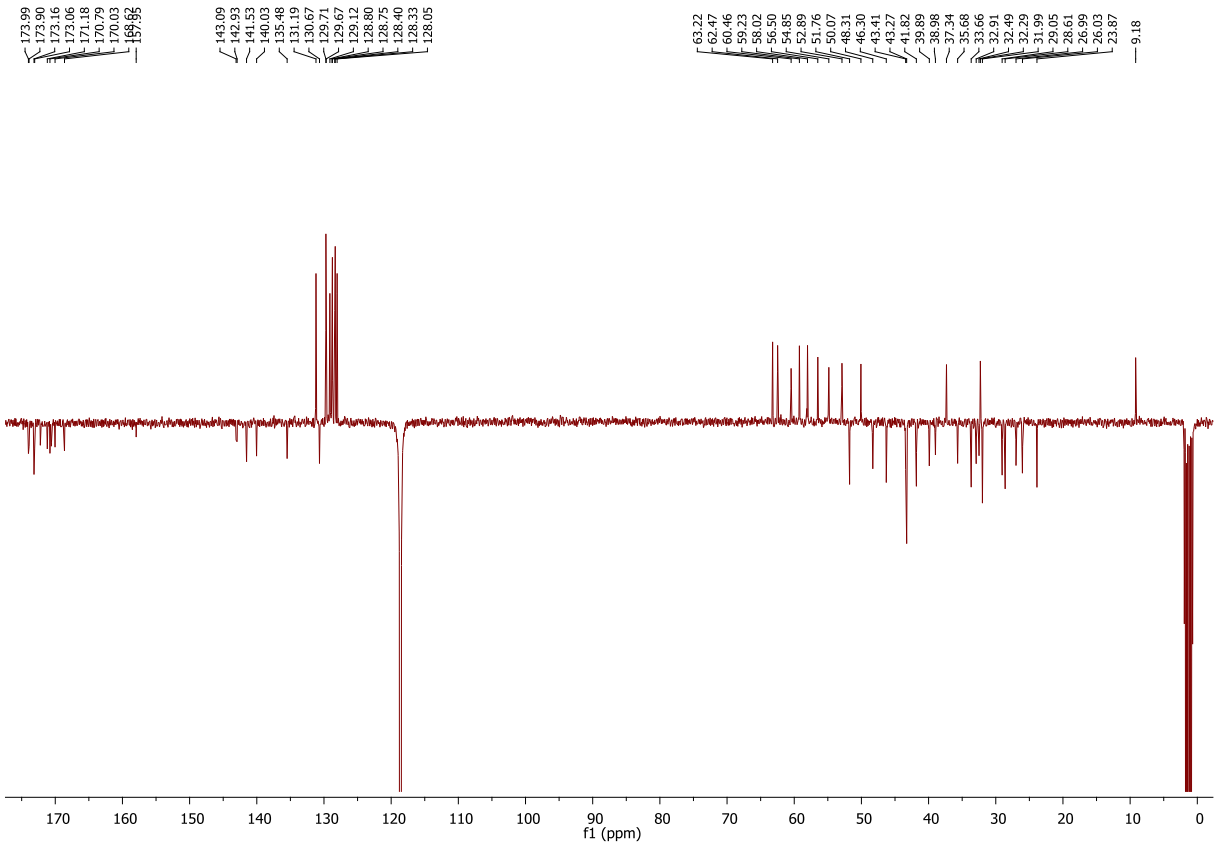

112:

^{1}H NMR (400 MHz, acetone-d_6)

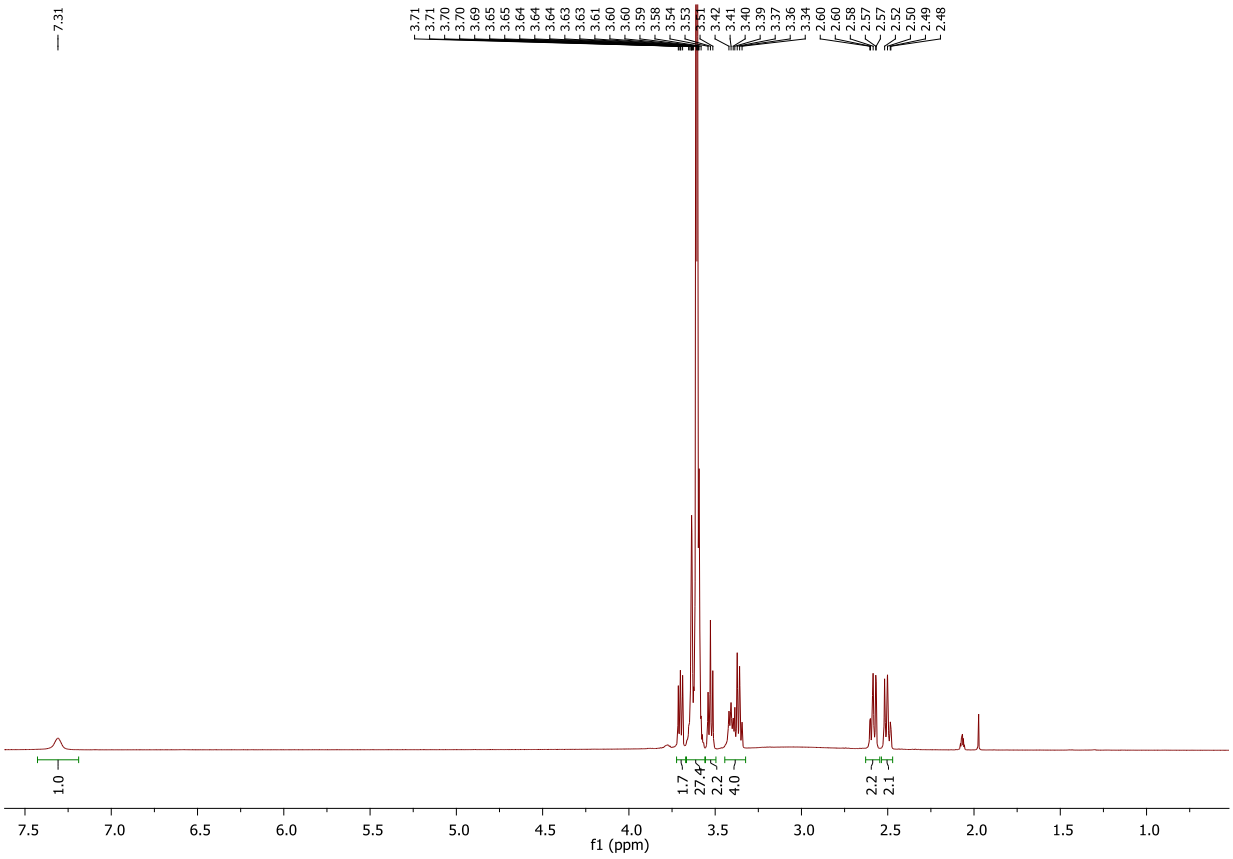

113:

^{1}H NMR (400 MHz, CD_3OD)

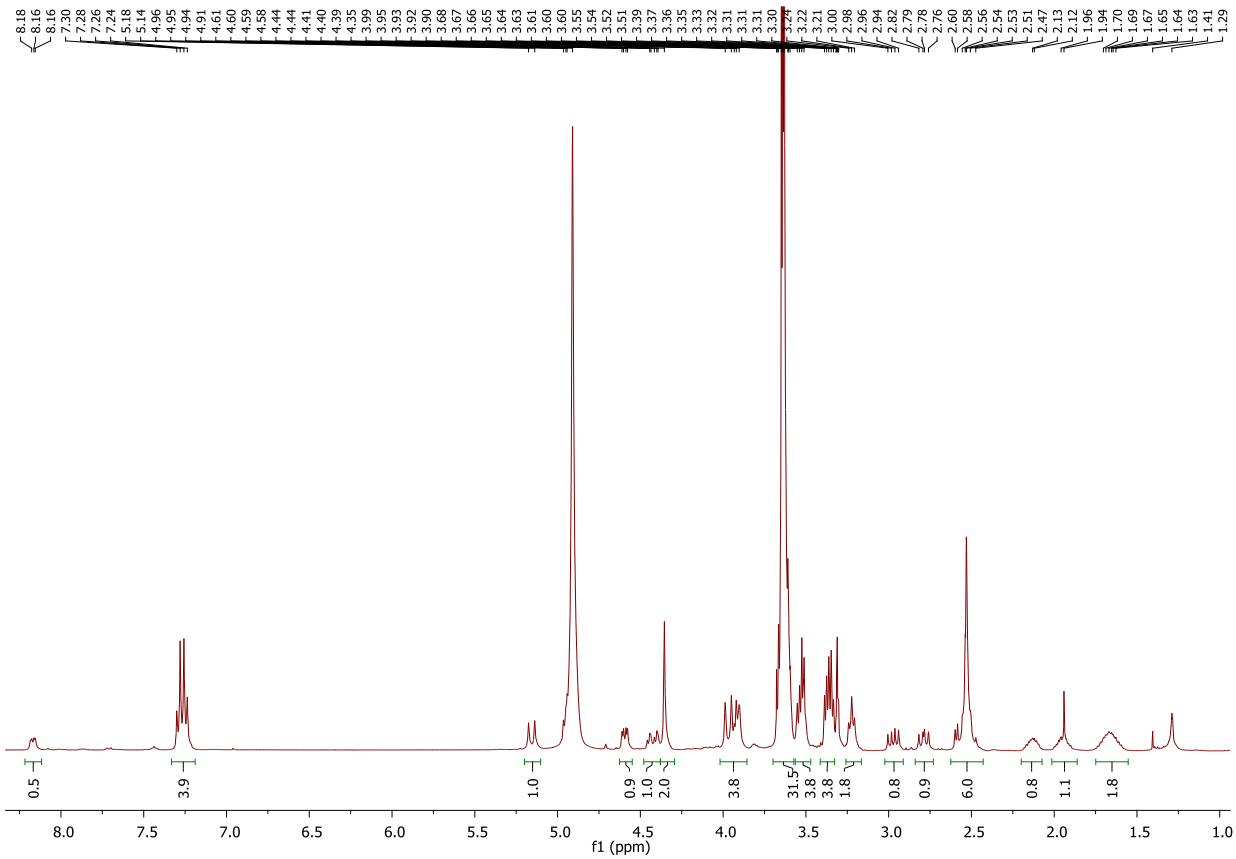

^{13}C NMR (101 MHz, CD_3OD)

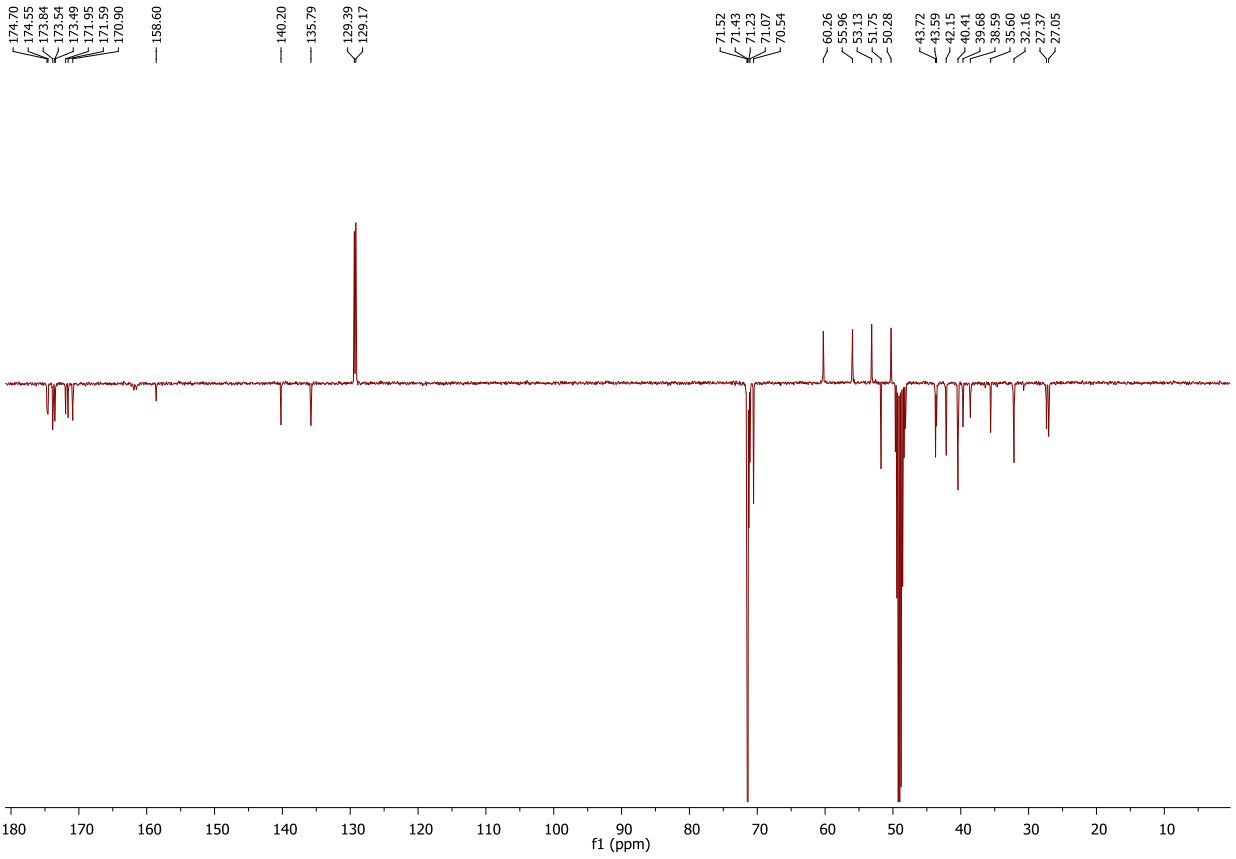

MA:

MS-MALDI-TOF (HCCA matrix)

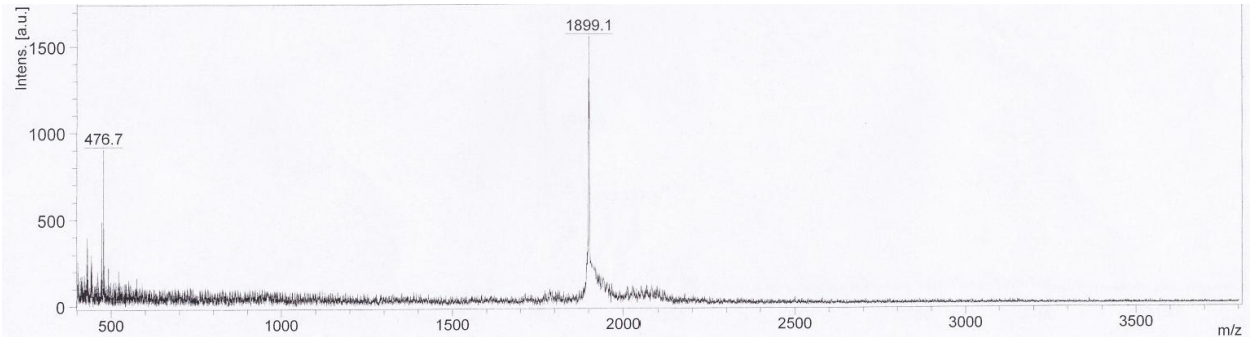

Ac-MA:

MS-MALDI-TOF (SIN matrix)

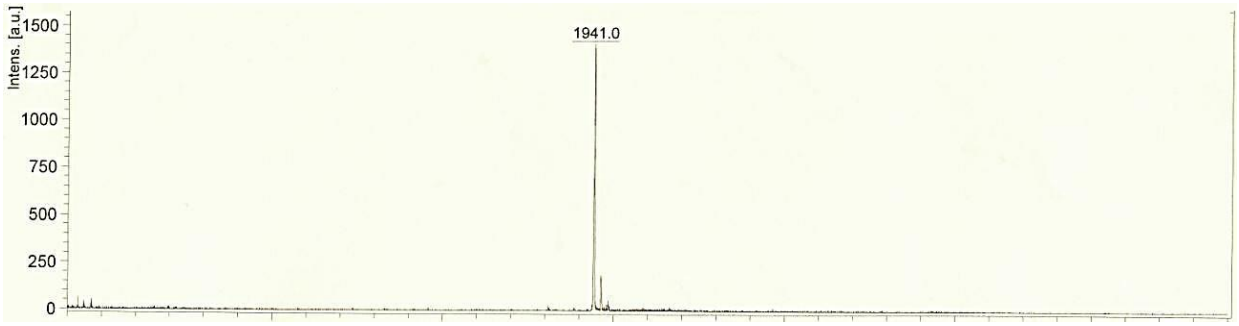

MA-RGD:

MS-MALDI-TOF (SIN matrix)

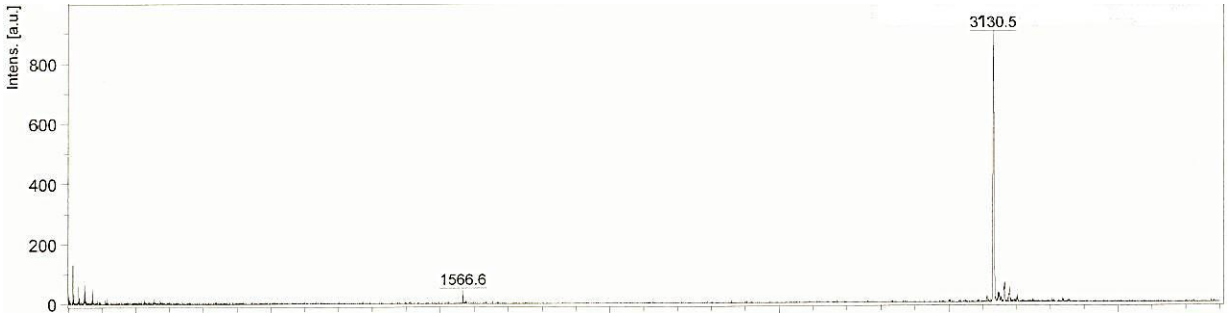

Ac-MA-RGD:

MS-MALDI-TOF (HCCA matrix)

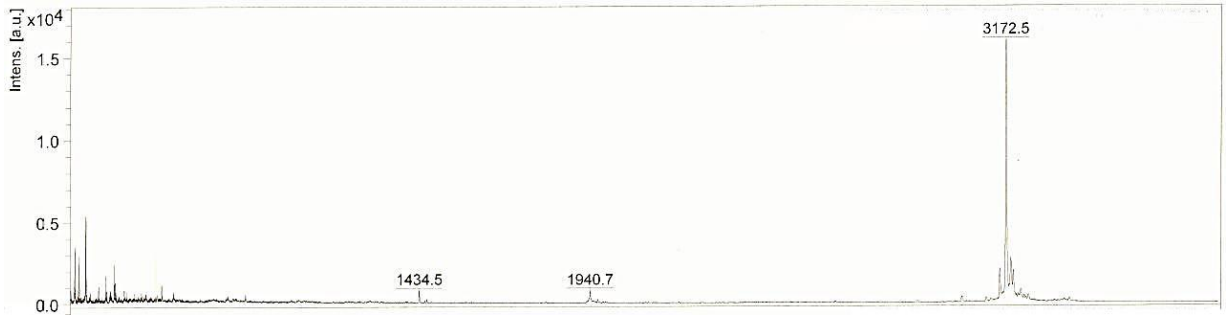

ABBREVIATIONS

Amino acid	One-letter code	Three-letter code
Alanine	A	Ala
Arginine	R	Arg
Asparagine	N	Asn
Aspartic	D	Asp
Cysteine	C	Cys
Glutamine	Q	Gln
Glutamic acid	E	Glu
Glycine	G	Gly
Histidine	H	His
Isoleucine	I	Ile
Leucine	L	Leu
Lysine	K	Lys
Methionine	M	Met
Phenylalanine	F	Phe
Proline	P	Pro
Serine	S	Ser
Threonine	T	Thr
Tryptophan	W	Trp
Tyrosine	Y	Tyr
Valine	V	Val
Unspecified amino acid	X	Xaa, Yaa

D-amino acids are described by D-Xaa in the three-letter code and with the small letter in the one-letter code.

1D, 2D, 3D	One / two / three- dimensional
Ac	acetyl
ACC	aminocyclopropanecarboxylic acid
AcOH	acetic acid
ACPC	aminocyclopentanecarboxylic acid
All	allyl
aq.	aqueous solution
Ar	aryl
Bn	benzyl
Boc	tert-butyloxycarbonyl-
Bu	Butyl
c-	cyclo
Cbz	Benzyloxycarbonyl-
CD	Circular Dichroism
Conc.	Concentrated
COSY	Correlation Spectroscopy
DBU	1,8-diazabicyclo[5.4.0]undec-7-ene
DCC	dicyclohexylcarbodiimide
DCM	dichloromethane
DIAD	diisopropylazadicarboxylate
DIC	diisopropylcarbodiimide
DIPEA	diisopropylethylamine
DKP	diketopiperazine
DMAP	dimethylaminopyridine
DMF	dimethylformamide
DMSO	dimethylsulfoxyde
DPPA	diphenylphosphoric acid azide
ECM	Extracellular matix
EDC	Ethyl-N,N-dimethyl-3-aminopropyl carbodiimide
eq.	equivalents
ESI	electrospray ionisation
Et	Ethyl
Fmoc	9-Fluorenylmethoxycarbonyl
Fn	Fibronectin
h	hours
HATU	O-(7-azabenzotriazol-1-yl)-tetramethyl-uronium hexafluorophosphate
ROESY	Rotating Frame NOE spectroscopy
sat.	saturated
SPPS	solid phase peptide synthesis
tBu	tert-butyl
TEA	triethylamine
tert	tertiary
Tf	triflate
TFA	trifluoroacetic acid
HBTU	O-benzotriazole-N,N,N′,N′-tetramethyl-uronium hexafluorophosphate
HMBC	heteronuclear multiple bond correlation
HOAt	1-Hydroxy-7-azabenzotriazole
HOBt	N-Hydroxybenzotriazole
HPLC	high performance liquid chromatography
HSQC	heteronuclear single quantum correlation
IC	inhibitory capacity
*i*PrOH	propan-2-ol
IR	Infrared Spectroscopy
J	Scalar coupling constants
KHMDS	potassium hexamethyldisilazane
MALDI	Matrix-assisted laser desorption ionization
MC	Monte Carlo
MD	molecular dynamics
Me	methyl
MeOH	methanol
MIDAS	Metal ion dependent site
min.	minutes
MS	Mass Spectroscopy
MW	Molecular weight
NMR	Nuclear Magnetic Resonance
NOE	Nuclear Overhauser Effect
PG	Protecting group
Ph	Phenyl
ppb	Part per billion
ppm	Part per million
Py	Pyridine
quant.	quantitative
quat.	quaternary
r.t.	room temperature
Rf	Retention faktor
RMSD	Root Mean Square Deviation
TFE	Trifluoroethanol
THF	tetrahydrofurane
TIS	triisopropylsilane
TMS	trimethylsilyl
TOCSY	Total Correlation Spectroscopy
tol	toluene
UV	Utraviolet Spectroscopy
δ	Chemical shift